

*McGraw-Hill* **HANDBOOKS**

# CAM DESIGN HANDBOOK



- Cam size and profile determination
- Numerical controls for manufacturing
- Computer-aided design techniques

HAROLD A. ROTHBART

---

# CAM DESIGN HANDBOOK

---

**Harold A. Rothbart** Editor

*Dean Emeritus  
College of Science and Engineering  
Fairleigh Dickinson University  
Teaneck, New Jersey*

**McGRAW-HILL**

New York Chicago San Francisco Lisbon London Madrid  
Mexico City Milan New Delhi San Juan Seoul  
Singapore Sydney Toronto

Copyright © 2004 by The McGraw-Hill Companies, Inc. All rights reserved. Manufactured in the United States of America. Except as permitted under the United States Copyright Act of 1976, no part of this publication may be reproduced or distributed in any form or by any means, or stored in a database or retrieval system, without the prior written permission of the publisher.

0-07-143328-7

The material in this eBook also appears in the print version of this title: 0-07-137757-3.

All trademarks are trademarks of their respective owners. Rather than put a trademark symbol after every occurrence of a trademarked name, we use names in an editorial fashion only, and to the benefit of the trademark owner, with no intention of infringement of the trademark. Where such designations appear in this book, they have been printed with initial caps.

McGraw-Hill eBooks are available at special quantity discounts to use as premiums and sales promotions, or for use in corporate training programs. For more information, please contact George Hoare, Special Sales, at [george\\_hoare@mcgraw-hill.com](mailto:george_hoare@mcgraw-hill.com) or (212) 904-4069.

## TERMS OF USE

This is a copyrighted work and The McGraw-Hill Companies, Inc. (“McGraw-Hill”) and its licensors reserve all rights in and to the work. Use of this work is subject to these terms. Except as permitted under the Copyright Act of 1976 and the right to store and retrieve one copy of the work, you may not decompile, disassemble, reverse engineer, reproduce, modify, create derivative works based upon, transmit, distribute, disseminate, sell, publish or sublicense the work or any part of it without McGraw-Hill’s prior consent. You may use the work for your own noncommercial and personal use; any other use of the work is strictly prohibited. Your right to use the work may be terminated if you fail to comply with these terms.

THE WORK IS PROVIDED “AS IS”. MCGRAW-HILL AND ITS LICENSORS MAKE NO GUARANTEES OR WARRANTIES AS TO THE ACCURACY, ADEQUACY OR COMPLETENESS OF OR RESULTS TO BE OBTAINED FROM USING THE WORK, INCLUDING ANY INFORMATION THAT CAN BE ACCESSED THROUGH THE WORK VIA HYPERLINK OR OTHERWISE, AND EXPRESSLY DISCLAIM ANY WARRANTY, EXPRESS OR IMPLIED, INCLUDING BUT NOT LIMITED TO IMPLIED WARRANTIES OF MERCHANTABILITY OR FITNESS FOR A PARTICULAR PURPOSE. McGraw-Hill and its licensors do not warrant or guarantee that the functions contained in the work will meet your requirements or that its operation will be uninterrupted or error free. Neither McGraw-Hill nor its licensors shall be liable to you or anyone else for any inaccuracy, error or omission, regardless of cause, in the work or for any damages resulting therefrom. McGraw-Hill has no responsibility for the content of any information accessed through the work. Under no circumstances shall McGraw-Hill and/or its licensors be liable for any indirect, incidental, special, punitive, consequential or similar damages that result from the use of or inability to use the work, even if any of them has been advised of the possibility of such damages. This limitation of liability shall apply to any claim or cause whatsoever whether such claim or cause arises in contract, tort or otherwise.

DOI: 10.1036/0071433287



# Professional

## Want to learn more?

We hope you enjoy this McGraw-Hill eBook! If you'd like more information about this book, its author, or related books and websites, please [click here](#).

*To Florence, Ellen, Dan and Jane,  
Candice, Michael, Jessica and Justine*

*This page intentionally left blank.*

[For more information about this title, click here.](#)

---

# CONTENTS

---

<b>Contributors</b>	<b>vii</b>
<b>Preface</b>	<b>ix</b>
<b>Chapter 1. Introduction</b>	<b>1</b>
<b>Chapter 2. Basic Curves</b>	<b>27</b>
<b>Chapter 3. Modified Cam Curves</b>	<b>55</b>
<b>Chapter 4. Polynomial and Fourier Series Cam Curves</b>	<b>89</b>
<b>Chapter 5. Cam Motion Synthesis Using Spline Functions</b>	<b>107</b>
<b>Chapter 6. Elements of Cam Profile Geometry</b>	<b>159</b>
<b>Chapter 7. Geometry of Planer Cam Profiles</b>	<b>175</b>
<b>Chapter 8. Cam Mechanism Forces</b>	<b>217</b>
<b>Chapter 9. Cam Materials and Lubrication</b>	<b>251</b>
<b>Chapter 10. Cam Manufacturing</b>	<b>285</b>
<b>Chapter 11. Cam System Modeling</b>	<b>315</b>
<b>Chapter 12. Cam System Dynamics—Analysis</b>	<b>357</b>
<b>Chapter 13. Cam System Dynamics—Response</b>	<b>399</b>
<b>Chapter 14. Special Cam Mechanisms</b>	<b>453</b>
<b>Chapter 15. Cams in Microelectromechanical Systems</b>	<b>505</b>
<b>Chapter 16. Automotive Camshaft Dynamics</b>	<b>529</b>
<b>Appendix A Basic Contours</b>	<b>545</b>
<b>Appendix B Basic Cam Curve Factors</b>	<b>551</b>
<b>Appendix C Polynomial Coefficients</b>	<b>557</b>
<b>Appendix D Cam Computer Software</b>	<b>561</b>
<b>Appendix E CAD/CAM for a Medical Instrument Cam Mechanism</b>	<b>565</b>
<b>Appendix F Optimal Control Theory Derivation for Two-Point Boundary Value Problem</b>	<b>585</b>
<b>Index</b>	<b>587</b>

*This page intentionally left blank.*

---

# CONTRIBUTORS

---

**G.K. Ananthasuresh** *Assistant Professor of Mechanical Engineering and Applied Mechanics, University of Pennsylvania, Philadelphia, Pennsylvania* (CHAP. 15)

**Jorge Angeles** *Professor of Mechanical Engineering, McGill University, Montreal, Canada* (CHAP. 7)

**J. Jesús Cervantes-Sánchez** *Professor, Departamento de Ingeniería Mecánica, Universidad de Guanajuato, Salamanca, Mexico* (CHAP. 7)

**Thomas L. Dresner** *Consulting Engineer, Mountain View, California* (CHAP. 13)

**Demitri Elgin** *D. Elgin Cams Co., Redwood City, California* (CHAP. 16)

**J. Christian Gerdes** *Assistant Professor of Mechanical Engineering, Design Division, Stanford University, Palo Alto, California* (CHAP. 11)

**Cecil O. Huey, Jr.** *Professor of Mechanical Engineering Clemson University, Clemson, South Carolina* (CHAP. 5)

**Harold A. Rothbart** *Dean Emeritus, College of Science and Engineering, Fairleigh Dickinson University, Teaneck, New Jersey* (CHAPS. 1, 2, 3, 4, 6, 8, 9, 10, 12, 14)

**Carlos Santiago Lopez-Cajún** *Professor de la Facultad, Departamento de Ingeniería, Universidad Autónoma de Querétaro, Querétaro, Mexico* (CHAP. 7)

**Dermin Tsay** *Professor, Department of Mechanical Engineering, National Sun Yat Sen University, Kaohsiung, Taiwan* (CHAP. 5)

*This page intentionally left blank.*

---

# PREFACE

---

A cam is a versatile, specially shaped part of a machine that is always in contact with a member called the follower. The name *cam* should not be confused with the common abbreviation *cam* for camera or camcorder, both used in the fields of photography and video, nor with the acronym CAM applied to computer-aided manufacturing, which utilizes computational facilities for machinery fabrication of all kinds.

The book is written for the designer concerned with creating or inventing a physical or mathematical function, a motion or an action, a mechanism or a machine. It would be valuable to the mechanical engineer, electrical engineer, physicist, and scientist aimed at developing cam-follower systems of all kinds, sizes, and speeds. In addition, shop machinists and toolmakers who make and assemble the machinery will find this book of value in their work. Automobile and racing car enthusiasts should find this book helpful in their aspirations. Last, the book can be an aid to students in engineering by introducing theoretical and practical applications of multifaceted ingenious mechanisms and machinery.

Cam design is constantly evolving. New techniques and information are available for cam synthesis, analysis, dynamics, and performance and the production of the actual cam body itself. The most significant advancement of cam systems has resulted from the application of the digital computer. Computer-aided design (CAD) and computer-aided manufacturing (CAM) have been invaluablely applied as software tools. CAD design is downloaded to CAM in discrete increments by computer numerical control (CNC) for actual cam production.

The content of the handbook may be considered in the following categories:

- Cam curves: basic trigonometric, modified or blended from basic curves, polynomial curves, Fourier series curves, and spline functions
- Cam profile geometry, consisting of pressure angle, curvature, and profile analysis
- Cam hardware, including materials, lubrication, and manufacturing
- Cam system dynamics, containing the elastic follower and drive systems, vibratory analysis, and response

This book is for use in the following fields of application:

- Industrial and commercial machinery, as a critical part of production equipment for goods and services, for example, shoe making, steel mill equipment, and paper printing presses
- Automotive performance and optimization, as a high-speed automotive valve operating system
- Cams in microelectromechanical systems (MEMS), for micromachinery in miniature control systems
- Cams as analog computers
- Gadgets, mechanisms, and machinery, as inventive, ingenious devices

Furthermore, this book contains the latest, most important techniques and test data available. The philosophy of the book is to present diversified applications for cams to aid the reader's understanding and design selection. This volume also contains many new examples, a listing of computer software, and an extensive list of references.

It should be noted that cams, gearing, rolling-element bearings, and traction (friction) drives are of the same basic mechanical family, the study of which is generically referred to as contact mechanics. These devices have in common rolling and/or sliding action coupled with reasonably high concentrated contact (Hertz) stresses. In the field of contact mechanics the failure mechanisms among these machine elements are similar and are related to material metallurgy and heat treatment, lubricant rheology and chemistry, surface topography and geometry, and applied contact load (stress). These machine components also have commonly related manufacturing requirements. Hence, they share a similar manufacturing technology and engineering analysis.

The significance of cam profile accuracy is emphasized. A surface may appear smooth to the eye and yet have poor dynamic properties. Depending on the application and loads the cam profile accuracy and its surface finish may affect the life, vibration, and noise of a cam-follower system. Poor manufacturing techniques can impede the functional ability of a mechanism or machine. Also, the choice of a lubricant and the lubrication system is pertinent on all designs.

We express our respect for the inventors, designers, engineers, scientists, toolmakers, and machinists who produced cam systems in the past. Our knowledge and experience are a result of the amazing contributions and successful machines these experts handed down over the years that they toiled. This evidence of their work is our fortunate heritage. We are surrounded with evidence of the high-quality performance of these machines, which was accomplished with less mathematical guidance, poor manufacturing facilities, and crude measurement tools. All the while, nature revealed her secrets, very slowly, bit by bit. It is to be noted that the Chinese exercise for health and combat, T'ai Chi Ch'uan, has a ritual that spiritually parallels the foregoing thought. The training performance classes conclude with the loud clapping of hands, which is speculated to be in deference to all those who went before.

Last, I wish to express my appreciation to Heather Tinsley, Washington, D.C., who edited and assisted in the production of this handbook. Also, grateful acknowledgment is due the elite chapter contributors whose dedication to the handbook is most noteworthy. I wish also to thank the many in academia and industry who were helpful in providing valuable guidance and information for the book, such as Samuel L. Doughty, Consulting Engineer, Mount Ephraim, New Jersey; Arthur F. Erdman, Professor of Mechanical Engineering, University of Minnesota, Minneapolis; Ralph Fusco, Consulting Engineer, Commack, New York; Grigor Kerdanyan, Consulting Engineer, Van Nuys, California; James A. Kurth, Senior Analytical Engineer, Commercial Cam Company, Inc., Wheeling, Illinois; Bernard Roth, Professor of Mechanical Engineering, Stanford University, Palo Alto, California; Michael Savage, Professor Emeritus of Mechanical Engineering, University of Akron, Akron, Ohio; and James L. Wiederrich, Manager, Modeling and Simulation, United Defense L.P., Santa Clara, California. Special recognition goes to Erwin V. Zaretsky, Branch Chief of Mechanical Components Branch, NASA Lewis Research Center, Cleveland, Ohio, for the many inspirational hours we spent discussing the subject of cams.

*Harold A. Rothbart*

---

# CHAPTER 1

---

# INTRODUCTION

---

Harold A. Rothbart, D.Eng.

1.1 INTRODUCTION	1	1.6 CAM PROFILE GRAPHICAL LAYOUT	15
1.2 CAM-FOLLOWER SYSTEM CRITERIA	2	1.7 CAM DEFINITIONS	17
1.3 FOLLOWER TYPES	4	1.8 OTHER METHODS THAN CAMS	20
1.4 CAM CLASSIFICATIONS	5	1.9 DESIGN CONSIDERATIONS	21
1.5 CAMS IN TERMS OF FOLLOWER MOTION	15		

---

## 1.1 INTRODUCTION

---

A cam is an element of the cam-follower mechanical system that compels the movement of the follower by direct contact. The motion of the follower is the result of a program. Just as a computer is programmed, so is a cam. Thus, the system can be thought of as a *mechanical information device*. Accordingly, the goal of the designers is to build a program, establish the locus of the contact points between the cam and follower, produce the cam profile coordinates system, and fabricate the cam within an acceptable accuracy. After all the parts are assembled the performance of the cam-follower system is observed.

No one is sure where and how cams got their start. The Sanskrit (Indo-Iranian) term *Jambha* (“cog,” “peg,” or “tooth”) may indicate the geographic area in which they had their beginnings, and so may the Teutonic “Kambr” (toothed instrument), which refers to cam mechanisms that have their origin in the wedge (a linear cam) and have been found in Paleolithic Age relics of about 10,000 years ago. The later construction of the great pyramids of Egypt also involved the use of the wedge. However, it was the genius of Leonardo da Vinci that produced a modern design cam applied to a machine for pumping water.

Cam-follower mechanisms are found in almost all mechanical devices and machines (i.e., agriculture, transportation equipment, textiles, packaging, machine tools, printing presses, automobile internal combustion engines, food processing machines, switches, ejection molds, and control systems, and more recently in micromachines such as micro-electromechanical systems [MEMS]). Figure 1.1 shows an automobile cam-driven overhead valve train linkage.

More recently, computer resources, known as CAD/CAM for cams, offer significant simplification in the design and fabrication of assembled cam and follower systems. CAD/CAM refers to computer-aided design and computer-aided manufacturing. Graphic workstations enable the design engineer to optimize the motion and geometry of a cam mechanism and also to incorporate the kinematic and dynamic performance requirements necessary over the entire range of operating speeds. In the manufacturing process, networked numerically controlled (NC) machines receive digitized geometric data from a CAD system. The downloaded file of cam coordinate data is forwarded directly to the machine tool controller, which eliminates the potential human error inherent in older techniques of manufacturing. The accuracy of the cam produced is frequently improved, and the costs are lowered.

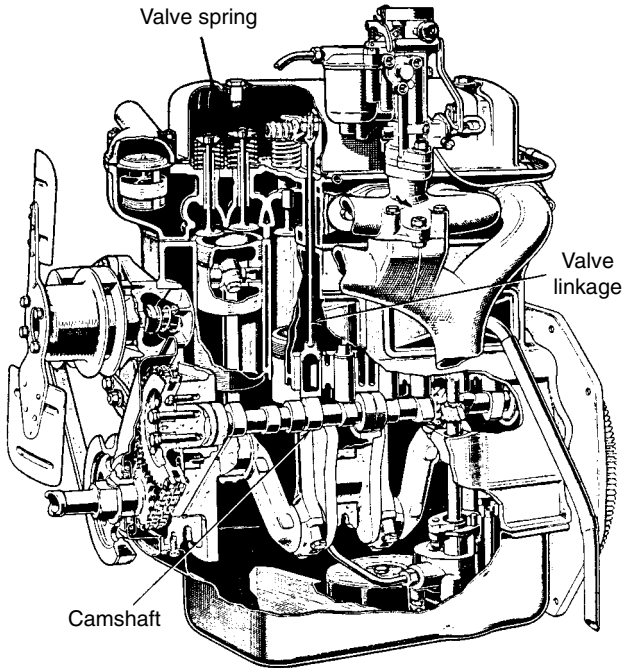


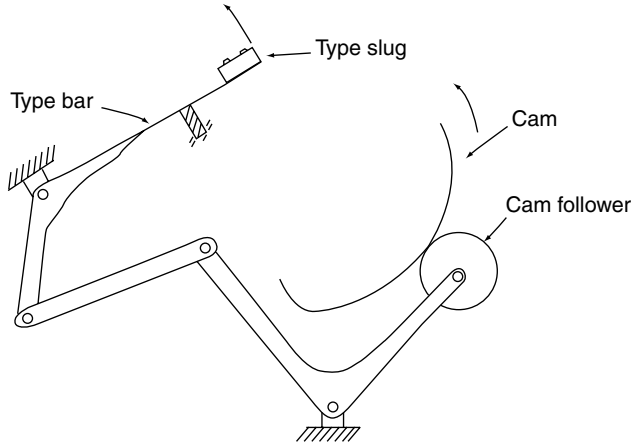
FIGURE 1.1. Automobile cam-driven overhead valve train linkage.

## 1.2 CAM-FOLLOWER SYSTEM CRITERIA

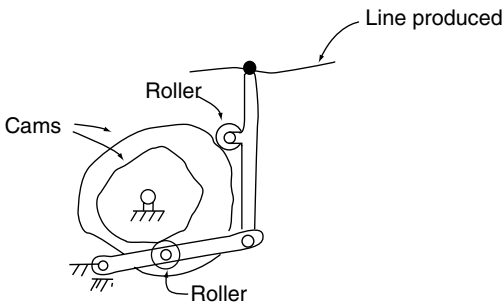
The cam-follower system may be designed for *path*, *motion*, or *function generation*. This book treats the cam and the follower almost totally as a function generator in which the output of the follower is a function of the cam input. Erdman and Sandor (1997) illustrate the three types of cam design functions in Figure 1.2. Figure 1.2a shows a function generator in which the cam drives a four-bar linkage to a type slug bar of an electric typewriter. The cam moves the linkage to impact the type slug to a platen roller (not shown). Figure 1.2b shows a path generator cam that uses a double cam to produce a line that is desired. Figure 1.2c shows a motion-generator cam in which a drift meter operates to define the aircraft direction of motion relative to the ground. The sight wire is aligned to follow an object on the earth that passes through the center. The instrument rotates about point  $O$  by two fixed guiding pins in a circular arc-shaped cam slot about its center. Without this design a physical pivot needed of point  $O$  would hinder the vision.

As stated previously, a cam is a mechanical member which transmits a desired action to a follower by direct contact. The driver is the cam (usually at constant speed), and the driven member is the follower. The cam may remain stationary, translate, oscillate, or rotate, whereas the follower may translate, oscillate, or index.

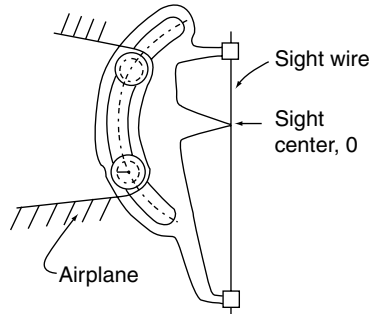
In its general form a cam mechanism (Fig. 1.3a) consists of two shaped bodies, 1 and 2, connected by a fixed third body, 3. Either body 1 or body 2 may be the driver with the other the follower. We may at each instant replace these shaped bodies by an equivalent mechanism having members as shown in Fig. 1.3b. These members are pin-jointed at the



(a) Function generator  
(cam-driven typewriter mechanism).

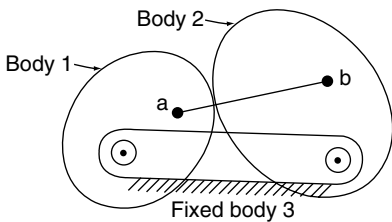


(b) Path generator  
(double cam line generator).

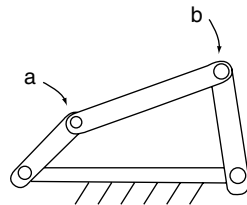


(c) Motion generator  
(aircraft drift meter).

FIGURE 1.2. Cam design functions.



(a) Mechanism  
(two shaped bodies in contact).



(b) Equivalent  
mechanism.

FIGURE 1.3. General cam mechanism. (Points *a* and *b* are the centers of curvature of point of contact.)

instantaneous centers of curvature,  $a$  and  $b$ , of the contacting surfaces. At any other instant, the points  $a$  and  $b$  are shifted and the links of the equivalent mechanism have different lengths. Grodinski (1947) and Jones (1967) have excellent compilations of practical cam mechanisms.

### 1.3 FOLLOWER TYPES

Cam follower systems are classified by referring to the follower or the cam or both. Let us consider the follower first. The follower movement is *translation*, *oscillation*, or *indexing*. The follower surface is *knife-edge*, *flat*, *curved*, or *roller*. The follower restraint to the cam is positive-driven by the use of *rollers in the cam groove* or *multiple conjugate cams*, is *spring-loaded*, or occurs by *gravity*. Also, the translating follower line of motion with reference to the cam center may be *radial* or *offset*.

The radial translating follower shown in Figure 1.4 will be used as an example. The popular oscillating follower and the rotating follower are discussed later.

The *knife-edge*, or *point*, follower (Fig. 1.4a), is, as the name implies, a sharp edge in contact with the cam. Although simple in construction, this type of follower is not practical because it results in excessive wear of the contact point. It is employed in design as the center of the roller follower.

For proper performance the follower is constrained to the cam at all speeds. The *roller follower*, Fig. 1.4b, is the most popular design for accomplishing this criterion. Commercially available roller followers use ball or needle bearings supported by a stem. *Positive drive action* is accomplished by a roller follower internally in a cam groove or track (Fig. 1.8), by followers on the opposite side of a single cam (yoke cam, Fig. 1.10), or by conjugate dual disk cams (Fig. 1.11). The roller follower has a low coefficient of friction when compared to the other followers and is most frequently used in production machinery and some automotive engines.

In contact with the cam surface the follower roller action at low speeds can be that of pure rolling; however, at higher speeds significant sliding is evident. In groove cams the fluctuation in roller speeds is the result of the driven rotational acceleration of the roller as it rides on different radial surfaces of the cam. Experience has shown that the grooved cam roller follower does not provide exact positive-driven action because of the neces-

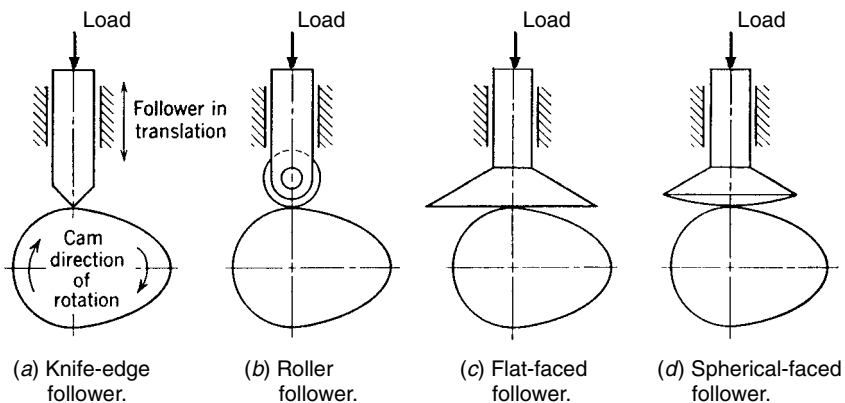
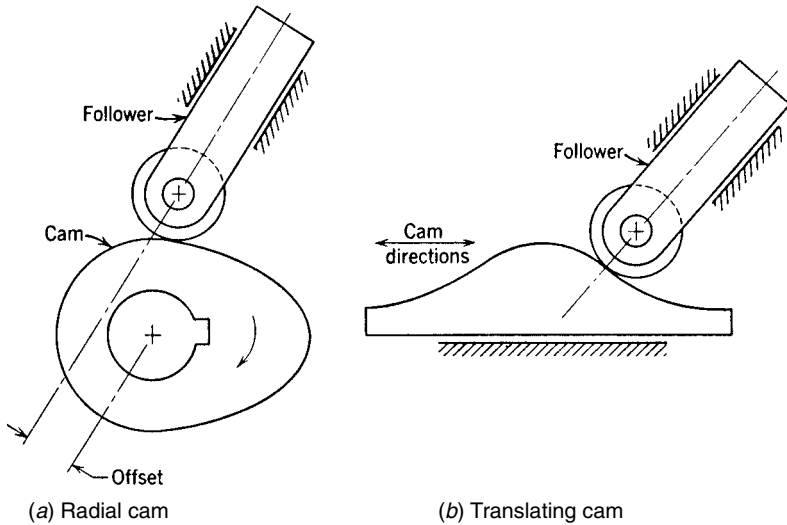


FIGURE 1.4. Types of follower contact surfaces.



**FIGURE 1.5.** Offset followers. (Movement of follower is different from shape of cam.)

sary clearance (backlash) between the roller sides and its groove. Sliding, wear, noise, vibration, and shock may be induced at high speeds. Furthermore, high speeds and high load may necessitate the use of crowned or conical rollers to accommodate the potential misalignment of contacting surfaces to avoid excessive surface stresses and wear. Figures 1.4c and 1.4d show *mushroom* followers in which the contacting surface is either *flat* or *spherical*. The spherical face of the Figure 1.4d mushroom follower has a large radius that compensates for detrimental deflection or misalignment that may occur with the flat mushroom follower.

The *radial follower* is one in which the follower translates along an axis passing through the cam center of rotation. This type, shown in Fig. 1.4, is the most common.

The *offset follower* is one in which the axis of the follower movement is displaced from the cam center of rotation. Offsetting often improves action by reducing force, stress, and also the cam's size. The eccentricity should be in the direction that improves force components tending to jam the translating follower in its bearing guide. Figure 1.5a shows a follower on a radial cam with an offset shown. Figure 1.5b shows the same relationship for a translating cam. In both cams, the follower path is not the profile displacement of the cam.

## 1.4 CAM CLASSIFICATIONS

Cams are classified in three ways:

1. In terms of their shape, such as wedge, radial, cylindrical, globoidal, conical, spherical, or three-dimensional;
2. In terms of the follower motion, such as dwell-rise-dwell (DRD), dwell-rise-return-dwell (DRRD), or rise-return-rise (RRR); or
3. In terms of the follower constraint, which is accomplished by either positive drive or spring load as mentioned previously.



**FIGURE 1.6.** Various types commercial of cams. (Courtesy Commercial Cam Co., Inc., Wheeling, Ill.)

The most popular industrial production cams (Fig. 1.6) are:

- positive drive, radial groove cam
- radial conjugate dual cams
- cylindrical groove cam

The most popular automotive cams are spring loaded. Figure 1.7 shows automotive camshafts. Let us discuss cams in terms of their shapes.

The *translating, wedge, or flat-plate* cam is one that moves back and forth driving a follower. The follower may either translate or oscillate, with its position established by the cam shape and location. This is the simplest of all cams. The follower is held in contact by a spring or a positive-drive groove and roller. Figure 1.8 shows a translating cam with a translating follower. Translating cams have been built as large as 15 feet long for turning the outside profile on gun barrels for milling and profiling work.



FIGURE 1.7. Automobile camshaft. (Courtesy of D. Elgin Cams, Redwood City, Calif.)

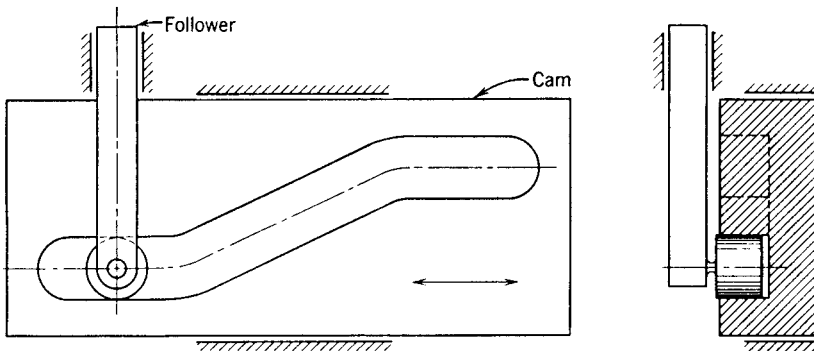
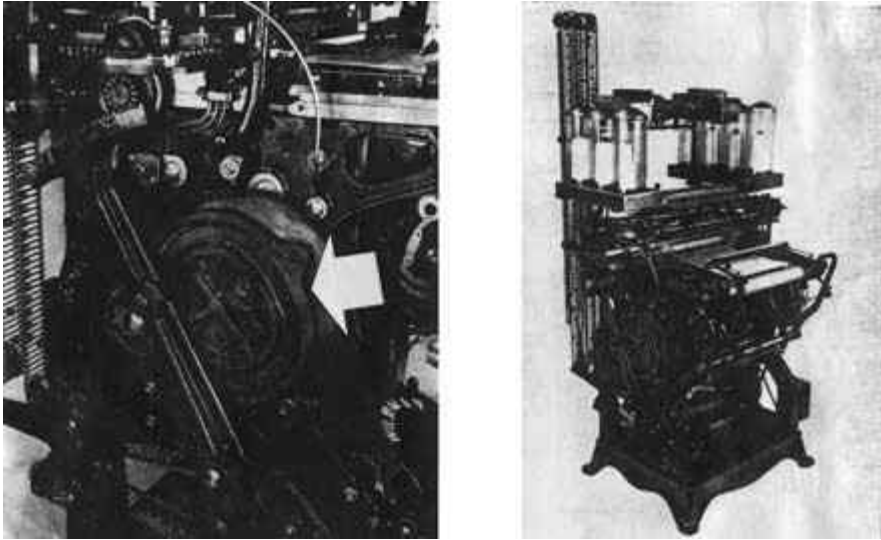


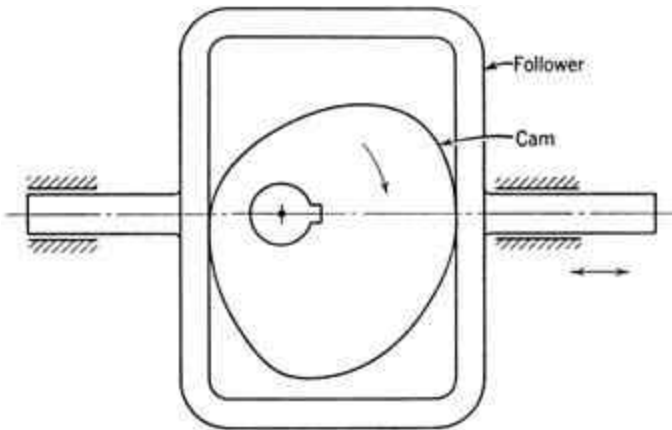
FIGURE 1.8. Translating cam. (Follower is a translating roller positive-drive type.)

The *radial, disk, or plate* cam is one in which the position of the follower is determined by radial distances from the cam axis. Figure 1.9 shows a radial open groove cam with oscillating roller follower used on a hosiery-making machine. The radial cam is by far the most popular because of its simplicity and compactness. Cams of this type are the yoke cams, conjugate cams, wiper cams, roller cams, and circular-arc cams.

The *yoke cam* is a positive-drive cam enclosed by a follower with opposite rollers or surfaces a constant distance apart. The rollers or surfaces may or may not be diametrically opposite of each other. The follower may translate or oscillate. Figure 1.10 shows a single-disk surface yoke cam with a translating follower. Control of follower action on single-disk cams is limited to 180 degrees of cam rotation. The other 180 degrees are



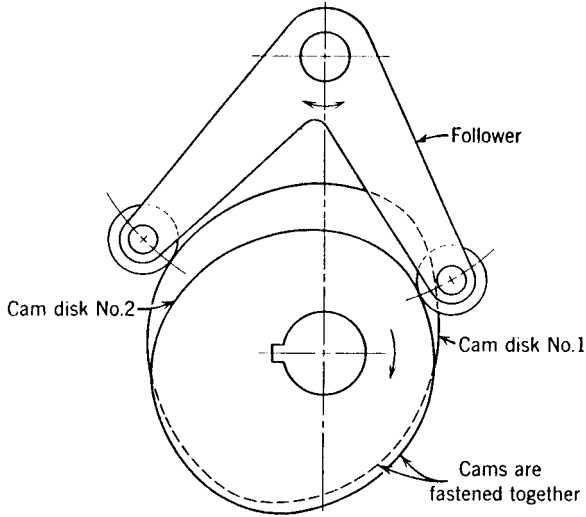
**FIGURE 1.9.** Radial open-groove cam—employed on a hosiery machine. Heat-treated meehanite cam; turns approximately 50 rpm and drives an extended gear quadrant, which in turn activates other parts of the machine to multiplied higher speeds. (Courtesy Wildman Manufacturing Co., Norristown, Pa.)



**FIGURE 1.10.** Yoke cam.

complementary to maintain the fixed distance contact on the other side of the cam. Another shortcoming of the single-disk yoke cam is that any wear produces clearance, which results in poor action at moderate to high speeds. Two roller followers may be utilized in lieu of surfaces to reduce this wear and detrimental backlash. The yoke cam is rarely utilized.

The *conjugate*, *complementary*, or *double-disk* cam is one having dual radial disks, each in contact with a roller on the follower. Figure 1.11 shows this type with an oscil-



**FIGURE 1.11.** Conjugate cam—oscillating follower (dual rollers and cams).

lating follower. Roller followers are generally used in this type of cam for optimum performance. The use of two followers allows one roller to be preloaded against the other to eliminate the backlash. This design effectively constrains the follower under high speed and high dynamic loads resulting in lower noise, vibration, and wear.

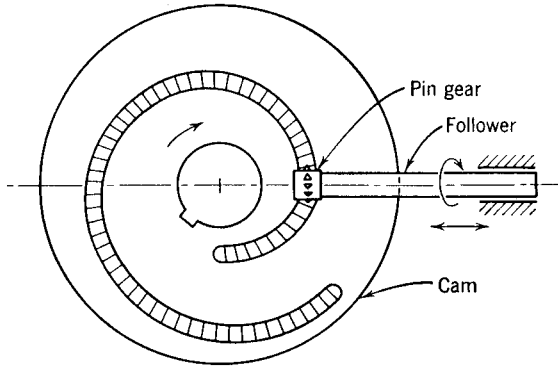
The *wiper* cam (Fig. 15.6) is one with a long, curved shape driving a curved or flat-faced follower with translation or oscillation. The follower is often called a toe by virtue of its shape. The cam usually oscillates but sometimes may be made to rotate. The wiper cam slides on the follower surface during its action. If the cam oscillates the cam and the follower will maintain contact at all times, but with complete cam rotation the surfaces will separate and the follower will, by spring action or gravity, have a quick return condition so that the cycle can be repeated. The rotating wiper cam has been used as an ore breaker in stamp mills.

The *rolling* cam is one with pure rolling between the cam and the follower. It is similar in appearance and application to the wiper cam, improved by alleviating the detrimental sliding and surface wear.

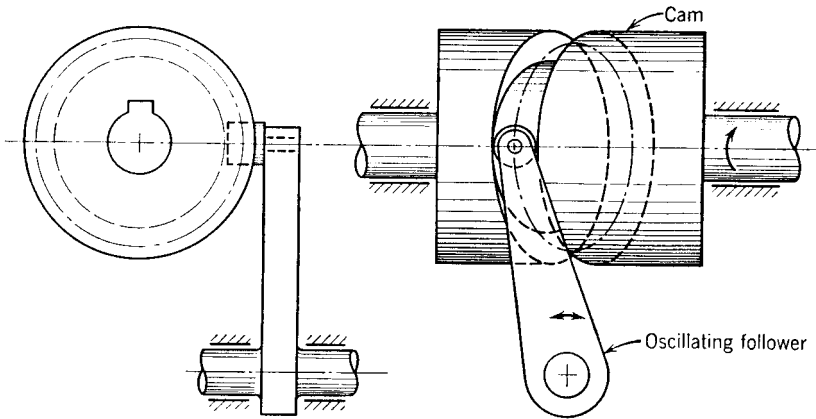
The *circular-arc* cam, as the name implies, is one composed of circular arcs (see Fig. 16.10). This cam is rarely utilized.

The *spiral* cam, shown in Fig. 1.12, has special grooves in its face that drive a translating and rotating follower. The pin gear follower is driven by teeth in the cam groove, and the angular velocity of the follower is determined by the cam radical distance. This cam has been employed in analog computing systems.

The *cylindrical, barrel, or drum* cam has a cylindrical shape that rotates about its axis, and the follower translates or oscillates. Cylindrical cams usually use cylindrical roller followers. Sometimes preloaded tapered conical rollers are applied to reduce the slippage and wear caused by the different driving radii and speeds. In addition, the cylindrical cam has been employed internally as well as externally. Also, in rare cases, the cylinder may operate as an “end” cam on its end surface. There are two types of cylindrical cams. The first type has a circumferential contour cut in its surface. Figure 1.13 shows this kind of cylindrical



**FIGURE 1.12.** Spiral cam. (Pin gear meshes with teeth in cam groove.)



**FIGURE 1.13.** Cylindrical cam—oscillating roller follower.

cam driving an oscillating roller follower. The second kind has a blade (blade cam) or thread projecting from its surface.

The *cylindrical blade* cam in Fig. 1.14 has two designs, the first type to drive a translating or oscillating follower (Fig. 1.14a) and the second type to index the intermittent action of a turret through its start-stop cycle (Fig. 1.14b), which indicates an indexing tapered roller turret.

The *globoidal* cam rotates about its axis driving a roller follower. It is similar in appearance and action to the cylindrical cam. The globoidal cam shape is determined by the arcs of an oscillating or indexing follower. There are two types of globoidal cams. The first kind has a groove with a circumferential contour cut in its surface for an oscillating roller follower. This type of globoidal cam is either convex (Fig. 1.15a), or concave (Fig. 1.15b). These cams are applied for small angles of follower oscillation. The second type of globoidal cam has a twisting “blade” or thread projecting from its surface. This blade cam is called the *roller gear drive* or *Ferguson drive* and has a roller follower on each side of the threads. The follower may oscillate or have intermittent rotation. Figure 1.16a shows a single-thread type with a globoidal body and an oscillating follower. Figure 1.16b is an

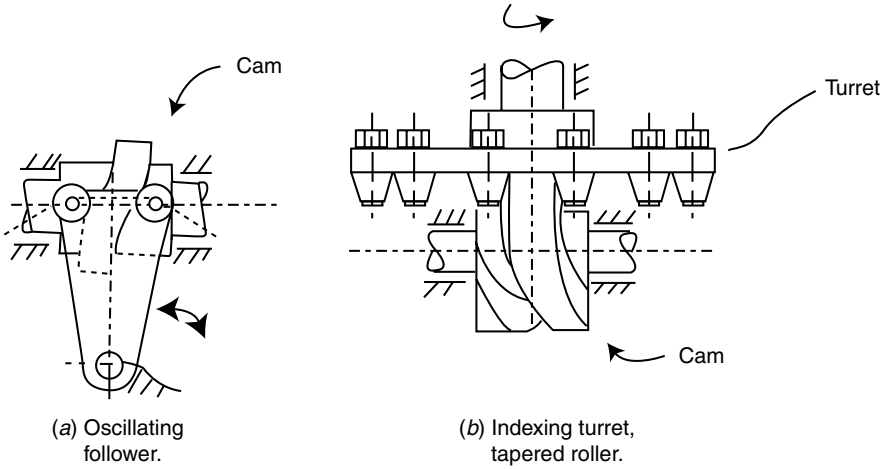


FIGURE 1.14. Cylindrical blade cam.

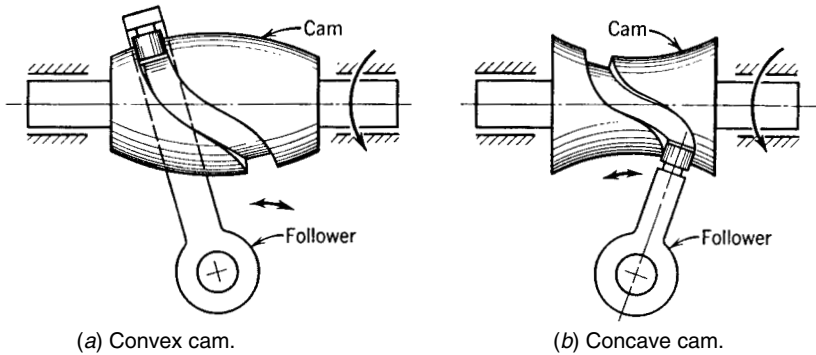
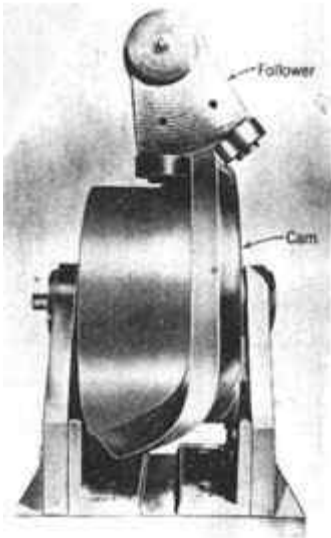


FIGURE 1.15. Globoidal cam-groove type, oscillating follower.

*indexing globoidal cam* with a turret follower. These blade-type globoidal indexing cams have high accuracy, long life, low vibration, low noise, and shockless performance under high speeds. For best action, the bearings should be preloaded so that the system has limited backlash. This cam and the follower can be obtained commercially. For indexing, they are often substituted for the familiar Geneva and star-wheel mechanisms, which have inherently poor high-speed dynamic properties.

The *conical cam* shown in Figure 1.17 has the shape of a cone driving the follower in a plane perpendicular to the base of the cone. The follower translates or oscillates, whereas the cam usually rotates. This cam is used infrequently because of its cost and the difficulty in cutting its contour. However, a conical cam may be necessary to change the direction of motion in a limited space. Grooves have been cut into conical cams for the positive-drive action of the follower.

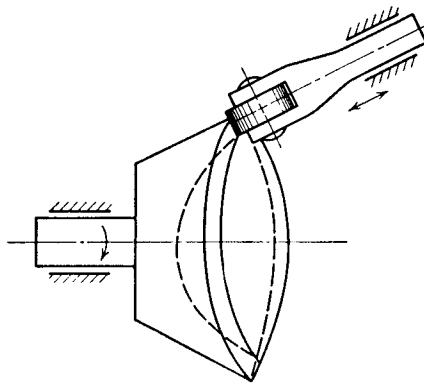


(a) Oscillating follower.



(b) Indexing turret follower.

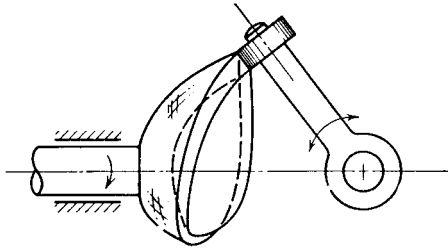
**FIGURE 1.16.** Globoidal cam-blade type (courtesy Ferguson Company St. Louis, Mo.).



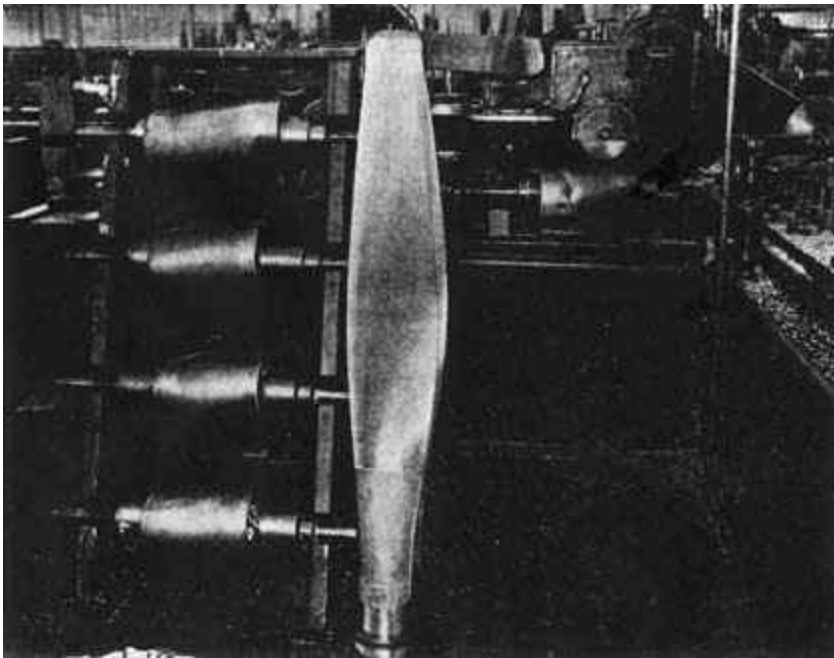
**FIGURE 1.17.** Conical cam—translating roller follower.

The *spherical cam* (Fig. 1.18) has a rotating portion of a sphere, which oscillates a follower having its axis perpendicular to the cam axis. This cam represents the limiting case of a conical cam. The realms and restrictions of the spherical cam are similar to that of the conical cam.

The *three-dimensional (3-D) cam* or *camiod* (Fig. 1.19), which has a curved face, both rotates about the longitudinal axis and moves relative to the follower along this



**FIGURE 1.18.** Spherical cam—oscillating roller follower.



**FIGURE 1.19.** Three-dimensional cam—Meehanite cams used in the manufacture of the solid aluminum blade shown. Employed as the master in cutting the proper contours in the face and side of the blade. (Courtesy United Aircraft Corp., East Hartford, Conn.).

axis. Thus, the position of the translating follower is dependent on both the angular and translational cam positions. The three-dimensional cam has limited application because of its high fabrication cost, high frictional forces that may be induced, and large space requirements.

The *inverse* cam is one in which the element corresponding to the follower of a cam mechanism is utilized as the driver. Figure 1.20 shows this cam mechanism with an oscillating roller driving a translating follower having a curved face. If the profile were a

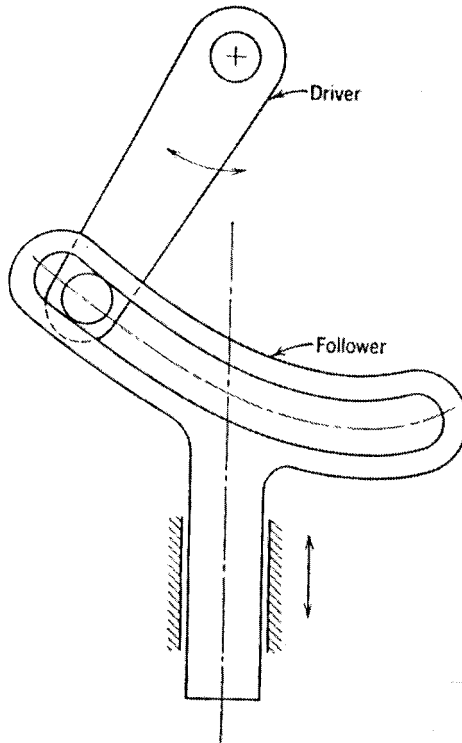


FIGURE 1.20. Inverse cam mechanism.

straight path perpendicular to the direction of follower motion, the familiar Scotch yoke mechanism would result (Ananthasuresh [2001]). Chapter 8 presents an inverse cam mechanism where the roller crank and the cam both complete a full rotation in each revolution having dwell action and intermittent motion.

*Stationary* cams are fixed and are machined with a curve or contour calculated to produce auxiliary motions on moving parts contacting them during traversal. Stationary cams are usually wedge cams and are used infrequently. They have been employed in high-speed wrapping machines.

The follower is constrained to the cam in either of two ways: via *open-track* (force closure) or *closed-track* (form closure) methods. The open-track cam utilizes a spring to load the cam (at all times) that is stronger than the sum of the outside forces of working action, inertia, friction, and impact, providing zero backlash in the system. Most automobile cam systems are of this type (see Fig. 1.1). The closed-track cam controls the follower on two surfaces with a roller or rollers in grooves. These cams have a small amount of backlash in the system. Most industrial machines are of this type. Automobile cams using this form are called desmodronic cams.

An *open* or *closed cam system* refers to whether the cam system is open or closed to the environment in reference to the lubrication system for the contacting surfaces of the cam and follower. Open cams (see Fig. 1.9) may be lubricated from the outside after dust

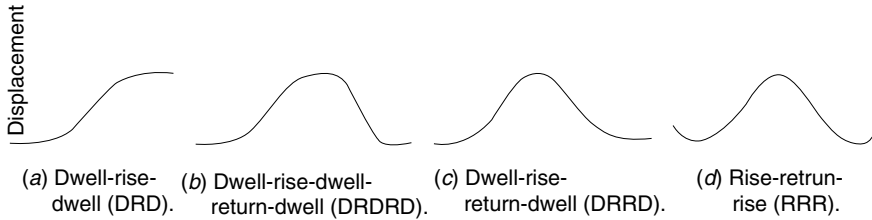


FIGURE 1.21. Types of cams in terms of follower motion.

and contamination are removed. Closed cams are sealed and lubricated by an oil bath, mist, or forced lubrication.

## 1.5 CAMS IN TERMS OF FOLLOWER MOTION

As previously stated, one of the special features of cam follower systems is that specific dwell action may be designed for the follower motion. A *dwell* is defined as a lack of follower movement while the cam maintains its input driving action. In production machinery, dwell occurs when the follower does not move while a secondary task is performed. Figure 1.21 shows the four basic types of cams for the follower action.

*Dwell-Rise-Dwell Cam (DRD)*. This cam type, Figure 1.21a, has a dwell followed by a rise contour followed by a dwell period at the maximum displacement. It also may have dwell-fall-dwell action, which is analyzed similarly. DRD cams are utilized in cylindrical and globoidal cams indexing a rotating turret. In rare cases multiple dwell actions may be necessary.

*A dwell-rise-dwell-return-dwell cam (DRDRD)*, Fig. 1.21b, incorporates the complete action cycle of a DRD cam.

*A dwell-rise-return-dwell cam (DRRD)*, Fig. 1.21c, has the rise and return preceded and followed by dwells. It has limited application in machinery.

The contour of the *rise-return-rise cam (RRR)*, Figure 1.21d, has no dwells. We will not analyze this type, because an eccentric mechanism (Chap. 15) is usually a better choice than the cam-follower mechanism. The eccentric mechanism is more accurate, less expensive, and easier to produce.

## 1.6 CAM PROFILE GRAPHICAL LAYOUT

The manual cam layout method described in this section is used primarily for information. In general, designers use CAD digitized packages to generate the cam profile on the drawing. Cam-follower designs begin with crude sketches using cartesian coordinates, as in Fig. 1.22. In this figure we see that the cam-follower action may be considered equivalent to a wedge action of infinite length.

The wedge is shown moving at a constant speed from right to left to raise the follower a maximum distance,  $h$ . The first cycle of the follower movement is the curve  $ABCA'$  continued to  $B'C'A''B''C''A'''B'''$ , and so forth. A radial cam may be considered a wedge rolled in the plane of the paper having a length of one cycle (wedge cam  $ABCA'$ ) equal to the

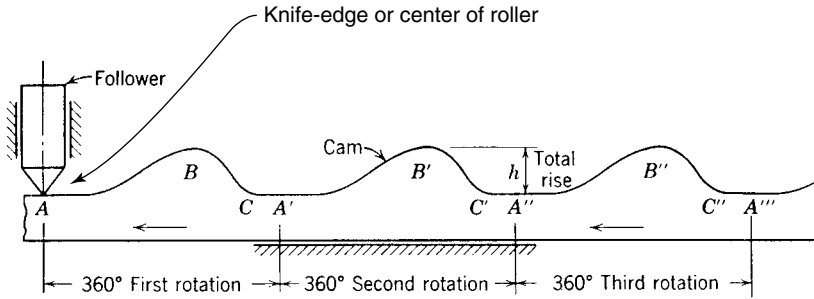


FIGURE 1.22. Wedge cam—equivalent to all cam actions.

circumference of a circle. A cylindrical cam is one in which the wedge  $ABCA'$  is twisted in a plane perpendicular to the paper with the length of the wedge cam  $ABCA'$  equal to the circumference of the cylinder. The contour  $AB$ , which is the rise portion of the cam, should not be too steep since this will produce jamming of the translating follower on the sides. This curve slope can be reduced by using a longer cam length for the same rise of the follower,  $h$ . A larger cam results. Also the speed of the wedge is pertinent to later investigation of the dynamics of the cam-follower action.

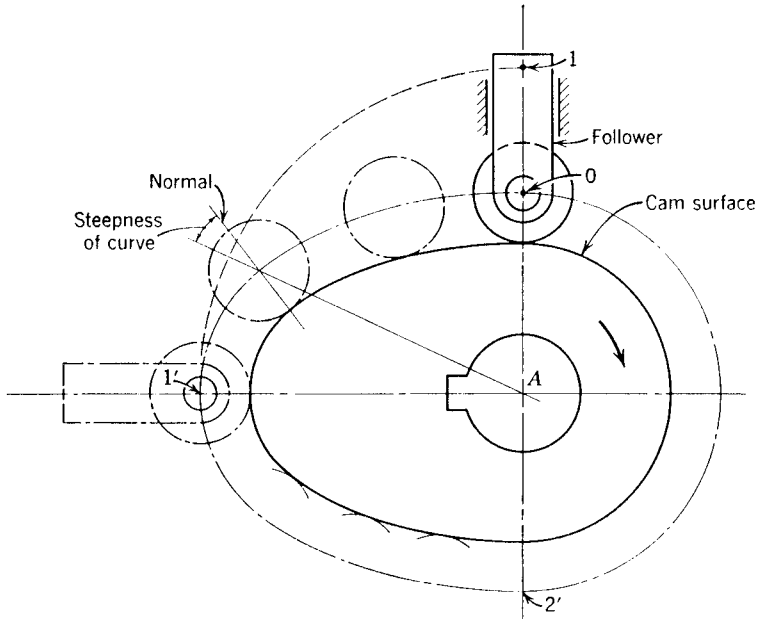
Let's construct a simple radial cam with a roller follower having a given rise in a given time. The means for finding the cam shape is one of inversion, that is, the profile is developed by fixing the cam and moving the follower around the cam at its respective relative positions. If we used an infinite number of points, the envelope of the cam contour would be formed. Also, the layout of a roller follower requires plotting the center of the roller and then drawing the curve tangent to the rollers. For clarity, only a few points will be shown.

**EXAMPLE** A radial cam rotating clockwise drives a  $1/2$  inch diameter roller follower as follows:

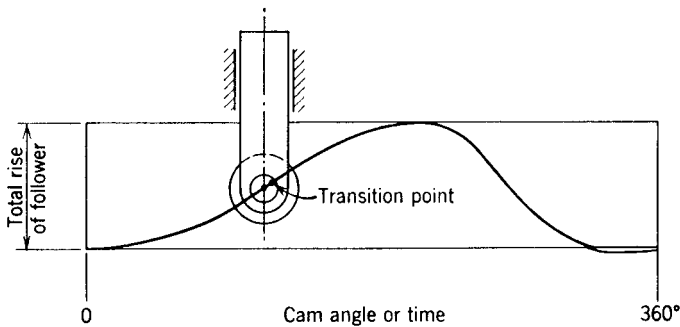
1. rise of  $5/8$  in. in 90 degrees of rotation
2. fall of  $5/8$  in. in 90 degrees of cam rotation
3. dwell for the last 180 degrees of the cam cycle

The procedure (Fig. 1.23), which consists of fixing the cam and moving the follower around it, is:

1. Draw two perpendicular axes locating the cam center at  $A$ .
2. Assume the location of the lowest point of the roller-follower center at point  $O$ , on one of the radial lines.
3. The maximum rise, point  $1$ , should be shown  $5/8$  in above point  $O$ .
4. With the cam center  $A$  and radius  $A1$ , swing an arc until it intersects line  $A1'$ , which is 90 degrees opposite the direction of cam rotation.
5. Draw a smooth curve through points  $O$  and  $1'$ , providing the rise portion of the cam.
6. Draw roller diameters and then a tangent curve to the rollers. This is the cam surface.
7. Check the steepness of the curve. If at any point it is excessive, redesign with larger radii  $A0$  and  $A1$ , which means a larger cam.
8. Repeat the process for the 90-degree fall portion  $1'2'$ . The last 180 degrees of cam action  $2'0$  is a dwell, a constant radial distance.



**FIGURE 1.23.** Graphical cam layout—Example. Rise is  $\frac{5}{8}$  in. in 90 degrees of cam rotation. Full scale.



**FIGURE 1.24.** Displacement diagram (shows cam action).

## 1.7 CAM DEFINITIONS

Let us define the terms necessary for the investigation of the cam shapes and actions.

The *displacement diagram* (Fig. 1.24) is a rectangular coordinate layout of the follower motion in one cycle of cam operation. The rise of the follower is shown as the ordinate with the length of the abscissa arbitrarily chosen. The abscissa is divided into equal cam angles or equal time divisions because the cam usually rotates at a constant speed. The displacement diagram is generally drawn or sketched as the first step in the development

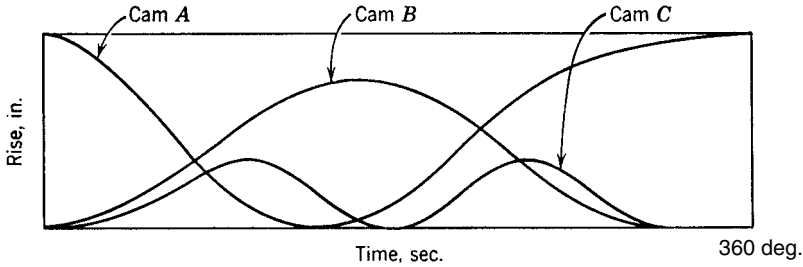


FIGURE 1.25. Time chart (showing compounding of three cams).

of the cam profile. It presents a quick picture of the follower motion. It will be shown that for radial cams the displacement diagram, if drawn to scale, does not show the true slopes of the cam contour. In other words, in transferring the cam contour from a rectangular to a polar layout the displacement diagram is distorted on radial cams, whereas no changes occur with cylindrical cams.

The *transition point* (see Fig. 1.24) is the point on the cam at which the follower is at maximum velocity. In the displacement diagram, the transition point (point of inflection) is located at the maximum cam slope.

The *time chart* or *timing diagram* is the superimposing of more than one displacement diagram on the same abscissa or time basis. This provides a comparison of the operation of interrelated cams. The initial plotting of this chart is essential in automatic machinery to establish the action of the cam followers and the proper timing of its members. By proper use of this chart, the designer can keep the idle time to a minimum and increase the production of the machine. Figure 1.25 shows the time charts used for the compounding of three cams. The usual development of high-speed automatic machinery requires the manipulation of the timing diagram until the ultimate design has been reached and the smallest cam possible has been attained.

The *cam profile* is the actual *working surface* contour of the cam. It is the surface in contact with the knife-edge, roller surface, or flat-faced follower. Figure 1.26 shows a popular cam profile consisting of a single-lobe, external radial cam. In an enclosed cam, an inner and outer cam profile constrain the roller follower. The cam profile may be of many shapes, external or internal, single or multilobe, and so forth.

The *base circle* (see Fig. 1.26) is the smallest circle drawn to the cam profile from the radial cam center. Obviously, the cam size is dependent on the established size of the base circle. We shall denote the radius of the base circle as  $R_b$ .

The *trace point* (see Fig. 1.26) is the point on the follower located at the knife-edge, roller center, or spherical-faced center.

The *pitch curve*, or *pitch profile*, is the path of the trace point. Figure 1.26 shows the pitch curve of a radial cam. In cam layout, this curve is often determined first and the cam profile is then established by tangents to the roller or flat-faced follower surfaces. For the elementary knife-edge follower, the pitch curve and cam profile are the same.

The *prime circle* (see Fig. 1.26) is the smallest circle drawn to the pitch curve from the cam center. It is similar to the base circle. We shall denote the radius of the prime circle in inches as  $R_a$ .

The *pressure angle* (see Fig. 1.26) is the angle (at any point) between the normal to the pitch curve and the direction of the follower motion. This angle is important in cam design because it represents the steepness of the cam profile, which if too large can affect the smoothness of the action.

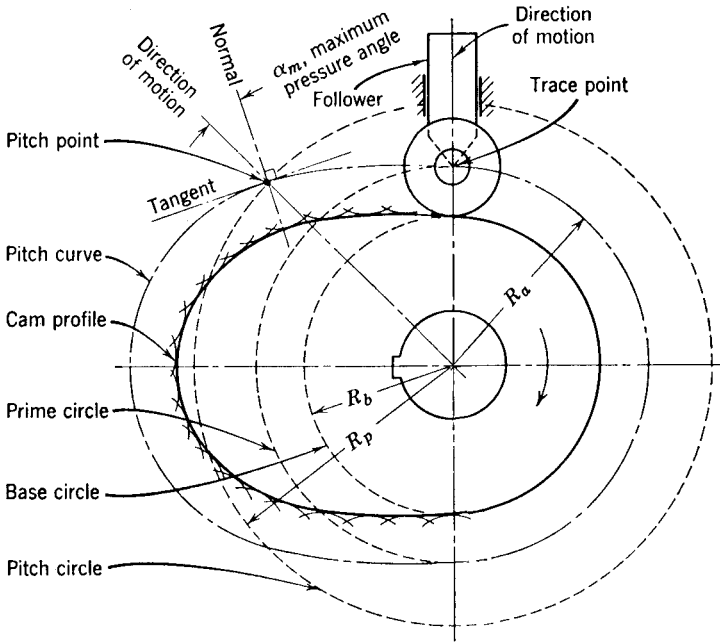


FIGURE 1.26. Cam nomenclature.

Suppose that, as in Figure 1.27a, the cam had a pressure angle of approximately 60 degrees. It can be seen that there is a strong possibility that clockwise rotation of the cam would not cause the translating follower to rise, but to jam against the guides and cause bending in the follower stem. Designers often empirically limit the pressure angle to 30 degrees or less for smooth cam-follower action. However, if the follower bearings are strong, the cam-follower is rigid, and the cam-follower overhang is small, the maximum pressure angle may be increased to more than 30 degrees. In flat-faced followers, this locking action does not exist. In Fig. 1.27b, we see a follower face normal to the translating follower motion in which the pressure angle is constant at zero degrees and thus no jamming occurs. Let us establish the following:  $\alpha$  = pressure angle and  $\alpha_m$  = maximum pressure angle.

The *pitch point* (see Fig. 1.26) is the point on the cam pitch having the maximum pressure angle,  $\alpha_m$ .

The *pitch circle* (see Fig. 1.26) is one with its center at the cam axis passing through the pitch point. The radius of the pitch circle is  $R_p$ .

The *radius of curvature* at any point on the pitch curve is the radius of curvature of the curve at that point. Here, we define the curvature as a measure of the rate of change of the angle of inclination of the tangent with respect to the arc length.

The *transition point* or *crossover point* is the position of maximum velocity where the acceleration changes from positive to negative and the inertia force of the follower changes direction accordingly.

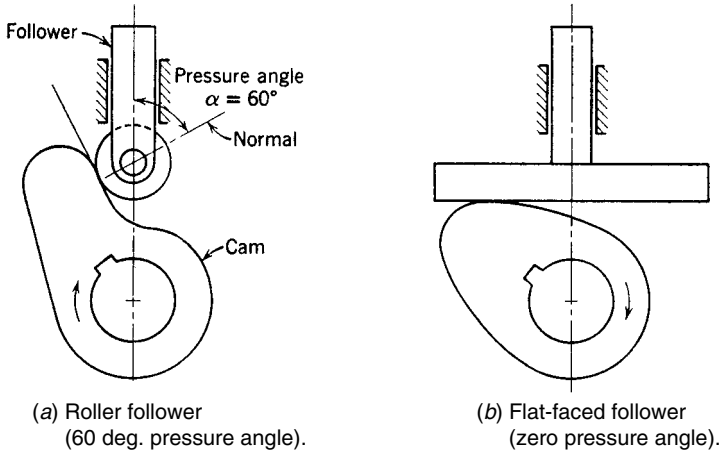


FIGURE 1.27. Significance of pressure angle.

## 1.8 OTHER METHODS THAN CAMS

Other methods than cams may employ mechanical, electrical, or fluid devices individually or in combination to satisfy the design requirements. Cam-follower systems and other methods have specific functional applications where they are selectively applied. The following are some of the major systems utilized and their performance compared to cam-follower systems: (a) linkage mechanisms; (b) servo valve-controlled hydraulic cylinder; (c) stepper motor and controller, and (d) industrial adjustable mechanism.

The *linkage mechanism* may be of either four-bar or multiple-bar construction depending on the complexity of the designed motion. These mechanisms cannot produce exact dwell action (only an approximation), with poor force transmission and high torque existing in the cyclical action.

A *servo valve-controlled hydraulic cylinder* yields equivalent performance to cam-follower systems for high force level requirements. This machinery has limited control and speed application.

The *servo motor* (stepping motor), *programmable servo controller* (stepper controller), and *ball-screw* combination is another replacement for cams. Motion controls can be changed easily. This mechanism has the advantage of programmability in small force and low power applications but has speed limitations.

The last alternate method involves the use of *adjustable mechanisms* in industrial applications. To achieve flexibility, the cams are replaced by multi-degree-of-freedom systems with multi-actuators and logic controllers. The adjustable or programmable mechanisms are utilized in flexible fixturing and flexible assembly systems. Their design is often complicated and costly.

In general these devices are easier to manufacture but have limited speeds and limited force levels and are more costly. Cam-follower systems in comparison are complex in construction, are smaller, have better dynamic properties, carry a heavier load, and transmit more power over a longer time period. The applications are high-speed automobile valve controls, indexing tables, and industrial machinery such as paper converting and textile machinery. Designing cams and forecasting their performance is easy.

## 1.9 DESIGN CONSIDERATIONS

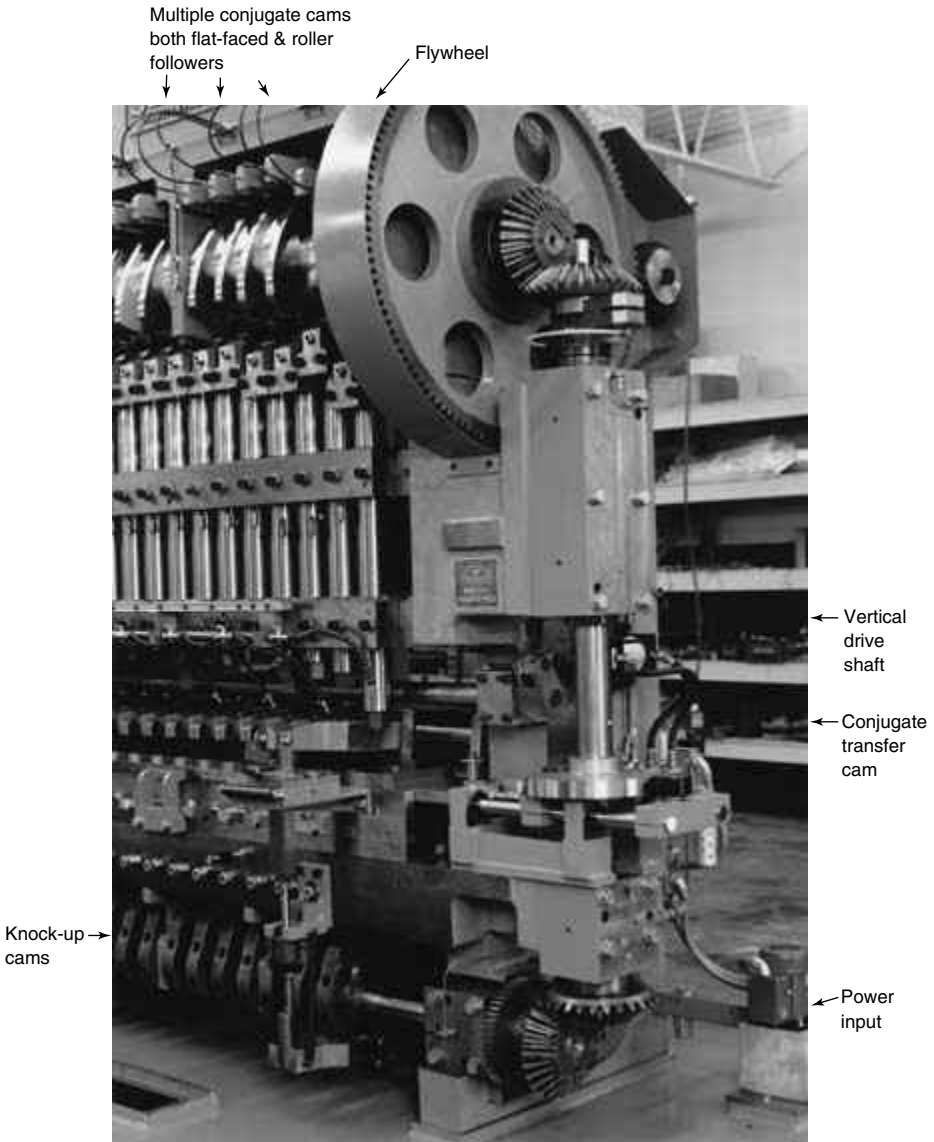
---

This section is a collection of introductory thoughts relating to the proper design and performance of cam-follower systems. Cam-follower systems have been built in an extreme range of sizes, from small mechanisms that have been produced in microelectromechanical systems (MEMS), in which forty of them could fit in the period at the end of this sentence, to the largest machine being a four-story high newspaper printing and folding press (heavy mass-moving parts) handling seventy thousand complete newspapers per hour. In between these extremes is a small high-speed punching mechanism running at 12,000rpm, with some dynamic loading and elasticity.

Figure 1.28 shows a high-production cam-operated press for sheet metal drawn parts (eyelets) for the cosmetic industry. This machine has multiple cam followers for each stage of operation and runs at 70rpm.

The following is a brief list of ideas to guide the engineer-designer in creating cam-follower machinery.

- The first step in designing a cam system is to establish the proposed design speed of the complete machine. This decision is a critical one and should be based on the best experience and judgment available. The customer should be helpful in this decision. After the design speed is determined, establish a time chart to synchronize the cam system with other actions of the machine.
- Positive drive, closed-track radial cams or conjugate dual cams with roller followers are the most popular choices.
- The cam contour should be smooth with no abrupt changes in its curvature. Note that curvature at any point on a cam is directly related to acceleration of the follower.
- The minimum curvature or sharpness of a convex cam contour is dependent on the value of the maximum negative acceleration of the follower. That is, the larger the negative acceleration, the sharper the cam surface will be.
- The cam size should be as small as possible to minimize the cam-follower sliding velocity, surface wear, torque on the camshaft, and cost and space requirements.
- The pressure angle should be kept to a minimum; 30 degrees is a general arbitrary limit for all followers.
- Proper dynamic cam-follower design necessitates the study of the cam-follower acceleration curve.
- The maximum follower acceleration should be as low as possible to keep the inertia forces and stresses small.
- The noise, surface wear, and vibration of a cam-follower system are dependent on the shape of the follower acceleration curve; hence, smoothness and continuity of the acceleration curve are essential.
- The moving parts of the cam-follower mechanism should be lightweight and as rigid as possible to keep the inertia forces, noise, and wear at a minimum, especially at high speeds.
- The torque curve should be investigated in addition to the force distribution of the system.
- Manufacturing methods and accuracy of cam cutting and inspection are of paramount importance in ensuring the anticipated performance of a system. Small surface errors that are imperceptible to the eye may produce high stress and vibrations in the follower linkages.



**FIGURE 1.28.** Production cam-operated press for sheet metal drawn parts (eyelets) for the cosmetic industry. (Cams run at 70 rpm.) (Courtesy Swanson Industries Mallory Industries, Farmington, Connecticut).

- The cam synthesis is usually done by a CAD package followed by a CAM package to produce the actual cam shape. Figure 1.29 shows a sample cam contour (App. E) and Fig. 1.30 presents a 3D wire frame representation of the cam contour. The solid model of Fig. 1.30 is used to calculate mass, center of gravity, and inertia properties to obtain static balancing requirements.

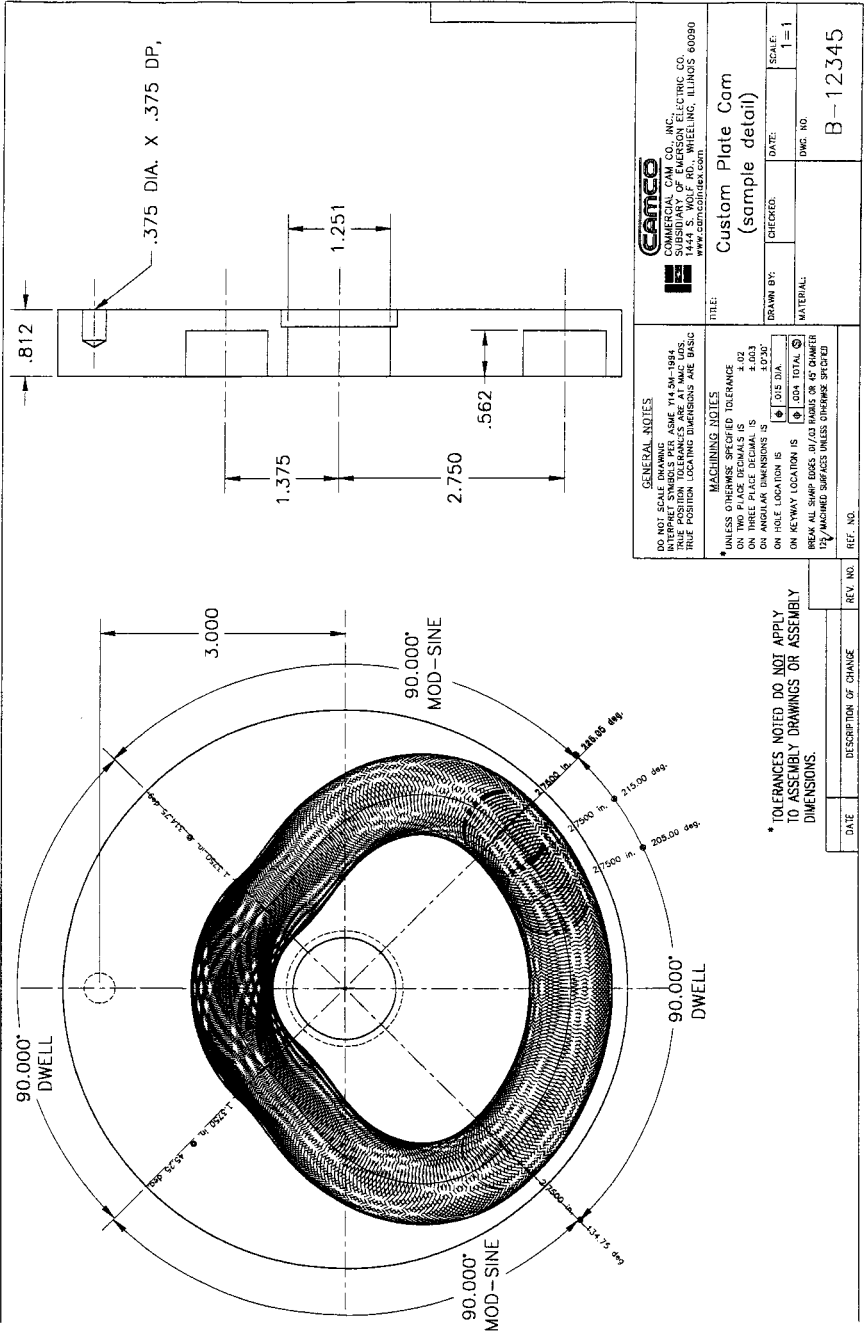
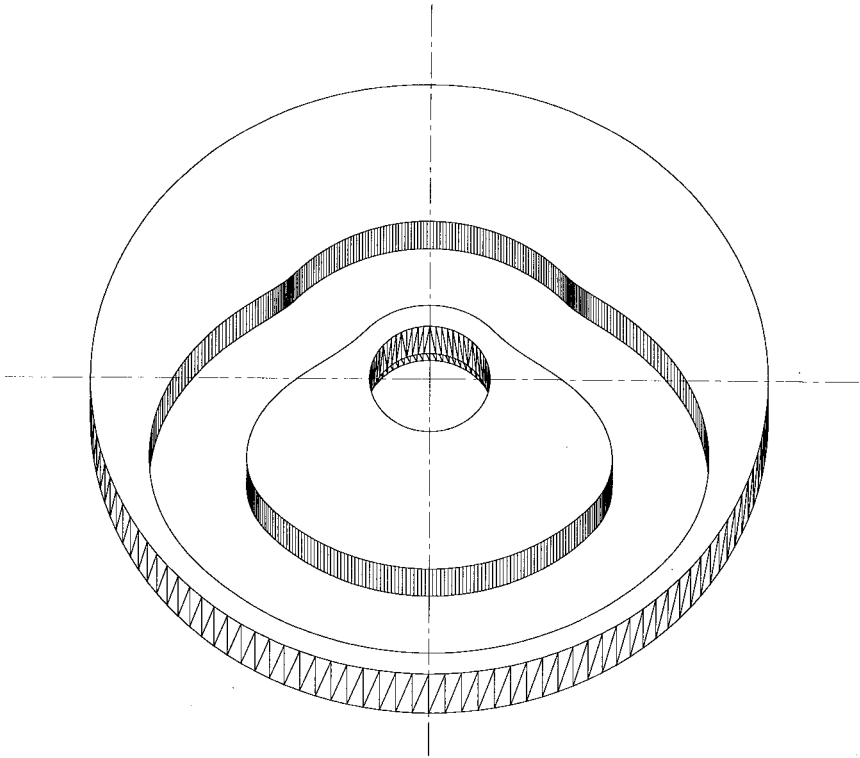


FIGURE 1.29. Sample Cam drawing with cam contour and tape check.



**FIGURE 1.30.** B-12345 Sample Cam with 3D Wire Frame representation of cam contour (Courtesy Commercial Cam Co. Inc. Wheeling, Illinois).

- In troubleshooting cam system performance, the first step of investigation is to *measure all the related action members of the machine* before initiating elaborate theoretical studies and changes.
- Cam-follower alignment and backlash (static and dynamic) should be controlled to keep surface stresses as small as possible. Note that slight deflections of cam-follower surfaces produce very high stresses.
- The lubrication of open and closed cam systems is a significant factor in the design of cam-follower systems. Environmental pollution, product dust, and particles are significant factors in the life of the cams.
- Choice of compatible cam and follower materials and selection of lubricant are critical in the life of both the cam and the follower. Dynamic fatigue and scuffing wear occur because of the rolling and skidding action of the roller-follower.
- In driving the cam, a flywheel should be located close to one of the rigid shaft bearings to maintain maximum support and minimize system vibrations.
- Other interesting design considerations include the unsuspected elasticity in the moving machine parts (especially under wear conditions), the effect of tolerances in performing parts, the worn parts backlash in the cam-follower, worn bearings, and the experience of the machinist in assembling the machine.

- Particular attention should be paid to the machine or toolmakers who make the parts and assemble the machine. These skilled artisans are talented and may apply innovation and invention working with all kinds of machinery.
- As soon as feasible, the machine should be forwarded to the customer for installation and appraisal. The designer should be in direct contact with the customer, to maximize the flow of ideas.
- The designer should be sensitive to the customer's suggestions on the performance of the machine, adaptability, strength, life, wear, corrosion, maintenance, and safety.
- The customer's machine operators may be strategically helpful in making the machine perform properly.
- In the end, frequent communication between all involved will produce the best design, with the customer being the final judge.
- For the designer, a list of computer software is in App. D.
- Additional references include Jensen (1987), and Jones (1978).
- For automotive camshaft design see Hubbard (2000).

## **REFERENCES**

---

- Ananthasuresh, G.K., "Design of Fully, Rotatable, Roller-Crank-driven Cam Mechanisms for Arbitrary Motion Specifications," *Mechanism and Machine Theory*, 36: 445–467, 2001.
- Erdman, A.G., and Sandor, G.N., *Mechanism Design*, third edition, Prentice Hall, Upper Saddle River, N.J., 1997.
- Grodzinski, P., *A Practical Theory of Mechanisms*, first edition, Emmott and Co., Ltd., Manchester, England, 1947.
- Hubbard, D., *Camshaft Reference Handbook*, Don Hubbard, Pub., Ft. Myers, Fla., 2000.
- Jensen P.W., *Cam Design and Manufacture*, Marcel Dekker, New York, 1987.
- Jones, S.R., *Cams and Cam Mechanisms*, Institute of Mechanical Engravers, London, 1978.
- Jones, F.P., *Ingenious Mechanisms for Designers and Inventors*, Industrial Press, New York, Vol. 1, 1930; Vol. 2, 1936; Vol. 3, 1951; Vol. 4, 1967.

*This page intentionally left blank.*

---

# CHAPTER 2

---

# BASIC CURVES

---

**Harold A. Rothbart, D.Eng.**

2.1 INTRODUCTION	28	2.9 CUBIC NO. 2 CURVE	40
2.2 FOLLOWER CHARACTERISTICS	28	2.10 SIMPLE HARMONIC MOTION CURVE	40
2.3 BASIC CURVE CLASSIFICATION	31	2.11 CYCLOIDAL MOTION CURVE	44
2.4 CONSTANT VELOCITY CURVE	33	2.12 DOUBLE HARMONIC MOTION CURVE	46
2.5 MODIFIED CONSTANT VELOCITY CURVE WITH CIRCULAR ARCS	34	2.13 ELLIPTICAL CURVE	47
2.6 CONSTANT ACCELERATION CURVE	34	2.14 COMPARISON OF BASIC CURVES	48
2.7 SKEWED CONSTANT ACCELERATION CURVE	37	2.15 CURVE APPLICATION TO DRRD CAM	49
2.8 CUBIC NO. 1 CURVE	38		

---

## ***SYMBOLS***

---

$a$  = acceleration in/rad<sup>2</sup>

$A$  = constant acceleration in/sec<sup>2</sup>

$a_e$  = semi-major axis of ellipse, in

$A$  = acceleration in/sec<sup>2</sup>

$b_e$  = semi-minor axis of ellipse, in

$C, C_1, C_2$  = constants

$h$  = total rise, in

$h_1$  = displacement at transition point, in

$n$  = any number

$n_e = \frac{a_e}{b_e}$  ratio

$V_0$  = initial velocity, in/sec

$y$  = follower displacement, in

$y' = \frac{dy}{d\theta}$  = follower velocity, dimensionless

$y'' = \frac{d^2y}{d\theta^2}$  = follower acceleration, dimensionless

$y''' = \frac{d^3y}{d\theta^3}$  = follower jerk, dimensionless

$\dot{y} = \frac{dy}{dt} = \omega y'$  = follower velocity

$\ddot{y} = \frac{d^2y}{dt^2} = \omega^2 y''$  = follower acceleration

$\ddot{y} = \frac{d^3y}{dt^3} = \omega^3 y'''$  = follower jerk

$y_1, y_2$  = displacement during acceleration periods 1 and 2, respectively, in

$\beta$  = cam angle for rise  $h$ , rad

$\beta_1$  = angle of rotation for rise  $h_1$ , rad

$\phi$  = angle of rotation for cycloidal curve, rad

$v_0$  = initial velocity, in/rad

$\omega$  = cam speed, rad/sec

$\theta$  = cam angle of rotation

## 2.1 INTRODUCTION

---

In Chapter 1, we saw that it is possible to construct a cam by blending crude increments and observing its appearance. This method is not acceptable in the design of today's cam machinery. Now it is necessary to provide accurate mathematical information for the cam characteristics of displacement velocity, acceleration, and sometimes the jerk. In so doing one can interpret and control the ultimate design performance. Also, the higher the cam speed, the more critical is the investigation. This is especially true of the acceleration data which is the important determining factor of the dynamic loads on cam-follower systems.

This chapter presents mathematically established *basic* curves which are the first selection to establish the follower action. They are easy to analyze and manipulate.

Cams can be designed for any acceptable curve or shape. Appendix A lists various kinds of geometric curves that have been used in the past. They include the ellipse, parabola, hyperbola, logarithmic spiral, and involute of a circle. Alternative combinations of these curves combined with the circle and straight line have also been constructed (see Chapter 15.)

## 2.2 FOLLOWER CHARACTERISTICS

---

As previously indicated, a cam can be considered similar to a wedge having a cyclical rise and fall which establishes the motion of the follower. In all cams, the displacement of the follower is given by the mathematical relationship

$$y = f(\theta) \text{ in} \quad (2.1)$$

where  $\theta$  = cam angle rotation in radians. However, since the cam rotates at a constant angular velocity, the displacement can also be written as

$$y = g(t) \text{ in} \quad (2.2)$$

and  $\theta = \omega t \quad (2.3)$

where  $t$  = time for cam to rotate through angle  $\theta$ , sec  
 $\omega$  = cam angular velocity, rad/sec

By the use of Eq. (2.1) the follower characteristics can be normalised (dimensionless) as follows:

The cam profile is usually given as a function of the angle  $\theta$ . Thus

$$y = \text{follower displacement.} \quad (2.4)$$

The instantaneous angular rate of change of displacement

$$y' = \frac{dy}{d\theta} = \text{follower velocity.} \quad (2.5)$$

The instantaneous angular rate of change of velocity

$$y'' = \frac{d^2y}{d\theta^2} = \text{follower acceleration.} \quad (2.6)$$

The instantaneous cam angle rate of change of acceleration

$$y''' = \frac{d^3y}{d\theta^3} = \text{follower jerk.} \quad (2.7)$$

By the use of Eq. (2.2) the follower characteristics can be expressed as direct time dependent as follows:

The follower velocity can be written as

$$\dot{y} = dy/dt = (d\theta/dt)(dy/d\theta) = \omega(dy/d\theta) = \omega y' \quad (2.8)$$

the follower acceleration

$$\begin{aligned} \ddot{y} &= d^2y/dt^2 = \frac{d}{dt} \left( \omega \frac{dy}{d\theta} \right) = \omega \frac{d}{d\theta} = \omega \frac{d}{d\theta} \left( \frac{dy}{d\theta} \right) \left( \frac{d\theta}{dt} \right) \\ &= \omega^2 (d^2y/d\theta^2) = \omega^2 y'' \end{aligned} \quad (2.9)$$

and the follower jerk

$$\ddot{\dot{y}} = \omega^3 \left( \frac{d^3y}{d\theta^3} \right) = \omega^3 y''' \quad (2.10)$$

These equations facilitate converting from one family of dimensional units to another. By having the cam profiles in the mathematical form of Eq. (2.1) or Eq. (2.2) we also can easily find the other characteristics, by differentiation.

From the foregoing equations, we see that each successive derivative can be determined from the slopes of any point on the previous curve. Thus, at any point the slope of the displacement curve yields the velocity of the follower. The slope of the velocity curve is the acceleration of the follower, and the slope of the acceleration curve is the jerk of the follower. This procedure is called the *graphical-slope* differentiating method. It is presented for a quick appraisal of the displacement, velocity, acceleration, and jerk curves. Utilizing the graphical-slope method, the velocity curve is reasonably accurate and the acceleration curve is at best only an approximation.

With the graphical-slope method, the determination of the signs (positive or negative) is essential for a fundamental understanding of the follower motion and dynamics. Let us establish as positive (+) the displacement of the follower above the lowest point in the displacement diagram (Fig. 2.1a). Therefore, the velocity is positive if the follower moves in the direction of positive displacement and negative if it moves in the opposite direction. That is, velocity is positive on the rise and negative on the fall. The acceleration follows a similar convention. Therefore the acceleration is positive when its direction is that of the positive displacement. Throughout this book, the word *deceleration* is not used because it does not indicate the direction of acceleration and would therefore cause confusion regarding the direction of inertia load. The slope of the curves at any point gives us another method for determining signs. Sloping upward to the top right the slope is positive, and sloping upward to the top left the slope is negative. Also, a vertical slope at a point in any of the curves has an infinite value and is called a *discontinuity* because it has two values at the point being studied.

Some concepts discussed in this chapter are:

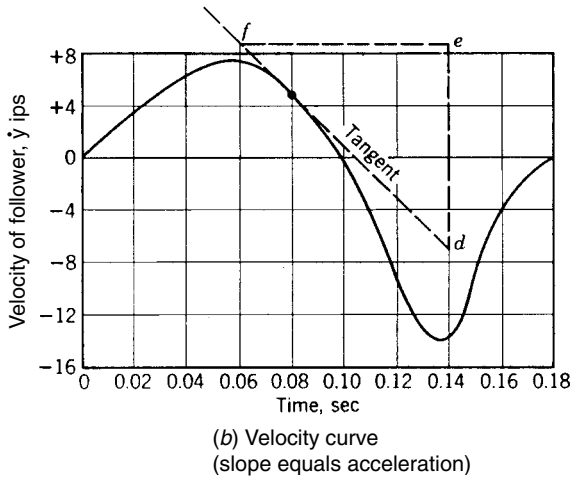
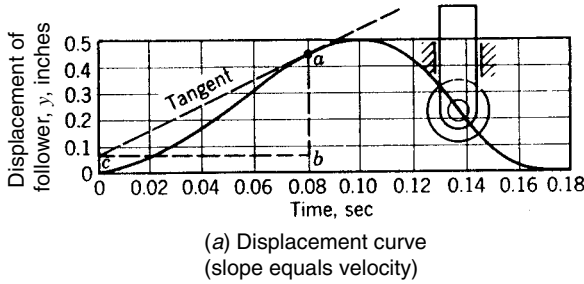


FIGURE 2.1. Graphical-slope method for follower characteristics.

- The follower *displacement* motion  $y$  refers to the knife-edge follower or the pitch curve center of the roller follower if employed.
- The follower *velocity*  $y'$  or  $\dot{y}$  is an indication of both the cam pressure angle and the cam torque.
- The follower *acceleration*  $y''$  or  $\ddot{y}$  is critically significant for design considerations.
- Acceleration values are related to the system inertia forces in which the maximum acceleration establishes the maximum inertia forces.
- The shape of the follower acceleration curve is of critical concern for the design of moderate- to high-speed machines. From it, analysis can be made for cam-follower system shock, noise, wear, and vibration.
- The acceleration curve shall have no discontinuities where it blends with the dwell action of the motion.
- Acceleration values at each point are related to the radius of curvature of the cam profile, which in turn relates to the surface stresses and wear.
- Over the complete rise-fall motion, the following is true:

$$\int y'' d\theta = 0 \text{ and } \int \ddot{y} dt = 0 \tag{2.11}$$

Therefore, the area of the acceleration curve for any cam has an area of positive action (+) equal to the area of the negative action (-). This observation could aid the designer in developing the optimum cam acceleration curve shape.

- The follower jerk  $y'''$  or  $\ddot{y}$  shall have the smallest values. Note that with industrial cams the jerk curve is not frequently of design control since the production tolerance is about  $\pm 0.001$  inch. The jerk curve is sensitive to much smaller deviations. However, in the automotive cam field the cam operates over a very small distance, requiring higher tolerance of about  $\pm 0.0001$  inch or better. In this case the jerk curve data is pertinent.

**EXAMPLE** Given the displacement diagram of a pitch curve in Fig. 2.1a, in which the follower has a total rise of  $\frac{1}{2}$  in. in 0.1 sec of cam rotation and falls in an additional 0.08 sec, plot the velocity curve and determine the velocity and acceleration after the initial 0.08 sec of cam rotation by applying the graphical-slope differentiating method.

**Solution** At the 0.08 sec point, we draw a tangent to the displacement curve. Caution is suggested. This is the instantaneous slope of the curve which equals the velocity.

$$\begin{aligned}\dot{y} &= dy/dt \\ &= \text{distance } ab/\text{distance } bc \\ &= \frac{0.371}{0.08} \\ &= 4.64 \text{ ips in a positive direction}\end{aligned}$$

Note that the distances  $ab$  and  $bc$  were arbitrarily chosen for reasonable measurement accuracy. In the same manner, other velocity points may be found and the curve plotted as in Fig. 2.1b. Here is the acceleration at 0.08 sec:

$$\begin{aligned}\ddot{y} &= d\dot{y}/dt \\ &= \text{distance } de/\text{distance } ef \\ &= -\frac{15.8}{0.08} \\ &= -198 \text{ in/sec}^2\end{aligned}$$

Again, the distances are chosen arbitrarily. Note, the acceleration is negative because the follower is reversing its acceleration in a minus, downward direction. Also, mathematically speaking, the slope is to the left (second quadrant), which means a negative value. The jerk values may be approximated in the same manner by plotting the acceleration curve and finding the slopes.

### 2.3 BASIC CURVE CLASSIFICATION

---

In this chapter we present some *basic curves* of the *DRD* type and their kinematic relationships.

In design, the first step is to sketch a time chart (discussed in Chap. 1). Then the basic cam curve may be chosen to satisfy the cam-follower requirements.

The basic curves of the rise-fall displacement diagram are primarily of two families: the *simple polynomial* and the *trigonometric*.

**SIMPLE POLYNOMIAL CURVES** *The displacement equations of simple polynomial curves are of the form*

$$y = C\theta^2 \quad (2.12)$$

where  $n = \text{any number}$   
 $C = \text{a constant}$

In this polynomial family, we have the following popular curves with integer powers: *straight line*,  $n = 1$ ; *parabolic or constant acceleration*,  $n = 2$ ; *cubic or constant jerk*,  $n = 3$ . High degree polynomial curves are shown in Chapter 3.

**TRIGONOMETRIC CURVES** *The curves of trigonometric form are: simple harmonic motion (SHM) or crank curve, which has a cosine acceleration curve; cycloidal, which has a sine acceleration curve; double harmonic; and elliptical. (Appendix B presents tabulated values of the simple harmonic motion curve and the cycloidal curve as a direct approach to follower characteristics.)*

**OTHER CURVES** *In addition to these two families are the miscellaneous, little-used curves: modified straight-line circular arc and the circular arc curves (see Chapter 14). These are employed primarily as an improvement over the characteristics of the straight-line curve and for special design requirements.*

**EXAMPLE** *A cam rotating at 120 rpm has the positive acceleration part of its rise of 3/8 in. in 40 degrees of cam rotation. A simple polynomial curve having  $n = 2.4$  is used. Find the velocity and acceleration values at the end of 30 degrees of cam rotation.*

**Solution** *The angular velocity of cam =  $\omega = 120 \times \frac{2\pi}{60} = 12.57 \text{ rad/sec}$ . The total cam angle =  $40\pi/180 = 0.698 \text{ radian}$ . Substituting into Eq. (2.12) gives the displacement*

$$y = C\theta^n = \frac{3}{8} = C(0.698)^{2.4}$$

Solving yields  $C = 0.888$ . Therefore, the basic equation is

$$y = 0.888\theta^{2.4}$$

The velocity by differentiating Eq. (2.12) is

$$\dot{y} = C\omega\theta^{n-1} \text{ ips}$$

Thus, the velocity after 30 degrees of rotation is

$$\dot{y} = 0.888(12.57)(2.4) \left( 30 \times \frac{\pi}{180} \right)^{1.4} = 10.8 \text{ ips}$$

The acceleration, differentiating again is

$$\ddot{y} = C\omega^2 n(n-1)\theta^{n-2}$$

The acceleration after 30 degrees of rotation is

$$\ddot{y} = 0.888(12.57)^2(2.4)(1.4) \left( 30 \times \frac{\pi}{180} \right)^{0.4} = 364 \text{ in/sec}^2$$

### 2.4 CONSTANT VELOCITY CURVE

The constant velocity or uniform displacement curve is the simplest of all ( $n = 1$ ). It has a straight-line displacement at a constant slope (Fig. 2.2) giving the smallest length for a given rise of all the curves. When the straight-line curve is developed for a radial cam, it becomes the *Archimedes spiral*; see App. A.

For a constant velocity curve

$$y = C_0 + C_1\theta$$

$$\text{at } \theta = 0, y = 0, \therefore C_0 = 0 \tag{2.13}$$

$$\text{at } \theta = \beta, y = h \therefore C_1 = \frac{h}{\beta}$$

$$\therefore \text{displacement } y = \frac{h}{\beta}\theta \tag{2.14}$$

$$\text{velocity } \dot{y} = \frac{h\omega}{\beta} = \text{a constant} \tag{2.15}$$

$$\text{acceleration } \ddot{y} = 0 \tag{2.16}$$

We see that the displacement is uniform, the velocity is constant, and the acceleration is zero during the rise. At the ends where the dwell meets the curve, however, we have an impractical condition. That is, as we go from the dwell (zero velocity) to a finite velocity, we have an instantaneous change in velocity, giving a theoretically infinite acceleration. This acceleration transmits high shock throughout the follower linkage, the magnitude of

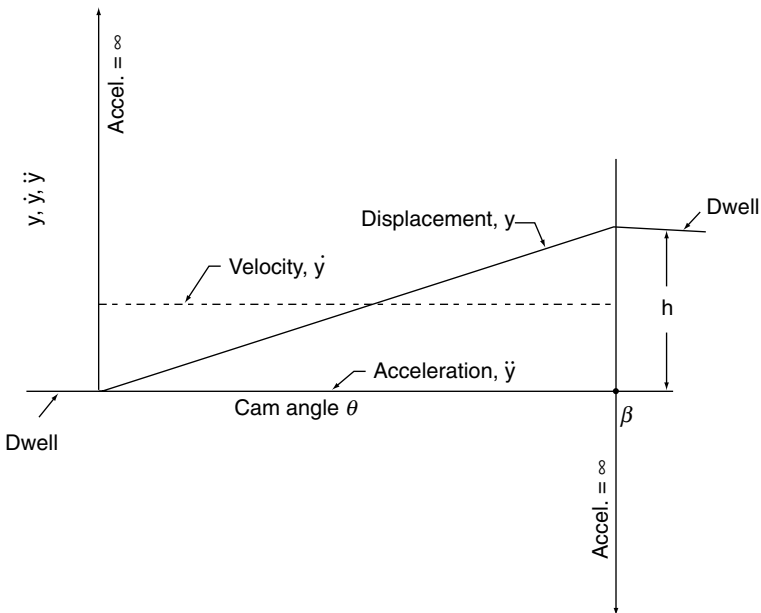


FIGURE 2.2. Constant velocity curve—DRD cam.

which depends on its flexibility. In other words, we have a “bump” in the contour that neither a roller nor other follower could follow. This curve is therefore impractical for a DRD cam.

## 2.5 MODIFIED CONSTANT VELOCITY CURVE WITH CIRCULAR ARCS

The constant velocity curve with its infinite acceleration and abrupt shock at the ends of the DRD cam is rarely used in industry. It can be applied with minor modifications. One such modification is made by utilizing circular arcs with a radius  $h$  and a tangent at the dwell ends (Fig. 2.3). In view of the poor characteristics of this curve, mathematical presentation is omitted.

## 2.6 CONSTANT ACCELERATION CURVE

This curve of the polynomial family is also known as the parabolic curve and has constant positive and negative acceleration values. The curve has the smallest maximum accelerations for all curves possible (Fig. 2.4). The displacement of the first half of motion of its symmetrical motion, the positive acceleration period is

$$y = C\theta^2 \quad (2.12)$$

$$0 \leq \theta \leq \frac{\beta}{2}$$

$$\text{at } \theta = \frac{\beta}{2} \quad y = \frac{h}{2}$$

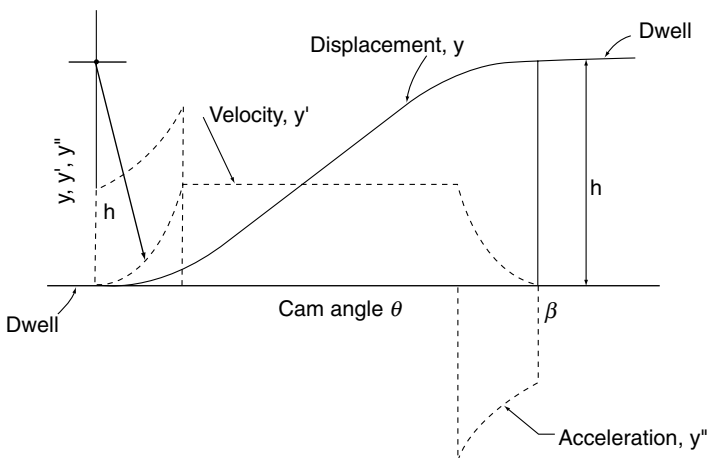


FIGURE 2.3. Modified constant velocity curve with circular area—DRD cam.

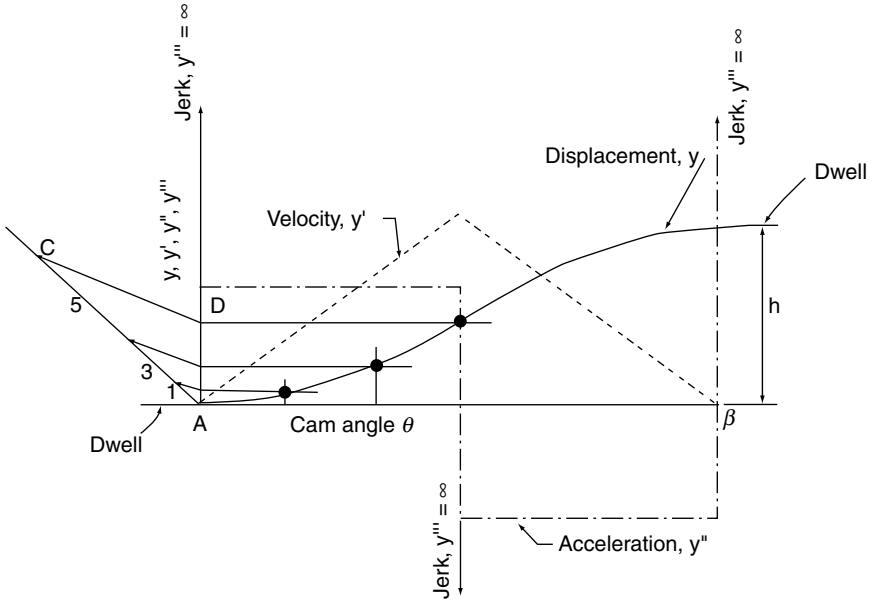


FIGURE 2.4. Constant acceleration curve—DRD cam.

substituting in Eq. (2.12)

$$C = \frac{2h}{\beta^2}$$

$$\text{displacement } y = \frac{2h}{\beta^2} \theta^2 \quad (2.17)$$

$$\text{velocity } y' = \frac{4h}{\beta^2} \theta \quad (2.18)$$

$$\text{acceleration } y'' = \frac{4h}{\beta^2} = \text{a constant} \quad (2.19)$$

jerk  $y''' = 0$  except at dwell ends and the midpoint

$$\frac{\beta}{2} \leq \theta \leq \beta$$

In the other half of the curve (negative acceleration), the displacement is

$$y = C_0 + C_1\theta + C_2\theta^2 \quad (2.20)$$

The boundary conditions are

$$\begin{aligned}\theta = \beta & \quad y = h \\ \theta = \frac{\beta}{2} & \quad y' = \frac{2h}{\beta} \\ \theta = \beta & \quad y' = 0\end{aligned}$$

yield constants

$$C_0 = -h, C_1 = \frac{4h}{\beta}, C_2 = \frac{-2h}{\beta}$$

Substituting in Eq. (2.20) yields

$$\text{displacement} \quad y = h - \frac{2h}{\beta^2}(\beta - \theta)^2 \quad (2.21)$$

$$\text{velocity} \quad y' = \frac{4h}{\beta} \left(1 - \frac{\theta}{\beta}\right) \quad (2.22)$$

$$\text{acceleration} \quad = -\frac{4h}{\beta^2} \quad (2.23)$$

jerk  $y''' = 0$  except at the changes in the acceleration where it equals infinity. Since the parabolic curve has discontinuities in the acceleration at the dwell ends and the transition point, it is primarily used for low-speed systems if at all.

Note that the data of this motion could have been accomplished by utilizing from physics (for constant acceleration action) such that the displacement

$$\begin{aligned}y &= v_0\theta + \frac{1}{2}a\theta^2 \\ &= V_0t + \frac{1}{2}At^2\end{aligned} \quad (2.24)$$

where

$v_0$  = initial velocity dimensionless

$V_0$  = initial velocity

$\theta$  = cam angle, radians

$t$  = time, sec

$a$  = acceleration, in/rad<sup>2</sup>

$A$  = acceleration, in/sec<sup>2</sup>

Furthermore, Eq. (2.24) will be used in Chap. 3 where the constant acceleration curve is blended with other curves to optimize the dynamics of the designed acceleration curve.

The construction for the constant acceleration curve is shown in Fig. 2.4. Draw line  $AC$ , which is made in odd number increments in this case three (i.e., 1, 3, 5), and draw line  $CD$  to the midpoint of the rise and draw parallel lines, which will be connected to the three cam increments. This establishes the cam profile since the steps are 1, 4, 9, and so forth as shown.

### 2.7 SKEWED CONSTANT ACCELERATION CURVE

The asymmetrical constant cam acceleration curve (follower motion) is shown in Fig. 2.5. The acceleration curve is made up of two parts, the positive and negative acceleration periods 1 and 2 connected at the transition point

$$y_1 = C_1\theta^2 \quad (0 \leq \theta \leq \beta_1) \tag{2.25}$$

$$h - y_2 = C_2(\beta - \theta)^2 \quad (\beta_1 \leq \theta \leq \beta) \tag{2.26}$$

where

$C_1$  and  $C_2$  are constants

$h_1$  = displacement at the transition point, in.

$\beta_1$  = angle of rotation for rise  $h_1$ , radians

Substituting in Eqs. (2.25) and (2.26) yields

$$h_1 = C_1\beta_1^2 \text{ and} \tag{2.27}$$

$$h - h_1 = C_2(\beta - \beta_1)^2 \tag{2.28}$$

Combining Eqs. (2.27) and (2.28) yields

$$C_1\beta_1^2 + C_2(\beta - \beta_1)^2 = h \tag{2.29}$$

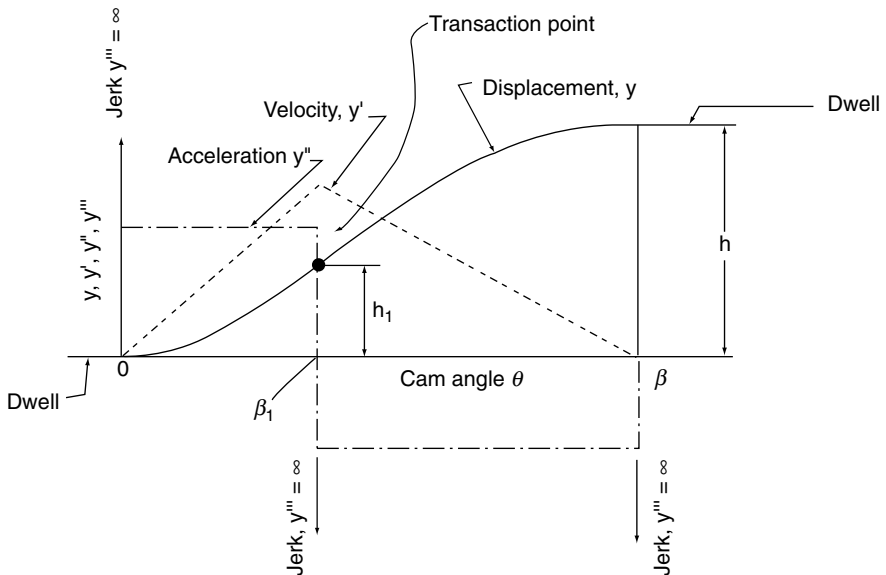


FIGURE 2.5. Skewed constant acceleration curve—DRD cam.

Since the velocities are equal at the point  $\theta = \beta_1$  differentiating Eqs. (2.25) and (2.26) yields

$$C_1 = C_2 \left( \frac{\beta}{\beta_1} - 1 \right) \quad (2.30)$$

Solving Eq. (2.29) and (2.30) gives

$$C_1 = \frac{h}{\beta_1 \beta}, \quad C_2 = \frac{h}{(\beta - \beta_1) \beta} \quad (2.31)$$

Therefore for  $0 < \theta \leq \beta_1$ ,

$$\text{displacement} \quad y_1 = \frac{h}{\beta_1 \beta} \theta^2 \quad (2.32)$$

$$\text{velocity} \quad y_1' = \frac{2h}{\beta_1 \beta} \theta \quad (2.33)$$

$$\text{acceleration} \quad y_1'' = \frac{2h}{\beta_1 \beta} \quad (2.34)$$

and for  $\beta_1 \leq \theta \leq \beta$ ,

$$\text{displacement} \quad y_2 = h - \frac{h}{(\beta - \beta_1) \beta} (\beta - \theta)^2 \quad (2.35)$$

$$\text{velocity} \quad y_2' = \frac{2h}{(\beta - \beta_1) \beta} (\beta - \theta) \quad (2.36)$$

$$\text{acceleration} \quad y_2'' = \frac{2h}{(\beta - \beta_1) \beta} \quad (2.37)$$

Note that the jerk values equal zero except where that value is infinite at the points of acceleration discontinuity.

## 2.8 CUBIC NO. 1 CURVE

---

This curve (follower motion) of the polynomial family has a triangular acceleration curve. It is a modification of the parabolic curve, eliminating the abrupt change in acceleration at the beginning and the end of the stroke. However it does have an acceleration discontinuity at the midpoint. This curve has limited applications since it also has high velocities and high acceleration values, giving excessive pressure angle and inertia forces. It is not very practical except when combined with other curves.

The construction of this curve (Fig. 2.6) is similar to that of the acceleration curve previously with the increments being 1, 7, 19, and so forth, which is a cubic relationship in lieu of 1, 3, 5 as with the constant acceleration curve. Thus it will not be shown here.

By methods shown for the parabolic curve, we can solve the cubic curve for

$$0 \leq \theta \leq \frac{\beta}{2}$$

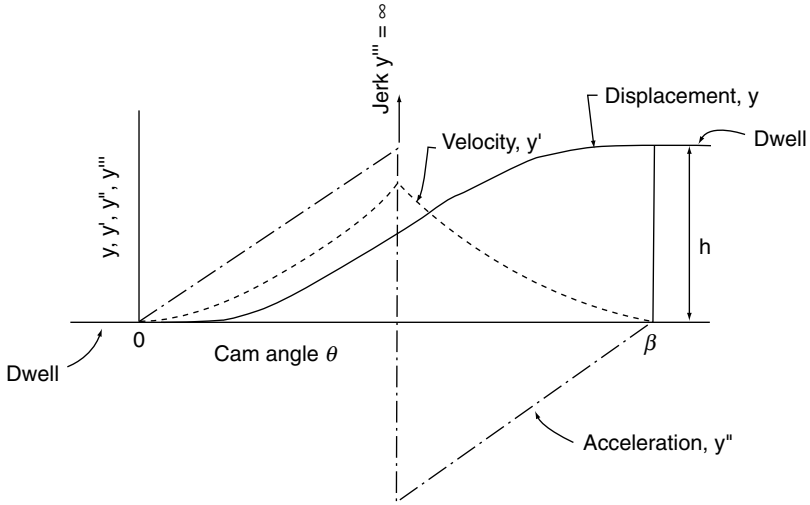


FIGURE 2.6. Cubic no. 1 curve—DRD cam.

$$\text{Displacement} \quad y = 4h\left(\frac{\theta}{\beta}\right)^3 \quad (2.38)$$

$$\text{Velocity} \quad y' = \frac{12h}{\beta}\left(\frac{\theta}{\beta}\right)^2 \quad (2.39)$$

$$\text{Acceleration} \quad y'' = \frac{24h}{\beta^2}\left(\frac{\theta}{\beta}\right) \quad (2.40)$$

$$\begin{aligned} \text{Jerk} \quad y''' &= \frac{24h}{\beta^3} \quad (2.41) \\ &= \text{constant} \end{aligned}$$

$$\frac{\beta}{2} \leq \theta \leq \beta$$

$$\text{Displacement} \quad y = h\left[1 - 4\left(1 - \frac{\theta}{\beta}\right)^3\right] \quad (2.42)$$

$$\text{Velocity} \quad y' = \frac{12h}{\beta}\left(1 - \frac{\theta}{\beta}\right)^2 \quad (2.43)$$

$$\text{Acceleration} \quad y'' = -\frac{24h}{\beta^2}\left(1 - \frac{\theta}{\beta}\right) \quad (2.44)$$

$$\text{Jerk} \quad y''' = \frac{24h}{\beta^3} = \text{constant} \quad (2.45)$$

## 2.9 CUBIC NO. 2 CURVE

---

This curve is similar to the constant acceleration and the cubic no. 1 curves. It differs from these, however, in that there is no discontinuity in acceleration at the transition point and also in that its acceleration is a continuous curve for the complete rise. Similar to the constant acceleration curve, it has the disadvantages of discontinuity in acceleration at the beginning and the end of the stroke. The cubic curve has characteristics similar to those of the simple harmonic motion curve presented next. It is not often employed but has advantages when used in combination with other curves. No simple construction method is available.

The characteristic formulas can be found by the same method as that shown for the parabolic curve.

$$\text{Displacement} \quad y = h \frac{\theta^2}{\beta^2} \left( 3 - \frac{2\theta}{\beta} \right) \quad (2.46)$$

$$\text{Velocity} \quad y' = \frac{6h\theta}{\beta^2} \left( 1 - \frac{\theta}{\beta} \right) \quad (2.47)$$

$$\text{Acceleration} \quad y'' = \frac{6h}{\beta^2} \left( 1 - \frac{2\theta}{\beta} \right) \quad (2.48)$$

$$\text{Jerk} \quad y''' = \frac{12h}{\beta^3} \quad (2.49)$$

= constant

The procedure used to plot Fig. 2.7 is similar to that for the previous curves.

## 2.10 SIMPLE HARMONIC MOTION CURVE

---

This curve (having a cosine acceleration curve) is a very popular choice in combination with other curves in Chap. 3. In Fig. 2.8, the projection of a radius point  $P$  starting at point  $O$  moves vertically at point  $Q$  along the diameter  $h$  of the circle with simple harmonic motion.

Let

$$\phi = \text{angle of rotations with radius } \frac{h}{2}$$

The basic harmonic motion displacement function is

$$y = \frac{h}{2} (1 - \cos \phi) \quad (2.50)$$

The construction of Fig. 2.8 uses a circle of radius  $\frac{h}{2}$ . Displacements are taken at angular increments moving through angle  $\phi$  the same increments along the displacement curve. The relationship between angle  $\phi$ , the generating circle, and the cam angle  $\theta$  is

$$\frac{\phi}{\theta} = \frac{\pi}{\beta} \quad (2.51)$$

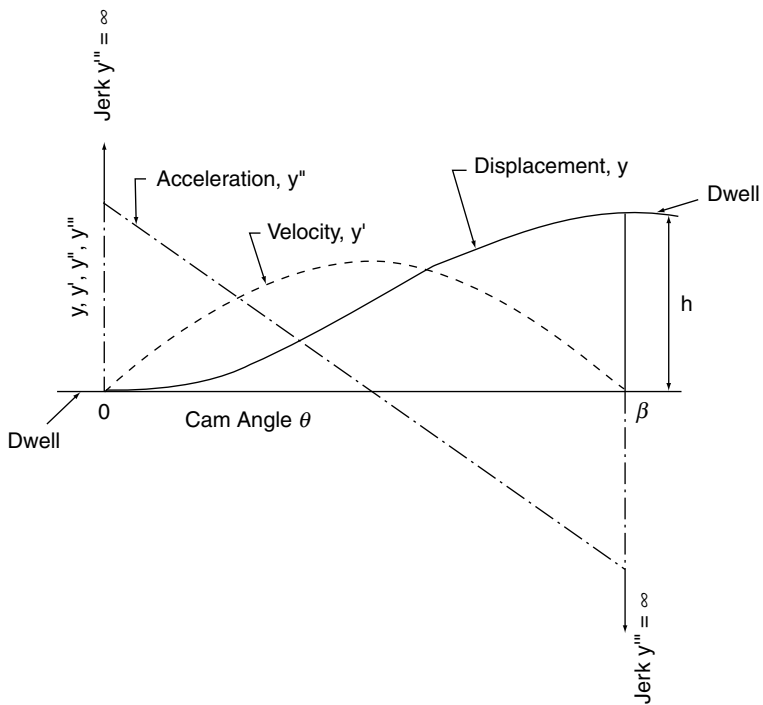


FIGURE 2.7. Cubic no. 2 curve—DRD cam.

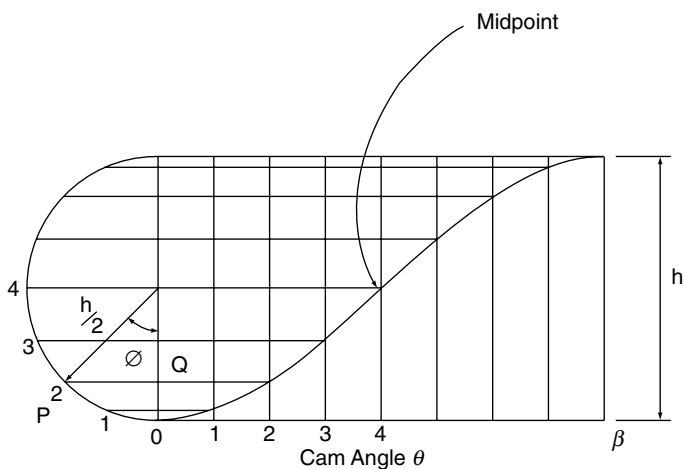


FIGURE 2.8. Simple harmonic motion curve construction.

Substituting in Eq. (2.50) gives

$$\text{Displacement } y = \frac{h}{2} \left( 1 - \cos \frac{\pi\theta}{\beta} \right), \tag{2.52}$$

from which we obtain

$$\text{Velocity } y' = \frac{h\pi}{2\beta} \sin \frac{\pi\theta}{\beta} \tag{2.53}$$

$$\text{Acceleration } y'' = \frac{h\pi^2}{2\beta^2} \cos \frac{\pi\theta}{\beta} \tag{2.54}$$

$$\text{Jerk } y''' = \frac{h\pi^3}{2\beta^3} \sin \frac{\pi\theta}{\beta} \tag{2.55}$$

Figure 2.9 shows the plotting of these equations. The simple harmonic motion has a smooth acceleration curve except at the dwell ends, where it has discontinuities (i.e., infinite jerk).

To simplify the cam calculations for displacement, velocity, and acceleration of the follower, tabulated data for the simple harmonic curve are shown in App. B.

**EXAMPLE** A cam rotates at a constant speed of 30rpm. The follower rises 1/2 in. with simple harmonic motion in 150 degrees of cam rotation. Find the displacement, velocity, and acceleration of the follower after 30 degrees of cam rotation (a) by use of formulas and (b) by employing the data in App. B.

**Solution (a)**

$$\text{Cam angle } \theta = 30 \times \frac{\pi}{180} = 0.524 \text{ rad}$$

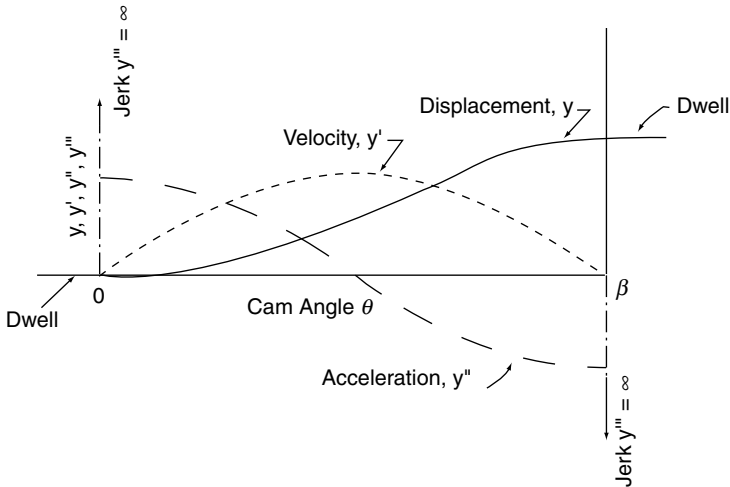


FIGURE 2.9. Simple harmonic motion curve—DRD cam.

$$\text{Cam angular velocity } \omega = 300 \times \frac{2\pi}{60} = 31.42 \text{ rad/sec}$$

$$\text{Total angle } \beta = 150 \times \frac{\pi}{180} = 2.62 \text{ rad}$$

From Eq. (2.51) the displacement

$$\begin{aligned} y &= \frac{h}{2} \left( 1 - \cos \frac{\pi\theta}{\beta} \right) \\ &= \frac{3}{4} \left( 1 - \cos \frac{\pi \times 0.524}{2.62} \right) = 0.143 \text{ in} \end{aligned}$$

Equation 2.52 gives velocity

$$\begin{aligned} y' &= \frac{h\pi}{2\beta} \sin \frac{\pi\theta}{\beta} \text{ in/rad and with Eq. 2.8, the velocity} \\ \dot{y} &= \frac{h\pi\omega}{2\beta} \sin \frac{\pi\theta}{\beta} \text{ in/sec} \\ &= \frac{1}{2} \times \pi \times 31.42 \sin \frac{\pi \times 0.524}{2.62} = 16.6 \text{ ips} \end{aligned}$$

Acceleration by Eq. (2.53)

$$\begin{aligned} y'' &= \frac{h\pi^2}{2\beta^2} \cos \frac{\pi\theta}{\beta} \text{ in/rad}^2 \text{ and with Eq.(2.9), the acceleration} \\ \ddot{y} &= \frac{h}{2} \left( \frac{\pi\omega}{\beta} \right)^2 \cos \frac{\pi\theta}{\beta} \text{ in/sec}^2 \\ &= \frac{3}{4} \left( \frac{\pi \times 31.42}{2 \times 2.62} \right)^2 \cos \frac{\pi \times 0.524}{2.62} = 862 \text{ in/sec}^2 \end{aligned}$$

### Solution (b)

In App. B-1 for simple harmonic motion

$$\text{Point \#} = \frac{\theta \times 120}{\beta} = \frac{30 \times 120}{150} = 24.0$$

$$\omega = \frac{360 \text{ deg/rev} \times 300 \text{ rpm}}{60 \text{ sec/min}} = 1800 \text{ deg/sec}$$

Displacement

$$\begin{aligned} y &= Kh \\ &= 0.9549 \cdot 1.5 = 0.14324 \text{ in} \end{aligned}$$

where  $K = 0.9549$  at point #24

Velocity

$$\begin{aligned} \dot{y} &= C_v h \left( \frac{\omega}{\beta} \right) \\ &= 0.9233 \times 1.5 \times \frac{1800}{150} \\ &= 16.6194 \text{ in/sec} \end{aligned}$$

Acceleration

$$\begin{aligned} \ddot{y} &= C_a h \left( \frac{\omega}{\beta} \right)^2 \\ &= 3.9924 \times 1.5 \times \left( \frac{1800}{150} \right)^2 \\ &= 862.3584 \text{ in/sec}^2 \end{aligned}$$

### 2.11 CYCLOIDAL MOTION CURVE

The cycloidal motion curve, as the name implies, is generated from a cycloid and has a sine acceleration curve. A cycloid is the locus of a point on a circle that is rolled on a straight line. The circumference of the circle is equal to the follower rise  $h$ . The cycloid is the first dwell-rise-dwell curve we discuss that does not have any discontinuities in the acceleration curve. Therefore, it can be applied to higher speeds than the foregoing curves even though its maximum acceleration is higher in some cases.

Designate point A (Fig. 2.10) as the center and draw a circle with the radius equal to  $\frac{h}{2\pi}$ . Divide this circle into the same number of parts used for the horizontal axis. From the projection of these points on the ordinate, draw lines that are parallel to the diagonal AD that intersect the vertical projections of the divisions of this abscissa. These intersections locate the necessary points for the displacement curve.

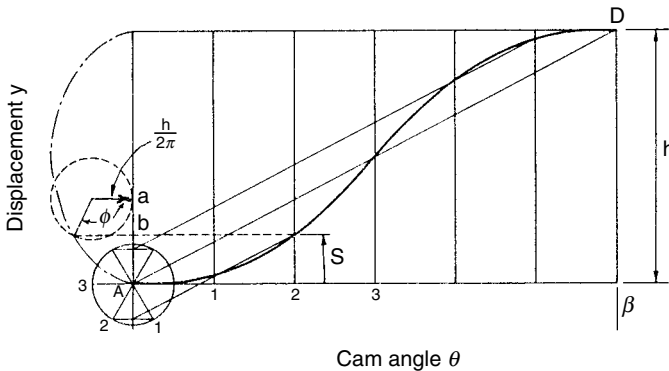


FIGURE 2.10. Cycloidal motion curve construction.

From Fig. 2.10, the radius is  $\frac{h}{2\pi}$  in which

$$\text{Displacement } y = \frac{h}{2\pi}\phi - \frac{h}{2\pi}\sin\phi \tag{2.56}$$

where  $\phi$  = angle of circle rotation, rad.  
We see

$$\frac{\theta}{\beta} = \frac{\phi}{2\pi}$$

Substituting in Eq. (2.56) yields

$$\text{Displacement } y = h\left(\frac{\theta}{\beta} - \frac{1}{2\pi}\sin\frac{2\pi\theta}{\beta}\right) \tag{2.57}$$

In Fig. 2.10, we see that the first term of the equation,  $\frac{h\theta}{\beta}$ , is the sloping line and the second term,  $\frac{h}{2\pi}\sin\frac{2\pi\theta}{\beta}$ , is the subtracted harmonic displacement. Thus

$$\text{Velocity } y' = \frac{h}{\beta}\left(1 - \cos\frac{2\pi\theta}{\beta}\right) \tag{2.58}$$

$$\text{Acceleration } y'' = \frac{2h\pi}{\beta^2}\sin\frac{2\pi\theta}{\beta} \tag{2.59}$$

$$\text{Jerk } y''' = \frac{4h\pi^2}{\beta^3}\cos\frac{2\pi\theta}{\beta}. \tag{2.60}$$

The above equations are plotted in Fig. 2.11. Note that this curve has no sudden change in acceleration for the complete cycle and thus has high-speed applications. To simplify

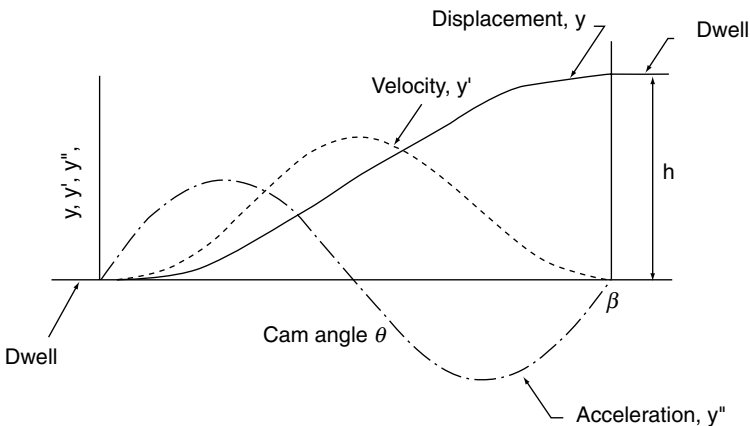


FIGURE 2.11. Cycloidal motion curve—DRD cam.

the cam calculations for displacement, velocity, and acceleration of the follower, tabulated data for the cycloidal curve are shown in Appendix B.

## 2.12 DOUBLE HARMONIC MOTION CURVE

This asymmetrical curve (Fig. 2.12) is composed of the difference between two harmonic motions, one being one-quarter of the amplitude and twice the frequency of the other. The construction is not shown. It has the advantages of the simple harmonic curve with almost complete elimination of the high shock and vibration at the beginning of the stroke. The rate of acceleration change at the beginning of the stroke is small, giving smooth action at the point. However, this slow start requires a larger cam to provide a sufficient minimum cam curvature. Note that as a dwell-rise-dwell cam, the limitation of the sudden change in acceleration at the maximum rise point allows only moderate cam speeds.

The relationships are

$$\begin{aligned} \text{Displacement} \quad y &= \frac{h}{2} \left[ (1 - \cos \phi) - \frac{1}{4}(1 - \cos 2\phi) \right] & (2.61) \\ &= \frac{h}{2} \left[ \left( 1 - \cos \frac{\pi\theta}{\beta} \right) - \frac{1}{4} \left( 1 - \cos \frac{2\pi\theta}{\beta} \right) \right] \end{aligned}$$

$$\text{Velocity} \quad y' = \frac{h}{2} \frac{\pi}{\beta} \left( \sin \frac{\pi\theta}{\beta} - \frac{1}{2} \sin \frac{2\pi\theta}{\beta} \right) \quad (2.62)$$

$$\text{Acceleration} \quad y'' = \frac{h}{2} \left( \frac{\pi}{\beta} \right)^2 \left( \cos \frac{\pi\theta}{\beta} - \cos \frac{2\pi\theta}{\beta} \right) \quad (2.63)$$

$$\text{Jerk} \quad y''' = \frac{h}{2} \left( \frac{\pi}{\beta} \right)^3 \left( \sin \frac{2\pi\theta}{\beta} - \sin \frac{\pi\theta}{\beta} \right) \quad (2.64)$$

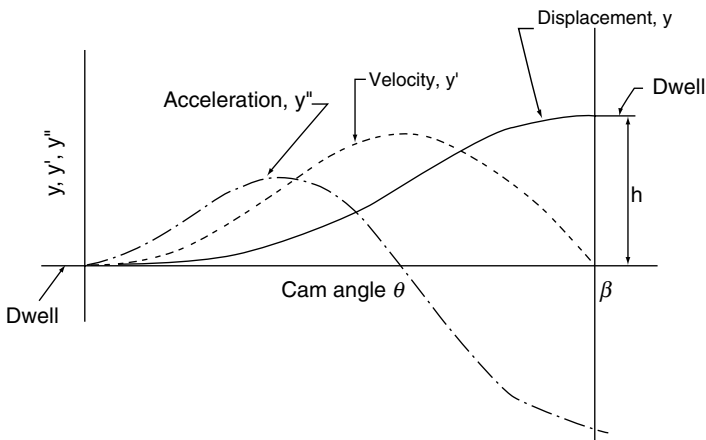


FIGURE 2.12. Double-harmonic motion curve—DRD cam.

### 2.13 ELLIPTICAL CURVE

This member of the trigonometric family is developed from projections of a semiellipse (Fig. 2.13). The contour of the elliptical curve and its characteristics depend on the assumed proportions of the major and minor axes. As the major axis increases the cam becomes larger with the velocities of start and stop slower. In other words, the curve is flatter at the top and the bottom as the ratio of the major axis to the minor axis is made larger. If the major axis of the ellipse is zero in length, the contour in the displacement diagram is a straight-line curve. A ratio of 2:4 gives a small cam for a given pressure angle. Increasing the ratio further to 11:8 makes the curve approach a parabolic curve. Further increase in the ratio is not practical, since velocity, acceleration, and cam size become prohibitive. Equations for the ellipse are in Appendix A.

The layout consists of the projections of equal arcs on an ellipse of assumed major to minor axis ratio (see Fig. 2.13):

1. Plot ordinate and abscissa axes with the total rise of the follower  $h$  equal to either the major or the minor axis of the ellipse.
2. Describe two circles whose diameters are equal to major and minor axes.
3. Draw any radius  $AE$  cutting circles at  $E$  and  $F$ .
4. Draw lines through  $E$  parallel to one axis and through  $F$  parallel to the other. The intersection  $G$  of these two lines is a point on the ellipse. Continue in this manner and draw the ellipse.
5. Divide both the abscissa of the displacement diagram and the arc of the ellipse into the same number of equal parts, usually 4, 6, 8, 10, 12, or 16. Note, no relation exists between the lengths of divisions on the displacement diagram and the divisions on the ellipse except that they must be the same in number.
6. Project these intercepts to their respective cam angle division, and connect points to yield the curve.

Next, we will establish the mathematical relationship for the elliptical curve of different major and minor axes. From descriptive geometry, the basic equation for the ellipse is

$$\frac{x_e^2}{a_e^2} + \frac{y_e^2}{b_e^2} = 1 \tag{2.65}$$

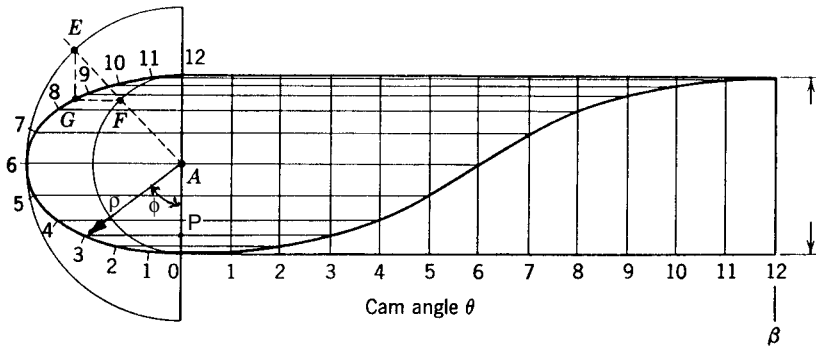


FIGURE 2.13. Elliptical curve construction.

where  $a_e$  and  $b_e$  are the semi-major and the semi-minor axes of the ellipse, respectively.

$$\text{If we let } n_e = \frac{a_e}{b_e} \text{ and} \quad (2.66)$$

$$\alpha = \frac{a_e^2 - b_e^2}{a_e^2} = \frac{n_e^2 - 1}{n_e^2} \quad (2.67)$$

It can be shown that

$$\text{Displacement } y = \frac{h}{2} \left( 1 - \frac{\cos \frac{\pi\theta}{\beta}}{\sqrt{1 - \alpha \sin^2 \frac{\pi\theta}{\beta}}} \right) \quad (2.68)$$

and

$$\text{Velocity } y' = \frac{\pi h}{2\beta} \frac{\sin \frac{\pi\theta}{\beta}}{n_e^2 \left( 1 - \alpha \sin^2 \frac{\pi\theta}{\beta} \right)^{3/2}} \quad (2.69)$$

$$\text{Acceleration } y'' = \frac{\pi^2 h}{2\beta^2} \cos \frac{\pi\theta}{\beta} \frac{1 + 2\alpha \sin^2 \frac{\pi\theta}{\beta}}{n_e^2 \left( 1 - \alpha \sin^2 \frac{\pi\theta}{\beta} \right)^{5/2}} \quad (2.70)$$

Figure 2.14 shows the velocity and acceleration curves for  $n = 1.0$  and  $n = 1.3$ . The kinematic characteristics of the elliptical curve depend on the assumed proportions of the major and the minor axes. Proper proportions in the ratio between major and minor axes produce cams of acceptable performance at moderate speeds similar to those of the simple harmonic motion curve, all having acceleration discontinuity at the beginning and end of the DRD action.

## 2.14 COMPARISON OF BASIC CURVES

The basic curves discussed can be applied for low to moderate speeds as a first design selection. For optimum cam follower performance, combinations of these basic curves and other mathematical curves for moderate to high speeds are presented in Chap. 3.

Comparing the curves most often used, the trigonometric ones (simple harmonic motion, cycloidal, and double harmonic curves) give better overall performance than those in the basic polynomial family (straight-line, parabolic, and cubic curves). The advantages are smaller cams and reduced translating follower ride thrust. In this chapter, the cycloidal curve, for most machine requirements, is the first choice. Since it has no abrupt change in acceleration, it gives the lowest vibrations, wear, stress, noise, and shock. It is easy to start, requires small springs, and induces low follower side thrust. However, the necessary accuracy of fabrication is higher than for low-speed curves. It has a slightly larger maximum acceleration than some others. Figure 2.15 shows the comparison of the basic curve characteristics of displacement, velocity, and acceleration. The data is that the

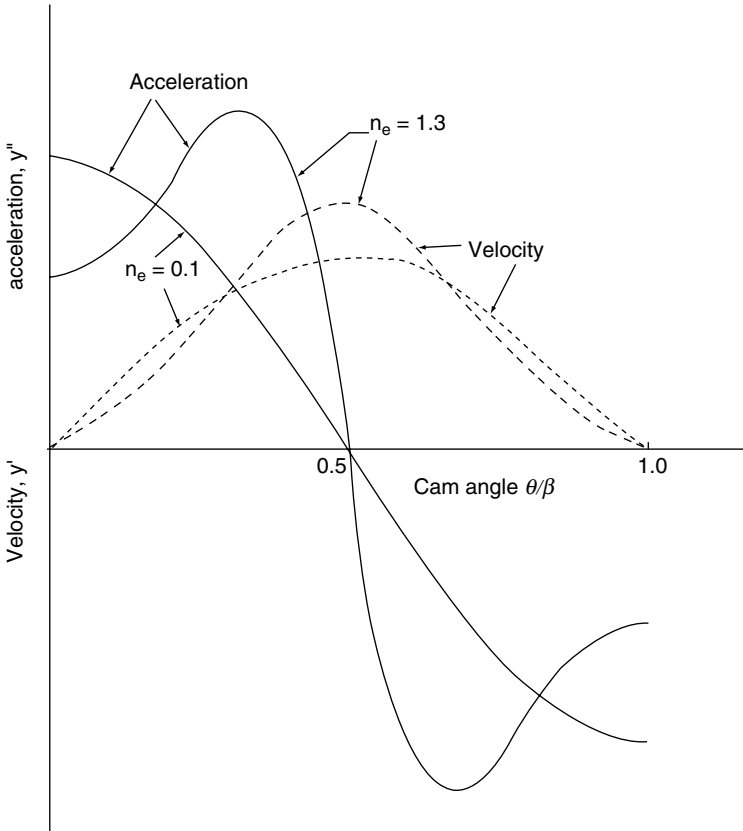


FIGURE 2.14. Elliptical curve velocity and acceleration ( $n = \frac{a_e}{b_e}$  ratio off axes).

follower rises 1-1/2 inches in 150 degrees of dwell-rise-dwell cam rotation at 300rpm. Table 2.1 presents the mathematical summary of the curve equations.

## 2.15 CURVE APPLICATION TO DRRD CAM

In this chapter we discussed the application of symmetrical basic curves to dwell-rise-return-dwell (DRRD) cams. Much of the previous information on the use of basic curves in dwell-rise-dwell cams applies to DRRD cams, with certain slight changes. DRRD cams using the basic curves of this chapter for both rise and return may be classified as:

- Symmetrical rise and fall displacement curve, in which both the rise and the fall take place in the same time or through the same cam angle.
- Asymmetrical rise and fall displacement curve (i.e., the cam angle of rise is different from the cam angle of fall).

**TABLE 2.1** Characteristic Equations of Basic Curves

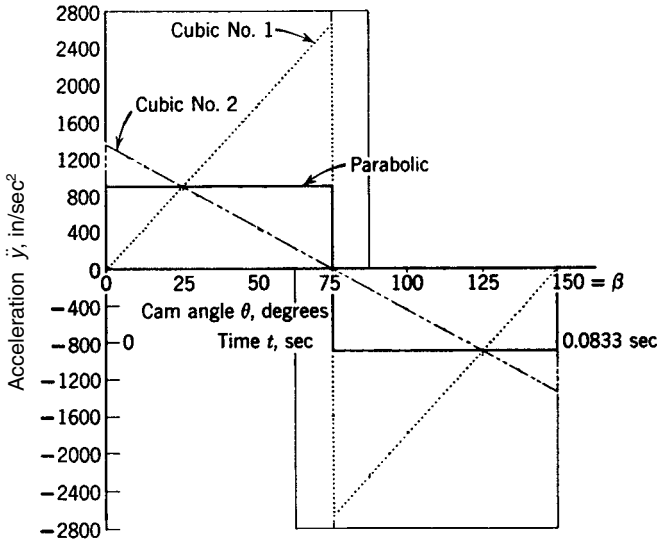
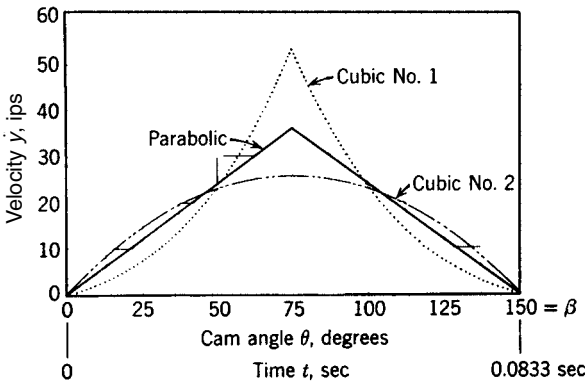
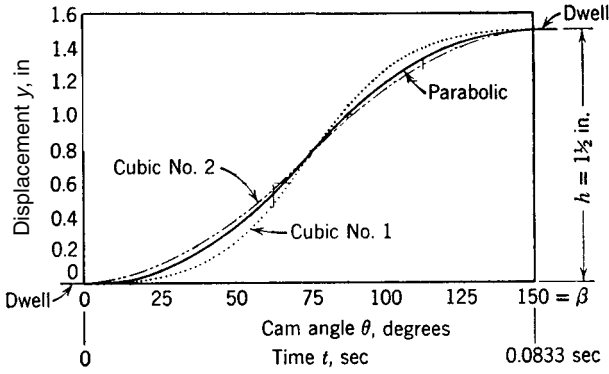
Curves	Displacement $y$ , in.	Velocity $\dot{y}$ , ips	Acceleration $\ddot{y}$ , in./sec <sup>2</sup>
Constant velocity	$\frac{h\theta}{\beta}$	$\frac{\omega h}{\beta}$	0
Simple harmonic motion (SHM)	$\frac{h}{2} \left( 1 - \cos \frac{\pi\theta}{\beta} \right)$	$\frac{h\pi\omega}{2\beta} \sin \frac{\pi\theta}{\beta}$	$\frac{h}{2} \left( \frac{\pi\omega}{\beta} \right)^2 \cos \frac{\pi\theta}{\beta}$
Double harmonic	$\frac{h}{2} \left[ \left( 1 - \cos \frac{\pi\theta}{\beta} \right) - \frac{1}{4} \left( 1 - \cos \frac{2\pi\theta}{\beta} \right) \right]$	$\frac{h\pi\omega}{2\beta} \left( \sin \frac{\pi\theta}{\beta} - \frac{1}{2} \sin \frac{2\pi\theta}{\beta} \right)$	$\frac{h}{2} \left( \frac{\pi\omega}{\beta} \right)^2 \left( \cos \frac{\pi\theta}{\beta} - \cos \frac{2\pi\theta}{\beta} \right)$
Cycloidal	$\frac{h}{\pi} \left( \frac{\pi\theta}{\beta} - \frac{1}{2} \sin \frac{2\pi\theta}{\beta} \right)$	$\frac{h\omega}{\beta} \left( 1 - \cos \frac{2\pi\theta}{\beta} \right)$	$\frac{2h\pi\omega^2}{\beta^2} \sin \frac{2\pi\theta}{\beta}$
Parabolic or constant acceleration	$2h \left( \frac{\theta}{\beta} \right)^2$	$\frac{4h\omega\theta}{\beta^2}$	$4h \frac{\omega^2}{\beta^2}$
	$h \left[ 1 - 2 \left( 1 - \frac{\theta}{\beta} \right)^2 \right]$	$\frac{4h\omega}{\beta} \left( 1 - \frac{\theta}{\beta} \right)$	$-4h \frac{\omega^2}{\beta^2}$
Cubic no. 1	$4h \left( \frac{\theta}{\beta} \right)^3$	$\frac{12h\omega}{\beta} \left( \frac{\theta}{\beta} \right)^2$	$\frac{24h\omega^2}{\beta^2} \left( \frac{\theta}{\beta} \right)$
	$h \left[ 1 - 4 \left( 1 - \frac{\theta}{\beta} \right)^3 \right]$	$\frac{12h\omega}{\beta} \left( 1 - \frac{\theta}{\beta} \right)^2$	$-\frac{24h\omega^2}{\beta^2} \left( 1 - \frac{\theta}{\beta} \right)$
Cubic no. 2	$h \left( \frac{\theta}{\beta} \right)^2 \left( 3 - 2 \frac{\theta}{\beta} \right)$	$\frac{6h\omega\theta}{\beta^2} \left( 1 - \frac{\theta}{\beta} \right)$	$\frac{6h\omega^2}{\beta^2} \left( 1 - 2 \frac{\theta}{\beta} \right)$

where  $h$  = maximum rise of follower, in.

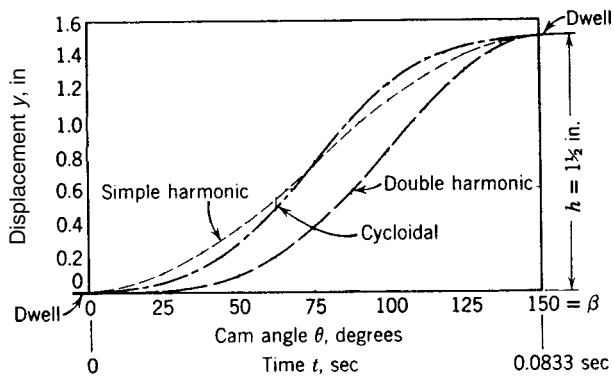
$\beta$  = cam angle of rotation to give rise  $h$ , radians.

$\omega$  = cam angular velocity, rad/sec.

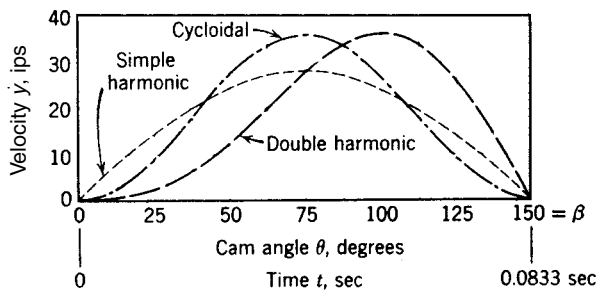
$\theta$  = cam angle rotation for follower displacement  $y$ , radians.



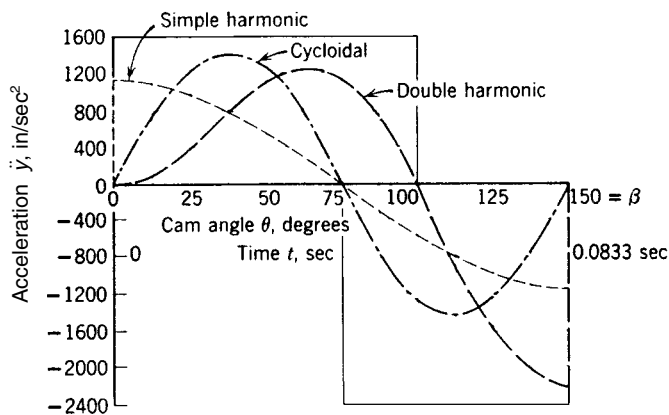
**FIGURE 2.15.** Comparison of basic curves—DRD cam. (Follower has  $1\frac{1}{2}$ -in. rise in 150 degrees of cam rotation at 30 rpm.)



(a) Displacement



(b) Velocity



(c) Acceleration

FIGURE 2.15. Continued

**DRRD Cams—Symmetrical Rise Return**

Let us now plot some basic curves for a DRRD cam. In Fig. 2.16*a*, for comparison, we see the symmetrical parabolic, simple harmonic motion, cycloidal, and double harmonic curves. We know that the displacement and velocity curves of all are smooth and continuous between the dwell ends. However, the parabolic and simple harmonic acceleration curves exhibit the same difficulty as those in the dwell-rise-dwell application, that is, sudden change at the ends. This shortcoming is known to produce inferior performance at high speeds. The cycloidal curve, on the other hand, which is one of the best dwell-rise-dwell curves, has an abrupt change in acceleration at the maximum rise point. This is not desirable, because vibration and difficult machining result. The magnitude of these factors, of course, depends on cam speed and flexibility of the parts. However, we note that at the maximum rise point neither the parabolic nor the simple harmonic curve has any abrupt change. We also see that the best high-speed curve, from the standpoint of slow starting

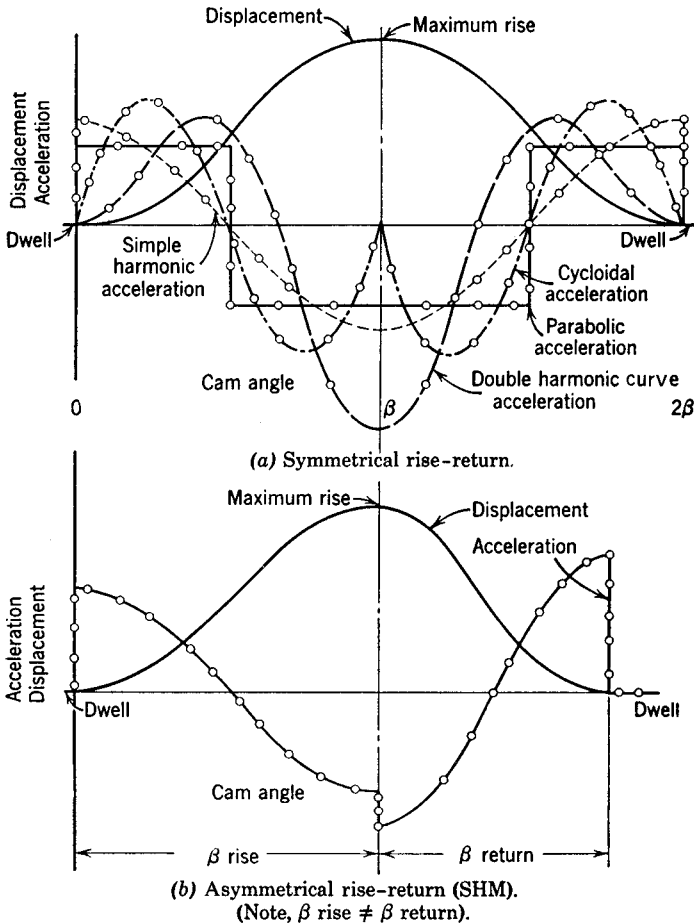


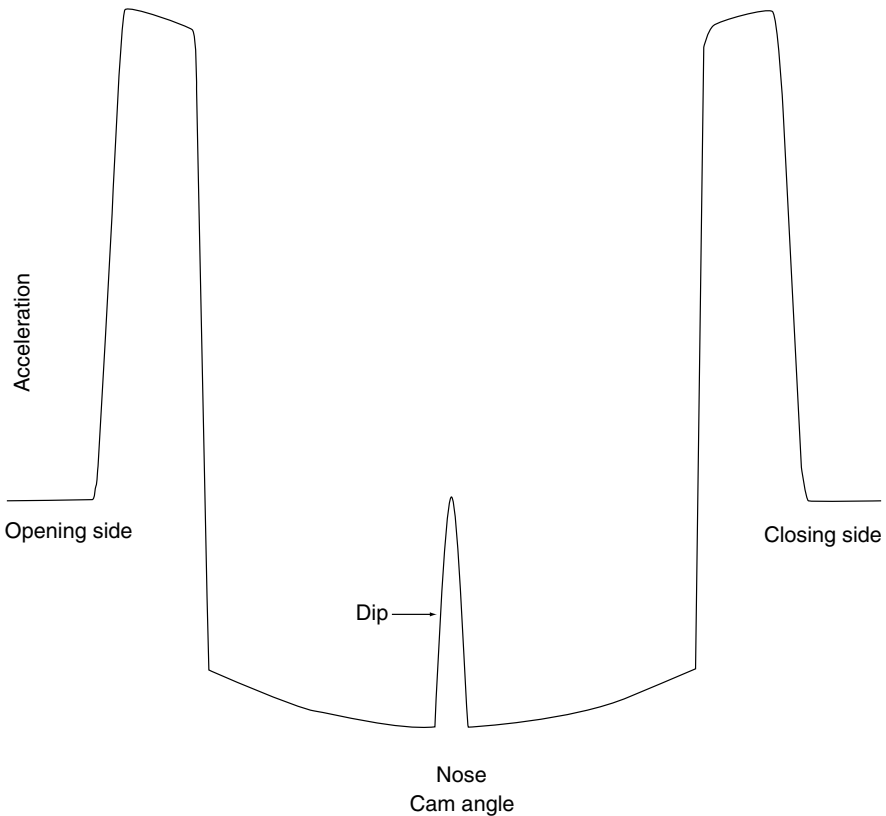
FIGURE 2.16. DRRD cam application of basic curves.

and stopping action and no abrupt change in acceleration, is the double harmonic curve. If it can be manufactured with the accuracy necessary, it is suggested as the best basic curve for the DRRD cam.

### DRRD Cam—Asymmetrical Rise Return

In this type of cam, we may observe another difficulty at the point of maximum rise, as shown in Fig. 2.16*b*. Using the simple harmonic motion curve as an example, we plot the action with the rise occurring in a shorter time or cam angle than the return. At the peak rise point, we observe an undesirable abrupt change in acceleration, and vibrations, noise, and wear result. This abrupt acceleration may be ignored at moderate or lower cam speeds.

Figure 2.17 shows the DRRD automotive racing car camshaft characteristic curves at the initial stage of development. There is an undesirable dip in the negative acceleration position. A final design had a smooth acceleration curve by modifying the exponents of the polynomials.



**FIGURE 2.17.** Automotive camshaft characteristic curves (preliminary design). (Courtesy Elgin Cam Company, Redwood City, Calif.) (Note, final design will have no dip.)

---

# CHAPTER 3

---

# MODIFIED CAM CURVES

---

**Harold A. Rothbart, D.Eng.**

3.1 INTRODUCTION	56	3.7 MODIFIED SINE CURVE	73
3.2 FUNDAMENTALS	57	3.8 MODIFIED CYCLOIDAL CURVE	76
3.3 MODIFIED CONSTANT VELOCITY CURVE	57	3.9 DWELL-RISE-RETURN-DWELL MOTION	78
3.4 TRAPEZOIDAL CURVE	61	3.10 COUPLED CURVE SIMPLIFICATION	81
3.5 MODIFIED TRAPEZOIDAL CURVE	61		
3.6 SKEWED MODIFIED TRAPEZOIDAL CURVE	70		

---

## **SYMBOLS**

$h$  = total rise of the follower, in

$h'$  = maximum rise of follower segment, in

$h$  = maximum follower displacement for full or half curve, in

$t$  = time, sec.

$y$  = follower displacement

$y' = \frac{dy}{d\theta}$  = follower velocity, dimensionless

$y'' = \frac{d^2y}{d\theta^2}$  = follower acceleration, dimensionless

$y''' = \frac{d^3y}{d\theta^3}$  = follower jerk, dimensionless

$\ddot{y} = \frac{d^2y}{dt^2} = \omega^2 y''$  = follower acceleration

$\dot{y} = \frac{dy}{dt} = \omega y'$  = follower velocity

$\ddot{y} = \frac{d^3y}{dt^3} = \omega^3 y'''$  = follower jerk

$A$  = follower acceleration, in/sec<sup>2</sup>

$V_{\max}$  = maximum velocity, ips

$V_0$  = follower initial velocity, in/sec

$a$  = follower acceleration, dimensionless

$\beta$  = cam angle for rise  $h$ , radians

$\beta$  = angle for maximum follower displacement, radians

$\beta_1, \beta_2$  = periods during positive and negative accelerations respectively, radians

$\theta$  = cam angle rotation, radians

$\omega$  = cam speed, rad/sec

$v_0$  = follower initial velocity, in/radians

### 3.1 INTRODUCTION

In Chap. 2, the characteristics of displacement, velocity, acceleration, and jerk of basic symmetrical curves were presented. These curves were employed because of their simplicity of mathematical analysis and ease of construction. However, for many machine performance requirements, as when the cam requires either special functional motions or must operate at high speeds, the basic symmetrical curves are inadequate and modifications in curve selection are necessary. These modifications can consist of blending, skewing, or combining sectors of the cubic curves, simple harmonic curves, cycloidal curves, constant velocity curves, and constant acceleration curves.

Last, it should be mentioned that cam curve development (not shown) can be accomplished by starting with the fourth derivative ( $d^4y/dy^4$ ) curve with numerical trial and error combined with past experience to find the ultimate desired cam shape. Computers are employed to perform the increment integration in determining the displacement velocity, acceleration, and jerk curves.

Curve development and selection is one of the primary steps in the design of any cam-follower system. Later chapters include investigation of the pressure angle, cam curvature, cam torques, lubrication, materials, and necessary fabrication tolerances, among other things. A typical design evolutionary process will proceed as a series of trade-offs to produce the final design.

This chapter has two parts:

- complete mathematical development for popular DRD curves
- a simplified procedure for combining sectors of various basic curves

The dwell-rise-dwell (DRD) and dwell-rise-return-dwell (DRRD) curves will be analyzed. The rise-return-rise (RRR) curve is not presented since the *eccentric mechanism* of Chap. 15 satisfies the action in a simple, reliable, less expensive way. The RRR curve is also best for high-speed requirements because it provides a motion curve having continuity in all of its derivatives.

Note that the DRD cam curve is a portion of the total action which could be a part of the dwell-rise-dwell-return-dwell (DRDRD) cam. Figure 3.1 shows the complete cycle of blended DRD cycloidal curve producing a DRDRD cam. The period of rise is smaller than the period of fall, producing higher rise maximum acceleration than the maximum fall acceleration.

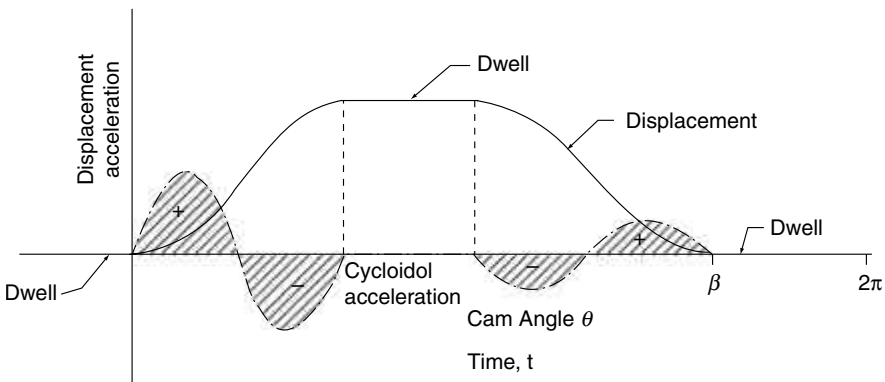


FIGURE 3.1. Dwell-rise-dwell-return-dwell cam with cycloidal acceleration curves.

### 3.2 FUNDAMENTALS

---

In this section, the fundamental conditions for shaping and combining curves are presented, and typical combinations of simple curves are shown. It is not practical to show all the possibilities, but it should be noted that any combination of sections of basic curves may be utilized to fulfill design requirements. The control conditions are:

- The sum of the displacements of the combining sectors shall equal the total rise of the follower.
- The sum of angles rotated of the combining sectors shall equal the total cam angle.
- The velocities at each sector junctions shall be equal.
- High-speed action requires that acceleration at all sector junctions be equal, that is, having no discontinuity in the acceleration and no infinite jerk value. Also, the acceleration curve should have the lowest maximum value with the value of jerk not too large.
- Sometimes special design requirements dictate the proportions of the acceleration curve. An example may be the controlling of the ratio of positive and negative acceleration periods and shapes. An asymmetrical acceleration curve, with the maximum positive acceleration larger than the negative maximum acceleration (ratio about 3:1) would be a good choice for spring-loaded high-speed cams. Smaller springs, larger cam curvatures, and longer surface life result.

On rare occasions limitations in the available manufacturing facilities may dictate the cam profile developed. For convenience, we have presented Fig. 3.2, which gives a comparison of important cam curves. Note that the velocity, acceleration, and jerk curves presented in this figure are all normalized (i.e., they have a unit total displacement  $h$  in a unit cam displacement  $\beta$ ).

To illustrate terminology we see that the trapezoidal acceleration curve (discussed later) is a continuous function whereas its derivative (jerk curve) has many discontinuities. Note that continuity of the jerk curve is of little value due to the usual tolerance limitations of cam profile machine tool fabrication.

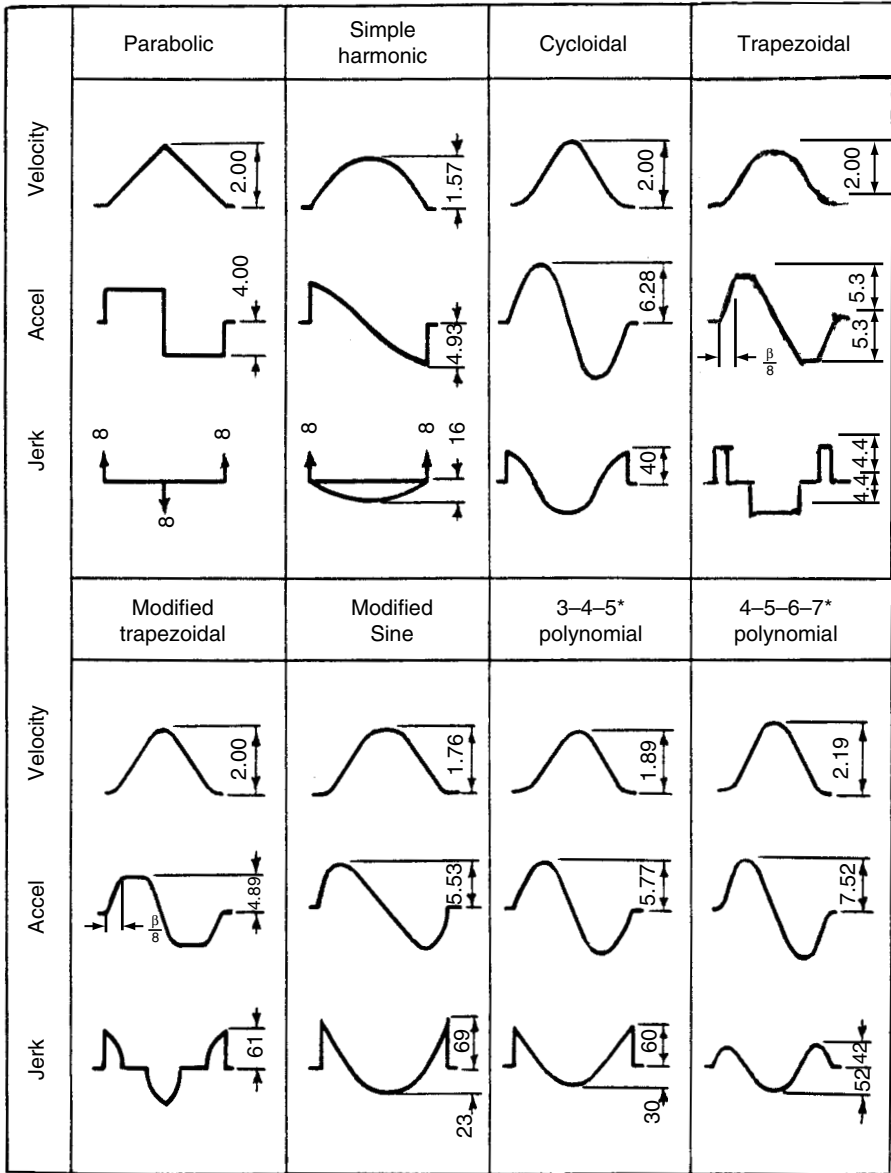
### 3.3 MODIFIED CONSTANT VELOCITY CURVE

---

In Chap. 2, we saw that the simplest curve is the constant velocity curve. It has a straight-line displacement at a constant slope. It also has the smallest cam for a given rise and provides a long stroke action. In this section we will blend any acceptable curve at the dwell ends for proper rise. The cycloidal curve or parabolic curves have been utilized depending on the cam speed, mass of the follower, and work performed by the machine.

As an example let us combine the parabolic motion curve blended with the straight-line displacement curve.

**EXAMPLE** *A cam having a rigid heavy-mass follower rotates at 300 rpm with a total DRD rise of 4 inches in 130 degrees of cam movement. As a preliminary study, use a parabolic curve modified with the constant velocity curve. The action is as follows: (a) for the first 40 degrees a positive parabolic curve acceleration; (b) for the next 30 degrees a straight-line displacement; and (c) for the last 60 degrees a negative parabolic curve acceleration. Find the ratio of accelerations, and plot all characteristic curves indicating pertinent values.*



\*In Chap. 4

FIGURE 3.2. Comparison of important DRD cam curves.

**Solution** The time for a revolution =  $60/300 = 0.2$  sec/rev. Let us divide the total action into three parts, as shown in Fig. 3.3 with  $T$  and  $Q$  the tangent points of the curves, giving the times

$$t_1 = 0.2 \left( \frac{40}{360} \right) = 0.0222 \text{ sec}$$

$$t_2 = 0.2 \left( \frac{30}{360} \right) = 0.0167 \text{ sec}$$

$$t_3 = 0.2 \left( \frac{60}{360} \right) = 0.0333 \text{ sec}$$

From the last chapter, we have the constant acceleration displacement

$$y = V_0 t + \frac{1}{2} A t^2 \text{ in} \quad (2.24)$$

where  $V_0$  = initial velocity, in./sec

$t$  = time, sec

$A$  = acceleration, in./sec<sup>2</sup>

Therefore, the displacements and the velocity for the parabolic motion of parts 1 and 3 are

$$\begin{aligned} y_1 &= \frac{1}{2} A_1 t_1^2 \\ y_3 &= v_Q t_3 + \frac{1}{2} A_3 t_3^2 \\ v_T &= A_1 t_1 \\ v_Q &= -A_3 t_3 \end{aligned} \quad (3.1)$$

For constant velocity of part 2

$$v_Q = v_T.$$

Combining yields

$$A_1 t_1 = -A_3 t_3.$$

Substituting yields

$$A_1 (0.0222) = -A_3 (0.0333)$$

or

$$A_1 = -1 \frac{1}{2} A_3.$$

Also, the displacement of part 2 is

$$y_2 = v_T t_2.$$

We are given that the total displacement

$$y_1 + y_2 + y_3 = 4.$$

Substituting gives

$$\frac{1}{2} A_1 t_1^2 + v_r t_2 + V_Q t_3 + \frac{1}{2} A_3 t_3^2 = 4.$$

Again substituting,

$$\frac{1}{2} A_1 t_1^2 + A_1 t_1 t_2 + A_1 t_1 t_3 - \frac{1}{3} A_1 t_3^2 = 4$$

$$\frac{1}{2} A_1 (0.0222)^2 + A_1 (0.0222)(0.0167) + A_1 (0.0222)(0.0333) - \frac{1}{3} A_1 (0.0333)^2 = 4.$$

Thus

$$A_1 = 4050 \text{ in/sec}^2$$

$$A_3 = -2700 \text{ in/sec}^2$$

The velocity at the points of intersection from Fig. 3.3 is

$$v_r = v_Q = A_1 t_1 = (4050)(0.0222) = 90 \text{ ips.}$$

The displacements for each part are

$$y_1 \frac{1}{2} A_1 t_1^2 = \frac{1}{2} (4050)(0.0222)^2 = 1 \text{ in}$$

$$y_2 A_1 t_1 t_2 = (4050)(0.0222)(0.0167) = 1.5 \text{ in}$$

$$y_3 = 1.5 \text{ in}$$

We can now plot the curves of displacement, velocity, and acceleration as shown in Fig. 3.3.

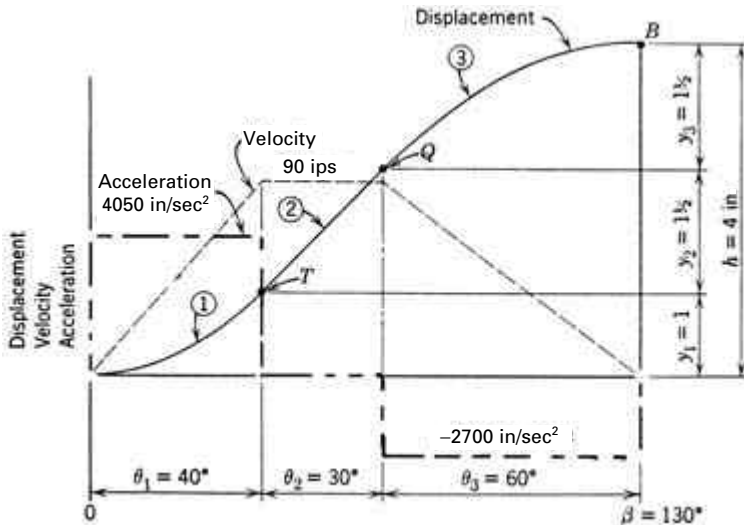


FIGURE 3.3. Example modified constant velocity curve.

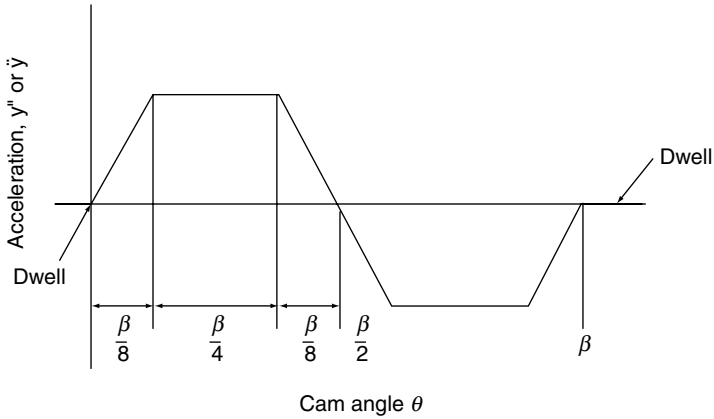


FIGURE 3.4. Trapezoidal acceleration curve—DRD cam.

### 3.4 TRAPEZOIDAL CURVE

The trapezoidal acceleration curve is a combination of the cubic and parabolic curves. It modifies the parabolic curve by changing its acceleration from a rectangular to a trapezoidal shape. It is an early composite that was first recognized by Neklutin (1969). He showed that the trapezoidal acceleration curve is an improvement over the parabolic curve and that it offers good dynamic response under high-speed operation. It is a slight improvement over the cycloidal curve with its lower maximum acceleration.

In trapezoidal curve motion, the fraction of the total rise angle used for the initial cubic segment is known as the  $b$  value for the motion. In Fig. 3.4 we see a trapezoidal acceleration curve (DRD cam) where  $b = 1/8$ . This choice of  $b = 1/8$  yields satisfactory cam-follower performance.

### 3.5 MODIFIED TRAPEZOIDAL CURVE

A combination cam curve (Chen, 1982) that has been used in lieu of the trapezoidal acceleration curve is the modified trapezoidal curve. It is composed of a parabolic motion combined with the cycloidal curve. This combination reduces the maximum acceleration at the expense of somewhat higher jerk values.

The modified trapezoidal curve is popular in industry. However, it has one objectionable characteristic: the torque (discussed in later chapters) goes from positive maximum to negative maximum in 20 percent of the travel time. If dynamic forces represent a significant part of the load on the cam, this sudden release of energy may be detrimental to the cam-follower system performance and limit the operating speeds. Much better torque characteristics can be obtained with the modified sine curve (see Sec. 3.7).

Figure 3.5a shows the basic cycloidal curve from which the modified trapezoidal curve is developed. The displacement and acceleration diagrams of the modified trapezoidal are also shown. The variables pertaining to the cycloidal curve are denoted by the primed symbols. At the start of the rise from  $A$  to  $B$  (Fig. 3.5b) the follower acceleration is a quarter sine wave; from  $B$  to  $C$  the acceleration is constant; and from  $C$  to  $D$  the acceleration decreases to zero with a quarter sine wave. After  $D$ , the follower has negative acceleration in the same way that it was positively accelerated.

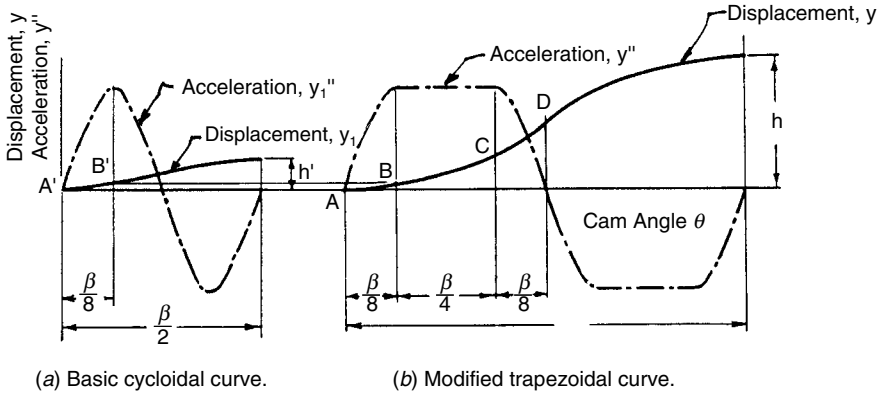


FIGURE 3.5. Modified trapezoidal acceleration curve.

Similar to the trapezoidal acceleration curve, we use  $b = \frac{1}{8}$  in the derivation. The equations of the curve from A to B are

$$\begin{aligned}
 \text{Displacement } y &= h' \left( \frac{2\theta}{\beta} - \frac{1}{2\pi} \sin 4\pi \frac{\theta}{\beta} \right), \\
 \text{Velocity } y' &= \frac{h'}{\beta} \left( 2 - 2 \cos 4\pi \frac{\theta}{\beta} \right), \\
 \text{Acceleration } y'' &= \frac{8\pi h'}{\beta^2} \sin 4\pi \frac{\theta}{\beta},
 \end{aligned} \tag{3.2}$$

where  $h'$  = maximum rise for cycloidal segment

When point B is reached,  $\theta = \frac{\beta}{8}$ . Substituting this value of  $\theta$  into Eq. (3.2) provides the characteristic equations at point B.

$$\begin{aligned}
 y_1 &= h' \left( \frac{1}{4} - \frac{1}{2\pi} \right) \\
 y'_1 &= \frac{2h'}{\beta} \\
 y''_1 &= \frac{8\pi h'}{\beta^2}.
 \end{aligned}$$

The general expression for displacement under constant acceleration has a displacement

$$y = v_0\theta + \frac{1}{2} a\theta^2 \tag{2.24}$$

where  $v_0$  = follower initial velocity, dimensionless  
 $a$  = follower acceleration, dimensionless  
 $\theta$  = cam angle rotation, radians

Therefore, the general equations of the curve from  $B$  to  $C$  are

$$y = y_1 + v_0 \left( \theta - \frac{\beta}{8} \right) + \frac{1}{2} a \left( \theta - \frac{\beta}{8} \right)^2$$

$$y' = v_0 + a \left( \theta - \frac{\beta}{8} \right)$$

$$y'' = a.$$

To get displacement, velocity, and acceleration to match at the junction  $B$ , it is necessary that

$$v_0 = \frac{2h'}{\beta}$$

$$a = \frac{8\pi h'}{\beta^2}$$

Therefore, the equations from  $B$  to  $C$  are

$$y = h' \left( \frac{1}{4} - \frac{1}{2\pi} \right) + \frac{2h'}{\beta} \left( \theta - \frac{\beta}{8} \right) + \frac{4\pi h'}{\beta^2} \left( \theta - \frac{\beta}{8} \right)^2 \tag{3.3}$$

$$y' = \frac{2h'}{\beta} + \frac{8\pi h'}{\beta^2} \left( \theta - \frac{\beta}{8} \right)$$

$$y'' = \frac{8\pi h'}{\beta^2}.$$

When point  $C$  is reached,  $\theta = \frac{3}{8}\beta$ . Substituting in Eq. (3.3), we obtain

$$y = \frac{3}{4}h' - \frac{h'}{2\pi} + \frac{\pi h'}{4}$$

$$\therefore y_2 = y - y_1 = \frac{h'}{2} - \frac{\pi h'}{4}$$

The cycloidal displacement is the sum of a constant velocity displacement and a quarter sine wave displacement. The displacement equation of the curve from  $C$  to  $D$  is

$$y = y_1 + y_2 + C_1 + C_2 \frac{\theta - \frac{3}{8}\beta}{\beta} + C_3 \sin \left( 4\pi \frac{\theta - \frac{\beta}{2}}{\beta} \right).$$

Hence,

$$y' = \frac{C_2}{\beta} + C_3 \frac{4\pi}{\beta} \cos 4\pi \frac{\theta - \frac{\beta}{2}}{\beta}$$

$$y'' = -C_3 \frac{16\pi^2}{\beta^2} \sin 4\pi \frac{\theta - \frac{\beta}{2}}{\beta} \tag{3.4}$$

where  $C_1$ ,  $C_2$ , and  $C_3$  are undetermined coefficients that can be obtained as follows:

An acceleration match at point  $C$  (when  $\theta = \frac{3}{8}\beta$ ) requires

$$\frac{8\pi h'}{\beta^2} = \left[ -C_3 \frac{16\pi^2}{\beta^2} \sin 4\pi \frac{\theta - \frac{\beta}{2}}{\beta} \right]_{\text{at } \theta = \frac{3}{8}\beta}$$

thus giving

$$C_3 = \frac{h'}{2\pi}.$$

A velocity match at point  $C$  requires

$$\left[ \frac{2h'}{\beta} + \frac{8\pi h'}{\beta^2} \left( \theta - \frac{\beta}{8} \right) \right]_{\theta = \frac{3}{8}\beta} = \left[ \frac{C_2}{\beta} + \frac{h'}{2\pi} \frac{4\pi}{\beta} \cos 4\pi \frac{\theta - \frac{\beta}{2}}{\beta} \right]_{\theta = \frac{3}{8}\beta}$$

from which we obtain

$$C_2 = 2h'(1 + \pi).$$

The total displacement at point  $C$  is

$$y = y_1 + y_2$$

or equivalently

$$\left[ C_1 = -2h'(1 + \pi) \frac{\theta - \frac{3}{8}\beta}{\beta} - \frac{h'}{2\pi} \sin 4\pi \frac{\theta - \frac{\beta}{2}}{\beta} \right]_{\theta = \frac{3}{8}\beta} = 0,$$

from which  $C_1$  can be obtained

$$C_1 = \frac{h'}{2\pi}.$$

Substituting the values of  $C_1$ ,  $C_2$ , and  $C_3$  in the displacement equation gives the curve from  $C$  to  $D$

$$y = \left( \frac{h'}{4} - \frac{h'}{2\pi} \right) + \left( \frac{h'}{2} + \frac{\pi h'}{4} \right) + \frac{h'}{2\pi} + 2h'(1 + \pi) \frac{\theta - \frac{3}{8}\beta}{\beta} - \frac{h'}{2\pi} \sin 4\pi \frac{\theta - \frac{\beta}{2}}{\beta}$$

or

$$y = h' \left[ -\frac{\pi}{2} + 2(1 + \pi) \frac{\theta}{\beta} - \frac{1}{2\pi} \sin 4\pi \frac{\theta - \frac{\beta}{2}}{\beta} \right]. \quad (3.5)$$

At point  $D$  (i.e., when  $\theta = \frac{\beta}{2}$ ) the total displacement can be found from this equation to be

$$y = h' \left( 1 + \frac{\pi}{2} \right).$$

The displacement of the final segment is

$$y_3 = y - y_1 - y_2$$

or

$$y_3 = h' \left( \frac{1}{4} + \frac{\pi}{4} + \frac{1}{2\pi} \right).$$

From the relationship

$$y_1 + y_2 + y_3 = \frac{h}{2},$$

we establish the relationship between  $h'$  and  $h$

$$h' = \frac{h}{2 + \pi}. \tag{3.6}$$

Therefore, the displacement equations of the first three segments are

$$\begin{aligned} y &= \frac{h}{2 + \pi} \left( \frac{2\theta}{\beta} - \frac{1}{2\pi} \sin 4\pi \frac{\theta}{\beta} \right) & 0 \leq \theta \leq \frac{\beta}{8} \\ y &= \frac{h}{2 + \pi} \left[ \frac{1}{4} - \frac{1}{2\pi} + \frac{2}{\beta} \left( \theta - \frac{\beta}{8} \right) + \frac{4\pi}{\beta^2} \left( \theta - \frac{\beta}{8} \right)^2 \right] & \frac{\beta}{8} \leq \theta \leq \frac{3}{8}\beta \\ y &= \frac{h}{2 + \pi} \left[ -\frac{\pi}{2} + 2(1 + \pi) \frac{\theta}{\beta} + \frac{1}{2\pi} \sin 4\pi \frac{\theta - \frac{\beta}{2}}{\beta} \right] & \frac{3}{8}\beta \leq \theta \leq \frac{\beta}{2}. \end{aligned} \tag{3.7}$$

Evaluating all constants, characteristic curve equations are:

for  $\theta \leq \frac{\theta}{\beta} \leq \frac{1}{8}$ , (3.8)

$$\begin{aligned} y &= 0.09724613h \left( 4 \frac{\theta}{\beta} - \frac{1}{\pi} \sin 4\pi \frac{\theta}{\beta} \right) \\ y' &= 0.3889845 \frac{h}{\beta} \left( 1 - \cos 4\pi \frac{\theta}{\beta} \right) \\ y'' &= 4.888124 \frac{h}{\beta^2} \sin 4\pi \frac{\theta}{\beta} \\ y''' &= 61.425975 \frac{h}{\beta^3} \cos 4\pi \frac{\theta}{\beta} \end{aligned}$$

$$\text{for } \frac{1}{8} \leq \frac{\theta}{\beta} \leq \frac{3}{8},$$

$$y = h \left( 2.444016188 \frac{\theta^2}{\beta} - 0.22203094 \frac{\theta}{\beta} + 0.00723406 \right)$$

$$y' = \frac{h}{\beta} \left( 4.888124 \frac{\theta}{\beta} - 0.222031 \right)$$

$$y'' = \frac{h}{\beta^2} (4.88124)$$

$$y''' = 0$$

$$\text{for } \frac{3}{8} \leq \frac{\theta}{\beta} \leq \frac{1}{2},$$

$$y = h \left( 1.6110155 \frac{\theta}{\beta} - 0.0309544 \sin \left( 4\pi \frac{\theta}{\beta} \right) - 0.3055077 \right)$$

$$y' = \frac{h}{\beta} \left( 1.6110155 - 0.3889845 \cos \left( 4\pi \frac{\theta}{\beta} \right) \right)$$

$$y'' = \frac{h}{\beta^2} \left( 4.88124 \sin \left( 4\pi \frac{\theta}{\beta} \right) \right)$$

$$y''' = -61.425975 \frac{h}{\beta^3} \cos \left( 4\pi \frac{\theta}{\beta} \right)$$

$$\text{for } \frac{1}{2} \leq \frac{\theta}{\beta} \leq \frac{5}{8},$$

$$y = h \left( 1.6110155 \frac{\theta}{\beta} + 0.0309544 \sin \left( 4\pi \frac{\theta}{\beta} \right) - 0.3055077 \right)$$

$$y' = \frac{h}{\beta} \left( 1.6110154 + 0.3889845 \cos \left( 4\pi \frac{\theta}{\beta} \right) \right)$$

$$y'' = \frac{h}{\beta^2} \left( -4.88124 \sin \left( 4\pi \frac{\theta}{\beta} \right) \right)$$

$$y''' = -61.425975 \frac{h}{\beta^3} \left( 4\pi \frac{\theta}{\beta} \right)$$

$$\text{for } \frac{5}{8} \leq \frac{\theta}{\beta} \leq \frac{7}{8},$$

$$y = h \left( 4.6660917 \frac{\theta}{\beta} - 2.44406188 \left( \frac{\theta}{\beta} \right)^2 - 1.2292650 \right)$$

$$y' = \frac{h}{\beta} \left( 4.6660928 - 4.888124 \frac{\theta}{\beta} \right)$$

$$y'' = \frac{h}{\beta^2} (-4.888124)$$

$$y''' = 0$$

for  $\frac{7}{8} \leq \frac{\theta}{\beta} \leq 1$ ,

$$\begin{aligned}
 y &= h \left( 0.6110155 + 0.3889845 \frac{\theta}{\beta} - 0.0309544 \sin \left( 4\pi \frac{\theta}{\beta} \right) \right) \\
 y' &= \frac{h}{\beta} \left( 0.3889845 - 0.3889845 \cos \left( 4\pi \frac{\theta}{\beta} \right) \right) \\
 y'' &= \frac{h}{\beta^2} \left( -4.888124 \sin \left( 4\pi \frac{\theta}{\beta} \right) \right) \\
 y''' &= 61.425975 \frac{h}{\beta^3} \cos \left( 4\pi \frac{\theta}{\beta} \right).
 \end{aligned}$$

A computer solution is employed to establish the incremental displacement value and the characteristic curves of the action.

The modified trapezoidal curve has the following peak values

$$\begin{aligned}
 y' &= 2 \frac{h}{\beta} \\
 y'' &= 4.888 \frac{h}{\beta^2} \\
 y''' &= 61.43 \frac{h}{\beta^3}.
 \end{aligned} \tag{3.9}$$

The nondimensional factors of the displacement, the velocity, and the acceleration of this curve are given in App. B.

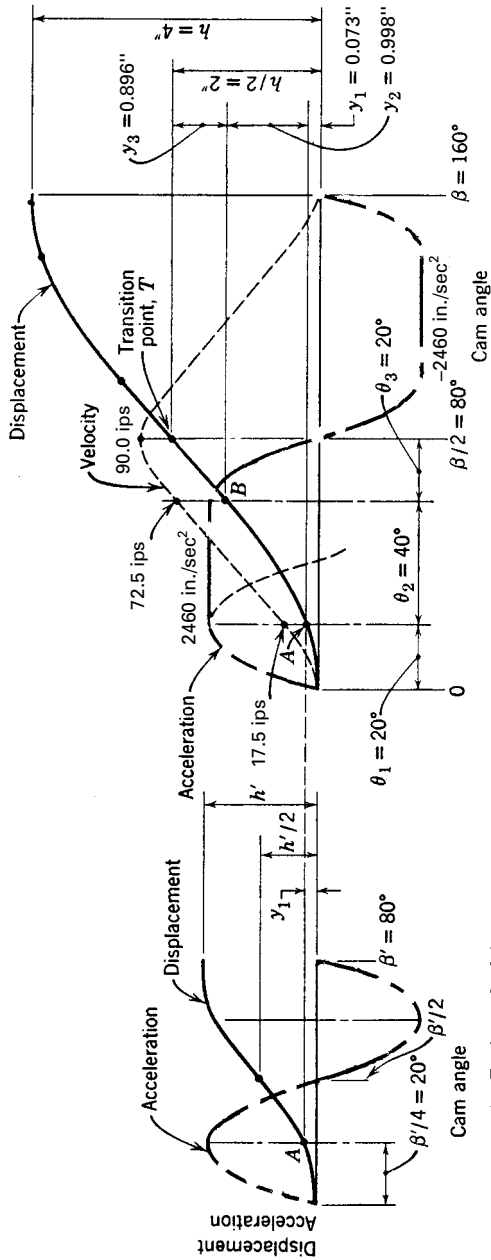
**EXAMPLE** A cam rotates at 300 rpm. A symmetrical modified trapezoidal acceleration curve (parabolic motion combined with the cycloidal curve) is to be drawn with the ratio  $b = 1/8$ . The total rise is 4 inches in 160 degrees of cam rotation. Find pertinent values of all the characteristics and plot the curves without the use of Eqs. (3.7) through (3.9).

**Solution** In Fig. 3.6 we see the basic cycloidal curve from which the combination curve is developed. This figure also shows the modified trapezoidal acceleration curve. The variables pertaining to the cycloidal sector will be denoted by the primed symbols (Fig. 3.6a). In Fig. 3.6b, let us divide one-half of the rise into its three component parts. Since  $b = 1/8$  and the angle  $\beta/2$  is 80 degrees, we see that the cam angle for parts 1 and 3 is  $\theta_1 = \theta_3 = 20$  degrees  $= \beta'/4$ . This gives  $\theta_2 = 40$  degrees. The angular velocity of the cam is

$$\omega = 300/60 \times 2\pi = 31.4 \text{ rad/sec}$$

The characteristics of the cycloidal curve from Eqs. (2.58), (2.59), and (2.60) are

$$\begin{aligned}
 \text{Displacement} \quad y &= h \left( \frac{\theta}{\beta} - \frac{1}{2\pi} \sin \frac{2\pi\theta}{\beta} \right) \text{in} \\
 \text{Velocity} \quad \dot{y} &= \omega y' = \frac{\omega h}{\beta} \left( 1 - \cos \frac{2\pi\theta}{\beta} \right) \text{ips} \\
 \text{Acceleration} \quad \ddot{y} &= \omega^2 y'' = \left( \frac{\omega^2 2h\pi}{\beta^2} \sin \frac{2\pi\theta}{\beta} \right) \text{in/sec}^2
 \end{aligned}$$



(a) Basic cycloidal curve.

(b) Modified trapezoidal curve.

FIGURE 3.6. Example modified trapezoidal acceleration curve.

At point A substituting

$$y_A = y_1 = \frac{h'}{4} - \frac{h'}{2\pi} = 0.091 h'$$

$$\dot{y}_A = \frac{h'\omega}{\beta'} = \frac{h'(31.4)}{\frac{80}{180}\pi} = 22.5 h'$$

$$\ddot{y}_A = A_2 = \frac{2\pi h'\omega^2}{(\beta')^2}$$

$$= \frac{2\pi h'(31.4)^2}{\left(\frac{80}{180}\pi\right)^2} = 3170 h'$$

The displacement of part 2, the parabolic curve, in Sec. 2.6

$$y_2 = v_A \frac{\theta_2}{\omega} + \frac{1}{2} A_2 \left(\frac{\theta_2}{\omega}\right)^2$$

Substituting, we obtain

$$y_2 = \frac{h'\omega}{\beta'} \frac{\theta_2}{\omega} + \frac{1}{2} \frac{2\pi h'\omega^2}{(\beta')^2} \left(\frac{\theta_2}{\omega}\right)^2$$

$$= \frac{h'\theta_2}{\beta'} + \frac{h'\pi\theta_2^2}{(\beta')^2}$$

$$= \frac{h'}{2} + h'\pi\left(\frac{1}{4}\right) = 1.285 h'$$

Also, the velocity at point B

$$\dot{y}_B = v_A + A_2 \frac{\theta_2}{\omega}$$

$$= 22.5 h' + 3170 h' \left(\frac{40\pi/180}{31.4}\right) = 93.3 h'$$

The displacement of part 3

$$\dot{y}_3 = v_3 \frac{\theta_3}{\omega} + \frac{h'}{2\pi} = 93.3 h' \left(\frac{20\pi/180}{31.4}\right) + \frac{h'}{2\pi} = 1.199 h'$$

we know that

$$y_1 + y_2 + y_3 = 2$$

Substituting,

$$0.091 h' + 1.285 h' + 1.199 h' = 2$$

$$h' = 0.7767 \text{ in}$$

Let us now find the displacements:

$$y_1 = 0.091(0.7767) = 0.071 \text{ in}$$

$$y_2 = 1.285(0.7767) = 0.998 \text{ in}$$

$$y_3 = 1.191(0.7767) = 0.896 \text{ in}$$

Substituting to find the velocity

$$\begin{aligned} v_A &= 22.5(0.7767) = 17.5 \text{ ips} \\ v_B &= 93.3(0.7767) = 72.5 \text{ ips} \\ v_T &= \text{maximum velocity} \\ &= v_B + \Delta v_{B \text{ to } T} \\ &= 72.5 + 17.5 = 900 \text{ ips} \end{aligned}$$

Also, the maximum acceleration

$$A_A = 3170(0.7767) = 2460 \text{ in/sec}^2$$

The curves may now be plotted in Fig. 3.6*b*. If they were to be compared with a trapezoidal acceleration curve, we would find that this curve has a slightly lower maximum acceleration and the advantage of lower required cutting accuracy in the initial and final rise portions. Also, the vibrations induced at high speeds should be slightly smaller than those of the trapezoidal curve.

### 3.6 SKEWED MODIFIED TRAPEZOIDAL CURVE

---

Occasionally, the follower requires a particular velocity and acceleration at some critical points in the machine motion. This can be accomplished by skewing the acceleration profile as seen in Fig. 3.7. Neklutin (1969) has treated the modified trapezoidal curve with unequal periods of acceleration, positive and negative. Ragsdell and Gilkey (1969) have related the skewed acceleration to a correspondingly symmetrical one. Before skewing is considered, the follower rise  $h$  and angle  $\beta$  have been determined and will be considered as constants.

Let  $\beta_1$  and  $\beta_2$  be the periods during positive and negative acceleration, respectively, and let  $p = \frac{\beta_1}{\beta_2}$  be the skew ratio (Fig. 3.7). Thus

$$\begin{aligned} \beta_1 + \beta_2 &= \beta \\ h_1 + h_2 &= h. \end{aligned}$$

The velocity match at the transition point that

$$(y'_{\max})_1 = (y'_{\max})_2$$

Substituting and equating from Eq. (3.9)

$$\begin{aligned} \frac{2h_1}{\beta_1} &= \frac{2h_2}{\beta_2} \\ \therefore \beta_1 &= \frac{p}{1+p} \beta \\ h_1 &= \frac{p}{1+p} h \end{aligned} \tag{3.10}$$

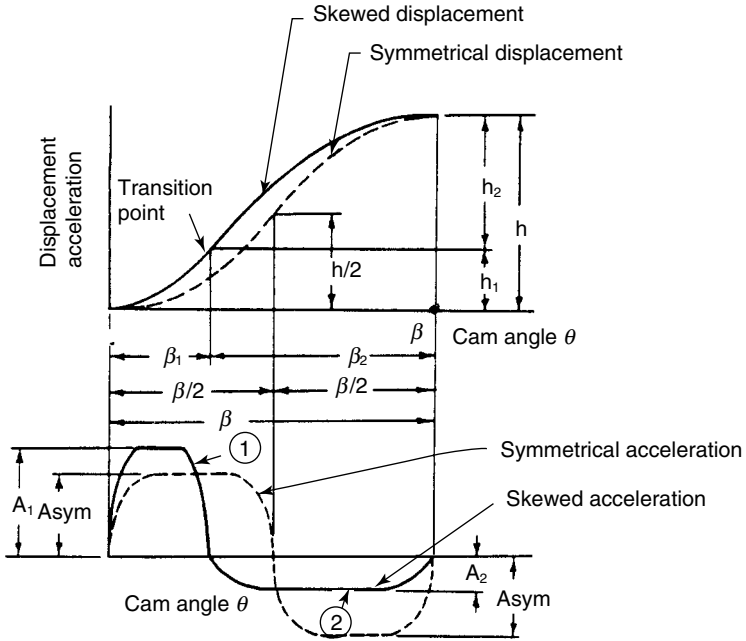


FIGURE 3.7. Skewed modified trapezoidal curve.

and

$$\beta_2 = \frac{p}{1+p} \beta \tag{3.11}$$

$$h_2 = \frac{p}{1+p} h.$$

The relationship between the skewed and corresponding symmetrical acceleration, since the maximum velocity is the same in both skewed and symmetric cases, is:

$$2\beta_1 a_1 = a_{sym} \beta = V_{max}$$

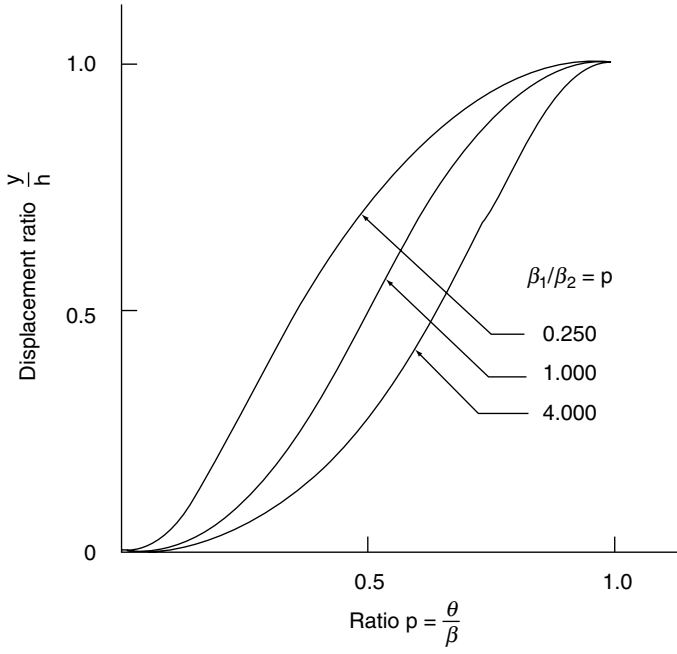
$$\therefore a_1 = a_{sym} \frac{\beta}{2\beta_1}$$

Thus using Eq. (3.10)

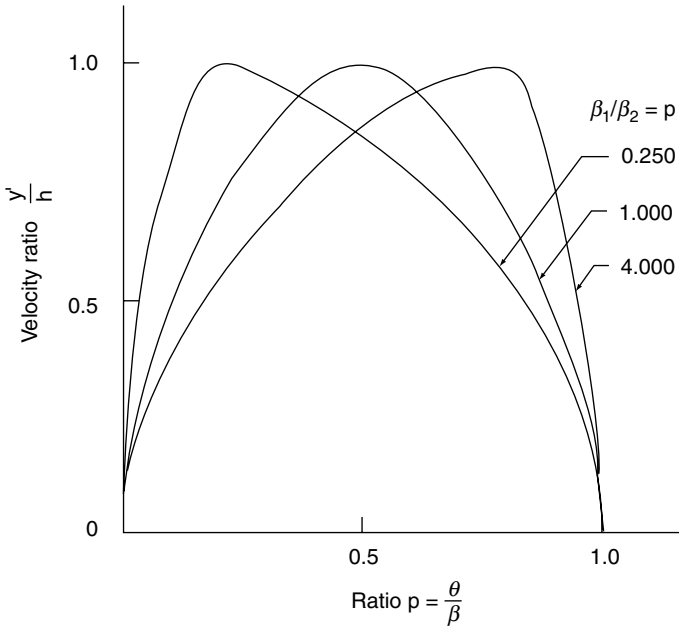
$$a_1 = \left( \frac{1+p}{2p} \right) a_{sym}. \tag{3.12}$$

Similarly

$$a_2 = \left( \frac{1+p}{2} \right) a_{sym}. \tag{3.13}$$



(a) Displacement.



(b) Velocity.

**FIGURE 3.8.** Skewed modified trapezoidal curve comparison (normalized  $h = 1, \beta = 1$ ).

Figure 3.8a shows the normalized displacement plot and Fig. 3.8b shows the normalized velocity plot where  $h = 1, \beta = 1$ .

### 3.7 MODIFIED SINE CURVE

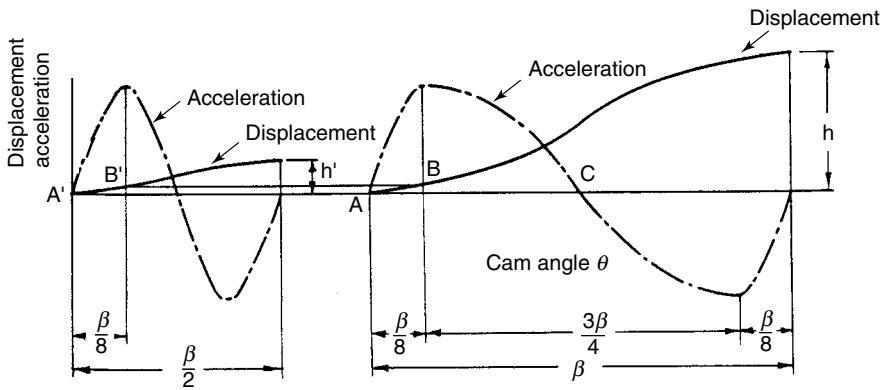
The modified sine curve (Chen, 1982; Schmidt, 1960) is a combination of quarter sine wave curves. In terms of its torsional action, the change from positive to negative torque occurs in over 40 percent of the travel time. This attribute makes this curve attractive as a choice in moving large masses such as indexing intermittent turrets. Its lower torque and power demand make the modified sine curve one of the best choices of curves.

Figure 3.9a shows the basic cycloidal curve from which the combination curve is developed, and Fig. 3.9b shows the displacement and the acceleration diagram of the modified sine curve. The primed symbols used in the drawing refer to the basic cycloidal curve. One-half of the rise is divided into the following segments; the follower is accelerated from A to B: (from  $\theta = 0$  to  $\theta = \frac{\beta}{8}$ ) with a quarter sine wave, and the acceleration decreased to zero from B to C (from  $\theta = \frac{\beta}{8}$  to  $\theta = \frac{\beta}{2}$ ), again with a quarter sine wave. The equations of cycloidal motion from A to B, given that  $\beta/8$  is the length of the initial quarter sine wave, are:

$$y = h' \left( \frac{2\theta}{\beta} - \frac{1}{2\pi} \sin 4\pi \frac{\theta}{\beta} \right)$$

$$y' = \frac{h'}{\beta} \left( 2 - 2 \cos 4\pi \frac{\theta}{\beta} \right)$$

$$y'' = \frac{8\pi h'}{\beta^2} \sin 4\pi \frac{\theta}{\beta}$$



(a) Cycloidal curve.

(b) Modified sine curve.

FIGURE 3.9. Modified sine curve.

At the end of the first segment  $\theta = \frac{\beta}{8}$ , and equations at point  $B$  are

$$\begin{aligned}y_1 &= h' \left( \frac{1}{4} - \frac{1}{2\pi} \right) \\y'_1 &= \frac{2h'}{\beta} \\y''_1 &= \frac{8\pi h'}{\beta^2}.\end{aligned}\tag{3.14}$$

The sine curve from  $B$  to  $C$  characteristics are:

$$\begin{aligned}y &= y_1 + C_1 + C_2 \frac{\theta - \frac{\beta}{8}}{\beta} + C_3 \sin \left( \frac{4\pi\theta}{3\beta} + \frac{\pi}{3} \right) \\y' &= \frac{C_2}{\beta} + C_3 \frac{4\pi}{3\beta} \cos \left( \frac{4\pi\theta}{3\beta} + \frac{\pi}{3} \right) \\y'' &= -C_3 \frac{16\pi^2}{9\beta^2} \sin \left( \frac{4\pi}{3} \frac{\theta}{\beta} + \frac{\pi}{3} \right)\end{aligned}\tag{3.15}$$

The acceleration boundary conditions give:

$$\begin{aligned}\frac{8\pi h'}{\beta^2} &= \left[ -C_3 \frac{16\pi^2}{9\beta^2} \sin \left( \frac{4\pi}{3} \frac{\theta}{\beta} + \frac{\pi}{3} \right) \right]_{\theta=\frac{\beta}{8}} \\C_3 &= -\frac{9h'}{2\pi}\end{aligned}$$

The velocity boundary conditions give:

$$\begin{aligned}\frac{2h'}{\beta} &= \left[ \frac{C_2}{\beta} - \frac{9h'}{2\pi} \left( \frac{4\pi}{3\beta} \right) \cos \left( \frac{4\pi}{3} \frac{\theta}{\beta} + \frac{\pi}{3} \right) \right]_{\theta=\frac{\beta}{8}} \\C_2 &= 2h'\end{aligned}$$

The displacement boundary conditions give:

$$\begin{aligned}\left[ C_1 + 2h' \frac{\theta - \frac{\beta}{8}}{\beta} - \frac{9h'}{2\pi} \sin \left( \frac{4\pi}{3} \frac{\theta}{\beta} + \frac{\pi}{3} \right) \right]_{\theta=\frac{\beta}{8}} &= 0 \\C_1 &= \frac{9h'}{2\pi}\end{aligned}$$

Then

$$\begin{aligned}
 y &= \left( \frac{h'}{4} - \frac{h'}{2\pi} \right) + \frac{9h'}{2\pi} + 2h' \left( \frac{\theta - \frac{\beta}{8}}{\beta} \right) - \frac{9h'}{2\pi} \sin \left( \frac{4\pi}{3} \frac{\theta}{\beta} + \frac{\pi}{3} \right) \\
 &= h' \left[ \frac{4}{\pi} + 2 \frac{\theta}{\beta} - \frac{9}{2\pi} \sin \left( \frac{4\pi}{3} \frac{\theta}{\beta} + \frac{\pi}{3} \right) \right].
 \end{aligned}
 \tag{3.16}$$

When  $\theta = \frac{\beta}{2}$ , the rise is

$$y = h' \left( 1 + \frac{4}{\pi} \right)$$

Hence,

$$y_2 = y - y_1 = \left( \frac{3}{4} + \frac{9}{2\pi} \right) h'.$$

Finally, from the relationship

$$y = y_1 + y_2 = \frac{h}{2}$$

we obtain  $h' = \frac{\pi}{2(\pi + 4)} h$ .

Therefore, the displacement equations of the modified sine curve are

$$\begin{aligned}
 y &= h \left[ \frac{\pi}{4 + \pi} \frac{\theta}{\beta} - \frac{1}{4(4 + \pi)} \sin \left( 4\pi \frac{\theta}{\beta} \right) \right] & 0 \leq \theta \leq \frac{\beta}{8} \\
 y &= h \left[ \frac{2}{4 + \pi} + \frac{\pi}{4 + \pi} \frac{\theta}{\beta} - \frac{9}{4(4 + \pi)} \sin \left( \frac{4\pi}{3} \frac{\theta}{\beta} + \frac{\pi}{3} \right) \right] & \frac{\beta}{8} \leq \theta \leq \frac{7}{8} \beta \\
 y &= h \left[ \frac{4}{4 + \pi} + \frac{\pi}{4 + \pi} \frac{\theta}{\beta} - \frac{1}{4(4 + \pi)} \sin \left( 4\pi \frac{\theta}{\beta} \right) \right] & \frac{7}{8} \beta \leq \theta \leq \beta.
 \end{aligned}
 \tag{3.17}$$

Evaluating all constants the characteristics equations for the modified sine curve are:

for  $0 \leq \frac{\theta}{\beta} \leq \frac{1}{8}$

$$\begin{aligned}
 y &= h \left( 0.43990 \frac{\theta}{\beta} - 0.35014 \sin 4\pi \frac{\theta}{\beta} \right) \\
 y' &= 0.43990 \frac{h}{\beta} \left( 1 - \cos 4\pi \frac{\theta}{\beta} \right) \\
 y'' &= 5.52796 \frac{h}{\beta^2} \sin 4\pi \frac{\theta}{\beta} \\
 y''' &= 69.4664 \frac{h}{\beta^3} \cos 4\pi \frac{\theta}{\beta}.
 \end{aligned}$$

for  $\frac{1}{8} \leq \frac{\theta}{\beta} \leq \frac{7}{8}$

$$\begin{aligned}
 y &= h \left[ 0.28005 + 0.43990 \frac{\theta}{\beta} - 0.351506 \cos \left( \frac{4\pi}{3} \frac{\theta}{\beta} - \frac{\pi}{3} \right) \right] \\
 y' &= \frac{h}{\beta} \left[ 0.43990 + 1.31970 \sin \left( \frac{4\pi}{3} \frac{\theta}{\beta} + \frac{\pi}{3} \right) \right] \\
 y'' &= 5.52796 \frac{h}{\beta^2} \sin \left( \frac{4\pi}{3} \frac{\theta}{\beta} + \frac{\pi}{3} \right) \\
 y''' &= 23.1555 \frac{h}{\beta^3} \cos \left( \frac{4\pi}{3} \frac{\theta}{\beta} + \frac{\pi}{3} \right).
 \end{aligned}$$

for  $\frac{7}{8} \leq \frac{\theta}{\beta} \leq 1$

$$\begin{aligned}
 y &= h \left[ 0.56010 + 0.43990 \frac{\theta}{\beta} - 0.03515006 \sin 4\pi \frac{\theta}{\beta} \right] \\
 y' &= \frac{h}{\beta} \left[ 0.43989 \left( 1 - \cos 4\pi \frac{\theta}{\beta} \right) \right] \\
 y'' &= 5.52796 \frac{h}{\beta^2} \sin 4\pi \frac{\theta}{\beta} \\
 y''' &= 69.4664 \frac{h}{\beta^3} \cos 4\pi \frac{\theta}{\beta}.
 \end{aligned} \tag{3.18}$$

A computer solution is employed to establish the incremental displacement values and the characteristic curves of the action. The maximum velocity of the modified sine curve is  $y'_{\max} = 1.760 \frac{h}{\beta}$ , the maximum acceleration is  $y''_{\max} = 5.528 \frac{h}{\beta^2}$ , and the maximum jerk is  $y'''_{\max} = 69.47 \frac{h}{\beta^3}$ . The nondimensionalized displacement, velocity, and acceleration factors are given in Table A-4, App. B. Figure 3.10 indicates the comparison (Erdman and Sandor, 1997) of the cycloidal, modified trapezoidal, and modified sine curves. The data shown is for a 3-inch pitch diameter cam having a 2-inch rise in 6 degrees of cam rotation.

### 3.8 MODIFIED CYCLOIDAL CURVE

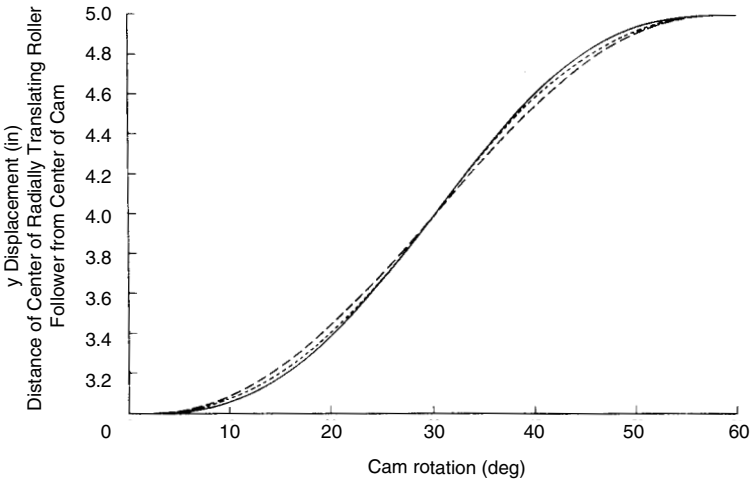
In this section we will reshape the cycloidal curve to improve its acceleration characteristics. This curve is the modified cycloidal curve that was developed by Wildt (1953). Figure 3.11 indicates the acceleration comparison between the true cycloidal curve and the Wildt cycloidal curve. The basic cycloidal curve equation for the displacement

$$y = h \left( \frac{\theta}{\beta} - \frac{1}{2\pi} \sin \frac{2\pi\theta}{\beta} \right) \tag{2.58}$$

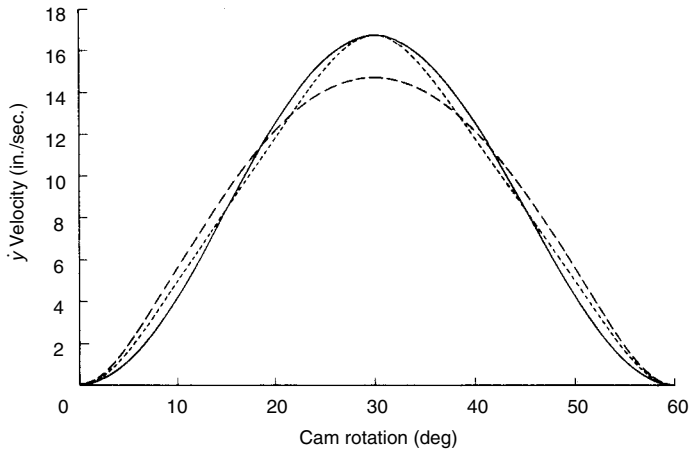
From this equation it is seen that the cycloidal curve is a combination of a sine curve and a constant velocity line. Figure 3.12a shows the pure cycloidal curve with point A

the beginning of motion, point *B* the end of motion, and point *P* the mid-stroke transition point. *APB* is the constant velocity line. *M* is the midpoint between *A* and *P*. The sine amplitudes are added to the constant-velocity line in this true cycloidal case.

The modified cycloidal curve was developed to maximize the orientation of the superimposed sine wave amplitude on the straight line; see geometric construction in Fig. 3.12*b*. In this figure, a point *D* equal to 0.57 the distance  $\frac{\beta}{2}$  is the first chosen and then is joined to *M* by a straight line. The base of the sine curve is then constructed

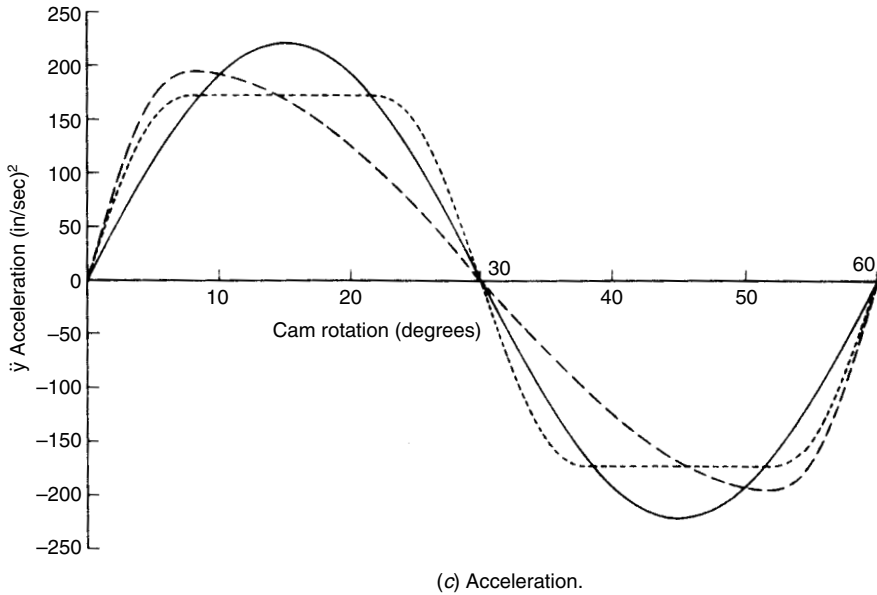


(a) Displacement.



(b) Velocity.

**FIGURE 3.10.** Comparison of popular curves (cam has 2-inch rise in 60-degree rotation and 3-inch pitch diameter). (Erdman and Sandor (1997) with permission by Prentice Hall, Upper Saddle River, N.J.)



— Cycloidal  
 - - Modified Sine  
 ···· Modified Trapezoidal

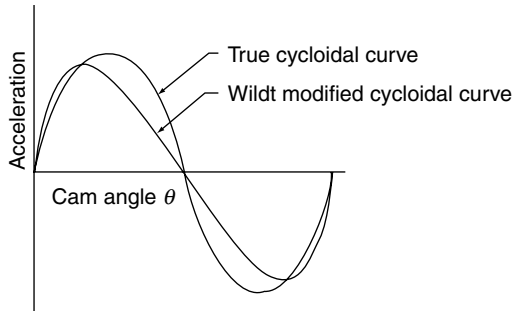
FIGURE 3.10. Continued

perpendicular to  $DM$ . This procedure results in the modified cycloidal curve having a maximum acceleration about 7 percent lower than that of the basic cycloidal curve.

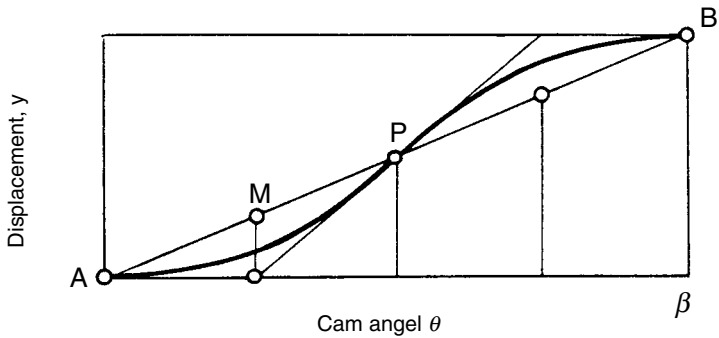
### 3.9 DWELL-RISE-RETURN-DWELL MOTION

Now, let us consider the dwell-rise-return-dwell curve, using a combination of curves to improve the high-speed action. To analyze the action, we shall use the symmetrical cycloidal curve (Fig. 3.13), although any of the high-speed shapes, such as trapezoidal and modified trapezoidal, introduce the same problem. A difficulty arises that did not prevail in the dwell-rise-dwell action, that is, an abrupt change or dip in the acceleration curve occurs at the maximum rise point. This dip is undesirable, because it produces sudden inertia loads and vibrations.

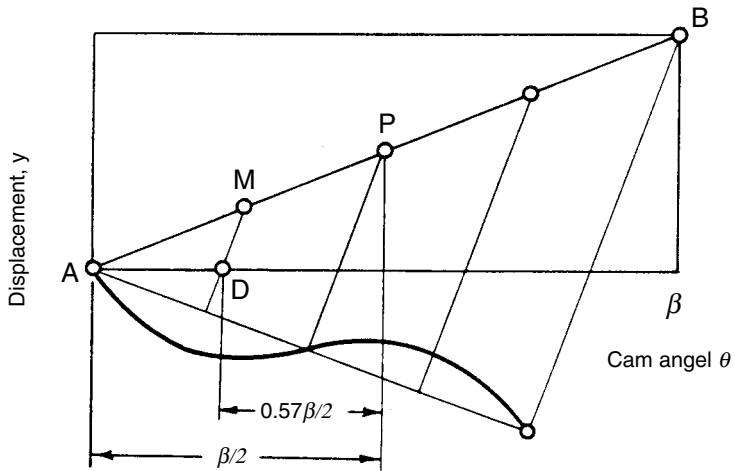
In Fig. 3.13, the problem is eliminated by blending a parabolic curve to the cycloidal curve portions. A modified total curve is produced. Also, a smoother, more desirable acceleration curve is developed with lower peak accelerations. An alternative solution, necessitating less mathematical work, is to employ polynomial equations as shown in Chap. 4.



**FIGURE 3.11.** Comparison of cycloidal acceleration curves.



(a) Pure cycloidal curve.



(b) Modified cycloidal curve.

**FIGURE 3.12.** Modified cycloidal curve construction.

**EXAMPLE** Derive the relationship for the dwell-rise-fall-dwell cam curve shown in Fig. 3.14 having equal maximum acceleration values. Portions I and III are harmonic; portions II and IV are horizontal straight lines.

**Solution** Let the  $\theta$ 's and  $\beta$ 's be the angles for each portion shown. Note that for velocity and acceleration one should multiply values by  $\omega$  and  $\omega^2$ , respectively, and the boundary conditions are  $y(0) = 0$ ,  $\dot{y}(0) = 0$ ,  $\dot{y}(\beta_4) = 0$ , and  $y(\beta_4) = \text{total rise } h$ . Use basic trigonometric relationships for

Portion I

$$\begin{aligned} \ddot{y} &= A \sin(\pi\theta/2\beta_1) \\ \dot{y} &= (2\beta_1 A/\pi)[1 - \cos(\pi\theta/2\beta_1)] \\ y &= -A(2\beta_1/\pi)^2 \sin(\pi\theta/2\beta_1) + (2A\beta_1/\pi)\theta \\ \dot{y}_1 &= 2A\beta_1/\pi \\ y_1 &= (2A\beta_1^2/\pi)(1 - 2/\pi) \end{aligned}$$

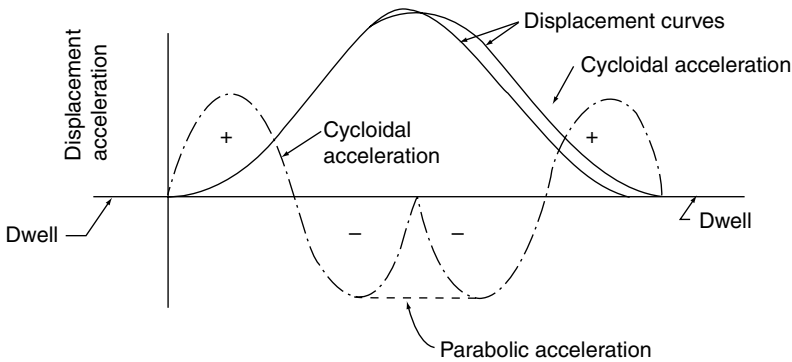


FIGURE 3.13. Dwell-rise-return-dwell curves, symmetrical rise-fall.

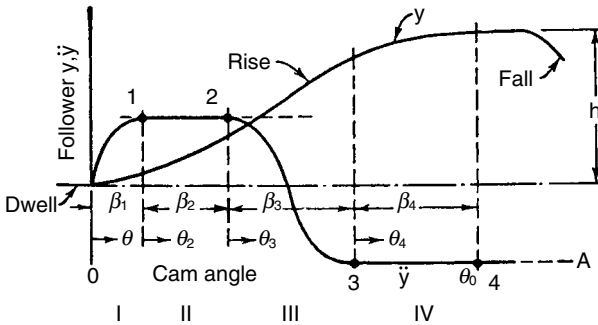


FIGURE 3.14. Example of asymmetrical dwell-rise-fall-dwell cam curve.

*Portion II*

$$\begin{aligned} \ddot{y} &= \dot{A} \\ \dot{y} &= A\theta_2 + \dot{y}_1 \\ y &= A(\theta_2)^2/2 + \dot{y}_1\theta' + y_1 \\ \dot{y}_2 &= A\beta_2 + 2A\beta_1/\pi \\ y_2 &= A\beta_2^2/2 + 2A\beta_1\beta_2/\pi + 2A\beta_1^2/\pi(1-2/\pi) \end{aligned}$$

*Portion III*

$$\begin{aligned} \ddot{y} &= A \cos(\pi\theta_3/\beta_3) \\ \dot{y} &= A\beta_3/\pi \sin(\pi\theta_3/\beta_3) + \dot{y}_2 \\ y &= -A(\beta_3/\pi)^2 [1 - \cos(\pi\theta''/\beta_3)] + \dot{y}_2\theta'' + y_2 \\ \dot{y}_3 &= \dot{y}_2 \\ y_3 &= 2A(\beta_3/\pi)^2 + A\beta_2\beta_3 + 2A\beta_1\beta_3/\pi + A\beta_2^2/2 + 2A\beta_1\beta_2/\pi + (2A\beta_1^2/\pi)(1-2/\pi) \end{aligned}$$

*Portion IV*

$$\begin{aligned} \ddot{y} &= -A \\ \dot{y} &= -A\theta_4 + \dot{y}_3 \\ y &= -[A(\theta_4)^2/2] + \dot{y}_3\theta''' + y_3 \\ \dot{y}_4 &= -A\beta_2 + \dot{y}_3 = -A\beta_4 + A\beta_2 + 2A\beta_1/\pi = 0 \\ \beta_4 &= \beta_2 + 2\beta_1/\pi \end{aligned}$$

*Total Rise*

$$h = y_4 = -(A\beta_4^2/2) + (A\beta_2 + 2A\beta_1/\pi)\beta_4 + y_3$$

Substituting

$$A = \frac{h}{[-\beta_4^2/2 + \beta_2\beta_4 + 2\beta_1\beta_4/\pi + 2(\beta_3/\pi)^2 + \beta_2\beta_3 + 2\beta_1\beta_3/\pi + \beta_2^2/2 + 2\beta_1\beta_2/\pi + (2\beta_1^2/\pi)(1-2/\pi)]}$$

For a given total rise  $h$  for angle  $\theta_0$  and any two of the  $\beta$  angles given one can solve for all angles and all values of the derivative curves.

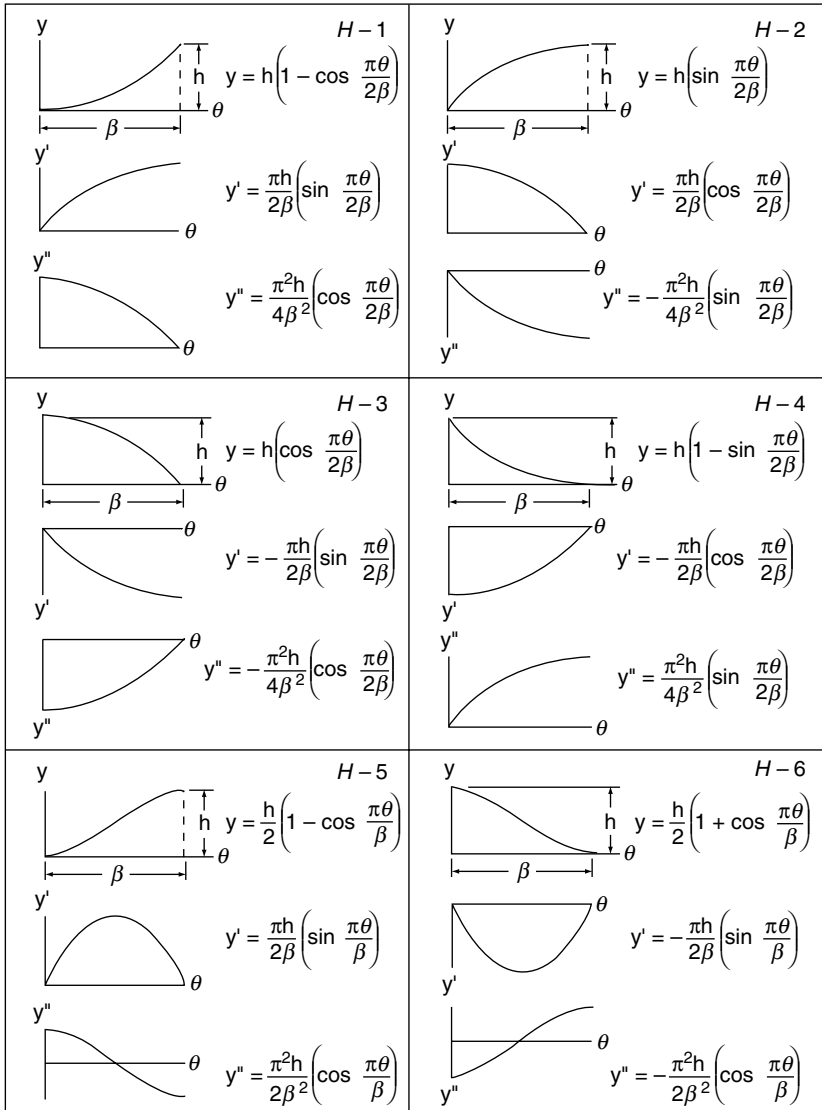
**3.10 COUPLED CURVE SIMPLIFICATION**

---

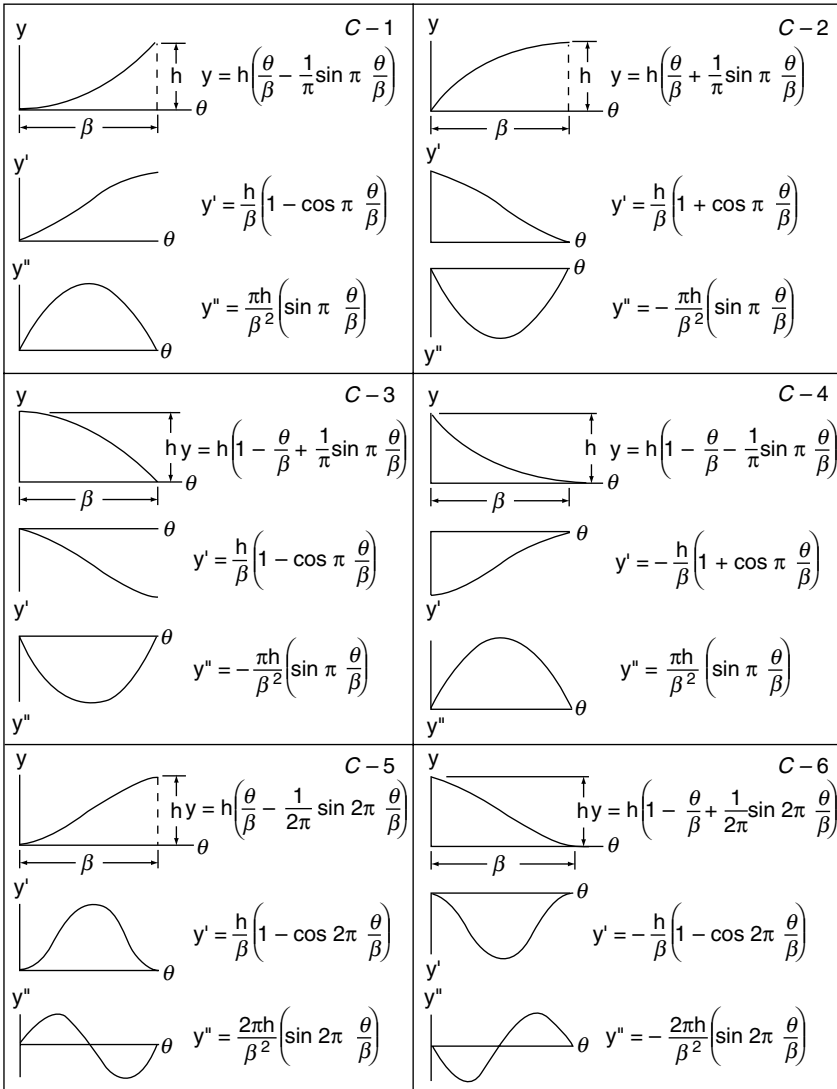
This section presents a convenient method for combining segments of basic curves to produce the required design motion. This procedure was developed by Klopmok and Muffley in Mabie and Ocvirk (1979), who selected three analytic functions of the simple harmonic, the cycloidal, and the eighth-degree polynomial (the latter described in Chapter 4). These curves, having excellent characteristics, can be blended with constant acceleration, constant velocity, and any other curve satisfying the boundary conditions stated in Sec. 3.2. Figures 3.15, 3.16, and 3.17 show the three curves including both half curve segments and full curve action in which

$h$  = total follower displacement for half curve or full curve action, and  
 $\beta$  = cam angle for displacement  $h$ , in

The displacement, velocity, and acceleration characteristics of the curves are indicated. The simple harmonic curve (Fig. 3.15) has a low maximum acceleration for a given rise. Its acceleration discontinuity at the ends of the DRD cycle can be matched with the cycloidal segments (Fig. 3.16) to produce the popular cycloidal coupling. The cycloidal segments are excellent choices to eliminate the acceleration curve discontinuities of any DRD curve by its blending segment. The eighth polynomial, Fig. 3.17, is a good choice



**FIGURE 3.15.** Harmonic motion characteristics.  
 Note:  $h$  = total follower displacement for half-curve or full-curve action, and  $\beta$  = cam angle for displacement  $h$ , in.

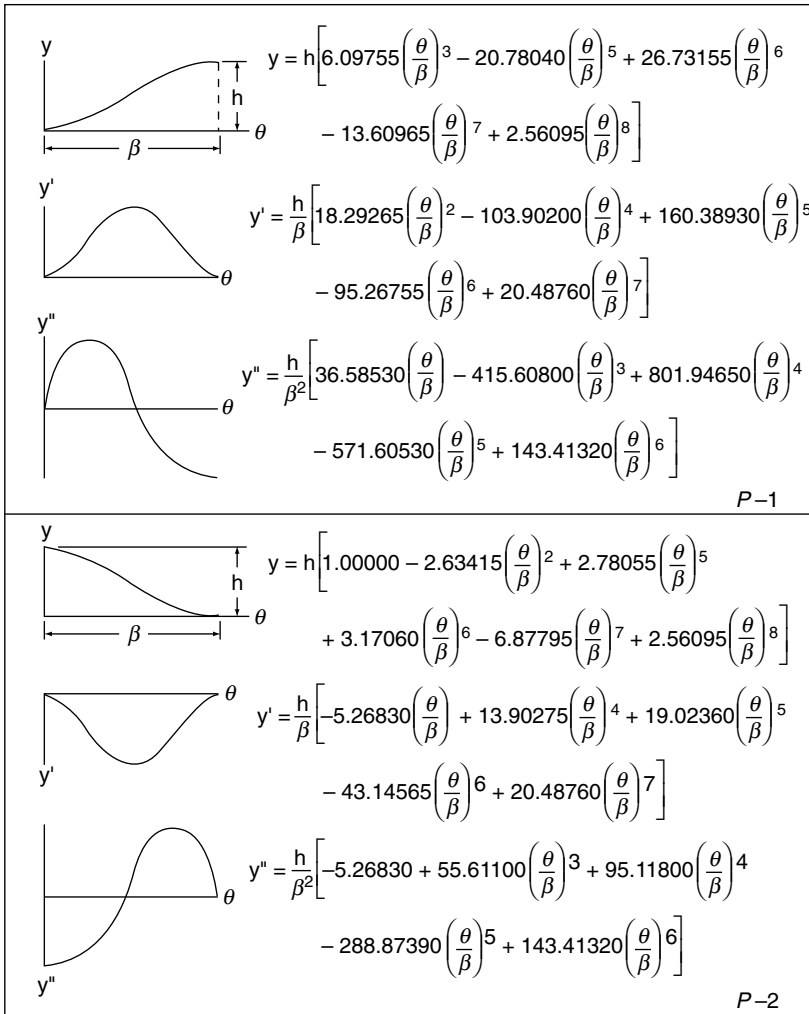


**FIGURE 3.16.** Cycloidal motion characteristics.

Note:  $h$  = total follower displacement for half-curve or full curve action, and  $\beta$  = cam angle for displacement  $h$ .

for blending with curves in general, especially with DRRD cam action. Chapter 4 shows an elaborate treatment of polynomials.

**EXAMPLE** A spring-loaded textile machine has a cam that rotates at 720 rpm in which the follower rises  $1\frac{3}{4}$  inches in 120 degrees. To keep the spring size small, the maximum positive acceleration is twice the maximum negative acceleration. Design (a) the rise portion of the DRRD system with harmonic and cycloidal coupling using the simplified



**FIGURE 3.17.** Eighth-degree polynomial motion characteristics.

Note:  $h$  = total follower displacement.

$\beta$  = cam angle for displacement  $h$ , in.

method of this section. Also find (b) at point the characteristic values of displacement, velocity, and acceleration.

**Solution (a)**

Angular velocity

$$\omega = \frac{720 \times 2\pi}{60} = 75.398 \text{ rad/sec}$$

$$h = 1.75 \text{ in.}$$

$$\beta = \frac{(120)2\pi}{360} = 2.094 \text{ rad}$$

From Fig. 3.16 for cycloidal motion (C1 segment), the characteristic curves are

$$y = h_1 \left( \frac{\theta}{\beta_1} - \frac{1}{\pi} \sin \frac{\pi\theta}{\beta_1} \right)$$

$$y' = \frac{h_1}{\beta_1} \left( 1 - \cos \frac{\pi\theta}{\beta_1} \right)$$

$$y'' = \frac{\pi h_1}{(\beta_1)^2} \sin \frac{\pi\theta}{\beta_1}$$

From Fig. 3.15 for harmonic motion (H2 segment) the characteristic curves are

$$y = h_2 \sin \frac{\pi\theta}{2\beta_2}$$

$$y' = \frac{\pi h_2}{2\beta_2} \cos \frac{\pi\theta}{2\beta_2}$$

$$y'' = -\frac{\pi^2 h_2}{4(\beta_2)^2} \sin \frac{\pi\theta}{2\beta_2}$$

We need velocity continuity at the end of the C1 curve and the beginning of the H2 curve (Fig. 3.18)

$$\frac{h_1}{\beta_1} \left( 1 - \cos \frac{\pi\beta_1}{\beta_1} \right) = \frac{\pi h_2}{2\beta_2} \cos \frac{\pi 0}{2\beta_2}$$

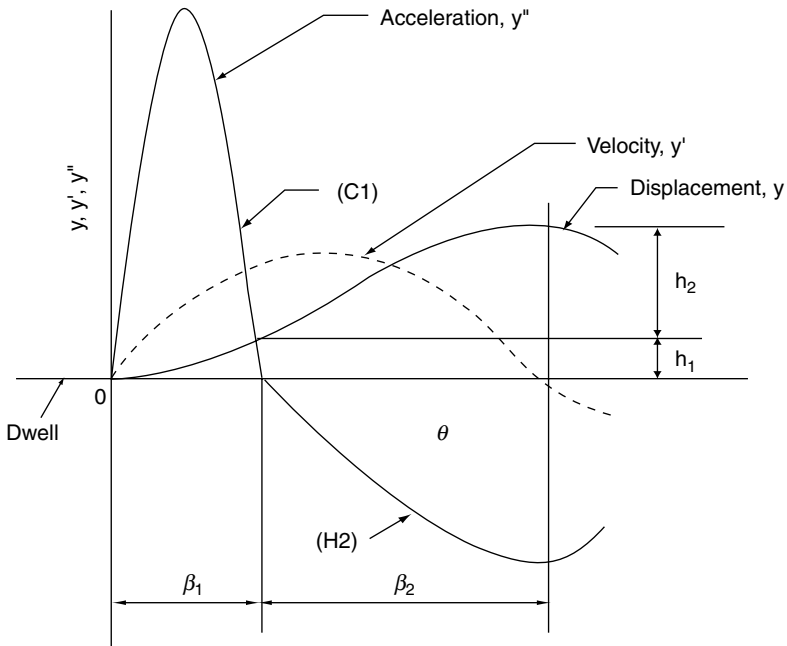


FIGURE 3.18. Cycloidal harmonic camplung example.

which yields

$$\frac{4h_1}{\pi h_2} = \frac{\beta_1}{\beta_2}$$

For the C1 curve the acceleration is

$$y''_{\max} = \frac{\pi h_1}{\beta_1^2}$$

And for the H2 curve, the acceleration is

$$y''_{\max} = \frac{\pi^2 h_2}{4\beta_2^2}$$

It is given that  $y''_{\max}$  for C1 curve =  $2 \times y''_{\max}$  for H2 curves.  
Therefore

$$\frac{\pi h_1}{\beta_1^2} = \left| -\frac{\pi^2 h_2}{2\beta_2^2} \right|$$

Now we have four equations to solve for  $h_1$ ,  $h_2$ ,  $\beta_1$ ,  $\beta_2$ .

$$\begin{aligned} h_1 + h_2 &= 1.75 \text{ in} \\ \beta_1 + \beta_2 &= 2.094 \text{ rad} \\ \frac{4h_1}{\pi h_2} &= \frac{\beta_1}{\beta_2} \\ \left| \frac{\pi h_1}{\beta_1^2} \right| &= \left| -\frac{\pi^2 h_2}{2\beta_2^2} \right| \end{aligned}$$

This solves to yield

$$\begin{aligned} h_1 &= 0.4934 \text{ in} \\ h_2 &= 1.2566 \text{ in} \\ \beta_1 &= 40 \text{ deg} \times \frac{\pi}{180} = 0.6981 \text{ rad} \\ \beta_2 &= 80 \text{ deg} \times \frac{\pi}{180} = 1.3963 \text{ rad} \end{aligned}$$

*By following the above principles, the designer may complete the DRRD curve (utilizing H3 and C4) and modify it to suit the design conditions of the machine.*

#### **Solution (b)**

The 15 degrees falls in the cycloidal curve C1 region

$$15 \text{ deg} = \frac{15\pi}{180} = 0.262 \text{ rad}$$

The displacement

$$y = 0.493 \left[ \frac{0.262}{0.698} - \frac{1}{\pi} \sin \frac{\pi(0.262)}{0.698} \right] = 0.400 \text{ in}$$

The velocity

$$y' = \frac{0.493}{0.698} \left[ 1 - \cos \frac{0.262\pi}{0.698} \right] = 0.437 \text{ in}$$

$$\dot{y} = \omega y' = 75.398(0.437) = 32.93 \text{ in/sec}$$

The acceleration

$$y'' = \frac{0.493\pi}{(0.698)^2} \left( \sin \frac{0.262\pi}{0.698} \right) = 2.938 \text{ in/rad}^2$$

$$\dot{y} = \omega^2 y'' = (75.398)^2 (2.938) = 6700 \text{ in/sec}^2$$

## REFERENCES

---

- Chen, F.Y., *Mechanics and Design of Cam Mechanisms*, Pergamon Press, New York, 1982.
- Erdman, A.G., and Sandor, G.N., *Mechanism Design*, Vol. 1, third edition, Prentice Hall, Upper Saddle River, N.J., 1997.
- Mabie, H.H., and Ocvirk, F.W., *Mechanisms and Dynamics of Machinery*, John Wiley & Sons, New York, 1979.
- Neklutin, C.N., *Mechanisms and Cams for Automatic Machines*, American Elsevier, New York, 1969.
- Ragsdell, K.M., and Gilkey, H.E., "Optimal Cam Design Using the Skewed Modified Trapezoidal Profile," *Proceedings of the Applied Mechanism Conference*, Paper 28, Oklahoma State University, Stillwater, 1969.
- Schmidt, E., "Continuous Cam Curves," *Machine Design* 32 (1): 127–132, 1960.
- Wildt, P., "Zwangläufige Triebkurvenherstellung," Dusseldorf, VDJ-Trungungsheft, 1: 11–20, 1953.

*This page intentionally left blank.*

---

# CHAPTER 4

---

## POLYNOMIAL AND FOURIER SERIES CAM CURVES

---

Harold A. Rothbart, D.Eng.

4.1 INTRODUCTION	89	4.6 POLYNOMIAL CURVE MODES OF CONTROL—DRRD CAM	96
4.2 THE 2-3 POLYNOMIAL CAM CURVE	90	4.7 POLYNOMIAL CURVE EXPONENT MANIPULATION	99
4.3 THE 3-4-5 POLYNOMIAL CAM CURVE	91	4.8 FOURIER SERIES CURVES—DRD CAM	103
4.4 THE 4-5-6-7 POLYNOMIAL CAM CURVE	92		
4.5 POLYNOMIAL CURVE GENERAL DERIVATION—DRD CAM	94		

---

### SYMBOLS

---

$C_i$ ,  $i = 0, 1, 2, \dots, n$  constant coefficients  
 $h$  = maximum follower rise normalized  
 $y$  = follower displacement, dimensionless  
 $y'$  = follower velocity, dimensionless  
 $y''$  = follower acceleration, dimensionless  
 $y'''$  = follower jerk, dimensionless  
 $\beta$  = cam angle for rise,  $h$ , normalized  
 $\theta$  = cam angle rotation normalized

---

### 4.1 INTRODUCTION

---

In Chap. 2, Basic Cam Curves, and Chapter 3, Modified Cam Curves, we presented two approaches for the engineers' selection of an acceptable curve design. Now, we will include a third choice of cam curve, that is, the use of algebraic polynomials to specify the follower motion. This approach has special versatility especially in the high-speed automotive field with its DRRD action. Also included in this chapter is a selection of important Fourier series curves that have been applied for high-speed cam system action.

The application of algebraic polynomials was developed by Dudley (1952) as an element of "polydyne" cams, discussed in Chap. 12, in which the differential equations of motion of the cam-follower system are solved using polynomial follower motion equations. Stoddart (1953) shows an application of these polynomial equations to cam action.

The polynomial equation is of the form

$$y = C_0 + C_1\theta + C_2\theta^2 + C_3\theta^3 + \dots + C_n\theta^n \quad (4.1)$$

For convenience Eq. (4.1) is normalized such that the rise,  $h$ , and maximum cam angle,  $\beta$ , will both be set equal to unity. Therefore, for the follower:

Displacement,  $y$ , dimensionless

Velocity,  $y' = \frac{dy}{d\theta}$ , dimensionless

Acceleration,  $y'' = \frac{dy'}{d\theta}$ , dimensionless

Jerk,  $y''' = \frac{dy''}{d\theta}$ , dimensionless

$\theta$  = cam angle rotation, dimensionless

$C_i$ ,  $i = 0, 1, 2, \dots, n$  constant coefficients

Note that  $C_i$  are chosen so that the displacement,  $y$ , and its derivatives satisfy the boundary conditions of the motion. Eq. (4.1) is utilized by establishing as many boundary conditions as necessary to define the mechanism motion. Polynomials can be employed to produce acceptable cam profiles, especially at high speeds. The number of terms to Eq. (4.1) should be properly limited to the desired design. Too many terms may add complications to the machine performance. Furthermore, the higher the order of terms, the slower will be the initial and final displacements and the more accurately the cam profile must be machined at these end points.

The simplest polynomial is the *constant velocity* polynomial,  $y = \frac{h}{\beta}\theta$ , Eq. (2.14) of Chap. 2, where the normalized displacement is

$$y = \theta \quad (4.2)$$

This primitive cam has control only at the ends,

$$\theta = 0, y = 0$$

$$\theta = 1, y = 1.$$

## 4.2 THE 2-3 POLYNOMIAL CAM CURVE

---

For the cubic 2-3 polynomial follower motion, the boundary conditions are:

$$\text{when } \theta = 0, y = 0, y' = 0$$

$$\theta = 1, y = 1, y' = 0.$$

The cubic polynomial is employed

$$y = C_0 + C_1\theta + C_2\theta^2 + C_3\theta^3$$

The first derivative is the velocity

$$y' = C_1 + 2C_2\theta + 3C_3\theta^2$$

Substituting the four boundary conditions into the polynomial equation and solving these equations, we obtain the coefficients:

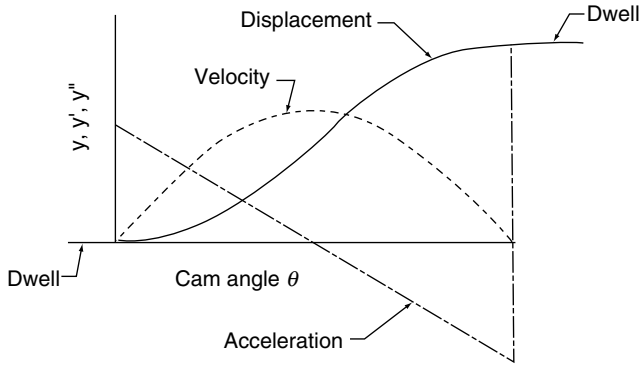


FIGURE 4.1. The 2-3 polynomial dwell-rise-dwell cam curve.

$$C_0 = 0$$

$$C_1 = 0$$

$$C_2 = 3$$

$$C_3 = -2.$$

Therefore, the resulting polynomial has the form

$$\begin{aligned} y &= 3\theta^2 - 2\theta^3 \\ y' &= 6\theta - 6\theta^2 \\ y'' &= 6 - 12\theta \\ y''' &= -12. \end{aligned} \quad (4.3)$$

Figure 4.1 shows the plots of curves. Note that the acceleration curve has a discontinuity at the end points for dwell-rise-dwell action which is unacceptable for high-speed cams.

### 4.3 THE 3-4-5 POLYNOMIAL CAM CURVE

With the 3-4-5 polynomial follower motion we will now control the acceleration at the terminals. This is an additional control of the displacement and velocity previously shown. The boundary conditions are:

$$\text{when } \theta = 0, y = 0, y' = 0, y'' = 0$$

$$\text{when } \theta = 1, y = 1, y' = 0, y'' = 0$$

The polynomial accommodates six conditions,

$$y = C_0 + C_1\theta + C_2\theta^2 + C_3\theta^3 + C_4\theta^4 + C_5\theta^5$$

in which the velocity and acceleration

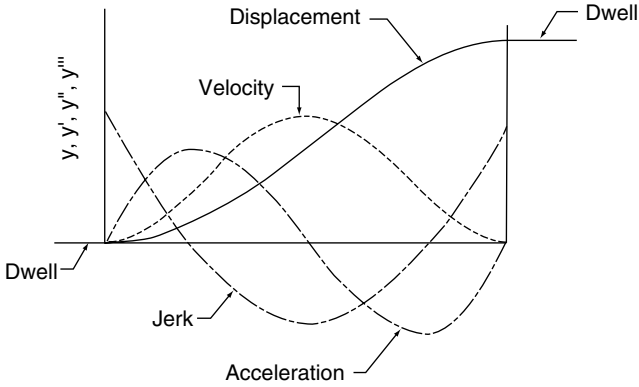


FIGURE 4.2. The 3-4-5 polynomial dwell-rise-dwell cam curve.

$$y' = C_1 + 2C_2\theta + 3C_3\theta^2 + 4C_4\theta^3 + 5C_5\theta^4$$

$$y'' = 2C_2 + 6C_3\theta + 12C_4\theta^2 + 20C_5\theta^3.$$

Substituting in the boundary conditions and solving yields

$$C_0 = C_1 = C_2 = 0$$

$$C_3 = 10$$

$$C_4 = -15$$

$$C_5 = 6.$$

This results in the following polynomial and its derivatives:

$$y = 10\theta^3 - 15\theta^4 + 6\theta^5$$

$$y' = 30\theta^2 - 60\theta^3 + 30\theta^4$$

$$y'' = 60\theta - 180\theta^2 + 120\theta^3$$

$$y''' = 60 - 360\theta + 360\theta^2. \tag{4.4}$$

Figure 4.2 shows the plots of these relationships. Note that this 3-4-5 polynomial has similar characteristics to the cycloidal motion curve.

#### 4.4 THE 4-5-6-7 POLYNOMIAL CAM CURVE

The foregoing derivative control will be extended to produce zero jerk at the ends. Therefore:

$$\text{when } \theta = 0, \quad y = 0, \quad y' = 0, \quad y'' = 0, \quad y''' = 0$$

$$\text{when } \theta = 1, \quad y = 1, \quad y' = 0, \quad y'' = 0, \quad y''' = 0.$$

**TABLE 4.1** Zero Coefficient Terms

Powers in general polynomials	Zero derivatives (at $\theta = 0$ )	Powers in remaining terms
0 and 1	None	1
0 to 3	$y$	2, 3
0 to 5	$y', y''$	3, 4, 5
0 to 7	$y', y'', y'''$	4, 5, 6, 7

These eight conditions establish the general polynomial

$$y = C_0 + C_1\theta + C_2\theta^2 + C_3\theta^3 + C_4\theta^4 + C_5\theta^5 + C_6\theta^6 + C_7\theta^7.$$

In dealing with high-degree polynomials, simplifications can be made if we realize that when  $\theta = 0$ ,  $\frac{d^n y}{d\theta^n} = 0$ . Subsequently, the coefficient for that derivative is  $C_n = 0$ . This is summarized in Table 4.1 for polynomials thus far derived for the DRD event.

For the 4-5-6-7 polynomial,  $C_0 = C_1 = C_2 = C_3 = 0$ . The remaining conditions at  $\theta = 1$  give the following equations:

$$\begin{aligned} C_4 + C_5 + C_6 + C_7 &= 1 \\ 4C_4 + 5C_5 + 6C_6 + 7C_7 &= 0 \\ 12C_4 + 20C_5 + 30C_6 + 42C_7 &= 0 \\ 24C_4 + 60C_5 + 120C_6 + 210C_7 &= 0. \end{aligned}$$

Solving these simultaneously for the 4-5-6-7 polynomial yields

$$\begin{aligned} y &= 35\theta^4 - 84\theta^5 + 70\theta^6 - 20\theta^7 \\ y' &= 140\theta^3 - 420\theta^4 + 420\theta^5 - 140\theta^6 \\ y'' &= 420\theta^2 - 1680\theta^3 + 2100\theta^4 - 840\theta^5 \\ y''' &= 840\theta - 5040\theta^2 + 8400\theta^3 - 4200\theta^4. \end{aligned} \tag{4.5}$$

Figure 4.3 shows a plot of these curves.

If we compare this acceleration curve with the lower order 3-4-5 polynomial, we see larger maximum acceleration and larger maximum jerk values. This indicates a possible inferiority to the 3-4-5 polynomial. A zero value of jerk is not required since manufacturing limits generally cannot meet this control. Next, let's compare the physical significance of the 4-5-6-7 polynomial. Table 4.2 shows the dynamic comparison with the 3-4-5 polynomial, basic simple harmonic, and cycloidal curves.

The physical meaning of this controlled acceleration is best depicted by large-scale plotting of the curves. Figure 4.4 compares these curves with an expanded view of the end points. The data is based on 2 percent of follower rise and 14 percent of cam rotation. Further control of fourth and higher derivatives raises the maximum acceleration and also the time consumed for the initial and final displacement of the cam, and manufacturing limits are often demanded.

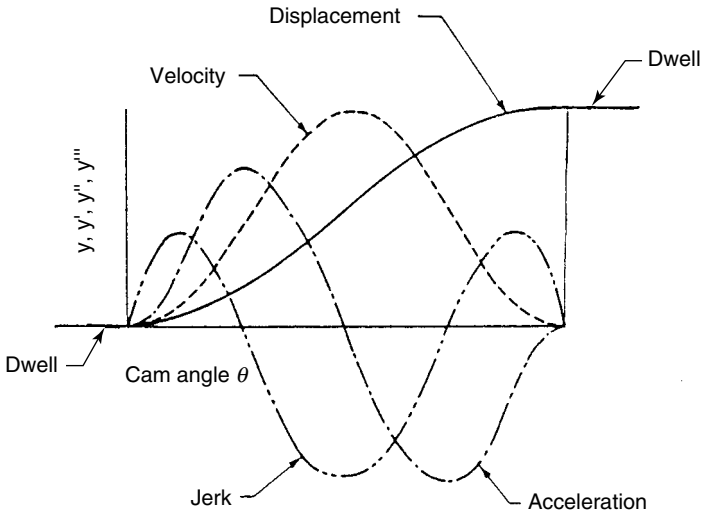


FIGURE 4.3. The 4-5-6-7 polynomial dwell-rise-dwell cam curve.

TABLE 4.2 Curve Comparison

Profile	Maximum acceleration
Harmonic	±4.9
3-4-5	±5.8
Cycloidal	±6.3
4-5-6-7	±7.3

### 4.5 POLYNOMIAL CURVE GENERAL DERIVATION DRD CAM

The successive derivative control for the DRD cam action can be generalized

$$y = C_p \theta^p + C_q \theta^q + C_r \theta^r + C_s \theta^s \dots$$

which can be shown (Stoddart, 1953) having the boundary control conditions equal to zero at the endpoints

$$C_p = \frac{C_0 qrs \dots}{(q-p)(r-p)(s-p) \dots}$$

$$C_q = \frac{C_0 prs \dots}{(p-q)(r-q)(s-q) \dots}$$

$$C_r = \frac{C_0 pqs \dots}{(p-r)(q-r)(s-r) \dots}$$

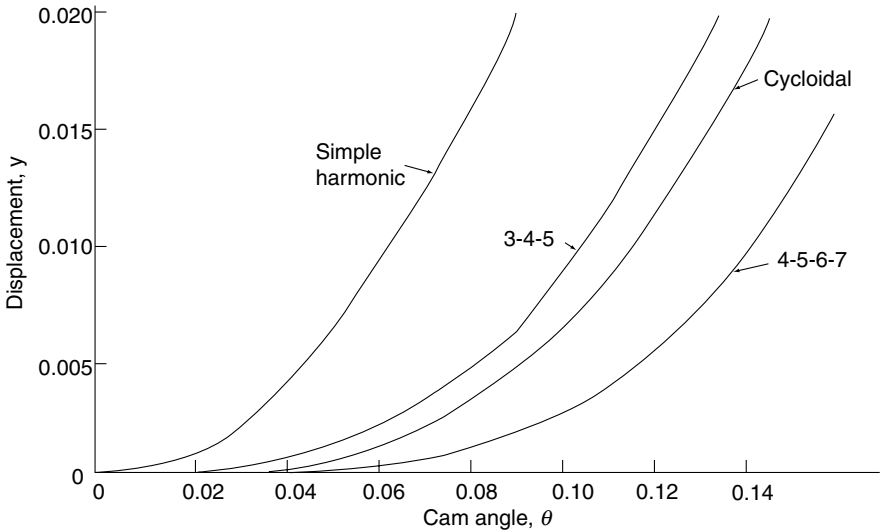


FIGURE 4.4. Comparison of displacement characteristics. (Graph range 2% of lift, 14% of cam rotation.)

$$C_s = \frac{C_0 p q r \dots}{(p-s)(q-s)(r-s) \dots} \quad (4.6)$$

**EXAMPLE** Find the displacement, velocity, and acceleration equations and values for the 4-5-6-7 follower motion for a DRD cam that has a rise of 0.5 in. in 60 degree of cam rotation.

**Solution** Using Eq. (4.6)

$$C_p = \frac{(5)(6)(7)}{(1)(2)(3)} = 35$$

$$C_q = \frac{(4)(6)(7)}{(4-6)(6-5)(7-5)} = -84$$

$$C_r = \frac{(4)(5)(7)}{(4-6)(5-6)(7-6)} = 70$$

$$C_s = \frac{(4)(5)(6)}{(4-7)(5-7)(6-7)} = -20$$

Thus characteristic curves are

$$y = 35\theta^4 - 84\theta^5 + 70\theta^6 - 20\theta^7, \text{ dimensionless}$$

$$y' = 140\theta^3 - 420\theta^4 + 420\theta^5 - 140\theta^6, \text{ dimensionless}$$

$$y'' = 420\theta^2 - 1680\theta^3 + 2100\theta^4 - 840\theta^5, \text{ dimensionless.}$$

This yields the same results as Eq. (4.5).

Let  $\beta =$  cam angle for maximum rise,  $h$ , degrees  
 $h =$  maximum follower rise, in

*Conversion to actual units from normalized equations requires multiplication of each polynomial term by ratio  $\frac{h}{\beta^n}$  giving  $hC_n\left(\frac{\theta}{\beta}\right)^n$ . Therefore each term of the 4-5-6-7 polynomial multiplied by  $\frac{0.5}{60^n}$  yields, with  $\theta$  in degrees.*

$$\text{Displacement, } y = \frac{35}{2}\left(\frac{\theta}{60}\right)^4 - 42\left(\frac{\theta}{60}\right)^5 + 35\left(\frac{\theta}{60}\right)^6 - 10\left(\frac{\theta}{60}\right)^7 \text{ in}$$

$$\text{Velocity, } y' = \frac{7}{6}\left(\frac{\theta}{60}\right)^3 - \frac{7}{2}\left(\frac{\theta}{60}\right)^4 + \frac{35}{10}\left(\frac{\theta}{60}\right)^5 - \frac{7}{6}\left(\frac{\theta}{60}\right)^6 \text{ in/deg}$$

$$\text{Acceleration, } y'' = \frac{7}{120}\left(\frac{\theta}{60}\right)^2 - \frac{7}{30}\left(\frac{\theta}{60}\right)^3 + \frac{7}{24}\left(\frac{\theta}{60}\right)^4 - \frac{7}{60}\left(\frac{\theta}{60}\right)^5 \text{ in/deg}^2$$

#### 4.6 POLYNOMIAL CURVE MODES OF CONTROL—DRRD CAM

In the foregoing example we have assigned one or more of the displacement derivatives to be zero at the boundary. In the dwell-rise-dwell cam, other modes of control may be required to optimize the cam curve. We can impose the following three modes of control:

1. no control
2. interior control
3. assignment of finite quantities to terminal point displacement derivations

The last category, the assignment of finite quantities to terminal point displacement derivations, will not be discussed here. For more see Stoddart (1953) and Chen (1982).

In **no control**, at the ends of a symmetrical DRRD cam (Fig. 4.5), the displacement, the velocity, and the acceleration are to be zero. However, at the midstation, displacement, of course, is 1, velocity is zero, and acceleration is left loose (no control). In addition, there is zero jerk at the midpoint. Thus the boundary conditions for the rise portion of the motion are

$$\text{when } \theta = 0, y = 0, y' = 0; y'' = 0$$

$$\text{when } \theta = 1 \text{ (midpoint), } y = 1, y' = 0, y'' = \text{no control, and } y''' = 0.$$

A polynomial

$$y = C_0 + C_1\theta + C_2\theta^2 + C_3\theta^3 + C_4\theta^4 + C_5\theta^5$$

is assumed which reduces to

$$y = C_3\theta^3 + C_4\theta^4 + C_5\theta^5.$$

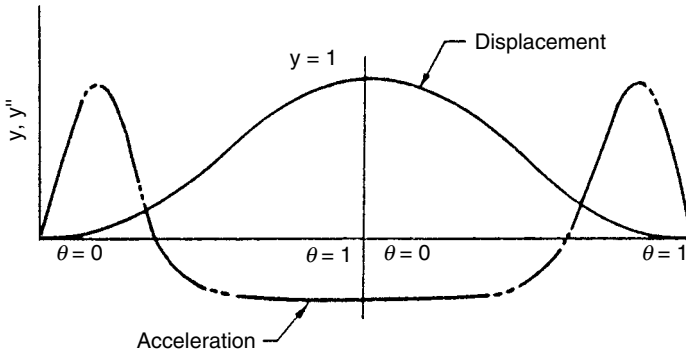


FIGURE 4.5. Fifth-degree polynomial curve for dwell-rise-return-dwell cam.

Substituting the end conditions yields

$$\begin{aligned} C_3 + C_4 + C_5 &= 1 \\ 3C_3 + 4C_4 + 5C_5 &= 0 \\ 6C_3 + 24C_4 + 60C_5 &= 0. \end{aligned}$$

Solving gives

$$\begin{aligned} y &= \frac{20}{3}\theta^3 - \frac{25}{3}\theta^4 + \frac{8}{3}\theta^5 \\ y' &= 20\theta^2 - \frac{100}{3}\theta^3 + \frac{40}{3}\theta^4 \\ y'' &= 40\theta - 100\theta^2 + \frac{160}{3}\theta^3. \end{aligned} \tag{4.7}$$

The return portion is symmetrical (see Fig. 4.5). In this figure we see the characteristic curves for the fifth-degree polynomial applicable as a DRRD cam.

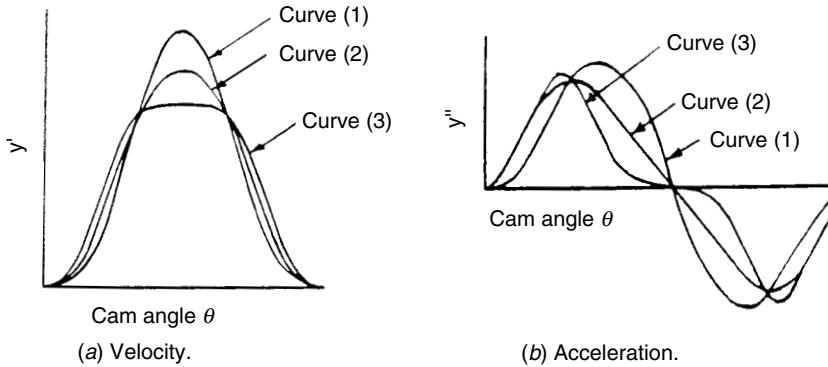
**Interior control** may be employed to shift the characteristic curves by manipulation of high-order polynomial equations. Chen (1982) elaborated on these different controls.

We see from the foregoing that controls at the beginning and terminal condition produce an asymmetrical acceleration curve. Interior control can elevate this situation. Let's assume boundary conditions

$$\begin{aligned} \theta = 0, y = 0, y' = 0, y'' = 0, y''' = 0, \frac{d^4}{d\theta^4} &= 0 \\ \theta = 1, y = 1, y' = 0, y'' = 0, y''' = 0, \frac{d^4}{d\theta^4} &= 0. \end{aligned} \tag{4.8}$$

In Fig. 4.6 the ninth-degree polynomial, curve (1), has a peak velocity of 2.46 and a peak acceleration of 9.37. Next let us apply symmetrical displacement controls

$$\theta = \frac{1}{2}, y = \frac{1}{2}$$



**FIGURE 4.6.** Comparison of velocity and acceleration characteristics of three polynomial motions:  
 curve (1) 9<sup>th</sup>-degree polynomial  
 curve (2) 11<sup>th</sup>-degree symmetric polynomial  
 curve (3) 11<sup>th</sup>-degree polynomial with midpoint velocity control.

$$\theta = \frac{1}{2}, y' = \text{no control.}$$

The polynomial becomes

$$y = 336\theta^5 - 1890\theta^6 + 4740\theta^7 - 6615\theta^8 + 5320\theta^9 - 2310\theta^{10} + 420\theta^{11}.$$

This is curve (2) in Fig. 4.6 with a peak velocity of 2.05 and a peak acceleration of 7.91.

Last we will apply additional velocity controls with the boundary conditions

$$\theta = \frac{1}{2}, y = \frac{1}{2}$$

$$\theta = \frac{1}{2}, y' = 1.75.$$

The resulting curve (3) in Fig. 4.6 is the displacement

$$y = 490\theta^5 - 2968\theta^6 + 7820\theta^7 - 11235\theta^8 + 9170\theta^9 - 4004\theta^{10} + 728\theta^{11}$$

which has a peak acceleration of 8.4.

As noted in this section, the polynomial techniques can be employed to satisfy any motion requirement. The designer has great flexibility in the final choice. Matthew (1979) has demonstrated the use of seventh-degree polynomials to minimize cam pressure angles, stresses, and torque for the ultimate final design choice. A trade-off is always necessary between the various criteria and specifications. Also, in high-speed action, the higher-order polynomials bring with them possible resonances with the follower system. This will be considered in the dynamic analysis of the later chapters.

### 4.7 POLYNOMIAL CURVE EXPONENT MANIPULATION

Curve shape adjustment can be accomplished by changing the exponents of the polynomial. This procedure at best is one of trial and error with some degree of predictability. For example, the fifth-order polynomial can have the powers 3-4-5, 3-5-7, 3-6-9, etc. The seventh-order polynomial can have powers of 4-5-6-7, 4-6-8-10, 4-8-12-16, 4-7-10-13, and so forth. Figures 4.7 and 4.8 show the progressive changes of the polynomials. Note that the higher the powers, the greater is the maximum acceleration that shifts toward the start of the displacement curve.

Polynomial curves having exponents as high as 50 have been used experimentally for automotive cams (see Thoren et al., 1952). Figure 4.9 shows some high-order DRRD polynomial curves. The rise boundary conditions are

$$\begin{aligned} \text{when } \theta = 0, y = 0, y' = 0, y'' = 0, y''' = 0, \frac{d^4y}{d\theta^4} = 0 \\ \theta = 1, y = 0.350, y' = 0, y'' = 0, y''' = 0. \end{aligned} \tag{4.9}$$

The general polynomial equation is of the form

$$y = C_0\theta^2 + C_p\theta^p + C_q\theta^q + C_r\theta^r + C_w\theta^w,$$

where the exponents  $p, q, r,$  and  $w$  may have values such that

$$8 \leq p < q < r < s \leq 50.$$

Now let us indicate some polynomial curves that have been developed. The following are four curves with excellent dynamic characteristics.

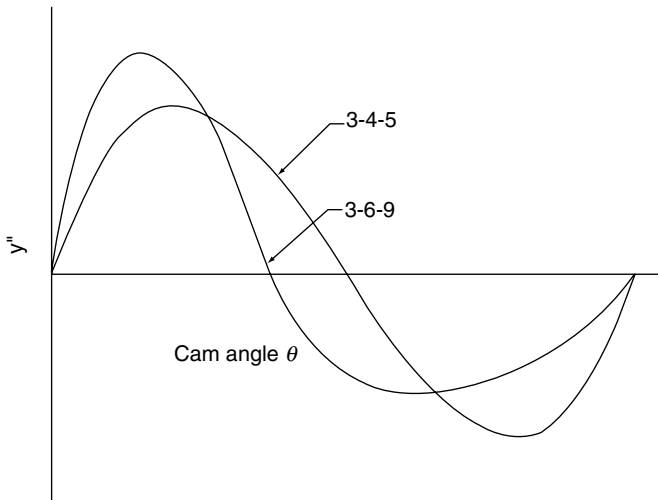


FIGURE 4.7. Acceleration of a family of fifth-order polynomial curves.

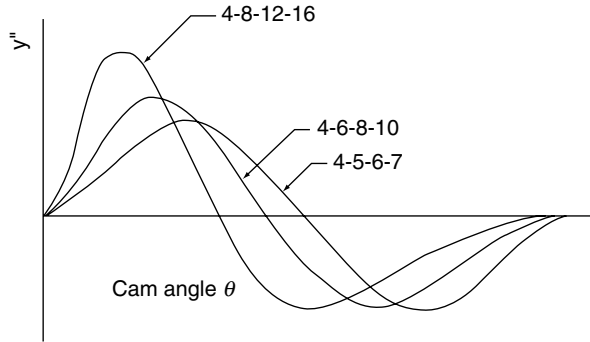


FIGURE 4.8. Acceleration of a family of seventh-order polynomial curves.

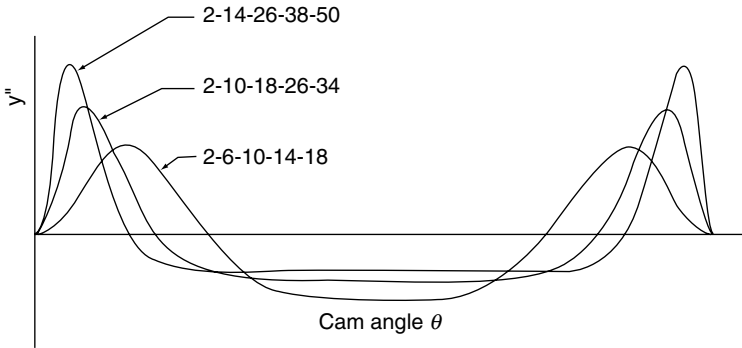


FIGURE 4.9. A family of high-order DRRD polynomial curves.

### Eighth-Degree Polynomial Curve

The eighth-degree polynomial has acceleration characteristics between the harmonic and cycloidal curves. It has an asymmetrical acceleration at the dwell rise or end. The curve can also be blended conveniently with other curves at its maximum rise point.

For the rise action:

$$y = h \left[ 6.09755 \left( \frac{\theta}{\beta} \right)^3 - 20.78040 \left( \frac{\theta}{\beta} \right)^5 + 26.73155 \left( \frac{\theta}{\beta} \right)^6 - 13.60965 \left( \frac{\theta}{\beta} \right)^7 + 2.56095 \left( \frac{\theta}{\beta} \right)^8 \right]$$

$$y' = \frac{h}{\beta} \left[ 18.29265 \left( \frac{\theta}{\beta} \right)^2 - 103.90200 \left( \frac{\theta}{\beta} \right)^4 + 160.38930 \left( \frac{\theta}{\beta} \right)^5 - 95.26755 \left( \frac{\theta}{\beta} \right)^6 + 20.48760 \left( \frac{\theta}{\beta} \right)^7 \right]$$

$$y'' = \frac{h}{\beta^2} \left[ 36.58530 \left( \frac{\theta}{\beta} \right) - 415.60800 \left( \frac{\theta}{\beta} \right)^3 + 801.94650 \left( \frac{\theta}{\beta} \right)^4 \right. \\ \left. - 571.60530 \left( \frac{\theta}{\beta} \right)^5 + 143.41320 \left( \frac{\theta}{\beta} \right)^6 \right]$$

For the fall action

$$y = h \left[ 1.00000 - 2.63415 \left( \frac{\theta}{\beta} \right)^2 + 2.78055 \left( \frac{\theta}{\beta} \right)^5 \right. \\ \left. - 3.17060 \left( \frac{\theta}{\beta} \right)^6 - 6.87795 \left( \frac{\theta}{\beta} \right)^7 + 2.56095 \left( \frac{\theta}{\beta} \right)^8 \right]$$

$$y' = \frac{h}{\beta} \left[ -5.26830 \left( \frac{\theta}{\beta} \right) + 13.90275 \left( \frac{\theta}{\beta} \right)^4 + 19.02360 \left( \frac{\theta}{\beta} \right)^5 \right. \\ \left. + 43.14565 \left( \frac{\theta}{\beta} \right)^6 + 20.48760 \left( \frac{\theta}{\beta} \right)^7 \right]$$

$$y'' = \frac{h}{\beta^2} \left[ -5.26830 + 55.61100 \left( \frac{\theta}{\beta} \right)^3 + 95.11800 \left( \frac{\theta}{\beta} \right)^4 \right. \\ \left. - 288.87390 \left( \frac{\theta}{\beta} \right)^5 + 143.41320 \left( \frac{\theta}{\beta} \right)^6 \right]$$

### Eleventh-Degree Polynomial Curve

$$y = h \left[ 336\delta - 1,890 \left( \frac{\theta}{\beta} \right)^6 + 4,740 \left( \frac{\theta}{\beta} \right)^7 - 6,615 \left( \frac{\theta}{\beta} \right)^8 \right. \\ \left. + 5,320 \left( \frac{\theta}{\beta} \right)^9 - 2,310 \left( \frac{\theta}{\beta} \right)^{10} + 420 \left( \frac{\theta}{\beta} \right)^{11} \right]$$

$$y' = \frac{h}{\beta} \left[ 1,680 \left( \frac{\theta}{\beta} \right)^4 - 11,240 \left( \frac{\theta}{\beta} \right)^5 + 33,180 \left( \frac{\theta}{\beta} \right)^6 - 52,920 \left( \frac{\theta}{\beta} \right)^7 \right. \\ \left. + 47,880 \left( \frac{\theta}{\beta} \right)^8 - 23,100 \left( \frac{\theta}{\beta} \right)^9 + 4,620 \left( \frac{\theta}{\beta} \right)^{10} \right]$$

$$y'' = \frac{h}{\beta^2} \left[ 6,720 \left( \frac{\theta}{\beta} \right)^3 - 56,700 \left( \frac{\theta}{\beta} \right)^4 + 199,080 \left( \frac{\theta}{\beta} \right)^5 - 370,440 \left( \frac{\theta}{\beta} \right)^6 \right. \\ \left. + 383,040 \left( \frac{\theta}{\beta} \right)^7 - 207,900 \left( \frac{\theta}{\beta} \right)^8 + 46,200 \left( \frac{\theta}{\beta} \right)^9 \right]$$

$$y''' = \frac{h}{\beta^3} \left[ 20,160 \left( \frac{\theta}{\beta} \right)^2 - 226,800 \left( \frac{\theta}{\beta} \right)^3 + 995,400 \left( \frac{\theta}{\beta} \right)^4 - 2,222,640 \left( \frac{\theta}{\beta} \right)^5 \right. \\ \left. + 2,681,280 \left( \frac{\theta}{\beta} \right)^6 - 1,663,200 \left( \frac{\theta}{\beta} \right)^7 + 415,800 \left( \frac{\theta}{\beta} \right)^8 \right]$$

The eleventh-degree polynomial function has a maximum velocity of  $2.05 \frac{h}{\beta}$  and a maximum acceleration of  $7.91 \frac{h}{\beta^2}$ .

### 3-4-5-6-7 Polynomial (D-curve; Berzak and Freudenstein 1979)

$$y = h \left[ 12.1 \left( \frac{\theta}{\beta} \right)^3 - 25.5 \left( \frac{\theta}{\beta} \right)^4 + 24.9 \left( \frac{\theta}{\beta} \right)^5 - 14.7 \left( \frac{\theta}{\beta} \right)^6 + 4.2 \left( \frac{\theta}{\beta} \right)^7 \right]$$

$$y' = \frac{h}{\beta} \left[ 36.3 \left( \frac{\theta}{\beta} \right)^2 - 102.0 \left( \frac{\theta}{\beta} \right)^3 + 124.5 \left( \frac{\theta}{\beta} \right)^4 - 88.2 \left( \frac{\theta}{\beta} \right)^5 + 29.4 \left( \frac{\theta}{\beta} \right)^6 \right]$$

$$y'' = \frac{h}{\beta^2} \left[ 72.6 \left( \frac{\theta}{\beta} \right) - 306.0 \left( \frac{\theta}{\beta} \right)^2 + 498.0 \left( \frac{\theta}{\beta} \right)^3 - 441.0 \left( \frac{\theta}{\beta} \right)^4 + 176.4 \left( \frac{\theta}{\beta} \right)^5 \right]$$

$$y''' = \frac{h}{\beta^3} \left[ 72.6 - 612 \left( \frac{\theta}{\beta} \right) + 1,494 \left( \frac{\theta}{\beta} \right)^2 - 1,764 \left( \frac{\theta}{\beta} \right)^3 - 882 \left( \frac{\theta}{\beta} \right)^4 \right]$$

This polynomial function has a maximum velocity of  $1.80 \frac{h}{\beta}$  and a maximum acceleration of  $5.60 \frac{h}{\beta^2}$ .

### 3-4-5-6-7 Polynomial (E-curve; Berzak and Freudenstein 1979)

$$y = h \left[ 5.35 \left( \frac{\theta}{\beta} \right)^3 + 8.20 \left( \frac{\theta}{\beta} \right)^4 - 35.74 \left( \frac{\theta}{\beta} \right)^5 + 32.46 \left( \frac{\theta}{\beta} \right)^6 - 9.27 \left( \frac{\theta}{\beta} \right)^7 \right]$$

$$y' = \frac{h}{\beta} \left[ 16.05 \left( \frac{\theta}{\beta} \right)^2 + 32.80 \left( \frac{\theta}{\beta} \right)^3 - 178.70 \left( \frac{\theta}{\beta} \right)^4 + 194.76 \left( \frac{\theta}{\beta} \right)^5 - 64.89 \left( \frac{\theta}{\beta} \right)^6 \right]$$

$$y'' = \frac{h}{\beta^2} \left[ 32.1 \left( \frac{\theta}{\beta} \right) + 98.40 \left( \frac{\theta}{\beta} \right)^2 - 741.8 \left( \frac{\theta}{\beta} \right)^3 + 973.8 \left( \frac{\theta}{\beta} \right)^4 - 389.34 \left( \frac{\theta}{\beta} \right)^5 \right]$$

$$y''' = \frac{h}{\beta^3} \left[ 32.1 + 196.8 \left( \frac{\theta}{\beta} \right) - 2144.4 \left( \frac{\theta}{\beta} \right)^2 + 3895.2 \left( \frac{\theta}{\beta} \right)^3 - 1946.70 \left( \frac{\theta}{\beta} \right)^4 \right]$$

This function has a maximum velocity of  $2.00 \frac{h}{\beta}$  and a maximum acceleration of  $6.50 \frac{h}{\beta^2}$ .

#### 4.8 FOURIER SERIES CURVES—DRD CAM

In Chap. 2 we discussed the basic parabolic, sinusoidal, and cycloidal curves for cam-follower DRD action. We also showed in Chap. 3 how these curves and others can be modified and combined to form a variety of cam profiles.

Ignoring the torsional aspect of the cam drive (assuming the cam runs at a constant speed), the two fundamental dynamic objectives in designing cam profiles are:

1. to have the smallest possible maximum acceleration and thus the minimum dynamic load on the high-speed follower;
2. To avoid resonant vibratory response in the follower caused by high harmonic content in the designed cam profile.

These fundamental objectives are not related. Let us compare the basic cam profiles as a means of describing the harmonic content that is addressed in the later paragraphs.

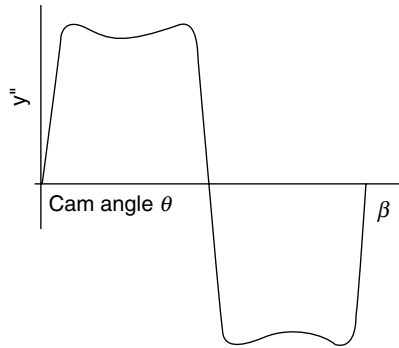
The parabolic curve has the smallest maximum acceleration but has a high harmonic content, since the Fourier expansion for a parabolic curve has an infinite number of terms. Because each term is associated with a certain forcing frequency, it may induce resonance vibrations in the follower at some of those frequencies at some speed as the system is brought up to speed. The cycloidal cam, on the other hand, having but a fundamental frequency in the acceleration curve, has a minimum harmonic content. The cycloidal profile is the least likely to excite vibration in the follower, but this occurs at the expense of high acceleration. Furthermore, it has a more than 50 percent higher maximum acceleration than does the parabolic profile. In design, it is necessary to find a cam profile that has the fewest and lowest possible harmonics, though, in the end, nature calls for a compromised balance of all factors, requiring judicial trade-offs. There is no perfect solution.

A number of acceptable harmonic curves have been developed in consideration of these thoughts. Note that for a DRD motion event, the Fourier series used must be an odd harmonic curve, which has polar symmetry with respect to the midpoint of the curve.

##### Gutman 1-3 Harmonic (Gutman, 1961)

$$\begin{aligned}
 y &= h \left[ \frac{\theta}{\beta} - \frac{15}{32\pi} \sin \frac{2\pi\theta}{\beta} - \frac{1}{96\pi} \sin \frac{6\pi\theta}{\beta} \right] \\
 y' &= \frac{h}{\beta} \left[ 1 - \frac{15}{16} \cos \frac{2\pi\theta}{\beta} - \frac{1}{16} \cos \frac{6\pi\theta}{\beta} \right] \\
 y'' &= \frac{h\pi}{8\beta^3} \left[ 15 \sin \frac{2\pi\theta}{\beta} + 3 \sin \frac{6\pi\theta}{\beta} \right] \\
 y''' &= \frac{h\pi^2}{4\beta^3} \left[ 15 \cos \frac{2\pi\theta}{\beta} + 9 \cos \frac{6\pi\theta}{\beta} \right]. \tag{4.11}
 \end{aligned}$$

Gutman's 1-3 harmonic curve can be obtained from the Fourier series expansion of the displacement of the parabolic curve by retaining the first two terms of the series. The resulting curve has a harmonic content triple the frequency of the cycloidal curve and a maximum acceleration of about 130 percent of the parabolic curve, or about 80 percent of the cycloidal curve (Fig. 4.10).



**FIGURE 4.10.** Gutman's [1961] 1-3 harmonic acceleration curve.

Similarly, if we retain the first three terms in the Fourier series expansion of the displacement of the parabolic curve, the equation of Gutman's fifth-order harmonic curve can be obtained.

#### Freudenstein 1-3 Harmonic Curve (Freudenstein, 1960)

$$\begin{aligned}
 y &= \frac{h\theta}{\beta} - \frac{h}{2\pi} \left( \frac{27}{28} \sin \frac{2\pi\theta}{\beta} + \frac{1}{84} \sin \frac{6\pi\theta}{\beta} \right) \\
 y' &= \frac{h}{\beta} \left( 1 - \frac{27}{28} \cos \frac{2\pi\theta}{\beta} - \frac{1}{28} \cos \frac{6\pi\theta}{\beta} \right) \\
 y'' &= \frac{2\pi h}{\beta^2} \left( \frac{27}{28} \sin \frac{2\pi\theta}{\beta} + \frac{3}{28} \sin \frac{6\pi\theta}{\beta} \right) \\
 y''' &= \frac{4\pi^2 h}{\beta^3} \left( \frac{27}{28} \cos \frac{2\pi\theta}{\beta} + \frac{9}{28} \cos \frac{6\pi\theta}{\beta} \right) \quad (4.12)
 \end{aligned}$$

In agreement with the foregoing design factors stated, Freudenstein's 1-3 harmonic curve has a maximum acceleration of about 135 percent of the acceleration of the parabolic curve, or 85 percent of the acceleration of the cycloidal curve.

#### Freudenstein 1-3-5 Harmonic Curve (Freudenstein, 1960)

$$\begin{aligned}
 y &= \frac{h\theta}{\beta} - \frac{hm}{2\pi} \left( \sin \frac{2\pi\theta}{\beta} + \frac{1}{54} \sin \frac{6\pi\theta}{\beta} + \frac{1}{1250} \sin \frac{10\pi\theta}{\beta} \right) \quad (4.13) \\
 m &= \frac{1125}{1192} \\
 y' &= \frac{h}{\beta} \left[ 1 - m \left( \cos \frac{2\pi\theta}{\beta} + \frac{1}{18} \cos \frac{6\pi\theta}{\beta} + \frac{1}{250} \cos \frac{10\pi\theta}{\beta} \right) \right]
 \end{aligned}$$

$$y'' = \frac{2\pi h}{\beta^2} m \left( \sin \frac{2\pi\theta}{\beta} + \frac{1}{6} \sin \frac{6\pi\theta}{\beta} + \frac{1}{50} \sin \frac{10\pi\theta}{\beta} \right)$$

$$y''' = \frac{4\pi^2 h}{\beta^3} m \left( \cos \frac{2\pi\theta}{\beta} + \frac{1}{2} \cos \frac{6\pi\theta}{\beta} + \frac{1}{10} \cos \frac{10\pi\theta}{\beta} \right)$$

This curve has a maximum acceleration of about 125 percent of the acceleration of the parabolic curve, or about 81 percent of the acceleration of the cycloidal curve.

In this way, other higher-order multiple harmonic curves can be generated. Baranyi (1970) has derived and tabulated the Fourier coefficients up to and including the seventeenth harmonic of the profile groups for the DRD cam. Unfortunately, these high-order harmonic curves do not generally produce a satisfactory dynamic response of the follower. Nevertheless, there is an advantage in using a harmonic series for cam motion design. This advantage is the direct knowledge of the harmonic content of the forcing function applied to the cam-and-follower system. With this knowledge, the designer can create a system that will avoid the resonance at certain critical harmonics.

In the foregoing discussion, we have studied the dwell-to-dwell curves including the transition between endpoints designed to have finite terminal velocities. Weber (1979) has presented an approximate method to generate Fourier series of cams with this transition. His method is based on the superposition principle in which simple curves are combined to develop a complex curve. In Weber's work, a curve is considered to be the composite of two elements: a chord (constant velocity line) connecting the endpoints and a Fourier sine series having terminal slopes equal and opposite to the chordal slope discontinuities such that the composite curve is slope-continuous.

## REFERENCES

- Baranyi, S.M., "Multiple-Harmonic Cam Profiles," ASME Paper 70-MECH-59, 1970.
- Berzak, N., and Freudenstein, F., "Optimization Criteria in Polydyne Cam Design," *Proceedings of 5<sup>th</sup> World Congress on Theory of Machine and Mechanisms*, pp. 1303–6, 1979.
- Chen, F.Y., *Mechanics and Design of Cam Mechanisms*, Pergamon Press, New York, 1982.
- Dudley, W.M., "A New Approach to Cam Design," *Machine Design* (184): 143–8, June 1952.
- Freudenstein, F., "On the Dynamics of High-Speed Cam Profiles," *Int J. Mech. Sci.* (1): 342–9, 1960.
- Gutman, A.S., "To Avoid Vibration—Try This New Cam Profile," *Prod. Eng.*: 42–8, December 25, 1961.
- Matthew, G.K., "The Modified Polynomial Specification for Cams," *Proceedings of 5<sup>th</sup> World Congress on Theory of Machine and Mechanisms*: 1299–302, 1979.
- Stoddart, D.A., "Polydyne Cam Design," *Machine Design* 25 (1): 121–35; 25 (2): 146–55; 25 (3): 149–62, 1953.
- Thoren, T.R., Engemann, H.H., and Stoddart, D.A., "Cam Design as Related to Valve Train Dynamics," *SAE Quart. Trans.* 1: 1–14, January 6, 1952.
- Weber, T., Jr. "Simplifying Complex Cam Design," *Machine Design*: 115–20, March 22, 1979.

*This page intentionally left blank.*

---

# CHAPTER 5

---

# CAM MOTION SYNTHESIS USING SPLINE FUNCTIONS

---

**Cecil O. Huey, Jr., PhD**

*Professor of Mechanical Engineering  
Clemson University, Clemson, South Carolina*

**Dermin Tsay, PhD**

*Professor, Department of Mechanical Engineering  
National Sun Yat Sen University  
Kaohsiung, Taiwan*

5.1 INTRODUCTION	108	5.5 THE SYNTHESIS OF FOLLOWER	
5.2 APPLICATION OF NONRATIONAL		MOTIONS OF THREE-	
B-SPLINES TO MOTION		DIMENSIONAL CAMS USING	
SYNTHESIS	109	NONPARAMETRIC B-SPLINES	144
5.3 APPLICATION OF RATIONAL		5.6 SUMMARY	154
B-SPLINES	117		
5.4 SPLINE FUNCTIONS APPLIED IN THE			
SYNTHESIS OF NONRIGID CAM-			
FOLLOWER SYSTEMS	127		

---

## SYMBOLS

---

- $a$  = Normal distance between the follower center and the axis of rotation of the cam at initial position
- $A_j$  = Constant coefficients ( $j = 1, \dots, n$ )
- $C_j$  = Viscous damping coefficient of follower (used in addressing nonrigid follower)
- $C_s$  = Viscous damping coefficient of the restoring damper
- $d$  = Deviation of cam-follower position from static equilibrium position
- $d'$  = First derivative of deviation
- $d''$  = Second derivative of deviation
- $E_{i,j}(x)$  = Spline function values at constraint locations ( $i, j = 1, \dots, n$ )
- $F_c$  = The contact force (used in addressing nonrigid follower)
- $F_j$  = Kinematic constraint values ( $j = 1, \dots, n$ )
- $F_{p'}$  = Preload (used in addressing nonrigid follower)
- $h$  = Rise of the follower
- $k$  = Order of spline function
- $K_f$  = Spring constant of follower (used in addressing nonrigid follower)
- $K_s$  = Spring constant of return spring (used in addressing nonrigid follower)
- $l$  = Length of the cam

- $M$  = Mass of follower (used in addressing nonrigid follower)  
 $M_{i,k2}(s_2)$  = B-spline basis functions of order  $k_2$  in the parametric directions,  $s_2$   
 $n$  = Number of kinematic constraints  
 $N_{i,k1}(\phi_2)$  = B-spline basis functions of order  $k_1$  in the parametric directions,  $\phi_2$   
 $N_{j,k}^{(m)}(x)$  =  $m^{\text{th}}$  derivative of B-splines of order  $k$   
 $N_{j,k}(x)$  = B-splines ( $j = 1, \dots, n$ ) of order  $k$   
 $P_{ij}$  = One of  $(n \times m)$  coefficients  
 $r$  = Follower radius  
 $R_j$  = Rational B-spline of order  $k$   
 $R_{j,k}^{(m)}$  =  $m^{\text{th}}$  derivative of rational B-spline of order  $k$   
 $s_2$  = Axial input displacement of three-dimensional cam  
 $S$  = Displacement of the follower  
 $S_f$  = Follower displacement of three-dimensional cam  
 $S^{(m)}$  =  $m^{\text{th}}$  derivative of the displacement of the follower  
 $t$  = Time  
 $T$  = Knot sequence  $T_1, \dots, T_{k+1}$   
 $U$  = Approximate solution of differential equation  
 $W_j$  = Weight sequence with positive values  
 $x$  = Cam rotational angle;  $x_{\min} \leq x \leq x_{\max}$ .  
 $Y$  = Displacement of follower (used in addressing nonrigid follower)  
 $Y^{(1)}$  = Velocity of follower (used in addressing nonrigid follower)  
 $Y^{(2)}$  = Acceleration of follower (used in addressing nonrigid follower)  
 $Y_c$  = Displacement of cam (used in addressing nonrigid follower)  
 $Y_c^{(1)}$  = Velocity of cam (used in addressing nonrigid follower)  
 $\beta$  = Total range of cam rotation  
 $\phi_2$  = Angular position of three-dimensional cam  
 $\tau$  = Normalized time,  $\tau = t/T_h$ , where  $T_h$  is the total time for the rise of  $h$   
 $\omega$  = Angular velocity of cam  
 $\omega_n$  = Natural frequency of the cam-follower system  
 $\xi$  = Damping ratio

## 5.1 INTRODUCTION

---

In synthesizing motion programs for cams the designer is faced with a variety of problems. Specific displacement, velocity, and acceleration constraints must be satisfied and continuity of the derivatives of displacement, at least through the second derivative, should be preserved. Expressions for displacement frequently must be refined to reduce acceleration peaks or to shift peak values of a particular kinematic parameter away from critical regions. Sometimes local adjustments must be made to reduce the pressure angle at a troublesome spot. On occasion, it is desirable to account for nonrigid behavior of the follower system when synthesizing the cam profile.

In the absence of especially demanding requirements, standard conventional motions defined by harmonic, modified harmonic, trapezoidal, cycloidal, modified trapezoidal, and the polynomial functions are applied directly or combined into piecewise functions. Sometimes polynomial functions that satisfy specified boundary conditions can, through manipulation of exponent values, be modified to improve motion characteristics by shifting peak acceleration values (Rothbart, 1956; Chen, 1982). Although the innovative combination and modification of standard analytical functions into effective motion programs is often a possibility, it is not sufficiently general nor is it a practical approach in the face of numerous constraints.

The use of polynomial functions is probably the most general scheme for interpolating a set of discrete constraints. In its basic form, the functions are applied by using a polynomial equation of a degree that is one less than the number of constraints to be satisfied. One of the polynomial coefficients can be established for each constraint that must be satisfied. If the number of constraints is sizable, then the polynomial will be of high degree. High-degree polynomials often display some undesirable characteristics between constraints. Sometimes the polynomial coefficients become computationally difficult to determine because of the large systems of ill-conditioned equations that may occur (Forsythe et al., 1977). The polynomial approach can be extended to address nonrigid follower behavior under certain conditions. The classic polydyne method is an example.

Early in the advent of computer-aided design (CAD) techniques, especially those used to define curves and surfaces, curve fitting methods were the subject of intense study. Farin (1988) offers a very readable treatment of the broad area of curves and surfaces, including several that have potential for cam applications. Of likely interest to cam designers are Bezier curves and splines. Both are piecewise continuous functions, and in certain circumstances are equivalent. Both are defined by control points but differ in the effects of changing these points. A change in a control point for a Bezier curve affects the entire curve, whereas a similar change in a spline function results in a local influence. Consequently, splines afford the designer greater local control and therefore are more adaptable when design constraints are defined locally. Such is usually the case with cams when the designer must satisfy discrete kinematic constraints and preserve continuity locally.

The methods described here employ splines, in particular piecewise continuous polynomials called basis splines (B-splines), to define displacement curves for cams. The basic approach is described and illustrated by example and then is extended to accommodate slightly more advanced forms of splines and is applied to nonrigid followers and to the synthesis of three-dimensional cam surfaces.

Spline functions are well known and well understood, and practical procedures for evaluating them have been long known (deBoor, 1972; Cox, 1972). An especially nice characteristic of spline functions for cam motion programs is that a piecewise polynomial constructed of B-splines can be made to have continuous derivatives up to any order. However, since continuity in the second derivative is usually adequate for cams, the B-splines often need only be cubic functions, regardless of the number of constraints present. There appears to be little practical difficulty in using splines of order five or six on a routine basis, though. (The order of spline functions will be more clearly defined later.) The reduction in the degree of the functions involved effectively avoids the numerical difficulties associated with high-degree polynomials mentioned earlier.

## 5.2 APPLICATION OF NONRATIONAL B-SPLINES TO MOTION SYNTHESIS

---

### 5.2.1 Basic Theory

A general expression for spline functions that can be applied to the problem of interpolating  $n$  kinematic constraints can be written as follows:

$$S(x) = \sum_{j=1}^n A_j N_{j,k}(x) \quad (5.1)$$

$$S^{(1)}(x) = \sum_{j=1}^n A_j N_{j,k}^{(1)}(x) \quad (5.2)$$

$$S^{(2)}(x) = \sum_{j=1}^n A_j N_{j,k}^{(2)}(x) \quad (5.3)$$

$$\vdots$$

$$S^{(m)}(x) = \sum_{j=1}^n A_j N_{j,k}^{(m)}(x) \quad (5.4)$$

Usually, the equations containing derivatives beyond acceleration are not needed.

Each spline function,  $N_{j,k}(x)$ ,  $j = 1, \dots, n$ , has a unique representation on the interval  $[x_{min}, x_{max}]$  (Curry and Schoenberg, 1966). The spline function of order  $k$  is continuous up to derivatives of order  $k - 2$ . Therefore, to obtain continuous acceleration, at least fourth-order splines must be used. If the coefficients,  $A_j$ , are known it is an easy matter to interpolate values of displacement, velocity, and acceleration on the interval  $[x_{min}, x_{max}]$  using established methods for evaluating the spline functions. As is the case with the conventional polynomial approach, one coefficient can be evaluated for each constraint that is given. For  $n$  constraints,  $n$  B-splines must be used.

Spline functions are defined by the variables  $k$ ,  $T$ ,  $n$ , and  $A_j$  (deBoor, 1978). The variable,  $T$ , referred to as the knot sequence, is a nondecreasing sequence of real points on the interval  $[x_{min}, x_{max}]$ . The order,  $k$ , of the spline functions and the selection of points in the knot sequence,  $T$ , are subject to the designer's control and consequently provide the means of refining the cam motion program mentioned earlier. Local adjustments in the knot sequence will cause local changes in the motion program. The examples that follow will illustrate this feature of the spline approach.

### Practical Implementation of the Basic Theory

The procedure for applying B-splines is really rather simple and is described in a stepwise fashion in the following outline. The means of determining the required values for the B-spline functions and derivatives appears later.

1. Establish the knot sequence on the interval  $[x_{min}, x_{max}]$ . A single B-spline of order  $k$  requires  $k + 1$  consecutive knots (de Boor, 1972). For cam design applications, there must be knots at  $x_{min}$  and at  $x_{max}$  and these knots must be repeated  $k$  times. For a series of B-splines to interpolate  $n$  constraints, the first spline will be located on the knot sequence  $T_1, \dots, T_{k+1}$ , the second on the sequence  $T_2, \dots, T_{k+2}$ , the third on the sequence  $T_3, \dots, T_{k+3}$ , and so on until the  $n^{\text{th}}$  spline on the sequence  $T_n, \dots, T_{k+n}$ . The total number of knots then is  $k + n$ .

2. Determine the values of each B-spline or B-spline derivative at all points where constraints are defined. For velocity constraints first derivatives are required; for acceleration constraints second derivatives are required, and so forth. In the expressions that follow, these values are referred to as  $E_{ij}$ , ( $i, j = 1, \dots, n$ ), where the first subscript identifies the constraint and the second the spline function.

3. Collect the constraint values,  $F_j$  ( $j = 1, \dots, n$ ), and form the linear system of equations

$$\begin{array}{ccccccc} A_1 E_{1,1} & + & A_1 E_{1,2} & + \cdots + & A_n E_{1,n} & = & F_1 \\ \vdots & & \vdots & & \vdots & & \\ A_1 E_{n,1} & + & A_2 E_{n,2} & + \cdots + & A_n E_{n,n} & = & F_n. \end{array} \quad (5.5)$$

As indicated in item 2, if the  $F_j$  is a velocity constraint, then the  $E_{ij}$  in the equation containing the  $F_j$  will be first derivatives. If the  $F_j$  is an acceleration, then the  $E_{ij}$  will be second derivatives, and so on. Written in matrix notation the system of equations above becomes

$$[E][A] = [F]. \quad (5.6)$$

4. Solve the system of equations above for the coefficients  $A_j$ .

5. Using the methods below, evaluate the B-splines or B-spline derivatives as needed to determine displacement, velocity, acceleration, jerk, and other elements between constraints.

**Evaluation of B-Splines and Their Derivatives.** B-splines can be evaluated by means of a well-known recurrence relation (Cox, 1972; deBoor, 1972). This relationship for the case here, in terms of the cam angle,  $x$ , and given the knot sequence,  $T$ , is

$$N_{j,k}(x) = \frac{x - T_j}{T_{j+k-1} - T_j} N_{j,k-1}(x) + \frac{T_{j+k} - x}{T_{j+k} - T_{j+1}} N_{j+1,k-1}(x) \quad (5.7)$$

for  $k > 1$  and  $j = 1, \dots, n$ . For  $k = 1$ , the relationship is

$$N_{j,1}(x) = \begin{cases} 1, & T_j \leq x < T_{j+1} \\ 0, & \text{otherwise.} \end{cases} \quad (5.8)$$

Similar relationships for the derivatives have been found (Butterfield, 1976) and are as follows:

$$N_{j,k}^{(m)}(x) = (k-1) \left[ \frac{N_{j,k-1}^{(m-1)}(x)}{T_{j+k-1} - T_j} - \frac{N_{j+1,k-1}^{(m-1)}(x)}{T_{j+k} - T_{j+1}} \right] \quad (5.9)$$

$$N_{j,k}^{(m)}(x) = \left( \frac{k-1}{k-m-1} \right) \left[ \frac{x - T_j}{T_{j+k-1} - T_j} N_{j,k-1}^{(m)}(x) + \frac{T_{j+k} - x}{T_{j+k} - T_{j+1}} N_{j+1,k-1}^{(m)}(x) \right]. \quad (5.10)$$

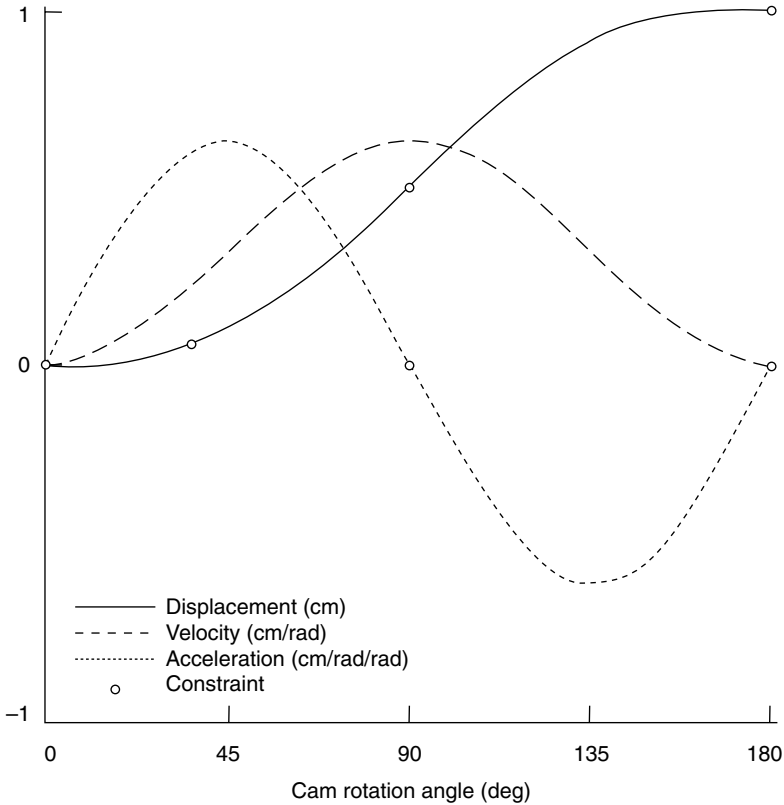
Many software packages contain procedures for evaluating B-splines (deBoor, 1977; Foy, 1977). Packages such as MatLab (The Math Works, Inc.) and the IMSL software (Visual Numerics) are easily accessed and widely used. At present MatLab is limited in its flexibility for handling spline functions, but the IMSL routines are fully capable of handling the procedures described here. Due to the general availability of these resources, the details of spline evaluation and equation solving will be omitted here and we will move directly to the issue of application.

**EXAMPLE APPLICATIONS:** A series of examples to illustrate the application of the spline method to cam motion synthesis follows. The examples, taken collectively, show how the approach provides a consistent and systematic procedure that can be used to accomplish several different aims that usually have to be approached using different procedures. It will be shown that the method is as easy to apply and is as effective in routine cases as are the more conventional approaches. It will also be shown that the same procedure can be applied in more demanding circumstances without modification. The examples also serve to demonstrate the mechanics of applying the spline approach.

**EXAMPLE 1: A Simple Case, with Comparison to the Use of Polynomial Functions** *In this example both the spline method and the conventional polynomial approach*

**TABLE 5.1** Constraints for Example 1

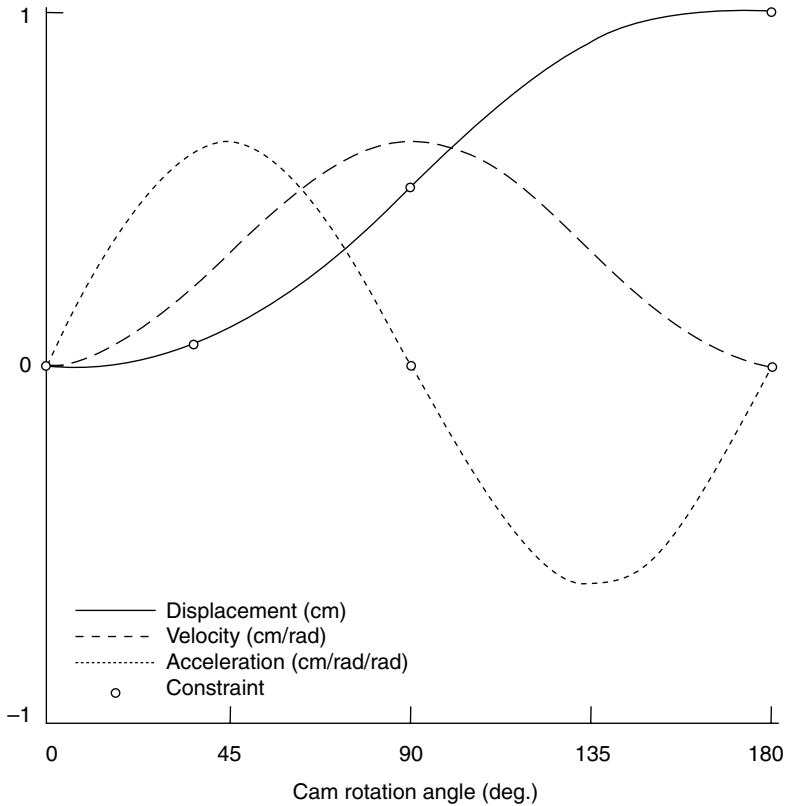
Cam angle (degrees)	Displacement (cm)	Velocity (cm/rad)	Acceleration (cm/rad/rad)
0.00	0.00	0.00	0.00
36.0	0.05	—	—
90.0	0.50	—	0.00
180.0	1.00	0.00	0.00



**FIGURE 5.1.** Cam follower displacement, velocity, and acceleration obtained by polynomial synthesis in Example 1.

are applied to a simple case. Table 5.1 contains a series of nine constraints governing the rise portion of a cam.

In applying the spline approach, B-splines of order 6 ( $k = 6$ ) defined on a knot sequence having uniform spacing were used. Since there are  $n + k$  knots, there are six knots located at  $x = 0$ , one each at  $x = 45$  deg,  $x = 90$  deg and  $x = 135$  deg, and six at  $x = 180$  deg. The results are shown in Figs. 5.1 and 5.2. At the scale plotted there is no discernable difference between the results obtained using either method.



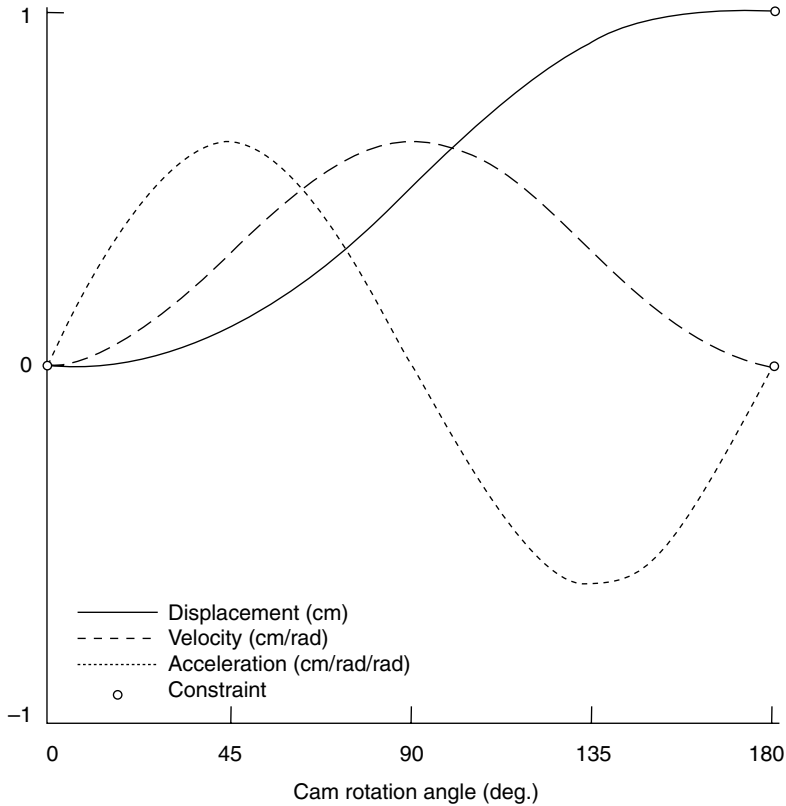
**FIGURE 5.2.** Cam follower displacement, velocity, and acceleration obtained by spline synthesis in Example 1.

**TABLE 5.2** Constraints for Example 2

Cam angle (degrees)	Displacement (cm)	Velocity (cm/rad)	Acceleration (cm/rad/rad)
0.00	0.00	0.00	0.00
180.0	1.00	0.00	0.00

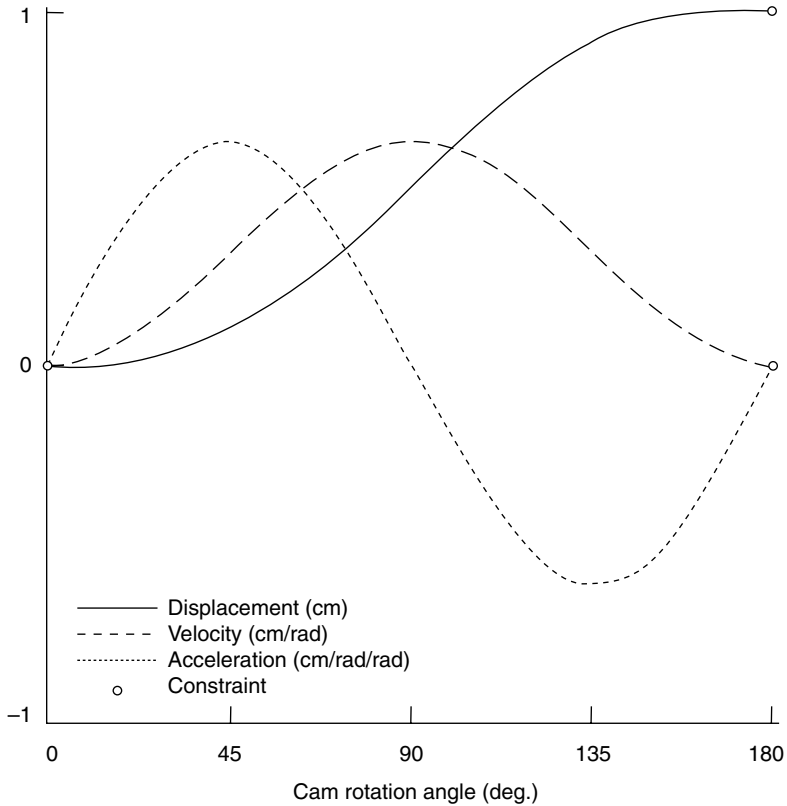
**EXAMPLE 2: A Simple Case, with Comparison to the Use of a Standard Function**

Here the spline method is used to satisfy boundary conditions that could also be satisfied by a standard (cycloidal) motion. The constraints are listed in Table 5.2. Splines of order 5 were used in this example. The results in Fig. 5.3 can be compared to standard cycloidal motion curves in Fig. 5.4. The results vary little between the two. However, since in this case splines of order 5 were used, derivatives are continuous through order 3 only.



**FIGURE 5.3.** Cam follower displacement, velocity, and acceleration obtained by spline synthesis in Example 2.

**EXAMPLE 3: A Case to Illustrate the Effects of Varying the Knot Sequence to Refine the Synthesized Motion** *In this case the constraints listed in Table 5.3 are to be satisfied in the rise portion of the cam profile. The differences between this example and the first are the displacement constraints at  $x = 36$  deg and at  $x = 90$  deg. Figures 5.5 and 5.6 show the results obtained by applying both the conventional polynomial approach and the spline method with uniform spacing of the knots, exactly as was done in the first example. In both cases all the constraints are satisfied, but there is a dip in the velocity curve and a reversal of acceleration near the end of the rise. This feature is more pronounced in the case of the polynomial function. Fig. 5.7 shows the result of adjusting the positions of the interior knots: the acceleration reversal is eliminated and the peak value of acceleration near 135 deg is reduced. If there is a rational approach to the selection of knots to achieve a specific effect in cases such as this, it has not yet been determined. However, in general, it is possible to introduce local adjustments in the synthesized cam motion by making adjustments in the knot sequence. Here, a simple trial-and-error procedure was used, and the results shown were obtained in only a few minutes. The results shown were obtained with the interior knots at  $x = 50$  deg,  $x = 95$  deg, and  $x = 100$  deg.*

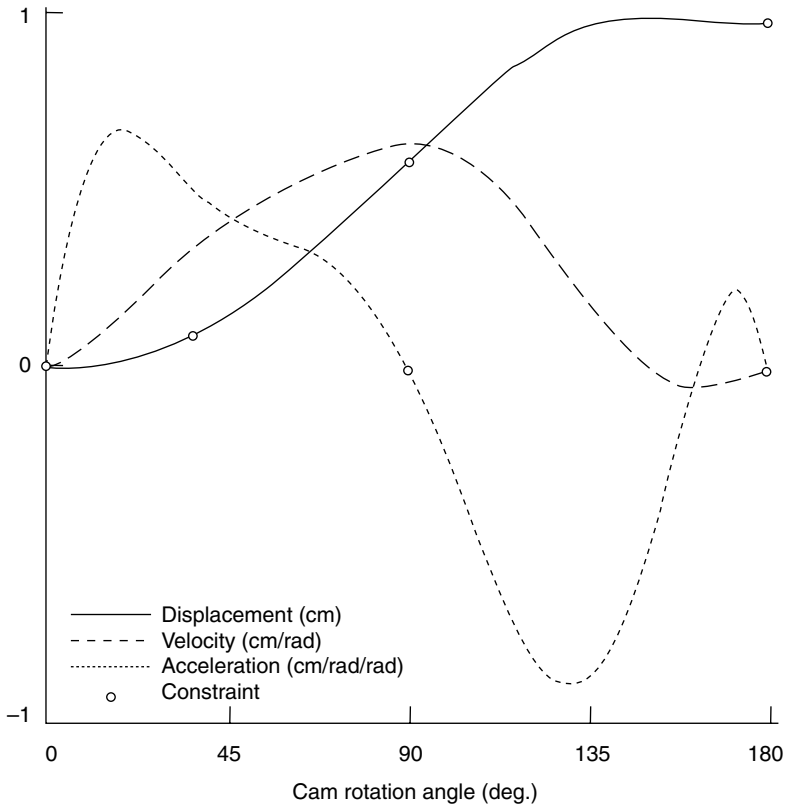


**FIGURE 5.4.** Cam follower displacement, velocity, and acceleration obtained from cycloidal motion in Example 2.

**TABLE 5.3** Constraints for Example 3

Cam angle (degrees)	Displacement (cm)	Velocity (cm/rad)	Acceleration (cm/rad/rad)
0.00	0.00	0.00	0.00
36.0	0.01	—	—
90.0	0.60	—	0.00
180.0	1.00	0.00	0.00

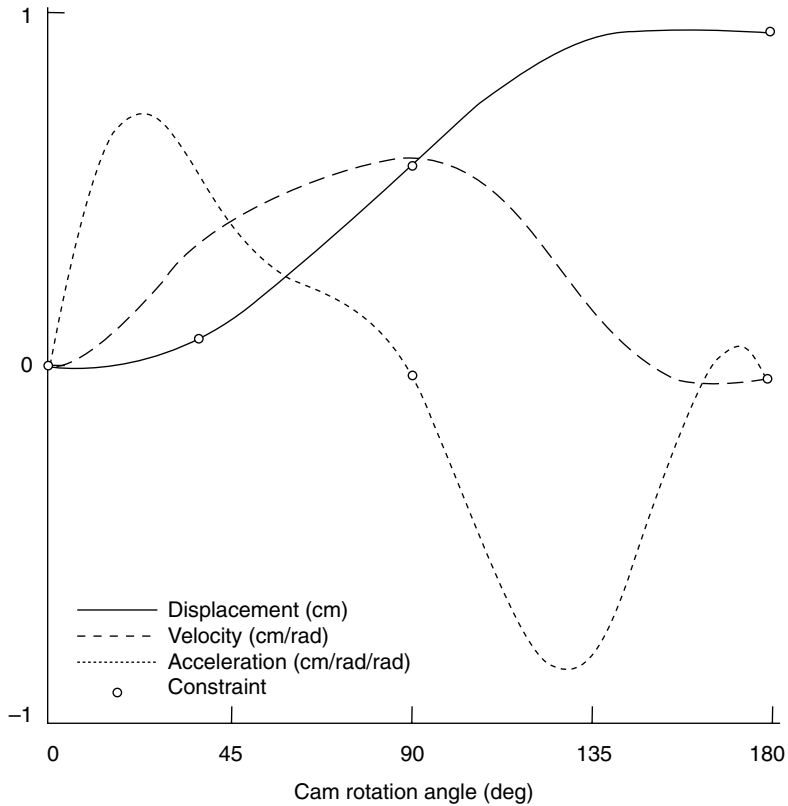
**EXAMPLE 4: A Case with a Large Number of Constraints** *In this example a total of 20 constraints has been specified. These constraints are listed in Table 5.4. The results obtained using a polynomial of degree 19 and sixth-order splines with uniform knot spacing are shown in Figs. 5.8, 5.9, and 5.10. The better characteristics of the spline function, particularly of the derivatives near the boundaries of the motion interval, are apparent. No attempt was made at further enhancement of the curves by adjusting the knot sequence.*



**FIGURE 5.5.** Cam follower displacement, velocity, and acceleration obtained by polynomial synthesis in Example 3.

Although cam synthesis problems in which the cam is constrained by the application to satisfy 20 kinematic conditions are rare, the capacity of the spline method to accommodate a large number of constraints is still important. It enables the designer to introduce constraints, in addition to those that are prescribed by the application, to obtain desirable qualitative characteristics in the follower motion. For example, it might be desired to ensure continuity of higher derivatives at the boundaries of a rise to improve the dynamic behavior (Wiederrich, 1981; Chew et al., 1983). In such a case constraints on jerk and the derivatives of jerk could be imposed at the boundary. Splines of a suitable order would have to be used, but the number of added constraints would not pose a problem. The addition of constraints to “tune” the motion to a specific need can easily yield a large array of constraints that cannot be reliably handled by other techniques.

As illustrated by the series of examples above, the spline approach to cam synthesis affords a systematic procedure that is versatile enough to accomplish many tasks that ordinarily require a variety of techniques. This approach can be conveniently used to satisfy the requirements of routine cam synthesis problems while remaining versatile enough to handle some cases that are very difficult by any other means. Implementation

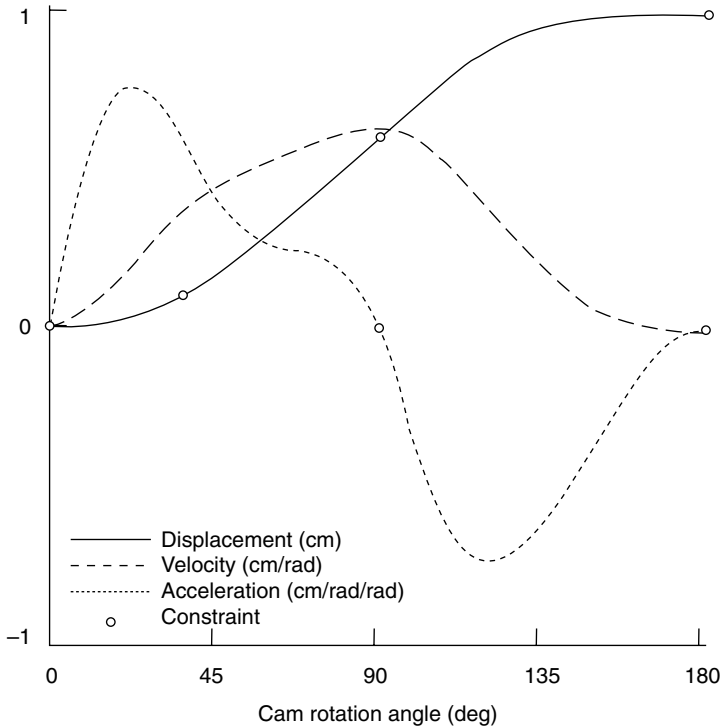


**FIGURE 5.6.** Cam follower displacement, velocity, and acceleration obtained by spline synthesis with uniform knot spacing in Example 3.

*of the computational aspects of the approach is largely procedural and can be accomplished using commonly available software to handle the major computational burden.*

### 5.3 APPLICATION OF RATIONAL B-SPLINES

Rational B-spline functions permit greater flexibility in refining motion programs than the method described above. As noted earlier, the spline method is sufficiently flexible and general to permit the motion programs to be refined or optimized while still satisfying motion constraints by adjusting certain spline function parameters that are independent of the kinematic constraints. It is with regard to this last feature of the generalized spline approach that rational B-splines offer an advantage over the methods described earlier. Rational B-splines incorporate additional function parameters and consequently offer additional degrees of design freedom. As was the case with nonrational B-splines, these parameters are independent of the motion constraints and can be controlled to refine and



**FIGURE 5.7.** Cam follower displacement, velocity, and acceleration obtained by spline synthesis with adjusted knot spacing in Example 3.

**TABLE 5.4** Constraints for Example 4

Cam angle (degrees)	Displacement (cm)	Velocity (cm/rad)	Acceleration (cm/rad/rad)
0.00	0.00	0.00	0.00
45.0	1.02	—	0.00
90.0	2.00	0.00	0.00
135.0	1.81	—	-1.17
150.0	1.61	—	—
180.0	1.00	-1.20	0.00
210.0	0.39	—	—
225.0	0.20	—	1.20
270.0	0.00	0.00	0.00

adjust motion characteristics without violating or adding to the constraints. The greater generality of this method can be easily grasped since nonrational B-splines are a special case of rational B-splines. The advantage of using rational B-splines will be illustrated in examples to follow.

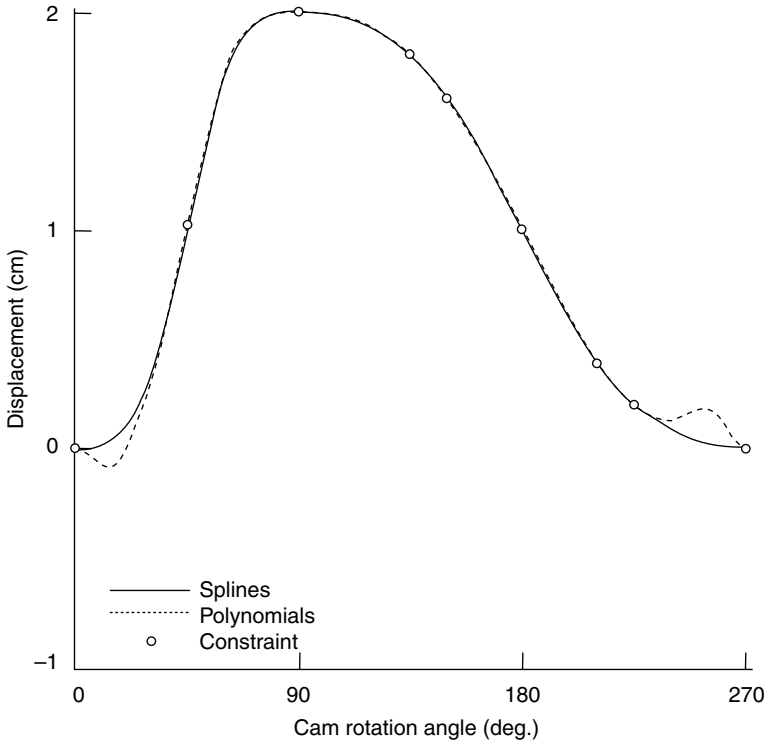


FIGURE 5.8. Comparison of the displacements obtained by both the polynomial and the spline synthesis techniques in Example 4.

**Practical Application of Rational B-Splines**

The rational B-spline method used to interpolate  $n$  motion constraints can be expressed as follows:

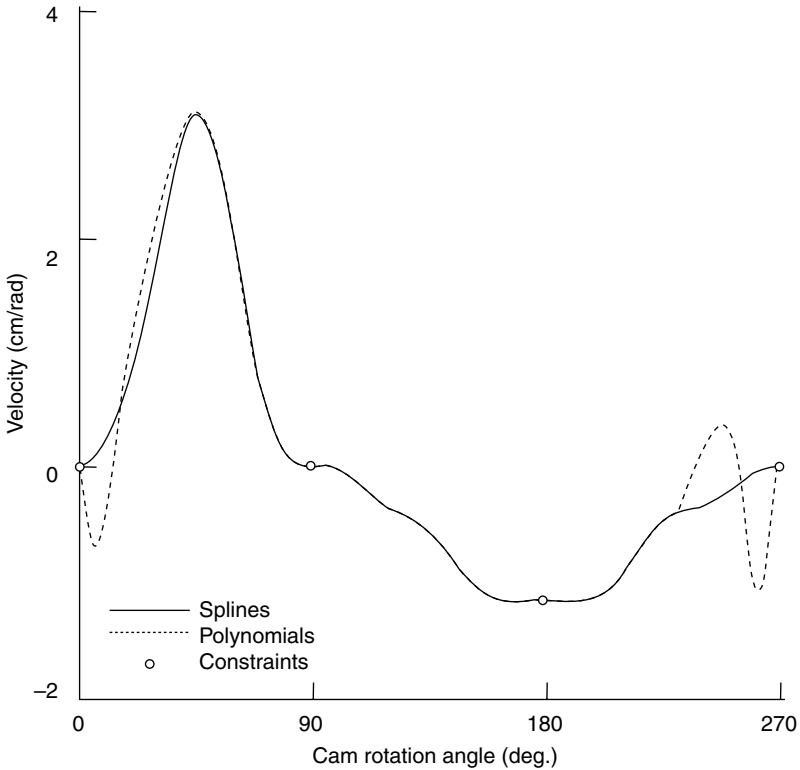
$$S(x) = \sum_{j=1}^n A_j R_{j,k}(x) \tag{5.11}$$

$$\begin{matrix} \cdot & \cdot \\ \cdot & \cdot \\ \cdot & \cdot \end{matrix}$$

$$S^{(m)}(x) = \sum_{j=1}^n S_j R_{j,k}^{(m)}(x). \tag{5.12}$$

The obvious difference between the rational B-spline method and the nonrational B-spline method is the use of rational B-spline basis functions. Therefore, the characteristics of rational B-splines and their evaluation must be addressed in detail.

**Evaluation of Rational B-Splines and Their Derivatives.** A single rational B-spline,  $R_{j,k}(x)$ , of order  $k$  is defined as follows (Versprille, 1975; Tiller, 1983):



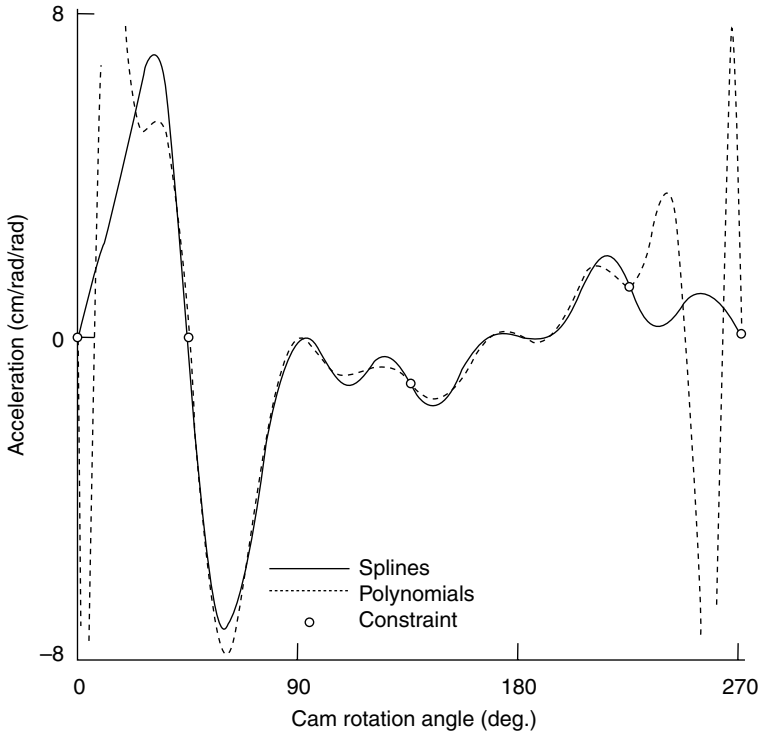
**FIGURE 5.9.** Comparison of the velocities obtained by both the polynomial and the spline synthesis techniques in Example 4.

$$R_{j,k}(x) = W_j N_{j,k}(x) / \sum_{j=1}^n W_j N_{j,k}(x) \tag{5.13}$$

where  $W_j$  is a weight sequence with positive values.

Equation (5.13) shows that a rational B-spline of order  $k$  can be obtained by modifying B-splines of order  $k$  (Versprille, 1975). Eq. (5.13) yields values of the  $R_{j,k}(x)$  for a specified order, knot sequence, and weight sequence in the domain of interest by repeatedly forming linear combinations of positive quantities.

Rational B-splines have a number of interesting properties, some of which are pertinent to the numerical procedures used in evaluating them and in applying them. The non-zero values of  $R_{j,k}(x)$  occur only on the interval  $[T_j, T_{j+k}]$  in the knot sequence. In other words, a rational B-spline of order  $k$  is non-zero only over  $k$  of the adjacent intervals between knots. A further characteristic of rational B-splines of order  $k$  is that for any given point,  $x$ , all but  $k$  adjacent  $R_{j,k}(x)$  are zero. These non-zero values of rational B-splines sum to 1 and can be written as



**FIGURE 5.10.** Comparison of the accelerations obtained by both the polynomial and the spline synthesis techniques in Example 4.

$$\sum_{j=1}^n R_{j,k}(x) = 1. \quad (5.14)$$

In Eq. (5.13), if all the  $W_j = 1$  ( $j = 1, \dots, n$ ),  $R_{j,k}(x) = N_{j,k}(x)$ , then, Eqs. (5.11) and (5.12) become the same as Eqs. (5.1) and (5.4), respectively. Adjustments to these weight values constitute the additional degrees of freedom mentioned earlier and provide additional design flexibility as well. Note that, in particular, a change in  $W_j$  affects the rational B-splines only in the interval of  $[T_j, T_{j+k}]$ . As a result, the designer can exercise local control of motion characteristics by adjusting a particular  $W_j$ . Hence, for a general case, the rational B-spline procedure permits the designer to refine the synthesized motion by adjusting the order of B-splines and the knot sequence and to exercise local control through the weight sequence, all without violating any of the motion constraints. Moreover, motion constraints can also be added or adjusted to “tune” motion programs.

When required for the equations above, derivatives of rational B-splines must be evaluated. They can be obtained by differentiating Eq. (5.13). For example, the first and the second derivatives of rational B-splines required for motion constraints of velocity and acceleration become:

$$R_{j,k}^{(1)}(x) = W_j N_{j,k}^{(1)}(x) \left/ \sum_{j=1}^n W_j N_{j,k}(x) - W_j N_{j,k}(x) \sum_{j=1}^n W_j N_{j,k}^{(1)}(x) \right/ \left/ \left[ \sum_{j=1}^n W_j N_{j,k}(x) \right]^2 \right., \quad (5.15)$$

$$R_{j,k}^{(2)}(x) = W_j N_{j,k}^{(2)}(x) \left/ \sum_{j=1}^n W_j N_{j,k}(x) - \left[ 2W_j N_{j,k}^{(1)}(x) \sum_{j=1}^n W_j N_{j,k}^{(1)}(x) + W_j N_{j,k}(x) \sum_{j=1}^n W_j N_{j,k}^{(2)}(x) \right] \right/ \left/ \left[ \sum_{j=1}^n W_j N_{j,k}(x) \right]^2 + 2W_j N_{j,k}(x) \left[ \sum_{j=1}^n W_j N_{j,k}^{(1)}(x) \right]^2 \right/ \left/ \left[ \sum_{j=1}^n W_j N_{j,k}(x) \right]^3 \right. \quad (5.16)$$

The derivatives of the B-splines required above can be evaluated using the recurrence relationships described earlier. The  $m^{\text{th}}$  derivative of rational B-splines at a given point  $x$  satisfy the following relationship:

$$\sum_{j=1}^n R_{j,k}^{(m)}(x) = 0. \quad (5.17)$$

This equation affords a convenient accuracy check when constructing the derivatives of rational B-splines.

**Implementation of the Procedure.** The systematic procedure for implementing the rational B-spline approach is very similar to the scheme for applying B-splines described earlier. The process is as follows, assuming the motion constraints have already been established:

1. Select the appropriate order of the rational B-splines to be used.
2. Choose the weight sequence.
3. Establish a knot sequence.
4. Determine the values of each rational B-spline or rational B-spline derivative at all points where motion constraints are imposed.
5. Collect the values of rational B-splines and/or rational B-spline derivatives and form a linear system of equations using the motion constraints in Eqs. (5.11) and (5.12).
6. Solve the solution of the linear system equations formed in the step above for the coefficients  $A_j$ .
7. Evaluate rational B-splines and/or their derivatives as needed to determine displacement and/or its derivatives between motion constraints using Eqs. (5.11) and (5.12).

**Example Applications.** The examples that follow illustrate the application of rational B-splines to the synthesis of the rise portion of a DRD motion program. The cases presented illustrate the effects that adjustments to the rational B-spline parameters have on the synthesized motion programs.

Note that in the cases below, normalized values for both displacement and time are used to provide a convenient basis for comparison of results. Accordingly in the examples  $S_c$  denotes a normalized value for cam displacement and  $\bar{s}$  the follower output motion dis-

placement. This expedient has no effect on the computations or conceptual basis. In practical applications, the actual displacement,  $Y$ , and its  $m^{\text{th}}$  derivative,  $Y^{(m)}$ , of the follower can be found from the normalized values as follows:

$$Y_c = S_c(\tau) \cdot h, \quad Y_c^{(m)}(x) = S_c^{(m)}(\tau) \cdot h \cdot (\omega/\beta)^{(m)}.$$

If time,  $t$ , starts at the beginning of the rise, then normalized time is  $\tau = t/T_h$ , where  $T_h$  is the total time for the rise of  $h$ .

#### EXAMPLE 5: A Simple Case Illustrating the Effect of Varying the Weight Sequence

*In this example, six boundary motion constraints for a follower system, listed in Table 5.5, are used to define a DRD motion program for a cam. With these six motion constraints, the velocities and accelerations of the cam will be continuous and will vanish at both ends of the normalized time domain. The cam profile can be determined by geometric methods (Hanson and Churchill, 1962) from the cam displacement curve and its derivatives. As described earlier, to ensure continuous cam acceleration curve, at least, cubic rational B-splines must be applied. In this example, the order  $k = 5$  is chosen so the cam has a quadratic acceleration curve. Hence, there is only one interior knot and it is placed at the midpoint of the time domain for this example. (The effect of varying knots on the B-spline method was illustrated in the earlier examples and so will not be repeated here.) To satisfy these six constraints, six rational B-splines are constructed. This is done with the three different weight sequences below to show the influence of this parameter.*

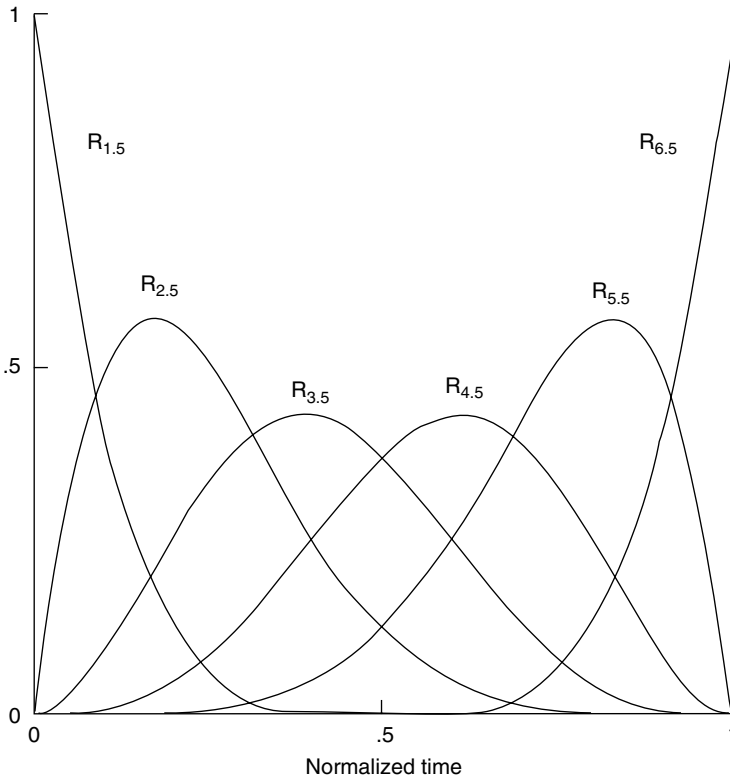
*Figures 5.11 to 5.13 show the series of rational spline functions that result from these weight sequences. Since the first sequence consists only of values of unity, the rational B-splines shown in Fig. 5.11 are identical to those that would be obtained by the B-spline method. In Fig. 5.12, the rational B-splines located in the range of  $[0.5, 1.0]$  are perturbed by the variation of  $W_6$ , which influences the basis functions constructed in the interval of  $[T_6, T_{11}]$ . This occurs, as can be seen from the equations, because the reduced value of  $W_6$  increases values for the fifth rational B-spline and decreases them for the sixth. As a result, the cam displacement and its derivatives in Figs. 5.14 to 5.16 are affected only in the range of  $[0.5, 1.0]$ . The change is small, illustrating the potential for exercising delicate local control over motion characteristics. The perturbed rational B-splines resulting from the third series of weights is shown in Fig. 5.13. Also, Figs. 5.14 to 5.16 show that the cam displacement and its derivatives are affected over the entire range  $[0.0, 1.0]$  and that these effects are much more pronounced than those of the second series of weights. The effect occurs over the entire range of motion because the affected spline functions (splines 2, 3, 4, and 5) span the entire range.*

#### EXAMPLE 6: Reduction of Peak Velocity and Acceleration by Adjusting the Weight Sequence

*Example 5 demonstrated that varying the weight sequence affects the peak values of the velocities and acceleration. The potential value of this characteristic will be shown by considering a spring-return cam-follower system in which it is desired to reduce*

**TABLE 5.5** Weight Sequences Used in Example 5

$[W]_1 = [1.0, 1.0, 1.0, 1.0, 1.0, 1.0]$
$[W]_2 = [1.0, 1.0, 1.0, 1.0, 1.0, 0.4]$
$[W]_3 = [1.0, 1.0, 1.0, 1.5, 1.0, 1.0]$

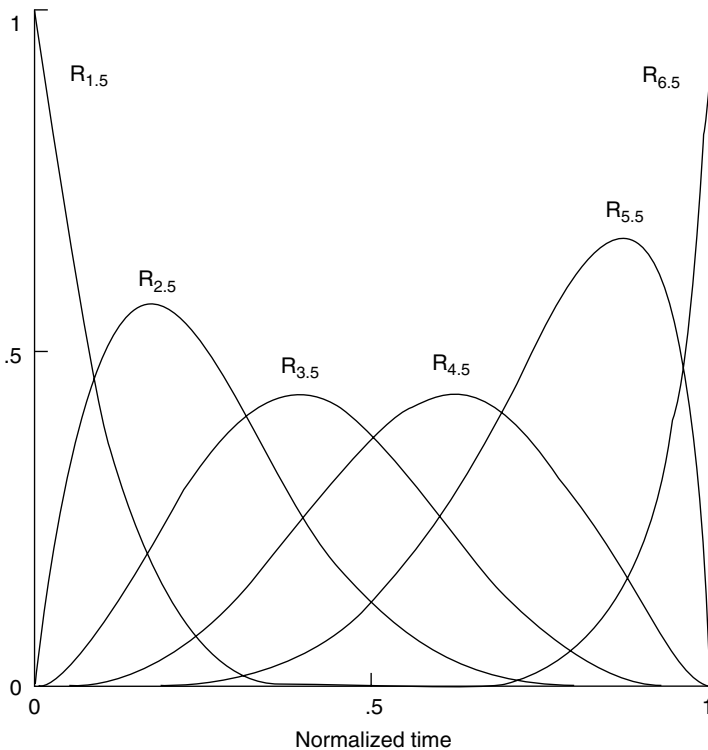


**FIGURE 5.11.** Rational B-splines ( $k = 5$ ) constructed with the weight sequence of [1, 1, 1, 1, 1, 1] in Example 5.

*the cam and follower contact forces during the rise. The following rationale was used in pursuing this end:*

1. The maximum acceleration values should be as low as possible.
2. The peak accelerations should occur early and late in the rise. The early peak will prevent simultaneous occurrence of high inertia forces and high return spring forces. The late negative peaks will occur when the return spring is compressed near its maximum and is best capable of producing the acceleration of the follower that is needed. The early and late peaks will also result in reduced magnitudes for the peak acceleration. The overall effect will be a reduction in the spring stiffness needed and an overall reduction in the contact forces.
3. The acceleration curves should remain smooth to avoid vibration problems.

*The same six motion constraints and order of the rational B-splines used for the last example are again applied. Also, the interior knot is fixed at the midpoint and only the weight sequence is adjusted to refine the synthesized motions. By maintaining a symmetrical sequence of weights, symmetrical velocity and acceleration curves are preserved. As*

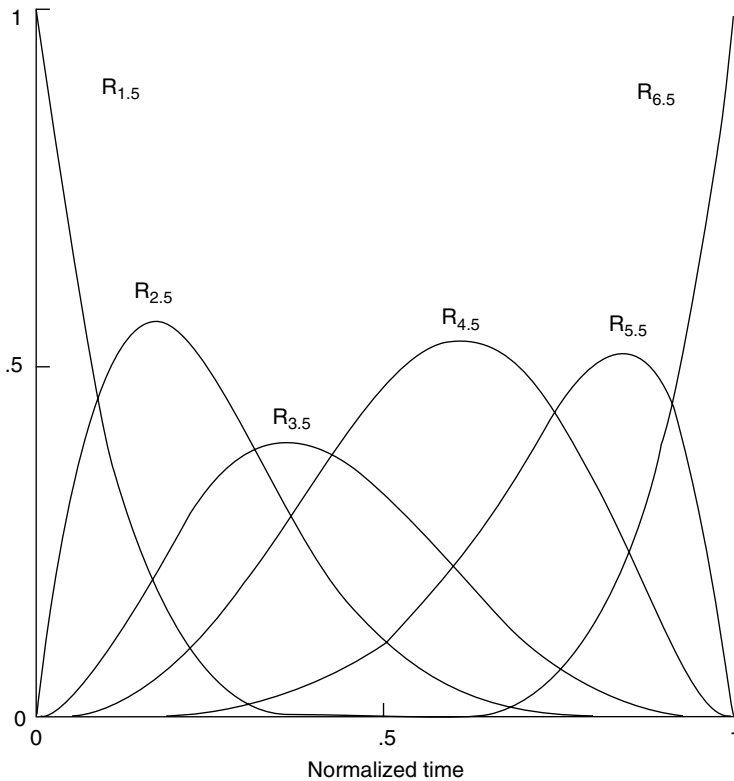


**FIGURE 5.12.** Rational B-splines ( $k = 5$ ) constructed with the weight sequence of  $[1, 1, 1, 1, 1, .4]$  in Example 5.

shown in the last example, an asymmetrical weight sequence could be used to tailor the motion for specific purpose if needed. The effects of the several different weight sequences are shown in Figs. 5.17 to 5.19. Careful consideration of the resulting contact forces could be used to refine the motion further.

**EXAMPLE 7: A Case Illustrating the Effect of Simultaneously Adjusting Both the Knot and Weight Sequences** In this example, both knots and weights will be adjusted to illustrate the flexibility of the rational spline method in refining the synthesized motion. The rise portion of a DRD motion program will be synthesized subject to the motion constraints in Table 5.6. In this example, splines of order  $k = 6$  will be used (resulting in a cubic acceleration curve) and will provide three interior knots that may be selected to adjust the synthesized motion. The different combinations of interior knots and weight sequences used in this example are listed in the table.

The kinematic properties of the synthesized motion are shown in Figs. 5.20 to 5.22. The displacement curve for the first set of spline parameters ( $[W]_1, [T]_1$ ) displays a dip near the end of the rise accompanied by a reversal in velocity and acceleration. The effect of changing the parameters is clearly indicated. The last set of parameters ( $[W]_2, [T]_2$ ) yields



**FIGURE 5.13.** Rational B-splines ( $k = 5$ ) constructed with the weight sequence of [1, 1, 1, 1.5, 1, 1] in Example 5.

**TABLE 5.6** Weight Sequences and Interior Knots Used in Example 7

$[W]_1 = [1.0, 1.0, 1.0, 1.0, 1.0, 1.0, 1.0, 1.0, 1.0]$
$[W]_2 = [1.0, 1.0, 1.0, 1.0, 0.8, 0.8, 1.2, 1.0, 1.0]$
$[T]_1 = [0.25, 0.50, 0.75]$
$[T]_2 = [0.30, 0.50, 0.55]$

much improved results in which the dip in displacement and the reversals of velocity and acceleration have all been removed. These improvements have been achieved without changing the original set of motion constraints, indicating the flexibility of the rational spline method in synthesizing motion programs for cams.

As illustrated by the foregoing examples, the rational B-spline interpolation approach to the synthesis of cam-follower motions affords a systematic procedure for cam synthesis that is versatile enough to accomplish many tasks that usually require a variety of techniques. The method is easy to apply, given algorithms to generate the rational spline values

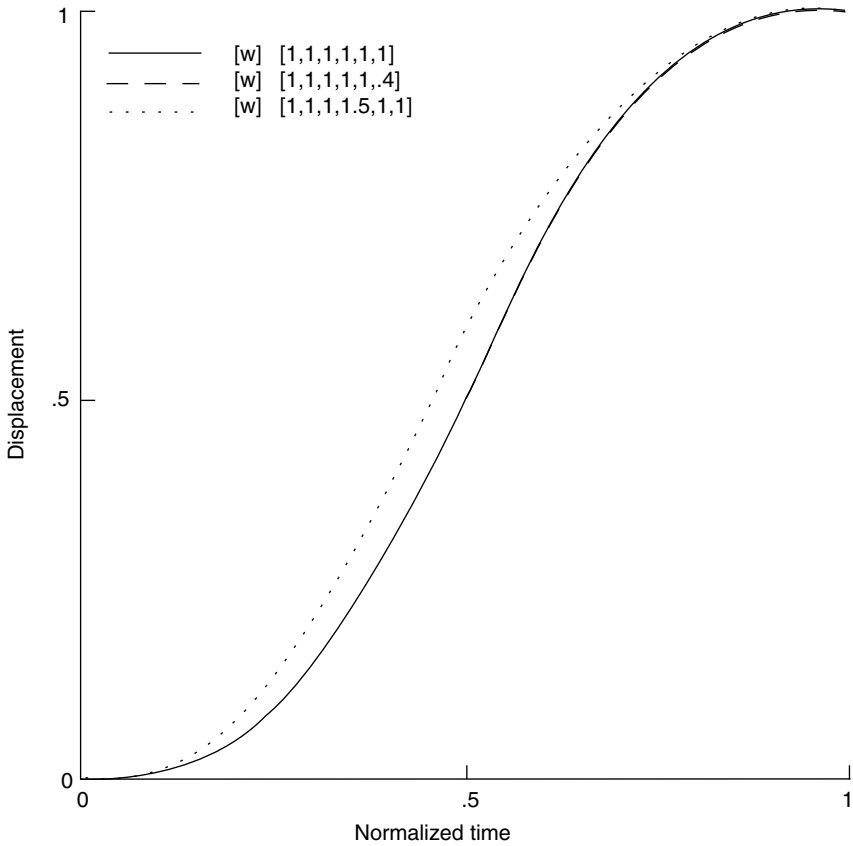


FIGURE 5.14. Comparison of cam-follower displacements in Example 5.

needed and to solve linear equations. The flexibility and versatility of the method enable the designer to refine motion programs to suit particular needs while still satisfying design constraints, without the need to disturb or add to the design constraints. The generality of the approach allows the same procedures to be applied readily to both simple and demanding cases with equal ease.

#### **5.4 SPLINE FUNCTIONS APPLIED IN THE SYNTHESIS OF NONRIGID CAM-FOLLOWER SYSTEMS**

When cams are used at high speeds and in demanding applications, the nonrigid nature of the follower sometimes must be considered. To synthesize a cam in such circumstances, the designer must do the following:

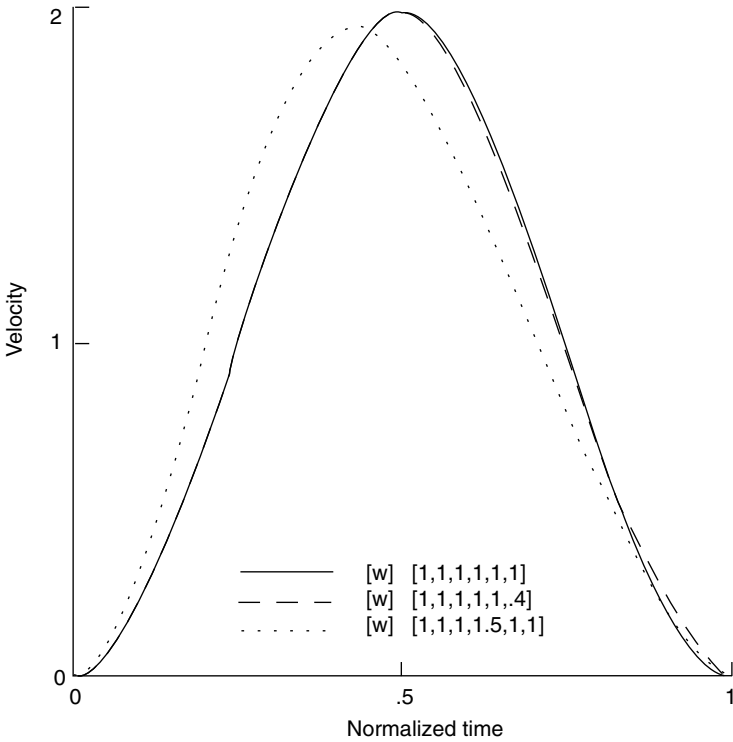


FIGURE 5.15. Comparison of cam-follower velocities in Example 5.

1. Synthesize an output motion to satisfy the kinematic constraints of the application and achieve desirable characteristics such as continuous accelerations, acceptable pressure angles, and so on.
2. Determine a cam profile that will best produce the desired output motion, considering the nonrigid nature of the follower system and the operating speed.
3. Evaluate the dynamic response of the system to assess vibration, contact force, and so forth, at the design operating speed or over a range of operating speeds.

These tasks do not constitute a sequence of steps but are functions that may have to be performed iteratively as part of the design process. Here, all three tasks are addressed by methods that can be readily integrated into a cam design procedure. To make this integrated procedure into a useful, reliable tool, it is necessary to use robust, general numerical procedures to accomplish each of these tasks.

Task 1 is accomplished conveniently by using the methods described earlier to synthesize output motions. Tasks 2 and 3 require the solution of ordinary differential equations, often a large number of times. These equations are usually stiff, making the solutions difficult and time-consuming by most methods. The approach described here uses the spline collocation method for this task. This method has proved to be efficient, effective, and nicely suited to the particular problems that occur in cam synthesis and allows the synthesis/analysis to be reduced to a systematic, general, and reliable procedure.

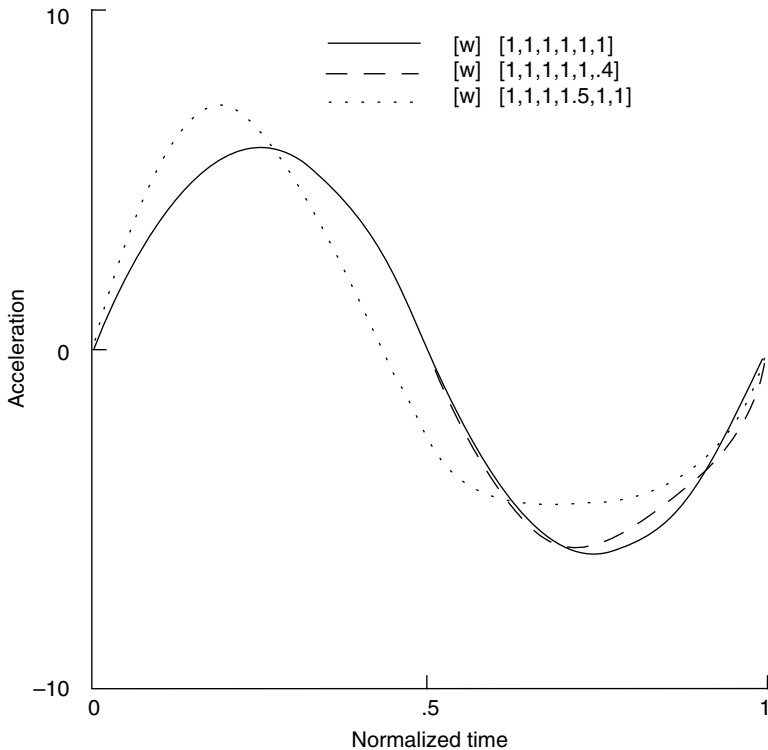


FIGURE 5.16. Comparison of cam-follower acceleration in Example 5.

### Linear Model of Single DOF System

The procedures that are described here are based on the linear, lumped parameter model shown in Fig. 5.23. It is composed of a single mass and massless springs and dampers. Such a model is usually satisfactory in addressing the dynamic effects of general cam-follower mechanisms (Barkan, 1953; Chew et al., 1983; Freudenstein et al., 1983; Kanzaki and Itao, 1972; Wiederrich and Roth, 1975). Further, follower models consisting of one or two degree-of-freedom systems will be adequate because the dynamic response of most cam-follower systems is dominated by the fundamental frequency and probably the second harmonic of the cam-follower system (Barkan, 1965). In fact, it has been shown (Koster, 1974) that a cam-follower system can be modeled by a single degree-of-freedom system without introducing significant errors if the system has a natural frequency equal to the frequency of the actual cam-follower system. As a consequence, single degree-of-freedom systems have been studied by most authors (Barkan, 1953; Chen, 1981; Chew et al., 1983; Freudenstein, 1960; Hrones, 1948; Kanesaka et al., 1978; Kanzaki and Itao, 1972; Kwakernaak and Smit, 1968; Mercer and Holowenko, 1958; Rees Jones and Reeves, 1978; Tesar and Matthew, 1976; Wiederrich and Roth, 1975) who have made general investigations of output motions or who have designed cam profiles. The general, simple model used in this work is shown in Fig. 5.23. Although it will not be explained here, the single degree-of-freedom can be extended to include nonlinear Coulomb friction damping

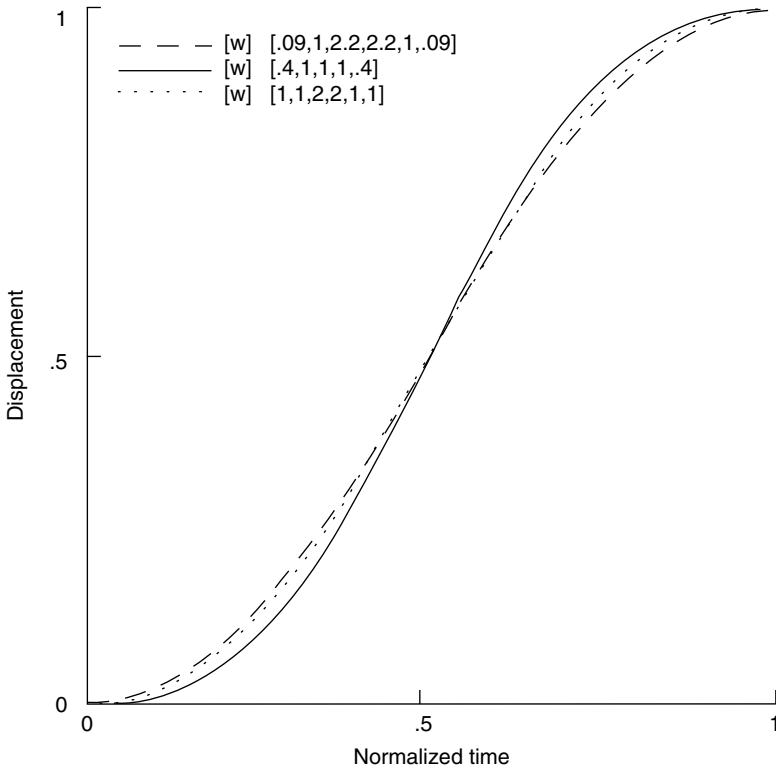


FIGURE 5.17. Comparison of cam-follower displacements in Example 6.

(Wiederrich, 1981; Rooney and Deravi, 1982). Multiple degree-of-freedom and combined lumped/distributed parameter models have been investigated for certain specific cam-follower mechanisms (Akiba et al., 1981; Chan and Pisano, 1987; Kosugi and Seino, 1986; Hanachi and Freudenstein, 1986; Pisano and Freudenstein, 1983). In the model described here, the cam and the camshaft operate at constant speed and are assumed to be rigid components so the cam contour and the camshaft are unaffected by the forces acting on them. It is also assumed that the cam is manufactured with precision so that machining errors can be neglected and that the spring will always prevent separation of the follower from the cam. Further, the effects of frictional forces are neglected.

**Output Motion and Cam Motion**

*Equations of Motion.* In the following discussions, the displacement,  $Y$ , and its derivatives will be referred to as the output motion. The displacement,  $Y_c$ , and its derivatives which define the cam pitch curve will be referred to as the cam motion. Correspondingly,  $Y_c^{(1)}$ , is referred to as the cam velocity,  $Y_c^{(2)}$ , the cam acceleration, etc. The equation of motion of the model of Fig. 5.23, written in terms of these variables, is as follows:

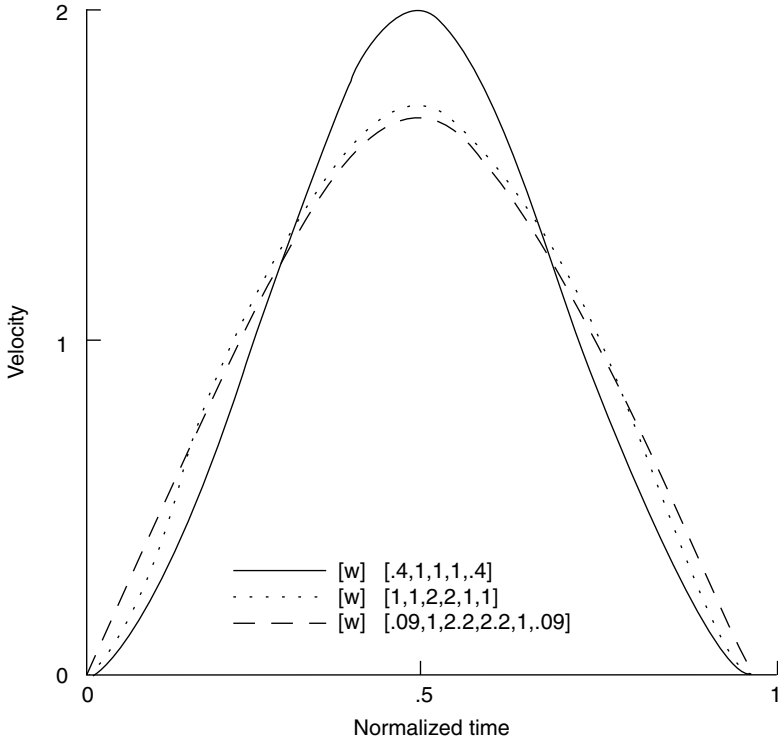


FIGURE 5.18. Comparison of cam-follower velocities in Example 6.

$$MY^{(2)}(t) + (C_s + C_f)Y^{(1)}(t) + (K_s + K_f)Y(t) = C_f Y_c^{(1)}(t) + K_f Y_c(t). \quad (5.18)$$

If the contact force is of interest it can be found easily. In the case of a flat-faced follower with a pre-load,  $F_p$ , the contact force,  $F_c$ , is given as:

$$F_c = C_f(Y_c^{(1)} - Y^{(1)}) + K_f(Y_c - Y) + F_p. \quad (5.19)$$

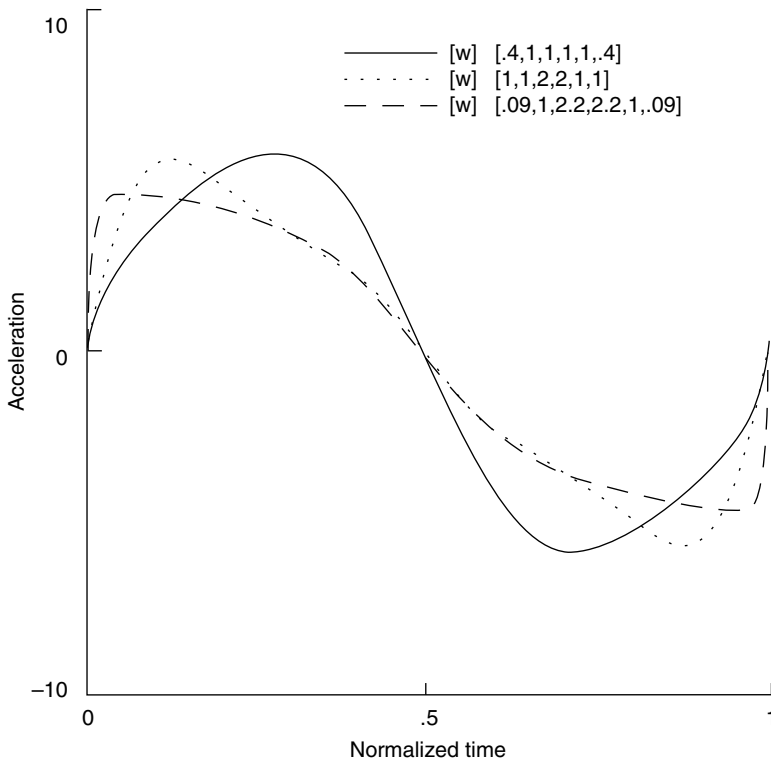
If, in Eq. (5.18), the damping,  $C_f = 0$  (the limiting case), then the cam displacement curve,  $Y_c(t)$ , can be arithmetically determined from the synthesized output motion. The quantity  $Y_c(t)$  can be found for this case as:

$$Y_c = [MY^{(2)} + C_s Y^{(1)} + (K_s + K_f)Y] / K_f. \quad (5.20)$$

Here, the contact force can be expressed as:

$$F_c = MY^{(2)} + C_s Y^{(1)} + K_s Y + F_p. \quad (5.21)$$

**Motion Constraints.** In defining a DRD output motion, the kinematic constraints must first be decided. These constraints would be determined both by the specific requirements of the application and by general requirements for good dynamic behavior. For example, the application itself may require only that several displacement constraints be satisfied.



**FIGURE 5.19.** Comparison of cam-follower acceleration in Example 6.

However, for the physical device to perform well dynamically it will probably be necessary to control velocities, accelerations, etc., at the boundaries. Also, from Eq. (5.20), note that if the displacement is differentiated twice, it is apparent that the acceleration of the cam,  $Y_c^{(2)}$  is governed by the second, third, and fourth derivatives of the output motion. Therefore, to ensure continuous first and second derivatives of the cam motion,  $Y_c$ , the following ten boundary constraints for the output motion must be imposed (Chew et al., 1983; Wiederrich, 1981):

$$\text{at } \tau = 0, Y = 0, Y^{(1)} = 0, Y^{(2)} = 0, Y^{(3)} = 0, Y^{(4)} = 0$$

$$\text{at } \tau = 1, Y = h, Y^{(1)} = 0, Y^{(2)} = 0, Y^{(3)} = 0, Y^{(4)} = 0.$$

Here  $\tau$  is the normalized time ( $0 \leq \tau \leq 1$ ), as defined earlier. Continuous cam motion acceleration is needed to improve the vibrational behavior of the follower. Boundary conditions for the cam profile curve that correspond to the above boundary conditions of the output motion are:

$$\text{at } \tau = 0, Y_c = 0, Y_c^{(1)} = 0, Y_c^{(2)} = 0,$$

$$\text{at } \tau = 1, Y_c = h(K_s + K_f)/K_f, Y_c^{(1)} = 0, Y_c^{(2)} = 0.$$

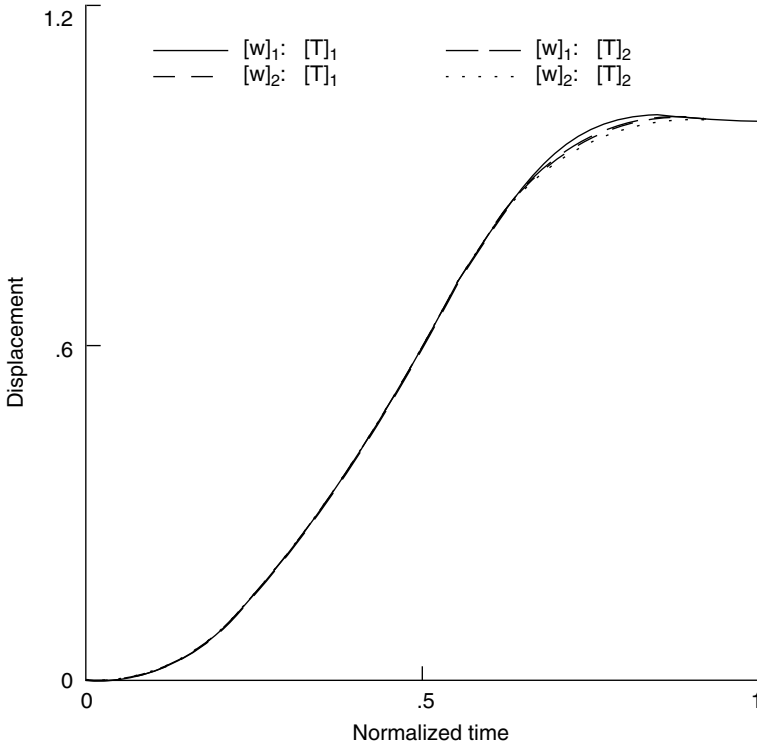


FIGURE 5.20. Comparison of cam-follower displacements in Example 7.

It is obvious, given the conditions above, that velocities and accelerations of the cam will be zero at both ends of the rise. As mentioned, additional kinematic constraints could be added to the output motion specification either to refine the output motion or to satisfy specific design requirements.

Again, in the cases that follow, normalized values for both displacements and time have been used to provide a convenient basis for comparison of results.

**Cam Motion in the General Model.** As mentioned earlier, if the damper,  $C_f$  is neglected, the cam motion can be determined from the output motion by geometric methods (Hanson and Churchill, 1962). However, when  $C_f$  is present, Eq. (5.18) becomes a first-order differential equation that must be solved to obtain the cam displacement,  $Y_c$ . The exact solution of this equation with the initial condition,  $S_c = 0$  at  $\tau = 0$ , is as follows:

$$S_c(\tau) = S_c(0)e^{-A\tau} + \left[ \frac{h/h_c/C_f}{(\omega_d/\beta)} e^{-A\tau} \right] \int_0^1 e^{A\lambda} \left[ M(\omega_d/\beta)^2 S''(\lambda) + (C_f + C_s)(\omega_d/\beta) S^{(1)}(\lambda) + (K_f + K_s)S(\lambda) \right] d\lambda \quad (5.22)$$

where  $A = K_f/C_f/(\omega/\beta)$  and  $\lambda =$  dummy variable for  $\tau$ .

Calculation of the exact solution above will often be difficult because  $S^{(2)}$ ,  $S^{(1)}$ , and  $S$  are complicated functions. As a result the integration required for each function becomes very time-consuming.

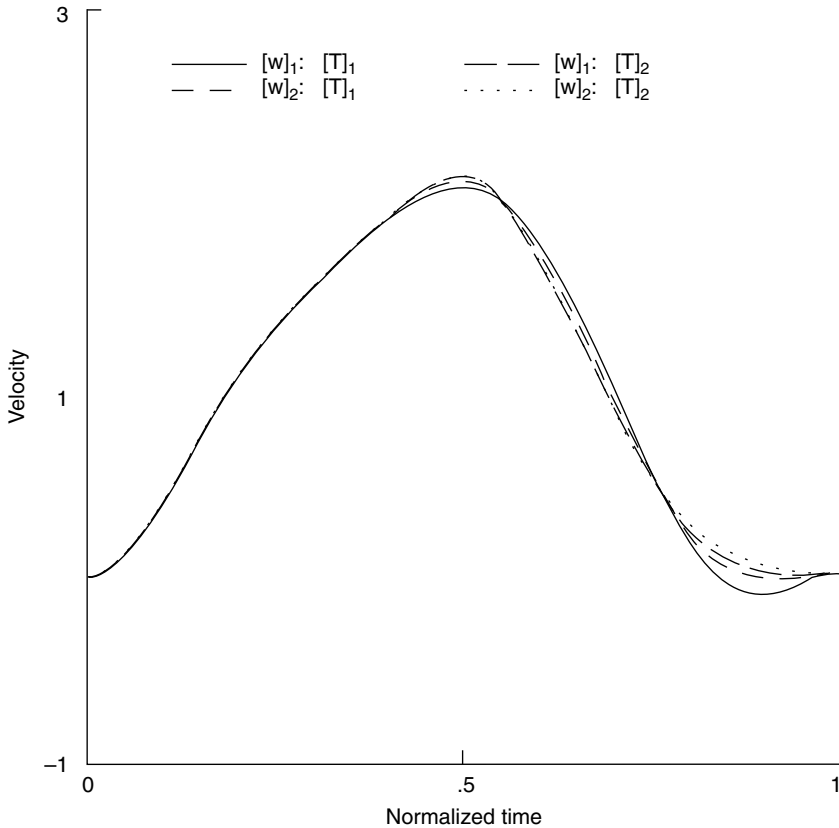


FIGURE 5.21. Comparison of cam-follower velocities in Example 7.

An alternative is to find a numerical procedure that will approximate the solution to Eq. (5.22), subject to the boundary conditions from the output motion. These boundary conditions result from the ten conditions listed earlier plus any additional ones that come from the applications. By considering the original ten constraints, the following conditions on the cam motion are obtained:

$$\begin{aligned}
 S_c^{(1)}(0) + (K_f/C_f/(\omega_d/\beta))S_c(0) &= 0 \\
 S_c^{(2)}(0) + (K_f/C_f/(\omega_d/\beta))S_c^{(1)}(0) &= 0 \\
 S_c^{(3)}(0) + (K_f/C_f/(\omega_d/\beta))S_c^{(2)}(0) &= 0 \\
 S_c^{(1)}(1) + (K_f/C_f/(\omega_d/\beta))S_c(1) &= S(1)h(K_s + K_f)/h_c/C_f/(\omega_d/\beta) \\
 S_c^{(2)}(1) + (K_f/C_f/(\omega_d/\beta))S_c^{(1)}(1) &= 0 \\
 S_c^{(3)}(1) + (K_f/C_f/(\omega_d/\beta))S_c^{(2)}(1) &= 0.
 \end{aligned} \tag{5.23}$$

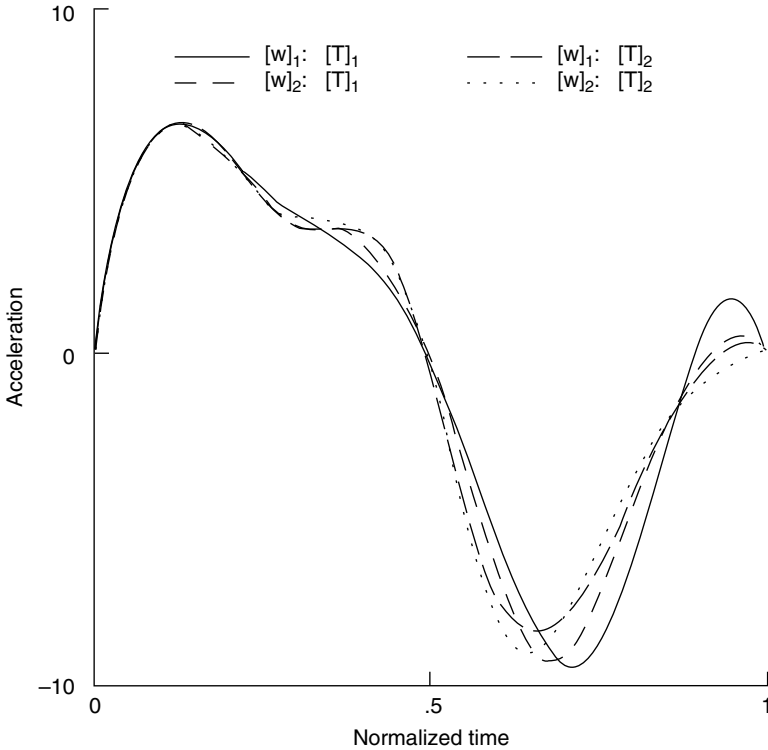


FIGURE 5.22. Comparison of cam-follower accelerations in Example 7.

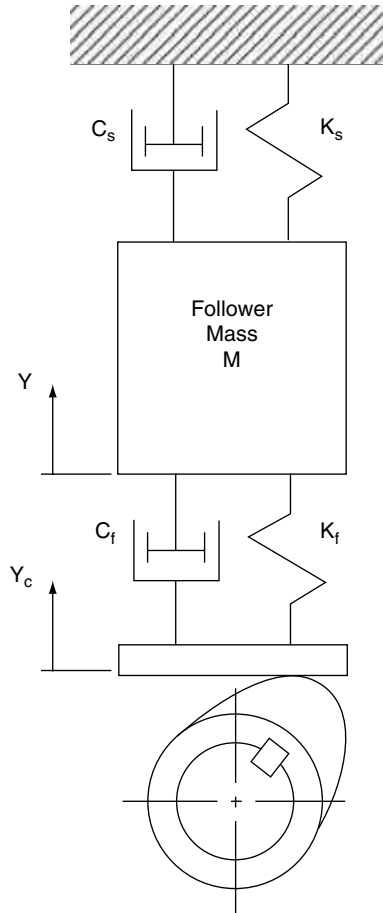
Since the rise portion of a DRD motion has  $S_c = 0$  at  $\tau = 0$ , the first three boundary conditions readily yield  $S_c(0) = 0$ ,  $S_c^{(1)}(0) = 0$ ,  $S_c^{(2)}(0) = 0$ , and  $S_c^{(3)}(0) = 0$ . These four simple boundary conditions at  $\tau = 0$ , the three remaining boundary conditions at  $\tau = 1$ , and additional ones from the applications must be satisfied when the cam displacement is found by a numerical approach.

To obtain a solution for  $S_c$  the cam rise,  $h$ , must be known. If the damper,  $C_f$ , is not present,  $h_c$  can be found directly by imposing the output motion constraints on Eq. (5.18). However, if  $C_f$  is present,  $h_c$  cannot be found so easily. Application of the boundary condition,

$$S^{(1)}(1) + (K_f/C_f)/(\omega_d/\beta)S_c(1) = S(1)h(K_s + K_f)/h_c/C_f/(\omega_d/\beta) \tag{5.24}$$

fails because  $S^{(1)}(1)$  is unknown. To overcome this difficulty, an iterative approach can be used. The value of  $h_c$  can be first approximated by  $h_c/h/(K_f + K_s)/K_f$  and then can be iteratively adjusted until the solution of the first order differential Eq. (5.18) yields the normalized value of  $S^{(1)}(1) = 1$ . A suitable value can usually be found in around a dozen iterations.

The spline procedure used for the interpolation of the kinematic constraints to yield output motion programs described previously can be used here as well.



**FIGURE 5.23.** System model for nonrigid follower.

### ***Cam Motion and Dynamic Behavior***

*Spline Collocation Method for the Solution of Differential Equations.* As indicated earlier, it is necessary to solve ordinary differential equations to investigate the follower motion and to find the cam motion. The method of collocation has been found to work very well in this application. The method has been explored by a number of authors (Ascher et al., 1979; Ascher, 1980; de Boor and Swartz, 1973; Carey and Finlayson, 1975; Cerutti, 1974, Russell and Shampine, 1972; Russell, 1974 and 1977). It is based on the simple concept that the solution of the differential equation can be represented as a linear combination of known functions. In forming the linear combination, coefficients are determined such that prescribed initial or boundary conditions together with the differential equation itself are satisfied at a series of points (the collocation points) on the range of interest.

Methods of this type have generally been used for boundary value problems because of the effort that is normally required to solve such equations by other means. The method is also applicable to initial value problems when the more usual explicit methods run into stability difficulties such as in cases involving stiff equations. Various suggestions for using

higher order implicit methods for stiff equations have been made in an effort to avoid step size limitations due to stability considerations. Both collocation and the implicit Runge-Kutta (Butcher, 1964) methods have been investigated for such cases (Wright, 1970).

It has been shown that the collocation method for the general first-order system yields results that are equivalent to those obtained by implicit Runge-Kutta methods (Weiss, 1974; Wright, 1970). However, the ease and generality of application of the collocation method make it very suitable for practical, difficult (stiff) ordinary differential equations (Shampine and Gear, 1979; Hulme and Daniel, 1974). Further, the solution requires only algebraic operations to find the unknown coefficients. In addition, for higher order differential equations the solution can be obtained without reducing the equation to a system of first-order equations (Cerutti, 1974).

In applying the method the domain of interest is divided into small elements (subdomains). Also it has been suggested that the roots (Gaussian points) of the  $P^{\text{th}}$  Legendre orthogonal polynomial be chosen as  $p$  collocation points within each of these elements (de Boor and Swartz 1973; Stroud and Secrest, 1986). When this is done, the resulting global truncation error in the solution of a  $q^{\text{th}}$  order differential equation will be of order  $O(\delta^{p+q})$ , where  $\delta$  is the maximum length of an element. At the ends of each element, the approximation solution and its first  $q - 1$  derivatives have errors of order  $O(\delta^{2p})$ .

As is the case in the synthesis of output motions, B-splines are used as the known functions. Evaluation of B-splines and their derivatives, using recurrence relations was discussed earlier. Because both the spline interpolation used in the output motion synthesis and spline collocation use B-splines as basis functions and because both require the solution of linear systems, much of the same software can be used for both procedures. In the collocation procedure, the solution ( $U(\tau)$ ) of a general differential equation is represented as a linear combination of B-splines, written as follows:

$$U(\tau) = \sum_{j=1}^n A_j N_{j,k}(\tau). \quad (5.25)$$

It is obvious that these expressions for the solution of a differential equation are similar to those of the spline interpolation procedure described earlier. The procedure for applying the spline collocation method to the solution of differential equations is very simple and is described in the following outline:

1. Discretize the domain of interest of the differential equation into  $e$  subdomains (elements). In each element,  $p$  Gaussian points are chosen as collocation points. The  $p$  Gaussian points in each element are the roots of the  $p^{\text{th}}$  orthogonal Legendre polynomial. Not including initial or boundary conditions, there are  $p \cdot e$  collocation points on the range of the differential equation.

2. Establish the knot sequence at both ends ( $\tau = 0$  and  $\tau = 1$ ) of the domain and at the ends of the  $e$  elements above. Following de Boor (1978), the knots at  $\tau = 0$  and at  $\tau = 1$  are repeated  $k$  times for a B-spline of order  $k$ . Also, at the ends, mesh points (not including points at  $\tau = 0$  and  $\tau = 1$ ) of each element have the knots repeated  $p$  times for  $p$  Gaussian points. Hence, there are a total of  $2k + p(e - 1)$  knots. For  $q$  conditions (initial or boundary) and  $p \cdot e$  collocation points to be satisfied,  $n$  B-splines are required and  $n = q + p \cdot e$ . The order of B-splines equals  $q + p$ . In addition, the number of knots,  $2k + p(e - 1)$ , equals  $k + n$ .

3. Determine the values of each B-spline and its derivatives at the points where conditions are given and at collocation points.

4. Formulate a linear system of equations that can be solved for the coefficients  $A_j$  in Eq. (5.25). For example, the differential equation  $ax''(\tau) + bx'(\tau) + cx(\tau) = F(\tau)$  with

boundary conditions  $x(0) = F_1$  and  $x'(1) = F_r$  is expressed, not including boundary conditions, using Eq. (5.25), as:

$$a \sum_{j=1}^n A_j N_{j,k}^{(2)}(\tau_i) + b \sum_{j=1}^n A_j N_{j,k}^{(1)}(\tau_i) + c \sum_{j=1}^n A_j N_{j,k}(\tau_i) = F(\tau_i) \tag{5.26}$$

where  $j = 1, \dots, n$  and  $i = 2, \dots, n - 1$ .

These two boundary conditions are satisfied by:

$$\sum_{j=1}^n A_j N_{j,k}^{(1)}(0) = F_1 \quad \text{and} \quad \sum_{j=1}^n A_j N_{j,k}^{(1)}(1) = F_r. \tag{5.27}$$

5. Collect the values of initial or boundary conditions  $F_j$ , ( $j = 1, \dots, n$ ) and the differential equation at collocation points, and form the linear systems of equations, in terms of the unknowns,  $A_j$  as follows (and as done earlier):

$$\begin{aligned} A_1 E_{1,1} + A_1 E_{1,2} + \dots + A_n E_{1,n} &= F_1 \\ \vdots & \\ A_1 E_{n,1} + A_2 E_{n,2} + \dots + A_n E_{n,n} &= F_n. \end{aligned} \tag{5.5, repeated}$$

Combine the equations above for the coefficients  $E_{i,k}$  ( $i, j = 1, n$ ). The first subscript identifies the initial or boundary condition or the collocation point, and the second identifies the spline. Written, in matrix notation, the system of equations above becomes

$$[E][A] = [F]. \tag{5.6, repeated}$$

6. Solve the system of equations above for the coefficients,  $A_j$ .

7. Evaluate the B-splines or their derivatives as needed to determine cam displacement and vibrational responses between collocation points.

*Dynamic Response of the Follower System.* Regardless of the precision of manufacture some departure of the actual output motion of a cam-follower system from the ideal will occur. The departure is likely to be of most concern in demanding applications in which the cam operates at high speed. The analysis given here addresses the vibrational responses of the follower system as the cam drives it.

During the rise portion of the output motion response a transient vibrational response exists. This response will be referred to as the primary vibration. This vibration may persist into the dwell phase that follows the rise. Additionally, the transient from the rise to the dwell may induce a response during the dwell. The departure from the ideal dwell will be referred to as the residual vibration. The severity of the vibration is of concern to the designer because the amplitude and intensity of the vibration produce impact, noise, wear, and potential damage to the follower system and the cam.

For calculating vibrational responses, the deviation,  $r$ , and its derivatives relative to its static equilibrium position are defined as follows (Wiederrich and Roth, 1975):

$$r = Y - Y_c K_f / (K_s + K_f) \tag{5.28}$$

$$r^{(1)} = Y^{(1)} - Y_c^{(1)} K_f / (K_s + K_f) \tag{5.29}$$

$$r^{(2)} = Y^{(2)} - Y_c^{(2)} K_f / (K_s + K_f) \tag{5.30}$$

Substituting Eqs. (5.28) to (5.30) into Eq. (5.18) with normalized values and replacing  $d^{(1)}$  by  $d' \omega$  and  $d^{(2)}$  by  $d'' \omega^2$ , the following vibrational response equation can be obtained:

$$\begin{aligned}
 d'' + d'(C_s + C_f)/(M\omega) + d(K_s + K_f)/(M\omega^2) &= -S_c^{(2)}h_c\omega_d^2K_f / \\
 (K_f + K_s)/\omega^2/\beta^2 - S_c^{(1)}h_c\omega_d & \\
 [K_f(C_s + C_f)/(K_s + K_f) - C_f]/(M\omega^2)/\beta. &
 \end{aligned} \tag{5.31}$$

Here initial conditions at the start of the rise are taken as  $d = 0$  and  $d' = 0$ .

If the cam-follower system is free from damping, then in terms of the synthesized output motion Eq. (5.31) becomes:

$$\begin{aligned}
 d'' + d(K_s + K_f)/(M\omega^2) &= -S^{(4)}(hM)(\omega_d/\beta)^4/(K_s + K_f)/\omega^2 \\
 - S^{(2)}(h/\omega^2)(\omega_d/\beta)^2. &
 \end{aligned} \tag{5.32}$$

It is obvious from Eq. (5.31) that the vibrational response is governed by the cam velocity and acceleration if the parameters for mass, springs, and dampers are fixed. Here,  $S_c^{(1)}$  and  $S_c^{(2)}$  are determined from the synthesized output motion based on the design speed  $\omega_d$  and cam angle  $\beta$ . The solution of Eq. (5.31) yields the primary vibration at any rotational speed  $\omega$ . As for residual vibration (when  $\tau > 1$ ), the right-hand side of Eq. (5.31) disappears. Therefore, from the homogeneous solution of Eq. (5.31) the amplitude of the residual vibration at any rotational speed  $\omega$  can be found as:

$$|d| = \left\{ d^2(1) + [d'(1)\omega + d(1)\xi\omega_n]^2 / (\omega_n\sqrt{1-\xi^2})^2 \right\}^{1/2} \tag{5.33}$$

where:

$\omega_n$  = the natural frequency of the cam-follower system,  $(\omega_n = \sqrt{(K_s + K_f)/M})$  and  $\xi$  = the damping ratio,  $(\xi = 0.5(C_s + C_f)/M/\omega_n)$ .

When the cam is rotating at the frequency of  $\omega = \omega_d/\beta$  the values of  $d(1)$  and  $d'(1)$  ( $\tau = 1$ ) in Eq. (5.32) will vanish and the amplitude of the residual vibration becomes zero. To assess vibrational responses, both primary and residual vibrations can be examined in a form of response spectrum for each synthesized output motion (Chen, 1981 and 1982; Mercer and Holowenko, 1958; Rees Jones and Reeves, 1978; Neklutin, 1954). The vibrational characteristic for the camshaft at various rotational speeds can be observed from the response spectrum even though the output motion is synthesized for the camshaft at a constant speed,  $\omega_d$ .

#### Example Application

**Example 8: Synthesis of Cam Motion with Nonrigid Follower** *An example application is provided here to illustrate the mechanics of applying the procedure described earlier. A DRD motion is synthesized using the spline interpolation procedure. The dynamic behavior of the follower system is then investigated and the cam motion is found using the spline collocation procedure. In preparing this example a case was selected from the literature for which a cam had been designed using an optimized polynomial (Peisakh, 1966; Chen, 1981). The solution obtained using the optimized polynomial gives a convenient basis for evaluating the performance of the methods described here, at least for one case. The results shown were refined iteratively by trying a total of ten different combinations of spline parameters and sets of constraints. Space limitations prevent the presentation of all the iterations; however, it should be clear that the procedures being used allow great freedom in specifying motion constraints and can easily evaluate the effects of changing these constraints and of altering the spline parameters.*

*In this example, each step of the process is illustrated even though some of the operations can be easily reduced to an algorithm and eliminated as a concern to the*

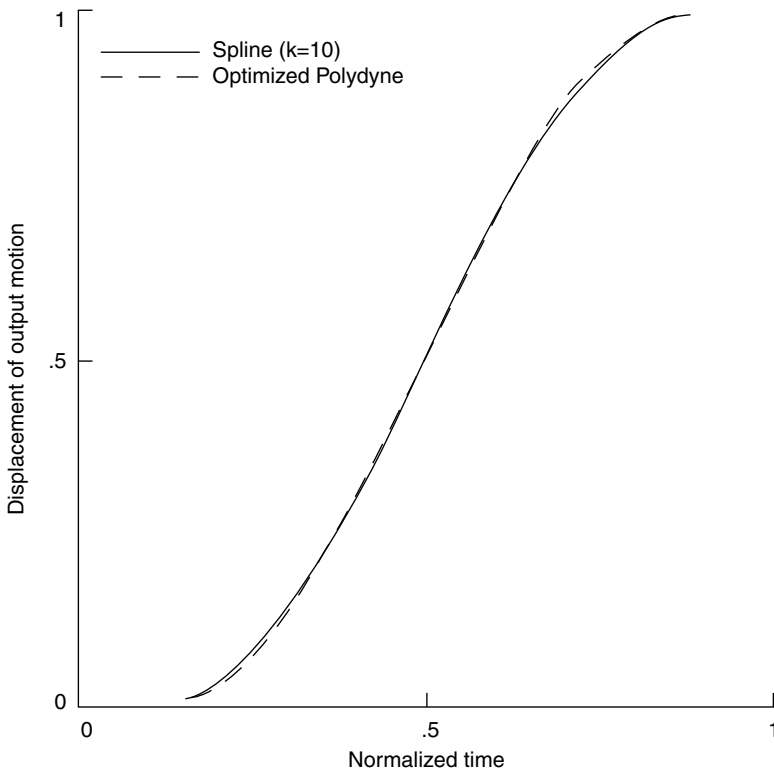
designer. For instance, selection of the collocation points is readily automated. Such operations are described in the example, however, for the sake of thoroughness.

**Synthesis of the Output Motion** In this illustration the basic goal is to satisfy the ten basic constraints at  $\tau = 0$  and at  $\tau = 1$  in the list of constraints that follows. These constraints are the primary design constraints. The two additional constraints at  $\tau = 0.5$  were added in the iterative process to refine the motion somewhat.

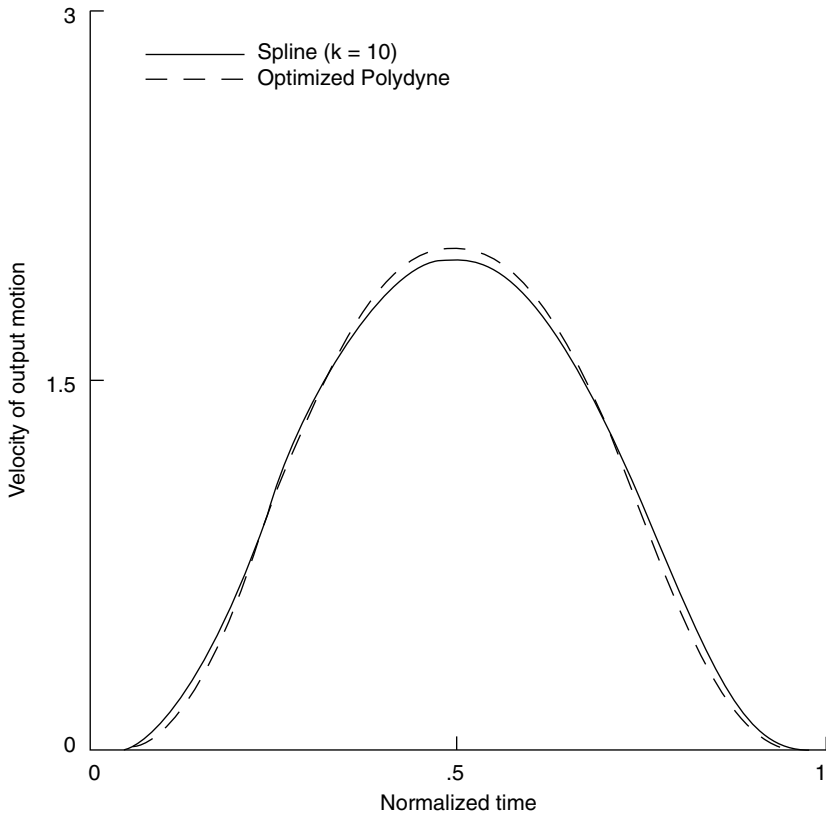
Since the degree of the spline curve is  $k - 1$ , splines of order  $k = 6$  are required for  $S^{(4)}$  to be continuous. It is necessary to achieve this continuity if the constraints on  $S^{(4)}$  are to be satisfied, as they must be if continuous cam acceleration is to be obtained.

The output motion that is synthesized using spline functions is shown in Figures 5.24 to 5.28 and compared to the motion produced by the optimized polynomial.

**Collocation Solution of the Differential Equations** To solve the differential Eqs. (5.18) and (5.31) for the cam displacements and for vibrational responses, the normalized time domain ( $\tau$ ) is divided into sixteen equal elements ( $e = 16$ ) and in each element four Gaussian points ( $p = 4$ ) are located. Both the number of elements used and the choice of



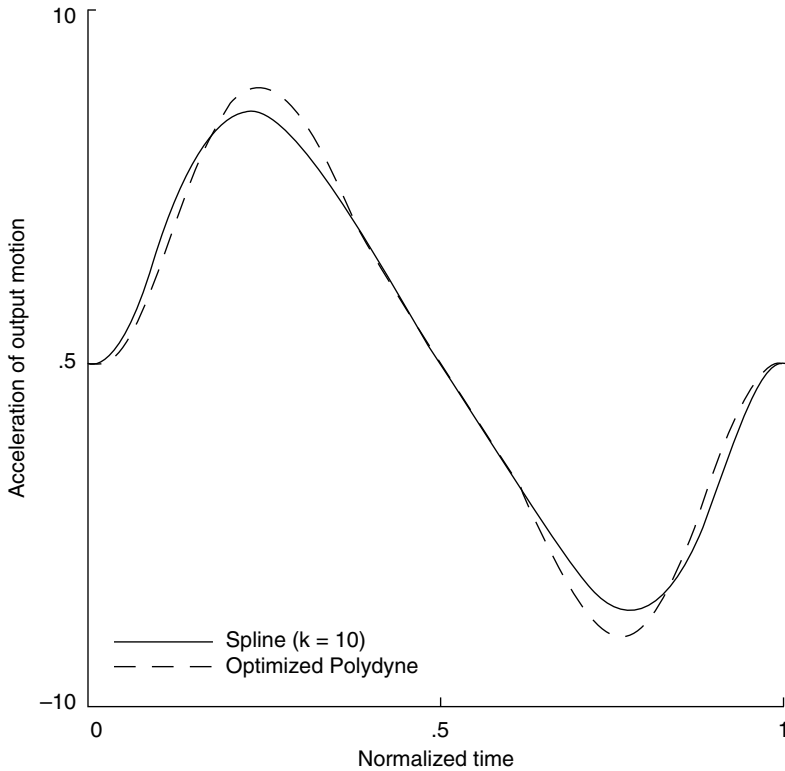
**FIGURE 5.24.** Normalized displacements of output motions for spline ( $k = 10$ ) and optimized polydyne in Example 8.



**FIGURE 5.25.** Normalized velocities of output motions for spline ( $k = 10$ ) and optimized polydyne in Example 8.

a uniform mesh for the elements are arbitrary. Based on the equal division, the first element is located on the normalized time subdomain  $[0, 1/16]$ , the second element on the subdomain  $[1/16, 2/16]$ , and so on through the sixteenth element on the subdomain  $[15/16, 1]$ . The four Gaussian points  $x = \pm 0.33992104$  and  $\pm 0.86113631$  of the fourth Legendre polynomial defined on  $[-1, 1]$  are scaled to  $\tau = ((b - a)x + b + a)/2$  on the subdomain  $[a, b]$  for each element (Stroud and Secrest, 1986). For example, the first four Gaussian points located on the subdomain,  $[0, 1/16]$ , of the first element are 0.00433949, 0.02062747, 0.04187253, and 0.05816051.

For Eq. (5.31), there are 66 constraints—the two end conditions and the sixty-four values for the right sides of the differential equations to be satisfied at the Gaussian points. Sixty-six B-splines of order six are used to formulate the system of linear equations in Eq. (5.6). The knot sequence used to evaluate the splines for the collocation process is established by repeating four knots at each mesh point,  $\tau = 1/16, 2/16, 3/16, \dots$ , and  $15/16$ . At the end points,  $\tau = 0$  and  $\tau = 1$ , the knots are repeated six times as necessary because of the order of the splines ( $k = 6$ ). After Eq. (5.6) is solved for the unknown coefficients, the solution of Eq. (5.31) is readily found for any point in the interval  $0 \leq \tau \leq 1$  enabling the dynamic behavior of the follower system to be determined.

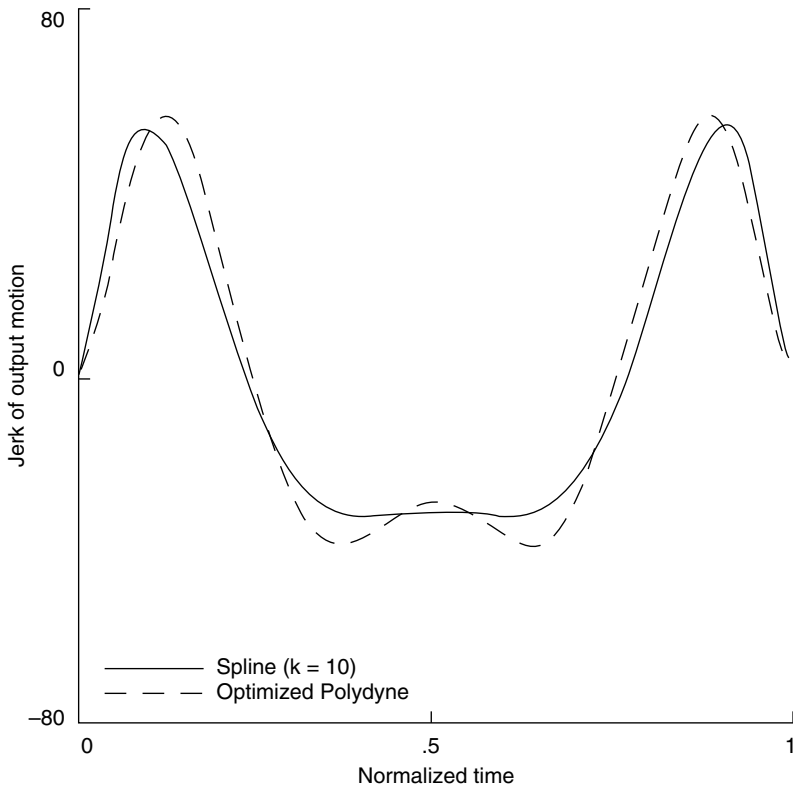


**FIGURE 5.26.** Normalized acceleration of output motions for spline ( $k = 10$ ) and optimized polydyne in Example 8.

**Evaluation of the Follower Response** *The physical parameters of the cam-follower system used are:  $M = 0.75$  lb,  $K_s = 200$  lb/in,  $K_f = 10000$  lb/in,  $\omega_d = 1000$  rpm,  $\beta = \pi/3$  rad.  $h = 0.5$  in. and  $F_p = 70$  lb. A damping ratio of  $0.5(C_s + C_f)/M/\omega_n = 0.2$  is used (Rothbart, 1958) and the damping coefficients  $C_s$  and  $C_f$  are set equal.*

*The performance of the spline-based motion as compared to the optimized polydyne motion is shown in the following figures. Table 5.7 shows the peak values of vibrations and contact forces for these two output motions. Figure 5.29 compares the amplitudes of primary and residual vibrations of the two motions with the damping values given above.*

**Finding the Cam Motion** *To solve differential Eq. (5.18) for the cam displacement and its derivatives, the spline collocation method is applied again. Here the seven boundary conditions cited earlier must be satisfied. Also the left side of Eq. (5.18) at the 64 collocation points must be satisfied. Application of these constraints yields a total of 71 conditions requiring 71 B-splines. Splines of order  $k = 11$  are used, requiring the knots at  $\tau = 0$  and 1 to be repeated eleven times. Again, at mesh points of  $\tau = 1/16, 2/16, \dots$ , and  $15/16$  the knots are repeated four times each. As before a system of linear equations is assembled and solved for the unknown coefficients in Eq. (5.6). Once this is done, the*



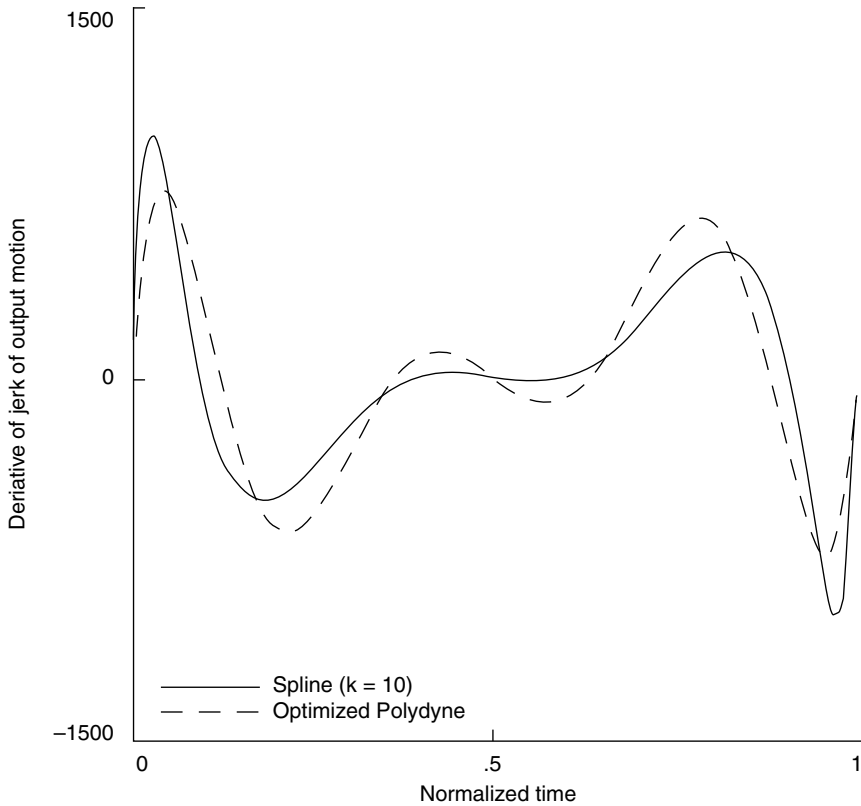
**FIGURE 5.27.** Normalized jerk of output motions for spline ( $k = 10$ ) and optimized polydyne in Example 8.

**TABLE 5.7** Peak Values of Dynamic Response with Damping Ratio = 0.2

Case	Damping	Residual vibration peak (in)	Primary vibration peak (in)	Interior peak contact force (lb)
Spline	$C_f = C_s$	0.01181	0.01539	213.42
Polydyne	$C_f = C_s$	0.01220	0.01604	216.38

cam motion is easily determined as described earlier. Figures 5.24 to 5.32 provide a convenient means of interpreting the outcome.

Figures 5.30 to 5.32 show the cam displacements, velocities, and accelerations found from Eq. (5.18) for the two cases being compared. It can be seen from Figure 5.32 that the cam accelerations of these output motions appear to have small discontinuities at  $\tau = 1$ . However, the motion carried on into the dwell period is continuous.

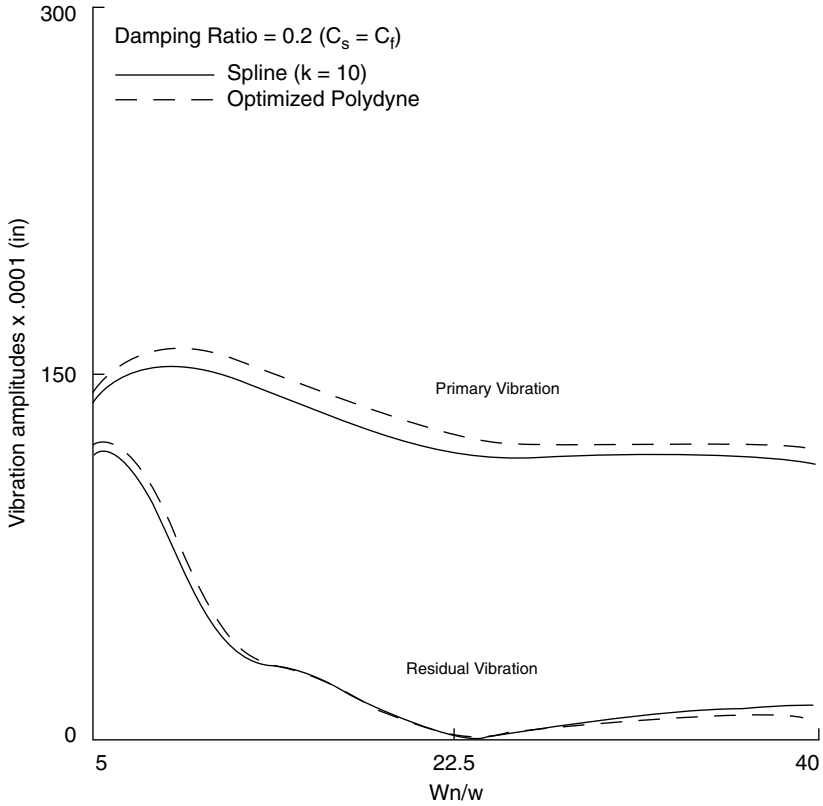


**FIGURE 5.28.** Normalized fourth derivative of output motions for spline ( $k = 10$ ) and optimized polydyne in Example 8.

*This example demonstrates that the combination of the spline interpolation procedure and the spline collocation approach to the solution of differential equations yield an effective approach to the synthesis and analysis of cams with nonrigid followers. It exploits the spline interpolation method described earlier to motion synthesis. The spline collocation approach to the solution of differential equations is accurate, efficient, and reliable and utilizes most of the same software resources that are used in the spline synthesis procedure.*

### **5.5 THE SYNTHESIS OF FOLLOWER MOTIONS OF THREE-DIMENSIONAL CAMS USING NONPARAMETRIC B-SPLINES**

A three-dimensional cam is shown in Fig. 5.33. In the case presented here, the follower position is a function of two input variables, the translation and rotation of the cam. Three-

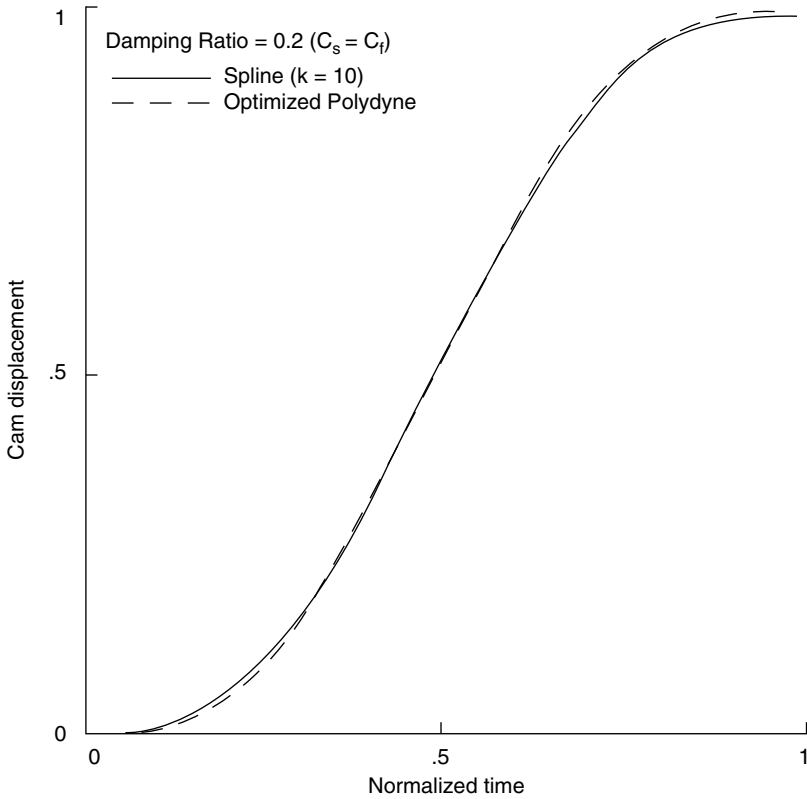


**FIGURE 5.29.** Amplitudes of primary and residual vibrations for both spline ( $k = 10$ ) optimized polydyne with damping ratio = 0.2 ( $C_s = C_f$ ) in Example 8.

dimensional cams have been used in machining fan blade surfaces (Nilson, 1980) and aircraft gas turbine blades (Thompson et al., 1983), and in controlling flow through an orifice (Mabie and Reinholtz, 1987). Variable valve timing systems used in internal combustion engines have also employed them (Titolo, 1991).

The problem of defining three-dimensional surfaces has been addressed (Dhande et al., 1975; Tsay and Hwang, 1994a, b). The analytical representation of the cam surface can be written as (Tsay and Hwang, 1994a)

$$\begin{Bmatrix} x \\ y \\ z \end{Bmatrix} = \begin{Bmatrix} A \cos \phi_2 - \frac{r(B \sin \phi_2 + A \cos \phi_2)}{D} \\ -A \sin \phi_2 - \frac{r(B \cos \phi_2 - A \sin \phi_2)}{D} \\ -s_2 - \frac{rAC}{D} \end{Bmatrix} \quad (5.34)$$



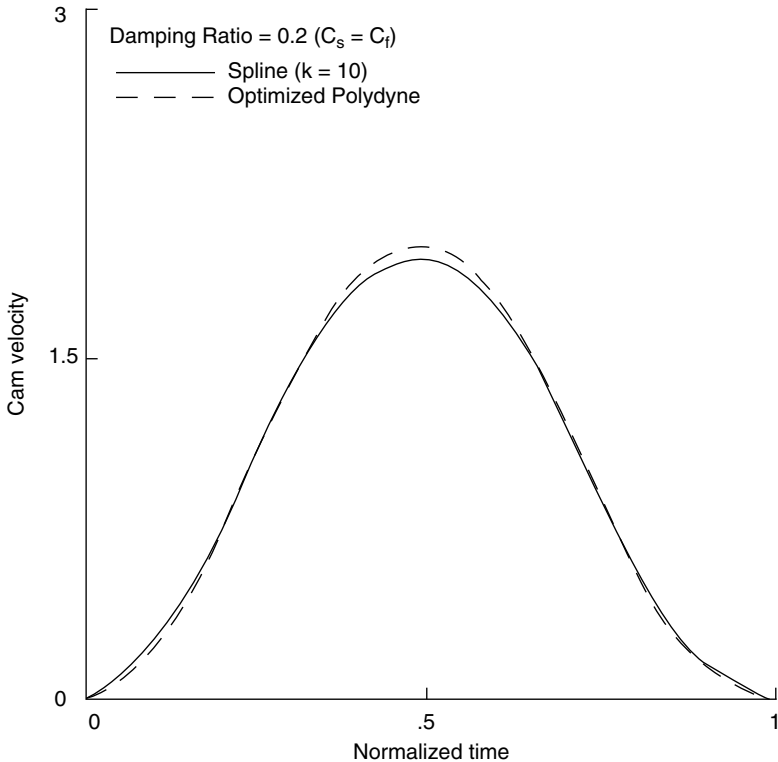
**FIGURE 5.30.** Cam displacements for both spline ( $k = 10$ ) and optimized polydyne with damping ratio = 0.2 ( $C_s = C_t$ ) in Example 8.

where

$$\begin{aligned}
 A &\equiv a + s_1 \\
 B &\equiv \frac{\partial s_1}{\partial \phi_2} \\
 C &\equiv \frac{\partial s_1}{\partial s_2} \\
 D &\equiv \sqrt{A^2 + B^2 + A^2 C^2} .
 \end{aligned}$$

The offset (pitch) surface of the cam, which is useful for the cutter path generation, can be described by the analytical expression

$$\begin{Bmatrix} x_R \\ y_R \\ z_R \end{Bmatrix} = \begin{Bmatrix} A \cos \phi_2 - \frac{(r-R)(B \sin \phi_2 + A \cos \phi_2)}{D} \\ -A \sin \phi_2 - \frac{(r-R)(B \cos \phi_2 - A \sin \phi_2)}{D} \\ -s_2 - \frac{(r-R)AC}{D} \end{Bmatrix} \quad (5.35)$$



**FIGURE 5.31.** Cam velocities for both spline ( $k = 10$ ) and optimized polydyne with damping ratio = 0.2 ( $C_s = C_f$ ) in Example 8.

where  $R$  is the offset distance (Faux and Pratt, 1979; Pharn, 1992).

From Eq. (5.34), we can observe that the profile equation of the cam is a function of the follower motion and its derivatives. Therefore, it is convenient to utilize the nonparametric B-spline functions to interpolate the motion function directly.

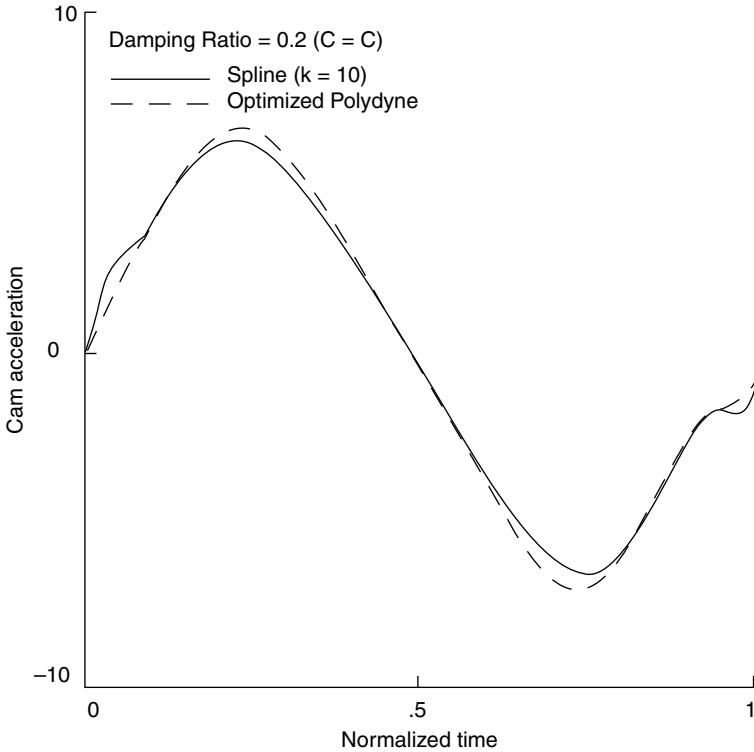
Here, the matter of determining the motion function will be addressed. Spline-based methods similar to those described earlier will be employed. However, they will be extended to yield functions of two variables.

As mentioned earlier, the position of the follower is directly dependent on the angular and the translating positions of the cam. Therefore, the follower motion function to be synthesized can be expressed as

$$S_1 = s_1(\phi_2, s_2). \quad (5.36)$$

As a result, the synthesis of the follower motion requires the formulation of a continuous surface that fits discrete follower motion constraints on the domain of the angular and the translating position parameters.

Spline methods applied to functions of two variables follow closely the methods described earlier and will be presented without lengthy discussion (Cox, 1972; de Boor, 1972; Farin, 1988; Faux and Pratt, 1979). Only displacement constraints will be addressed at this point.



**FIGURE 5.32.** Cam accelerations for both spline ( $k = 10$ ) and optimized polydyne with damping ratio = 0.2 ( $C_s = C_t$ ) in Example 8.

Assuming the motion constraints are defined in an  $n \times m$  array, a recursive definition of nonparametric B-spline surface  $S_1(\phi_2, s_2)$  can be defined as follows (de Boor, 1978):

$$\begin{aligned}
 S_1(\phi_2, s_2) &= \sum_{i=1}^n \sum_{j=1}^m N_{i,k_1}(\phi_2) M_{j,k_2}(s_2) p_{i,j} \\
 2 \leq k_1 &\leq n \\
 2 \leq k_2 &\leq m.
 \end{aligned}
 \tag{5.37}$$

The maximum order of the surface in each parametric direction is equal to the number of motion constraints in that direction ( $n$  or  $m$ , respectively). The continuity of the surface in each parametric direction is two less than the order in that direction. The B-splines in Eq. (5.37) can be computed using the following recurrence relations (Cox, 1972; de Boor, 1972). (Note the similarity to earlier, one-dimensional formulations.)

$$N_{i,1}(\phi_2) = \begin{cases} 1 & \text{if } x_i \leq \phi_2 < x_{i+1} \\ 0 & \text{otherwise} \end{cases}
 \tag{5.38}$$

$$N_{i,k_1}(\phi_2) = \frac{(\phi_2 - x_i)N_{i,k_1-1}(\phi_2)}{x_{i+k_1-1} - x_i} + \frac{(x_{i+k_1} - \phi_2)N_{i+1,k_1-1}(\phi_2)}{x_{i+k_1} - x_{i+1}}
 \tag{5.39}$$

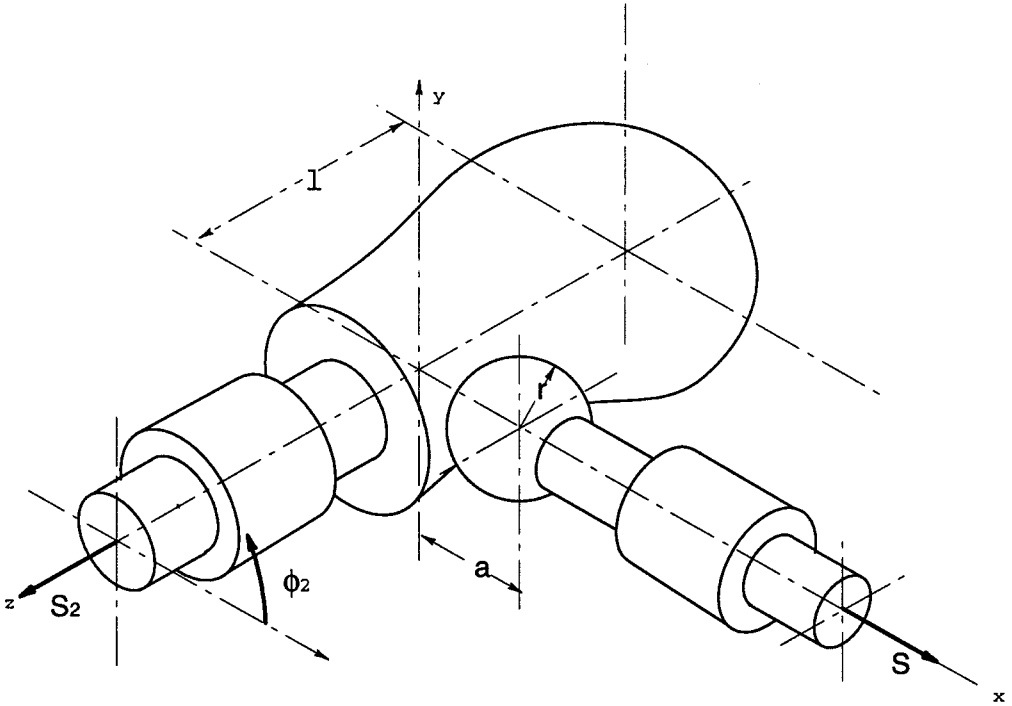


FIGURE 5.33. Three-dimensional cam with translating spherical follower.

$$M_{j,1}(s_2) = \begin{cases} 1 & \text{if } y_i \leq s_2 < y_{i+1} \\ 0 & \text{otherwise} \end{cases} \quad (5.40)$$

$$M_{j,k_2}(s_2) = \frac{(s_2 - y_j)M_{j,k_2-1}(s_2)}{y_{j+k_2-1} - y_j} + \frac{(y_{j+k_2} - s_2)M_{j+1,k_2-1}(s_2)}{y_{j+k_2} - y_{j+1}} \quad (5.41)$$

where  $x_i$  and  $y_j$  are used here to denote elements of the knot sequences in each direction. It should be clear from the earlier discussions that the knot sequences must be nondecreasing series of real numbers that satisfy the relations  $\phi_{2min'} \leq x_i \leq x_{i+1} \leq \phi_{2max'}$  and  $s_{2min'} \leq y_i \leq y_{i+1} \leq s_{2max'}$ . Two types of knot sequences must be used. The first, used for the angular position of the cam, is a uniform knot sequence, for instance [0, 1, 2, 3, 4]. This sequence will ensure continuity at  $\phi_2 = 0$  and at  $\phi_2 = 2\pi$ . A knot sequence having a multiplicity of values at the ends equal to the order of the B-spline with the internal knot values evenly spaced is used in the other direction, for example, [0, 0, 1, 2, 3, 3] for B-splines of order  $k = 2$ .

The recursive representation for the derivative of a nonparametric B-spline surface can be obtained by differentiating Eq. (5.36) to yield (Butterfield, 1976)

$$\frac{\partial^{(w+v)}}{\partial \phi_2^w \partial s_2^v} S_1(\phi_2, s_2) = \sum_{i=1}^n \sum_{j=1}^m N_{i,k_1}^{(w)}(\phi_2) M_{j,k_2}^{(v)}(s_2) p_{i,j} \quad (5.42)$$

$$N_{i,k_1}^{(w)}(\phi_2) \equiv \frac{\partial^w N_{i,k_1}(\phi_2)}{\partial \phi_2^w} = (k_1 - 1) \left[ \frac{N_{i,k_1-1}^{(w-1)}(\phi_2)}{x_{i+k_1-1} - x_i} - \frac{N_{i+1,k_1-1}^{(w-1)}(\phi_2)}{x_{i+k_1} - x_{i+1}} \right] \quad (5.43)$$

$$N_{i,k_1}^{(w)}(\phi_2) = \left( \frac{k_1 - 1}{k_1 - w - 1} \right) \times \left[ \frac{(\phi_2 - x_i) N_{i,k_1-1}^{(w)}(\phi_2)}{x_{i+k_1-1} - x_i} + \frac{(x_{i+k_1} - \phi_2) N_{i+1,k_1-1}^{(w)}(\phi_2)}{x_{i+k_1} - x_{i+1}} \right] \quad (5.44)$$

$$M_{j,k_2}^{(v)}(s_2) \equiv \frac{\partial^v M_{j,k_2}(s_2)}{\partial s_2^v} = (k_2 - 1) \left[ \frac{M_{j,k_2-1}^{(v-1)}(s_2)}{y_{j+k_2-1} - y_j} - \frac{M_{j+1,k_2-1}^{(v-1)}(s_2)}{y_{j+k_2} - y_{j+1}} \right] \quad (5.45)$$

$$M_{j,k_2}^{(v)}(s_2) = \left( \frac{k_2 - 1}{k_2 - v - 1} \right) \times \left[ \frac{(s_2 - y_j) M_{j,k_2-1}^{(v)}(s_2)}{y_{j+k_2-1} - y_j} + \frac{(y_{j+k_2} - s_2) M_{j+1,k_2-1}^{(v)}(s_2)}{y_{j+k_2} - y_{j+1}} \right]. \quad (5.46)$$

The B-spline surface interpolation can also be expressed by matrix as

$$[S_i(\phi_2, s_2)] = [N(\phi_2)] \cdot [p] \cdot [M(s_2)] \quad (5.47)$$

where

$$[S_i(\phi_2, s_2)] = \begin{bmatrix} S_1(\phi_{2_1}, s_{2_1}) & S_1(\phi_{2_1}, s_{2_2}) & \cdots & S_1(\phi_{2_1}, s_{2_m}) \\ S_1(\phi_{2_2}, s_{2_1}) & S_1(\phi_{2_2}, s_{2_2}) & \cdots & S_1(\phi_{2_2}, s_{2_m}) \\ \vdots & \vdots & \ddots & \vdots \\ S_1(\phi_{2_n}, s_{2_1}) & S_1(\phi_{2_n}, s_{2_2}) & \cdots & S_1(\phi_{2_n}, s_{2_m}) \end{bmatrix}_{n \times m}$$

$$[N(\phi_2)] = \begin{bmatrix} N_{1,k_1}(\phi_{2_1}) & \cdots & N_{n,k_1}(\phi_{2_1}) \\ \vdots & \ddots & \vdots \\ N_{1,k_1}(\phi_{2_n}) & \cdots & N_{n,k_1}(\phi_{2_n}) \end{bmatrix}_{n \times n}$$

$$[p] = \begin{bmatrix} p_{1,1} & \cdots & p_{1,m} \\ \vdots & \ddots & \vdots \\ p_{n,1} & \cdots & p_{n,m} \end{bmatrix}_{n \times m}$$

$$[M(s_2)] = \begin{bmatrix} M_{1,k_2}(s_{2_1}) & \cdots & M_{1,k_2}(s_{2_m}) \\ \vdots & \ddots & \vdots \\ M_{m,k_2}(s_{2_1}) & \cdots & M_{m,k_2}(s_{2_m}) \end{bmatrix}_{m \times m}$$

### Follower Motion Synthesis for the Three-Dimensional Cam

Before examining the synthesis process, some basic requirements should be noted:

1. The number of motion constraints is not limited. However, for the nonparametric forms of the B-spline surface interpolation used here, the pattern of the motion constraints must be a rectangular grid data form.

2. To guarantee jerk continuity, the synthesized motion function in each parametric direction must be of at least degree = 4. This means that the order of the B-spline functions must be greater than or equal to 5.

3. Since the profile is a closed surface in the parametric direction of rotation, the motion function along that parametric direction, i.e.,  $\phi_2$ , which is used to form the must

be continuous everywhere, including the ends (as noted earlier). The general form of the B-spline surface interpolation can guarantee the continuity only of the internal region of the interpolated surface but not between the two ends. Closed periodic B-spline functions produced from uniform knot sequences cited earlier solve this problem.

4. No special consideration of continuity is required at the surface edges in the direction of translation so the multiple uniform knot sequence is used.

The systematic procedure for implementing the B-spline surface interpolation can be established as follows:

1. Set up the motion constraints in a  $n \times m$  rectangular grid. If any data are absent in the rectangular grid, they can be filled in by using the B-spline interpolation applied along either the rotating or the translating directions.
2. Select the appropriate order of the B-spline functions. As shown in Eq. (5.37), the proper value of the order is between two and the number of motion constraints. Recall that the degrees of the functions are one less than the order.
3. Construct the knot sequence according to the demand of each parametric direction. The knot sequence,  $x_i$ , for the closed periodic B-spline (along the rotation coordinate) can be obtained by

$$x_i = \begin{cases} \phi_{2_{\min}} & i = 1 \\ x_{i-1} + \frac{\phi_{2_{\max}} - \phi_{2_{\min}}}{n} & 2 \leq i \leq n + 1. \end{cases} \quad (5.48)$$

The knot sequence in the translation coordinate can be found as

$$y_j = \begin{cases} s_{2_{\min}} & 1 \leq j \leq k_2 \\ y_{j-1} + \frac{s_{2_{\max}} - s_{2_{\min}}}{m - k_2 + 1} & k_2 + 1 \leq j \leq m \\ s_{2_{\max}} & m + 1 \leq j \leq m + k_2. \end{cases} \quad (5.49)$$

4. Determine the values of B-spline functions corresponding to motion constraints by using Eqs. (5.38) to (5.41).
5. Collect the values of B-splines and motion constraints to form the matrices

$$[N(\phi_2)], [S_1], \text{ and } [M(s_2)].$$

6. Obtain the coefficient matrix  $[p]$  as follows:

$$[p] = [N(\phi_2)]^{-1} \cdot [S_1(\phi_2, s_2)] \cdot [M(s_2)]^{-1}.$$

7. Evaluate the complete follower motion function by applying Eq. (5.47).

After the follower motion function is determined, kinematic properties for the velocity  $v_f(\phi_2, s_2)$ , the acceleration  $A_f(\phi_2, s_2)$ , and the jerk  $J_f(\phi_2, s_2)$  of the synthesized follower motion can be derived by differentiating Eq. (5.37). When the angular and linear velocities of the cam are constant, the derivatives can be expressed as

$$\begin{aligned}
 v_1(\phi_2, s_2) &= \frac{dS_1}{dt} = \frac{\partial S_1}{\partial \phi_2} \frac{d\phi_2}{dt} + \frac{\partial S_1}{\partial s_2} \frac{ds_2}{dt} \\
 &= \frac{\partial S_1}{\partial \phi_2} \omega_2 + \frac{\partial S_1}{\partial s_2} v_2 \\
 &= [N(\phi_2)]^{(1)} \cdot [p] \cdot [M(s_2)] \omega_2 + [N(\phi_2)] \cdot [p] \cdot [M(s_2)]^{(1)} v_2 \quad (5.50)
 \end{aligned}$$

$$\begin{aligned}
 A_1(\phi_2, s_2) &= [N(\phi_2)]^{(2)} \cdot [p] \cdot [M(s_2)] \omega_2^2 + 2[N(\phi_2)]^{(1)} \cdot [p] \cdot [M(s_2)]^{(1)} \omega_2 v_2 \\
 &\quad + [N(\phi_2)] \cdot [p] \cdot [M(s_2)]^{(2)} v_2^2 \quad (5.51)
 \end{aligned}$$

$$\begin{aligned}
 J_1(\phi_2, s_2) &= [N(\phi_2)]^{(3)} \cdot [p] \cdot [M(s_2)] \omega_2^3 + 3[N(\phi_2)]^{(2)} \cdot [p] \cdot [M(s_2)]^{(1)} \omega_2^2 v_2 \\
 &\quad + 3[N(\phi_2)]^{(1)} \cdot [p] \cdot [M(s_2)]^{(2)} \omega_2 v_2^2 + [N(\phi_2)] \cdot [p] \cdot [M(s_2)]^{(3)} v_2^3 \quad (5.52)
 \end{aligned}$$

where  $[N(\phi_2)]^{(i)} = -i[N(\phi_2)]/\phi_2^i$  is the  $i^{\text{th}}$  order partial derivative. With respect to  $(\phi_2, [M(s_2)])^{(j)} = j[M(s_2)]$ ,  $s_2^j$  is the  $j^{\text{th}}$  order partial derivative, and with respect to  $s_2$ ,  $\omega_2 = d\phi_2/dt$  is the angular velocity of the cam, and  $v_2 = ds_2/dt$  is the linear velocity of the cam. Note that the elements in the matrices above for the derivatives of B-splines in the rotating and translating directions are found in Eqs. (5.43) to (5.46).

*Example Application.* The following numerical examples demonstrate the feasibility of synthesizing the follower motions. In these two cases, a cam with a translating spherical follower is considered. The dimensional parameters used for the cam-follower mechanism in both examples are:

$$a = 22 \text{ mm}$$

$$l = 50 \text{ mm}$$

$$r = 5 \text{ mm.}$$

**EXAMPLE 9: Synthesis of a Three-Dimensional Surface** A rectangular grid data set of  $7 \times 7$  displacement constraints for the follower is assumed as in Table 5.8.

To guarantee continuity of the fourth derivative of the motion function (i.e., to ensure that derivative of jerk is continuous), the orders of the B-spline surface are chosen to be six in both parametric directions of rotation and translation. A uniform knot sequence in the  $\phi_2$  direction is adopted as

$$[0, 2\pi/7, 4\pi/7, 6\pi/7, 8\pi/7, 10\pi/7, 12\pi/7, 2\pi].$$

The knot sequence in the  $s_2$  direction is taken as

$$[0, 0, 0, 0, 0, 0, 25, 50, 50, 50, 50, 50, 50].$$

The result of the interpolated motion function is plotted in Fig. 5.34.

As mentioned, should the constraint data array be incomplete, the methods described earlier could be used to fill in the gaps. For example, had the data table been incomplete, as in Table 5.9, the missing points could be supplied by interpolating along the rows and columns. The results of doing so appear in Tables 5.10 and 5.11.

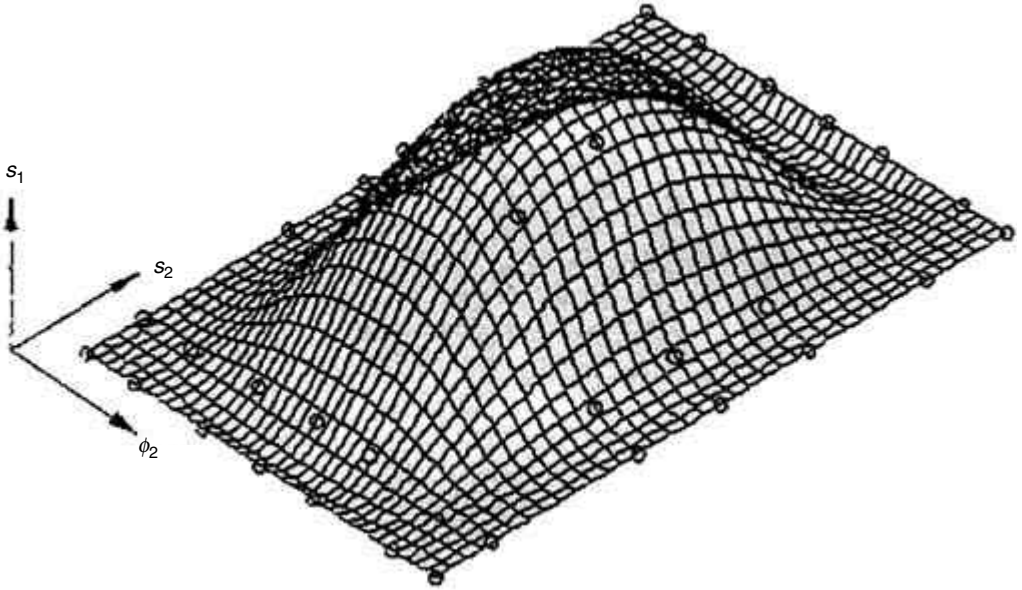


FIGURE 5.34. Interpolated follower motion function for Example 9.

TABLE 5.8 Displacement Constraints for Example 9

Cam translation $s_2$ (mm)	Cam rotation $\phi_2$ (deg)						
	0	50	120	180	235	315	360
0	0	0	0	0	0	0	0
5	0	0.03	0.20	0.24	0.21	0.02	0
18	0	0.53	3.53	4.38	3.70	0.40	0
25	0	0.61	4.03	5.00	4.22	0.45	0
33	0	0.50	3.31	4.12	3.48	0.37	0
43	0	0.07	0.50	0.62	0.52	0.06	0
50	0	0	0	0	0	0	0

TABLE 5.9 Incomplete Table of Displacement Constraints

Cam translation $s_2$ (mm)	Cam rotation $\phi_2$ (deg)						
	0	50	120	180	235	315	360
0	0	0	0	0	0	0	0
5	0	0.03	0.20	—	0.21	0.02	0
18	0	0.53	—	4.38	3.70	0.40	0
25	0	0.61	4.03	5.00	—	0.45	0
33	0	0.50	3.31	4.12	3.48	0.37	0
43	0	0.07	—	0.62	0.52	—	0
50	0	0	0	0	0	0	0

**TABLE 5.10** Displacement Constraints, Missing Values Supplied by Interpolating Along the Rows of Table 5.9

Cam translation		Cam rotation $\phi_2$ (deg.)						
$s_2$ (mm)								
	0	50	120	180	235	315	360	
0	0	0	0	0	0	0	0	0
5	0	0.03	0.20	<b>0.88</b>	0.21	0.02	0	0
18	0	00.53	<b>3.01</b>	4.38	3.70	0.40	0	0
25	0	0.61	4.03	5.00	<b>4.09</b>	0.45	0	0
33	0	0.50	3.31	4.12	3.48	0.37	0	0
43	0	0.07	<b>0.38</b>	0.62	0.52	<b>0.07</b>	0	0
50	0	0	0	00	0	0	0	0

**TABLE 5.11** Displacement Constraints, Missing Values Supplied by Interpolating Along the Columns of Table 5.9

Cam translation		Cam rotation $\phi_2$ (deg)						
$s_2$ (mm)								
	0	50	120	180	235	315	360	
0	0	0	0	0	0	0	0	0
5	0	0.03	0.20	<b>1.68</b>	0.21	0.02	0	0
18	0	00.53	<b>3.04</b>	4.38	3.70	0.40	0	0
25	0	0.61	4.03	5.00	<b>4.43</b>	0.45	0	0
33	0	0.50	3.31	4.12	3.48	0.37	0	0
43	0	0.07	<b>1.10</b>	0.62	0.52	<b>0.17</b>	0	0
50	0	0	0	00	0	0	0	0

## 5.6 SUMMARY

The methods described here afford a convenient and systematic means of developing motion curves. As illustrated they work very well in the face of numerous constraints and enable the designer to conveniently refine the synthesized motion when needed, often without modifying basic design constraints. Only familiar numerical methods are required to implement the procedures. Handling nonrigid followers is a bit challenging for designers who are unfamiliar with splines and the solution of differential equations but should not be beyond the reach of most engineers, given a little time and effort.

## REFERENCES

- Akiba, K., Shimizu, A., and Sakai, H., "A Comparison Simulation of High Speed Driven Valve Trains," SAE Technical Paper Series 810865, 1981.

- Angeles, J., "Synthesis of Plane Curves with Prescribed Local Geometric Properties Using Periodic Splines," *Computer-Aided Design*, 15 (3): 147–155, 1983.
- Angeles, J., and Lopez-Cajun, C., "Optimal Synthesis of Cam Mechanisms with Oscillating Flat-Face Followers," *Mechanisms and Machine Theory*, 23 (1): 1–6, 1988.
- Ascher, U., "Solving Boundary-Value Problems with a Spline-Collocation Code," *Journal of Computational Physics*, 34: 401–413, 1980.
- Ascher, U., Christiansen, J., and Russell, R. D., "A Collocation for Mixed Order Systems of Boundary Value Problems," *Mathematics of Computation*, 33: 659–679, 1979.
- Barkan, P., "Calculation of High-Speed Valve Motion with a Flexible Overhead Linkage," *SAE Trans.*, 61: 678–700, 1953.
- Barkan, P., Discussion in: *ASME Journal of Engineering for Industry*, 87: 191–204, 1965.
- Butcher, J. C., "Implicit Runge-Kutta Processes," *Mathematics of Computation*, 18: 50–64, 1964.
- Butterfield, K. R., "The Computation of All the Derivatives of a B-Spline Basis," *J. Inst. Math. Appl.*, 17: 15–25, 1976.
- Carey, G. F., and Finlayson, B. A., "Orthogonal Collocation on Finite Elements," *Chemical Engineering Science*, 30: 587–596, 1975.
- Cerutti, J. H., "Collocation for Systems of Ordinary Differential Equations," Computer Sciences Technical Report #230, University of Wisconsin, Madison, WI, 1974.
- Chan, C., and Pisano, A. P., "Dynamic Model of a Fluctuating Rocker-Arm Ratio Cam System," *ASME Journal of Mechanisms, Transmissions, and Automation in Design*, 109: 357–365, 1987.
- Chen, F. Y., "Assessment of the Dynamic Quality of a Class of Dwell-Rise-Dwell Cams," *ASME Journal of Mechanical Design*, 13: 793–802, 1981.
- Chen, F. Y., *Mechanics and Design of Cam Mechanisms*, Pergamon Press, New York, 1982.
- Chew, M., Freudenstein, F., and Longman, R. W., "Application of Optimal Control Theory to the Synthesis of High-Speed Cam-Follower Systems-Part 1: Optimality Criterion," *ASME Journal of Mechanisms, Transmissions, and Automation in Design*, 105: 576–584, September 1983.
- Cox, M. G., "The Numerical Evaluation of B-Splines," *J. Inst. Math. Appl.*, 10: 134–149, 1972.
- Curry, H. B., and Schoenburg, I. J., "On Polya Frequency Functions IV: The Fundamental Spline Functions and Their Limits," *J. Analyse Math.*, 17: 71–107, 1966.
- Dhande, S. G., Bhadoria, B. S., and Chakraborty, J., "A Unified Approach to the Analytical Design of Three-Dimensional Cam Mechanisms," *ASME Journal of Engineering for Industry*, pp. 327–333, 1975.
- de Boor, C., "On Calculating with B-Splines," *J. Approximation Theory*, 6: 50–62, 1972.
- de Boor, C., *A Practical Guide to Splines*, Springer-Verlag, 1978.
- de Boor, C., "Package for Calculating with B-Splines," *SIAM Journal of Numerical Analysis*, 14 (3): 441–472, June 1977.
- de Boor, C., and Swartz, B., "Collocation at Gaussian Points," *SIAM Journal of Numerical Analysis*, 10: 582–606, 1973.
- Dudley, W. M., "A New Approach to Cam Design," *Machine Design*, 19: 143–184, July 1947.
- Farin, G., *Curves and Surfaces for Computer Aided Geometric Design: A Practical Guide*, Academic Press, London, 1988.
- Faux, L. D., and Pratt, M. J., *Computational Geometry for Design and Manufacture*, Ellis Horwood Limited, London, 1979.
- Forsythe, G. E., Malcolm, M. A., and Moler, C. B., *Computer Methods for Mathematical Computations*, Prentice-Hall, Upper Saddle River, N.J., 1977.
- Foy, P. A., Ed., *The Port Mathematical Subroutine Library*, Bell Laboratories, Murray Hill, N.J., 1977.
- Freudenstein, F., "On the Dynamics of High-speed Cam Profiles," *Int. J. Mech. Sci.*, 1: 342–349, 1960.

- Freudenstein, F., Mayourian, M., and Maki, E. R., "Energy Efficient Cam-Follower Systems," *ASME Journal of Mechanisms, Transmissions, and Automation in Design*, 105: 681–685, 1983.
- Gonzalez-Palacios, M. A., and Angeles, J., *Cam Synthesis*, Kluwer Academic Publishers, Dordrecht, Netherlands, 1993.
- Hanachi, S., and Freudenstein, F., "The Development of a Predictive Model for the Optimization of High-Speed Cam-Follower Systems with Coulomb Damping Internal Friction and Elastic and Fluidic Elements," *ASME Journal of Mechanisms, Transmissions, and Automation in Design*, 108: 506–515, 1986.
- Hanson, R. S., and Churchill, F. T., "Theory of Envelopes Provides New Cam Design Equations," *Product Engineering*, pp. 45–55, August 20, 1962.
- Hrones, J. A., "An Analysis of the Dynamic Forces in a Cam-Driven System," *ASME Transactions*, 70: 473–482, 1948.
- Hulme, B. L., and Daniel, S. L., "COLODE: A Collocation Subroutine for Ordinary Differential Equations," Rep. SAND 74-0380, Sandia Laboratories, Albuquerque, N.M., 1974.
- Kanesaka, H., Akiba, K., and Sakai, H., "A New Method of Valve Cam Design-HYSYDNE Cam," SAE Paper 770777, 1978.
- Kanzaki, K., and Itao, K., "Polydyne Cam Mechanisms for Typehead Positioning," *ASME Journal of Engineering for Industry*, 94: 250–254, 1972.
- Koster, M. P., *Vibrations of Cam Mechanisms*, Macmillan Press, London, 1974.
- Kosugi, T., and Seino, T., "Valve Motion Simulation Method for High-Speed Internal Combustion Engines," SAE Paper 850179, 1986.
- Kwakernaak, H., and Smit, J., "Minimum Vibration Cam Profiles," *Journal of Mechanical Engineering Science*, 10: 219–227, 1968.
- Mabie, H. H., and Reinholtz, C. E., *Mechanisms and Dynamics of Machinery*, John Wiley & Sons, New York, 1987.
- Mercer, S., Jr., and Holowenko, A. R., "Dynamic Characteristics of Cam Forms Calculated by the Digital Computer," *ASME Transactions*, 80: 1695–1705, 1958.
- Neklutin, C. N., "Vibration Analysis of Cams," *Machine Design*, pp. 190–198, December 1954.
- Nilson, E. N., "Integrating CAD and CAM-Future Directions," *CADI CAM*, SME, pp. 115–131, 1980.
- Peisakh, E. E., "Improving the Polydyne Cam Design Method," *Russian Engineering Journal*, XLVI, (12): 25–27, 1966.
- Pham, B., "Offset Curves and Surfaces: A Brief Survey," *Computer-Aided Design*, 24 (4): 223–229, 1992.
- Pisano, A. P., and Freudenstein, F., "An Experimental and Analytical Investigation of the Dynamic Response of a High-Speed Cam-Follower System. Part 2: A Combined, Lumped/Distributed Parameter Dynamic Model," *ASME Journal of Mechanisms, Transmissions, and Automation in Design*, 105: 699–704, 1983.
- Rees Jones, J., and Reeves, J. E., "Dynamic Response of Cam Curves Based on Sinusoidal Segments," *Cams and Cam Mechanisms*, J. Rees Jones ed., Mechanical Engineering Publications, London, pp. 14–24, 1978.
- Rogers, D. F., and Adams, J. A., *Mathematical Elements for Computer Graphics*, 2nd edition, McGraw-Hill Inc., New York, 1990.
- Rooney, G. T., and Deravi, P., "Coulomb Friction in Mechanism Sliding Joints," *Mechanism and Machine Theory*, 17: 207–211, 1982.
- Rothbart, H. A., Discussion. *ASME Transactions*, 80: 1695–1705, 1958.
- Rothbart, H. A., *Cams*, John Wiley and Sons, New York, 1956.
- Russell, R. D., "Collocation for Systems of Boundary Value Problems," *Numerical Mathematics*, 23: 119–133, 1974.
- Russell, R. D., "A Comparison of Collocation and Finite Differences for Two-Point Boundary Value Problems," *SIAMJ of Amer. Anal.*, 14: 19–39, 1977.

- Russell, R. D., and Shampine, L. F., "A Collocation Method for Boundary Value Problems," *Numerical Mathematics*, 19: 1–28, 1972.
- Sanchez, N. M., and de Jalon, J. G., "Application of B-Spline Functions to the Motion Specification of Cams," ASME paper 80-DET-28, 1980.
- Sandgren, E., and West, R. L., "Shape Optimization of Cam Profiles Using a Representation," *ASME Journal of Mechanisms, Transmissions, and Automation in Design*, 1 (11): 195–201, 1989.
- Shampine, L. F., and Gear, C. W., "A User's View of Solving Stiff Ordinary Differential Equations," *SIAM Review*, 21: 1–17, 1979.
- Stroud, A. H., and Secrest, D., *Gaussian Quadrature Formulas*, Prentice-Hall, Upper Saddle River, N.J., 1986.
- Tesar, D., and Matthew, G. K., *The Dynamic Synthesis, Analysis, and Design of Modeled Cam Systems*, D. C. Heath Company, Lexington, Mass., 1976.
- Thompson, B. S., Mass, D. J., and Jiang, J., "Cam-Follower, Cutter-Workpiece Interaction in Airfoil Milling Machines," Oklahoma State University's 8th Applied Mechanisms Conference, September 19–21, Saint Louis, Mo., pp. 39-1–39-7, 1983.
- Thoren, T. R., Engemann, H. H., and Stoddart, D. A., "Cam Design as Related to Valve Train Dynamics," *SAE Quarterly Transactions*, 6 (1): 1–14, 1952.
- Tiller, W., "Rational B-Splines for Curve and Surface Representation," *IEEE CG&A*, pp. 61–69, September 1983.
- Titolo, A., "The Variable Valve Timing System—Application on a V8 Engine," SAE paper 910009, pp. 35–42, 1991.
- Tsay, D. M., and Hwang, G. S., "Application of the Theory of Envelope to the Determination of Camoid Profiles with Translating Followers," *ASME Journal of Mechanical Design*, 116: 320–325, 1994a.
- Tsay, D. M., and Hwang, G. S., "The Profile Determination and Machining of Camoids with Oscillating Spherical Followers," *ASME Journal of Engineering for Industry*, 116: 355–362, 1994b.
- Versprille, K., *Computer Aided Design Applications of the Rational B-spline Approximation Form*, Ph.D. Thesis, Syracuse University, Syracuse, N.Y., 1975.
- Weiss, R., "The Application of Implicit Runge-Kutta and Collocation Methods to Boundary Value Problems," *Mathematics of Computation*, 28: 449–464, 1974.
- Wiederrich, J. L., "Residual Vibration Criteria Applied to Multiple Degree of Freedom Cam Followers," *ASME Journal of Mechanical Design*, 103: 702–705, October 1981.
- Wiederrich, J. L., and Roth, R., "Dynamic Synthesis of Cams Using Finite Trigonometric Series," *ASME Journal of Engineering for Industry* 97: 287–293, 1975.
- Wright, K., "Some Relationships Between Implicit Runge-Kutta, Collocation and Lanczos T Methods, and Their Stability Properties," *BIT*, 10: 217–227, 1970.
- Yoon, K., and Rao, S. S., "Cam Motion Synthesis Using Cubic Splines," *ASME Journal of Mechanical Design*, 115: 441–446, 1993.

*This page intentionally left blank.*

---

# CHAPTER 6

---

## ELEMENTS OF CAM PROFILE GEOMETRY

---

Harold A. Rothbart, D.Eng.

6.1 INTRODUCTION	160	6.4 CAM RADIUS OF CURVATURE	169
6.2 CAM PROFILE GRAPHICAL LAYOUT	160	6.4.1 Radius of Curvature	169
6.3 CAM PRESSURE ANGLE	162	6.4.2 Undercutting of Cam—Roller Follower	170
6.3.1 Introduction	162	6.4.3 Undercutting of Cam— Flat-Faced Follower	173
6.3.2 Pressure Angle Forces— Translating Roller Follower	163	6.4.4 Hub Design	173
6.3.3 Pressure Angle Forces— Oscillating, Roller Follower	166	6.5 SUMMARY	174
6.3.4 Pressure Angle Forces— Translating Flat-Faced Follower	168		

---

### SYMBOLS

---

$A$  = follower overhang, in  
 $B$  = follower bearing length, in  
 $d_h$  = hub diameter, in  
 $d_s$  = shaft diameter, in  
 $F$  = force normal to cam profile, lb  
 $l$  = distance from force  $F_n$  to follower axis, in  
 $L_o$  = external load on follower  
 $N_1N_2$  = forces normal to follower stem, lb  
 $Q_oQ_b$  = reactions at pivot point  $Q$ , in  
 $r$  = radius to cutter center, in  
 $r_b$  = base circle radius, in  
 $R_g$  = cutter or grinder radius, in  
 $R_r$  = roller follower radius, in  
 $s$  = follower rise, in (other chapters usually shown as  $y$ )  
 $T$  = total torque on system, lb/in  
 $W$  = radius of follower stem, in  
 $\alpha$  = pressure angle, deg  
 $\alpha_m$  = maximum pressure angle, deg  
 $\chi$  = angle for radius  $r$ , rad  
 $\kappa$  = distance from normal force  $F_n$  to pivot point  $Q$ , in  
 $\mu$  = coefficient of friction  
 $\mu_c$  = coefficient of friction between cam and flat-faced follower  
 $\rho$  = radius of curvature, in  
 $\rho_c$  = radius of curvature of cam profile, in  
 $\rho_k$  = radius of curvature of pivot curve, in  
 $\theta$  = cam angle for rise,  $s$ , rad

## 6.1 INTRODUCTION

---

This chapter introduces the physical factors and forces involved with the development of the proper cam profile shape. This chapter is complemented by Chap. 7, which contains algorithms for the establishment of the cam profile including manufacturing information.

The three basic factors for this kinematic study are:

- cam profile
- cam pressure angle
- cam curvature

In the past the cam profile was developed by observing the cam shape from the graphical construction method explained below.

## 6.2 CAM PROFILE GRAPHICAL LAYOUT

---

Simple cam motions are easily produced by the graphical layout method. The graphic construction is based on the principle of “inversion,” in which the cam is considered the fixed member and the follower is then moved to its proper position (same relative motion) corresponding to the number of cam angles selected. The cam profile is thus the envelope of the follower profile as the follower is positioned around the cam. Note that the conjugate cam follower layout is similar, with the additional cam developed from the first cam shape.

The cam and follower are shown in Fig. 6.1. Developing the cam profile by the graphical layout method:

- Sketch the timing chart Fig. 6.1*a*, showing the cam follower action in 30 degree increments.
- Locate cam center *A*, Fig. 6.1*b*, follower pivot *B*, and location of initial point *O* to maximum rise point 4.
- At lowest point *O* draw the cam base circle (smallest circle to cam profile) and the prime circle to cam center.
- Draw reference arc through follower center *C*.
- Locate points on reference arc *C* according to divisions in timing chart and number accordingly.
- Draw a pivot circle through follower pivot *B*.
- Locate pivot points on pivot circle pertinent to each point on the reference circle and number.
- From each of the pivot points, draw an arc with radius *BC*.
- Lay off the angle or arc on follower arc *C* related to points 0, 1, 2, 3, 4.
- Rotate each of the points on the arc to its proper position around the cam.
- Draw the roller follower outline at each of the points located.
- Draw a smooth curve tangent to the follower outline.

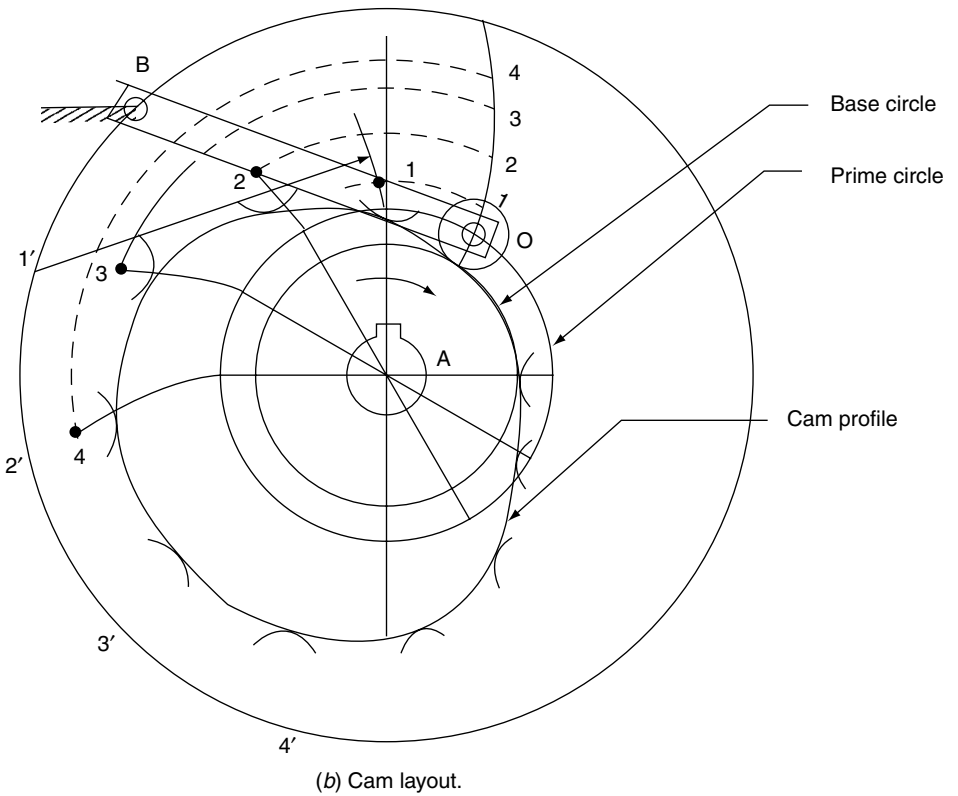
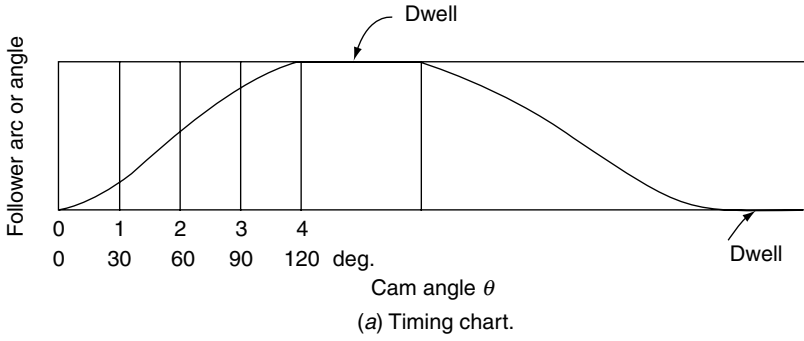


FIGURE 6.1 Cam with oscillating follower.

### 6.3 CAM PRESSURE ANGLE

#### 6.3.1 Introduction

The *cam pressure angle* indicates the steepness and forces of the cam surface. The pressure angle is the angle (at any point) between the normal to the pitch profile and the direction of follower motion; see Fig. 6.2.

The size of the cam directly affects the pressure angle, the curvature of the cam profile, and the proportions of the supporting cam shaft and hub. In all machinery design minimum size is desired to reduce weight and the inertia effects of all moving parts. So it is too with cam-follower systems. As the cam is made smaller the pressure angle increases and the radius of curvature decreases. The pressure angle is limited to minimize forces and deflections in the machine and for CNC increment manufacturing.

Let us discuss the transferring of the cam displacement curve to the radial plate cam, Fig. 6.3. If the pitch curve of the displacement diagram is plotted on a radial cam, we see that it is distorted toward the cam center. As an example, in Fig. 6.3a, let us take a straight-line pitch curve *OB* in the displacement diagram. This pitch curve has a constant pressure angle  $\alpha$  for a total rise *h* in  $\beta$  cam degrees. Let point *T* be the midpoint of rise *OB*, and, in Fig. 6.3b, let *A* be the cam center. By trial and error, choose a radius *AT* so that the pressure angle of the pitch curve at point *T* is equal to  $\alpha$ . The pressure angle is changed when laid out on the radial cam. It is larger than  $\alpha$  below point *T* and smaller than  $\alpha$  above point *T*. It can be reduced by using a larger cam.

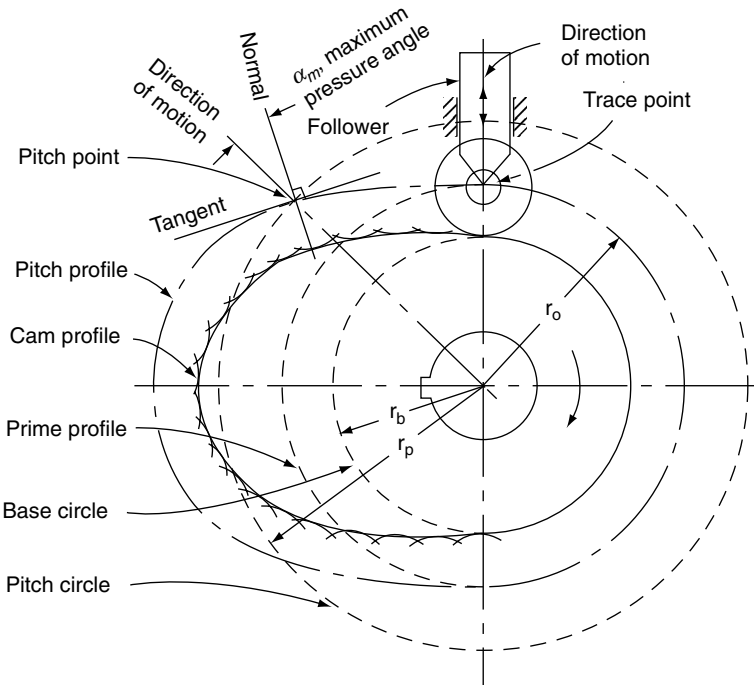


FIGURE 6.2 Cam nomenclature.

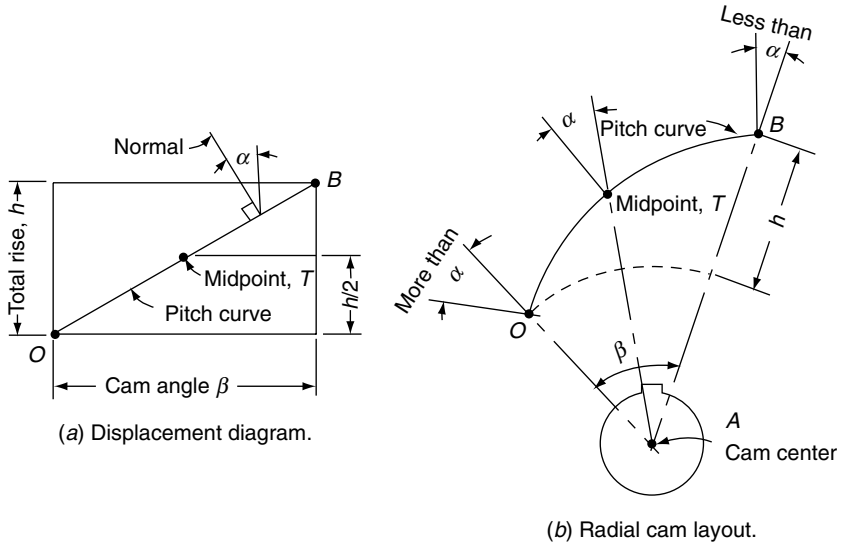


FIGURE 6.3 Radial cam layout distortion.

### 6.3.2 Pressure Angle Forces—Translating Roller Follower

Let us analyze the *side thrust* due to an excessive pressure angle on a translating radial follower. It will be shown that the allowable pressure angle is limited by the length of the follower overhang, its guide bearing length, the coefficient of friction of the follower, and the follower stem rigidity and backlash. First assume that the effect of the roller bearing and its rolling on the cam are negligible. Let

$A$  = follower overhang, in

$B$  = follower bearing length, in

$F$  = force normal to cam profile, lb

$L_o$  = external load on follower (includes working load, weight, spring force, inertia and friction, lb)

$N_1$  and  $N_2$  = forces normal to follower stem, lb

$W$  = radius of follower stem, in.

$\alpha$  = pressure angle, deg

$\alpha_m$  = maximum pressure angle, deg

$\mu$  = coefficient of friction

Figure 6.4 shows the direction of cam rotation, the normal forces on the follower, and the frictional forces opposing the motion of the follower. For static equilibrium, the sum of forces along the vertical axis is

$$\Sigma F_y = 0 = -L_o + F \cos \alpha - \mu N_1 - \mu N_2. \quad (6.1)$$

Let point  $p$  and  $q$  be the intersection of  $N_1$  and  $N_2$  on the line of follower motion. From statics the sum of the moments is

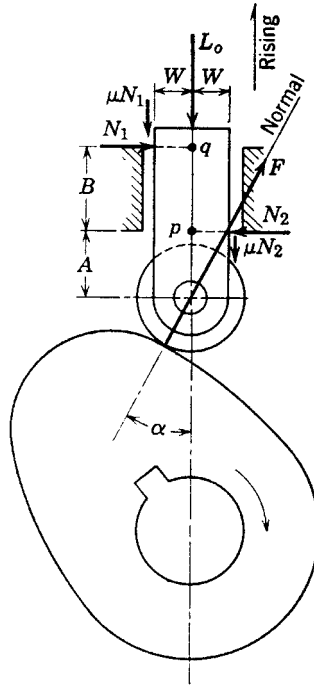


FIGURE 6.4 Radial cam translating roller-follower force distribution.

$$\Sigma M_p = 0 = -FA \sin \alpha + NB - \mu N_1 W + \mu N_2 W \tag{6.2}$$

$$\Sigma M_q = 0 = -F(A + B) \sin \alpha + N_2 B - \mu N_1 W + \mu N_2 W. \tag{6.3}$$

Simplifying Eq. (6.2) and Eq. (6.3) and assuming  $\mu N_1 W$  and  $\mu N_2 W$  equal zero since they are negligible yields

$$N_1 = \frac{A}{B} F \sin \alpha \tag{6.4}$$

$$N_1 = \frac{A+B}{B} F \sin \alpha. \tag{6.5}$$

Substituting Eq. (6.4) in Eq. (6.1) and eliminating  $N_1$

$$0 = -L_0 + F \cos \alpha - \mu F \frac{A}{B} \sin \alpha - \mu N_2 \tag{6.6}$$

Substituting gives the external load

$$L_0 = F \left[ \cos \alpha - \mu \left( \frac{2A+B}{B} \right) \sin \alpha \right]$$

Solving for the force normal to the cam

$$F = \frac{L_0}{\cos\alpha - \mu\left(\frac{2A+B}{B}\right)\sin\alpha} \quad (6.7)$$

The normal force  $F$  is a maximum (equals infinity) which means that the follower will jam in its guide when the denominator of Eq. (6.7) equals zero. Therefore,

$$\cos\alpha_m - \mu\left(\frac{2A+B}{B}\right)\sin\alpha_m = 0$$

The maximum pressure angle without locking the follower in its guide is

$$\alpha_m = \tan^{-1} \frac{B}{\mu(2A+B)}. \quad (6.8)$$

Let us substitute some trial values to compare the magnitude of the results. If we let  $A = B$  and assume the values for the coefficient of friction of bronze on steel to be

$$\mu(\text{kinetic}) = 0.10 \text{ and } \mu(\text{static}) = 0.15$$

Substituting in Eq. (6.8), we find the maximum pressure angle for each condition:

$$\alpha_m = \tan^{-1} \frac{B}{(0.10)(2B+B)} = 73 \text{ degrees for } \mu = 0.10$$

$$\alpha_m = \tan^{-1} \frac{B}{(0.15)(2B+B)} = 66 \text{ degrees for } \mu = 0.15.$$

Note that these values and the derivation of Eq. (6.8) are based on the ideal assumption that the follower is perfectly rigid. Thus, the coefficient of friction may actually reach a value of 0.25 or more depending on relative elasticity and backlash of the follower. A flexible stem may “dig” into the lower corner of the bearing. Therefore, the suggested guide in practice is to keep the coefficient of friction  $\mu$ , the follower overhang  $A$ , and the backlash as small as possible with the bearing length  $B$  as large as possible, in the range of  $B = 2A$ . Generally the safe limiting pressure angle in practice is 30 degrees. However, for light loads with accurate low-friction bearings, the author was successful using a pressure angle as high as 48 degrees. Note that commercially available ball bushings for the linear moving stem have provided low friction and little backlash; see Chap. 10.

We may observe that the follower jamming is of concern only when the follower moves in the direction opposite that of the external load  $L$ . As shown in Figure 6.4, jamming occurs during the rise period only. During the fall period, the size of the maximum pressure angle is generally not limited in proper cam design. However, the author has seen machine installations in which the follower drove the cam during the fall action. It occurred with a chain-driven cam and a spring-loaded follower. The spring force, acting on an excessive pressure angle of fall, produced detrimental shock and fluctuating action in absorbing the backlash of the system.

Also, if the load  $L_0$  varies according to the inertia acceleration in both the rise and fall, the pressure angle should be considered in both. Chapter 9 discusses load fluctuations and reflected torque curve which should be an initial point of analysis in all pressure angle investigations.

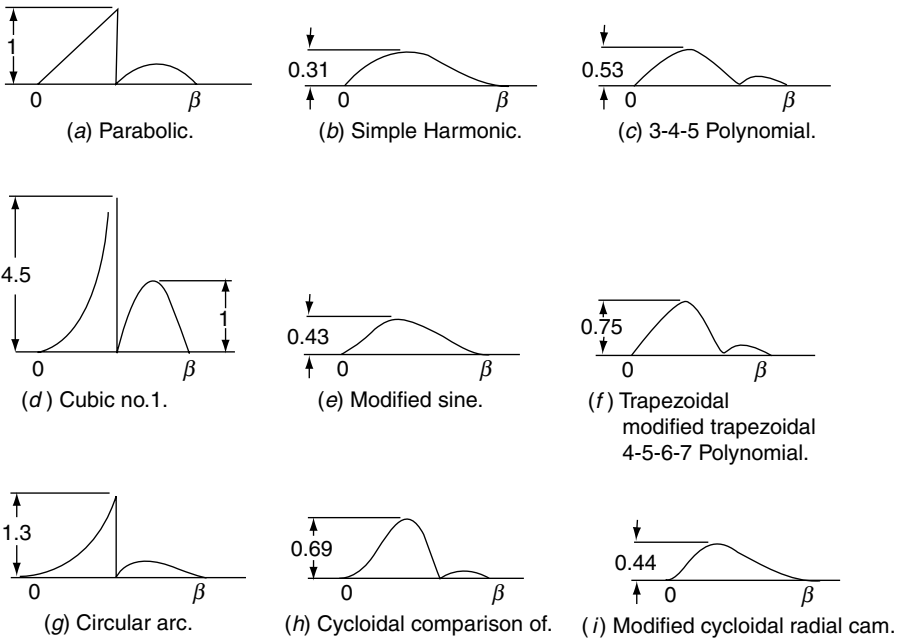


FIGURE 6.5 Side thrust comparison of cam curves.

Let us discuss the side thrust effect on different cam curves. In Fig. 6.4, it has been shown that the greater the pressure angle, the greater the magnitude of the side thrust on the follower. During action, the side thrust varies continuously, depending on the cam curve used. Let's compare cam curves on the basis of the magnitudes of the side thrust they produce. Fig. 6.5 presents such a comparison for a number of cam curves under the same conditions, i.e., equal base circle size, equal range of cam rotation  $\beta$ , and equal loading condition. In addition, all cams had unity lift and unity follower weight. Also, the maximum side thrust of the parabolic curve is to serve as a basis of comparison with the side thrust of all other curves.

From Fig. 6.5, it is apparent that the trigonometric function and the modified trigonometric function curves are superior to the others, and that the trapezoidal, the modified trapezoidal, and the 4-5-6-7 polynomial curves produce about the same magnitude of side thrust. The cubic no. 1 curve and the circular-arc-tangent curve give the greatest amount of side thrust.

### 6.3.3 Pressure Angle Forces—Oscillating Roller Follower

The oscillating roller follower is generally an improvement over the translating type in that the distribution of forces allows a much larger limiting pressure angle for satisfactory performance. Thus, with an oscillating follower, a smaller cam may be used. It is suggested for best performance and highest accuracy that the trace point arc of motion should pass near or through the cam center. Also, by proper location of the follower pivot, it becomes virtually impossible to jam the follower, no matter how steep the cam surface. The extreme limiting condition is to make the pressure angle small enough to prevent the

cam normal force from passing through the follower pivot. Locking results from this detrimental force distribution. Often, for ultimate performance, frequent trials must be made to determine the performance and establish the best dimensional proportions for the given design conditions. Therefore, the side thrust will not exist with the properly designed oscillating roller follower in which the maximum pressure angle is much smaller than a locking condition.

As shown in Fig. 6.6, the forces acting on a swinging arm are the normal reaction at the cam  $F$  and the bearing reactions  $Q_a$  and  $Q_b$  at the pivot point  $Q$  of the swinging arm. Static force balance yields

$$F = \sin \alpha - Q_a = 0 \quad (6.9)$$

$$F \cos \alpha - Q_b = 0 \quad (6.10)$$

$$F \cos \alpha - T = 0 \quad (6.11)$$

where  $k$  = distance from normal force  $F_n$  to pivot point  $Q$ , in

$Q_a, Q_b$  are the reactions at pivot point  $Q$ , in

$T$  = the total torque on the system, lb-in

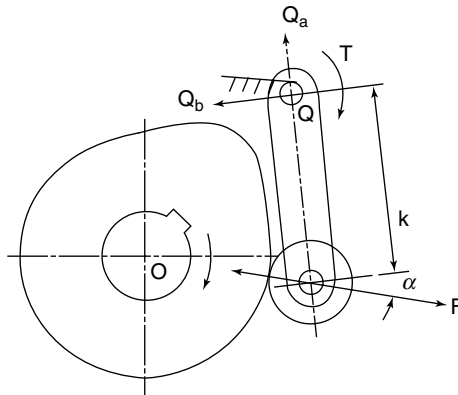
Torque includes the torque due to the effects of springs, inertia, etc. The solutions of Eqs. (6.9), (6.10), and (6.11) are

$$F_n = \frac{T}{k \cos \alpha} \quad (6.12)$$

$$Q_a = \frac{T}{k} \tan \alpha \quad (6.13)$$

$$Q_b = \frac{T}{k} \quad (6.14)$$

With the proper design location of the oscillating arm pivot it is not possible to jam the follower. The pressure angle has less effect on the performance of the system which



**FIGURE 6.6** Forces for radial cam, oscillating roller follower.

is one of the reasons oscillating followers are a more popular design choice than translating followers.

**6.3.4 Pressure Angle Forces—Translating Flat-Faced Follower**

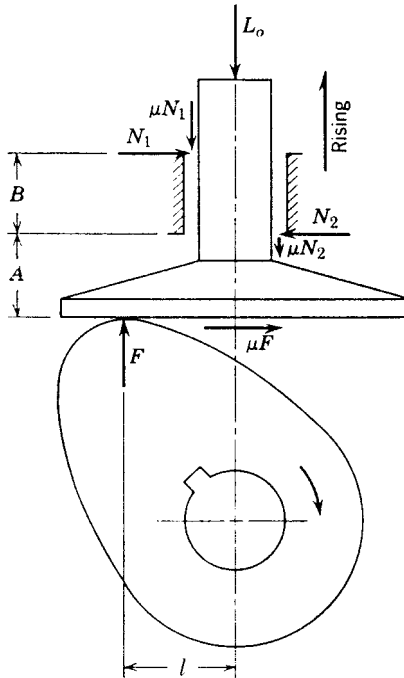
The pressure angle of a radial cam with a translating flat-faced follower has the advantage of being zero at all times. Thus the side thrust or jamming effect on translating flat-faced followers is inconsequential compared to that of translating roller followers. Nevertheless a force analysis is presented for comparison. The normal forces to the follower are  $N_1$  and  $N_2$  with their respective frictional components; Fig. 6.7. The new symbols are:

- $l$  = the distance from the normal force  $F$  to the axis of the follower, in
- $\mu_c$  = coefficient of friction between the cam and the flat-faced follower surface
- $\mu$  = coefficient of friction of follower bearing

For the “follower,”  $\Sigma F_x = 0, \Sigma F_y = 0$  and the moments about point  $q$  are for the rising cycle with

$$\Sigma F_x = 0 = -\mu_c F + N_1 + N_2. \tag{6.15}$$

$$\Sigma F_y = 0 = -L + F - \mu N_2 - \mu N_1 \tag{6.16}$$



**FIGURE 6.7** Forces for radial cam, translating flat-faced follower.

$$\Sigma N_q = 0 = 1F - AN_2 + (A + B)N_1 - \mu N_1 W + \mu N_2 W. \quad (6.17)$$

Solving these equations and eliminating  $\mu_c N_1 W$  and  $\mu N_2 W$ , whose differences are negligible, gives

$$F = \frac{BL}{B + 2l\mu - \mu\mu_c(2A + B)} \quad (6.18)$$

$$N_2 = \frac{(\mu_c A - l)L}{B + 2l\mu - \mu\mu_c(2A + B)} \quad (6.19)$$

$$N_1 = \frac{[\mu_c(2A + B) - l]L}{B + 2l\mu - \mu\mu_c(2A + B)}. \quad (6.20)$$

For best action, the overhang  $A$  (which varies through the complete cycle) should be as small and rigid as possible and the coefficient of friction  $\mu_c$  should be kept as small as possible, such as by a good lubricant and minimization of contaminants.

## 6.4 CAM RADIUS OF CURVATURE

### 6.4.1 Radius of Curvature

In the previous discussion, we saw that the pressure angle and cam size are directly related and the size of the cam should be as small as possible. However, as the cam size is reduced, another design parameter, *radius of curvature* is affected. The radius of curvature has a limiting value for the following reasons:

1. Undercutting could be introduced to yield an erroneous cam shape.
2. Surface contact stresses may be exceeded.
3. Heat treatment could produce cracks.

In other words, the cam surface radius of curvature will have a minimum allowable design value that will satisfy the other design factors. The shape of a curve at any point (its flatness or sharpness) depends on the rate of change of direction called curvature. We may construct for each point of the curve a tangent circle whose curvature is the same as that of the curve at that point. The radius of this circle is called radius of curvature. Figure 6.8 shows the center  $C$  of the radius of curvature of a point  $p$  of the curve. Note that the radius of curvature is continuously changing as we move toward other points on the curve.

From calculus we know that if the curve is in the Cartesian coordinate form  $y = f(x)$ , the radius of curvature

$$\rho = \frac{\{1 + [f'(x)]^2\}^{3/2}}{f''(x)}. \quad (6.21)$$

If a curve is given in polar coordinate form  $r = f(\theta)$ , the radius of curvature

$$\rho = \frac{\{f^2(\theta) + [f'(\theta)]^2\}^{3/2}}{[f(\theta)]^2 + 2[f'(\theta)]^2 - f(\theta)f''(\theta)}. \quad (6.22)$$

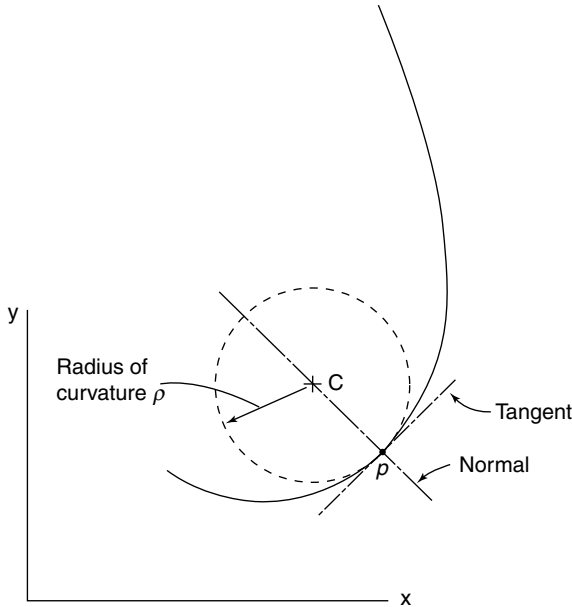


FIGURE 6.8 Curvature of a curve.

The radius of curvature is positive (+) for convex cam surfaces and negative (-) for concave cam surfaces (see Fig. 6.9).

### 6.4.2 Undercutting of Cam-Roller Follower

*Undercutting* is a phenomenon in which the constructed cam profile has a faulty shape. Cam undercutting is dependent on the radius of curvature, the follower acceleration, and the size of the cam. The easiest way to avoid undercutting is to make a larger cam. To investigate for undercutting one must find the radii of curvature at every point in the cam profile. For concave cams using roller followers the acceleration at the initial point of rise generally controls. In convex profiles utilizing either the roller or flat-faced followers the maximum negative acceleration controls.

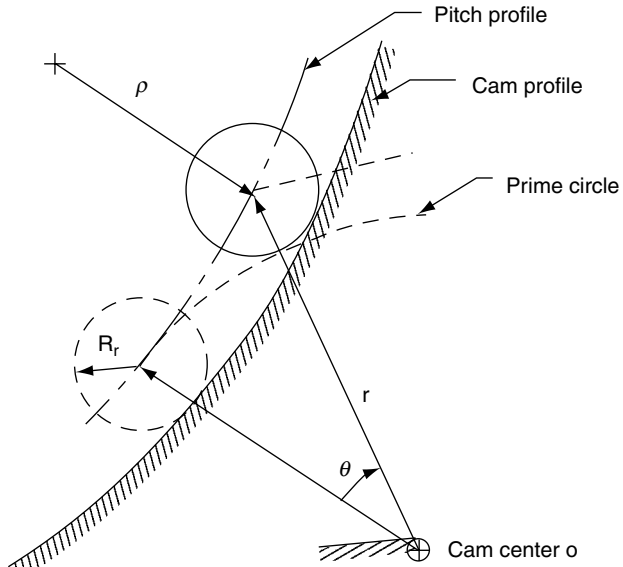
Let

$\rho_k$  = radius of curvature of pitch curve, in

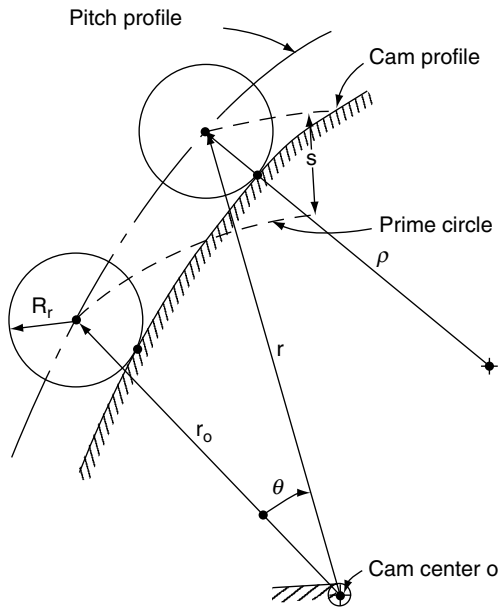
$\rho_c$  = radius of curvature of cam profile, in

$R_r$  = radius of follower roller, in

Figure 6.10 shows the different possibilities of roller action. At point (a) on the figure the concave segment of the curve has proper action where the radius of curvature  $\rho_k > 0$ . At point (b) on the convex segment curve we have a condition  $\rho_k = R_r$  and the center of the roller radius  $R_r$  moves on the pitch curve about a single point on the cam profile. A sharp point is produced which is not acceptable because of excessive stresses.



(a) Concave cam.



(b) Convex cam.

FIGURE 6.9 Typical cam contours.

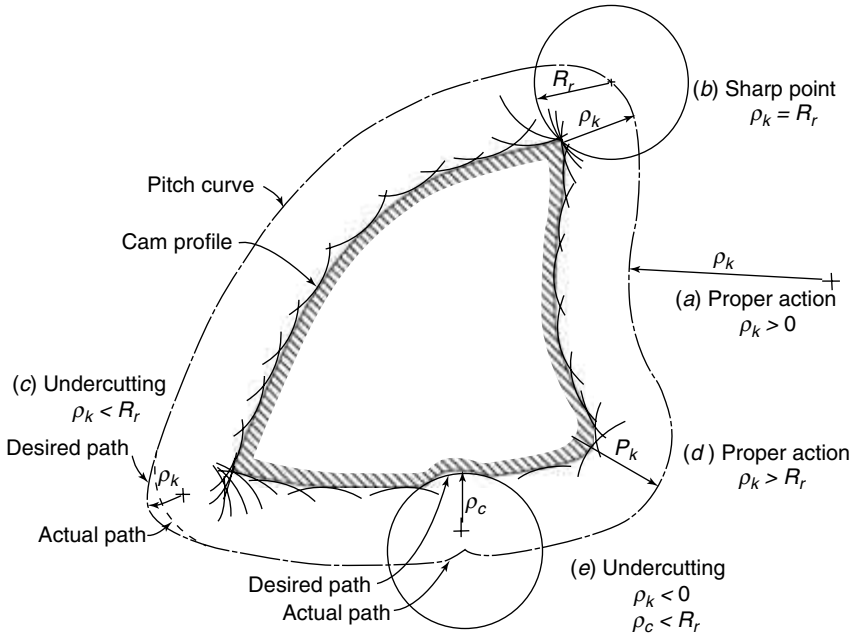


FIGURE 6.10 Effect of curvature on cam and roller follower.

At the convex curve, point (c),  $\rho_k$  of the pitch curve is less than  $R_r$ . Undercutting occurs, and the developed cam profile will not constrain the trace point to the pitch curve. The motion of the follower (dotted path) will not be as planned. At the concave curve, point (d),  $\rho_k$  is less than zero and a cusp is formed. Again, a form of undercutting occurs in which the follower cannot follow the path desired. But, at points (d) and (e), the radius of curvature  $\rho_k$  is adequate in size and the action is proper. The following suggestions are offered to alleviate the serious condition of undercutting or sharp corners on the cam.

Undercutting rarely occurs on the concave portion of the cam curve. However, the radius of curvature of the actual cam profile should always be larger than the roller radius by a margin of design safety. The following summarizes the design needs:

- Examination of Eqs. (6.21) and (6.22) shows that the radius of curvature  $\rho$  and the acceleration factor  $f''(x)$  are inversely related to each other and that an increase in the acceleration factor  $f''(x)$  will result in a decrease in the radius of curvature. Thus, the minimum radius of curvature usually occurs in the region where the negative acceleration is a maximum.
- The radius of curvature decreases with decreases in the prime circle radius of the roller follower. The radius of curvature must be greater than the follower roller radius. Use a roller size that is as small as possible within design limitations of roller wear and life. The minimum recommendation  $\rho_k < 3R_r$ , or  $\rho_k < 5$  to  $7R_r$ , is suggested.
- The curvature effect is not as critical in internal cams as in external cams because of lower stresses.

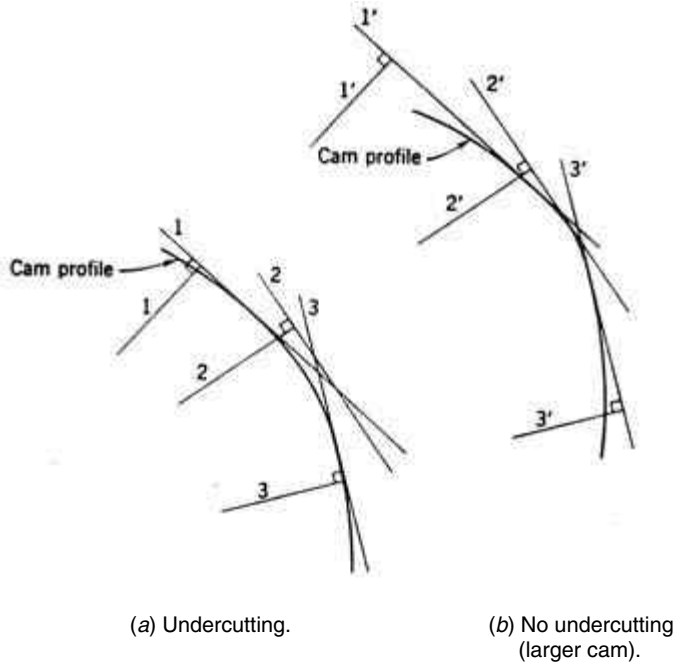


FIGURE 6.11 Undercutting of cam by flat-faced follower.

### 6.4.3 Undercutting of Cam—Flat-Faced Follower

It has been shown that the size of the pressure angle is always zero and thus has no effect on the required cam size of the flat-faced follower. Therefore, the only limiting factor of the size of the cam for the follower is the phenomenon of undercutting. In Fig. 6.11, a flat-faced follower is shown tangent to the cam at its respective positions 1, 2, and 3 to construct the cam. The cam profile, drawn tangent to the flat-faced follower, cannot be made to contact the follower at position 2. In other words, follower positions 1 and 3 eliminate or undercut position 2. The cam thus developed is incapable of driving the follower in the desired manner. Figure 6.11*b* shows a larger cam without undercutting. Thus undercutting limits the cam size to a minimum value in flat-faced followers.

### 6.4.4 Hub Design

Obviously, the cam must have a hub large enough to accommodate the shaft upon which it turns. The first step in the design of a cam-follower system is to establish the size of the cam shaft and the hub key necessary. Stresses and deflections are the controlling factors in this choice. For a cast iron cam, the hub diameter is

$$d_h = 1\frac{3}{4}d_s + \frac{1}{4} \text{ in} \tag{6.21}$$

where  $d_s$  is the shaft diameter in inches (see Fig. 6.12).

For steel cams, the hub may be made slightly smaller. For additional strength, locate the key in the largest portion of the cam body, which will also easily establish the proper

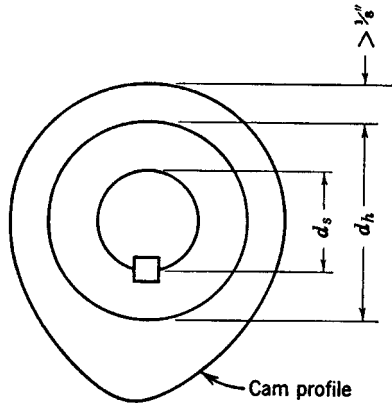


FIGURE 6.12 Hub size.

relative position of the follower and the cam in assembling the mechanism. In practice, the cam profile is made larger than the hub by at least 1/8 in. This is to prevent stress concentrations and short life in the cam surface.

## 6.5 SUMMARY

The three pertinent factors involved in determining the minimum cam size are pressure angle, profile curvature, and hub size. The pressure angle is the steepness of the cam and therefore determines the side thrust or wear of the translating roller follower in its bearing guide and the performance of an oscillating roller follower. This side thrust exists only during the rise, i.e., when the follower motion is in the opposite direction to the follower load. The maximum pressure angle should be made as small as possible during this action. For the roller follower, this is done by having the coefficient of friction and the follower stem overhang small, and the follower bearing long, with the stem as rigid as possible. With flat-faced followers, the pressure angle, being constant (usually equal to zero), is not of design consideration. Also, the side thrust pressure angle effects do not exist with properly designed oscillating followers.

For most machines having translating roller followers, the maximum pressure angle is  $30^\circ$  or less, but the author has gone as high as  $47.5^\circ$  with light loads and rigid, low-friction linkages, such as linear ball bearings. Reduction in pressure angle may be achieved by using a larger cam, an offset follower, a different cam curve, or a secondary follower. Equation 6.13 may be used to establish the roller follower cam size for cylindrical cams and for yielding acceptable accuracy for radial cams.

We have seen that not all cams can be constructed to give the desired motion to the followers. This condition, called undercutting, is attributed to the follower surface radius of curvature, the follower acceleration, and the cam size. In concave profiles using roller followers, the acceleration at  $\theta = 0$  generally controls. In convex profiles, using either a roller or flat-faced follower, the maximum negative acceleration controls. The easiest solution to this problem of undercutting is to employ a larger cam. Furthermore, without undercutting, sharp corners may be produced in the cam profile. Last, the hub or shaft size is another limiting factor in determining the minimum cam size.

---

# CHAPTER 7

---

# GEOMETRY OF PLANAR CAM PROFILES

---

**Jorge Angeles, Ph.D.**

*Dept. of Mech. Eng. McGill University CANADA  
angeles@cim.mcgill.ca*

**Carlos S. López-Cajún, Ph.D.**

*Depto. de Ing Mecánica Universidad A. de Querétaro MEXICO  
carlos@citlali.imt.mx*

**J. Jesús Cervantes-Sánchez, Ph.D.**

*Depto. de Ing. Mecánica Universidad de Guanajuato MEXICO  
jecer@salamanca.ugto.mx*

7.1 INTRODUCTION	177	7.4 COMPUTATIONAL SCHEMES	186
7.2 LOCAL PROPERTIES OF THE CAM PROFILE	177	7.5 COMMERCIAL SOFTWARE PACKAGES	203
7.3 GLOBAL PROPERTIES OF THE CAM PROFILE	184	7.6 CASE STUDIES	204

---

## ***SYMBOLS***

---

$a$  = radius of camshaft  
 $a_i$  = scalar component of  $\mathbf{w}_i$   
 $A$  = cam area  
 $A_i$  = component of  $\mathbf{w}_i$   
 $A \dots G$  = cubic spline matrices  
 $A_{xi} \dots D_{yi}$  = cubic spline coefficients at the  $i$ th point  $P_i$   
 $\mathbf{b}_i$  = vector component of  $\mathbf{w}_i$   
 $c$  = radius of balancing hole  
 $c$  = fixed component of follower displacement  
 $\mathbf{c}$  = centroid vector  
 $c_1$  = x component of centroid location  
 $c_2$  = y component of centroid location  
 $c_3$  = z component of centroid location  
 $C$  = closed cam surface contour  
 $d$  = component location along axis of rotation  
 $e$  = follower offset  
 $e$  = counterweight radius component  
 $\mathbf{e}_n$  = unit normal vector  
 $\mathbf{e}_t$  = unit tangential vector  
 $\mathbf{e}_\theta$  = polar circumferential unit vector  
 $\mathbf{e}_\rho$  = polar radial unit vector  
 $E$  = 90 degree CCW rotation matrix

$f$  = counterweight centroid location  
 $f_s$  = centrifugal force  
 $F(O,x,y,z)$  = 3D cam coordinate frame  
 $h_{ik}$  = polynomial coefficient  
 $h$  = radial difference vector  
 $I_o$  = cam inertia matrix  
 $I_{xx}$  = inertia component about x axis  
 $I_{yy}$  = inertia component about y axis  
 $I_{xy}$  = product of inertia  
 $I_{xz}$  = product of inertia  
 $I_{yz}$  = product of inertia  
 $I_{zz}$  = polar moment of inertia  
 $I^o$  = inertia about O  
 $J^o$  = polar moment of inertia about O  
 $K$  = center of cam curvature  
 $l$  = distance from cam center to oscillating follower pivot  
 $m$  = radial difference vector  
 $m_s$  = centrifugal moment  
 $n$  = position index count  
 $n_i$  = unit outward normal vector of  $\Gamma$   
 $O$  = center of cam rotation  
 $O_\lambda$  = start of arc  
 $p$  = cam surface position, length  
 $p$  = position vector  
 $q$  = first moment of cam area  
 $q^o$  = first moment about O  
 $Q^o$  = first moment about O  
 $r$  = cam radius of curvature  
 $r$  = position vector  
 $r_i$  = position vector to surface  
 $R$  = cam region  
 $s_i$  = cam surface length  
 $s(\psi)$  = follower displacement function  
 $S$  = solid boundary  
 $S_i$  = polygon segment  
 $t$  = thickness  
 $v_i$  = third moment of  $\Gamma_i$  segment  
 $V$  = cam volume  
 $V_j$  = solid volume  
 $w_i$  = inertia evaluation component  
 $x$  = Cartesian coordinate  
 $x_i$  = location of balancing hole center  
 $x_i$  = center of mass location  
 $y$  = Cartesian coordinate  
 $y$  = output displacement  
 $z$  = Cartesian coordinate  
 $'$  = first spatial derivative  
 $''$  = second spatial derivative  
 $||$  = absolute value  
 $\alpha$  = pressure angle  
 $\alpha_m$  = minimum pressure angle  
 $\alpha_M$  = maximum pressure angle  
 $\psi$  = angle of cam rotation

$\Delta$  = difference angle  
 $\Delta$  = incremental area  
 $\gamma$  = angle between tangent to cam and radius  
 $\Gamma$  = cam surface or curve  
 $\kappa$  = cam surface curvature  
 $\lambda$  = arc length  
 $\mu$  = angle between velocity vector and cam radius  
 $\mu$  = ramp function from 0 to 1  
 $\rho$  = radius to point Q on cam profile  
 $\rho$  = mass density  
 $\sigma(\psi)$  = positive definite follower displacement function  
 $\theta$  = angle to point Q on cam profile  
 $\varphi(\psi)$  = follower oscillation function  
 $\omega$  = camshaft speed

## 7.1 INTRODUCTION

---

The geometric properties of the profile of disk cams is studied here. To produce accurate values of both *local* and *global* properties of the contour, a suitable number of points  $\{P_i\}_1^m$  on the cam profile, with Cartesian coordinates  $(x_i, y_i)$ , for  $i = 1, \dots, m$ , is required. Local properties pertain to slope and curvature values throughout the contour; global properties involve area or, correspondingly, volume, centroid location, and moments and products of inertia of the cam.

Thus, global geometric properties require the calculation of integrals, which, broadly speaking, involve numerically stable computations. That is, truncation errors induced by the discretization of the contour are attenuated due to the *filtering* effect of integrations, although care must be taken to produce results that are accurate enough. Various techniques are currently available for the systematic evaluation of the integrals that arise in this context, those yielding the highest accuracy for a fixed value of  $m$  being techniques based on spline representations of the contour.

However, regarding the calculation of local properties, the truncation errors due to the contour discretization are amplified by virtue of the differentiations involved. Various techniques are available to cope with these problems; the techniques favored in this chapter are those based on a spline representation of the contour.

Thus, a methodology for handling the discrete points via nonparametric and parametric cubic splines is described. In Sec. 7.2 various concepts of differential geometry are outlined; these involve local properties such as slope, which is needed in the calculation of the pressure angle, and cam curvature, which arises in avoiding cusps and *undercutting*. In Sec. 7.3, the computation of the global properties of the cam is studied.

The computational issues around the calculation of the local and global geometric properties of planar cam plates are addressed in Sec. 7.4. An outline of relevant commercial software is included in Sec. 7.5, and Sec. 7.6 closes with some case studies.

## 7.2 LOCAL PROPERTIES OF THE CAM PROFILE

---

The differential-geometry relationships pertaining to cam profiles are discussed in this section. These relationships will be used later for determining the cam profile and some related variables, such as the tangent orientation, required to evaluate the pressure angle, and the curvature of the cam profile, required to verify the occurrence of cusps and under-

cutting. This information is also needed in planning the trajectory of the cutter of an NC machine tool.

### 7.2.1 Tangent at a Point of a Cam Profile

To systematically obtain a relationship for determining the angle between the position vector of a point on the cam profile and the tangent at that point, we refer to Fig. 7.1. In that figure,  $\lambda$  measures the arc length from a reference point  $O_\lambda$ , and  $\mathbf{e}_t$  is a unit vector parallel to line  $T$ , the tangent at point  $Q$  of the curve  $\Gamma$ . Note that  $\mathbf{e}_t$  points in the direction in which  $\lambda$  grows.

It would be desirable to obtain an expression for vector  $\mathbf{e}_t$  as a parametric representation of the position vector  $\mathbf{p}$  of an arbitrary point of the contour, of components  $x$  and  $y$ , that is,  $\mathbf{p} = [x, y]^T$ . However,  $x$  and  $y$  are usually available as functions of a parameter  $q$  different from  $\lambda$ . Hence, derivatives with respect to  $\lambda$  will be obtained using the *chain rule*. First, from elementary differential geometry, Marsden and Tromba (1988), we have

$$\mathbf{e}_t = \frac{d\mathbf{p}}{d\lambda} = \frac{d\mathbf{p}}{dq} \frac{dq}{d\lambda} = \frac{\mathbf{p}'(q)}{\lambda'(q)} \tag{7.1}$$

where

$$\mathbf{p}(q) = \begin{bmatrix} x(q) \\ y(q) \end{bmatrix} \quad \text{and} \quad \mathbf{p}'(q) = \begin{bmatrix} x'(q) \\ y'(q) \end{bmatrix}. \tag{7.2}$$

Next, since  $\mathbf{e}_t$  is a unit vector, we have

$$\lambda'(q) = \pm \|\mathbf{p}'(q)\| = \pm \sqrt{x'^2(q) + y'^2(q)} \tag{7.3}$$

where, obviously, the negative sign is used if  $\lambda'(q) < 0$ . Thus,

$$\mathbf{e}_t = \begin{cases} \mathbf{p}'(q) / \|\mathbf{p}'(q)\|, & \text{if } \lambda'(q) > 0 \\ -\mathbf{p}'(q) / \|\mathbf{p}'(q)\|, & \text{if } \lambda'(q) < 0 \end{cases} \tag{7.4}$$

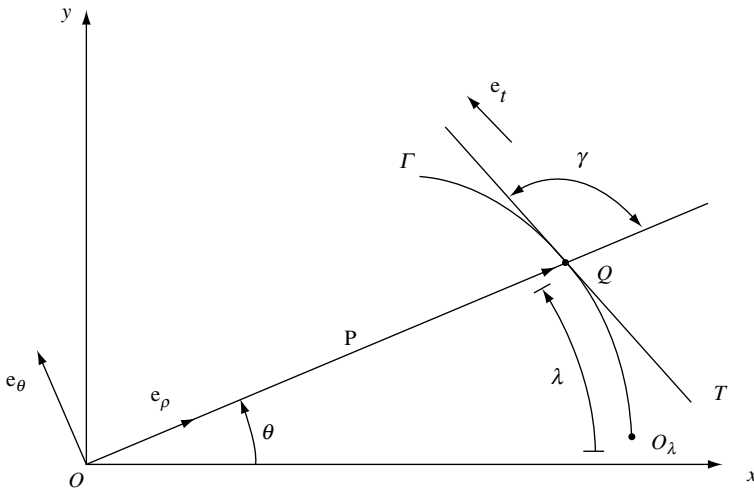


FIGURE 7.1. Geometric variables of a planar curve.

Sometimes the cam contour is given in polar coordinates  $\rho$  and  $\theta$  in the form  $\rho = \rho(\theta)$  or, equivalently, in parametric form as  $\rho = \rho(\psi)$  and  $\theta = \theta(\psi)$ , where  $\psi$  denotes the angular displacement of the cam plate. In this case, the position vector of a point on the cam profile is given in terms of two mutually orthogonal unit vectors,  $\mathbf{e}_\rho$  and  $\mathbf{e}_\theta$ , pointing in the directions in which  $\rho$  and  $\theta$  increase, respectively. Thus,

$$\mathbf{p} = \rho(\theta)\mathbf{e}_\rho \tag{7.5}$$

Differentiating both sides of Eq. (7.5) with respect to the arc length  $\lambda$  yields

$$\frac{d\mathbf{p}}{d\lambda} \equiv \mathbf{e}_t = \rho(\theta) \frac{d\theta}{d\lambda} \mathbf{e}_\theta + \frac{d\rho}{d\theta} \frac{d\theta}{d\lambda} \mathbf{e}_\rho \tag{7.6}$$

where the *chain rule* and the relation  $d\mathbf{e}_\rho/d\theta = \mathbf{e}_\theta$  have been used. On dot-multiplying both sides of Eq. (7.5) by  $\mathbf{e}_\theta$  and  $\mathbf{e}_\rho$ , one obtains

$$\mathbf{e}_\theta \cdot \mathbf{e}_t \equiv \sin \gamma = \rho(\theta) \frac{d\theta}{d\lambda}, \quad \mathbf{e}_\rho \cdot \mathbf{e}_t = \cos \gamma = \frac{d\rho}{d\theta} \frac{d\theta}{d\lambda}. \tag{7.7}$$

Furthermore, combining Eq. (7.7) yields

$$\tan \gamma = \frac{\rho(\theta)}{\rho'(\theta)}, \quad \rho'(\theta) \equiv \frac{d\rho}{d\theta}. \tag{7.8}$$

These results are used in deriving the synthesis equations of the cam profile (Angeles and Lopez-Cajún, 1991).

### 7.2.2 Pressure Angle

The direction of the tangent to the cam profile, given by the angle  $\gamma$  between the tangent and the radius vector  $\rho$ , is used to determine the *pressure angle of the profile*. This variable can be defined as the angle between the normal to the cam profile and the velocity of the point of the follower at which the force exerted by the cam is applied. Let us assume in this discussion that the velocity of the point of interest is parallel to line  $L$ , which is shown in Fig. 7.2, the normal to the cam profile being denoted by  $N$ .

Since we assume  $L$  to be known, we know the angle between  $L$  and line  $OP$ , called  $\mu$  here. With this information, we should be able to calculate the pressure angle  $\alpha$  in terms of  $\gamma$  and  $\mu$ . In fact, from Fig. 7.2, if the difference  $\Delta$  between  $\mu$  and  $\alpha$  is subtracted from  $\gamma$ , the angle between  $N$  and  $T$  is obtained, which is  $\pi/2$ , i.e.,

$$\gamma - \Delta = \pi/2$$

where

$$\Delta = \mu - \alpha$$

and hence,

$$\alpha = \frac{\pi}{2} - (\gamma - \mu)$$

which is the desired relation. Expressions for  $\mu$  vary from case to case, but the principle is the same. In particular,  $\mu$  depends on the angle of rotation of the cam,  $\psi$ , and the position of the follower, whether translational or angular.

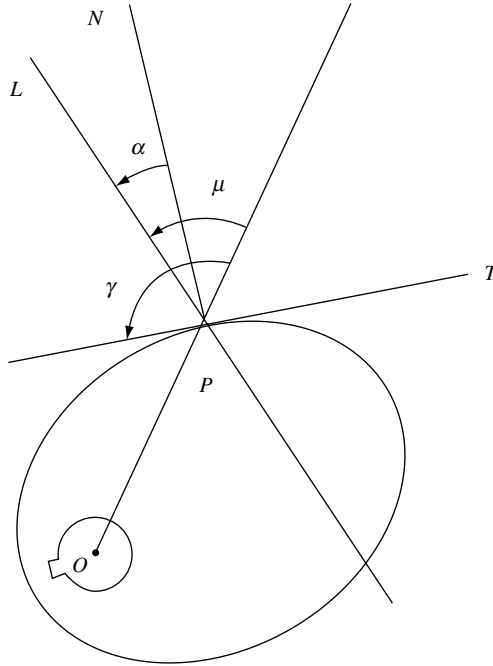


FIGURE 7.2. Notation for pressure-angle determination.

**7.2.3 Cam Curvature**

The shape of a planar curve  $\Gamma$  depends on the rate of change of the direction of its tangent with respect to the arc length, a measure that is called the *curvature* of  $\Gamma$ , and designated hereafter as  $\kappa$ . This variable plays an important role in the design of cam mechanisms, for it is directly related to the occurrence of cusps and the already mentioned effect known as *undercutting*. The reciprocal of the curvature  $\kappa$  is the radius of curvature  $r$ , i.e.,

$$r = \frac{1}{\kappa}. \tag{7.9}$$

The radius of curvature at a point of the cam profile is the radius of a circle tangent at that point to the cam profile, on the concave side, as shown in Fig. 7.3. The curvature of that circle is the same as that of the cam profile. For our purposes, the radius of curvature is positive if the center  $K$  of the circle is located between the center of rotation  $O$  and the point of tangency  $Q$ ; otherwise, the radius of curvature is negative. In the discussion that follows, formulas for calculating the curvature at any point of a cam profile are derived.

Let us consider a planar curve, as shown in Fig. 7.4. At any point  $P$  on the curve, whose position vector is denoted by  $\mathbf{p}$ , a unique orthonormal pair of vectors is defined, namely, the tangent and the normal vectors indicated in that figure as  $\mathbf{e}_t$  and  $\mathbf{e}_n$ . Let  $\lambda$  measure the arc length as in Fig. 7.4.

Unit vectors  $\mathbf{e}_t$  and  $\mathbf{e}_n$ , their derivatives with respect to  $\lambda$ , and the curvature  $\kappa$  are related by the Frenet-Serret formulas, Brand (1965), namely,

$$\frac{d\mathbf{e}_t}{d\lambda} = \kappa \mathbf{e}_n \tag{7.10}$$

$$\frac{d\mathbf{e}_n}{d\lambda} = -\kappa \mathbf{e}_t \tag{7.11}$$

Now, let the position vector  $\mathbf{p}$  be a function of a parameter  $q$  that, in general, is different from  $\lambda$ . Differentiation of  $\mathbf{p}$  with respect to  $q$  twice yields

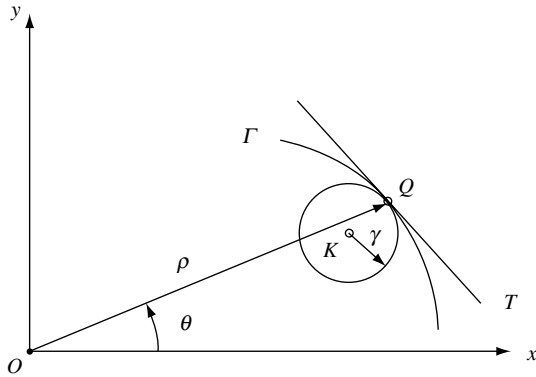


FIGURE 7.3. Visualization of the radius of curvature.

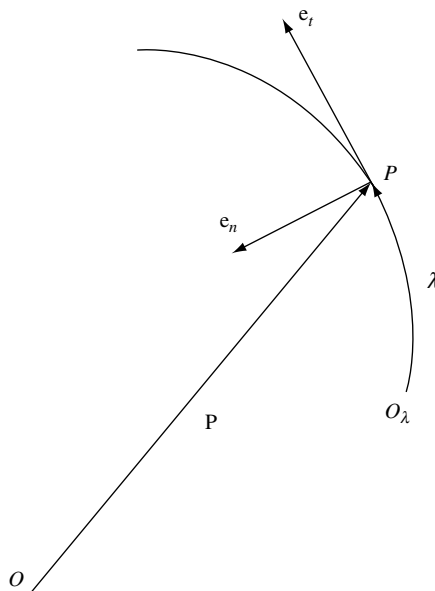


FIGURE 7.4. Planar curve and the orthonormal vectors  $\mathbf{e}_t$  and  $\mathbf{e}_n$ .

$$\mathbf{p}'(q) \equiv \frac{d\lambda}{dq} \frac{d\mathbf{p}}{d\lambda} = \lambda'(q)\mathbf{e}_t \quad (7.12a)$$

$$\mathbf{p}''(q) = \lambda''(q)\mathbf{e}_t + \lambda'^2(q)\kappa\mathbf{e}_n \quad (7.12b)$$

where Eq. (7.10) has been used.

An expression for  $\kappa$  can now be derived in terms of the geometric variables of the cam profile from Eqs. (7.12a and b). It is apparent that the expression sought is a scalar, which calls for a scalar operation between the vectors of those equations. However, the dot product of the right-hand side of those equations will not be very helpful. Indeed, on dot-multiplying those two sides, the term in  $\kappa$  will vanish because vectors  $\mathbf{e}_n$  and  $\mathbf{e}_t$  are mutually orthogonal. An alternative consists in first rotating vector  $\mathbf{e}_t$  through an angle of  $90^\circ$  counterclockwise, which can be done by multiplying both sides of Eq. (7.12b) by matrix  $\mathbf{E}$ , defined as

$$\mathbf{E} = \begin{bmatrix} 0 & -1 \\ 1 & 0 \end{bmatrix} \quad (7.13)$$

Thus,

$$\mathbf{E}\mathbf{p}''(q) = \lambda''(q)\mathbf{E}\mathbf{e}_t + \lambda'^2(q)\kappa\mathbf{E}\mathbf{e}_n \quad (7.14)$$

where

$$\mathbf{E}\mathbf{e}_t = \mathbf{e}_n \quad \text{and} \quad \mathbf{E}\mathbf{e}_n = -\mathbf{e}_t \quad (7.15)$$

Hence,

$$\mathbf{E}\mathbf{q}''(q) = -\lambda'^2(q)\kappa\mathbf{e}_t + \lambda''(q)\mathbf{e}_n \quad (7.16)$$

Second, on dot-multiplying the corresponding sides of Eqs. (7.12a) and (7.16), we obtain

$$\mathbf{p}'(q)^T \mathbf{E}\mathbf{p}''(q) = -\lambda'^3(q)\kappa \quad (7.17)$$

and, if we recall Eq. (7.3),

$$\mathbf{p}'(q)^T \mathbf{E}\mathbf{p}''(q) = -\|\mathbf{p}'(q)\|^3 \operatorname{sgn}[\lambda'(q)]\kappa \quad (7.18)$$

where  $\operatorname{sgn}(\cdot)$  is the *signum* function of  $(\cdot)$ , which is defined as +1 if its argument is positive and -1 if its argument is negative. If the argument vanishes, then we can define  $\operatorname{sgn}(\cdot)$  arbitrarily as zero. Therefore,

$$\kappa = -\operatorname{sgn}[\lambda'(q)] \frac{\mathbf{p}'(q)^T \mathbf{E}\mathbf{p}''(q)}{\|\mathbf{p}'(q)\|^3} \quad (7.19a)$$

or, if we realize that  $\mathbf{E}$  is skew symmetric, i.e.,  $\mathbf{E}^T = -\mathbf{E}$ , then we can also write

$$\kappa = \operatorname{sgn}[\lambda'(q)] \frac{\mathbf{p}''(q)^T \mathbf{E}\mathbf{p}'(q)}{\|\mathbf{p}'(q)\|^3} \quad (7.19b)$$

Either of Eqs. (7.19a and b) is the expression sought for the curvature of the cam profile. A visualization of Eq. (7.19b) is displayed in Fig. 7.5. In that figure, notice that  $\kappa > 0$  at  $P_1$ , which indicates a convexity at this point. Likewise,  $\kappa < 0$  at  $P_2$ , thereby indicating a concavity at  $P_2$ .

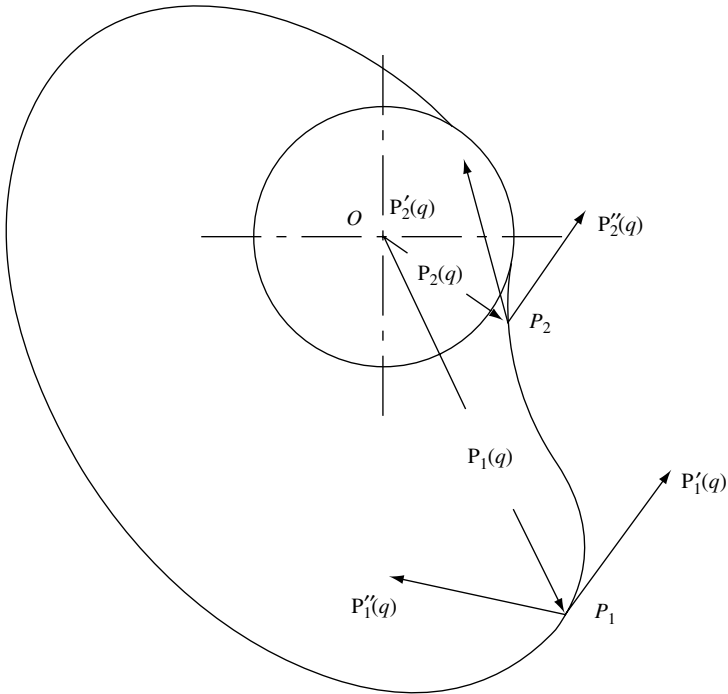


FIGURE 7.5. Concave and convex points of a cam profile.

Now, if we recall the components of vector  $\mathbf{p}(q)$  and its derivatives with respect to  $q$ , as given in Eq. (7.2), the curvature can be expressed as

$$\kappa = \text{sgn}(\lambda') \frac{x'y'' - y'x''}{(x'^2 + y'^2)^{3/2}}$$

where the argument  $q$  has been dropped for brevity.

If the cam profile is given instead in polar coordinates  $\rho = \rho(\theta)$ , then  $\theta$  can be considered as a parameter, and the position vector of any point of the curve can be expressed as

$$\mathbf{p}(\theta) = \rho(\theta)\mathbf{e}_\rho \tag{7.20}$$

where  $\mathbf{e}_\rho$  and  $\mathbf{e}_\theta$  are shown in Fig. 7.4. After differentiating both sides of Eq. (7.20) with respect to  $\theta$  twice, one has

$$\mathbf{p}'(\theta) = \rho(\theta)\mathbf{e}_\theta + \rho'(\theta)\mathbf{e}_\rho \tag{7.21}$$

$$\mathbf{p}''(\theta) = [\rho''(\theta) - \rho(\theta)]\mathbf{e}_\rho + 2\rho'(\theta)\mathbf{e}_\theta. \tag{7.22}$$

By substituting Eqs. (7.21) and (7.22) into Eqs. (7.12a and b), one obtains further

$$\kappa = \operatorname{sgn}(\lambda') \frac{\rho^2 + 2\rho'^2 - \rho\rho''}{(\rho^2 + \rho'^2)^{3/2}}$$

where the argument  $\theta$  has been dropped for compactness.

### 7.3 GLOBAL PROPERTIES OF THE CAM PROFILE

The global properties of a planar contour are its area, the position vector of its centroid, and its moments and products of inertia about a certain point, e.g., its centroid. Likewise, the global geometric properties of a closed region of the 3-D space are its volume, the position vector of its centroid, and its  $3 \times 3$  inertia matrix about a certain point such as its centroid. Below we recall the formal definitions of these items.

#### 7.3.1 Planar Contours

Let  $\mathcal{R}$  denote the region bounded by a closed contour  $C$  in the  $x$ - $y$  plane, and  $\mathbf{p}$  the position vector of a point  $P$  of  $\mathcal{R}$  in a frame  $\mathcal{F}(O, x, y, z)$ . Moreover, its area is denoted by  $A$ , its *first moment* by vector  $\mathbf{q}$ , and its inertia matrix about the given origin  $O$  by  $\mathbf{I}_O$ . Thus,

$$A = \int_{\mathcal{R}} dA \quad (7.23a)$$

$$\mathbf{q} = \int_{\mathcal{R}} \mathbf{p} dA \quad (7.23b)$$

$$\mathbf{I}_O = \int_{\mathcal{R}} (\|\mathbf{p}\|^2 \mathbf{1} - \mathbf{p}\mathbf{p}^T) dA \quad (7.23c)$$

where  $dA = dx dy$ ,  $\mathbf{1}$  is the  $2 \times 2$  identity matrix,  $\|\mathbf{p}\|^2$  denotes the square of the magnitude of  $\mathbf{p}$ , that is,

$$\|\mathbf{p}\|^2 = x^2 + y^2$$

and  $\mathbf{p}\mathbf{p}^T$  is the  $2 \times 2$  matrix *external product* recalled below:

$$\mathbf{p}\mathbf{p}^T = \begin{bmatrix} x \\ y \end{bmatrix} \begin{bmatrix} x & y \end{bmatrix} = \begin{bmatrix} x^2 & xy \\ xy & y^2 \end{bmatrix}.$$

Moreover, from the *mean-value theorem* of integral calculus [1], a vector  $\mathbf{c}$  exists such that

$$\mathbf{q} = A\mathbf{c}.$$

Vector  $\mathbf{c}$  thus defines the position of the *centroid*  $C$  of  $\mathcal{R}$ . Henceforth, the two components of  $\mathbf{c}$  in  $\mathcal{F}$  are denoted by  $c_1$  and  $c_2$ , i.e.,  $\mathbf{c} = [c_1, c_2]^T$ .

The moment of inertia of  $\mathcal{R}$  about  $C$  is then defined as

$$\mathbf{I}_C \equiv \int_{\mathcal{R}} [\|\mathbf{p} - \mathbf{c}\|^2 \mathbf{1} - (\mathbf{p} - \mathbf{c})(\mathbf{p} - \mathbf{c})^T] dA.$$

Moreover,  $\mathbf{I}_C$  reduces to

$$\mathbf{I}_C = \begin{bmatrix} I_{xx} & I_{xy} \\ I_{xy} & I_{yy} \end{bmatrix}$$

where

$$I_{xx} \equiv \int_{\mathcal{R}} (y - c_2)^2 dx dy$$

$$I_{yy} \equiv \int_{\mathcal{R}} (x - c_1)^2 dx dy$$

$$I_{xy} \equiv - \int_{\mathcal{R}} (x - c_1)(y - c_2) dx dy.$$

The quantities  $I_{xx}$  and  $I_{yy}$  are usually referred to as the centroid moments of inertia of  $\mathcal{R}$  about the  $x$  and  $y$  axes, respectively, whereas  $I_{xy}$  is termed the product of inertia of  $\mathcal{R}$  about its centroid. Moreover, the quantity  $I_{zz}$ , defined as

$$I_{zz} = I_{xx} + I_{yy}$$

is known as the *polar moment of inertia* of  $\mathcal{R}$  about its centroid.

The integral appearing in Eq. (7.23b) is called the *first moment* of  $\mathcal{R}$ , whereas  $\mathbf{I}_C$  is referred to as the *second moment* of  $\mathcal{R}$  about the centroid  $C$ . By extension, the integral of Eq. (7.23a) is also termed the *zeroth moment* of  $\mathcal{R}$ .

Calculating the three moments of  $\mathcal{R}$  directly as given above calls for a double integration, one in  $x$  and one in  $y$ . This is not practical, the foregoing integrals being more readily calculated if suitable transformation formulas are introduced, as indicated in Sec. 7.4, thereby reducing those calculations to line integrals. Furthermore, if the cam profile is described in polar coordinates as  $\rho = \rho(\theta)$ , then the area is given by

$$A = \frac{1}{2} \int_0^{2\pi} \rho^2(\theta) d\theta$$

which is a simple integral with similar expressions for  $\mathbf{q}$  and  $\mathbf{I}_C$ .

### 7.3.2 Solid Regions

Although the global geometric properties of cam disks can be described as those of a planar contour, the presence of nonsymmetric hubs, keyways, and the like render the cam plate a 3-D solid of a general shape. By the latter we mean a solid that cannot be generated by a simple *extrusion* or *sweeping* of the planar contour in a direction perpendicular to its plane. In this case, the global properties are those of a 3-D region  $\mathcal{R}$  bounded by a closed surface  $S$ , namely, its volume  $V$ , its vector first-moment  $\mathbf{q}$ , and its  $3 \times 3$  inertia matrix about point  $O$ . These are defined

$$\begin{aligned} V &\equiv \int_{\mathcal{R}} dV \\ \mathbf{q} &\equiv \int_{\mathcal{R}} \mathbf{p} dV \\ \mathbf{I}_O &\equiv \int_{\mathcal{R}} (\|\mathbf{p}\|^2 \mathbf{1} - \mathbf{p}\mathbf{p}^T) dV \end{aligned}$$

where, now,  $\mathbf{1}$  is the  $3 \times 3$  identity matrix,  $\mathbf{p} \equiv [x, y, z]^T$ , and hence,

$$\|\mathbf{p}\|^2 = x^2 + y^2 + z^2$$

while

$$\mathbf{pp}^T \equiv \begin{bmatrix} x \\ y \\ z \end{bmatrix} \begin{bmatrix} x & y & z \end{bmatrix} = \begin{bmatrix} x^2 & xy & xz \\ xy & y^2 & yz \\ xz & yz & z^2 \end{bmatrix}.$$

Again, from the mean-value theorem of integral calculus, a vector  $\mathbf{c}$  exists such that

$$\mathbf{q} = V\mathbf{c}$$

and vector  $\mathbf{c}$ , once more, defines the location of the *centroid*  $C$  of  $\mathcal{R}$ . Correspondingly, the three components of  $\mathbf{c}$  in a frame  $\mathcal{F}(O, x, y, z)$  are given by  $c_i$ , for  $i = 1, 2, 3$ , that is,  $\mathbf{c} = [c_1, c_2, c_3]^T$ .

The moment of inertia of  $\mathcal{R}$  about  $C$  is then defined as

$$\mathbf{I}_C \equiv \int_{\mathcal{R}} [\|\mathbf{p} - \mathbf{c}\|^2 \mathbf{1} - (\mathbf{p} - \mathbf{c})(\mathbf{p} - \mathbf{c})^T] dV$$

which then reduces to

$$\mathbf{I}_C = \begin{bmatrix} I_{xx} & I_{xy} & I_{xz} \\ I_{xy} & I_{yy} & I_{yz} \\ I_{xz} & I_{yz} & I_{zz} \end{bmatrix}$$

where

$$I_{xx} \equiv \int_{\mathcal{R}} [(y - c_2)^2 + (z - c_3)^2] dx dy dz$$

$$I_{yy} \equiv \int_{\mathcal{R}} [(x - c_1)^2 + (z - c_3)^2] dx dy dz$$

$$I_{zz} \equiv \int_{\mathcal{R}} [(x - c_1)^2 + (y - c_2)^2] dx dy dz$$

$$I_{xy} \equiv - \int_{\mathcal{R}} (x - c_1)(y - c_2) dx dy dz$$

$$I_{xz} \equiv - \int_{\mathcal{R}} (x - c_1)(z - c_3) dx dy dz$$

$$I_{yz} \equiv - \int_{\mathcal{R}} (y - c_2)(z - c_3) dx dy dz.$$

As in the case of planar contours, the foregoing calculations involve multiple integrals, in this instance, three. Reduced formulas transforming these calculations into surface and even line integrals are provided later.

## 7.4 COMPUTATIONAL SCHEMES

For static and dynamic balancing, and also for dynamic analysis (Koloc and Vaclacik, 1993), the determination of the cam global geometric properties is of the utmost importance. For example, very often the cam axis of rotation and the principal axis of inertia perpendicular to the cam disk are skew. Therefore, to balance the cam statically and dynamically, their global volumetric properties must be calculated. The calculation of these and the local properties requires the introduction of suitable numerical techniques that will be discussed later.

### 7.4.1 Cubic Splines

We focus here on the representation of the closed contours of planar cam mechanisms using the simplest geometric splines, namely, cubic splines.

A spline curve is an *interpolation tool* fully developed in the second half of the twentieth century (Dierckx, 1993). As applied to functions  $y = y(x)$ , for  $x \in [x_1, x_2]$ , classical interpolation tools include orthogonal polynomials of various kinds that go by names such as Legendre, Chebyshev, etc. (Kahaner et al., 1989). It is well known that, as the variations of  $y(x)$  in the interpolation interval become more pronounced, the order of the interpolating polynomial must be increased. However, the larger this order, the larger will be the condition number (Golub and Van Loan, 1983) of the underlying linear system of equations that must be solved for the polynomial coefficients. The larger the condition number, the larger is the roundoff-error amplification and, hence, the smaller the accuracy of the computed coefficients.

As a matter of fact, the use of a nonorthogonal polynomial readily leads to unacceptably high roundoff-error amplifications. Orthogonal polynomials offer a remedy to these amplifications but only to some extent. As an alternative to polynomial interpolation, spline functions were developed by numerical analysts to allow for lower-degree interpolating polynomials. Lower-degree interpolating polynomials are possible if they are defined *piecewise*. Thus, a cubic spline function is a piecewise cubic polynomial. Quintic spline functions are piecewise quintic polynomials.

As applied to geometric curves of the form  $F(x, y) = 0$ , spline functions, also called *nonparametric splines*, are not sufficient. Here is where parametric splines  $x = x(p)$ ,  $y = y(p)$  come into the picture. Notice that geometric curves, as opposed to curves representing functions, can have slopes making arbitrary angles with the coordinate axes, can cut themselves, thus giving rise to *double points*, and can have cusps. Not so curves representing functions. While we limit ourselves to cubic parametric splines, other spline curves are available that go by names such as Bézier curves, rational Bézier curves (Srinivasan and Ge, 1997), and NURBS, which stands for *non-uniform rational Bézier splines* (Rogers, 2001), as required for more advanced applications.

The cam profiles of interest are assumed to be closed smooth curves of the  $G^2$  type, i.e., with uniquely defined tangent and curvature everywhere, except for, possibly, some isolated points. Moreover, functions describing the Cartesian coordinates of a cam profile, i.e.,  $x = x(\psi)$  and  $y = y(\psi)$ , are also periodic functions of  $\psi$ . In the following discussion we introduce an alternative parameter,  $p$ , as yet to be defined, and regard  $x$  and  $y$  as functions  $x(p)$  and  $y(p)$ .

Let  $(x_i, y_i)$ , where  $x_i \equiv x(\psi_i)$  and  $y_i \equiv y(\psi_i)$ , for  $i = 1, \dots, n$ , be a discrete set of points generated on the cam profile. Since we need a closed smooth curve<sup>1</sup> the pertinent periodic boundary conditions must be satisfied, namely,

$$x_1 = x_n, \quad x'_1 = x'_n, \quad x''_1 = x''_n, \quad y_1 = y_n, \quad y'_1 = y'_n, \quad y''_1 = y''_n \tag{7.24}$$

where  $x'_i$  and  $x''_i$  are defined as

$$x'_i \equiv \left. \frac{dx}{dp} \right|_{x=x_i}, \quad x''_i \equiv \left. \frac{d^2x}{dp^2} \right|_{x=x_i} \tag{7.25}$$

with similar definitions for  $y'_i$  and  $y''_i$ . Conditions in Eq. (7.24) can be satisfied by resorting to a periodic parametric cubic spline, as discussed in Rogers (2001) and outlined below.

---

<sup>1</sup> If cusps are allowed at the endpoints  $P_1(x_1, y_1)$  and  $P_2(x_2, y_2)$ , then the slope and curvature conditions of Eq. (7.24) must be relaxed.

Let  $(x, y)$  be the coordinates of one point of the cam profile. The curve describing the cam profile can be represented in parametric form as

$$x(p) = A_{xi}(p - p_i)^3 + B_{xi}(p - p_i)^2 + C_{xi}(p - p_i) + D_{xi} \quad (7.26a)$$

$$y(p) = A_{yi}(p - p_i)^3 + B_{yi}(p - p_i)^2 + C_{yi}(p - p_i) + D_{yi} \quad (7.26b)$$

for  $p_i \leq p \leq p_{i+1}$  and  $i = 1, \dots, n - 1$ , with further definitions:

$$p_i = 0, \quad p_{i+1} = p_i + \Delta p_i \quad (7.27a)$$

$$\Delta p_i = \sqrt{\Delta x_i^2 + \Delta y_i^2} \quad (7.27b)$$

$$\Delta x_i = x_{i+1} - x_i, \quad \Delta y_i = y_{i+1} - y_i. \quad (7.27c)$$

Notice that parameter  $p$  represents a length measured along the perimeter of the polygon defined by the set of vertices  $\{P_i\}_1^m$ . In the foregoing description,  $x_i$  and  $y_i$  represent, additionally, the Cartesian coordinates of the  $i$ th supporting point (SP)  $P_i$  of the spline, while coefficients  $A_{ui}$ ,  $B_{ui}$ ,  $C_{ui}$ ,  $D_{ui}$ , for  $u = x, y$ , and  $i = 1, \dots, n - 1$ , are determined as explained presently. Let us define the  $n'$  ( $\equiv n - 1$ )-dimensional vectors

$$\mathbf{x} \equiv [x_1, \dots, x_{n'}]^T, \quad \mathbf{y} \equiv [y_1, \dots, y_{n'}]^T \quad (7.28a)$$

$$\mathbf{x}' \equiv [x'_1, \dots, x'_{n'}]^T, \quad \mathbf{y}' \equiv [y'_1, \dots, y'_{n'}]^T \quad (7.28b)$$

and

$$\mathbf{x}'' \equiv [x''_1, \dots, x''_{n'}]^T, \quad \mathbf{y}'' \equiv [y''_1, \dots, y''_{n'}]^T. \quad (7.28c)$$

The relationships between  $\mathbf{x}$  and  $\mathbf{x}''$  and  $\mathbf{y}$  and  $\mathbf{y}''$  are linear (Rogers, 2001), namely,

$$\mathbf{Ax}'' = 6\mathbf{Cx}, \quad \mathbf{Ay}'' = 6\mathbf{Cy}. \quad (7.29)$$

Note that the  $\mathbf{A}$  and  $\mathbf{C}$  matrices appearing above are themselves functions of the coordinates of the SP. In fact the  $n' \times n'$  matrices  $\mathbf{A}$  and  $\mathbf{C}$  are defined as

$$\mathbf{A} = \begin{bmatrix} 2\alpha_{1,n'} & \alpha_1 & 0 & 0 & \cdots & \alpha_{n'} \\ \alpha_1 & 2\alpha_{1,2} & \alpha_2 & 0 & \cdots & 0 \\ 0 & \alpha_2 & 2\alpha_{2,3} & \alpha_3 & \cdots & 0 \\ \vdots & \vdots & \ddots & \ddots & \ddots & \vdots \\ 0 & 0 & \cdots & \alpha_{n''} & 2\alpha_{n'',n''} & \alpha_{n''} \\ \alpha_{n'} & 0 & 0 & \cdots & \alpha_{n''} & 2\alpha_{n'',n'} \end{bmatrix}$$

and

$$\mathbf{C} = \begin{bmatrix} -\beta_{1,n'} & \beta_1 & 0 & 0 & \cdots & \beta_{n'} \\ \beta_1 & -\beta_{1,2} & \beta_2 & 0 & \cdots & 0 \\ 0 & \beta_2 & -\beta_{2,3} & \beta_3 & \cdots & 0 \\ \vdots & \vdots & \ddots & \ddots & \ddots & \vdots \\ 0 & 0 & \cdots & \beta_{n''} & -\beta_{n'',n''} & \beta_{n''} \\ \beta_{n'} & 0 & 0 & \cdots & \beta_{n''} & -\beta_{n'',n'} \end{bmatrix}$$

where

$$\alpha_k = \Delta p_k, \quad \alpha_{i,j} = \alpha_i + \alpha_j, \quad \beta_k = 1/\alpha_k, \quad \beta_{i,j} = \beta_i + \beta_j$$

for  $i, j, k = 1, \dots, n'$ , and

$$n' = n - 1, \quad n'' = n - 2, \quad n''' = n - 3.$$

On the other hand, the relations between  $\mathbf{x}$  and  $\mathbf{x}'$ , and between  $\mathbf{y}$  and  $\mathbf{y}'$  can be written as

$$\mathbf{x}' = (\mathbf{F} - \mathbf{GC})\mathbf{x}, \quad \mathbf{y}' = (\mathbf{F} - \mathbf{GC})\mathbf{y} \tag{7.30}$$

where the  $n' \times n'$  matrices  $\mathbf{F}$  and  $\mathbf{G}$  are given by:

$$\mathbf{F} = \begin{bmatrix} -\alpha_1 & \alpha_1 & 0 & 0 & \cdots & 0 \\ 0 & -\alpha_2 & \alpha_2 & 0 & \cdots & 0 \\ 0 & 0 & -\alpha_3 & \alpha_3 & \cdots & 0 \\ \vdots & \vdots & \ddots & \ddots & \ddots & \vdots \\ & & & & & \alpha_{n''} \\ \alpha_{n'} & & & & & -\alpha_{n'} \end{bmatrix}$$

$$\mathbf{G} = \begin{bmatrix} 2\beta_1 & \beta_1 & 0 & 0 & \cdots & 0 \\ 0 & 2\beta_2 & \beta_2 & 0 & \cdots & 0 \\ 0 & 0 & 2\beta_3 & \beta_3 & \cdots & 0 \\ \vdots & \vdots & \ddots & \ddots & \ddots & \vdots \\ & & & & & \beta_{n''} \\ \beta_{n'} & & & & & 2\beta_{n'} \end{bmatrix}.$$

For the synthesis of the cam profile, the SPs, and hence, the spline coefficients are available. In fact, with the SPs known, the coefficients  $A_{ui}, B_{ui}, C_{ui}, D_{ui}$ , for  $u = x, y$ , and  $i = 1, \dots, n - 1$  can be calculated, the coordinates of the interpolated points then following from Eqs. (7.26a and b). These points are meant for the actual display of the cam profile and the generation of the cutter path of the machine tool, if the follower is of the flat-face type. If the follower is of the roller type, the interpolated points represent the pitch curve, the cam profile then being obtained as the *envelope* (Angeles and Lopez-Cajun, 1991) of the set of positions of the roller. This procedure is illustrated in Sec. 7.6.

### 7.4.2 Local Properties

In the design phase one has information only about the displacement program, i.e., one knows  $s(\psi)$  in the case of translational followers, or  $\phi(\psi)$  in the case of their oscillating counterparts, but the dimensions of the cam are, as yet, to be determined. Hence, the local geometric properties of the cam profile are to be computed based on  $s(\psi)$  or, correspondingly, on  $\phi(\psi)$  and its derivatives with respect to  $\psi$ . Thus, in this subsection we introduce formulas for calculating the curvature and the pressure angle of the cam profile in terms of the displacement program and its derivatives.

**7.4.2.1 Translating Flat-Face Followers.** Apparently, the pressure angle for translating flat-face followers is constantly equal to zero and needs no further discussion.

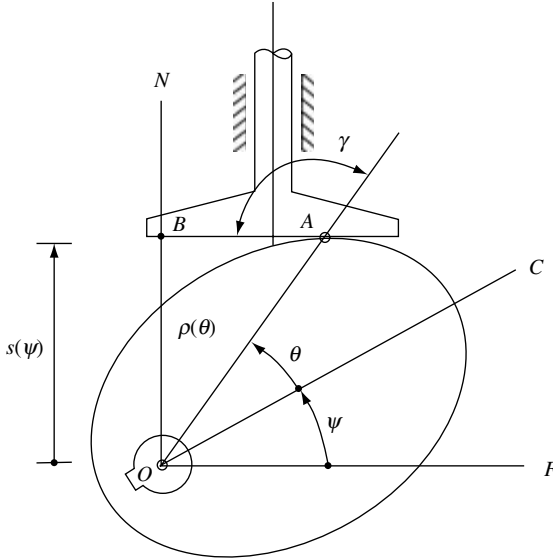


FIGURE 7.6. Layout of a translating flat-face follower cam mechanism.

On the other hand, the curvature of the cam profile can be calculated by means of the formula (Angeles and Lopez-Cajun, 1991)

$$\kappa = \frac{1}{s + s''} \tag{7.31}$$

where  $s$  and  $s''$  are, respectively, the translational displacement of the follower and its second derivative with respect to the angular displacement of the cam. The parameters involved are displayed in Fig. 7.6.

**7.4.2.2 Oscillating Flat-Face Followers.** As in the previous case, the pressure angle for oscillating flat-face followers is also constantly equal to zero. On the other hand, the formula for calculating the curvature of the cam profile is given by Angeles and Lopez-Cajun (1991)

$$\kappa = \frac{(1 + \phi')^3}{|F(\psi)|} \tag{7.32a}$$

where

$$F(\psi) \equiv \phi'' \cos \phi + (1 + \phi') [(1 + 2\phi') \sin \phi + \bar{e}(1 + \phi')^2], \quad \bar{e} \equiv \frac{e}{l} \tag{7.32b}$$

$\phi$  being the angular displacement of the follower and  $e$  as shown in Fig. 7.7.

**7.4.2.3 Translating Knife-Edge and Roller Followers.** The translating knife-edge follower shown in Fig. 7.8 is not usually found in practice, because of the large contact stresses that it produces. However, it has theoretical and practical importance because its

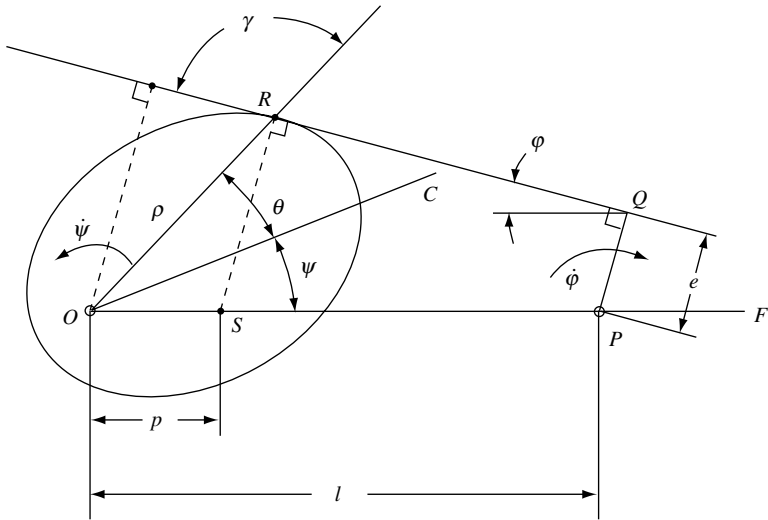


FIGURE 7.7. Layout of a disk cam with oscillating flat-face follower.

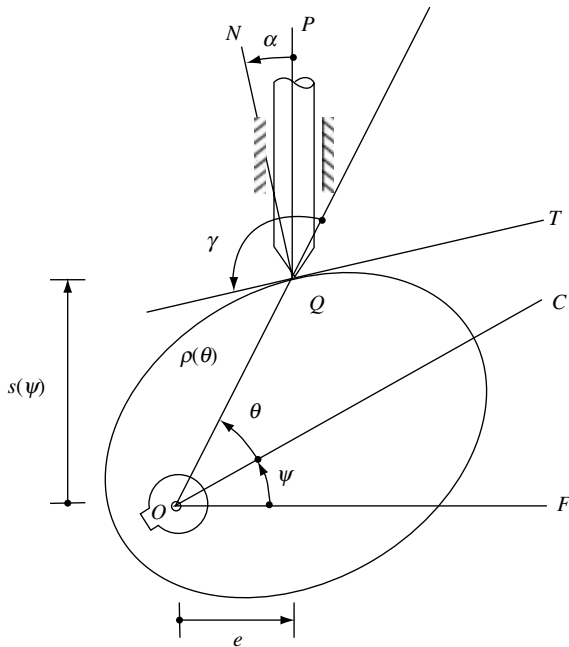


FIGURE 7.8. Geometry of a cam mechanism with a translating knife-edge follower.

associated cam profile is the trajectory of the center of the roller follower, which is known as the *pitch curve*. Moreover, if the roller-follower cam is machined with a mill having a radius identical to that of its roller, then the pitch curve is identical to the trajectory of the cutter center, the curve needed for the programming of the NC machine tool used to produce the cam disk. Thus, for translating knife-edge and roller followers, the pressure-angle  $\alpha$  can be obtained by:

$$\tan \alpha = \frac{s' - e}{s} \quad (7.33)$$

where  $s'$  is the first derivative of the displacement  $s$  with respect to the angle  $\psi$  and  $e$  as shown in Fig. 7.8.

On the other hand, for both the knife-edge and the roller-follower, the curvature of the pitch curve is given by

$$\kappa_k = \frac{N}{D} \quad (7.34a)$$

where (Angeles and Lopez-Cajun, 1991)

$$N \equiv s(s - s'') + (s' - e)(2s' - e) \quad (7.34b)$$

and

$$D \equiv [s^2 + (s' - e)^2]^{3/2}. \quad (7.34c)$$

**7.4.2.4 Oscillating Roller Followers.** For the oscillating roller follower, the formula given below can be used to calculate the pressure angle (Angeles and Lopez-Cajun, 1991)

$$\tan \alpha = \frac{l\rho'(\theta)\sin\phi + \rho(l\cos\phi - e)}{\rho'(\theta)(l\cos\phi - e) - l\rho\sin\phi} \quad (7.35a)$$

where

$$\rho'(\theta) = \frac{\rho'(\psi)}{\theta'(\psi)} \quad (7.35b)$$

$$\rho'(\psi) = \frac{e l \phi'(\psi) \sin \phi}{\rho} \quad (7.35c)$$

$$\theta'(\psi) = \frac{l \varepsilon \phi'(\psi) - \rho^2 [1 + \phi'(\psi)]}{\rho^2} \quad (7.35d)$$

and the parameters involved are shown in Fig. 7.9.

Finally, the formula for calculating the curvature of the pitch curve of the oscillating roller follower is (Angeles and Lopez-Cajun, 1991)

$$\kappa_k = \frac{e^2(1 + \phi')^3 - e l [(1 + \phi')(2 + \phi') \cos \phi + \phi'' \sin \phi] + l^2}{[e^2(1 + \phi')^2 - 2e l (1 + \phi') \cos \phi + l^2]^{3/2}} \quad (7.36)$$

where the argument  $\psi$  of  $\phi'$  and  $\phi''$  have been omitted for simplicity.

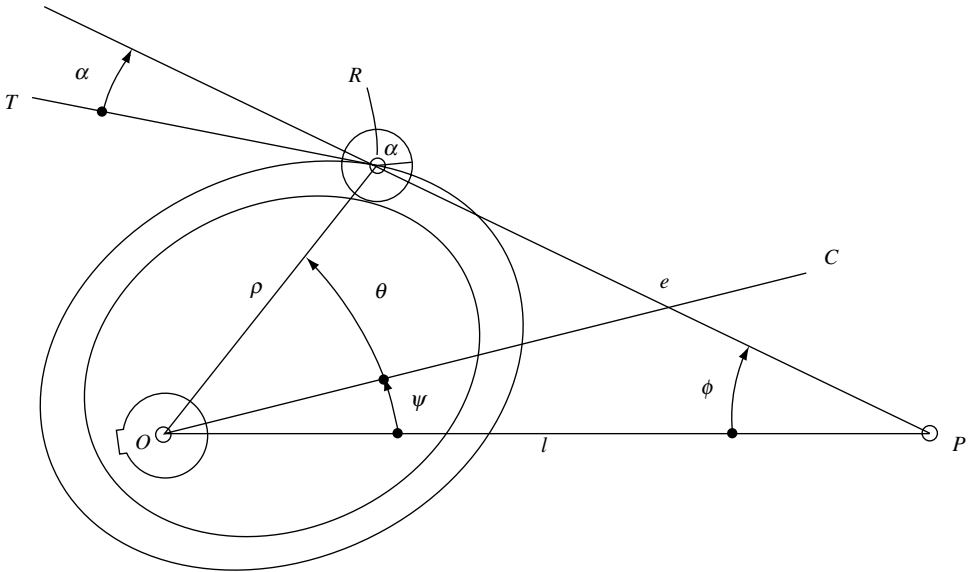


FIGURE 7.9. Cam mechanism with oscillating roller follower.

**7.4.2.5 Computation of the Local Properties.** As shown above, the curvature and the pressure angle depend on the displacement program and its derivatives. Thus, an adequate synthesis procedure of the displacement program is required.

The synthesis of the displacement program has been traditionally based on a limited set of functions giving rise to parabolic, harmonic, cycloidal, trapezoidal, and polynomial motions. More complex motions, such as those appearing in indexing cam mechanisms, can be synthesized using spline functions, which are also known as *nonparametric splines*.

Nonparametric cubic splines, when applied to the displacement programs  $s(\psi)$  or  $\phi(\psi)$ , take the simple forms

$$y(\psi) = A_i(\psi - \psi_i)^3 + B_i(\psi - \psi_i)^2 + C_i(\psi - \psi_i) + D_i, \quad \psi_i \leq \psi \leq \psi_{i+1} \quad (7.37)$$

for  $i = 1, \dots, n - 1$ , and with  $y$  representing  $s$  in the case of translating followers,  $\phi$  in the case of their oscillating counterparts. Now, if we define the  $(n - 1)$ -dimensional vectors  $\mathbf{y}$ ,  $\mathbf{y}'$ , and  $\mathbf{y}''$  in exactly the same way as defined in Subsec. 7.4.1, then the counterparts of relations (7.29) and (7.30) take the forms

$$\mathbf{A}\mathbf{y}'' = 6\mathbf{C}\mathbf{y} \quad (7.38)$$

$$\mathbf{y}' = (\mathbf{F} - \mathbf{G}\mathbf{C})\mathbf{y} \quad (7.39)$$

where  $\mathbf{A}$ ,  $\mathbf{C}$ ,  $\mathbf{F}$ , and  $\mathbf{G}$  are formally identical to their counterparts in Subsec. 7.4.1. Their differences are that  $\alpha_i$  and  $\beta_i$  in the entries of these matrices in that subsection change to  $\Delta\psi_i$  and  $1/\Delta\psi_i$ , respectively. In this case, obviously,

$$\Delta\psi_i \equiv \psi_{i+1} - \psi_i$$

The calculation of the pressure angle and the curvature of the profile at an arbitrary value of  $\chi$  outside of the set  $\{\psi_i\}_i^n$  calls for values of  $s'(\psi)$  and  $s''(\psi)$  or, correspondingly,  $\phi'(\psi)$  and  $\phi''(\psi)$  outside of the values arrayed in vectors  $\mathbf{y}'$  and  $\mathbf{y}''$ . These derivative values can be readily calculated by means of Eq. (7.37), namely, as

$$y'(\psi) = 3A_i(\psi - \psi_i)^2 + 2B_i(\psi - \psi_i) + C_i, \quad \psi_i \leq \psi \leq \psi_{i+1} \quad (7.40)$$

$$y''(\psi) = 6A_i(\psi - \psi_i) + 2B_i, \quad \psi_i \leq \psi \leq \psi_{i+1}. \quad (7.41)$$

With the foregoing interpolated derivative values, the calculation of the pressure angle and the curvature at arbitrary values of  $\psi$  is straightforward.

### 7.4.3 Global Properties

The computation of the global geometric properties—area for 2-D contours and volume for 3-D surfaces, centroid location, and inertia matrix—of cam plates is the subject of this subsection. Rather than using *directly* the definitions of these concepts, as given in Sec. 7.3, we resort to the Gauss divergence theorem (GDT) (Marsden and Tromba, 1988) to transform volume integrals into surface integrals. One second application of the GDT readily leads to algorithms based on line integrals, which are computationally more economical than the direct formulas.

**7.4.3.1 Two-Dimensional Regions.** In this subsection the general formulas introduced in Angeles et al. (1990) and recalled below are applied to 2-D regions. Thus, line-integration formulas will be derived for the computation of the area, the centroid position vector, and the inertia matrix of planar regions  $\mathcal{R}$  bounded by a closed contour  $\Gamma$ .

Let  $A$ ,  $\mathbf{q}^O$ , and  $\mathbf{I}^O$  denote the area, the vector first moment, and the matrix second moment of  $\mathcal{R}$ ,  $\mathbf{q}^O$ , and  $\mathbf{I}^O$  being defined with respect to a given point  $O$  in the plane of the region. The computation of these quantities can be reduced to integration on the boundary  $\Gamma$ , by application of the GDT, namely,

$$A = \frac{1}{2} \int_{\Gamma} \mathbf{r} \cdot \mathbf{n} d\Gamma \quad (7.42a)$$

$$\mathbf{q}^O = \frac{1}{2} \int_{\Gamma} (\mathbf{r} \cdot \mathbf{r}) \mathbf{n} d\Gamma = \frac{1}{3} \int_{\Gamma} \mathbf{r}(\mathbf{r} \cdot \mathbf{n}) d\Gamma \quad (7.42b)$$

$$\mathbf{I}^O = \int_{\Gamma} \mathbf{r} \cdot \mathbf{r} \left[ \frac{3}{8} \mathbf{1}(\mathbf{r} \cdot \mathbf{n}) - \frac{1}{2} \mathbf{r}\mathbf{n}^T \right] d\Gamma \quad (7.42c)$$

where  $\mathbf{1}$  denotes the  $2 \times 2$  identity matrix and  $\mathbf{n}$  is the unit outward normal of  $\Gamma$ , the products  $\mathbf{r} \cdot \mathbf{n}$  and  $\mathbf{r}\mathbf{n}^T$  being the inner product and the outer product of vectors  $\mathbf{r}$  and  $\mathbf{n}$ , already introduced in Sec. 7.3. Their products are reproduced below for quick reference, with  $r_i$  and  $n_i$ , for  $i = 1, 2$ , denoting the components of vectors  $\mathbf{r}$  and  $\mathbf{n}$ , correspondingly, in the given reference frame, i.e.,

$$\mathbf{r} \cdot \mathbf{n} = r_1 n_1 + r_2 n_2$$

and

$$\mathbf{r}\mathbf{n}^T = \begin{bmatrix} r_1 \\ r_2 \end{bmatrix} \begin{bmatrix} n_1 & n_2 \end{bmatrix} = \begin{bmatrix} r_1 n_1 & r_1 n_2 \\ r_2 n_1 & r_2 n_2 \end{bmatrix}.$$

The foregoing formulas, Eqs. (7.42a–c), are applied below to planar regions with piecewise-linear and cubic-spline approximations of their boundaries, respectively. Note that  $\mathbf{q}^o$  can be computed with two alternative formulas, which are given in Eq. (7.42b). We recall here that the second of these formulas is more suitable for applications involving piecewise linear approximations, given the simple forms that the  $\mathbf{r} \cdot \mathbf{n}$  term produces in such cases. Both formulas will prove to be useful in deriving practical simple formulas, as shown below.

**7.4.3.2 Piecewise-Linear Approximation of the Boundary.** If  $\Gamma$  in Eqs. (7.42a to 7.42c) is approximated by a closed  $n$ -sided polygon, then

$$\Gamma \approx \bigcup_1^n \Gamma_i, \tag{7.43}$$

where  $\Gamma_i$  denotes the  $i$ th side of the polygon. The aforementioned formulas, thus, can be approximated as

$$A \approx \frac{1}{2} \sum_1^n \int_{\Gamma_i} \mathbf{r} \cdot \mathbf{n}_i d\Gamma_i \tag{7.44a}$$

$$\mathbf{q}^o \approx \frac{1}{2} \sum_1^n \int_{\Gamma_i} (\mathbf{r} \cdot \mathbf{r}) \mathbf{n}_i d\Gamma_i = \frac{1}{3} \sum_1^n \int_{\Gamma_i} \mathbf{r} (\mathbf{r} \cdot \mathbf{n}_i) d\Gamma_i. \tag{7.44b}$$

$$\mathbf{I}^o \approx \sum_1^n \int_{\Gamma_i} \mathbf{r} \cdot \mathbf{r} \left[ \frac{3}{8} \mathbf{1} (\mathbf{r} \cdot \mathbf{n}_i) - \frac{1}{2} \mathbf{r} \mathbf{n}_i^T \right] d\Gamma_i. \tag{7.44c}$$

where  $\mathbf{n}_i$  denotes the outward normal unit vector of  $\Gamma_i$ , and hence is a constant along this side of the approximating polygon.

Furthermore, let  $A_i$ ,  $\mathbf{q}_i^o$ , and  $\mathbf{I}_i^o$  be the contributions of  $\Gamma_i$ , the  $i$ th side of the polygon, to the corresponding integral,  $s_i$  and  $\bar{\mathbf{r}}_i$  denoting its length and the position vector of its centroid, as shown in Fig. 7.10. From this figure, the reduced calculations are readily derived, namely,

$$A_i = \frac{1}{2} \mathbf{n}_i \cdot \int_{\Gamma_i} \mathbf{r} d\Gamma_i = \frac{1}{2} \mathbf{n}_i \cdot \bar{\mathbf{r}}_i s_i. \tag{7.45}$$

Using each of the two formulas of Eq. (7.44b), one obtains two alternative expressions for  $\mathbf{q}_i^o$  namely,

$$\mathbf{q}_i^o = \frac{1}{2} \left( \int_{\Gamma_i} \mathbf{r} \cdot \mathbf{r} d\Gamma_i \right) \cdot \mathbf{n}_i \tag{7.46a}$$

$$\mathbf{q}_i^o = \frac{1}{3} \left( \int_{\Gamma_i} \mathbf{r} \mathbf{r}^T d\Gamma_i \right) \cdot \mathbf{n}_i. \tag{7.46b}$$

By subtracting two times both sides of Eq. (7.46a) from three times both sides of Eq. (7.46b), one obtains

$$\mathbf{q}_i^o = -\mathbf{n}_i \cdot \int_{\Gamma_i} [(\mathbf{r} \cdot \mathbf{r}) \mathbf{1} - \mathbf{r} \mathbf{r}^T] d\Gamma_i. \tag{7.47}$$

The right-hand side of Eq. (7.47) is readily recognized—see Eq. (7.23c)—as the projection onto  $-\mathbf{n}_i$  of the matrix second moment of segment  $\Gamma_i$ , with respect to  $O$ , represented here as  $\mathbf{J}_i^o$ . Thus,

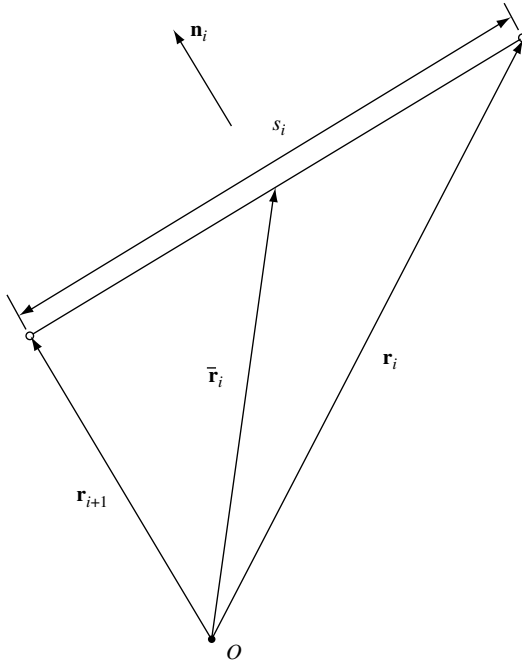


FIGURE 7.10. Segment  $\Gamma_i$  of the boundary.

$$\mathbf{q}_i^O = -\mathbf{n}_i \cdot \mathbf{J}_i^O \tag{7.48}$$

Furthermore,

$$\mathbf{I}_i^O = \int_{\Gamma_i} \mathbf{r} \cdot \mathbf{r} \left[ \frac{3}{8}(\mathbf{r} \cdot \mathbf{n}_i) - \frac{1}{2} \mathbf{r} \mathbf{n}_i^T \right] d\Gamma_i = \frac{3}{8} \mathbf{1}(\mathbf{n}_i \cdot \mathbf{v}_i) - \frac{1}{2} \mathbf{v}_i \mathbf{n}_i^T \tag{7.49}$$

with  $\mathbf{v}_i$ , a *third moment* of  $\Gamma_i$ , defined as

$$\mathbf{v}_i = \int_{\Gamma_i} (\mathbf{r} \cdot \mathbf{r}) \mathbf{r} d\Gamma_i \tag{7.50}$$

Now, vector  $\mathbf{r}$  appearing in the integrand of Eq. (7.50) is expressed as

$$\mathbf{r} = \mathbf{r}_i + \mu(\mathbf{r}_{i+1} - \mathbf{r}_i), \quad 0 \leq \mu \leq 1 \tag{7.51}$$

where  $\mathbf{r}_i$  and  $\mathbf{r}_{i+1}$  denote the position vectors of the endpoints of  $\Gamma_i$ . Thus, the foregoing vectors are the position vectors of the  $i$ th and the  $(i + 1)$ st vertices of the approximating polygon, which are assumed to be numbered in counterclockwise order. Moreover, since the polygon is closed,  $i + 1 = 1$ , for  $i = n$  in Eq. (7.51) and below. Substitution of Eq. (7.51) into Eq. (7.50) yields, for  $i = 1, \dots, n$ ,

$$\mathbf{v}_i = \int_0^1 [ \|\mathbf{r}_i\|^2 + 2\mu \mathbf{r}_i \cdot (\mathbf{r}_{i+1} - \mathbf{r}_i) + \mu^2 \|\mathbf{r}_{i+1} - \mathbf{r}_i\|^2 ] [ \mathbf{r}_i + \mu(\mathbf{r}_{i+1} - \mathbf{r}_i) ] d\mu$$

whence

$$\mathbf{v}_i = \frac{S_i}{3}(A_i \mathbf{r}_i + B_i \mathbf{r}_{i+1}) \tag{7.52a}$$

where  $A_i$  and  $B_i$  are the scalars defined as

$$A_i \equiv \mathbf{r}_i \cdot \mathbf{r}_{i+1} + \frac{1}{2} \mathbf{r}_i \cdot \mathbf{r}_i + \frac{S_i^2}{4} \tag{7.52b}$$

$$B_i \equiv 2\mathbf{r}_i \cdot \mathbf{r}_{i+1} - \frac{1}{2} \mathbf{r}_i \cdot \mathbf{r}_i + \frac{3}{4} S_i^2. \tag{7.52c}$$

Equations (7.45), (7.48), and (7.49 to 7.52c) are the relations sought.

7.4.3.2.1 *Spline Approximation of the Boundary.* The formulas introduced in Angeles et al. (1990) are now applied to regions whose boundary is approximated by periodic parametric cubic splines. Recalling expressions (7.26a and b), the  $(x, y)$  coordinates of one point on the boundary are represented as functions of parameter  $p$ , while  $x_i$  and  $y_i$  represent the Cartesian coordinates of the  $i$ th supporting point of the spline. Moreover, integrals (7.42a to c) are approximated as

$$A \approx \sum_1^{n-1} A_i \tag{7.53a}$$

$$Q_x^o \approx \sum_1^{n-1} Q_{xi}^o, \quad Q_y^o \approx \sum_1^{n-1} Q_{yi}^o \tag{7.53b}$$

$$I_x^o \approx \sum_1^{n-1} I_{xi}, \quad I_{xy}^o \approx \frac{1}{2} \left( \sum_1^{n-1} I_{xyi} + \sum_1^{n-1} I_{yxi} \right), \quad I_y^o \approx \sum_1^{n-1} I_{yi} \tag{7.53c}$$

with

$$A_i = \frac{1}{2} \int_{p_i}^{p_{i+1}} (xy' + x'y) dp = \sum_{k=1}^5 a_{ik} (\Delta p_i)^k \tag{7.53d}$$

$$Q_{xi}^o = \frac{1}{2} \int_{p_i}^{p_{i+1}} (x^2 + y^2) y' dp = \sum_{k=1}^9 q_{xik} (\Delta p_i)^k \tag{7.53e}$$

$$Q_{yi}^o = -\frac{1}{2} \int_{p_i}^{p_{i+1}} (x^2 + y^2) x' dp = \sum_{k=1}^9 q_{yik} (\Delta p_i)^k \tag{7.53f}$$

where

$$x' \equiv \frac{dx}{dp}, \quad y' \equiv \frac{dy}{dp}.$$

The polynomial coefficients  $a_{ik}$ ,  $q_{xik}$ , and  $q_{yik}$  appearing in Eqs. (7.53d to 7.53f) are included in App. C: Polynomial Coefficients. The components  $I_{xi}$ ,  $I_{yi}$ ,  $I_{xyi}$ , and  $I_{yxi}$  of the inertia matrix are computed as

$$\begin{aligned} I_{xi} &= \frac{1}{8} \int_{p_i}^{p_{i+1}} (x^2 + y^2)(xy' + 3x'y) dp \\ &= \frac{1}{8} \int_{p_i}^{p_{i+1}} (x^2 + y^2) xy' dp + \frac{3}{8} \int_{p_i}^{p_{i+1}} (x^2 + y^2) x'y dp \end{aligned} \tag{7.54a}$$

$$\begin{aligned}
 I_{yi} &= -\frac{1}{8} \int_{p_i}^{p_{i+1}} (x^2 + y^2)(3xy' + x'y) dp \\
 &= -\frac{3}{8} \int_{p_i}^{p_{i+1}} (x^2 + y^2)xy' dp - \frac{1}{8} \int_{p_i}^{p_{i+1}} (x^2 + y^2)x'y dp.
 \end{aligned} \tag{7.54b}$$

In the calculation of the product of inertia appearing in Eq. (7.53c), one summation would suffice to compute the product of inertia  $I_{xy}^O$ , given the symmetry of the inertia matrix. The two summations are computed here and then averaged to diminish roundoff or measurement errors that could be introduced if, for instance, the coordinates of the cam profile—the supporting points—were digitized or picked up with a coordinate measuring machine. Thus, the terms of both summations are given by

$$I_{xyi} = \frac{1}{2} \int_{p_i}^{p_{i+1}} (x^2 + y^2)xx' dp \tag{7.55}$$

$$I_{yxi} = -\frac{1}{2} \int_{p_i}^{p_{i+1}} (x^2 + y^2)yy' dp. \tag{7.56}$$

From Eqs. (7.54a to 7.56) it is noted that all components of the inertia matrix are given as linear combinations of four integrals, namely,

$$I_i^{(1)} \equiv \int_{p_i}^{p_{i+1}} (x^2 + y^2)xx' dp = \sum_1^{12} h_{ik}^{(1)}(\Delta p_i)^k \tag{7.57a}$$

$$I_i^{(2)} \equiv \int_{p_i}^{p_{i+1}} (x^2 + y^2)yy' dp = \sum_1^{12} h_{ik}^{(2)}(\Delta p_i)^k \tag{7.57b}$$

$$I_i^{(3)} \equiv \int_{p_i}^{p_{i+1}} (x^2 + y^2)x'y dp = \sum_1^{12} h_{ik}^{(3)}(\Delta p_i)^k \tag{7.57c}$$

$$I_i^{(4)} \equiv \int_{p_i}^{p_{i+1}} (x^2 + y^2)xy' dp = \sum_1^{12} h_{ik}^{(4)}(\Delta p_i)^k. \tag{7.57d}$$

The polynomial coefficients  $h_{ik}^{(1)}, \dots, h_{ik}^{(4)}$ , appearing in Eqs. (7.57a to 7.57d), are also included in App. C: Polynomial Coefficients.

**7.4.3.3 Three-Dimensional Regions.** For solid regions, the general relations of Angeles et al. (1990) reduce to

$$V_3 = \frac{1}{3} \int_S \mathbf{r} \cdot \mathbf{n} dS \tag{7.58}$$

$$\mathbf{q}_3^O = \frac{1}{2} \int_S (\mathbf{r} \cdot \mathbf{r}) \mathbf{n} dS = \frac{1}{4} \int_S \mathbf{r}(\mathbf{r} \cdot \mathbf{n}) dS \tag{7.59}$$

$$\mathbf{I}_3^O = \int_S \mathbf{r} \cdot \mathbf{r} \left[ \frac{3}{10} \mathbf{1}(\mathbf{r} \cdot \mathbf{n}) - \frac{1}{2} \mathbf{r}\mathbf{n}^T \right] dS. \tag{7.60}$$

Next, explicit formulas are discussed that are applicable to piecewise-linear approximations of boundaries of solids of arbitrary shapes.

One simple approximation of the boundary can be obtained by means of a polyhedron formed by polygonal faces. The integrals appearing in Eqs. (7.58 to 7.60), therefore, can be expressed as sums of integrals over the polyhedral faces, the whole boundary  $S$  thus being approximated as

$$S \approx \bigcup_1^n S_i \tag{7.61}$$

where each part  $S_i$  is a polygonal portion of a plane. The integral formulas thus can be approximated as

$$V_3 \approx \sum_1^n \frac{1}{3} \int_{S_i} \mathbf{r} \cdot \mathbf{n}_i dS_i \tag{7.62}$$

$$\mathbf{q}_3^O \approx \frac{1}{2} \sum_1^n \int_{S_i} (\mathbf{r} \cdot \mathbf{r}) \mathbf{n}_i dS_i = \frac{1}{4} \sum_1^n \int_{S_i} \mathbf{r} (\mathbf{r} \cdot \mathbf{n}_i) dS_i \tag{7.63}$$

$$\mathbf{I}_3^O \approx \sum_1^n \int_{S_i} \mathbf{r} \cdot \mathbf{r} \left[ \frac{3}{10} \mathbf{1} (\mathbf{r} \cdot \mathbf{n}_i) - \frac{1}{2} \mathbf{r} \mathbf{n}_i^T \right] dS_i. \tag{7.64}$$

Now, let  $V_{3i}$ ,  $\mathbf{q}_{3i}$ , and  $\mathbf{I}_{3i}^O$  be the contribution of the  $i$ th face  $S_i$  of the polyhedron to the corresponding integral,  $\Delta_i$ ,  $\bar{\mathbf{r}}_i$ , and  $\mathbf{I}_{\Delta_i}^O$  being the area, the position vector of the centroid, and the inertia matrix of the polygon  $S_i$ , respectively. (The last two quantities are taken with respect to  $O$ .) Then,

$$V_{3i} = \frac{1}{3} \mathbf{n}_i \cdot \int_{S_i} \mathbf{r} dS_i = \frac{1}{3} \mathbf{n}_i \cdot \bar{\mathbf{r}}_i \Delta_i. \tag{7.65}$$

We calculate the polygon area  $\Delta_i$  and its centroid  $\bar{\mathbf{r}}_i$  in a plane defined by the polygon, using the method applied to 2-D regions, as outlined earlier in this subsection.

By subtracting twice the rightmost-side of Eq. (7.63) from the middle one, we readily obtain an expression for  $\mathbf{q}_{3i}^O$  as a summation of terms  $\mathbf{q}_{3i}^O$  having the form

$$\begin{aligned} \mathbf{q}_{3i}^O &= -\frac{1}{2} \int_{S_i} [(\mathbf{r} \cdot \mathbf{r}) \mathbf{n}_i - (\mathbf{r} \cdot \mathbf{n}_i) \mathbf{r}] dS_i \\ &= -\frac{1}{2} \mathbf{n}_i \cdot \int_{S_i} [(\mathbf{r} \cdot \mathbf{r}) \mathbf{1} - \mathbf{r} \mathbf{r}^T] dS_i. \end{aligned} \tag{7.66}$$

The second integral of Eq. (7.66) is readily identified as  $\mathbf{I}_{\Delta_i}^O$ —the second moment of polygon  $S_i$ . Hence,

$$\mathbf{q}_{3i}^O = -\frac{1}{2} \mathbf{n}_i \cdot \mathbf{I}_{\Delta_i}^O \tag{7.67}$$

that is, the contribution of  $S_i$  to the first moment of  $\mathcal{R}$  is recognized as one-half the projection onto  $-\mathbf{n}_i$  of the second moment of  $S_i$ , both moments being taken, of course, with respect to the same point  $O$ . We calculate the centroidal inertia matrix of the polygon at hand using the formulas derived for 2-D regions in the plane defined by the polygon. Using the parallel-axis theorem and a rotation of axes, we then find  $\mathbf{I}_{\Delta_i}^O$  from the calculated centroidal inertia matrix.

Additionally, the contribution of the  $i$ th polygonal face to the second moment of the 3-D region under study takes the form

$$\mathbf{I}_{3i}^o = \frac{1}{2} \int_{S_i} \mathbf{r} \cdot \mathbf{r} \left[ \frac{3}{5} (\mathbf{r} \cdot \mathbf{n}_i) \mathbf{1} - \mathbf{r} \mathbf{n}_i^T \right] dS_i = \frac{3}{10} (\mathbf{n}_i \cdot \mathbf{w}_i) \mathbf{1} - \frac{1}{2} \mathbf{w}_i \mathbf{n}_i^T \quad (7.68)$$

with  $\mathbf{w}_i$  defined as:

$$\mathbf{w}_i \equiv \int_{S_i} (\mathbf{r} \cdot \mathbf{r}) \mathbf{r} dS_i. \quad (7.69)$$

The integral appearing in Eq. (7.69) is evaluated below. To this end,  $\mathbf{r}$  is expressed as:

$$\mathbf{r} = \bar{\mathbf{r}}_i + \mathbf{p} \quad (7.70)$$

where  $\mathbf{p}$  is a vector lying in the plane of the polygon  $S_i$  and stemming from the polygon centroid, as shown in Fig. 7.11. Now,  $\mathbf{w}_i$  becomes

$$\mathbf{w}_i = \bar{\mathbf{r}}_i^2 \Delta_i \bar{\mathbf{r}}_i + \bar{\mathbf{r}}_i \cdot \int_{S_i} (2\mathbf{p}\mathbf{p}^T + \mathbf{p}^2 \mathbf{1}) dS_i + \int_{S_i} \mathbf{p}^2 \mathbf{p} dS_i \quad (7.71)$$

where an exponent  $k$  over a vector quantity indicates the  $k$ th power of the magnitude of the said vector, that is,  $\mathbf{r}^2 \equiv \mathbf{r} \cdot \mathbf{r} = \|\mathbf{r}\|^2$ .

Three surface integrals over  $S_i$  are needed in the expression for  $\mathbf{w}_i$ , namely,

$$\mathbf{A}_i = \int_{S_i} \mathbf{p}\mathbf{p}^T dS_i \quad (7.72a)$$

$$a_i = \int_{S_i} \mathbf{p}^2 dS_i \quad (7.72b)$$

$$b_i = \int_{S_i} \mathbf{p}^2 \mathbf{p} dS_i. \quad (7.72c)$$

Since  $\mathbf{p}$  is a vector lying entirely in the plane  $\Pi_i$  defined by the polygon  $S_i$ , it can be represented uniquely in the 2-D subspace as a 2-D vector of that plane. Consequently, the GDT can be applied in this 2-D subspace to reduce the surface integrals (7.72a to c) to line integrals (Al-Daccak and Angeles, 1993), namely,

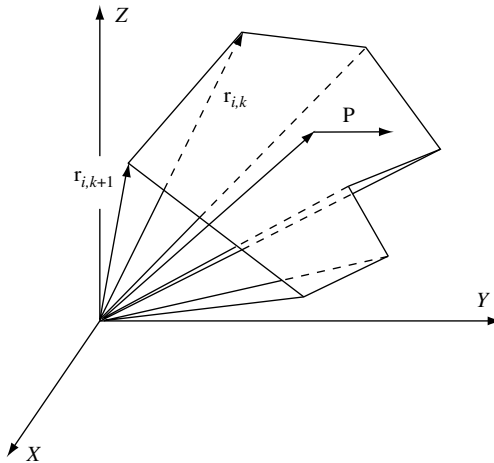


FIGURE 7.11. Polygon  $S_i$  representing one face of a polyhedron approximating a closed surface.

$$\mathbf{A}_i = \frac{1}{4} \int_{S_i} \text{div}(\mathbf{P}) dS_i = \frac{1}{4} \int_{\Gamma_i} \mathbf{p} \mathbf{p}^T (\mathbf{p} \cdot \bar{\mathbf{n}}) d\Gamma_i \tag{7.73a}$$

$$a_i = \frac{1}{4} \int_{S_i} \text{div}(\mathbf{p}^2 \mathbf{p}) dS_i = \frac{1}{4} \int_{\Gamma_i} \mathbf{p}^2 (\mathbf{p} \cdot \bar{\mathbf{n}}_i) d\Gamma_i \tag{7.73b}$$

$$\mathbf{b}_i = \frac{1}{5} \int_{S_i} \text{div}(\mathbf{p}^2 \mathbf{p} \mathbf{p}^T) dS = \frac{1}{5} \int_{\Gamma_i} \mathbf{p}^2 \mathbf{p} (\mathbf{p} \cdot \bar{\mathbf{n}}_i) d\Gamma_i \tag{7.73c}$$

where  $\mathbf{P}$  is a *third-rank* tensor that is cubic and homogeneous in  $\mathbf{p}$ . It is omitted here, the interested reader being referred to Al-Daccak and Angeles (1993) for further details. Moreover,  $\Gamma_i$  denotes the polygonal boundary of  $S_i$  contained in the plane  $\Pi_i$ . Note that, just as the GDT is used in 3-D to reduce volume integrals, it is used in 2-D to reduce surface integrals to line integrals.

Now let  $\Gamma_{i,k}$  denote the  $k$ th side of the  $m$ -sided polygon  $S_i$  that joins the  $k$ th and the  $(k + 1)$ st vertices, numbered counterclockwise when the face of interest is viewed from outside the polyhedron. Moreover, a sum over subscript  $k$  is to be understood, henceforth, as being *modulo*  $m$ . Furthermore, the position vector  $\mathbf{p}$ , shown in Fig. 7.12, of any point of  $\Gamma_{i,k}$  is defined in the plane  $\Pi_i$  as

$$\mathbf{p} = \mathbf{m}_{i,k} + \mathbf{h}_{i,k S_{i,k}}, \quad \mathbf{p} \in \Gamma_{i,k}, \quad 0 \leq s_{i,k} \leq 1 \tag{7.74}$$

where  $\mathbf{m}_{i,k}$  and  $\mathbf{h}_{i,k}$  are the vectors  $\mathbf{r}_{i,k} - \bar{\mathbf{r}}$  and  $\mathbf{r}_{i,k+1} - \mathbf{r}_{i,k}$ , respectively,  $\mathbf{r}_{i,k}$  being the position vector of the  $k$ th vertex of the polygon  $S_i$ . Similar to vector  $\mathbf{p}$ , vectors  $\mathbf{m}_{i,k}$  and  $\mathbf{h}_{i,k}$  lie solely in the plane  $\Pi_i$ . Consequently, their representation as 2-D vectors in that plane is used to apply the GDT to reduce the surface integrals defined over  $S_i$  to line integrals defined over  $\Gamma_{i,k}$ .

Let  $\mathbf{n}_{i,k}$  be the unit normal vector to  $\Gamma_{i,k}$  pointing outward of  $S_i$  and  $s_{i,k}$  be the length of the  $k$ th side of  $\Gamma_i$ . Thus, quantities  $\mathbf{A}_i$ ,  $a_i$ , and  $\mathbf{b}_i$  can be evaluated as indicated below, keeping in mind that  $s_{i,k} = \|\mathbf{h}_{i,k}\|$  and  $\mathbf{p} \cdot \mathbf{n}_{i,k} = \mathbf{m}_{i,k} \cdot \mathbf{n}_{i,k}$ , since  $\mathbf{h}_{i,k} \cdot \mathbf{n}_{i,k} = 0$ . Then

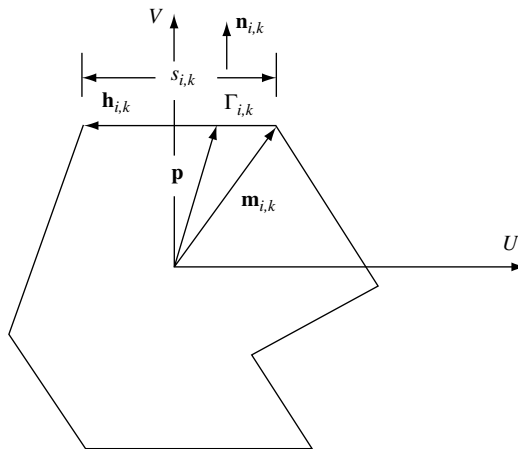


FIGURE 7.12. The  $i$ th polygon  $S_i$  contained in the plane  $\Pi_i$ .

$$\mathbf{A}_i = \frac{1}{4} \sum_{k=1}^m s_{i,k} (\mathbf{m}_{i,k} \cdot \mathbf{n}_{i,k}) \int_0^1 \mathbf{p} \mathbf{p}^T ds, \quad \mathbf{p} \in \Gamma_{i,k}. \quad (7.75a)$$

where

$$\mathbf{p} \mathbf{p}^T = (\mathbf{m}_{i,k} \mathbf{m}_{i,k}^T) + (\mathbf{m}_{i,k} \mathbf{h}_{i,k}^T + \mathbf{h}_{i,k} \mathbf{m}_{i,k}^T) + (\mathbf{h}_{i,k} \mathbf{h}_{i,k}^T) s^2 \quad (7.75b)$$

and hence

$$\int_0^1 \mathbf{p} \mathbf{p}^T ds = (\mathbf{m}_{i,k} \mathbf{m}_{i,k}^T) + \frac{1}{2} (\mathbf{m}_{i,k} \mathbf{h}_{i,k}^T + \mathbf{h}_{i,k} \mathbf{m}_{i,k}^T) + \frac{1}{3} (\mathbf{h}_{i,k} \mathbf{h}_{i,k}^T). \quad (7.75c)$$

Also

$$a_i = \frac{1}{4} \sum_{k=1}^m s_{i,k} (\mathbf{m}_{i,k} \cdot \mathbf{n}_{i,k}) \int_0^1 \mathbf{p}^2 ds, \quad \mathbf{p} \in \Gamma_{i,k}.$$

where

$$\mathbf{p}^2 = \mathbf{m}_{i,k}^2 + 2 \mathbf{m}_{i,k} \cdot \mathbf{h}_{i,k} s + \mathbf{h}_{i,k}^2 s^2$$

and hence,

$$\int_0^1 \mathbf{p}^2 ds = \mathbf{m}_{i,k}^2 + \mathbf{m}_{i,k} \cdot \mathbf{h}_{i,k} + \frac{1}{3} \mathbf{h}_{i,k}^2.$$

Furthermore,

$$\mathbf{b}_i = \frac{1}{5} \sum_{k=1}^m s_{i,k} (\mathbf{m}_{i,k} \cdot \mathbf{n}_{i,k}) \int_0^1 \mathbf{p}^2 \mathbf{p} ds, \quad \mathbf{p} \in \mathbf{G}_{i,k}$$

where

$$\mathbf{p}^2 \mathbf{p} = \mathbf{p}^2 \mathbf{m}_{i,k} + \mathbf{p}^2 \mathbf{h}_{i,k} s.$$

Therefore,

$$\begin{aligned} \int_0^1 \mathbf{p}^2 \mathbf{p} ds &= \mathbf{m}_{i,k} \left( \mathbf{m}_{i,k}^2 + \mathbf{m}_{i,k} \cdot \mathbf{h}_{i,k} + \frac{1}{3} \mathbf{h}_{i,k}^2 \right) \\ &+ \mathbf{h}_{i,k} \left( \frac{1}{2} \mathbf{m}_{i,k}^2 + \frac{2}{3} \mathbf{m}_{i,k} \cdot \mathbf{h}_{i,k} + \frac{1}{4} \mathbf{h}_{i,k}^2 \right). \end{aligned} \quad (7.76)$$

Once the three surface integrals given in Eqs. (7.72a) to 7.72c) have been reduced to line integrals and evaluated in plane  $\Pi_i$ , the results obtained in this 2-D subspace should be mapped to produce the results necessary for calculating  $\mathbf{w}_i$  in the 3-D space, Eq. (7.71). The scalar quantity  $a_i$  poses no problem and is readily multiplied by the  $3 \times 3$  identity matrix  $\mathbf{1}$  in the expression for  $\mathbf{w}_i$ . Furthermore, matrix  $\mathbf{A}_i$  and vector  $\mathbf{b}_i$  in the 2-D subspace are transformed to their matrix and vector counterparts, respectively, in the 3-D space, before being substituted into the expression for  $\mathbf{w}_i$ .

This completes the calculation of  $\mathbf{w}_i$ , in terms of which we can calculate the matrix second moment of the piecewise-linear approximation of  $\mathcal{R}$ . See Eqs. (7.68) and (7.69).

## 7.5 COMMERCIAL SOFTWARE PACKAGES

---

The synthesis and design of cam mechanisms can be eased by using the capabilities offered by CAD packages. Extensive CAD software is commercially available, with new packages and new features appearing every year. Among these features, we can mention the plotting of functions, the rotation and translation of planar rigid figures, and the determination of intersections of lines, curves, and surfaces. This function is important, because to start with the design process we assume that the displacement program of the follower is given as a smooth, explicit function of the input variable so that its derivative is available.

If only a discrete set of points is specified for the functions needed in the synthesis procedures, an interpolation is needed, which can be implemented by using software packages as well.

A representative list of commercial packages is given below.

- **AUTOCAD:** Comprehensive package for mechanical design and geometric analysis. Runs mostly on Windows. Old versions run also on Unix. Vendor: Autodesk, Inc. Its Web site is: <http://info.autodesk.com/>.
- **VERSACAD:** Basically a production-level CAD software. However, the 3DJoy module is a modeler that offers high-powered spline-based modeling. Also, the Rhino module can create, edit, analyze, and translate NURBS, surfaces, and solids. Runs on Windows. Vendor: Archway Systems, Inc. Web site: <http://www.versacad.com/>

Other pertinent CAD software packages have more advanced features in terms of solid modeling, assembly, and motion animation, e.g.,

- **PRO/ENGINEER:** Comprehensive package for mechanical design and analysis at large. Its PRO/MECHANICA module provides motion analysis, simulation, and animation of fairly complex mechanisms. Runs on Windows and Unix. Vendor: Parametric Technology, Inc. Web site is: <http://www.ptc.com/>
- **CATIA:** This software package has advanced features that can be used for creating and modifying free-form surfaces, complex solids, parametric modifications, and the use of solids in a multimodel environment. Vendor: TBM Technologies. Web site is <http://www.catia.com/>
- **UNIGRAPHICS:** High-end, comprehensive package with modules for finite-element analysis, CAD/CAM, etc. It feature ADAMS, a general tool for mechanism and multi-body-system analysis. No synthesis features are supported. Vendor: Unigraphics Solutions. Web site: <http://www.openitx.com/>

Finally, general-purpose software for numerical and symbolic computations is included below. This software becomes quite useful in the computation and plotting of the local geometric properties, whereby some statistics are occasionally needed, like mean value and standard deviation of pressure-angle of curvature values. We thus have

- **MATLAB:** General-purpose numerical analysis package with excellent routines for equation-solving and optimization. To be used as a support for linkage synthesis. Vendor: The Mathworks Inc. ([www.mathworks.com/feex](http://www.mathworks.com/feex)).
- **MACSYMA** ([www.macsyma.com](http://www.macsyma.com)), **MAPLE** ([www.maplesoft.com](http://www.maplesoft.com)), and **MATHEMATICA** ([www.wolfram.com](http://www.wolfram.com)): commercial packages for symbolic computations. These packages feature capabilities for numerical computations.

## 7.6 CASE STUDIES

We introduce below two case studies illustrating the application of the concepts introduced in this chapter.

### 7.6.1 Cam-Size Minimization

We illustrate here a methodology that allows the designer to minimize the overall size of planar cam mechanisms while maintaining an acceptable force-transmission performance on imposing bounds on the pressure angle. This methodology has some improvements over other techniques, e.g., the exploratory search method proposed in Chan and Kok (1996).

The cam mechanism to be synthesized is shown in Fig. 7.13. In this figure,  $b$  represents the radius of the base circle,  $c$  is the smallest displacement of the follower,  $e$  denotes the offset of the path of the follower tip,  $N$  is the line normal to the cam profile at the contact point,  $s(\psi)$  is the displacement of the follower,  $\alpha(\psi)$  denotes the pressure angle, and  $\psi$  represents the angular displacement of the cam. In this figure, line  $OF$  is fixed to the mechanism frame, while line  $OC$  is fixed to the cam plate.

The follower-displacement program of a cam mechanism is given as the addition of a constant  $c$  and a positive-definite function  $\sigma(\psi)$ . Thus, the displacement of the follower can be written as

$$S(\psi) = c + \sigma(\psi), \quad \sigma(\psi) \geq 0, \quad 0 \leq \psi \leq 2\pi \tag{7.77}$$

with the derivatives

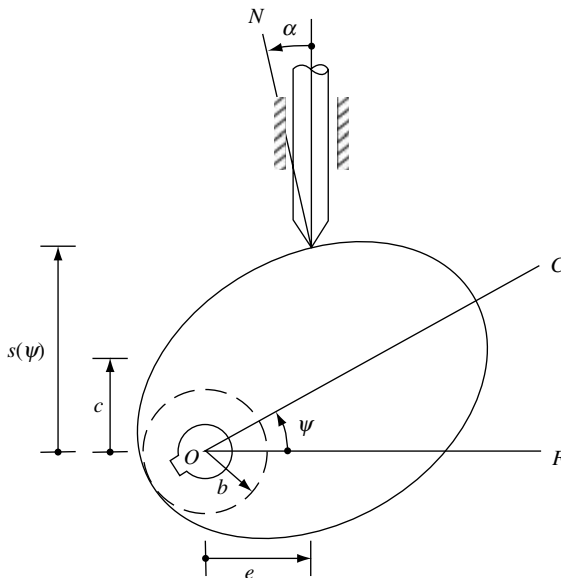


FIGURE 7.13. Knife-edge translating follower.

$$s'(\psi) = \sigma'(\psi), \quad s''(\psi) = \sigma''(\psi), \quad s'''(\psi) = \sigma'''(\psi). \quad (7.78)$$

On the other hand, the tangent of the pressure angle was derived in Angeles and Lopez-Cajun (1991) as

$$\tan \alpha(\psi) = \frac{s'(\psi) - e}{s(\psi)}. \quad (7.79)$$

Now, substituting Eqs. (7.77) and (7.78) into Eq. (7.79) yields

$$\tan \alpha(\psi) = \frac{\sigma'(\psi) - e}{\sigma(\psi) + c}. \quad (7.80)$$

If, moreover,  $\psi_1$  and  $\psi_2$  are the values at which the pressure angle attains a maximum  $\alpha_M$  and a minimum  $\alpha_m$ , the corresponding *extremality conditions* take the form

$$\sigma''(\psi) - \sigma'_1(\psi) \tan \alpha_M = 0 \quad (7.81a)$$

$$\sigma''_2(\psi) - \sigma'_2(\psi) \tan \alpha_m = 0 \quad (7.81b)$$

with  $\sigma_i = \sigma(\psi_i)$ , for  $i = 1, 2$ , and  $\sigma'_i(\psi_i)$  and  $\sigma''_i(\psi_i)$  defined likewise. The problem thus reduces to solving two independent nonlinear equations, (7.81a) and (7.81b), for the two unknowns  $\psi_1$  and  $\psi_2$ . Furthermore, we have, from Eq. (7.80),

$$c \tan \alpha_M + e = \sigma'_1 - \sigma_1 \tan \alpha_m \quad (7.82)$$

$$c \tan \alpha_m + e = \sigma'_2 - \sigma_2 \tan \alpha_M. \quad (7.83)$$

Equations (7.82) and (7.83) thus suggest a graphical solution of the optimization problem at hand, for each of these equations represents a line in the  $c$ - $e$  plane.

The optimum values of  $c$  and  $e$  are found as the coordinates of the intersection of these two lines, as illustrated in Fig. 7.14, where we have assumed that  $\alpha_m = -\alpha_M$  and  $\alpha_M = 30^\circ$ . Moreover, the optimum values  $c_{\text{opt}}$  and  $e_{\text{opt}}$  can be obtained by solving for these parameters from Eqs. (7.82) and (7.83), namely,

$$c_{\text{opt}} = \frac{\sigma'_1 - \sigma_1 \tan \alpha_M - \sigma'_2 + \sigma_2 \tan \alpha_m}{\tan \alpha_M - \tan \alpha_m} \quad (7.84a)$$

$$e_{\text{opt}} = \frac{-\tan \alpha_m (\sigma'_1 - \sigma_1 \tan \alpha_M) + \tan \alpha_M (\sigma'_2 - \sigma_2 \tan \alpha_m)}{\tan \alpha_M - \tan \alpha_m}. \quad (7.84b)$$

Finally, from the geometry of the translating cam mechanism, the optimum radius of the base circle of the optimum cam is

$$b_{\text{opt}} = \sqrt{e_{\text{opt}}^2 + c_{\text{opt}}^2} \quad (7.85)$$

which can be readily computed using Eqs. (7.84a and b).

Now we apply the foregoing relations to the size-minimization of the cam plate of a quick-return mechanism. This mechanism is a mechanical transmission that produces a slow feed motion under a load in one direction, followed by a fast return stroke under no load in the opposite direction. Quick-return mechanisms are frequently used in manufacturing processes, e.g., in pick-and-place operations, metal-cutting, and metal-forming. Cam mechanisms are well suited for this type of task, because they can readily produce such a type of motion. The required motion for this case is the *dwell-rise-dwell-return* dis-

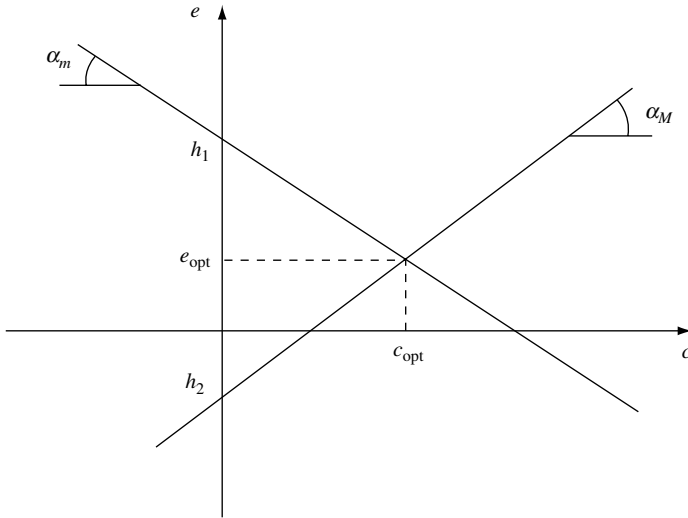


FIGURE 7.14. Graphical determination of the optimum values of  $c$  and  $e$ .

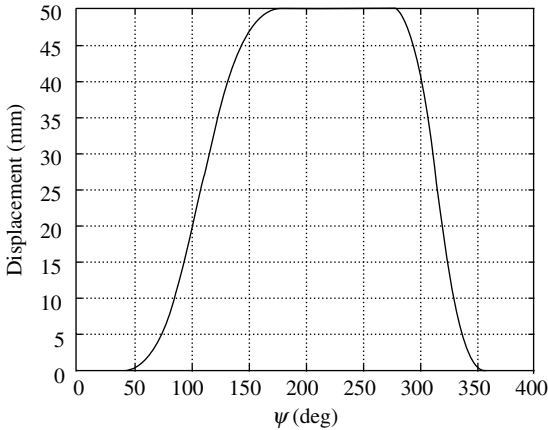


FIGURE 7.15. Prescribed displacement program.

placement, as shown in Fig. 7.15 and described in Table 7.1. Moreover, the displacement of the follower has an amplitude of  $\pm 50$  mm, and the phase and return phases are produced using a *cycloidal motion* (Angeles and Lopez-Cajún, 1991). For quick reference, the *normal cycloidal motion* is given as

$$\sigma(\psi) = \psi - (1/2\pi)\sin 2\pi\psi, \quad 0 \leq \psi \leq 1. \tag{7.86}$$

The parameters for the optimum cam with translating follower were found to be  $e_{opt} = -11.5525$  mm and  $c_{opt} = 67.5378$  mm, which are graphically shown in Fig. 7.16.

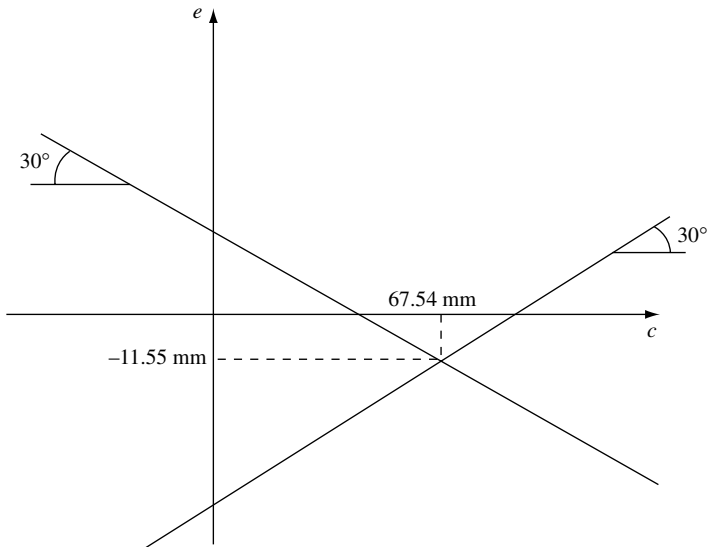


FIGURE 7.16. Numerical determination of the optimum values of  $c$  and  $e$ .

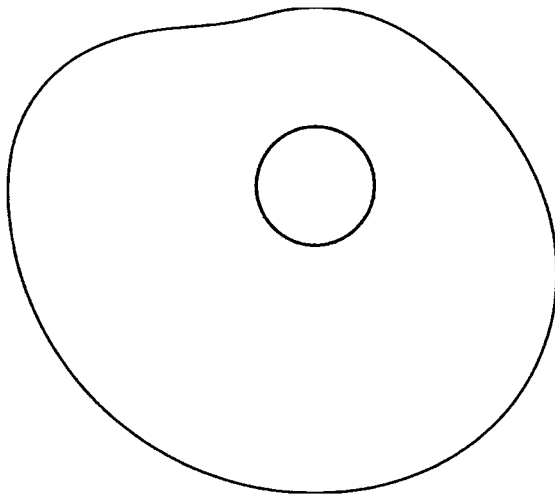


FIGURE 7.17. Cam profile.

TABLE 7.1 Displacement program

Phase	Angle of rotation $\psi$	Translating follower $s(\psi)$
$D_1$ (dwell)	$36^\circ$	0
$R_1$ (rise)	$144^\circ$	+50mm
$D_2$ (dwell)	$90^\circ$	0
$R_2$ (return)	$90^\circ$	-50mm

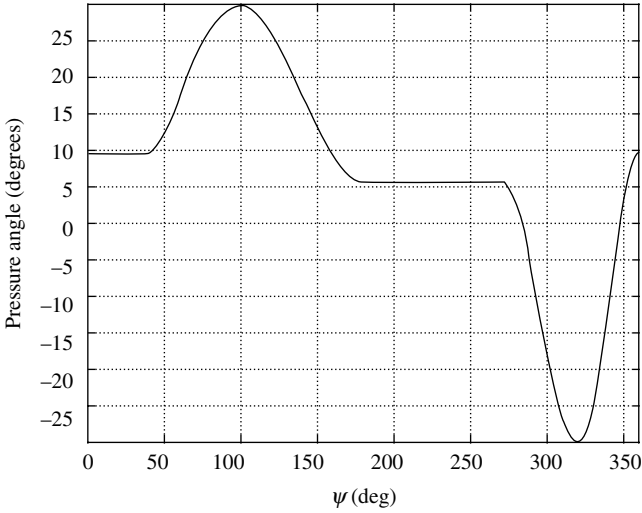


FIGURE 7.18. Pressure-angle distribution.

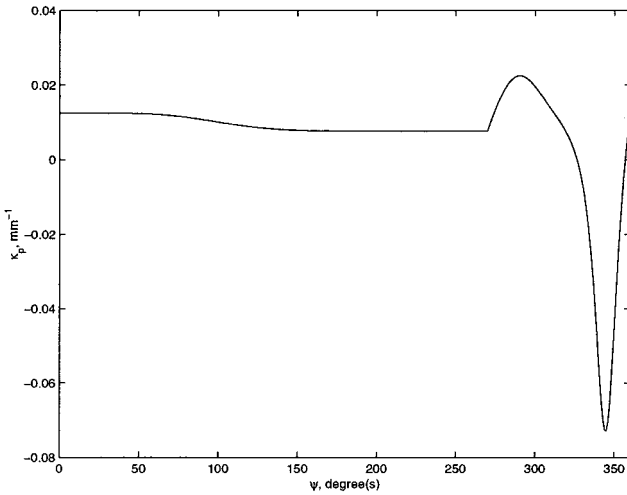


FIGURE 7.19. Curvature of the pitch curve.

Other interesting features are the cam profile and the pressure-angle distribution, which are shown in Figs. 7.17 and 7.18. Moreover, to complete the description of the problem at hand, Fig. 7.19 shows the curvature of the pitch curve. From this figure, one can obtain the maximum value of the curvature of the pitch curve as  $\kappa_M = 0.07283 \text{ mm}^{-1}$ , which corresponds to a roller radius  $r_R = 12 \text{ mm}$ . Once we know the value of the roller radius, we can plot the pitch curve as shown in Fig. 7.20, which is displayed using a dash line.

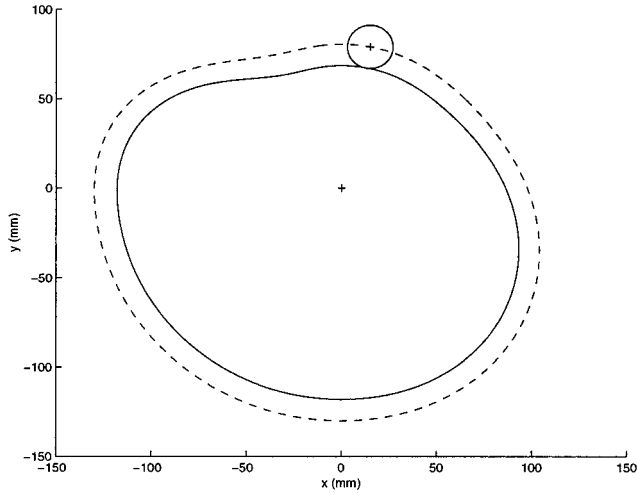


FIGURE 7.20. Pitch curve.

### 7.6.2 Balancing of the Camshaft of a Speed-Reduction Mechanism

The design of a speed-reduction mechanism based on cams was reported in Gonzalez-Palacios and Angeles (1999). This application calls for the use of two identical, symmetric, conjugate cams rotated 180° and axially translated with respect to each other, as displayed in Fig. 7.21. Note that the cams and the shaft are treated as a single, rigid body. Moreover, the mass of the keys is neglected. Since the centers of mass of the cams do not coincide with the axis of rotation, a shaking moment normal to the shaft axis will appear by virtue of centrifugal forces. Moreover, by virtue of the symmetry of the cams, the mass center of the pair lies in the axis of the shaft, the camshaft thus being statically balanced but dynamically unbalanced.

This study aims at imposing the dynamic performance of the prototype of Fig. 7.21 by suitably dynamically balancing the camshaft of that prototype.

The basic idea in balancing the camshaft lies in a redistribution of the mass, which involves removal or addition of mass, or a combination of both. To minimize the total mass of the shaft and the conjugate cams, we attempt first mass removal and then mass addition, if balancing is not possible solely with mass removal.

Since we are dealing with planar parts and, furthermore, a single material, the relationship between the area  $A$  and the mass  $m$  is simply

$$m = \delta tA$$

where  $\delta$  is the mass density of the material and  $t$  is the uniform thickness of the part. Hence, we focus below on the area properties instead of mass properties.

**7.6.2.1 Material removal.** If the center of mass of the cams can be moved such that it coincides with the axis of rotation of the cam, then the camshaft is dynamically balanced, i.e., the moment of the inertia forces the cams in a direction normal to the axis of rotation vanishes. To achieve this, a circular hole must be drilled on the cam plate to translate the mass center of the cam to the axis of rotation of the camshaft, if possible; otherwise, we attempt to shift this center as near as possible to that axis, as shown in Fig. 7.22.

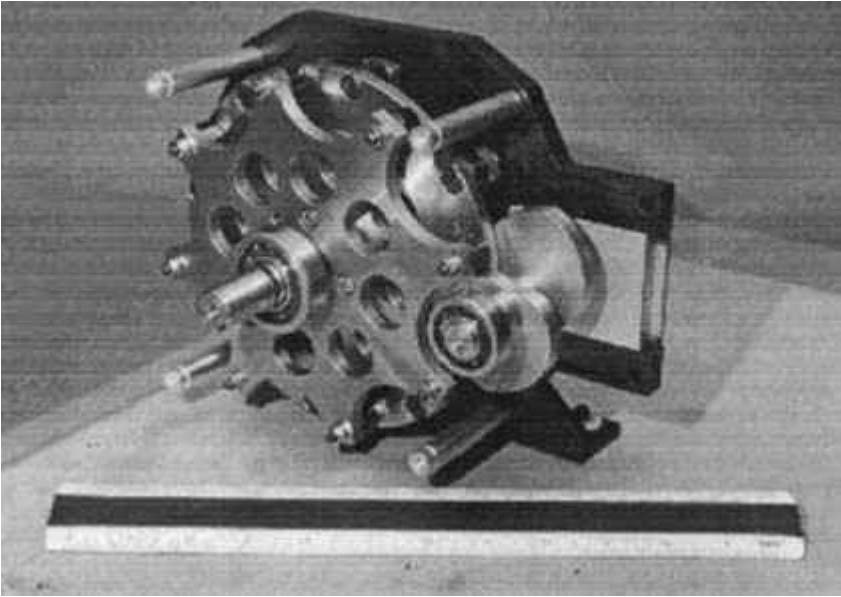


FIGURE 7.21. The prototype.

Referring to Fig. 7.22,  $C_1$  is the cross section of the camshaft;  $C_2$  is a circular hole with its center located on the  $x$ -axis, so that the center of mass of the cam is shifted only in the  $x$ -direction. Moreover,  $a$  and  $c$  are the radii of  $C_1$  and  $C_2$ , respectively, and  $x_2$  is the distance between the center of  $C_2$  and the origin  $O$ , i.e., the center of the camshaft cross section.

Now we recall that our reason for removing material from the cam plate is to shift the centroid of the cam plate to the axis of rotation, namely, the axis perpendicular to the  $x$  and  $y$  axes through point  $O$ . Hence, we compute the centroid of the new cam plate. The centroid of a planar object composed of  $n$  given shapes of known centroids can be obtained using

$$x_c = \frac{1}{A} \sum_{i=1}^n A_i x_i, \quad A = \sum_{i=1}^n A_i \quad (7.87)$$

where

$x_c$  = center of mass of the overall object

$x_i$  = center of mass of the  $i$ th part

$A_i$  = area of the  $i$ th part

for  $i = 1, 2, \dots, n$ .

From Fig. 7.22, the centroid location of the cam with removed material is found to be

$$x_c = \frac{A_{\text{cam}} x_{\text{cam}} - A_2 x_2}{A_c - A_2} \quad (7.88)$$

with the notation

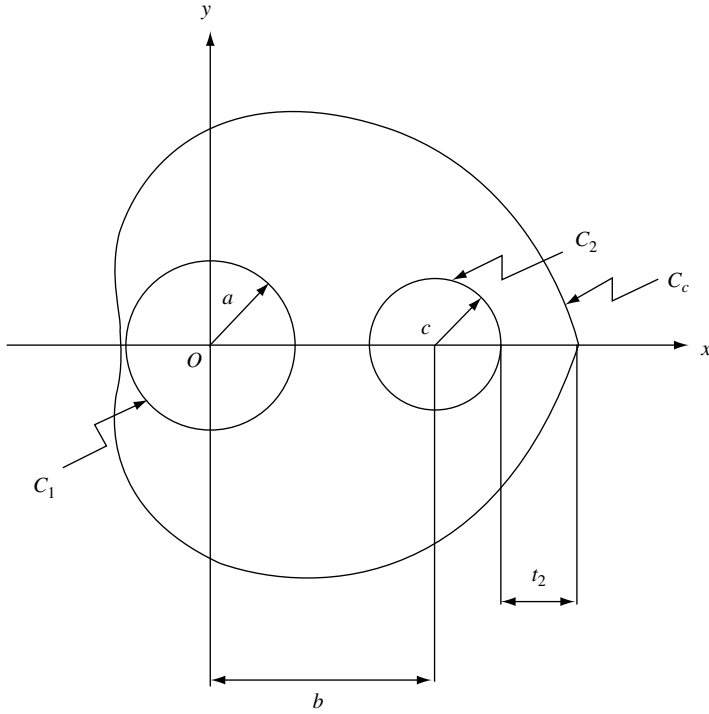


FIGURE 7.22. Cam plate with a hole drilled.

- $A_{cam}$  = total area enclosed by the cam profile
- $A_2$  = area of circle  $C_2$ ;  $A_2 = \pi c^2$
- $x_{cam}$  = centroid abscissa of the cam plate
- $x_2$  = abscissa of the center of  $C_2$

To have the centroid coincide with the axis of rotation, we set  $x_c = 0$  in Eq. (7.88) and solve for  $x_2$ , thereby obtaining

$$x_2 = \frac{A_{cam} x_{cam}}{\pi c^2}. \tag{7.89}$$

Choosing a suitable value of  $c$  constrained by the geometric conditions will balance the camshaft. In the case of a speed reduction of 8 : 1, there is no feasible set of solutions that can balance the camshaft. Therefore, we proceed to adding counterweights to the camshaft.

**7.6.2.2 Material Addition** The notation used in Fig. 7.23 is described below:

- $A_{cw}$  = the area of the two identical counterweights
- $A_{cam}$  = the area of the two identical conjugate cams
- $t_{cw}$  = the uniform thickness of the two identical counterweights
- $t_{cam}$  = the uniform thickness of the two identical cams
- $\mathbf{c}_{cw_1}$  and  $\mathbf{c}_{cw_2}$  = the position vectors of the centroids of the two identical counterweights

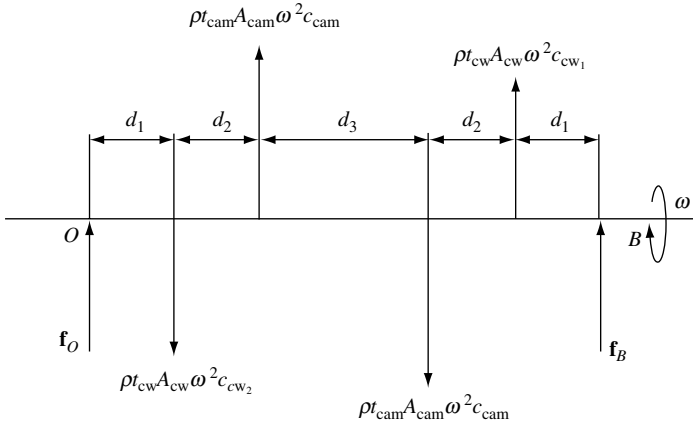


FIGURE 7.23. Free-body diagram of the camshaft.

- $\mathbf{c}_{cam_1}$  and  $\mathbf{c}_{cam_2}$  = the position vectors of the centroids of the two identical cams
- $\omega$  = the constant angular velocity of the camshaft
- $\delta$  = the mass density of the material of the camshaft

Consider the force-balance and the moment-balance conditions, the latter taken with respect to point  $O$ , namely,

$$\mathbf{f}_s = \delta t_{cam} A_{cam} \omega^2 \mathbf{c}_{cam} + \delta t_{cam} A_{cam} \omega^2 \mathbf{c}_{cam} + \delta t_{cw} A_{cw} \omega^2 \mathbf{c}_{cw_1} + \delta t_{cw} A_{cw} \omega^2 \mathbf{c}_{cw_2} + \mathbf{f}_O + \mathbf{f}_B = \mathbf{0} \tag{7.90a}$$

$$\mathbf{m}_s = \delta t_{cw} A_{cw} \omega^2 (d_1 + 2d_2 + d_3) \mathbf{c}_{cw_1} + \delta t_{cam} A_{cam} \omega^2 (d_1 + d_2 + d_3) \mathbf{c}_{cam} + \delta t_{cam} A_{cam} \omega^2 (d_1 + d_2) \mathbf{c}_{cam} + \delta t_{cw} A_{cw} \omega^2 d_1 \mathbf{c}_{cw_2} = \mathbf{0}. \tag{7.90b}$$

Note that simplifications arise from the symmetric geometry of the camshaft, i.e.,  $\mathbf{c}_{cw_1} = -\mathbf{c}_{cw_2}$  and  $\mathbf{c}_{cam_1} = -\mathbf{c}_{cam_2}$ . Henceforth we denote by  $c_{cw}$  the magnitude of  $\mathbf{c}_{cw}$ , and  $c_{cw_2}$ . Substituting these parameters into Eqs. (7.90a) and (7.90b), and referring to Fig. 7.24, we obtain, for the force-balance equation,

$$\mathbf{f}_O = -\mathbf{f}_B \tag{7.91}$$

and two scalar equations in  $x$  and  $y$  for the moment-balance condition. For the  $x$ -component,

$$t_{cw} A_{cw} (d_1 + 2d_2 + d_3) c_{cw} \cos \theta_1 + t_{cam} A_{cam} (d_1 + d_2 + d_3) c_{cam} \cos 270^\circ + t_{cam} A_{cam} (d_1 + d_2) c_{cam} \cos 90^\circ + t_{cw} A_{cw} d_1 c_{cw} \cos \theta_2 = 0 \tag{7.92}$$

where  $\delta$  has been deleted. After expansion, the above relation reduces to

$$t_{cw} A_{cw} (2d_2 + d_3) c_{cw} \cos \theta_1 = 0. \tag{7.93}$$

We obtain the  $y$ -component expression likewise, as

$$A_{cw} t_{cw} (2d_2 + d_3) c_{cw} \sin \theta_1 - A_{cam} t_{cam} d_3 c_{cam} = 0. \tag{7.94}$$

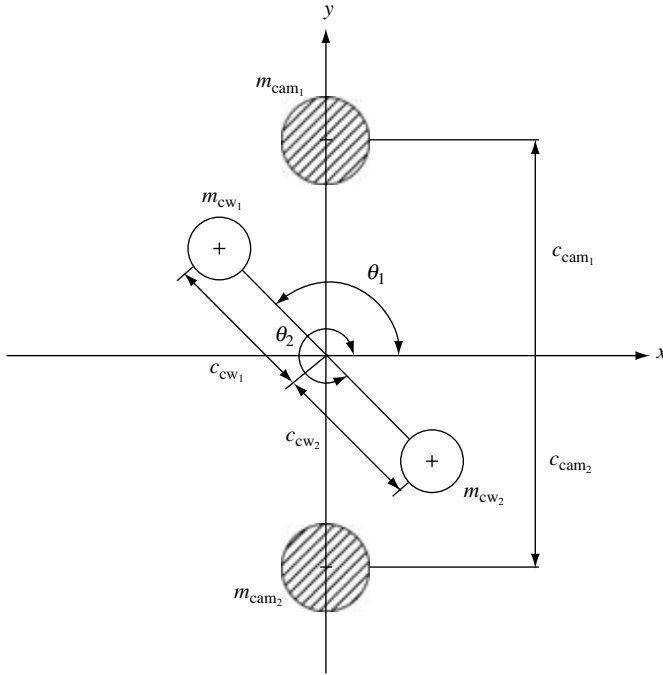


FIGURE 7.24. Diagram for moment balance.

It follows that  $\theta_1 = 90^\circ$  verifies Eq. (7.93). Now, substituting this value of  $\theta$  into Eq. (7.94) leads to

$$c_{cw} = \frac{A_{cam} t_{cam} c_{cam}}{A_{cw} t_{cw}} \frac{d_3}{2d_2 + d_3} c_{cam}. \tag{7.95}$$

For manufacturability purposes, circular counterweights are proposed, since a circle is the simplest contour to machine. We introduce parameters  $a$ ,  $e$ , and  $f$ , as defined in Fig. 7.25.

From Fig. 7.25, the centroid of the counterweight lies a distance  $f$  from  $O$ , in the  $-y$  direction, i.e.,

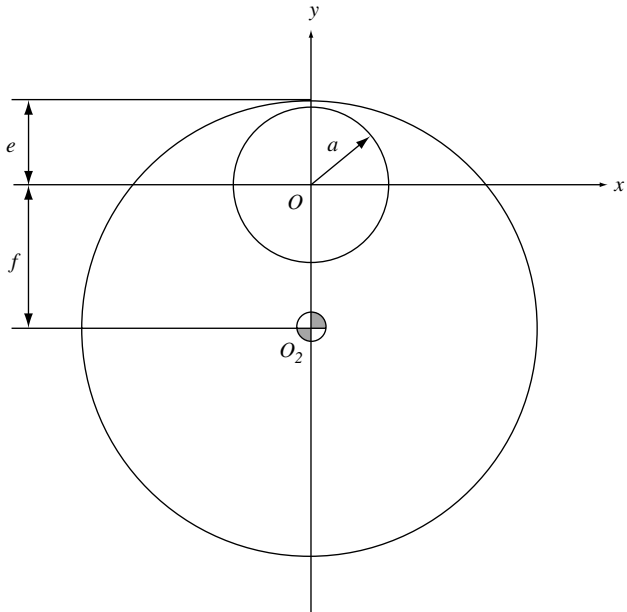
$$c_{cw} = f. \tag{7.96}$$

Apparently,

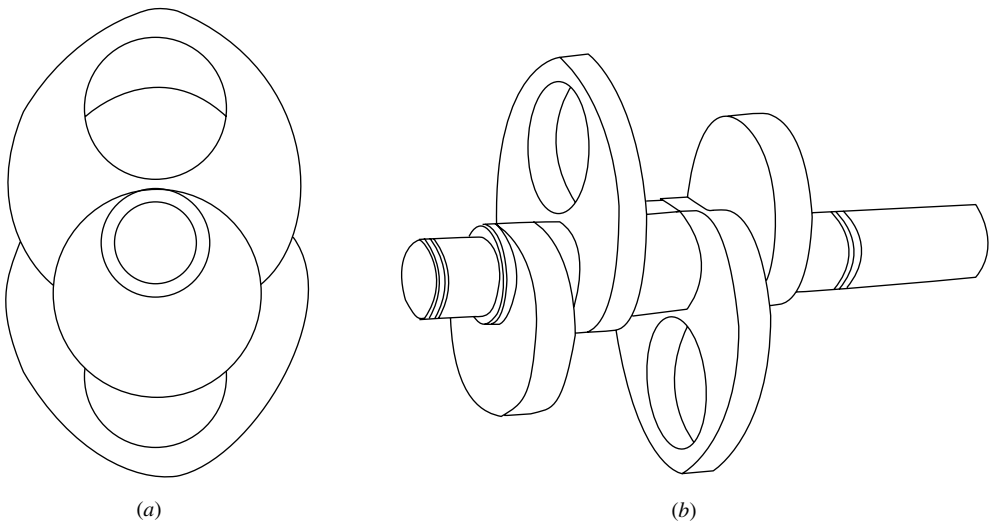
$$A_{cw} = \pi(e + f)^2 \tag{7.97}$$

With Eqs. (7.95), (7.96), and (7.97), and taking into account the sign of the ordinate of  $O_2$ , we obtain a cubic equation to determine  $f$ :

$$f^3 + 2ef^2 + e^2f - \frac{d_3 A_{cam} t_{cam} c_{cam}}{\pi t_{cw} (2d_2 + d_3)} = 0. \tag{7.98}$$



**FIGURE 7.25.** Circular counterweight proposed.



**FIGURE 7.26.** Camshaft with counterweights, created in Pro/Engineer: (a) side view; (b) perspective.

It is apparent that having  $e > a$  would lead to more unbalance, since this would be equivalent to adding material to the cams, a minimum value of  $e$  being preferred in this case. Choosing  $e = a$  and using the maximum value of  $t_{cw}$ , we minimize the counterweight size; in other words, we minimize the radius of the counterweight. With these constraints, the value of  $f$  can be readily computed.

For the case of a speed reduction of 8:1, we computed the counterweight and created a solid model in Pro/Engineer, as displayed in Fig. 7.26, with the parameters  $t_2 = 5$  mm,  $a = e = 9.5$  mm,  $b = 23.5$  mm,  $c = 12.5$  mm,  $d_2 = 9.85$  mm,  $d_3 = 27$  mm,  $t_{cam} = 6$  mm,  $t_{cw} = 8$  mm,  $c_{cam} = 9.8235$  mm,  $A_{cam} = 1.6253 \times 10^6$  mm<sup>2</sup>, and  $f = 8.7866$  mm.

## REFERENCES

---

- Al-Daccak, M., and Angeles, J., "The Calculation of the Volumetric Properties of Sweep-Generated Solids Via Line Integration," *ASME, J. of Mechanical Design*, 115 (1): 110–118, 1993.
- Angeles, J., Chaoming, Z., Duarte, R., and Ning, H., "The Evaluation of Moments of 3-D Solids of Revolution Using Spline Approximations of the Boundary," *ASME, J. of Mechanical Design*, 112: 108–110, 1990.
- Angeles, J., and Lopez-Cajún, C.S., *Optimization of Cam Mechanisms*, Kluwer Academic Publishers, Dordrecht, 1991.
- Brand, L., *Advanced Calculus*, John Wiley, New York, 1965.
- Chan, Y.W., and Kok, S.S., "Optimum Cam Design," *Int. J. Comput. Appl. Technol.*, 9 (1): 34–47, 1996.
- Dierckx, P., *Curve and Surface Fitting with Splines*, Oxford University Press, New York, 1993.
- Golub, G.H., and Van Loan, C.F., *Matrix Computations*, Johns Hopkins University Press, Baltimore, 1983.
- González-Palacios, M.A., and Angeles, J., "The Design of a Novel Mechanical Transmission for Speed Reduction," *ASME, Journal of Mechanical Design*, 121 (4): 538–551, 1999.
- Kahaner, D., Moler, C., and Nash, S., *Numerical Methods and Software*, Prentice Hall, Englewood Cliffs, N.J., 1989.
- Koloc, Z., and Václavík, M., *Cam Mechanisms*, Elsevier, New York, 1993.
- Lee, M.K., Design for Manufacturability of Speed-Reduction Cam Mechanisms, M. Eng. Thesis, Department of Mechanical Engineering, McGill University, Montreal, 2001.
- Marsden, J.E., and Tromba, A.J., *Vector Calculus*, W.H. Freeman and Company, New York, 1988.
- Navarro-Martínez, O.R., The Synthesis of Speed-Rectifying Mechanisms for Mechatronic Applications, M.Eng. Thesis, Department of Mechanical Engineering, McGill University, Montreal, 1999.
- Rogers, D.F., *An Introduction to NURBS: With Historical Perspective*, Academic Press, San Francisco, Calif., 2001.
- Srinivasan, L.N., and Ge, Q.J., "Fine Tuning of Rational B-Spline Motions," *Proc. ASME Design Engineering Technical Conferences*, September, Sacramento, Calif., 1997.

*This page intentionally left blank.*

---

# CHAPTER 8

---

## CAM MECHANISM FORCES

---

Harold A. Rothbart, D. Eng.

8.1 INTRODUCTION	218	8.11.2 Translating Flat-faced Follower Torque	230
8.2 WORKING LOADS	218	8.11.3 Torque-Controlled Cams	232
8.3 IMPACT FORCES	219	8.11.4 Torque-Controlled Wrapping Cams	235
8.4 INERTIA FORCES	219	8.12 ROTATABLE INVERSE CAM MECHANISM	236
8.5 VIBRATORY FORCES	220	8.12.1 Kinematic Principles	237
8.6 FRICTIONAL FORCES	220	8.12.2 Cam Output Motion	238
8.7 SPRING FORCES	222	8.12.3 Design Procedure	244
8.8 COMPARISON OF CAM CURVES FOR SPRING DESIGN	223	8.12.4 Force Closure	245
8.9 OPERATING FORCES	224	8.12.5 Quasikinestatic Analysis	245
8.10 CAM SURFACE LOADS	225		
8.11 TORQUE	228		
8.11.1 Translating Roller-Follower Torque	228		

---

### SYMBOLS

---

$A$  = follower acceleration, in/sec<sup>2</sup>  
 $F$  = friction force to cam surface, lb  
 $F_a$  = inertia force, lb  
 $F_k$  = kinetic friction force, lb  
 $F_n$  = force normal to cam surface, lb  
 $F_s$  = static friction force, lb  
 $h$  = maximum rise of follower, in  
 $I$  = moment of inertia of body about center of rotation lb-in-sec<sup>2</sup>  
 $\bar{k}$  = radius of gyration, in  
 $k_s$  = spring index, ib/in  
 $L$  = external load on cam, lb  
 $L_o = m\ddot{y} + L$  = total load on cam, lb  
 $m$  = follower mass, lb-sec<sup>2</sup>/in  
 $N$  = normal component of velocity, ips  
 $r$  = distance from cam center to roller follower center, in  
 $r_b$  = base circle radius, in  
 $S$  = spring force, lb  
 $T$  = torque, in-lb  
 $T_a$  = inertia torque, in-lb  
 $T_G$  = tailgate torque, in-lb  
 $v_s$  = sliding component of velocity, ips  
 $w$  = equivalent weight, lb  
 $y$  = follower displacement, in  
 $\dot{y}$  = follower velocity, ips  
 $\ddot{y}$  = follower acceleration in/sec<sup>2</sup>  
 $\alpha$  = angular acceleration radians/sec<sup>2</sup>

$\alpha_p$  = pressure angle, deg

$\beta$  = cam angle rotation for rise,  $h$ , radians

$\delta$  = deflection, in

$\mu$  = coefficient of friction

$\theta$  = cam angle rotation, radians

$\omega$  = cam rotational speed, rad/sec

## 8.1 INTRODUCTION

---

We shall discuss the cam-follower system forces driven by constant speed cam. The forces listed are generally superimposed on each other during the cam-follower system action.

- working loads
- impact forces
- inertia forces
- vibratory forces
- frictional forces
- spring forces
- operating forces (braking, start/stop, and overload shock actions)

Information on these forces is necessary to determine (at a designed speed) the structural sizes of the machine moving parts for strength and rigidity, the proper choice of and life materials, the bearing sizes, the spring sizes and loads, and the system performance and power consumption, among other things. Note that impact forces may produce forces that far exceed all others. Also, a torque analysis of the system is usually necessary to understand the transfer of energy throughout the system under conditions of operation.

Often the follower system is remotely located with reference to the cam (cam modulated system) and the dynamic analysis becomes quite complex. For dynamic analysis of these cam modulated systems, see Paul (1979) (1996) and Sandor and Erdman (1984).

## 8.2 WORKING LOADS

---

Working loads, or applied loads, represent the useful work performed by a machine. Working loads may be classified in these relative categories: gradually applied, suddenly applied, and impact forces.

Note that these three categories may not be directly related to the speed of the cam. For example, a slow-speed cam mechanism, having a large flywheel, punching holes in tough sheet metal may have an impact load, while a high-speed system pumping chemically processed air can have gradually applied loads. It is the responsibility of the engineer to make an experienced judgment about the designed effect of the working load on the system. Also, the application of working loads in a positive drive cam follower may augment or reduce the other forces in a system. For example, if applied during the initial cam stroke, they add to the inertia forces during the positive acceleration period. During the negative acceleration period they tend to reduce the load by absorbing some of the energy stored in the follower mechanism.

The static force analysis (*gradually applied*) was presented in Chapter 7 where the cam pressure angle and its forces were investigated. *Suddenly applied* loads may be considered during a slow impact on the system with a load amplification factor of up to two times the static force value. Bear in mind that discontinuity of the cam acceleration curve yields the same amplification factor as suddenly applied loads. This is discussed in the cam action descriptions of Chap. 10.

### 8.3 IMPACT FORCES

---

Impact is often called mechanical shock, referring to an extreme abruptly applied force. It is a velocity shock transient force. Impact phenomena are especially important to the designer since in all machines the highest forces and stresses arise as a consequence of impact. In cam-follower systems the impact forcing functions are not precisely known. Thus, the design for these forces requires an approximation of the idealized functions of velocity changes on impact. As stated, practical design data for impact calculation are not directly available, necessitating a larger design safety factor in considering its effects. Impact or velocity shock factors have a load amplification factor of two to four times the static force values. This is discussed in the cam action discussion of Chap. 10 in which a “bump” on the cam profile is a discontinuity in the velocity curve, producing an impact in the follower. For more on impact see Barkan (1996) and Zuleas (1982).

For more precise data on impact the designer could resort to experimental measurement employing such powerful tools as strain gauges, high-speed photography, and velocity and motion transducers. The sources of impact in cam-follower mechanisms could be the result of: (a) backlash in a positive-drive cam and roller follower, (b) high-speed systems which are nonlinearly elastic so that abrupt changes occur with results similar to impact, and (c) the working load action as a cam-driven punching mechanism. To minimize impact, the following is suggested, if possible: (a) minimize the velocity of impact, (b) minimize the mass of impacting bodies, and (c) minimize sensitivity to local stress concentrations by employing a ductile material with some capacity for plastic deformation.

### 8.4 INERTIA FORCES

---

Inertia forces in most cam-follower systems are the most important of all the forces analyzed, especially at high speeds. Inertia forces are caused by the necessity of moving the follower masses linearly or rotationally. The inertia force on a linearly moving follower is

$$F_a = \frac{w}{g} A \quad \text{lb} \quad (8.1)$$

where  $A$  = acceleration, in/sec<sup>2</sup>  
 $w$  = equivalent follower weight, lb.

The inertia force, passing through the center of gravity of the body, has a direction opposite to that of the acceleration. By D’Alembert’s principle, we may make a free-body diagram of all forces and analyze the dynamic condition as a static problem, Fig. 8.1*a*. For rotating bodies, the analysis is similar. If the body has an unbalanced torque, it will have an angular acceleration which will be resisted by a torque reaction. The direction of this torque will be opposite to the direction of acceleration (Fig. 8.1*b*). The torque is:

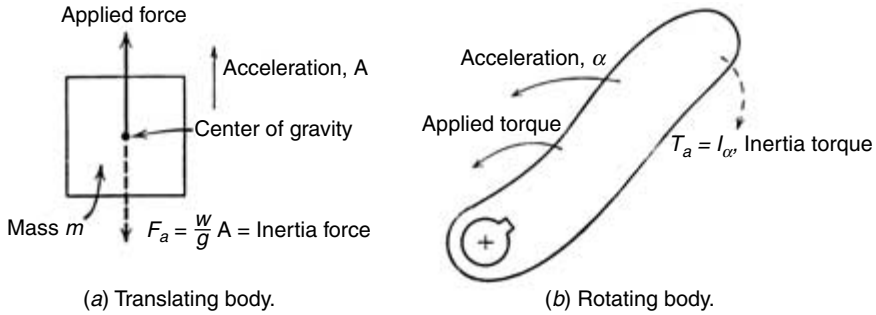


FIGURE 8.1. Free-body diagrams of accelerated bodies.

$$T_a = I\alpha, \text{ lb-in} \quad (8.2)$$

where  $I$  is the moment of inertia of the body about the center of rotation, and

$$I = m\bar{k}^2 \text{ lb-in-sec}^2$$

$\bar{k}$  = radius of gyration, in

$\alpha$  = angular acceleration, radians/sec<sup>2</sup>

## 8.5 VIBRATORY FORCES

Vibrations are generally caused by forces whose magnitudes, directions, and/or point of application vary with time. These forces produce variations in elastic deformations. These vibrations in turn produce stresses and forces that are superimposed on the inertia and other forces in the follower systems. The magnitudes of the vibratory stresses and forces are influenced by the acceleration characteristics, as well as the rigidity and the damping of the follower mechanism. This topic is separately treated in Chaps. 12 and 13.

## 8.6 FRICTIONAL FORCES

Friction opposes the relative movement of contacting bodies in all machinery. It is a surface phenomenon. In cam-follower systems, we have both sliding and rolling friction to consider. The accurate way to include frictional resistance in a design is to measure it on the actual machine or prototype. Handbooks list these resistances for some combinations of materials, but the conditions under which the values are obtained seldom fit the specific conditions. This is especially true in cam and follower action. Also, differences in friction may be obtained under apparently similar conditions.

Here are the three broad categories of frictional action in cam-follower mechanisms:

- Pure sliding that occurs between the cam and flat-faced and spherical-faced followers
- Rolling and some sliding in rolling-element followers and cams
- Linear ball-bearing guiding mechanisms that support translating followers

The friction force between two bodies is defined as the force at their surface that resists their relative movement. The coefficient of friction

$$\mu = \frac{F}{F_n} \quad (8.3)$$

where  $F$  = the friction force, lb

$F_n$  = normal reaction of one body on another, lb.

To initiate the relative motion, the static coefficient of friction is

$$\mu_s = \frac{F_s}{F_n}$$

where  $F_s$  is the friction force between bodies not sliding on each other. To maintain the motion the kinetic coefficient of friction is

$$\mu_k = \frac{F_k}{F_n}$$

where  $F_k$  is the friction force between bodies sliding on each other.

### 8.6.1 Flat-Faced and Spherical-Faced Followers

These kinds of followers are selected from materials compatible with the cam surface materials. The following factors affect the coefficient of friction between the cam and follower surfaces: (a) cleanliness of the surfaces; (b) wear of the parts; and (c) surrounding environmental contaminants such as particles of ink, paper, dust, and textiles which may result in lubrication starvation, (d) kind of lubrication system, (e) cavitation of lubricant, (f) elastohydrodynamic lubricant film on surfaces, and (g) windage due to moving parts. Also, multiple startups and shutdowns cause metal-to-metal contact, resulting in wear debris and affecting friction. Sliding followers have a coefficient of friction  $\mu_k = 0.12$  to 0.20. The starting coefficient of friction  $\mu_s$  is about 40 percent more than the kinetic  $\mu_k$ .

### 8.6.2 Rolling Element Cam Followers

Rolling-element cam followers are made up of either ball, roller, or needle bearings encased in a steel ring and supported by a steel stem (See Fig. 8.2). They are most popular because of their small size and low friction. In addition to the factors affecting the previ-



**FIGURE 8.2.** Commercial roller follower (needle bearing) (Courtesy of McGill Manufacturing Co., South Bend, Indiana).



**FIGURE 8.3.** Linear ball bearing for translating follower (Courtesy Warner Electric, South Beloit, Ill.).

ous sliding followers, we have the following frictional losses: (a) oil viscosity, (b) hysteresis loss due to the damping of the rolling materials, (c) excessive working load impact (if it exists), (d) number of follower rollers (either one or two) affected by change in inertia force, (e) number of times of rotation of roller, (f) deflection of the follower stem, producing misalignment and wear on the roller, (g) skidding loss of bearing in its container, (h) flinging oil from rotating bearings, and (i) excessive oil in the bearing. Rolling-element followers have a coefficient of friction  $0.01 < \mu_k < 0.15$ . This wide range is due to the uncertainty as to the actual performance of this kind of follower.

### 8.6.3 Linear Ball Bearings

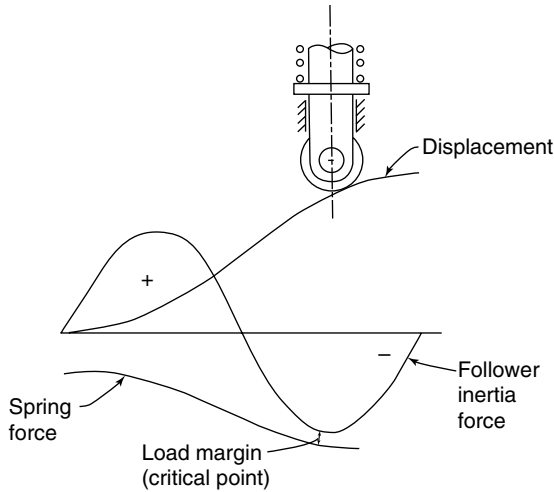
These commercially produced low-friction ball mechanisms are available in many applications, as they specifically are used for linear translation followers and have a coefficient of friction  $\mu_k > 0.010 < \mu_k < 0.050$ , depending on the lubrication adversities previously discussed. Fig. 8.3 shows a picture of a linear ball bearing used to guide and support a translating follower.

## 8.7 SPRING FORCES

In cam-follower systems the follower must be held in contact with the cam at all times to counteract the follower inertia. The follower inertia follows the acceleration curve with the magnitude of the negative acceleration being of concern. The constraint of the follower should be accomplished by utilizing a preloaded compression spring, usually a helical coil.

The spring force is directly proportional to the follower displacement. If the force is too small it will allow the follower to jump off the cam. On the other hand, an excessive spring force is reflected throughout the system during the total cycle of operation. This excessive force will require a stronger design system and more wear of parts will result. Also, one of the disadvantages of spring-loaded systems is that the spring force produces an additional load on the system.

Figure 8.4 shows a cam-follower mechanism with its displacement and inertia force curves, which are shaped as the acceleration curve. Also shown is a properly designed



**FIGURE 8.4.** Spring critical design point (inertia force only).

spring force curve. The critical point is where the inertia and spring forces are closest to each other. This point occurs in the vicinity of the maximum negative acceleration. Jump will occur when the negative inertia force of the system exceeds the available spring force. The spring force should exceed the total external load by 30 to 50 percent, depending on the mass and elasticity of the mechanism. Note, a small percent of spring load is to include the spring strength loss that will occur over a period of use. Also, in the design of a spring-loaded system the spring should be located at the farthest part of the follower to eliminate all backlash and clearances.

Surging, or coil flutter, at high speeds is the common manifestation of spring performance. The surging of the spring is the result of forced vibration waves advancing and reflecting throughout the length of the spring. Thus, a complicated series of vibrations may be continually reinforcing and partially canceling each other during the action, further reducing the effective spring force. A multi-degree-of-freedom system for spring surge phenomenon is discussed in Chap. 12.

## **8.8 COMPARISON OF CAM CURVES FOR SPRING DESIGN**

For inertia loading, let us compare spring sizes necessary to constrain the follower to the cam during the complete cycle of operation. The following basic curves are considered: parabolic, simple harmonic, cycloidal, and double harmonic. In Fig. 8.5 we see that the simple harmonic curve has a spring force that is 68 percent of the parabolic curve, the cycloidal curve has a spring force of 95 percent of the parabolic curve, and the double harmonic is 110 percent of the parabolic curve value. Among the curves compared, the cycloidal cam gives the smoothest force variation. For further information see Jennings (1941).

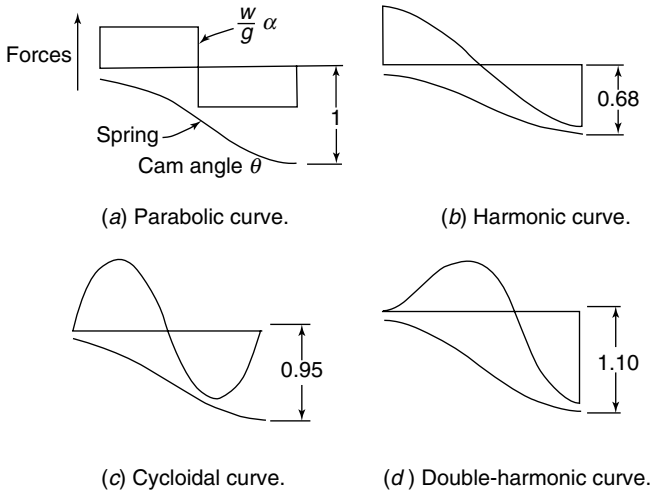


FIGURE 8.5. Spring forces for basic cam curves (inertia force only).

## 8.9 OPERATING FORCES

Let's consider the operating forces of the complete cam mechanism system from the input (usually an electrical motor) to the cam-follower working output. There are transient forces that are more severe than the normal design (running) speed forces presented in latter chapters. The following actions will be discussed:

- start and stop
- emergency stop
- interrupted drive

Every cam-follower machine has specific needs to control these transient operating forces. Generally, smaller machines with lower inertias require simple equipment and heavy-mass machines need more elaborate controls of the actions. Usually clutches or brakes are chosen. They engage or activate by mechanical, pneumatic, hydraulic, electrical, or automatic means. The operating principle of the brake clutch is positive contact (either jawed or toothed), friction contact, overruning (by wedge relief), overload safety by shear pins (to be replaced), and magnetic and fluid couplings.

In *normal* operation the machine must start, run at full speed, and stop. These steps produce positive and negative inertia forces and inertia torques that influence the input transmission. The clutch/brake system can have a no-load start, manually or automatically controlled or have gradual, smooth pickup of speed and load. It can also, when at full speed, have control of variable torque load and be stopped by dynamic braking.

In *emergency operation*, we have overload protection and stopping of the machine. The clutch functions, reacting to transient and infrequent overloads, to limit the speed and the torque, and for automatic overload release, dynamic braking and backstopping. Also, positive-drive shear pins may be utilized to protect the system. These pins are designed to break and are replaced after every failure.

*Interrupted drive* operation carries a special design need for cam mechanisms to be

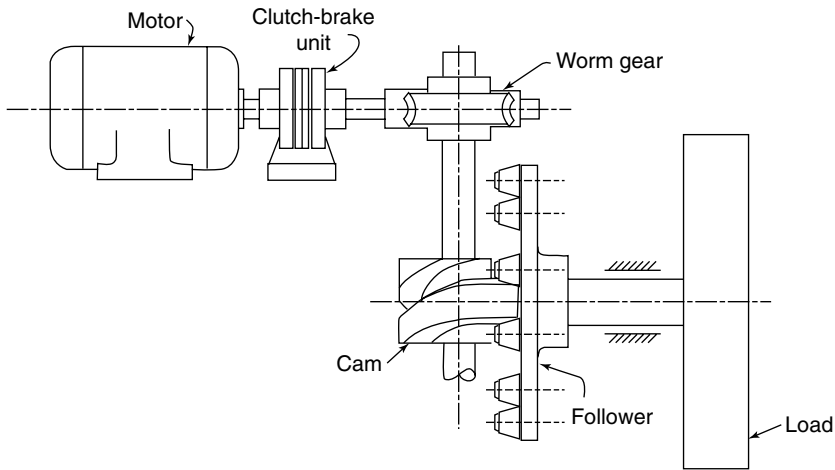


FIGURE 8.6. Cam indexing mechanism.

deliberately and rapidly started and stopped for functional reasons. A case in point is a cam-driven indexing mechanism whose input is interrupted by an electromagnetic clutch/brake unit, either to make the mechanism cycle on demand or to produce an extended dwell period. The same system can also be applied when inching and jogging is desired and also indexing and load positioning.

Figure 8.6 shows a simplified sketch of a cam indexing mechanism. These connected parts are the motor, clutch/brake, worm gear speed reducer, cam and follower, and the output load indexing disk. A typical indexing system of this kind is used to explain the dynamics of an interrupted drive. The same principles apply to any means of accelerating or decelerating the input of any cam system, provided that a constant input torque is used for the purpose. Any friction clutch or friction brake can be assumed to apply a torque that is approximately constant. A common device used for interrupting a cam drive is a braked motor for which, although its start-up torque varies considerably as it speeds up, its peak start-up torque can be used as if it were constant to arrive at a safe design.

## 8.10 CAM SURFACE LOADS

**EXAMPLE** A helical-spring-loaded cam rotates at 1200 rpm with a translating roller follower. The actions are: (a) the follower rises  $1\frac{1}{4}$  in. in  $160^\circ$  of cam rotation; (b) a dwell for  $20^\circ$ ; (c) the fall same as the rise; (d) a dwell again for  $20^\circ$ . Furthermore, an asymmetrical parabolic curve will be utilized having the positive acceleration three times the negative acceleration to keep the spring size and surface stresses small. The parabolic curve, which is of course a poor choice on the basis of vibratory effect, is presented for ease of calculations. The follower linkage weighs 2 lb, and the external force on the system is constant at 10 lb.

Design the spring with a margin of safety of at least 7 lb in excess of the forces tending to eliminate constraint of the follower on the cam. This will compensate for friction, errors, etc.

**Solution** In Fig. 8.7a we see a schematic picture of the mechanism. The time is  $60/1200 = 1/20$  sec/rev; the time for total rise of  $1\frac{1}{4}$  in. is  $160/360 \times 1/20 = 1/45$  sec.

In Fig. 8.7b the displacement diagram divides into two parts, denoted by 1 and 2. We are given  $\theta_1 + \theta_2 = 160$  degrees. Since the ratio of acceleration is 3:1, we see that

$$\theta_1 = 40 \text{ degrees}$$

$$\theta_2 = 120 \text{ degrees}$$

The time

$$t_1 = \frac{40}{160} \left( \frac{1}{45} \right) = \frac{1}{180} \text{ sec}$$

$$t_2 = \frac{120}{160} \left( \frac{1}{45} \right) = \frac{1}{60} \text{ sec.}$$

Also, we know that the displacements

$$y_1 + y_2 = 1\frac{1}{4}.$$

For the parabolic curve from Eq. (2.24) the follower displacement

$$y = \frac{1}{2} At^2 \text{ in}$$

where

$$A = \text{follower acceleration, in/sec}^2$$

The displacement

$$y_1 = \frac{1}{2} (20,200) \left( \frac{1}{180} \right)^2 = \frac{5}{16} \text{ in}$$

$$y_2 = \frac{1}{2} (6750) \left( \frac{1}{60} \right)^2 = \frac{15}{16} \text{ in.}$$

The displacement diagram is shown plotted in Fig. 8.7b. The inertia loads from Eq. (8.1)

$$F_i = \frac{w}{g} \ddot{y}$$

where  $w$  is the equivalent weight:

$$\begin{aligned} w &= \frac{\text{weight of spring}}{3} + \text{weight of linkage} \\ &= \text{assumed negligible} + 2 = 2 \text{ lb.} \end{aligned}$$

The inertia force which increases the cam surface load

$$F_i = \frac{2}{386} (20,200) = +104 \text{ lb.}$$

The critical inertia force tending to remove follower from cam

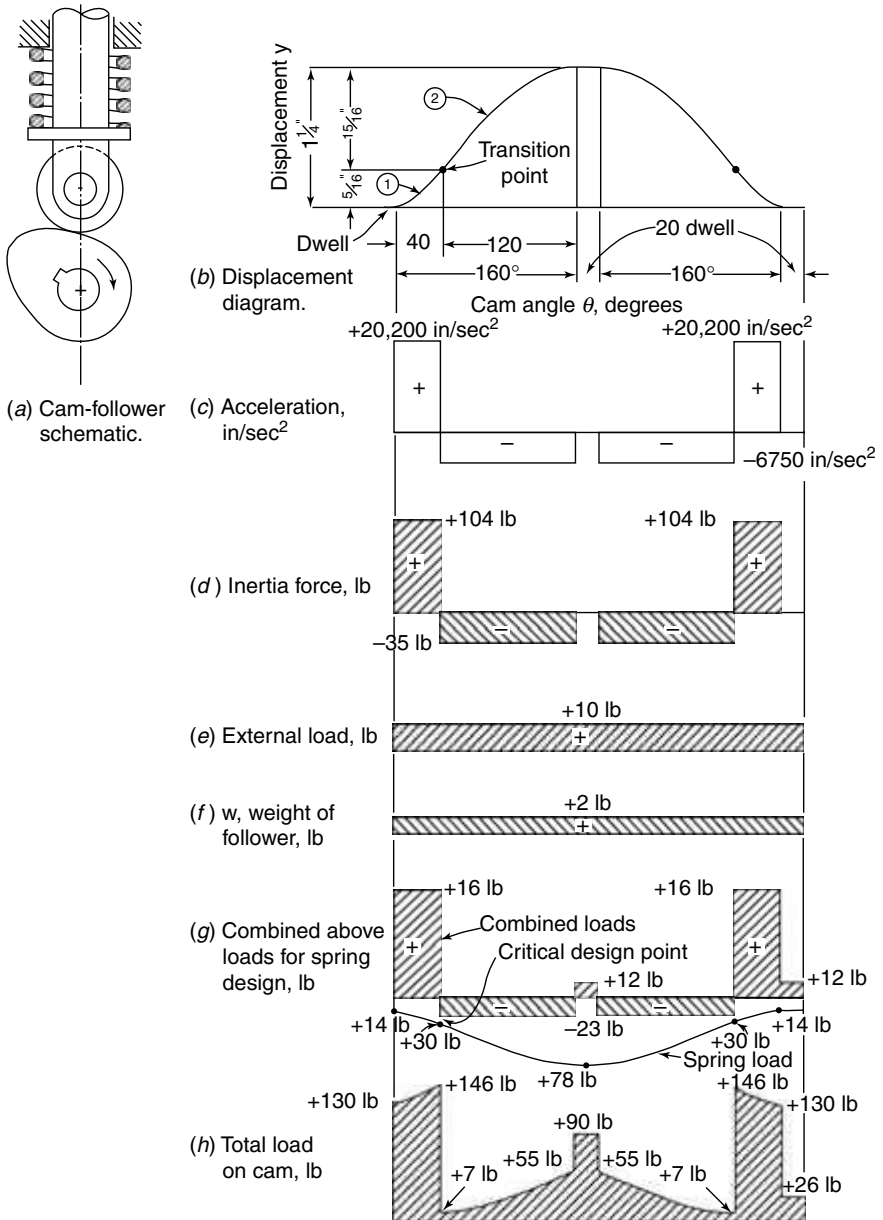


FIGURE 8.7. Cam surface load example.

$$F_i = \frac{2}{386}(-6750) = -35 \text{ lb.}$$

The acceleration curves and inertia are shown in Figs. 8.7*c* and 8.7*d*. The external load on the follower is +10 lb in Fig. 8.7*c*. The weight of follower linkage is +2 lb, Fig. 8.7*f*. Now, we shall combine these forces. Fig. 8.7*g* shows the superimposed values to give a combined force diagram. We see a fluctuating load from +116 lb to -23 lb, etc. It was stated that the spring must exceed the net negative loads by a margin of 7 lb. In Fig. 8.7*g*, we shall plot the spring load curve. At the transiting point, the spring force must equal 23 lb + 7 lb = 30 lb. At the lowest point, let us assume an initial spring preload of 14 lb.

The spring has a spring index

$$k_s = \frac{\Delta S}{\Delta \delta} = \frac{30 - 14}{\frac{5}{16}} = +51.2 \text{ lb/in}$$

where  $\Delta S$  = spring force, lb  
 $\delta$  = deflection, in

and the spring force at maximum rise

$$\frac{S_2 - 14}{1 \frac{1}{4}} = 51.2$$

$$S_2 = 78.0 \text{ lb.}$$

Superimposing the spring force in Fig. 8.7*g*, we see that the spring force curve rises appreciably as the cam rises. Note that the spring force is +( $\downarrow$ ) although it is now plotted in reverse for better understanding of margin safety. Also, this spring may have to be redesigned to fit the mechanism or to eliminate any spring surge. Last, it must be remembered that the highest cam speed requires the largest spring since at any lower speed the inertia forces are reduced.

Let us now combine all the forces. This is shown in Fig. 8.7*h*, in which we see a fluctuating load curve. The critical load point is the transition point where the minimum difference of 7 lb exists between the spring load and the external load. A slightly stronger spring could have been chosen with a negligible effect on the system.

It should be noted that the foregoing problem serves primarily as a guide since recalculations are necessary. One of the factors for redesign would be to include the spring weight of the follower. Note that the use of a spring-loaded system produces a load on the cam regardless of the speed and accordingly affects the size and wear of the designed parts.

## 8.11 TORQUE

### 8.11.1 Translating Roller-Follower Torque

An important part of the cam-follower system design is the determination of the torque, which is continually changing through the performance of any machine. From the torque we can determine the running performance of the machine, the size of the motor drive, and the proportions of the drive shaft and related parts. The torque is especially significant with:

- mechanisms having heavy masses or loads such as an indexing turret mechanism
- mechanisms having high-speed and thus high-inertia loads
- mechanisms having high pressure angles.

Let

$N$  = normal component of velocity, ips

$\ddot{y}$  = follower acceleration in/sec<sup>2</sup>

$F_n$  = force normal to cam surface, lb

$\alpha_p$  = pressure angle, deg

$W$  = cam rotational speed, rad/sec

$T$  = torque, lb-in

$\beta$  = angle of cam rotation for maximum rise, h rad

$h$  = maximum rise of follower, in

$\theta$  = cam angle rotation, rad

$\dot{y}$  = follower velocity, ips

$L$  = external load on cam, lb

$L_o = m\dot{y} + L$  = total load on cam, lb  
(friction is negligible)

$m$  = mass of follower, lb sec<sup>2</sup>/in

Figure 8.8 shows a radial cam with a roller follower. The normal component

$$N = r\omega \sin \alpha_p$$

also the follower velocity

$$\dot{y} = r\omega \tan \alpha_p \quad (8.4)$$

and the torque load

$$L_o = F_n \cos \alpha_p$$

also the torque

$$T = F_n r \sin \alpha_p$$

combining yields

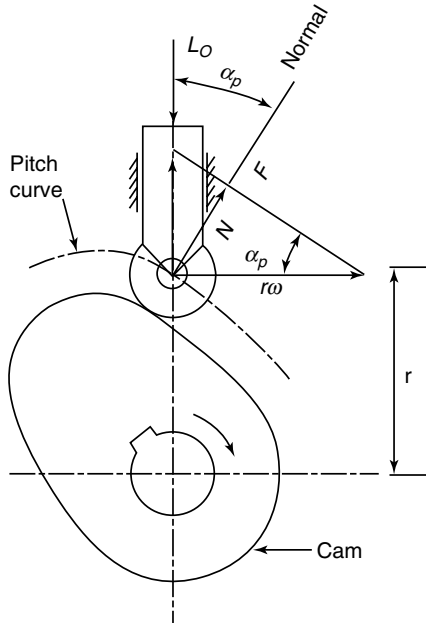
$$T = L_o r \tan \alpha_p. \quad (8.5)$$

Substituting Eq. (8.4) in Eq. (8.5) we find torque

$$T = \frac{L_o \dot{y}}{\omega} \quad (8.6)$$

$$= \frac{(L + m\ddot{y})\dot{y}}{\omega}. \quad (8.7)$$

From Eq. (8.7) we see for the dwell-rise-dwell action that the torque is continually changing, being proportional to the follower velocity and the load. Also, if these cams are



**FIGURE 8.8.** Translating roller follower velocity and forces.

driven by a motor or other power unit, the torque rating of the prime mover would have to be larger than the value of the maximum torque.

Figure 8.9 shows the roller follower comparisons for the simple harmonic, cycloidal, and modified sine curves. These were obtained by substituting values in Eq. (8.7) for the dwell-rise-dwell cam. Figure 8.9a shows the torque with a constant external load,  $L$  and the inertia load  $m\ddot{y} = 0$  for a slow-speed cam. Figure 8.9b shows the high-speed system with inertia load  $m\ddot{y}$  and zero external load,  $L = 0$ . It can be seen that the modified sine curve is most advantageous when inertia loads dominate, giving the lowest maximum value of torque.

**8.11.2 Translating Flat-Faced Follower Torque**

A cam with a reciprocating flat-faced follower is shown in Fig. 8.10a.

Let

$r_b$  = base circle radius, in

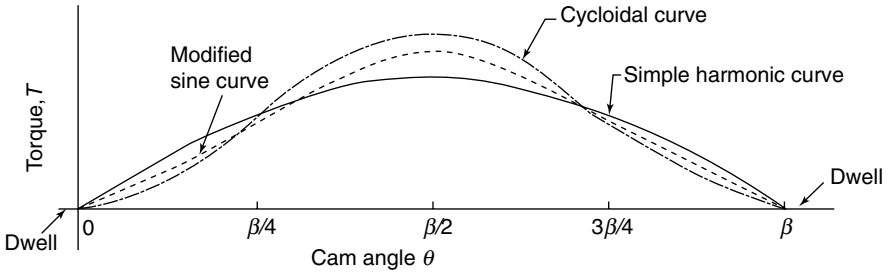
$V_s$  = sliding component of velocity, ips

$\mu$  = coefficient of friction between the follower and the cam.

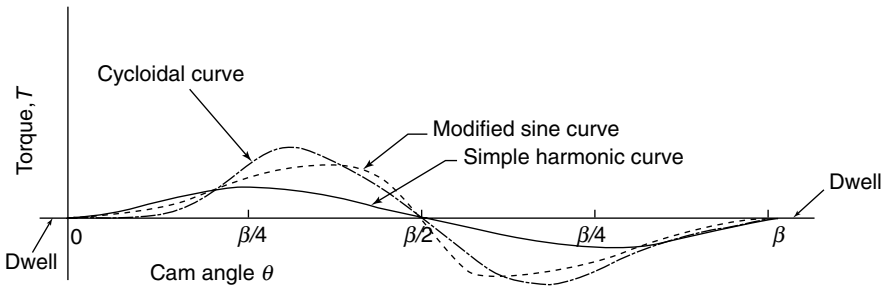
By the principle of virtual work

$$T\omega = F_n \dot{y} + \mu F_n V_s$$

or

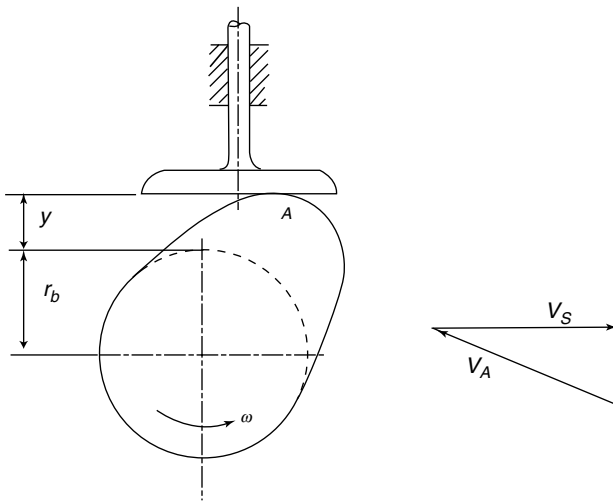


(a) External load,  $L$ , only  
(Inertia load  $\sim \ddot{y} = 0$ ).



(b) Inertia load only  
(external load  $L = 0$ ).

FIGURE 8.9. Torque comparison of cam curves (DRD cam).



(a) Cam follower.

(b) Velocity vector diagram.

FIGURE 8.10. Cam and reciprocating flat-faced follower.

$$T = \frac{F_n}{\omega}(\dot{y} + \mu V_s). \quad (8.8)$$

From the velocity diagram, Fig. 8.10b, it is seen that the sliding component velocity

$$V_s = \omega(y + r_b). \quad (8.9)$$

Substituting Eq. (8.9) into Eq. (8.8) gives

$$T = F_n \left[ \frac{\dot{y}}{\omega} + \mu(y + r_b) \right]. \quad (8.10)$$

Equation 8.10 shows that the torque is a variable function of the displacement of the follower and the converted velocity  $\frac{\dot{y}}{\omega}$  (or the slope of the cam surface) and is also dependent on the coefficient of friction and on the base circle radius of the cam.

In Eq. 8.10 the total load  $F_n$  is variable: it is the result of the weight and the loading of the follower and the resistance, the inertia, and the spring forces. If the relationship between  $F_n$  and the displacement of the follower is known, the cam-driving torque at each instant, its maximum and minimum values, and the average torque can easily be found.

### 8.11.3 Torque-Controlled Cams

In many slow-speed cam-activated mechanisms, we can design the cam profile to the desired input force and output torque relationships for a finite range of operation. We will use a radial cam with a roller follower to illustrate this; see Chen (1982) and Garrett (1962).

From Fig. 8.11 we see that pressure angle

$$\tan \alpha_p = \frac{dr}{rd\theta}$$

where  $r$  = distance from cam center to roller follower center, in.

Substituting this into Eq. (8.5) gives torque

$$T = \frac{Ldr}{d\theta}. \quad (8.11)$$

If a design requires that the output torque  $T$  be proportional to the angle of rotation  $\theta$  while the input force be proportional to the follower displacement, then

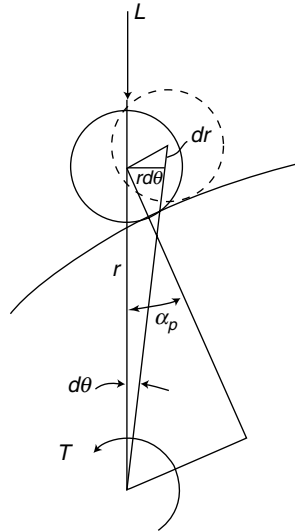
$$T = T_i + C_1\theta \quad (8.12)$$

$$L = L_i + C_2(r - r_i) \quad (8.13)$$

where  $T_i$ ,  $L_i$ , and  $r_i$ , are initial values of torque (lb-in), force (lb), and radial distance (in), respectively.  $C_1$  and  $C_2$  are constants of proportionality.

Substituting Eqs. (8.12) and (8.13) into Eq. (8.11) and integrating we obtain

$$T_i\theta + \frac{C_1\theta^2}{2} = L_i r + \frac{C_2}{2}(r - r_i)^2 + C_3.$$



**FIGURE 8.11.** Torque-controlled cam angle relationship.

When  $r = r_i$  at  $\theta = 0$

$$C_3 = -L_i r_i.$$

The final equation relationship is

$$r^2 + \frac{2}{C_2}(L_i - C_2 r_i)r + r_i^2 - \frac{2L_i r_i}{C_2} - \frac{C_1}{C_2}\theta^2 - \frac{2T_i\theta}{C_2} = 0. \quad (8.14)$$

Equation (8.14) is a quadratic equation in  $r$  when angle  $\theta$  and other values are specified.

Next, suppose a constant torque is required in the output, ignoring the change in the spring force as the follower moves. Then  $C_1$  is equal to zero in Eq. (8.14). Subsequently Eq. (8.14) becomes

$$r^2 + \frac{2}{C_2}(L_i - C_2 r_i)r + r_i^2 - \frac{2L_i r_i}{C_2} - \frac{2T_i\theta}{C_2} = 0.$$

In this way, we can find the cam profile with a prescribed torque pattern.

Furthermore, we know that the size of the motor drive is dependent on the maximum value of the torque demands of the system. For slow-speed systems it could be shown that a smaller torque and smaller prime mover can supply the same energy requirement by using constant-torque cams developed by employing the foregoing equations. Reduced size of parts, such as gears, shafts, belts, etc., results. These constant-torque cams have found application in activating mechanisms for motor-drive spring compression, circuit breakers, and others. Similarly, a unique, hydraulically driven, inverse cylindrical cam has been applied in controlling the inclination of aircraft propeller blades as required by the changing speed of the plane. The cam profile was established to provide a constant excess of torque over a complex resistance torque curve.

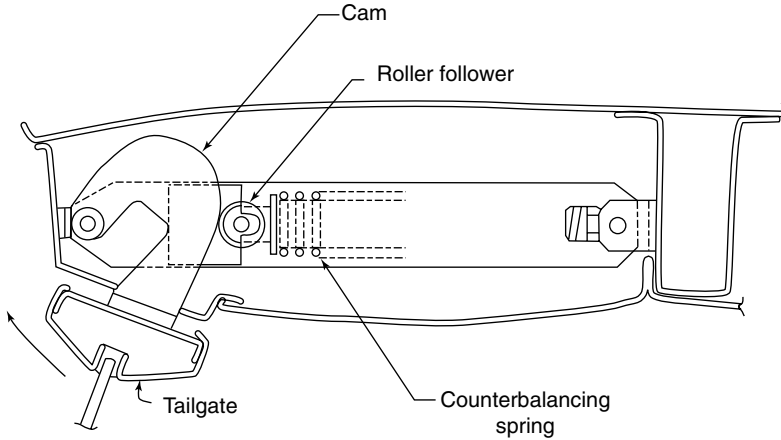


FIGURE 8.12. Automobile station wagon tailgate counterbalance mechanism.

**EXAMPLE** Figure 8.12 shows a cam that might be used to raise the upper section of an automobile station wagon tailgate. The desired cam output torque used to balance the gate varies sinusoidally with respect to angle  $\theta$  according to

$$T = C_1 \sin\left(\theta + \frac{\pi}{6}\right).$$

This is shown in Fig. 8.13. The input torque is supplied by the spring-loaded follower. The spring force decreases as the gate rises, but the torque supplied by the spring increases to a maximum, then gradually drops off to balance the gate. The spring force may be described by

$$L = L_1 - C_2(r_i - r).$$

From the principal of virtual work

$$Td\theta = Ldr.$$

When the torque equation and the spring-force equation are substituted into this equation, and when the results are integrated and evaluated with the boundary condition  $r = r_1$  when  $\theta = 0$ , the resulting quadratic equation in  $r$  is

$$r^2 - 2rr_i + r_i^2 + \frac{2L_1}{C_2}(r - r_i) - \frac{C_1}{C_2}[\sqrt{3}(1 - C) + 5] = 0$$

when  $C_2$ ,  $L_1$ , and  $r_1$  are given.

Also, with reference to Fig. 8.12, the fully open tailgate torque caused by the weight of the tailgate is 125 lb-in. This tailgate torque is

$$T_G = C_3 \sin\left(\theta + \frac{\pi}{12}\right) \text{ lb-in.}$$

When

$$\theta = \frac{\pi}{2}, \text{ we want } T = T_G, \text{ and}$$

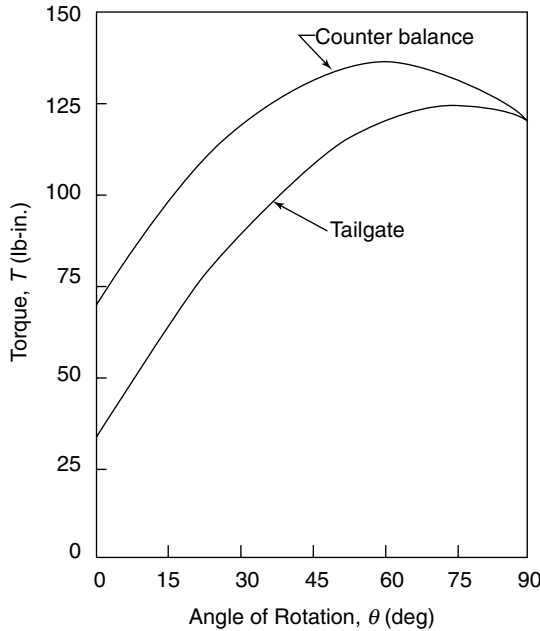


FIGURE 8.13. Automobile station wagon tailgate torque.

$$C_1 = C_3 \frac{\sin\left(\frac{\pi}{2} + \frac{\pi}{12}\right)}{\sin\left(\frac{\pi}{2} + \frac{\pi}{6}\right)}.$$

Since  $C_3 = (T_G)_{\max} = 125 \text{ lb per in.}$ ,  $C_1 = 139 \text{ lb-in.}$

Assume that  $C_2 = 50 \text{ lb per in.}$ ,  $r_1 = 3 \text{ in.}$ , and  $F_1 = 200 \text{ lb}$  are given which yields

$$r = [16 - 4.815(i - \cos\theta) - 278\sin\theta]^{\frac{1}{2}} - 1.$$

*This is the required pitch profile of the cam as a function of  $\theta$ , and a reversal of the pressure angle near the closed position permits the mechanism to hold the tailgate closed. Also, the equations express the paths of the centers of the rollers, not the surfaces of the cams. If a cutter of the same diameter as the roller is used on the prescribed path of the roller center, the desired cam surface will be generated.*

#### 8.11.4 Torque-Controlled Wrapping Cams

Tidwell et al. (1994) describe a technique for synthesizing a force-generating mechanism composed of a cam wrapped by a belt or chain, referred to as “wrapping cams.” Synthesis methods for two configurations of this mechanism are presented in Tidwell [1994]. In the simplest case, the cam is wrapped by a belt or chain under constant tensile force, producing a nonlinear torque at the cam. In the second case, the cam is under constant torque, producing a nonlinear belt or chain force. Although wrapping cams are far less common

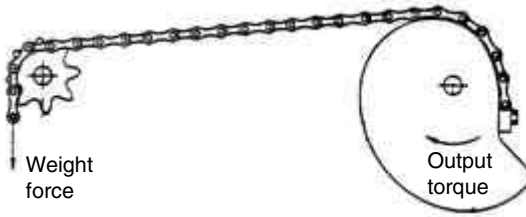


FIGURE 8.14. Wrapping cam mechanism.

than cams that generate specified follower displacement functions, applications for wrapping cams exist in counterbalancing mechanisms, exercise equipment, and process machines.

A wrapping cam mechanism consists of a planar disk in the shaped of a cam profile. However, instead of a conventional follower, a belt or chain is wrapped around the profile (Fig. 8.14).

Although conventional cam-and-follower systems can be used for force generation, wrapping cams have the advantage of low hertzian contact stresses with no relative sliding. Sliding between the cam and the belt or chain is prohibited either by using sprocket-type teeth on the cam or by permanently attaching the chain or belt to a smooth cam.

The cam does not generally rotate continuously but rather oscillates back and forth, typically through less than one revolution. The belt or chain reciprocates through less than one revolution. A weight can be used in conjunction with a wrapping cam to convert a constant force input to a precisely controlled, nonlinear output torque function, as shown in Fig. 8.14.

## 8.12 ROTATABLE INVERSE CAM MECHANISM

The content of this section, developed by Ananthasuresh (2001 with special permission from Pergamon Press, N.Y.), shows an inverse cam mechanism in which the follower drives the cam. Both cam and follower complete a full rotation in each cycle and remain in contact throughout. It is noted that to have the cam fully rotate for every full rotation of the roller crank, the cam cannot be a closed profile; rather the roller traverses the open cam profile twice in each cycle. Using kinematic analysis, the angular velocity of the cam when the roller traverses the cam profile in one direction is related to the angular velocity of the cam when the roller retraces its path on the cam in the other direction. Thus, one can specify any arbitrary function relating the motion of the cam to the motion of the roller crank for only  $180^\circ$  of rotation in the angular velocity space. The motion of the cam in the remaining portion is then automatically determined. In specifying the arbitrary motion, many desirable characteristics such as low acceleration and jerk can be obtained. Using the kinematic inversion technique, the cam profile is readily obtained once the motion is specified in the angular velocity space. The only limitation to the arbitrary motion specification is making sure that the transmission angle never gets too low, so that the force will be transmitted efficiently from roller to cam. This is addressed by incorporating a *transmission index* into the motion specification in the synthesis process. Consequently, in this method we can specify a permissible zone, such that the transmission index is higher than the specified minimum value.

**SYMBOLS**

- $a$  = length of the roller-crank, in  
 $d$  = distance between the roller-crank and cam pivots, in  
 $k$  = spring constant of the force-closure spring, lb/in  
 $m_c$  = cam mass, lb  
 $n$  = angular velocity ratio of the cam and the roller-crank in the first half of the cycle  
 $n^*$  = angular velocity ratio of the cam and the roller-crank in the second half of the cycle  
 $r$  = transmission index  
 $r_{Fc}$  = moment arm of contact force, in  
 $r_s$  = moment arm of spring force, in  
 $F_s$  = spring force, lb  
 $F_c$  = contact force between roller and cam, lb  
 $I_c$  = moment of inertia of cam, lb-in<sup>2</sup>  
 $I_r$  = moment of inertia of roller crank, in-lb-sec<sup>2</sup>  
 $R_c^2$  = distance from pivot to com mass center, in  
 $R_{Fc}$  = moment arm of contact force, in  
 $R_s$  = moment arm of spring force, in  
 $R_r^2$  = distance from pivot to roller crank mass center, in  
 $T$  = torque in-lb  
 $\alpha$  = angular acceleration, rad/sec<sup>2</sup>  
 $\alpha_c$  = angular acceleration of cam, rad/sec<sup>2</sup>  
 $\beta$  = angle between the common normal and the line joining the cam and roller-crank pivots, rad  
 $\psi$  = angular position of the force-closure spring location of the cam, deg  
 $\phi$  = rotation of the cam, rad  
 $\eta$  = angle between the line joining the cam and the roller-crank pivots and the line joining the cam pivot and the center of the roller, rad  
 $\lambda$  = pressure angle, deg  
 $\mu$  = transmission angle, deg  
 $\theta$  = rotation of the roller-crank, rad  
 $\omega$  = angular velocity, rad/sec

**8.12.1 Kinematic Principles**

The physical arrangement of the planar cam-follower system considered here is shown schematically in Fig. 8.15. The roller-crank and the cam are pivoted about two fixed points,  $A_0$  and  $B_0$ , respectively. A roller mounted at the free end of the roller crank is in contact with the cam. The rotations of the roller crank and cam are denoted by  $\theta$  and  $\phi$ , respectively. For the purpose of the kinematic analysis that follows, we will use the pitch curve of the cam. The design objectives are:

- Both cam and roller-crank must rotate through 360° in each cycle.
- They should always be in contact with each other.
- Arbitrary specification of motion relating  $\theta$  and  $\phi$  should be possible including finite dwells and reversal of motion.
- Transmission criteria should be adequately satisfied to be of practical use.

In mechanism synthesis, it is necessary to have a suitable transmission criterion to be able to judge the efficiency of transmission of motion and force. The pressure angle is the

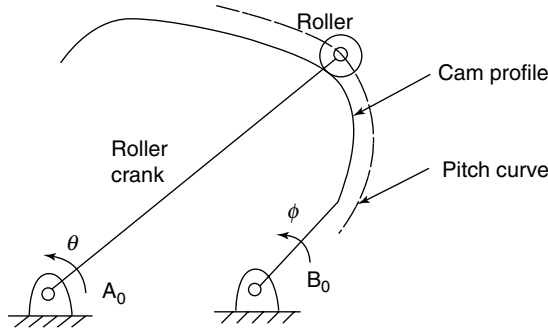


FIGURE 8.15. Schematic of cam-follower mechanism.

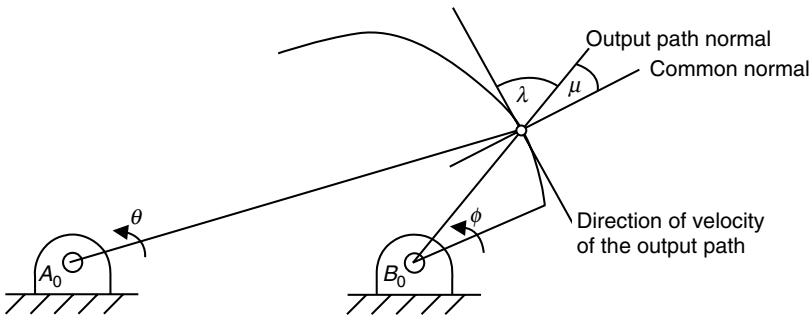


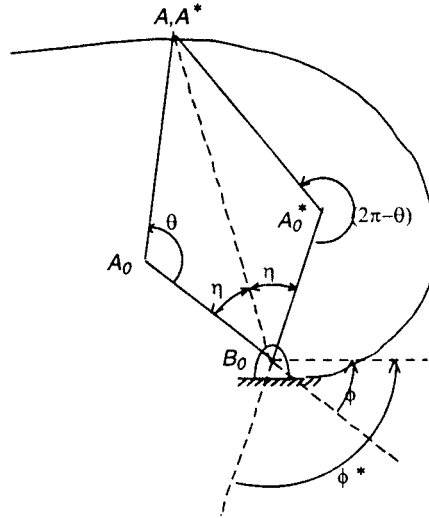
FIGURE 8.16. Pressure angle  $\lambda$ , and transmission angle  $\mu$  for the mechanism when the cam is the output member.

acute angle between the direction of the contact force between the cam follower and the direction of the velocity of the output point where the contact force is applied. Since the transmission angle is the complement of the pressure angle, the former can be defined as the acute angle between the common normal and the output point path normal. In cam-follower systems, the direction of force is along the common normal at the point of contact. The pressure angle and transmission angle are indicated in Fig. 8.16 when the roller crank drives the cam. The smaller the pressure angle the better the transmission and vice versa. Likewise, if the ideal transmission angle is 90 deg, the closer it is to 90 deg the better will be the transmission. In this paper, the above definition of transmission angle will be used as the criterion for the efficiency of transmission in the following discussions. A more suitable *transmission index* based on the transmission angle will be defined later.

It has been stated that for a full rotation of the cam and roller crank, the cam cannot have a closed profile. Consequently the roller must traverse the open profile twice in each revolution. An important feature of the mechanism is that we can prescribe the functional relationship between  $\theta$  and  $\phi$  for only half the cycle. Barring this limitation and proper transmission criteria, there is no other restriction to specify the basic design.

### 8.12.2 Cam Output Motion

As discussed above, if the input member roller crank completes one revolution, the roller must traverse the open-cam profile twice. Consequently, the output motion of the cam



**FIGURE 8.17.** Kinematic inversion of the mechanism to determine the motion in the second part of the cycle.

while the roller retraces its path is governed by the profile that prescribes the motion of the cam in the first part of the cycle. It is now clear that we can specify the motion of the cam in only half the cycle and that the remaining half is determined automatically, thus limiting control over the complete motion. However, by studying the motion in the second half we can design the cam profile to have better control over its motion.

Figure 8.17 shows a kinematic inversion of the basic arrangement of Fig. 8.15, where  $B_0A_0A$  is the configuration during the initial traverse of the roller on the cam.  $B_0A_0^*A^*$  is the configuration when the roller returns to the same point during the reverse traverse on the cam. The angle between  $A_0B_0$  extended beyond  $B_0$  and a reference (horizontal) line on the fixed link (i.e., the cam in this inversion)  $\phi$ , indicates the rotation of the cam in the basic arrangement. Figure 8.17 shows the same angle  $\phi^*$  for the reverse traverse. The following relationships can be observed from the figure:

$$\theta^* + \theta = 2\pi \quad (8.15a)$$

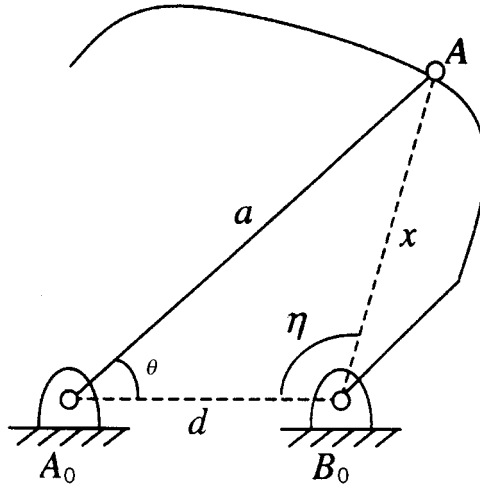
$$\phi^* - \phi = 2\eta \quad (8.15b)$$

where  $\eta$  is the angle between the line joining the cam-pivot and the roller center, and the line joining the cam pivot and roller-crank pivot. By differentiating Eq. 8.14b with respect to input  $\theta$ , we get

$$\frac{d\phi^*}{d\theta} - \frac{d\phi}{d\theta} = 2 \frac{d\eta}{d\theta}. \quad (8.16)$$

Eq. (8.15) can be rewritten as

$$\frac{d\phi^*}{d\theta^*} \frac{d\theta^*}{d\theta} - \frac{d\phi}{d\theta} = 2 \frac{d\eta}{d\theta}. \quad (8.17)$$



**FIGURE 8.18.** Schematic to derive an expression for  $\eta$  and its derivative.

Denoting  $d\phi/d\theta$  as  $n$  and  $d\phi^*/d\theta^*$  as  $n^*$ , and using the fact that  $d\theta^*/d\theta = -1$ , Eq. (8.17) becomes

$$n^* + n = -2 \frac{d\eta}{d\theta}.$$

It should be noted that  $n$  refers to the part of the motion that we specify and  $n^*$  refers to the motion in the remaining part. The integration of  $n$  and  $n^*$  gives the cam rotation  $\phi$ . Therefore, the area under the  $-2d\eta/d\theta$  vs  $\theta$  gives the sum of the motion of the cam in both halves of the cycle. Thus, using Eq. (8.17), we can predict and control the motion in the second half of the cycle.

Denoting the distance between the cam and the roller-crank pivots by  $d$ , and the length of the roller-crank as  $a$ , applying the cosine rule to the triangle  $A_0B_0A$  in Fig. 8.18,  $\eta$  can be written as

$$\eta = \cos^{-1} \left( \frac{d^2 + x^2 - a^2}{2dx} \right) \quad (8.18)$$

where

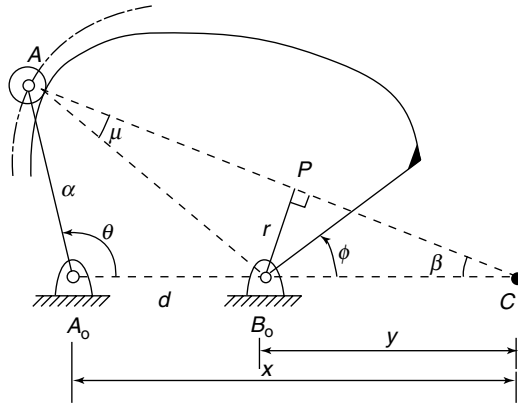
$$x = \sqrt{a^2 + d^2 - 2ad \cos \theta}.$$

Differentiating  $\eta$  in Eq. (8.18) with respect to  $\theta$ , we get

$$\frac{d\eta}{d\theta} = \frac{-1}{\sin \eta} \frac{\sin \theta (1 - (d/a) \cos \theta)}{(1 + (d/a)^2 - 2(d/a) \cos \theta)^{3/2}}. \quad (8.19)$$

The above expression is useful in specifying the desired motion as well as in generating the cam profile.

Although the transmission angle is a useful measure to quantify the performance of a given mechanism, it is not always the most convenient measure to use while designing a



**FIGURE 8.19.** Schematic sketch of the mechanism for the purpose of writing the design equations.

new mechanism. Here, we use a more appropriately defined index of transmission as shown in Fig. 8.19. The torque exerted on the output member, the cam, is the moment due to the contact force between the roller and the cam, which acts along the common normal. The moment arm is given by  $r$ , which is the perpendicular distance to the common normal from the cam pivot. The higher the value of  $r$  is, the better the transmission and vice versa. As shown the nondimensionalized  $r$  is a convenient measure of transmission for the mechanism considered here. The ratio  $(r/d)$  is the nondimensional transmission index for this mechanism.

As shown in Fig. 8.19, point  $C$  is the instantaneous center of the roller crank and the cam. Therefore, this point has the same velocity on both the cam and the roller crank. This leads to the following relationship:

$$n = \frac{d\phi}{d\theta} = \frac{x}{y}. \quad (8.20)$$

Further, since  $x = y + d$ , Eq. (8.20) can be rewritten as

$$\frac{1}{y} = \frac{n-1}{d}. \quad (8.21)$$

Now, applying the sine rule to the triangle  $A_0AC$  of Fig. 8.19, we get

$$\frac{\sin(180^\circ - \theta - \beta)}{x} = \frac{\sin \beta}{a} \quad (8.22)$$

which, after eliminating  $x$ , can be simplified to

$$\sin \theta \cot \beta + \cos \theta = \frac{y+d}{a}. \quad (8.23)$$

From the right-angled triangle  $B_0PC$ ,

$$\cot \beta = \frac{\sqrt{y^2 - r^2}}{r} = \sqrt{\left(\frac{y}{r}\right)^2 - 1}. \quad (8.24)$$

Combining Eqs. (8.23) and (8.24) yields

$$\sin \theta \sqrt{\left(\frac{y}{r}\right)^2 - 1} = \frac{y}{a} + \frac{d}{a} - \cos \theta. \quad (8.25)$$

Squaring both sides of Eq. (8.25) and rearranging, we get

$$\sin^2 \theta - \sin^2 \theta \left(\frac{r}{y}\right)^2 = \left(\frac{r}{a}\right)^2 + \left(\frac{r}{y}\right)^2 \left(\frac{d}{a} - \cos \theta\right)^2 + \frac{2r^2}{ay} \left(\frac{d}{a} - \cos \theta\right). \quad (8.26)$$

Substituting for  $(1/y)$  from Eq. (8.21) into the above equation gives a quadratic equation in  $n$

$$\left(\frac{r}{d}\right)^2 \left\{ \left(\frac{d}{a} - \cos \theta\right)^2 + \sin^2 \theta \right\} (n-1)^2 + \frac{2r^2}{ad} \left(\frac{d}{a} - \cos \theta\right) (n-1) + \left(\frac{r}{a}\right)^2 - \sin^2 \theta = 0. \quad (8.27)$$

Several observations can be made about the above equation.

1. Since Eq. (8.27) remains the same if we replace  $\theta$  with  $(2\pi - \theta)$ , the two solutions of  $n$  for a given value of  $\theta$  correspond to the angular velocity ratios of the cam and the roller crank during the initial and reverse traversal of the roller on the cam. That is,

$$\begin{aligned} n_{\text{solution1}} &= n = \left(\frac{d\phi}{d\theta}\right)_{\text{at } 0} \\ n_{\text{solution2}} &= n^* = \left(\frac{d\phi^*}{d\theta^*}\right)_{\text{at } 0^*=(2\pi-0)}. \end{aligned} \quad (8.28)$$

2. When  $\theta = 0$  or  $\pi$ , Eq. (8.27) becomes independent of  $r$

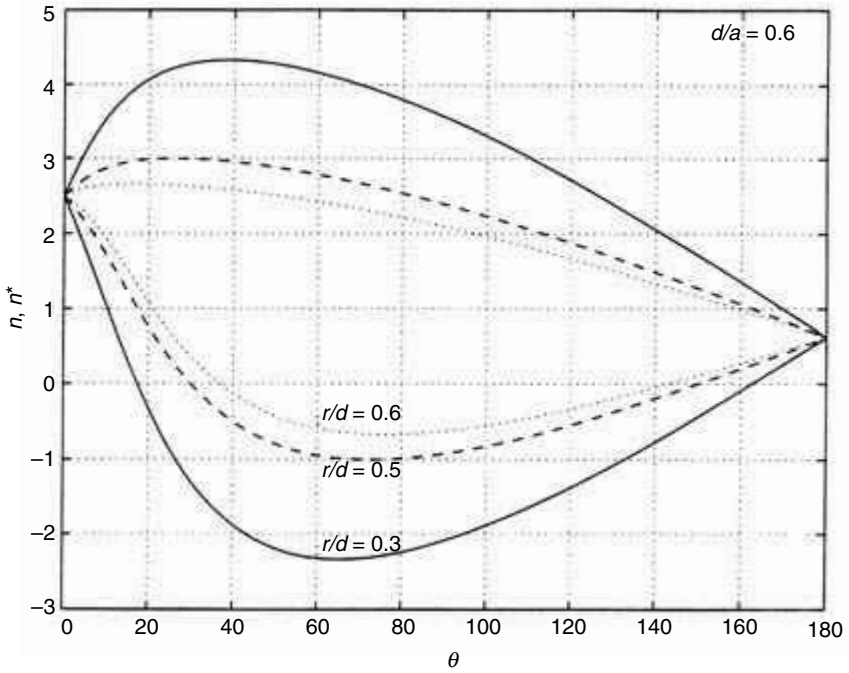
$$\left(\frac{d}{a} \mp 1\right)^2 (n-1)^2 + \frac{2d}{a} \left(\frac{d}{a} \mp 1\right) (n-1) + \left(\frac{d}{a}\right)^2 = 0. \quad (8.29)$$

This can be seen in Fig. 8.20 which shows the solution curves for  $n$  for different  $(r/d)$  ratios. It can also be observed in this figure that the region bounded by the two solution curves for one value of the  $(r/d)$  ratio contains similar curves of a larger ratio. As mentioned earlier a larger value of  $(r/d)$  implies better transmission. Therefore, the region between two solution curves can be used to specify the angular velocity ratio  $n$  so that the transmission index  $(r/d)$  is larger than a minimum specified value. This is a useful feature in designing the mechanism.

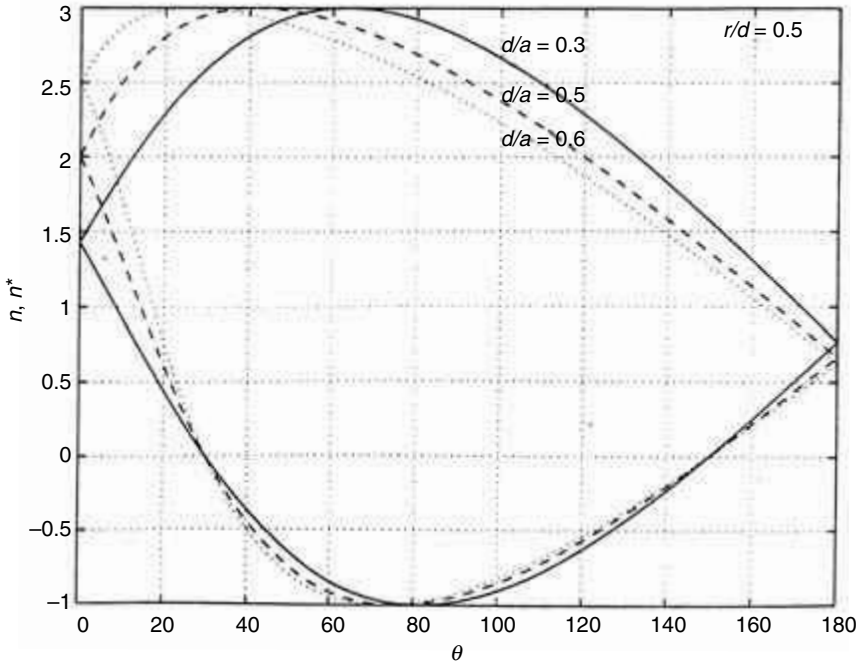
3. Figure 8.21 shows the solutions curves for  $n$  for a fixed ratio of  $(r/d)$  and varying ratios of  $(d/a)$ . It can be seen that  $n = 0$  occurs at the same two points. This is also evident from Eq. (8.27) if we substitute  $n = 0$  and solve for  $\theta$

$$n = 0 \Rightarrow \theta = \sin^{-1}(r/d) \text{ or } \pi - \sin^{-1}(r/d) \quad (8.30)$$

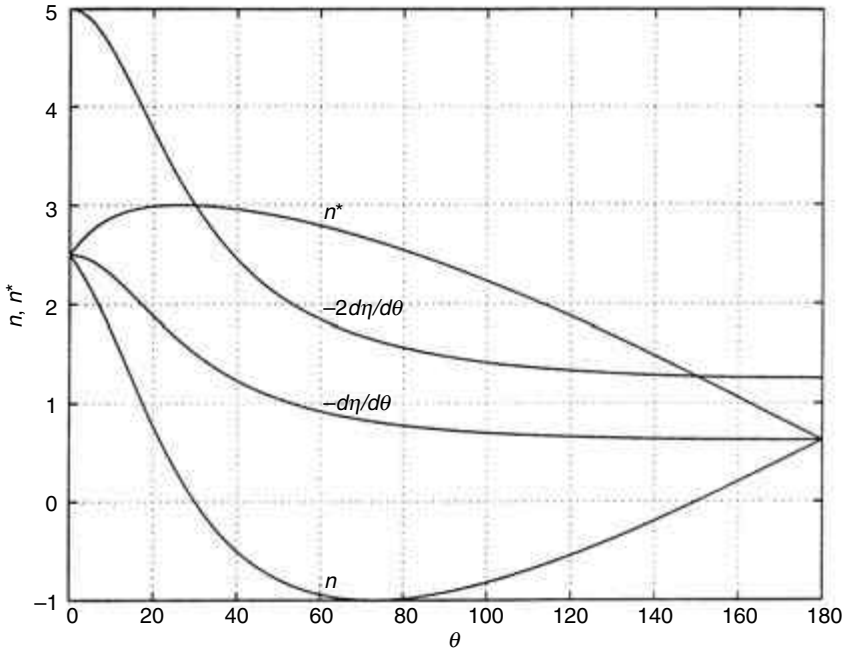
which is clearly independent of the ratio  $(d/a)$ . This feature of the design (see Eq. [8.27]) has an important significance if a long dwell or reversal of motion of the cam is desired. That is, if we specify a lower bound on the transmission index  $(r/d)$ , then the permissible region for  $n$  has zero or a negative value over only a limited range of  $\theta$ . For example, the maximum possible single dwell in the initial traversal of the roller on the cam is  $(\pi - 2\sin^{-1}(r/d))$ . It should be noted that this is a minimum value of  $r$  here, not  $r$  generically. Thus, the ratio is useful not only to achieve a prescribed minimum



**FIGURE 8.20.** Solutions of Eq. (8.27) for a constant value of  $(d/a) = 0.6$  and varying values of  $(r/d) = 0.3, 0.5,$  and  $0.6$ .



**FIGURE 8.21.** Solutions of Eq. (8.27) for a constant value of  $(r/d) = 0.5$  and varying values of  $(d/a) = 0.3, 0.5,$  and  $0.6$ .



**FIGURE 8.22.** Design curves for specifying the desired motion of the mechanism;  $(d/a) = 0.6$ ,  $(r/d) = 0.5$ .

transmission index but also in selecting the longest possible dwell or reversal of motion. It is also worth noting that unless the transmission index is zero, a single dwell of  $180^\circ$  or more is not possible. Furthermore, shorter dwell or no dwell at all implies that the transmission index is greatly improved. This is a useful feature in designing a mechanism for prescribed function generation without a dwell.

4. Figure 8.22 shows a  $(-d\eta/d\theta)$  vs  $\theta$  curve drawn along with the solution curves for  $n$  for sample values of  $(r/d)$  and  $(d/a)$ . Recalling Eq. (8.17), it can be seen that the  $(-d\eta/d\theta)$  vs  $\theta$  curve is the average of two segments of the solution curves for  $n$ . Therefore, by reflecting the  $n$  curve for the range  $(0 \leq \theta \leq \pi)$  about  $(-d\eta/d\theta)$  vs  $\theta$  curve, we get  $n$  curve for the range  $(\pi \leq \theta \leq 2\pi)$ . This makes the prediction and control of the output motion of the cam in the second half of the cycle possible, as Eq. (8.17) is true for any value of  $n$ , not just the solutions of Eq. (8.27). It should be noted that  $(-d\eta/d\theta)$  is independent of the transmission index  $(r/d)$ . It is also worth noting that by choosing  $n$  along the  $(-2d\eta/d\theta)$  curve,  $n^*$  can be made zero to get a dwell in the second half of the cycle.

5. The area under the  $n$  vs  $\theta$  curve gives  $\phi$ , the rotation of the cam that can be used to generate the cam profile by using the kinematic inversion shown in Fig. 8.17.

### 8.12.3 Design Procedure

Using the results of the foregoing analysis, a systematic procedure for designing a fully rotatable, roller-crank driven cam mechanism for arbitrary motion specifications is described in this section. An important design specification is *the minimum value the trans-*

*mission index can take throughout the motion of the mechanism.* The overall size of the mechanism is not important as this is a function generation problem. Consequently, the nondimensional ratios of  $(r/d)$  and  $(d/a)$  are used. The value of  $d$  determines the size of the mechanism. The procedure consists of the following steps.

*Step 1:* For the specified minimum value of  $(r/d)$  and a chosen value of  $(d/a)$ , using Eq. (8.27), the two segments of  $n$  vs  $\theta$  curve are drawn. This determines the permissible zone as the region enclosed between the two curves for specifying the motion in the first half of the cycle. Drawing the  $(-d\eta/d\theta)$  vs  $\theta$  curve in the same graph aids the visualization of the motion in the remaining half of the cycle.

*Step 2:* Depending on the nature of the desired function  $\phi(\theta)$ , the  $n$  vs  $\theta$  can be specified within the permissible region. The  $(d/a)$  ratio can be changed if necessary. Second-order (acceleration) and third-order (jerk or shock) derivatives of the function  $\phi(\theta)$  can be controlled in this process. Continuity of the function  $\phi(\theta)$  and its derivatives can also be ensured. Harmonic, cycloidal, polynomial, spline, and other types of curves can be used to specify the  $n$  vs  $\theta$  curve to satisfy all of the design objectives in the design of the cam. Then, the motion in the second half of the cycle is easily computed using Eq. (8.17). The  $(-d\eta/d\theta)$  vs  $\theta$  curve should be appropriately used to control the motion in the second half of the cycle by specifying a curve in the first half.

*Step 3:* The rotation of the cam in the entire  $360^\circ$  range can be readily obtained by computing the cumulative area under the  $n$  vs  $\theta$  curve from  $0$  to  $360^\circ$ . This can be done either analytically or numerically depending on how the  $n$  vs  $\theta$  curve is specified. Note that the analytical expression for  $(-d\eta/d\theta)$  is readily available from Eq. (8.19).

*Step 4:* Using the kinematic inversion technique the endpoint of the two-link open serial chain can be made to trace the pitch curve of the cam profile as per the function  $\phi(\theta)$  obtained in step 3. The finite radius of the roller is then used to obtain the actual profile of the cam as an envelope of all the positions of the rollers. This can be done by computing the equidistant offset curve of the pitch profile of the cam using the numerically determined normal at the point of contact. In practice, by choosing a milling cutter of the same radius as the roller, the pitch profile is sufficient.

All of the above steps are implemented in Matlab (2000) and the entire design procedure automated. The Matlab scripts generate the  $G$ -code for the computer numerically controlled Fadal vertical machining center to manufacture the cam.

### 8.12.4 Force Closure

Form closure and force closure are two ways in which the cam and roller can be kept in constant contact even at high speeds. Force closure with a helical extension spring is discussed here.

Figure 8.23 shows the arrangement of the spring. Three parameters— $s_1$ ,  $s_2$ , and  $\psi$ —are identified to locate the spring on the roller crank and the cam. These three parameters are determined to meet the following objectives. As the mechanism is in motion, the length of the spring should not change excessively as this will impose additional loads on the mechanism. The direction of the spring force should be such that it counteracts the separative forces acting on the cam and roller. An optimization problem was solved for the single dwell cam to minimize the maximum variation of the spring length with  $s_1$ ,  $s_2$ , and  $\psi$  as the design variables. The Nelder-Mead simplex algorithm was used for this purpose.

### 8.12.5 Quasikinestatic Analysis

In this section, the expressions for computing the input torque required at the roller crank are presented. If the mechanism operates at high speeds, inertia forces should also be taken

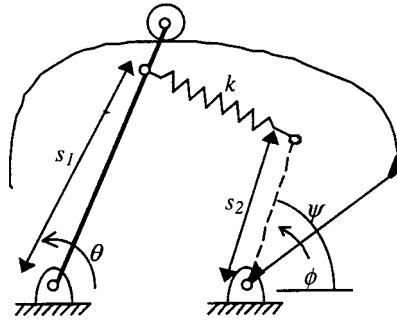


FIGURE 8.23. Force closure for the mechanism using a spring.

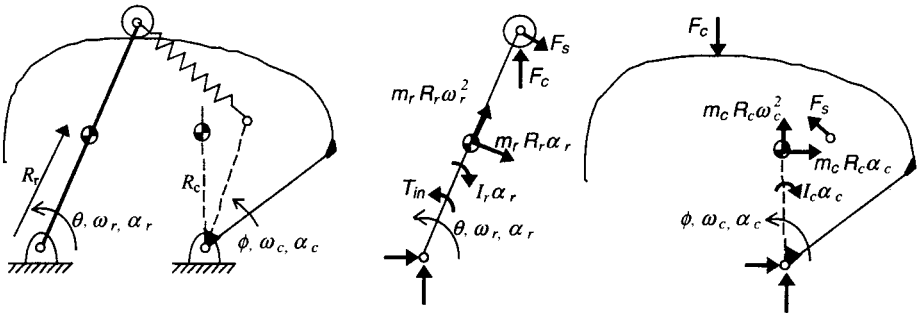


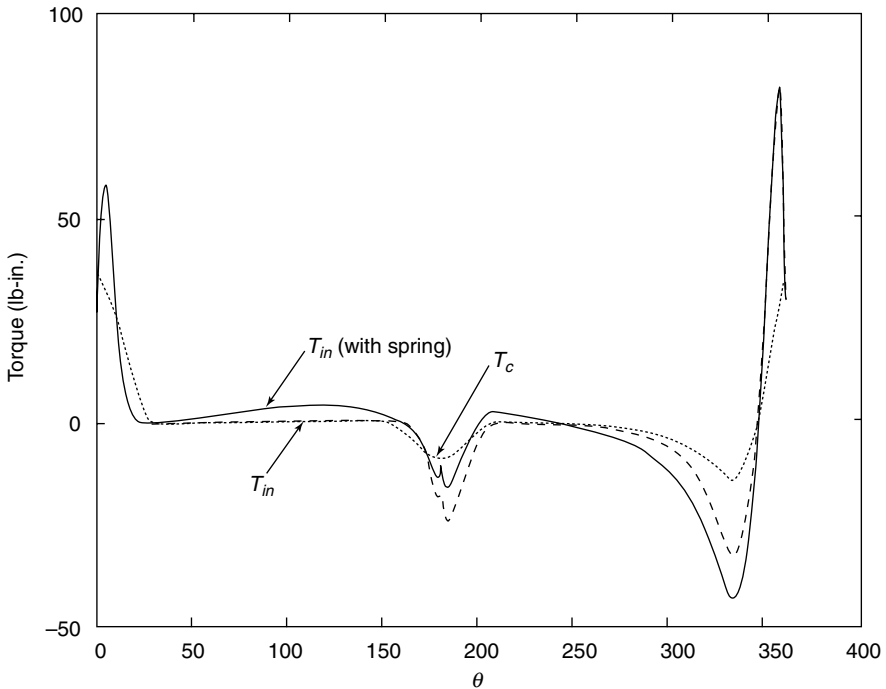
FIGURE 8.24. Contact, spring, and inertia forces acting on the roller crank and the cam.

into account. The following quasikinestostatic analysis is also useful in selecting the correct value of the spring constant for the force closure spring by way of optimization. Figure 8.24 shows the forces acting on the roller crank and the cam.  $F_c$  is the contact force between the roller and the cam and acts in the direction of the common normal.  $F_s$  is the spring force whose direction is also known at every instant during the motion. No load other than the inertia force is shown on the cam. Radial, tangential, and angular acceleration components of the inertia forces are shown on both the cam and the roller crank. From the results of the kinematic analysis and the mass properties of the roller crank and the cam, all inertia forces can be computed at every instant. Therefore, the unknown in the force analysis are the four ground reaction forces (two at each fixed pivot),  $F_c$ , and  $T_{in}$ . Since this is a planar problem, three Newtonian force/moment balance equations arise for each body, here the roller crank and the cam. Thus, the six equations in six unknowns are easily solved. The contact force and the required input torque are given by:

$$-I_c \alpha_c - m_c R_c^2 \alpha_c + F_c R_{Fc} + F_s R_s = 0, \tag{8.31}$$

$$T_{in} - I_r \alpha_r - m_r R_r^2 \alpha_r + F_c r_{Fc} + F_s r_s = 0 \tag{8.32}$$

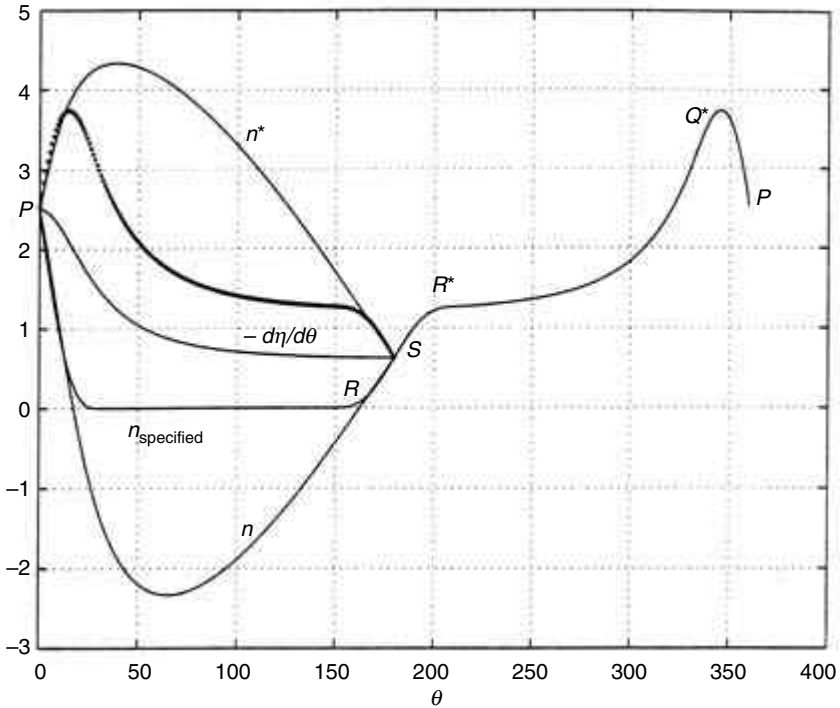
where  $I_c$  = the moment of inertia of the cam about its center of mass  
 $\alpha_c$  = the angular acceleration of the cam



**FIGURE 8.25.** Inertia torque of the cam  $T_c$  and the required input torque on the roller crank with and without the spring.

- $m_c$  = the mass of the cam
- $R_c$  = the distance from the pivot to the center of mass of the cam
- $R_{Fc}$  = the moment arm of the contact force about the cam pivot
- $R_s$  = the moment arm of the spring force about the cam pivot
- $I_r$  = the moment of inertia of the roller crank about its center of mass
- $m_r$  = the mass of the roller crank
- $R_r$  = the distance from the pivot to the center of mass of the roller crank
- $r_{Fc}$  = the moment arm of the contact force about the roller crank pivot
- $r_s$  = the moment arm of the spring force about the roller crank pivot

Figure 8.25 shows  $T_{in}$  as a function of the roller crank position for the single-dwell mechanism. In this calculation, a constant angular velocity of 30rpm was assumed for the roller crank. Other properties estimated for the single-dwell prototype were: density of the cam material =  $0.04 \text{ lb/in}^3$ ;  $m_c$  = mass of the cam =  $0.32 \text{ lb}$ ;  $I_c$  = moment of inertia of the cam about its center of mass =  $1.7264 \text{ lb} - \text{in}^2$ ;  $R_c$  = distance from the cam pivot to its center of mass =  $2.2 \text{ in}$ . Inertia forces of the roller crank were neglected. Figure 8.25 shows the input torque requirement with and without the force-closure spring. The next step is to optimize the location of the spring and the spring constant to decrease the peak input torque to improve the performance of the device at high speeds based on the quasi-static analysis.



**FIGURE 8.26.** Design curves and the specification of single-dwell motion using half-cycloidal curves.

**EXAMPLE** In this single-dwell motion design example, the objective is to obtain a mechanism with the longest possible dwell in the first half of the cycle while satisfying the requirements of good transmission and smoothness of motion. A minimum transmission index ( $r/d$ ) of 0.5 is desired.

**Solution** The design procedure begins with choosing  $(d/a)$  equal to 0.6. Figure 8.26 shows the design curves and the specified curve for  $n$  in the range  $0 \leq \theta \leq 180^\circ$ . Since  $n$  is zero or negative from  $30^\circ$  to  $150^\circ$ , the maximum possible dwell period is  $120^\circ$ . It should be noted that the specified  $n$  must lie in the area enclosed by the  $n$  and  $n^*$  curves to meet the minimum value specification for  $(r/d)$ . To meet the smoothness of motion requirements, the half-cycloidal motion is specified in the range  $0 \leq \theta \leq 30^\circ$  and  $150^\circ \leq \theta \leq 180^\circ$ . This ensures that the second derivative of  $n$  (i.e., the jerk) is also smooth. In Fig. 8.26

PQ\* = half-cycloidal motion

Q\*R = dwell portion

RS = half-cycloidal motion.

The motion in the second half of the cycle is obtained by reflecting  $n$  about the  $-(d\eta/d\theta)$  curve. Therefore, it retains the smoothness at the transition points. The segment  $SR^*Q^*P$  corresponds to this part of the motion as seen in Fig. 8.26. The  $n$  curve is then used to

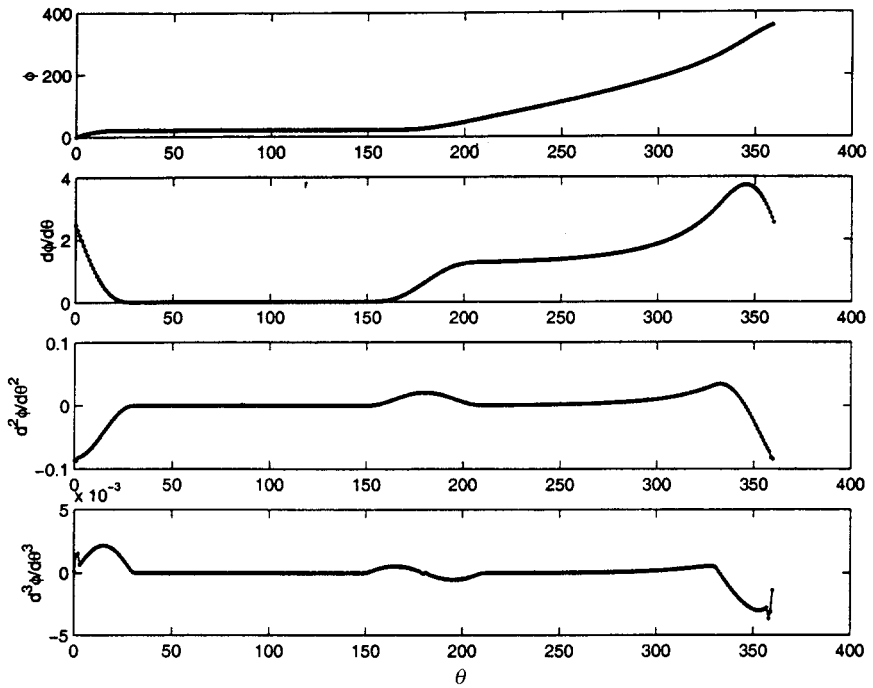


FIGURE 8.27. Single-dwell motion of the cam and its derivatives.

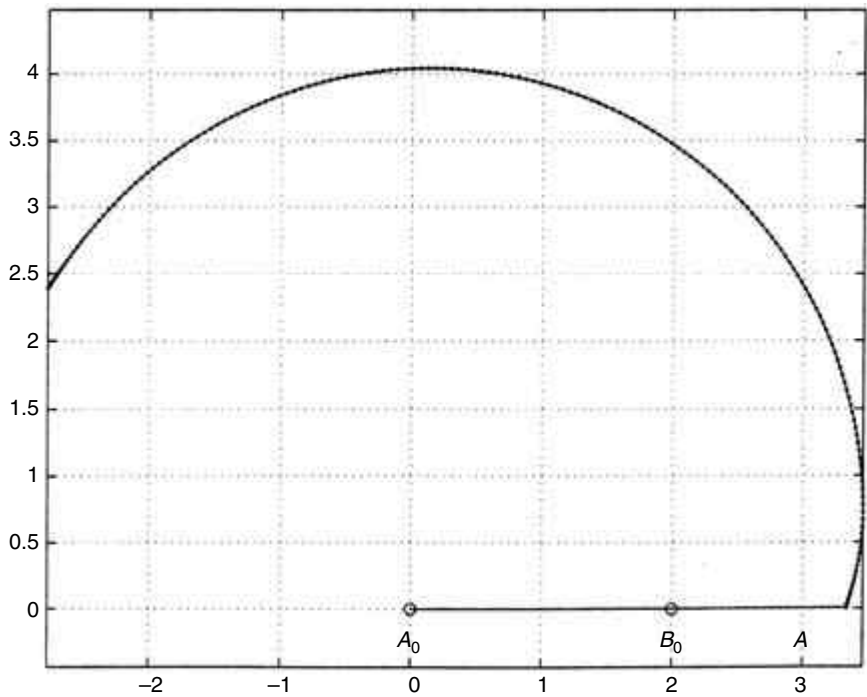


FIGURE 8.28. Cam profile obtained using the inversion technique for the single-dwell motion.

obtain the cam rotation,  $\phi$ . Figure 8.27 shows the resulting cam motion along with its three derivatives. By knowing the function  $\phi(\theta)$ , kinematic inversion is used to obtain the cam profile, which is shown in Fig. 8.28. A laboratory prototype confirmed the action.

## REFERENCES

---

- Ananthasuresh, G.K., "Design of Fully Rotatable, Roller-Crank-Driven Cam Mechanisms for Arbitrary Motion Specifications," *Mechanism and Machine Theory* (36): 445–67, Pergamon Press, N.Y., 2001.
- Barkan, P., *Impact Design in Mechanical Design Handbook*, H. Rothbart, Ed., McGraw-Hill, Chapter 31, New York, 1996.
- Chen, F.Y., *Mechanics and Design of Cam Mechanisms*, Pergamon Press, New York, 1982.
- Garrett, R.E., "Force Cams," *Machine Design*, pp 174–76, August 16, 1962.
- Jennings, J., "Calculating Springs for Cams," *Mach. London*. 57: 433. January 16, 1941.
- Paul, B., *Kinematics and Dynamics of Planar Machinery*, Prentice-Hall, Englewood Cliffs, N.J., 1979.
- Paul, B., *Machine Systems in Mechanical Design Handbook*, H. Rothbart, Ed., McGraw-Hill, Sec 6, New York, 1996.
- Sandor, G.N., and Erdman, A.G., *Advanced Mechanism Design, Analysis and Synthesis*, Vol. II, Prentice-Hall, Englewood Cliffs, N.J., 1984.
- Tidwell, P.H. et al., "Synthesis of Wrapping Cams," *Trans ASME, J. Mech. Des.* 116: 634–38, June 1994.
- Zuleas, J.A. et al., *Impact Dynamics*, John Wiley and Sons, New York, 1982.

---

# CHAPTER 9

---

# CAM MATERIALS AND LUBRICATION

---

Harold A Rothbart, D. Eng.

9.1 INTRODUCTION	252	9.4.5 Materials Selection	269
9.2 ELASTIC CONTACT THEORY	253	9.4.5.1 Plastics	270
9.3 CONTACT STRESSES	256	9.4.5.2 Bronze Alloys	270
9.4 WEAR	260	9.4.5.3 Cast Iron	271
9.4.1 Wear Phenomena	260	9.4.5.4 Hardened Steels	271
9.4.1.1 Surface Definition	260	9.5 LUBRICATION	273
9.4.2 Adhesive Wear	261	9.5.1 Introduction	273
9.4.3 Abrasive Wear and Corrosive Wear	263	9.5.2 Elastohydrodynamic Film	274
9.4.3.1 Corrosive Wear	263	9.5.3 Lubricant Selection	277
9.4.4 Surface Fatigue	263	9.5.3.1 Grease	277
9.4.4.1 Introduction	263	9.5.3.2 Extreme-Pressure Lubricants	278
9.4.4.2 Design	264	9.5.3.3 Contaminants	281
		9.6 SUMMARY	281

---

## SYMBOLS

---

$a$  = semiaxes of elliptical boundary  
 $b$  = semiaxes of elliptical boundary  
 $E'$  = effective Young's modulus, lb/in<sup>2</sup>  
 $E_1, E_2$  = elastic moduli of bodies 1 and 2, lb/in  
 $E_c, E_f$  = moduli of elasticity of cam and follower respectively, lb/in<sup>2</sup>  
 $G$  = materials parameter, dimensionless  
 $h$  = film thickness of the medium  
 $h_1, h_2$  = depressed depth of contact, in  
 $H$  = film thickness, dimensionless  
 $m$  = values in Table 9.1  
 $n$  = values in Table 9.1  
 $N$  = velocity of the medium  
 $p$  = intensity of pressure over surface of contact  
 $p_0$  = maximum pressure of contacting surfaces  
 $P$  = normal force of contacting bodies  
 $P'$  = normal force per unit cylinder length, in  
 $P'$  = normal force per cylinder length, lb/in  
 $R_x$  = equivalent radius in rolling direction, in  
 $R_{x1}, R_{x2}$  = radii of bodies 1 and 2 in rolling direction, in  
 $t_n$  = thickness of contacting cam and follower, in  
 $v$  = speed parameter, dimensionless  
 $\nu_1, \nu_2$  = Poisson's ratio of bodies 1 and 2  
 $W'$  = load parameter, dimensionless  
 $z$  = viscosity of the medium

$\alpha$  = pressure viscosity coefficient of fluid,  $\text{lb/in}^{-1}$   
 $\Delta$  = relationship between  $\mu_1$ ,  $\mu_2$ , and  $E_1$ ,  $E_2$  of materials  
 $\eta_0$  = lubricant absolute viscosity,  $\text{lbf-s/in}^2$   
 $\Lambda$  = film parameter  
 $\mu_1$ ,  $\mu_2$  = Poisson's ratio  
 $\mu_c$ ,  $\mu_f$  = Poisson's ratio for cam and follower, respectively, in  
 $\rho_c$ ,  $\rho_f$  = radii of curvature of cam and follower, respectively, in  
 $\sigma_{\max}$  = maximum compressive stress  $\text{lb/in}^2$   
 $\tau_1$ ,  $\tau_2$  = rms roughness of two surfaces in contact  
 $\omega$  = load per unit cylinder length,  $\text{lb/in}$

## 9.1 INTRODUCTION

---

This chapter considers the mating cam and follower surfaces to determine the optimum performance, wear, and life of these moving parts. Note that no general methodology is available for the design of the cam and follower surfaces even though they have been around for a long time. The lack of reliable design data is primarily due to the special complexity of cam-follower systems. In this chapter, selected methods and available data are presented that should be used with discretion.

Some of the factors involved in cam-follower surface contact are: (a) for the system: choice of mating materials, lubricant and additive used, contaminants in the lubricant, lubrication system chosen, fluctuating external load, and reversal of the inertia and torques (affecting the crossover shock in the backlash); (b) for the cam: materials selected, surface roughness, surface finish, surface hardness, changing radius of curvature, and the prior history of machining; and (c) for the follower: materials used, surface hardness and finish, and the roller diameter and inertia (affecting rolling and sliding due to the changing roller acceleration). Therefore, experience and performance in the laboratory or field is the critical need in all designs.

Despite the numerous variables listed, the design information in this chapter presents an acceptable approach to optimizing cam material life performance. It is suggested that selective periodic replacement of the follower roller be done in the field. Adding new rollers, rather than replacing the cam, is an easy and the least costly method of extending the life of the contacting cam and roller follower.

It should be stated that cams and the following are of the same basic mechanical family, the study of which is generically referred to as "contact mechanics":

- cams
- gearing
- rolling-element bearings
- traction friction drives
- intermittent motion mechanisms
- chains
- belts
- wire rope.

All the foregoing have in common rolling and/or sliding action coupled with reasonably high concentrated contact (hertz) stresses. In the field of contact mechanics the failure mechanism among these various machine elements is similar and is related to material

metallurgy and heat treatment, lubricant rheology and chemistry, surface topography and geometry, and applied contact load (stress). These machine components also have commonly related manufacturing requirements. Hence, they share similar manufacturing technology and engineering analysis.

Specifically much knowledge is now compiled to solve materials problems of rolling-element bearings and gearing, which is relevant to the needs of the cam-follower designer. This is because cams, rolling bearings, and gearing are similar in their performance applications. All three are heavily loaded, surface-contact moving machine elements supported by lubricated surfaces, and much of their action is primarily of a rolling nature. Studying the design analysis, data, and application of rolling-element bearings and gearing will be of distinct value in optimizing the materials and lubrication of cam-follower mechanisms.

To date, the ultimate material design data is: ball bearings have a finite fatigue life that is subject to wide fluctuations of life, while gears have a unified theory of surface life within a limited range of sizes. Zaretsky (1997) and Hamrock and Dawson (1981) are excellent sources of information for the tribology of gearing and bearings. Zaretsky is at the National Aeronautics and Space Agency (NASA) in Cleveland, Ohio where in the past 45 years engineers have contributed significantly to the reliability and life of bearings and gearing. This information is valuable to the study of cam-follower machinery. Therefore, this chapter contains the latest information on rolling element bearings and gearing, which could be applied at the designer's discretion to specific optimized cam-follower systems.

## 9.2 ELASTIC CONTACT THEORY

Hertz (1882, 1895) established the state of stress and strain between two contacting elastic bodies. In this section we present two cases: (a) two *crowned rollers* and (b) two *cylindrical rollers*.

Figure 9.1 shows two *crowned rollers* of different sizes in elastic contact. A plane tangent to each body at the touching point forms the tangent plane. If the bodies are now pressed together so that the collinear force is normal to the tangent plane, deformation takes place and a small contact area will replace the contact point  $O$  of the unloaded state. First, we will find the size and shape of this contact area and distribution of normal pressure. Then we can calculate the stresses and strains that the interfacial pressure induces in the contacting members.

Hertz assumed that (a) the two contacting bodies are isotropic and elastic in accordance with Hooke's law, (b) the contact area is quite small compared to the radii of curvature of the undeformed bodies, and (c) only normal pressures that exist during contact are prevalent. Displacements in the  $xy$  plane and shearing tractions are neglected.

In Fig. 9.1, the pressure distribution between the two contacting bodies form a semiellipsoid, and the surface of contact traced on the tangent plane will have an elliptical boundary. The intensity of pressure over the surface of contact is represented by the coordinates of the semiellipsoid

$$p = p_0 \left[ 1 - \frac{x^2}{a^2} - \frac{y^2}{b^2} \right]^{1/2} \quad (9.1)$$

where  $a$  and  $b$  denote the semiaxes of the elliptical boundary. The maximum pressure is situated at the center of the surface of contact above point  $O$

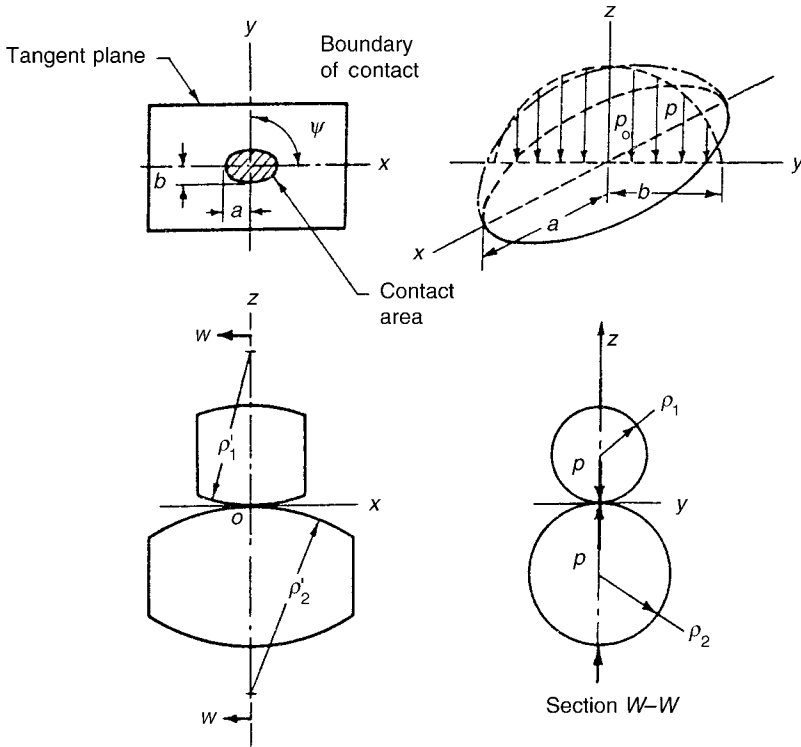


FIGURE 9.1. Crowned rollers in elastic contact.

$$p_0 = \frac{3p}{2\pi ab}. \tag{9.2}$$

The semiaxes  $a$  and  $b$  of the ellipse of contact are

$$a = m \left[ \frac{3}{4} \frac{P\Delta}{A+B} \right]^{1/3} \tag{9.3}$$

$$b = n \left[ \frac{3}{4} \frac{P\Delta}{A+B} \right]^{1/3} \tag{9.4}$$

where the values of  $m$  and  $n$  are given in Table 9.1.

In Eqs. (9.3) and (9.4),  $\Delta$  is a factor determined by the relationship between the materials where the subscripts 1 and 2 refer to the first and the second contacting bodies

$$\Delta = \frac{1-\mu_1^2}{E_1} + \frac{1-\mu_2^2}{E_2}. \tag{9.5}$$

$A$  and  $B$  are factors determined by various radii of curvature of the contacting bodies. If we designate  $\rho_1, \rho_2$  as the minimum radii of curvature,  $\rho'_1, \rho'_2$  as the maximum radii of

**TABLE 9.1** Constants for Contact Ellipse

$\theta$	$m$	$n$	$\theta$	$m$	$n$
35°	2.397	0.530	65°	1.378	0.759
40°	2.136	0.567	70°	1.284	0.802
45°	1.926	0.604	75°	1.202	0.846
50°	1.754	0.641	80°	1.128	0.893
55°	1.611	0.678	85°	1.061	0.944
60°	1.486	0.717	90°	1.000	1.000

$$\text{Note: } \cos \theta = \frac{B-A}{B+A}$$

curvature at the point of contact, and  $\psi$  as the angle between the planes containing the curvatures  $\frac{1}{\rho}$  and  $\frac{1}{\rho'}$ , then

$$A+B = \frac{1}{2} \left( \frac{1}{\rho_1} + \frac{1}{\rho'_1} + \frac{1}{\rho_2} + \frac{1}{\rho'_2} \right) \quad (9.6)$$

$$B-A = \frac{1}{2} \left[ \left( \frac{1}{\rho_1} - \frac{1}{\rho'_1} \right)^2 + \left( \frac{1}{\rho_2} - \frac{1}{\rho'_2} \right)^2 + 2 \left( \frac{1}{\rho_1} - \frac{1}{\rho'_1} \right) \left( \frac{1}{\rho_2} - \frac{1}{\rho'_2} \right) \cos 2\psi \right]^{1/2}. \quad (9.7)$$

Therefore, the dimensions  $a$  and  $b$  of the ellipse depend on the shape, applied force, and material properties of the two contacting bodies.

Next, let us consider *two cylinders* of infinite length in contact. For two long elastic cylinders having radii  $\rho_1$  and  $\rho_2$  aligned so that their axes are parallel (Fig. 9.2), the “elliptical boundary” of contact degenerates into parallel lines. The contact area thus becomes a “rectangle” of infinite length (in practice, the length of the cylinder) and of width  $2b$  given by

$$2b = \left( \frac{16P'\rho}{\pi E} \right)^{1/2} \quad (9.8)$$

where  $P'$  is the normal force per unit length of the cylinder  $\rho = \frac{\rho_1\rho_2}{(\rho_1 + \rho_2)}$ . Note that the contact zone’s dimension varies as the one-half power of the load, rather than the one-third power as in the previous case. The normal pressure distribution is given as

$$p = p_0 \left( 1 - \frac{y^2}{b^2} \right)^{1/2} \quad (9.9)$$

where  $p_0 = \frac{2P'}{\pi b}$ .

From the geometry of circles (see Fig. 9.2) the depressed depths of contact are

$$h_1 = \rho_1 - \sqrt{\rho_1^2 - b^2} \quad (9.10)$$

$$h_2 = \rho_2 - \sqrt{\rho_2^2 - b^2}.$$

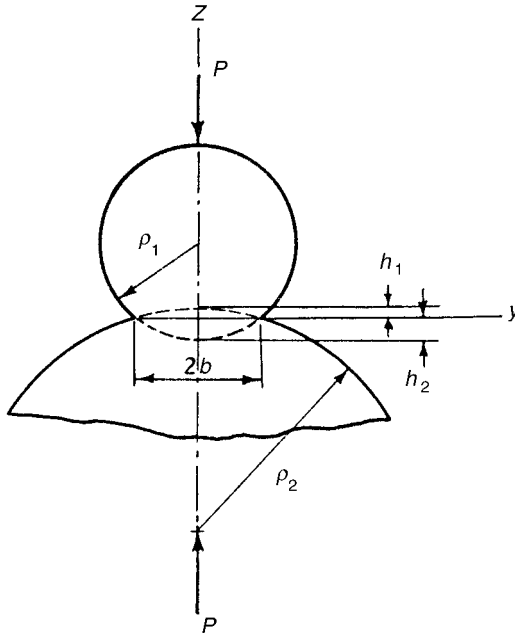


FIGURE 9.2. Cylinders in elastic contact.

### 9.3 CONTACT STRESSES

Using the newtonian potential function, the equations for the total stress field of two elastic bodies in contact can be established (Lundberg and Odquist [1932]).

The results of the stress distribution in the case of two cylinders, i.e., a disk cam with a roller follower, are plotted in Fig. 9.3. This is a plot of the three principal normal stresses ( $\sigma_x, \sigma_y, \sigma_z$ ) in the direction of the applied load and the corresponding three shear stresses. The highest shear stress is  $\tau_{yz}$  ( $45^\circ$ ), which has a maximum value of approximately  $0.3 \rho_0$  at a depth of  $0.786b$ . Note that the yielding of steel depends on shearing stress, and it is necessary to determine the point within the body at which the principal stresses combine to produce maximum shear. Thus, in the case of a disk cam with a roller follower made of steel, the maximum stress occurs below the cam surface. Failure results at the approximate depth of the point of a maximum shearing stress.

When sliding is present, a combined rolling and sliding action makes the problem more complicated.

Any *cam and roller follower* (two cylinders in contact and in alignment) produce a maximum compressive stress below the surface within the elastic limit

$$\sigma_{\max} = 0.564 \left[ \frac{P \left( \frac{1}{\rho_c} + \frac{1}{\rho_f} \right)}{t_h \left( \frac{1 - \mu_c^2}{E_c} + \frac{1 - \mu_f^2}{E_f} \right)} \right]^{1/2} \tag{9.11}$$

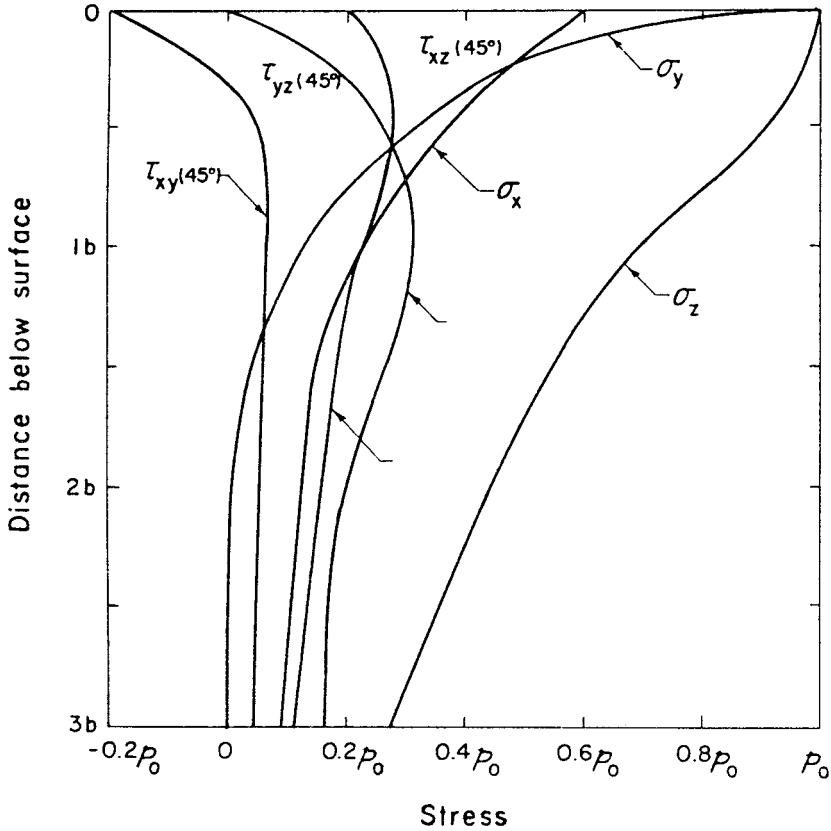


FIGURE 9.3. Hertzian stresses below surface for two cylinders.

where  $\sigma_{max}$  = maximum compressive stress at any point, lb/in<sup>2</sup>  
 $P$  = normal load on cam profile, lb  
 $\rho_c$  and  $\rho_f$  = radii of curvature of cam and follower, respectively, in  
 $t_n$  = thickness of contacting cam and follower, in  
 $\mu_c$  and  $\mu_f$  = Poisson's ratio for cam and follower, respectively, having average values: steel = 0.30; cast iron = 0.27; bronze = 0.34.  
 $E_c$  and  $E_f$  = modulus of elasticity of cam and follower, respectively, psi. Average values are: steel = 30,000,000; cast iron = 12,000,000 to 23,000,000, depending on class; brass or bronze = 15,000,000; nylon = 400,000.

Note that the radius of curvature of any point on the cam can be obtained from Chap. 6 and is positive when the profile is convex and negative when the profile is concave. Also, at any cam speed the load and cam radius of curvature and stress are different at every point along the profile. Usually, the nose of the cam with its small radius of curvature presents the largest compressive stress. Also, it was shown in Chap. 6 that the smallest cam radius of curvature can be increased by reducing the maximum negative acceleration. Thus, an asymmetrical cam acceleration curve having the positive accelera-

tion greater than the negative acceleration will reduce the nose stresses and the size of the compression spring needed.

Hertz indicated the stress distribution of two contacting cylinders; as shown in Fig. 9.4a with perfect alignment of the contacting bodies, we see that the surface compressive stress is a maximum at the center of the contact area and decreases to zero at the ends. The area of contact of the two cylinders is rectangular. However, the deflection and misalignment of the cam shaft will cause additional stresses. Fig. 9.4b shows this extreme stress condition. Some manufacturers alleviate this condition in roller followers by grinding a crown on the roller surface. The automobile cam has a taper ground on its surface of a few thousandths of an inch over the cam width to give a more uniform stress distribution to compensate for the camshaft deflection.

For the *flat-faced follower* the designer should substitute in Eq. (9.11) its radius of curvature  $\rho_f$  equal to infinity. Also, the value of the thickness  $t_h$  depends on the rigidity of the cam shaft and its misalignment. For automotive applications, the stress value of  $t_h$  no greater than  $1/2$  in is usually appropriate. For a similar relatively flexible cam shaft, the value of  $t_h \leq 1/2$  in should be applied to Eq. (9.11). The designer should decide the proper value according to the rigidity of his system.

The *disk cam* with *spherical* or *crown-face follower* of dissimilar metals has a maximum compressive stress (Thomas and Hoerch [1930] and Turkish [1946])

$$\sigma_{\max} = \frac{0.0469P^{1/3}}{\left(1 + \frac{\rho_f}{\rho_c}\right)^{0.237}} \left[ \frac{\frac{2}{\rho_f} + \frac{1}{\rho_c}}{\frac{1-\mu_c^2}{E_c} + \frac{1-\mu_f^2}{E_f}} \right]^{2/3} \quad (9.12)$$

In Fig. 9.5a, we see the ideal stress distribution in which the load or stress on the follower is symmetrical with the cam. The area of contact has an elliptical shape. Figure 9.5b shows the stress distribution of a cam with extreme misalignment and deflection. We see

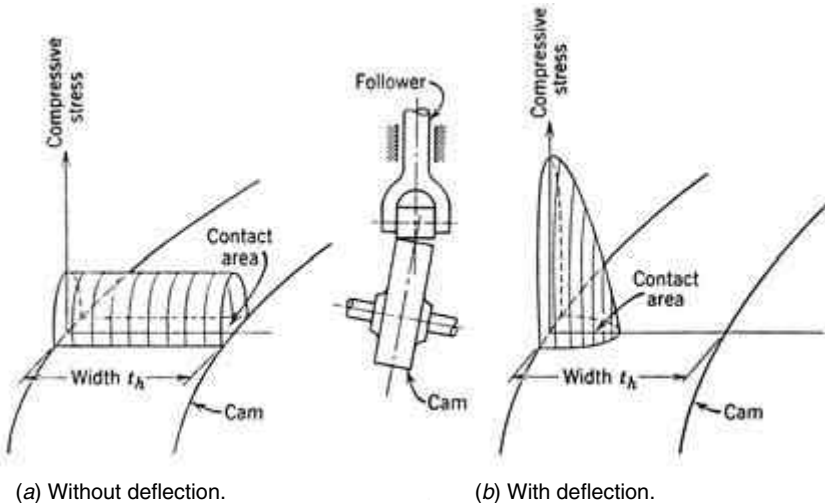


FIGURE 9.4. Stress distribution on cam—cylindrical roller and flat-faced followers.

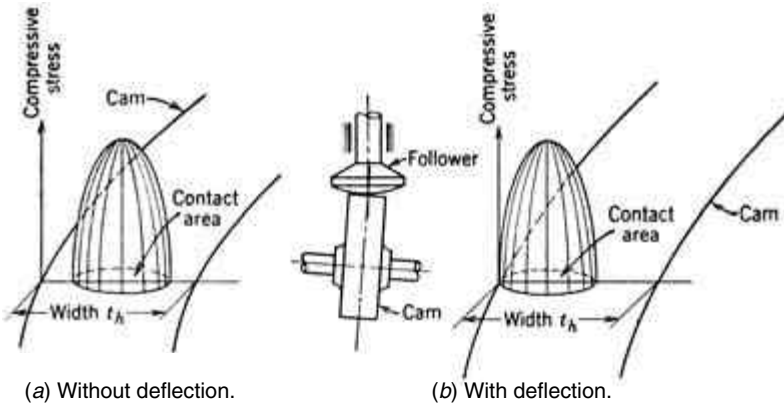


FIGURE 9.5. Stress distribution on cam—spherical-faced follower.

that the same stress values exist, which are shifted from the deflected side of the cam. This is the primary advantage of a spherical follower as compared to the serious stress increase exhibited with the cylindrical roller or flat-faced follower. The spherical radii used are from 10 in to 300 in.

**EXAMPLE** The nose of a cam has a radius of curvature of 1/4 in. At 1200 rpm, the translating roller-follower has an axial force at this point of 132 lb, with a pressure angle of  $20^\circ$  and a roller-follower diameter of 3/4 in. The cam thickness is 3/4 in. Both the cam and the follower are made of steel. The cam shaft and bearing supports are relatively rigid. Find the maximum compressive stress on the cam nose at this speed.

**Solution** The force distribution gives the normal force on the cam surface

$$P = \frac{132}{\cos 20} = 140 \text{ lb.}$$

From Eq. (9.11), the maximum compressive stress at this point

$$\sigma_{\max} = 0.564 \left[ \frac{P \left( \frac{1}{\rho_c} + \frac{1}{\rho_f} \right)}{t_h \left( \frac{1 - \mu_c^2}{E_c} + \frac{1 - \mu_f^2}{E_f} \right)} \right]^{1/2}$$

$$\sigma_{\max} = 0.564 \left[ \frac{140 \left( \frac{1}{\frac{3}{8}} + \frac{1}{\frac{1}{4}} \right)}{4 \left( \frac{1 - 0.3^2}{30 \times 10^6} + \frac{1 - 0.3^2}{30 \times 10^6} \right)} \right]^{1/2} = 801,800 \text{ lb/in}^2$$

Note that for a complete study, all points on the cam should be investigated to find the maximum stress on the cam. This stress should be below the elastic limit of the cam steel material with a proper factor of safety.

## 9.4 WEAR

---

### 9.4.1 Wear Phenomena

The action between two surfaces in contact is complicated, involving the statistical relationships between many variables. Among the parameters are the surface roughness, waviness, and stresses; prior history of machining; modules of elasticity; friction (rolling and sliding); materials; lubrication; corrosion; and loads. Wear, in a broad sense, is related to the friction between the two surfaces in contact.

Simply, wear may be considered the undesirable removal of solid material from rubbing surfaces. Basically, the four kinds of wear in cam-follower mechanisms are: adhesive wear, abrasive wear, corrosive wear, and surface fatigue wear. Each of these will be articulated in the following sections. Also, other, less significant types of surface failure do not fit into these four categories, such as erosive wear, cavitation wear, and fretting corrosion wear. In cam-follower material design, test data will be presented including different perspectives for design. Much of the material in the following sections must be utilized with discretion. Wear testing and experience of a particular design is critical to optimizing the performance of the mechanism.

For the engineer, the study of wear mechanisms on a specific machine may be possible by three methods: examination of wear debris, examination of worn surfaces, and metallographic examination of surface and subsurface structures.

In the examination of the wear debris, usually collected from the lubricating oil, large lumps imply adhesive wear; fine particles, oxidative wear; chiplike particles, abrasive wear; and flakelike particles, delamination wear.

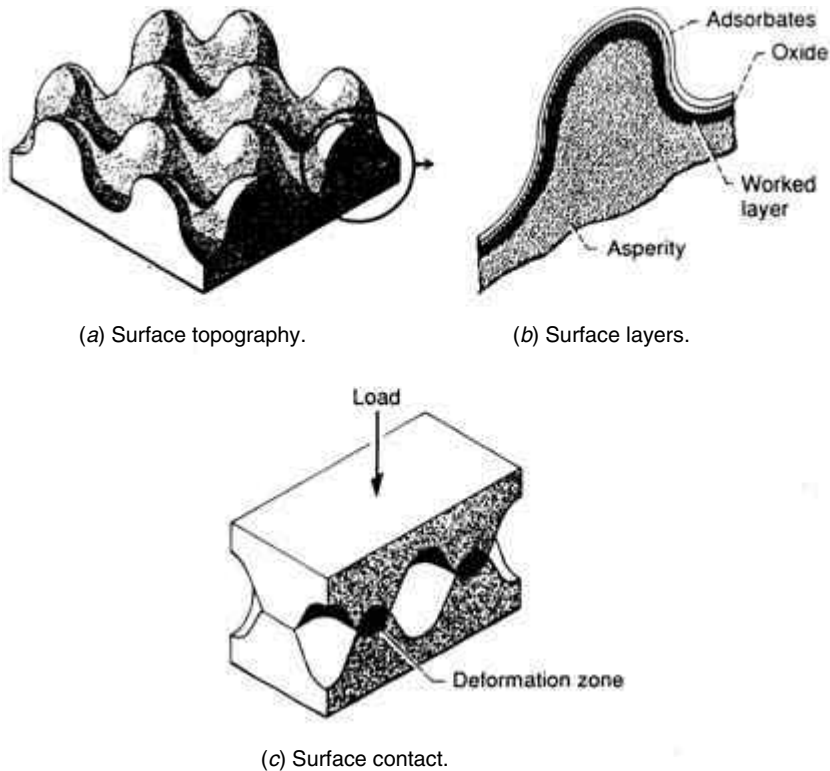
In the examination of the worn surface heavy tearing implies adhesive wear; scratches, abrasive wear; and burnishing, nonadhesive wear.

Metallographic examination of the surface structure may reveal the type of deformation to the sliding process, the generation of subsurface crack, incipient delamination, and other things.

**9.4.1.1 Surface Definition.** A fundamental understanding of the mechanisms interacting with the tribological surface is of utmost importance in lubrication. A solid surface is not a flat or smooth surface. When a surface is examined with an electron microscope or surface profilometer, it is found to contain irregularities called asperities; see Buckley (1997) and Fig. 9.6a.

The asperity surfaces contain surface films—they are not clean (Fig. 9.6b). For metals, these films consist of oxides and absorbed gases—usually water vapor, carbon monoxide, and carbon dioxide. Nonmetals may contain other adsorbates. All film materials strongly affect the mechanical and metallurgical behavior of contacting solids. Also, the near surface (surficial) layers of the solid itself may vary from the bulk of the solid. Crystalline solids may have recrystallized material and strain hardening. In metals, polishing or finishing the operation of a surface produces these surficial layers. These layers are generally rich in impurities.

When the two solids touch, the area of contact is at the points of the contacting asperities across the interface, Fig. 9.6c. Initial contact of the solids deforms the asperities elastically, later followed by plastic deformation when the load is increased. It is at



**FIGURE 9.6.** Surface topography and contact. (Adapted from Buckley, D.H., "Tribology Fundamentals," *Tribology for Aerospace Applications*, E.V. Zaretsky, Ed., copyrighted by the Soc. of Trib. and Lub. Eng., Park Ridge, Ill., with permission.)

the asperities that the adhesion between two solids occurs. Today, surface profiles can be established on an atomic level by use of a scanning electron tunneling microscope. In this way, a surface can be examined tribologically to study the structural, physical, and chemical change in the surface.

### 9.4.2 Adhesive Wear

*Adhesive wear*, often called *galling*, *scuffing*, or *scoring wear*, occurs between two sliding solid surfaces. It exists as an attraction between the surface atoms of contacting materials, leading to a transfer of material from one surface to the other and eventually to the formation of loose fragments.

Strong adhesive forces develop at the interface formed by the solids. The magnitude of the forces relates to the surface condition (cleanliness, etc.) and fundamental properties of the two solids. The surface contact is established in deep areas. High local pressure combined with the relative sliding motion along crystallographic planes causes roughening of the interface of contact. When a pair of firmly interlocked high spots is forced apart, breakage will occur where the section is weakest.

Most of the energy released during the process of breaking the high spots is transformed into heat, which causes a sudden temperature flash. When the heat of the temperature flash is conducted through the interface, momentary diffusion occurs rapidly. If the diffusion process is rapid enough to cause welding of the sheared-off peak to the opposite high spot, a piece of transferred metal is formed. If the conditions are such that no appreciable diffusion occurs, the adhesive force can still keep the metal particles on the opposite high spot. The small piece of metal sheared from the high spot will leave a "loose particle" when both diffusion and adhesion are weak. Also, the amount of adhesive transfer and wear can be profoundly affected by the surface friction and ambient conditions. Figure 9.7 shows adhesive wear on a shaft with an example of surface failure which is similar for cams and followers.

A significant factor affecting adhesion is the compatibility of the mating materials. Tests show that some combinations of metals are compatible for long wear life, whereas others are poor. Table 9.2 indicates some interesting metal combinations' wearing on unlubricated surfaces. Note that these material combinations relate to adhesive properties only.

Adhesive bonding can occur if the materials surfaces have contaminants. These contaminants could be forms of oxide, oils from human skin, moisture coatings, or lubricants. Obviously the lubricant is of positive value in isolating the two potentially adhesive bonding surfaces.

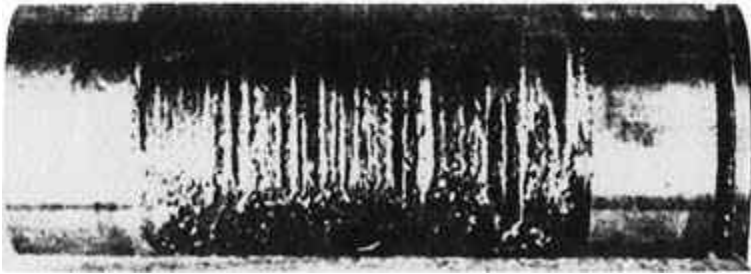


FIGURE 9.7. Example of adhesive wear (shaft).

TABLE 9.2 Metal Combinations

<i>Good</i>	<i>Poor</i>
Cast iron and phosphor bronze	Hardened steel and hardened bronze
Hardened steel and phosphor bronze	Hardened nickel steel and hardened nickel steel
Cast iron and soft steel	Soft steel and bronze
Babbitt and soft steel	Soft steel and soft steel
Soft brasses and soft steel	Soft steel and laminated thermoset resins
Hardened steel and soft bronze	Soft steel and nylon
Hardened steel and brass	
Hardened steel and cast iron	
Hardened steel and laminated thermoset resins	
Hardened steel and nylon	

### 9.4.3 Abrasive Wear and Corrosive Wear

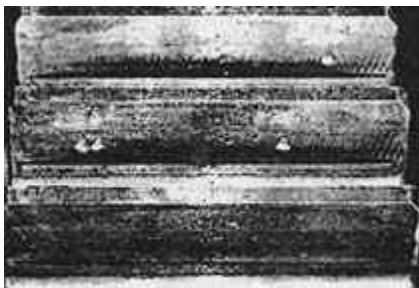
*Abrasive wear* occurs when two surfaces are in contact and one is considerably harder than the other. Free particles of the harder surface are produced that by interaction remove materials from the softer surfaces. This type of wear produces the removal of solid material by gouging by the much harder body. In general these harder particles are the result of the machinery action such as the cam and follower system. In addition, hard particles may be found outside the system, such as dust, grinding action, and special contaminants. One of the responsibilities of the lubrication system is the removal of these abrasive materials from the machine surfaces.

**9.4.3.1 Corrosive Wear.** *Corrosion* occurs in normal environments, and the most common form is oxidation. Most metals react with oxygen in the atmosphere of air and water and form oxides. In cam-follower surface action, the wear occurs due to the sliding or rolling contact of the two bodies. As these oxides are loosely attached to the metal surface, rubbing serves to remove them. These loose particles remove themselves and contribute to the abrasive wear action. Proper lubrication can be utilized to keep corrosive wear to a minimum. Adequate lubrication will protect the vulnerable surface from the corroding environment and also react favorably and chemically with the surface.

### 9.4.4 Surface Fatigue

**9.4.4.1 Introduction.** *Surface fatigue* is produced by rolling elements in repeated loaded contact. Fatigue is affected by many variables such as speed, load, material, temperature, geometry of surfaces, lubricant, and amount of sliding. Rolling-element fatigue can be of either surface or subsurface origin. General dislocation theory provides a tool for understanding the rolling-element fatigue process. During rolling action, the accumulation of dislocations will act as a stress raiser by concentrating the stress field in a small local contact area. The result is to initiate a crack (called *pitting*) which in time will produce a crack network and subsequently a spall. Figure 9.8a shows the phenomenon of fatigue, producing mild pitting.

*Spalling* is the loss of large pieces from the surface and occurs when the pits are joined and the metal surface is flaked. In other words, pitting produces spalling with the action occurring rather suddenly after many cycles of operation. Surface fatigue exists with rolling-element bearings, gearing, and cams. Figure 9.8b shows severe pitting and spalling.



(a) Mild pitting



(b) Severe pitting and spalling

**FIGURE 9.8.** Example of surface failure by pitting and spalling (gear teeth). (Source: Graham, J.D., "Pitting of Gear Teeth," *Handbook of Mechanical Wear*, C. Lipson, Ed., U. Mich. Press, pp. 138–43, 1961, with permission.)

Rolling-element fatigue can be initiated by hard inclusions in the material; corrosion; surface stress raisers such as dents, grinding imperfections, or geometric stress concentrations; microspalling; and surface interactions dependent on roughness and lubrication film thickness. Sometimes thin layers of case hardening, surface checks from heat treatment and high sliding velocities, excessive temperature, type of lubricant, or contamination can accelerate the action of fatigue.

If the surface is stressed in a corrosive environment, a phenomenon called *corrosion fatigue* or *stress corrosion* occurs. Corrosion on either the cam or roller follower will initially most frequently by surface fatigue. Corrosion on either the cam or roller follower will start due to the local stress concentration. The use of a lubricant has another function besides the reduction of friction of the surfaces, which is to prevent corrosion and ensure longer fatigue life.

**9.4.4.2 Surface Fatigue Design.** As mentioned previously cams, rolling-element bearings, and gearing are machine elements that are similar in their performance, and they fail most frequently by surface fatigue. Unfortunately statistical wear data have been developed for rolling-element bearings and gearing but not for cam-follower systems. The diversity and complexity of cam-follower systems has prevented a complete wear design methodology to evolve.

Nevertheless, this section presents a simplified design procedure for the cam engineer. The data presented will be of initial value as a guide in selecting compatible material combinations for the cam and follower. Ultimately, the proper materials, wear performance, and lubricant must be confirmed in the field under actual operating conditions.

Test data are presented for the comparison of cam and follower fatigue under pure rolling and rolling with some sliding conditions. Experience has shown that some sliding may occur, even at low speeds, affecting the wear life of the contacting surfaces.

Life surface fatigue tests were conducted by Talbourdet (1950), Morrison (1968), and Cram (1956) utilizing radially loaded contacting cylinders with (a) pure rolling and (b) rolling with 9 percent sliding. Three-inch diameter mating rollers were used; one roller had a hardened steel surface (60-62 RC) and the other, softer roller was cast iron, steel (of different hardnesses), bronze, and nonmetallic materials. The weaker roller material wore out under the cyclical loading which established the life of the materials in combination.

The stress test data algorithm relates  $\sigma_{\max}$  to the hertzian compressive stress Eq. (9.11) for dissimilar metals in surface contact.

For a Poisson's ratio  $\mu = 0.3$  and the normal force per cylinder length

$$P' = \frac{K}{\left(\frac{1}{\rho_1} + \frac{1}{\rho_2}\right)} \text{ lb/in} \quad (9.13)$$

where

$$K = \frac{\sigma_{\max}^2}{0.35} \left(\frac{1}{E_1} + \frac{1}{E_2}\right) \quad (9.14)$$

which is called the load-stress factor for cylinders in contact. Table 9.3 lists values of  $K$  for 100 million stress repetitions for pure rolling and rolling plus 9 percent sliding action. One roll is of hardened steel 60-62RC while the other is of various selected materials. Values of  $K$  have been determined as a function of the number of stress cycles necessary for surface failure. The test lubricant was mineral oil 280-320 SSU and 100°F at a surface

**TABLE 9.3** Surface Fatigue Strength for Various Materials (Run against Tool Steel Roller 60–62 Rc)

Material	Pure Rolling						Rolling & 9% sliding					
	$K_1$	$\sigma$ max*	A	B	$K_1$	B	$K_1$	$\sigma$ max*	A	B		
1020 steel, carburized, 0.045 in min. depth, 50–60 Rc	12,700	256,000	7.39	38.33	10,400	99,000	13.20	61.06				
1020 steel, 130–150 BHN	—	—	—	—	1,720	94,000	4.78	23.45				
1117 steel, 130–150 BHN	1,500	89,000	4.21	21.41	1,150	77,000	3.63	19.12				
X1340 steel, induction-hardened, 0.045 in min. depth, 45–58 Rc	10,000	227,000	6.56	34.24	8,200	206,000	8.51	41.31				
Blue tempered spring-steel stampings, 40–50 Rc	2,470	113,000	4.00	21.57	—	—	—	—				
4140/4150 steel, 350–370 BHN (etd 180)	—	—	—	—	11,300	242,000	17.76	80.00				
4150 steel, heat-treated, 270–300 BHN, phosphate-coated	12,000	249,000	11.40	54.52	8,660	211,000	15.47	68.92				
4150 steel, heat-treated, 270–300 BHN, flash chromium-plated	6,060	177,000	11.18	50.29	—	—	—	—				
4150 steel, heat-treated, 270–300 BHN, phosphate-coated	9,000	216,000	8.80	42.81	6,260	180,000	11.56	51.92				
4150 ceramic cast steel, heat-treated, 270–300 BHN	—	—	—	—	2,850	121,000	17.86	69.72				
4340 steel, induction-hardened	—	—	—	—	—	—	—	—				
0.045 in. min. depth, 50–58 Rc	13,000	259,000	14.15	66.22	9,000	216,000	14.02	63.44				
4340 steel, heat-treated, 270–300 BHN	—	—	—	—	5,500	169,000	18.05	75.55				
6150 steel, 300–320 BHN	1,170	78,000	3.10	17.51	—	—	—	—				
6150 steel, 270–300 BHN	—	—	—	—	1,820	97,000	8.30	35.06				
18% Ni maraging tool, air-hardened, 48–50 Rc	—	—	—	—	4,300	146,000	3.90	22.18				
Gray-iron, class 20,	—	—	—	—	—	—	—	—				
160–190 BHN, phosphate-coated	940	53,000	3.90	19.60	—	—	—	—				
Gray-iron, class 20, 140–160 BHN	790	49,000	3.83	19.09	740	47,000	4.09	19.72				
Gray-iron, class 30, 200–220 BHN	1,120	63,000	4.24	20.92	—	—	—	—				
Gray-iron, class 30,	—	—	—	—	—	—	—	—				

**TABLE 9.3** *Continued*

Material	Pure Rolling				Rolling & 9% sliding			
	$K_1$	$\sigma$ max*	A	B	$K_1$	$\sigma$ max*	A	B
heat-treated (austempered), 255–300 BHN, phosphate-coated Gray-iron, class 30,	2,920	102,000	5.52	27.11	2,510	94,000	6.01	28.44
oil-quenched, 270–415 BHN	1,850	81,000	5.45	25.79	—	—	—	—
Gray-iron, class 35, 225–255 BHN	2,000	86,000	11.62	46.35	1,900	84,000	8.39	35.51
Gray-iron, class 45, 220–240 BHN	—	—	—	—	1,070	65,000	3.77	19.41
Nodular-iron, Grade 80-60-03, 270–241 BHN	2,100	96,000	10.09	41.53	1,960	93,000	5.56	26.31
Nodular-iron, Grade 100-70-03, heat-treated, 240–260 BHN	—	—	—	—	3,570	122,000	13.04	54.33
High-strength yellow brass, drawn, 157–162 BHN	1,280	67,000	3.69	19.45	—	—	—	—
Nickel bronze, 80–90 BHN	1,390	73,000	6.01	26.89	—	—	—	—
SAE 65 phosphor-bronze sand casting, 65–75 BHN	730	52,000	2.84	16.13	350	36,000	2.39	14.08
SAE 660 continuous-cast bronze, 75–80 BHN	—	—	—	—	320	33,000	1.94	12.87
Aluminum bronze	2,500	98,000	5.87	27.97	—	—	—	—
Zinc die casting, 70 BHN	250	28,000	3.07	15.35	220	26,000	3.11	15.29
Random-fiber cotton-base phenolic	1,000	—	6.03	26.11	900	—	5.95	25.60
Graphitized laminated phenolic	900	—	6.58	27.43	—	—	—	—
Nema Grade L laminated phenolic	880	—	9.39	35.64	830	—	5.53	24.13
Linen-base laminated phenolic	830	—	8.54	32.90	670	—	6.46	26.25
Acetal resin	620	—	—	—	580	—	—	—
Polyurethane rubber	240	—	—	—	—	—	—	—
Polycarbonate resin	60	—	—	—	—	—	—	—
High-molecular-weight polyethylene	—	—	—	—	370	—	8.03	28.61

BHN—Brinell hardness number.

Re—Rockwell hardness number.

\* for 100,000,000 cycles.

velocity of 600 ft/min. Table 9.3 also includes static hertzian stress values, which are presented for information and comparison only and do not relate to the fatigue tests.

In plotting  $K$  versus life, a least-square curve fitting line is drawn through the normal scatter of significant points obtained from tests. The equation for the  $K$  factor as a function of life is derived from the slope of these fitting lines

$$\log_{10} K = \frac{B - \log_{10} N}{A} \quad (9.15)$$

where constants  $A$  and  $B$  are given in Table 9.3 and  $N$  is the number of stress cycles for which a  $K$  value is required. For numbers other than 100 million cycles the load stress factors can be interpreted from the load-life curves similar to Fig. 9.9. Figure 9.9 presents typical load-life test data obtained from the roll test machine. Comparisons are given for pure rolling and up to 300 percent sliding to indicate trends and slope comparison of the materials. Figure 9.9a shows nodular iron and class 45 cast iron and Fig. 9.9b shows cast bronze.

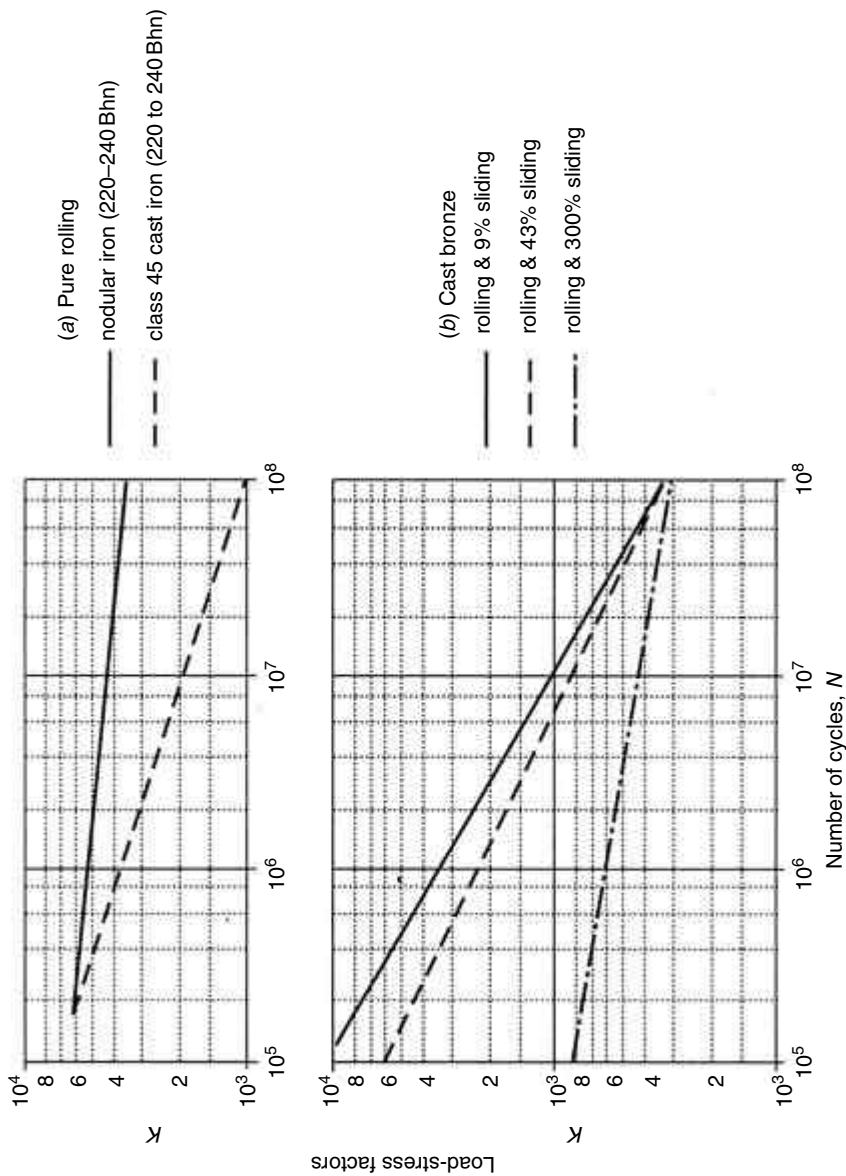
Let us consider the design approach for choosing the optimum combination of materials. In fatigue design criteria, this choice is a modification of *Fail-Safe Design* by Fuchs and Stephens (1980).

Fail-safe design recognizes that fatigue cracks may occur and arranges the structure so that cracks will not lead to a failure before they are detected. In cam-follower system design we design and operate the machine so that the roller follower will wear out before the cam is ever affected. In this manner the rollers will be periodically replaced. This is the easiest and least expensive solution to the fatigue problem. Therefore the roller diameter should be *measured periodically* and replaced when it has shown a reduction in size but before destructive wear of either the roller or cam occurs. Experience over time will be necessary to succeed with this approach *to discover compatible materials for each particular machine*. It is suggested that dependent on the size and reliability of the system a reduction of the roller diameter from  $-0.0004$  to  $-0.002$  in requires a replacement. For example, the author designed a newspaper folding mechanism run at 70,000 papers per hour with commercial ball-bearing rollers SAE 52100 hardened RC60-62. They were measured every six months and if the diameters were reduced by  $-0.001$  in they were replaced. The cam material is SAE 8620 air-hardened die steel RC 58-60 and still running with accuracy and some surface polish over 35 years as well as operating properly and at a minimum cost.

Next, let us discuss some of the test data in Table 9.3 in which it was stated that the rollers were of equal size and the softer material of the combination failed first. However, this is not the case with cam-follower machines which use a roller smaller than the cam by a ratio of between 1 and 6 or 1 and 10 depending on the design. Accordingly the follower roller surface has more fatigue stress cycles than the cam surface and will tend to fail first. This fact slants the test data of Table 9.3 positively to the periodic replacement of the roller follower. Also, it may be noted that the roller will wear out first even though it is a harder and more expensive surface material than that of the cam.

Occasionally, a soft metal ring may be added to the commercial roller follower as a choice over the manufactured bearing surface. A shortcoming is the larger rotational moment of inertia of the roller and more skidding produced in contact with the cam.

**EXAMPLE** *A cam is loaded by a roller follower with about 9 percent sliding. The cam is 4340 steel and 280 BHN hardness. The roller follower (tool steel 60-62 RC) is 1-in diameter and has a width of 3/4 in. At a point on the cam which has a radius of curvature of 2 in find the allowable contact forces to prevent significant wear before 100 million cycles.*



**FIGURE 9.9.** Typical curves of load-life relationships for cam materials run on tool steel rollers, Rc 60-62 (Rabinowicz, 1965).

**Solution** Equation 9.13

$$P' = \frac{k}{\frac{1}{\rho_1} + \frac{1}{\rho_2}}$$

From Table 9.3  $K = 5500$ ,  $\rho_1 = 0.5$  in,  $\rho_2 = 2.0$  in  
Therefore

$$P'_2 = \frac{5500}{\frac{1}{0.5} + \frac{1}{2}} = 2200 \text{ lb/in}$$

which gives an allowable load

$$P' = 2200 \times 3/4 = 1650 \text{ lb.}$$

Note that after 100 million cam cycles the roller will wear out first since it has more cycles than the cam.

#### 9.4.5 Materials Selection

A wide variety of materials are available for the cam designer; see Table 9.3. Depending on the application, the designer may choose from materials such as plastics; bronze; gray cast iron; nodular and malleable iron; Meehanite iron; a range of low-, medium-, and high-alloy steels; and stainless steels. In addition, there are different ways of modifying or processing the materials to improve their properties or to reduce the cost of manufacture (Zaretsky, 1997). These include reinforcements for plastics, processing for titanium, and hardening for many of the iron-based materials.

When selecting a material for an application, the cam designer will first determine the requirements for the cams being considered. The design requirements for a cam in a given application will depend on such things as accuracy, load, speed, material, and noise limitations. The more stringent these requirements are, the more costly the cam will become.

Some of the considerations in the choice of a material include allowable hertzian stress, wear resistance, impact strength, water and corrosion resistance, manufacturing cost, size, weight, reliability, and lubrication requirements. Steel, under proper heat treatment, meets most of these qualifications for roller followers, while cast iron is excellent for sliding followers.

Furthermore, these tests reveal that the *rate of stress cycling* has no significant effect on the surface wear of metals. This is not the case for nonmetallic materials with low heat conduction properties. Under these conditions, high speed was found to cause blistering or excessive material in test specimens.

Also, although surface endurance usually increases with hardness in a given material, hardness alone is a dangerous criterion for comparing different materials. For example, SAE 6150 steel at 300 BHN shows a surface endurance strength only slightly greater than the much less expensive and easier to machine SAE 1020 at 130 BHN.

Nevertheless, it is generally an established practice to harden materials to resist wear. Although the surface hardness of a material is not always the sole criterion for wear resistance, it is not possible to abandon hardness as an important factor. We shall outline in the following subsections the commonly used cam materials and their surface treatments, starting with those materials with the least hardness.

*Soft metals* are bronze, cast iron, and cold-rolled steel. Soft cams require the same degree of manufactured tolerance and accuracy as hardened cams. Profiles are milled and good surface finish is required.

The most widely acceptable metal characteristic reducing the tendency to gall is *self-lubrication*. Self-lubrication is exemplified by porous powder metals (oil-impregnated), gray cast iron, Meehanite, ductile cast iron, graphitic steels (graphite-lubricated), and leaded bronze (lead-lubricated). These materials suffer less damage when galling takes place. Other materials with much sliding and high loads may have their wear life increased by the frequent addition of various coatings and electrographite especially during run-in periods.

**9.4.5.1 Plastics.** There has always been a need for lightweight, low-cost cam material for light-duty applications. In the past, cams were made from phenolic-resin-impregnated cloth. However, in recent years, with the development of new polymers, many cams are made of various plastic materials. Table 9.4 lists plastic materials used for molded cams. The most common molded plastic cams are made of acetate and nylon resins. These materials are limited in strength, temperature resistance, and accuracy. The nylon and acetate resins have a room-temperature yield strength of approximately 10,000 lb/in<sup>2</sup>. This is reduced to approximately 4000 lb/in<sup>2</sup> at their upper temperature limit of 250°F. Nylon resin is subject to considerable moisture absorption, which reduces its strength and causes considerable expansion. Plastic cams can operate for long periods in adverse environments, such as dirt, water, and corrosive fluids, where other materials would tend to wear excessively. They can also operate without lubrication or can be lubricated by the processed material as in the food industry. Plastic cams are run in combination with a steel roller follower to give dimensional control and quiet operation.

Polyimide is a more expensive plastic material than nylon or acetate resin, but it has an operating temperature limit of approximately 600°F. This makes polyimides suitable for many adverse applications that might otherwise require metal cams. Polyimides can be used very effectively in combination with a metal follower without lubrication because of polyimide's good sliding properties.

**9.4.5.2 Bronze Alloys.** Several bronze alloys are used for cams. Most of the bronze alloys contain varying amounts of tin, zinc, manganese, aluminum, phosphorus, silicon, lead, nickel, and iron. The bronze alloys are most often used in combination with a steel

**TABLE 9.4** Properties of Plastic Cam Materials

Property	ASTM	Acetate	Nylon	Polyimide
Yield strength, lb/in <sup>2</sup>	D 638	10,000	11,800	10,500
Shear strength, lb/in <sup>2</sup>	D 732	9,510	9,600	11,900
Impact strength (Izod)	D 256	1.4	0.9	0.9
Elongation at yield, percent	D 638	15	5	6.5
Modulus of elasticity, lb/in <sup>2</sup>	D 790	410,000	410,000	460,000
Coefficient of linear thermal expansion, in/in·°F	D 696	$4.5 \times 10^{-5}$	$4.5 \times 10^{-5}$	$2.8 \times 10^{-5}$
Water absorption (24 h), percent	D 570	0.25	1.5	0.32
Specific gravity	D 792	1.425	1.14	1.43
Temperature limit, °F	—	250	250	600

**TABLE 9.5** Properties of Bronze Alloy Cam Materials

Material	Modulus of elasticity, 10 <sup>6</sup> lb/in <sup>2</sup>	Yield strength, lb/in <sup>2</sup>	Ultimate strength, lb/in <sup>2</sup>
Phosphor bronze	15	40,000	75,000
Aluminum bronze	19	50,000	100,000
Manganese bronze	16	45,000	80,000
Silicon bronze	15	30,000	60,000
Nickel-tin bronze	15	25,000	50,000
Leaded bronze	—	—	—

roller follower to give good wear and load capacity, especially where there is a high sliding component.

Bronze cams are also used where corrosion and water are a problem. The bronze alloys listed in Table 9.5 are aluminum bronze, manganese bronze, silicon bronze, leaded bronze, or phosphorous bronze. These bronze alloys have yield strengths ranging from 20,000 to 60,000 lb/in<sup>2</sup> and all have good machinability. Bronze cams are excellent for shock, noise reduction, inaccuracies in the fabricated contour, excessive inertia and wear due to frequent start and stop actions, and special contaminants in the lubricated operating system.

**9.4.5.3 Cast Iron.** Cast iron is used for cams because of its low cost, good machinability, and moderate mechanical properties. Many cam applications use cast iron because of its good sliding and wear properties, which are in part a result of the free graphite and porosity. The three basic cast irons are distinguished by the structure of graphite in the matrix of ferrite: (1) gray cast iron, where the graphite is in flake form; (2) malleable cast iron, where the graphite consists of uniformly dispersed, fine, free-carbon particles or nodules; and (3) ductile iron, where the graphite is in the form of tiny balls or spherules. The malleable iron and ductile iron have more shock and impact resistance. The cast irons can be heat treated to give improved mechanical properties. The bending strength of cast iron ranges from 5000 to 25,000 lb/in<sup>2</sup> and the surface fatigue strength ranges from 50,000 to 115,000 lb/in<sup>2</sup>. Nodular iron, chilled cast iron (heat treatable) and Meehanite are materials in the categories indicated. Both chilled cast iron and Meehanite have good shock resistance and good vibratory damping; both are attributes that help reduce noise. In many drives, a cast iron cam can be used to replace a bronze cam at a lower cost because of the better sliding properties of the cast iron.

Although the class 20 gray irons have a low endurance limit, classes 30, 45, and others have shown considerable advantages over free-machining steel. Austempering of Meehanite or class 30 iron approximately doubles surface endurance strength over untreated iron of similar hardness and thus is well suited for cams, probably because of the fine grain structure, excellent dispersion of graphite, and conversion of retained austenite.

The cam is supported by bearings on a frame generally of steel or cast iron. A frame of cast iron is usually a first choice because it provides greater rigidity and vibratory damping in the performance of the moving parts. The frame should be as heavy and rigid as possible.

**9.4.5.4 Hardened Steels.** A large variety of iron or steel alloys are used for cams. When operating conditions are moderate, such as medium loads and ambient temperatures, a

low-alloy steel can be used without the added cost of heat treatment and additional processing. The low-alloy material in the non-heat-treated condition can be used for bending stresses in the 20,000 lb/in<sup>2</sup> range and surface durability hertzian stresses of approximately 85,000 lb/in<sup>2</sup>. As the operating conditions become more severe, it becomes necessary to harden the cam for improved strength and to case harden the cam surface by case carburizing or case nitriding for longer pitting fatigue life, better scoring resistance, and better wear resistance. Several medium-alloy steels can be hardened to give good load-carrying capacity with bending stresses of 50,000 to 60,000 lb/in<sup>2</sup> and contact stresses of 160,000 to 180,000 lb/in<sup>2</sup>.

The higher alloy steels are much stronger and must be used in heavy-duty applications. AISI 9310, AISI 8620, and Nitralloy N are good materials for these applications and can operate with bending stresses of 70,000 lb/in<sup>2</sup> and maximum contact (hertzian) stresses of 200,000 lb/in<sup>2</sup>. These high-alloy steels should be case carburized (AISI 8620 and 9310) or case nitrided (Nitralloy) for a very hard, wear-resistant surface. Cams that are case carburized will usually require grinding after the hardening operation because of distortion during the heat-treating process. The nitrided materials offer the advantage of much less distortion during nitriding and therefore can be used in the as-nitrided condition without additional finishing. This is very helpful for large cams with small cross sections where distortion can be a problem. Since case depth for nitriding is limited to approximately 0.020 in, case crushing can occur if the load is too high. Selection of the nitriding process requires careful consideration of cost because of the long time involved in the case formation. A very hard case having a hardness about Rockwell C 70 ensures excellent wear resistance. Nitrided parts have good corrosion resistance and improved fatigue properties. Nitriding follows the finish-machining and grinding operations, and many parts can be nitrided without distortion. AISI 8620 steel (die steel) is an excellent choice for an accurate cam under heavy loads and endurance at a reasonable cost. With 8620 steel, an inherent core hardness of approximately 36 Rockwell C and a surface hardness of 60-62 Rockwell C or higher is achieved. It is an oil-quench material that has less heat-treating distortion than a water quench and less danger of cracking. It is sometimes carburized. In general, the case depth of case-hardened materials varies between 0.030 in and 0.060 in to be slightly below the point of maximum shear stress.

AISI 4140, 4150, 4320 (usually carburized), 4340, and 4615 steels have been chosen as cam materials. AISI 4140 is particularly selected as it can be (a) flame hardened, (b) through hardened Rockwell C 52-54, or (c) nitrided. The nitriding process produces a thin, very hard surface Rockwell C 70 about a few ten thousandths of an inch thick. This very hard thin case ensures excellent wear resistance. Below that surface is a case depth 0.020 to 0.035 in with a hardness Rockwell C 52 to 54. AISI 4140 is plate or bar stock and provides for good machinability and hardening properties.

The low- and medium-alloy steels have a limited operating temperature above which they begin to lose their hardness and strength, usually around 300°F. Above this temperature, the material is tempered and surface pitting failures or scoring will occur. The generally accepted minimum hardness required at higher operating temperature is Rockwell C 58.

In rare cases, Tungsten Carbide Stellite and AISI 52100 have been chosen as the cam material or as an insert to the cam at high points of undesirable wear. Also, although hardened tool steel is a satisfactory choice as a cam material, here the selection is either an oil-quench steel or air-hardened tool steel. The air-hardened steel is best, giving less distortion under heat treatment.

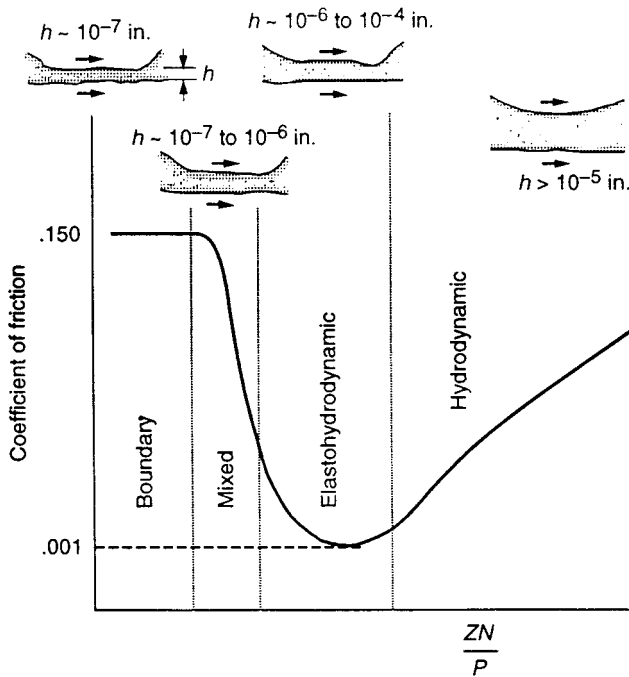
Stainless steel 360 and 440 C have been utilized for medical purposes. Nitriding of stainless steels is sometimes employed.

## 9.5 LUBRICATION

### 9.5.1 Introduction (Buckley, 1997)

The purpose of lubrication is to separate surfaces in relative motion, by a material that has a low shear resistance to friction and wear and also to minimize damage or prevent major damage of the surfaces. The material can be of any variety, such as adsorbed gases, chemical reaction products, films, liquids, or solid lubricants. The lubricating film (Stribeck, 1902) is classified first by the well-known Stribeck-Hersey curve (1902) in which the coefficient of friction is plotted as a function of the  $ZN/P$  parameter where  $Z$  is the viscosity of the medium,  $N$  is the velocity,  $P$  is the load, and  $h$  is the film thickness (Fig. 9.10).

The fluid film regimes are: hydrodynamic, elastohydrodynamic, and mixed-lubrication regimes as well as boundary lubrication. *Hydrodynamic lubrication* or fluid-film lubrication occurs at high speeds and low loads or high viscosities in which the surfaces are completely separated by a thick film  $h > 10^{-5}$  in. This rheology of the lubricant determines the friction in this hydrodynamic regime. *Elastohydrodynamic lubrication* (EHD) implies a fluid-film regime where the loads of the surfaces and the pressure-viscosity of the lubricant occur at  $h \sim 10^{-6}$  to  $10^{-4}$  in. In *mixed-lubrication regime*, which is thinner, surface asperity interactions occur with increased friction and fluid film effects, with  $h \sim 10^{-7}$  to  $10^{-6}$  in. Last, with low values of the  $ZN/P$  parameter  $h \sim 10^{-7}$  in is the realm of *boundary lubrication*. The most important aspect of the boundary lubrication regime is the forma-



**FIGURE 9.10.** Coefficient of friction as a function of viscosity-velocity-load parameter (Stribeck-Hersey curve). From Stribeck (1902).

tion of protective surface films to reduce wear and surface damage. The effectiveness of the films is established by their physical properties, which include shear strength, thickness, surface adhesion, film cohesion, melting point, and solubility. Operating variables that affect the lubricant include load, speed, temperature, and environmental atmosphere. Additions in the lubricant include antiwear and antifoam agents, antioxidants, and viscosity improvers.

### 9.5.2 Elastohydrodynamic Film (EHD)

This section applies to roller followers only. Sliding followers are assumed to function in the boundary and mixed lubrication regimes. The elastohydrodynamic film is experienced by cast iron (with its free graphite and porosity) which operates with limited lubrication and gives good sliding and wear properties. Also, this section is written based on theories and tests from both rolling-element bearings and gearing (Zaretsky, 1997). Specific design data is not available for cam-follower elements. However, the information contained here is of a fundamental nature (rolling fatigue) so it can be applied to cams and followers since all these systems show similar surface fatigue wear. In application, some modifications and refinements may be necessary to account for the skidding action of the follower roller at high speeds and for larger cams. The information is presented as a potential design basis for the cam designer in selecting the best material and lubricant available and to optimize the performance of the machine. *The important point is that the film that separates rolling-contact surfaces is elastohydrodynamic (EHD) film.*

Grubin (1949) solved the EHD problem by assuming that the elastic displacements of contacting lubricating surfaces, heavily loaded, would be similar to the dry hertzian contact, Fig. 9.11.

The dimensionless minimum film thickness is written as a function of the other three parameters

$$H = f(U, W', G)$$

which develops to

$$H = \frac{h}{R_x} = 1.95G^{0.73}(W')^{-0.091} \quad (9.16)$$

in which  $G$  is the material parameter,  $U$  is speed parameter, and  $W'$  is the load parameter. The variables are related in Eq. (9.16) by four dimensionless groupings.

$$\text{Film thickness } H = \frac{h}{R_x}, \text{ dimensionless}$$

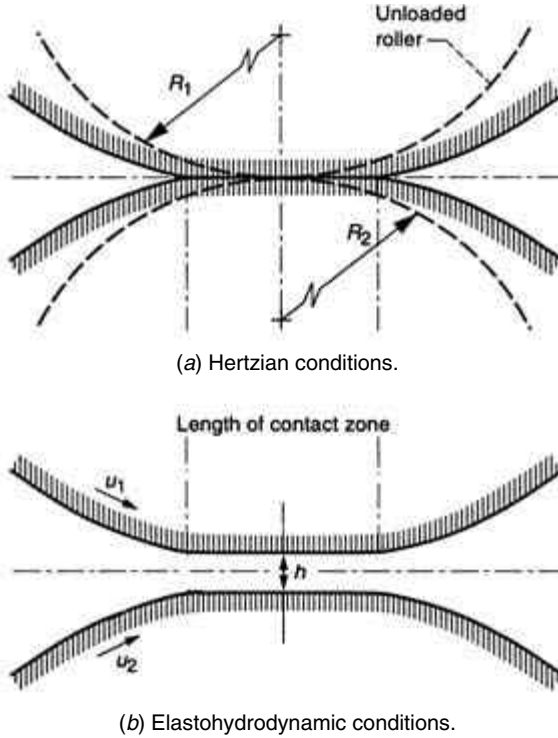
$$\text{Load parameter } W' = \frac{w}{E'R_x}, \text{ dimensionless}$$

$$\text{Speed parameter } U = u_{\eta_0}/E'R_x, \text{ dimensionless}$$

$$\text{Materials parameter } G = \alpha'E', \text{ dimensionless}$$

where

- $h$  = EHD film thickness, in
- $R_x$  = equivalent radius in the rolling direction, in
- $W'$  = EHD load parameter,  $w/E'R_x$
- $w$  = load per unit cylinder length, lb/in
- $E'$  = effective Young's modulus, lb/in<sup>2</sup>



**FIGURE 9.11.** Grubin's model of elastohydrodynamic contact. From Zaretsky (1997).

$\eta_0$  = lubricant absolute viscosity (atmospheric pressure)  $1 \text{ bf} - \text{s/in}^2$   
 $\alpha'$  = pressure-viscosity coefficient of fluid,  $\text{psi}^{-1}$

and

$$\frac{1}{R_x} = \frac{1}{R_{x1}} + \frac{1}{R_{x2}} \quad (9.17)$$

when

$R_{x1}, R_{x2}$  = radii of bodies 1 and 2 in rolling direction, in

$$E' = \frac{2}{(1 - \nu_1^2)/E_1 + (1 - \nu_2^2)/E_2} \quad (9.18)$$

where

$E_1, E_2$  = elastic moduli for bodies 1 and 2, psi

$\nu_1, \nu_2$  = Poisson's ratios of bodies 1 and 2, psi

For typical steels,  $E' = 33 \times 10^6 \text{ lb/in}^2$  and for mineral oils, a typical value of  $\alpha' = 1/5 \times 10^{-4} \text{ in}^2/\text{lb}$ . Thus for mineral oils, lubricated rolling elements  $G = 5000$ .

**TABLE 9.6** Pressure-Viscosity Coefficient and Materials Parameter for Representative Lubricants\*

Type (specification)	Pressure-viscosity coefficient, <sup>†</sup> $\alpha$ , m <sup>2</sup> /N (psi <sup>-1</sup> )			Materials parameter, $G = \alpha E'$		
	40°C (104°F)	100°C (212°F)	150°C (302°F)	40°C (104°F)	100°C (212°F)	150°C (302°F)
Automatic transmission fluid (GM6137-M)	$1.54 \times 10^{-8}$ ( $1.06 \times 10^{-4}$ )	$1.17 \times 10^{-8}$ ( $0.81 \times 10^{-4}$ )	$1.02 \times 10^{-8}$ ( $0.70 \times 10^{-4}$ )	3498	2673	2310
Superrefined mineral oil	$2.5 \times 10^{-8}$ ( $1.73 \times 10^{-4}$ )	$1.54 \times 10^{-8}$ ( $1.06 \times 10^{-4}$ )	$1.27 \times 10^{-8}$ ( $0.87 \times 10^{-4}$ )	5709	3498	2871
Type II ester (MIL-L-23699)	$1.24 \times 10^{-8}$ ( $0.85 \times 10^{-4}$ )	$0.99 \times 10^{-8}$ ( $0.68 \times 10^{-4}$ )	$0.87 \times 10^{-8}$ ( $0.60 \times 10^{-4}$ )	2805	2244	1980
Diester (polyolester) (MIL-L-7808)	$1.15 \times 10^{-8}$ ( $0.79 \times 10^{-4}$ )	$0.93 \times 10^{-8}$ ( $0.63 \times 10^{-4}$ )	$0.80 \times 10^{-8}$ ( $0.55 \times 10^{-4}$ )	2607	2079	1815
Synthetic hydrocarbon plus 20 percent polyolester (MIL-L-2104C, MIL-L-46152)	$1.38 \times 10^{-8}$ ( $0.95 \times 10^{-4}$ )	$1.13 \times 10^{-8}$ ( $0.79 \times 10^{-4}$ )	$1.04 \times 10^{-8}$ ( $0.72 \times 10^{-4}$ )	3135	2607	2376
Synthetic hydrocarbon	$1.77 \times 10^{-8}$ ( $1.77 \times 10^{-4}$ )	$1.51 \times 10^{-8}$ ( $1.04 \times 10^{-4}$ )	$1.09 \times 10^{-8}$ ( $0.75 \times 10^{-4}$ )	3861	3432	2475
Mineral oil (MIL-L-6081)	$2.19 \times 10^{-8}$ ( $1.51 \times 10^{-4}$ )	$1.54 \times 10^{-8}$ ( $1.06 \times 10^{-4}$ )	$1.07 \times 10^{-8}$ ( $0.74 \times 10^{-4}$ )	4983	3498	2442

<sup>†</sup>The values given are representative values of  $\alpha$  and may vary from batch to batch or from one lubricant brand to another.

\*Zaretbhy, E. V. Ed., "Tribology for Aerospace Applications" *Soc. of Trib. and Lub. Emgrs.*, Park Ridge, Ill. Sec., 1997 (with permission).

Table 9.6 shows pressure-viscosity coefficient  $\alpha$  and materials parameter  $G$  for representative lubricants.

Grubins' film thickness, Eq. (9.16) has been successfully related to surface topography. Design comparisons will provide information on fatigue life of contacting materials. The EHD theory assumed that the surfaces were perfectly smooth, which of course is not true. The calculated film might be less than the combined surface roughness of the contacting bodies. Note that an EHD film of several millionths of an inch can support highly loaded rolling elements.

A measure of the performance of the lubricant film is a surface-roughness criterion to determine the extent of asperity contact. The film parameter

$$\Lambda = \frac{h}{\tau} \quad (9.19)$$

when composite roughness

$$\tau = (\tau_1^2 + \tau_2^2)^{1/2} \quad (9.20)$$

and  $\tau_1$  and  $\tau_2$  are the *rms* roughness of the two surfaces in contact. For comparison, the roughness  $\tau$  can be taken as  $10 \mu$  in for most commercial bearings.

The lubricant film parameter  $\Lambda$ , Eq. (9.19), can be applied as an indicator of rolling element performance and life. At values the ratio of  $3 < \Lambda < 10$ , minimal wear and long life would prevail with failure eventually being caused by classical subsurface rolling-element pitting fatigue. That is the ideal suggested design range for the value of  $\Lambda$ . For  $\Lambda$

$< 1$ , surface smearing or deformation will occur on the rolling surface accompanied by 20 times more wear. For  $1 < \Lambda < 1.5$ , surface distress will exist accompanied by superficial surface pitting with about 4 times more wear than  $\Lambda > 3$ . For  $1.5 < \Lambda < 3$ , some surface glazing can occur with eventual surface failure by subsurface rolling pitting fatigue with about  $1\frac{1}{2}$  times more wear than  $\Lambda > 3$ . In other words, when  $\Lambda$  is below 3 mixed film or boundary lubrication may occur.

The easiest way to raise the  $\Lambda$  ratio is to change the lubricant necessary, using a higher viscosity lubricant or raising the lubricant viscosity at operating temperature. Producing a high-quality surface finish on the rolling elements is, of course, more expensive.

Zaretsky (1997) states that the  $\Lambda$  ratio Eq. (9.19) can be used as an indicator of gearing and rolling-element bearing life. For aerospace gears, the composite surface finish is  $23\ \mu$  in ms and most gears operate at  $\Lambda < 1.5$  with either a mixed or boundary lubrication regime. The surface distress may have superficial pitting without proper additive in the lubricant. With proper lubrication, failure will eventually occur by classical subsurface-originated rolling (pitting) fatigue.

### 9.5.3 Lubricant Selection

A liquid lubricant has several functions in cam-follower system performance. It is the medium for the separating film (a) between the roller follower and its mating cam surface elastodynamically and also the rolling-element inner bearing and (b) between the slider and the cam surface of a sliding follower. The lubricant also serves to absorb the shock of the roller on the cam during the roller acceleration action as it rolls and slides. It should maintain the best rolling action and reduce the sliding to a minimum. The lubricant also serves as a coolant to the contacting bodies. A lubricant serves to flush out wear debris and carry it to a filter where it can be removed from the system. Last, it provides corrosion protection.

The best choice of lubricant is difficult to determine depending on the load and speed conditions of the cam-follower mechanism. A lubricant should be selected along with the cam follower materials in an early part of the design process to eliminate costly redesign necessities that may occur otherwise. The equilibrium temperature of a lubricating system is also an important consideration.

This section presents a study of lubricants in nonrecirculatory systems of (a) grease (which contains the liquid lubricant) and (b) oil lubricants. Recirculating systems may be used for cam and follower mating surfaces and other parts of the total machine. It is also important to decide whether to feed the lubricant on the entering side of the cam or the exit side. The author has observed early cam fatigue wear in heavily loaded systems using entering lubricants. Experience is critically important. Note that the Ferguson Company of St. Louis, Missouri uses Chevron SAE 80W90 for its high-speed, heavily loaded cam systems, especially the roller-gear drive. This lubricant contains numerous additives for surface protection and wear.

**9.5.3.1 Grease.** The least expensive mode of lubrication is grease. In the commercial roller follower, the bearing (a) is packed with grease or (b) is unsealed and supplied with a liquid lubricant; see Chap. 10. The use of grease requires a simplified housing and seals with a Zerk fitting for feed. Grease is not a liquid, but the liquid or fluid constituent in the grease is the lubricant. Greases consist of a fluid phase of either a petroleum oil or a synthetic oil and a thickener. The most common thickeners are sodium-, calcium-, or lithium-based soaps, although thickeners of inorganic materials such as bentonite clay have been used in synthetic greases. Since there is no recirculating fluid, grease-lubricated bearings must reject their heat by conduction and convection. The heat transfer requirements of

**TABLE 9.7** Greases

Type	Specification	Recommended temp. range, °F	General composition
High-speed, ball and roller bearing	MIL-G-38220	-40 to +400	Thickening agent and fluorocarbon
Synthetic, extreme pressure	MIL-G-23827	-100 to +250	Thickening agent, low-temperature synthetic oils, or mixtures EP additive
Synthetic, molybdenum disulfide	MIL-G-21164	-100 to +250	Similar to MIL-G-23827 plus MoS <sub>2</sub>
General purpose, wide temp. range	MIL-G-81322	-65 to +350	Thickening agent and synthetic hydrocarbon
Oscillating, bearing	MIL-G-25537	-65 to +160	Thickening agent and mineral oil
Gasoline- and oil-resistant, plug valve	MIL-G-6032	+32 to +200	Thickening agent, vegetable oils glycerols and/or polyesters
Fuel- and oil-resistant	MIL-G-27617	-30 to +400	Thickening agent and fluorocarbon or fluorosilicone
Ball and roller bearing: Extreme high temperature	MIL-G-25013	-100 to +450	Thickening agent and silicone fluid

cams and followers dictate whether a grease lubricant can be utilized. Grease lubricants are listed in Table 9.7.

*Liquid Lubrication Systems.* At low to moderate speeds, when the use of grease lubrication is not suitable, other methods of supplying lubricant to the bearing can be used. These include hand lubrication with open-cam follower systems, splash or bath lubrication, and wick, oil-ring, or oil-air mist lubrication. Felt wicks can be used to transport oil by capillary action from a nearby reservoir. Oil rings, which are driven by frictional contact with the rotating shaft, run partially immersed in an oil reservoir and feed oil mechanically to the shaft, which is adjacent to the bearing. The cam may be partially immersed in an oil reservoir to splash-lubricate itself. All of these methods require very modest ambient temperatures and thermal conditions as well as speed conditions.

The most commonly used lubricant is mineral oil both in liquid and grease form (Table 9.8). As a liquid, mineral oil usually has an antiwear or extreme pressure (EP) additive, an antifoam agent, and an oxidation inhibitor. Grease does not require an antifoam agent.

Oil-air mist lubrication supplies atomized oil in an airstream to the bearing, where a reclassifier increases the droplet size, allowing it to condense on the bearing surfaces. Feed rates are low and a portion of the oil flow escapes with the feed air to the atmosphere. Friction losses and heat generation with mist lubrication are low, but ambient temperatures and cooling requirements must be moderate because oil-air mist systems provide minimal cooling.

**9.5.3.2 Extreme-Pressure Lubricants.** Extreme-pressure (EP) lubricants can significantly increase the load-carrying capacity of cams. The extreme-pressure additives in the lubricating fluid form a film on the surfaces by a chemical reaction, adsorption, and/or chemisorption. These boundary films can be less than 1  $\mu$  in to several microinches thick

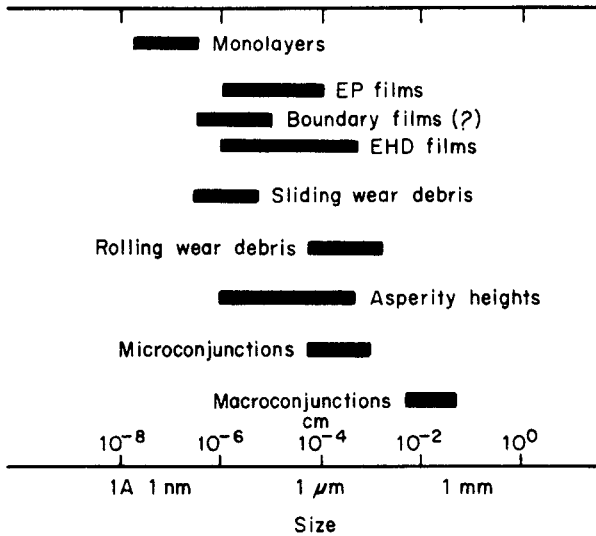
**TABLE 9.8**  
Mineral Oil Classification and Comparative Viscosities

Category	SAE number	ASTM grade*	AGMA gear oil	Temperature	
				38°C (100°F)	99°C (210°F)
				Approximate viscosity, cSt	
	—	32	—	2	—
	—	40	—	3 to 5.5	—
	—	60	—	8.5 to 12	—
	—	75	—	12 to 16	—
	—	105	—	19 to 24	—
	—	150	—	29 to 35	—
Extra light	—	215	—	42 to 51	—
	10 W	—	1	45	4.2
	—	315	—	61 to 75	—
Light	20 W	—	2	69	5.7
	—	465	—	90 to 110	—
Medium	30 W	—	—	—	10
	—	—	3	128	—
	—	700	—	130 to 166	—
Medium heavy	40	—	—	—	13
	—	—	4	183	—
Heavy	50	—	—	—	17
	—	1000	—	194 to 237	18
	—	—	5	—	—
	—	1500	—	291 to 356	—
	—	2150	—	417 to 525	—
	—	—	6	—	24
	140	—	—	—	25
	—	3150	—	630 to 780	—
Super heavy	—	—	7 <sup>†</sup>	—	29
	—	4650	—	910 to 1120	—
	—	—	8 <sup>†</sup>	—	36
	250	—	—	—	43
	—	—	8A <sup>†</sup>	—	47
	—	7000	—	1370 to 1670	—
	—	—	9	—	97
	—	—	10	—	227
	—	—	11	—	464

\*Grade number is equivalent to average Saybolt universal viscosity (SUV) at 38°C (100°F).

<sup>†</sup> Compounded with fatty oil.

and may be formed by the chemical reaction of sulfur or from the chemisorption of iron stearate. Figure 9.12 shows the range of film thicknesses for various types of films (Godfrey, 1968). The films can provide separation of the metal surfaces when the lubricant becomes thin enough for the asperities to interact. The boundary film prevents contact of the asperities and at the same time provides low shear-strength properties that prevent shearing of the metal and reduce the friction coefficient over that of the base metal. These boundary films provide lubrication at different temperature conditions, depending on the



**FIGURE 9.12.** Range of film thickness for various types of lubricant films with relation to roughness and wear.

material used. In extreme-pressure lubrication, the failure temperature is the temperature at which the boundary film melts. Many extreme-pressure lubricants contain more than one chemical for protection over a wide temperature range. Phosphorus compounds are superior to chlorine and sulfur at slow speeds, while sulfur is superior at high speeds. Some metals such as zinc and copper have to be removed from their systems when using certain extreme-pressure additives.

Some of the extreme-pressure additives commonly used are those containing one or more compounds of chlorine, phosphorus, sulfur, or lead soaps. Some lubricants are made with chlorine-containing molecules where the  $Cl_3-C$  linkage is used. For example, tri(trichlorethyl) phosphate additive has shown high load-carrying capacity. Other chlorine-containing additives are chlorinated paraffin or petroleum waxes and hexachlorethene. The phosphorus-containing compounds are perhaps the most commonly used additives for cam oils with other active elements. The sulfur-containing extreme-pressure additives are believed to form iron sulfide films that prevent wear for high loads and speeds. Lead soaps have been used in lubricants for many years. They inhibit the wiping and sliding action in cams and help prevent corrosion of steel in the presence of water.

Other additive compounds contain combinations of these elements and most extreme-pressure lubricants contain more than one extreme-pressure additive. The selection of a proper extreme-pressure additive is a complicated process. Factors such as solubility, volatility, stability, compatibility, load-carrying capacity, and cost must be considered.

Many gear oil companies depend on the use of proprietary or packaged extreme-pressure additives. As a result, the lubricant manufacturer does not evaluate the additives' effectiveness. Because of this, any selection of extreme-pressure additives should be supported by an evaluation program to determine their effectiveness for a given application. However, a few firms have considerable background in their manufacture and use of extreme-pressure additives for cam lubrication, and their recommendations are usually accepted without question by users of gear oils.

**9.5.3.3 Contaminants.** Contaminants in both fluid-film and gas-film systems can significantly affect cam performance, life, and reliability. Contaminant particles can brinell the shaft (journal) and bearing surfaces, causing stress raisers that can act as nuclei for surface pitting (spalling). Hard particles act as an abrasive medium and wear the softer surface. The particles can also act to clog lubricant orifices and jets, resulting in lubricant starvation of the bearing surfaces. The particles in a lubricant are the result of (a) manufacturing (chips and grit); (b) machine performance (wear particles); (c) environment result (dust, sand, paper, etc.); and (d) lubricant breakdown products (precipitates). Even in systems that are initially clean, multiple startups and shutdowns cause metal-to-metal contact, resulting in wear debris. Over time this debris can cause damage. As a result, good filtration is required in the lubrication system for long life and reliability.

## 9.6 SUMMARY

---

Limited explanation or theory is available for a full understanding of the life of surfaces in contact. Therefore, it is no surprise that in cam-follower surface actions there is somewhat of a lack of agreement concerning service performance. However, certain basic thoughts are presented for the proper use of materials for the system.

- Much of the knowledge now available to solve problems in rolling-element bearings and gearing is relevant to the needs of the cam designer.
- Section 9.4.4.2, Surface Fatigue Design, and Sec. 9.4.5, Materials Selection, provide information about the cam-follower material choices.
- Selecting materials and lubricants to fulfill the requirements of smooth cam followers with minimum wear is ultimately governed by experience in the field.
- Improve the cam-follower action by changing materials and lubricant only after measurement of parts, alignment, and cam contour accuracy has been established.
- In cam roller-follower systems, the design basis is for the roller follower to be the first-destroyed material for easy replacement and least cost.
- Roller-follower and cam surface failures are primarily fatigue failures with some adhesive wear evident. As the percent of rolling increases, the amount of adhesive wear decreases.
- Gray cast iron in combination with hardened steel is probably the cheapest choice for high-sliding galling action. Chilled cast iron and alloyed cast iron are among the best materials for galling. Meehanite in contact with hardened steel is an excellent choice, giving long life, good internal preparatory damping characteristics, and easy machining.
- Bronze or nylon in combination with hardened steel has good wear life, especially under high shock loads. It gives less noise, less vibration, and smoother action and compensates for inaccuracies in the contour surface. Plastics are excellent for noise reduction. A lubricant coolant is generally necessary.
- Hardened tool steel in contact with hardened steel gives the best combination under rolling action when shock and sliding action occur under high loads.
- Good surface finish with a lapping and polishing action is essential with hardened materials. It is not as important with ductile materials.
- Excellent choices for hardened steels are AISI 4140 and 8620. AISI 4140 can be through hardened, flame hardened, and nitrided, producing a thin, hard skin a few ten thou-

sandths of an inch thick, Rockwell 65-70. AISI 8620 (inherent core hardness of 35 Rockwell C) is an oil-quench material that is sometimes carburized.

- Spherical, curved, or flat-faced followers with pure sliding have adhesive wear action.
- Offsetting the mushroom follower gives a corkscrew motion to the follower and distributes wear.
- Surface quality after machining is almost always changed by the destructive action of metal removal, especially in grinding. In general, surface destruction is related to the pressure and the speed of the metal-finishing operation and the metal being affected to an appreciable distance below the surface. The effects on the surface are high stresses due to cold working, higher susceptibility to corrosive action, and metallurgical change due to high cutting temperatures.
- Cleanliness of the oil lubricant system is critical.
- Shot peening of steel cams increases their fatigue life by 50 percent.

## REFERENCES

---

- Buckley, D.H., "Tribology Fundamentals," *Tribology for Aerospace Applications*, pp. 1-67, E.V. Zaretsky, Ed., Soc. of Trib. and Lub. Engrs, Park Ridge, Ill, 1997.
- Cram, W.D., "Practical Approach to Cam Design," *Machine Design*, pp. 92-103, November 1, 1956.
- Fuchs, H.O., and Stephens, R.I., "Metal Fatigue in Engineering," *Fail-Safe Design*, John Wiley: New York, 1980.
- Godfrey, D., "Boundary Lubrication," *Interdisciplinary Approach to Friction and Wear*, pp. 335-84, SP-181. NASA: Washington, DC, 1968.
- Graham, J.D., "Pitting of Gear Teeth," *Handbook of Mechanical Wear*, pp. 138, 143, C. Lipson, Ed., University of Michigan Press, 1961.
- Grubin, A.N., "Fundamentals of the Hydrodynamic Theory of Lubrication of Heavily Loaded Cylindrical Surfaces," *Investigation of the Contact Machinery Components*. Kh. F. Ketova, Ed., translation of the Russian Book No. 30, Central Scientific Institute of Technology and Mechanical Engineering, Moscow, 1949. (Available from Special Libraries Association, Chicago, Trans. R-3554.)
- Hamrock, B.J., and Dawson, D., *Ball Bearing Lubrication—The Elastodynamics of Elliptical Contacts*, John Wiley & Sons, New York, 1981.
- Hertz, H., "Über die Berührung Fester Elastischer Körper," 1881; "Über die Berührung Fester Elastischer Körper und Über die Harte," 1882.
- Hertz, H., *Gesammelte Werke*, Vol. 1, J.A. Barth: Leipzig, 1895.
- Hubbard, D., *Camshaft Reference Handbook*, Don Hubbard Pub., Ft. Myers, Fla., dhubbard@peaonet.com, 2000.
- Lundberg, G., and Odquist, F.G., "Studies on Stress Distributions in the Vicinity of the Contact Region between Bodies with Applications," *Ing. Vetensk Akad. Handl.*, 116, 1932.
- Morrison, R.A., "Load/Life Curves for Gear and Cam Materials," *Machine Design*, 40: 102-8, August 1, 1968.
- Rabinowicz, E., *Friction and Wear of Materials*, p. 110, John Wiley and Sons, New York, 1965.
- Stribeck, R., "Characteristics of Plain and Roller Bearings," *Z.V.D.I.*, 56 (38): 1345-8; 1432-8; 56 (39): 1463-70, 1902.
- Talbourdet, G.J., "A Progress Report on the Surface Endurance Limits of Materials," p. 289, *ASM Conference on Mechanical Wear*, M.I.T., 1950.

- Thomas, H.R., and Hoerch, U.A., "Stresses Due to the Pressure of One Elastic Solid on Another," *Eng. Ext. Sta. Illinois Bulletin* 212: 1930.
- Turkish, M.C., *Valve Gear Design*, first edition, p. 100, Eaton Mfg. Co., Detroit, 1946.
- Wulpi, D.J., *Understanding How Components Fail*, American Society of Metals, Ponk, Ohio, 1990.
- Zaretsky, E.V., Ed., *Tribology for Aerospace Applications*, Soc. of Trib. and Lub. Engrs, Park Ridge, Il, 1997.

*This page intentionally left blank.*

---

# CHAPTER 10

---

# CAM MANUFACTURING

---

Harold A. Rothbart, D. Eng.

10.1 MANUFACTURING METHODS	285	10.5 CAM SHAPES VERSUS ACCELERATION CURVE	296
10.2 MASTER CAM ANALOG DUPLICATION CAMS	287	10.6 DYNAMIC ERRORS BY FINITE DIFFERENCES	297
10.3 CONTINUOUS NUMERICAL CONTROL (CNC) CAMS	288	10.7 MATERIAL PROCESSES	301
10.4 MANUFACTURING ERRORS AND DISCUSSION	291	10.7.1 Melting Practice	302
10.4.1 Structural Errors	293	10.7.2 Heat Treatment	302
10.4.2 Fixed Backlash Errors	293	10.7.3 Metalworking	302
10.4.3 Variable Backlash Errors	293	10.8 SPARE PARTS LISTING	303
10.4.4 Miscellaneous Errors	293	10.9 CAM FOLLOWERS	305
10.4.5 Probabilistic Model of Cam Profile	294	10.9.1 Roller Followers	305
10.4.6 Manufacturing Discussion	295	10.9.2 Roller-Follower Installations	306
		10.9.3 Sliding Followers	312
		10.10 CONCLUSION	312

---

## SYMBOLS

---

$r_c$  = distance from center to cam, in  
 $y$  = follower displacement, in  
 $\ddot{y}$  = follower acceleration, in/sec<sup>2</sup>  
 $\ddot{y}_m$  = maximum follower acceleration, in/sec<sup>2</sup>  
 $\ddot{y}_\sigma$  = follower deviation from theoretical cam curve, in  
 $F$  = normal force, lb  
 $I$  = moment of inertia of roller, lb-in-sec<sup>2</sup>  
 $R_c$  = radius of cutter or grinder, in  
 $R_r$  = roller radius, in  
 $\alpha$  = angular acceleration of roller, rad/sec<sup>2</sup>  
 $\mu_s$  = static coefficient of friction between cam and roller  
 $\sigma$  = error or deviation from theoretical cam profile, in  
 $\theta$  = increment angle, rad  
 $\omega$  = cam speed, rad/sec

---

## 10.1 MANUFACTURING METHODS

---

It is important that engineers be aware of the fabrication techniques involved in manufacturing and inspecting the actual cam produced from the design information. They should be knowledgeable about the experience and level of dedication of the machine shop workers in making and assembling the parts. To ensure quality (1) errors in fabrication and misalignment in assembly should be eliminated; (2) cam fabrication should be usefully monitored, and (3) tool wear, vibrations, and chatter should be eliminated. Necessary periodic inspection also should be minimized.

Let us consider the overall machine tool system next. The kinds and ages of the machine tools are important factors. New equipment always functions with greater precision than old equipment. Also, in cutting cams, the cams' surface and accuracy are to be controlled. Another factor is the cam pressure angle effect on the machine tool-cutting accuracy due to the elastic deflection of the parts during machining. Furthermore, the cutting increments vary according to the pressure angle of the cam being machined. In addition, the tool cutter material and hardness should be selected for the cam material being produced, and the tool cutter life and wear should be known at all times. Many other factors are not included here. One might say that the making of a cam approaches that of an art. In somewhat technical abstraction, one could relate that the *cam fabricating machine tool cutting action is a dynamic elastic system performing in a fundamentally similar manner to the operation of the cam-follower system* discussed in this book. In both cases, experience is necessary to understand and control performance.

The main areas of concern in this chapter are:

- manufacturing
- inspection
- assembly

Inspection and assembly are discussed in Sec. 10.3, CNC cams.

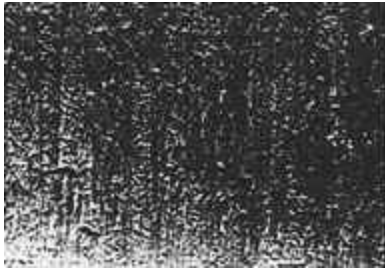
The method employed to produce a particular cam is a function of the cam's contour, application, and quantity of production. One would certainly not manufacture a cam for a simple clamping fixture using the same degree of precision and wear characteristics as those used for a high-speed textile machine cam. Present-day common cam manufacturing methods can be categorized as:

- manual or numerical control (NC) machining to cam coordinates
- analog duplication of a hand-dressed master cam
- computer numerical control (CNC) with linear, circular, spherical, or Bezier curve interpolation (Special computer software is usually developed for this purpose.)
- electrodischarge machining (EDM)
- miscellaneous methods, such as flame cutting, die casting, die forging, stamping, and powder metallurgy

In the first three methods, the cam profiles are formed on prepared cam blanks by the appropriate machine tool, such as milling and grinding machines. Heat-treated steel cams usually require a grinding operation to correct geometric distortions. Figure 10.1 shows milled and ground cam surfaces at 100× magnification. Standard milling machines are accurate to  $\pm 0.001$  in tolerance range. High-quality tooling, expensive jig borers, and grinders are accurate from 0.001 to 0.0005 in. Sometimes, the final stage of a cam-making operation consists of the machinist lightly "touching up" the cam and removing the burrs from the edges.

In *manual or numerical control (NC)*, the cam is mounted on a milling machine or precision jig borer for the cutter to plunge cut the cam from tabulated data. This step-by-step process creates finely scalloped surfaces and hand finishing is necessary to remove the asperities.

*Electrodischarge machining (EDM)* utilizes a hot wire to electrically cut the cam profile while the cam plank is fixed on the CNC table. Electrodischarge machining is a process similar to CNC and allows a prehardened cam blank to be machined to size without significant grinding. The practice is to EDM leaving approximately 0.003 in grinding stock. The local hardening effect of the hot wire and the fact that the wire can have a tendency



(a) Milled cam surface.



(b) Hardened and ground cam surface

**FIGURE 10.1.** Cam surface scanning electron microscope photographs (100×).

to bow across the face width of the cam requires that a minimal stock be left on for finish grinding. These minimal finish grinding passes will “true up” the cam surface as well as cam bores and dowel holes and does not add significant manufacturing time.

The significance of cam profile accuracy is emphasized. A surface may appear smooth to the eye and yet have poor dynamic properties. Depending on the application and loads the cam profile accuracy and its surface finish may affect the life, vibration, and noise of a cam-follower system. Poor manufacturing techniques can impede the satisfactory functional ability of a mechanism or machine.

Many have assumed that the accuracy of the cam profile does not affect its mating performance with the follower (dependent on Hertz stress). This may be acceptable for limited loads, dependent on the follower compliancy or high-frequency errors that often exist. For example, it has been found that vibrations and noise can be a significant result of a waviness-type error in the cam profile. In summation, vigilance in fabrication control (dependent on cost) is a pertinent philosophy to maintain at all times.

## 10.2 MASTER CAM ANALOG DUPLICATION CAMS

The master cam analog duplication method was universally applied to the making of cams before the introduction of numerically controlled (NC) machine tools. The method of master cam duplication is utilized today in small shops, for low production cams, and for special cams. The first step is the formation of the master cam in which the master cam blank is placed on a jig bore machine. The blank is incrementally plunge cut as defined by radial and angular coordinates, usually at 0.5 degree increments. Sometimes  $x$ - $y$  coordinates are utilized. Note that the cutter is generally the same size as the follower roller.

Master cam production is a slow, tedious, costly operation. The result of the cutting action leaves a series of scalloped edges. The scalloped master is next covered with a blue die and hand filed or ground until the die is observed only at the valley of the scallops that were removed. Using 0.5 degree increments for the cutting, a master cam with an approximate diameter of 12 in would have a profile accuracy of about  $\pm 0.0001$  in. The magnitude of the scallops, Fig. 10.2, is shown with the increment angle, by triangulation

$$\Delta\theta = \left( \frac{8R_c\sigma}{r_c^2} \right)^{1/2}, \quad \text{radians} \quad (10.1)$$

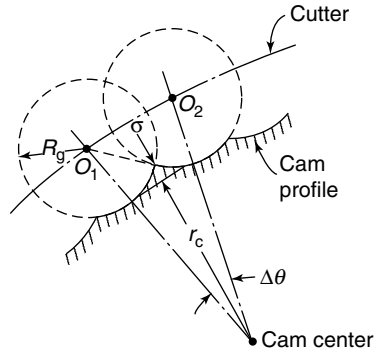


FIGURE 10.2. Increment cutting scallops.

where

$r_c$  = distance from center to cam profile, in

$R_c$  = radius of cutter or grinder, in

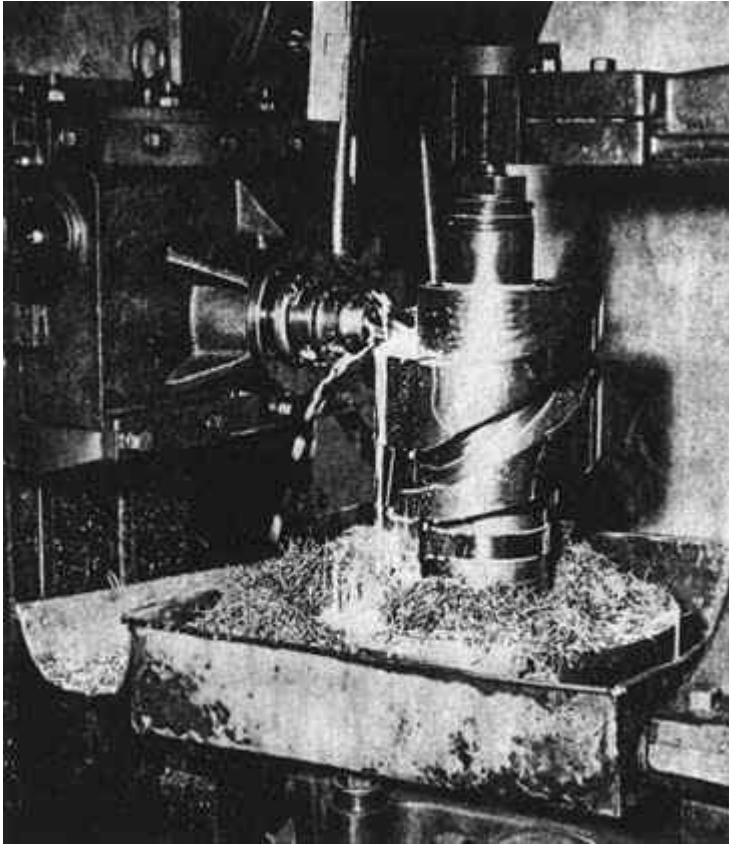
$\sigma$  = error or deviation from theoretical cam profile, in

After the master cam is completed and deemed acceptable, it is placed in an analog machine tool (milling machine or otherwise) and run to duplicate the desired production cams. The accuracy of the production cams is about  $\pm 0.001$  in tolerance; Fig 10.3 shows the master cam analog cutting of a cylindrical cam.

### 10.3 CONTINUOUS NUMERICAL CONTROL (CNC) CAMS

Except in special cases, the use of the master cam analog duplication method for production cams has been replaced by CNC milling and CNC grinding of cam profiles. In the CNC machine, the tool is continuously cutting the workpiece. The computer controls the movement of the workpiece from position to position and provides a continuous cutting process. The cam profile is usually discretized, commonly at 0.25 to 0.5 degree increments, for  $x$ ,  $y$  locations around the cam. The information line is connected from the personal computer (PC) to the cam production machine. The cutter-compensated cam chart is produced in several seconds.

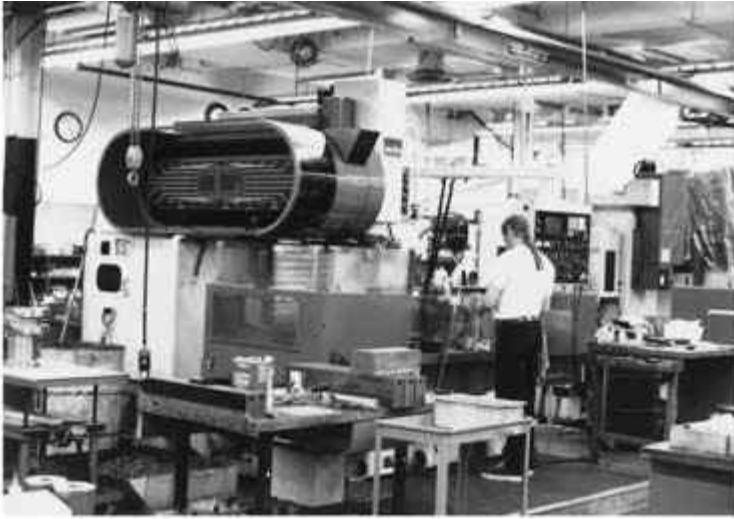
Norton (1988) has shown that in well-conditioned machine tools, the CNC methods of cam manufacturing yield better results than do analog duplication methods of cam manufacturing. Figure 10.4 presents a CNC machining center in operation. Figure 10.4a shows the machinist observing the milling operation. Note the carousel tool changer at the top left above the machine. Figures 10.4b and c are milling operations of cylindrical and radial cams, respectively. Usually, the cutting increments are 0.5 deg; increments may be larger for large cams. The increments are dependent on the pressure angle of the cam being cut. For high pressure angles, the increments may be reduced to correct for the flexibility in the smaller tool support structure. Figure 10.5 is an acceleration measurement of a ground 4-5-6-7 polynomial cam showing high-frequency vibratory errors. Last, the reader is referred to App. E, "CAD/CAM for a Medical Instrument Cam Mechanism," for more on CNC cam manufacturing.



**FIGURE 10.3.** Master cam analog cutting—cylindrical cam. (Courtesy Rowbottom Machine Co., Waterbury, Conn.)

Cams vary in difficulty from simple 3-axis ( $x, y, z$ ) plate cams to 5-axis ( $x, y, z$ ) and rotary axis globoidal cams. The design of the proper contour must include an accurate dimensional representation of the linkage (roller-follower mechanism) with which the cam will be engaged. If the cam has pivoting or offset linkages, an accurate model must be provided to ensure that the cam does what it is intended to do. A modified-sine profile, Chapter 3, which consists of cycloid and harmonic curves, is an industry standard for cam contours and provides for the least amount of power demand. A standard material used is a preheat-treated AISI 4140 plate or bar stock which provides for good machinability and hardening properties.

CNC plays a significant role in the ability to machine a cam component to theoretical dimensions. Based on the size of the part a part program is generated (typically with 4 increments per degree) and allows the operator the ability to cutter compensate the cam track if different cutters are more readily available. Cutter compensation can be applied only to plate cams (2-D) as roller gear and right-angle (barrel) cams must be milled on center only. These part programs allow the operator to ensure proper milling directions (climb or conventional machining) to minimize table vibrations and cutter wear.



(a) Machining center (note carousel tool changer at top left).



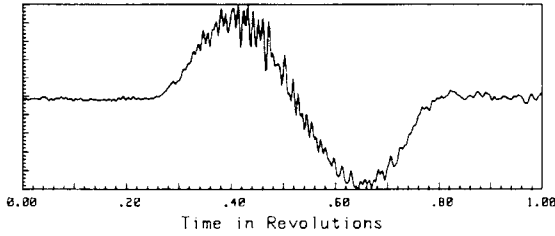
(b) Milling cylindrical cam.



(c) Milling radial cam.

**FIGURE 10.4.** CNC cam machining. (Courtesy Mallory Industries Inc., Farmington Conn.)

Standard plate and barrel cams are typically rough milled, leaving approximately 0.012 in grinding stock per side, are stress relieved to remove residual machining stresses, and then are hardened and finally ground to finish dimensions. Grinding is usually required to remove distortions from the heat treating phase. Some of the smaller cams can be milled to size and ion-nitrided. Proper feeds and spindle speeds must be maintained to prevent excessive cutter wear and deflections. Also grinding wheel breakdown must be monitored and is usually compensated by eccentric grinding wheels. Operators must peri-



**FIGURE 10.5.** Ground cam (DRD) 4-5-6-7 polynomial acceleration curve measured by Accelerometer (Norton, 1988).

odically check the cam track dimensions between rough grinding passes and after the final grinding pass to ensure that significant wheel breakdown is not present. As far as heat treating is concerned, distortions can be minimized if proper hardening practices are followed.

A vital step in cam manufacturing is the ability to *inspect* the part after machining and heat treating to ensure that distortions are minimized. There will always be some distortion due to cutter or grinding wheel deflection and heat treating, but they can be tolerated if kept to a minimum. A precision measuring machine (PMM) (Fig. 10.6 shows an example) can produce a variation analysis of theoretical and measured contours. The analysis would show full center axis translation ( $x$ ,  $y$ ,  $z$ ) and angular offset in degrees (timing). The timing feature is commonly a jig-bored manufacturing hold in line with a cam feature such as a keyway or scribe line. Typically the cam dwells are the most important features since this is where a positive stop is provided for external work to commence. Cam dwell location and runout (from one end to the other) are important concepts.

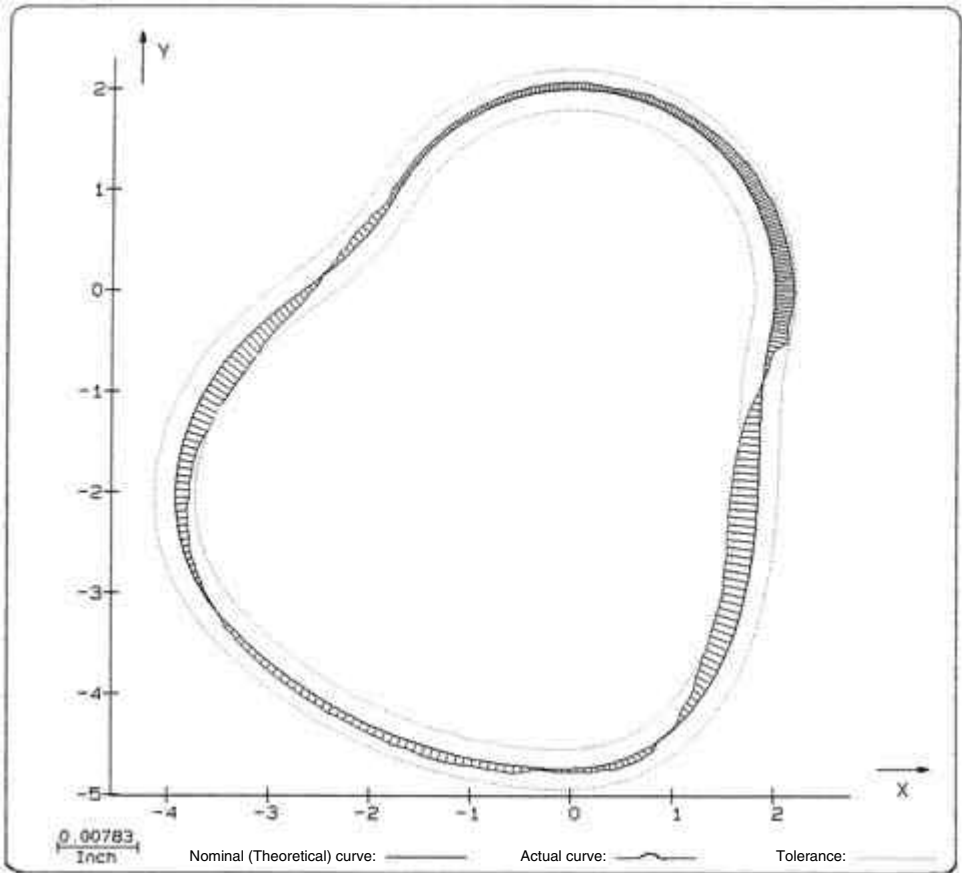
*Assembly* of cam mechanisms still requires significant experience as to the proper engagement of the cam and cam-follower mechanisms. To ensure proper fit and preload, assembly torques are measured at all bearing surfaces including the cam and follower wheel set.

## 10.4 MANUFACTURING ERRORS AND DISCUSSION

Parts cannot be made to ideal or design dimensions because inaccuracies are inherent in manufacturing processes. In this section we recognize these imperfections as *errors*. Manufacturing errors are important because poor manufacturing techniques can seriously impede the functional ability of the machine. Thus the best and newest machine tools plus the most experienced machinists and operators are of particular need. Accuracies for industrial production machinery are in the range of  $\pm 0.001$  in. However, accuracies as close as  $\pm 0.0003$  in may be necessary in some of these high-speed machines. Automotive valve gear system cams are often controlled to a tolerance of  $\pm 0.0001$  in.

In this section we are concerned with the methods for relating dimensions and tolerances to conditions affecting assembly or operation. Determining value for conditions controlling assembly or operation is one of the principal activities of designers. This activity may be accomplished on the basis of the theory, experiment, or experience and carried out to reduce or eliminate the errors in manufacturing the parts. Also, mechanism errors in high-speed machinery can cause early wear, noise, and fracture.

This section presents the accuracy (deviation from theoretical) of cam-follower fabrication and assembly. Only major manufacturing errors will be emphasized. Note that



**FIGURE 10.6.** Precision measuring machine example—Leitz PMM, Browne Sharpe Corp. (Courtesy CAMCO Corporation, Wheeling, Ill.)

acceptable accuracy of fabrication is determined by the experience of the shop artisans and the availability of effective machine tool equipment. The subject of proper cam production is most significant to the ultimate performance and acceptability by the customer.

Errors in any machining operation are statistical phenomena and the probabilistic approach to their study will produce meaningful results. Kim and Newcombe (1978, 1982) applied probabilistic techniques in the study of the effect of manufacturing tolerance in high-speed cams. Grewal and Newcombe (1988) and Newcombe and Kim (1983) applied the same techniques, separating the size and waviness components of the errors.

The actual manufactured cam-follower system to perform its theoretical design function is critically desired. The deviation of the actual follower's action from the theoretical can be listed in four categories of manufacturing in which in each mechanism can be the source of more than one type of error:

- structural errors
- fixed backlash errors

- variable backlash errors
- miscellaneous errors

#### 10.4.1 Structural Errors

Structural errors are mistakes in the dimension of the part or the utilization of wrong parts in building the machine. Another error of this type is one in the computer programming data, for example, in the case of a cam driving an oscillating follower. If the lever were the wrong length it would give the follower the wrong information because it would rest on the improper part of the cam curve.

#### 10.4.2 Fixed Backlash Errors

Most mechanisms have clearances necessary for assembly and operation, i.e., clearance between gear teeth and clearance between the roller follower and the cam groove. The smallest necessary clearance will result in a minimum backlash error. For cam-follower systems, backlash is a major source of error and the designs should be established to reduce it as much as possible.

#### 10.4.3 Variable Backlash Errors

Variable backlash errors are due to the additional clearance caused by *tolerances*. Tolerances are the differences between the limits of a dimension. Tolerances are assigned so that even when not made to ideal dimensions parts still assemble and operate satisfactorily. Statistically, if the tolerances controlling the amount of this additional clearance are normally distributed, then the amount of additional backlash will also be normally distributed. In this case the total backlash error is a combination of fixed and probable values.

#### 10.4.4 Miscellaneous Errors

*Cyclic errors* are associated with the eccentricity of rotating elements, the wobble of the cam faces, etc. The amplitude of cyclic errors is normally distributed.

*Cam profile errors* are deviations from the theoretical cam curve. Depending on the installation, speeds, and load, this surface error may produce operational difficulties of excessive noise and wear of the parts. These errors can be produced by an incorrect setting of the milling cutter, by a file scratch, or by holding the grinding wheel at a point on the cam for too long a time. Errors on the cam are often observed at points where the milling cutter or grinding wheel starts or stops as it travels around the cam. Also, the grinding machine may chatter in grinding which may affect the cam. In addition, the start and stop of the cutter or grinder as it sweeps in cutting around the cam contour sometimes leaves an error on the cam. This is often seen on acceleration tests of the cam profile as a “blip.”

Most cams require no operation after the jig borer, milling, or grinding machine cutting stages. Others may occasionally need hand filing or stoning of scallops or flats, especially for the master NC cams. Any hand operation is subject to error and is completely dependent on the operator’s skill and experience.

*Waviness* in the cam surface is a periodic imperfection or error. It is a uniform distribution of high and low points of longer duration than roughness. Waviness of a surface is the vertical distance between peaks and valleys of relatively long wavelengths. It may be

produced by a milling cutter taking too large a feed in the continuous generation of a cam. See Harris (1991) for the effect of waviness on vibration and noise.

Another kind of error is the *misalignment* of assembled parts. Misalignment of parts is a fault that should not be tolerated. The parts should be fitted properly for machine running conditions. The sources of misalignment include inaccurate machining or large tolerances in the mounting surfaces. Misalignment produces a reduced fatigue life in cam-follower contacting surfaces. In the roller follower there are two types of misalignment: (1) the cam follower axis is not parallel to the plane of rolling, e.g., the axis is lifted on one end. This condition will shift the contact area to one end of the outer ring. (2) Also, the cam-follower axis is not perpendicular to the direction of motion; in other words, the axis is skewed. Misalignment can be accommodated by using crowned followers. Straight rollers produce an elliptical contact stress surface, and crowned runners produce a circular stress surface. Also, a large radius crown should be used.

#### 10.4.5 Probabilistic Model of Cam Profile

The stochastic nature of the cam profile used by Kim and Newcombe (1982) is presented in this section. Also, the designer is referred to Chap. 12, which shows the combined effects of the cam follower dynamics and the probabilistic model of the cam profile.

In Fig. 10.7, we see that the desired location of the cutter is within a tolerance band in both the  $x$  and the  $y$  directions. Thus, the resulting profile shape will have a random waviness, and surfaces produced by milling, turning, grinding, and honing have an almost gaussian, or normal, distribution. For the cam profile, a normally distributed random value with a given mean and a standard deviation is generated from a sequence of uniform random numbers. To obtain a smooth acceptable shape, the random points that lie within a selected tolerance band are connected by a cubic spline curve, Fig. 10.8.

Kim and Newcombe (1982) applied a spline curve on displacement values from the two-dimensional tolerance of the cam profile and the roughness of the roller surface, assuming both obey the gaussian distribution, Fig. 10.9. The resulting continuous spline function was differentiated to obtain the theoretical characteristic acceleration, pressure angle, and radius of curvature of the cam profile so that the dynamic simulation may be investigated, Fig. 10.9.

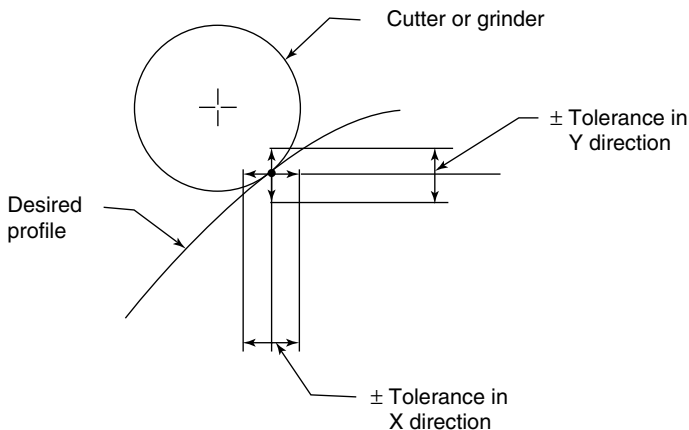


FIGURE 10.7. Tolerance band for setting cutter.

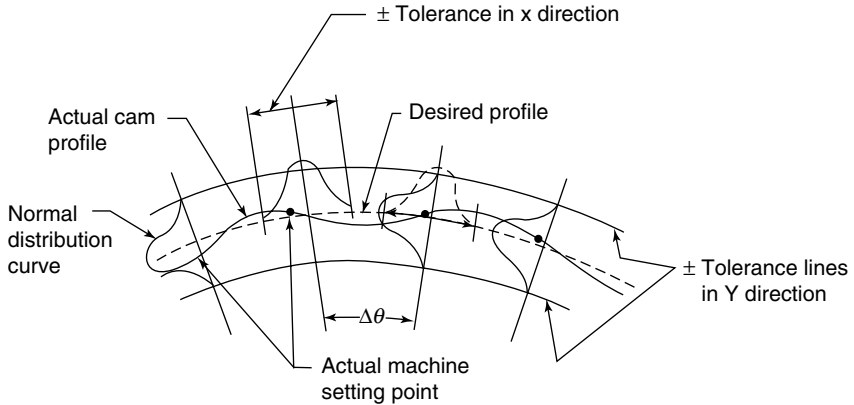


FIGURE 10.8. Cam profile waviness produced by tolerance band in setting cutter.

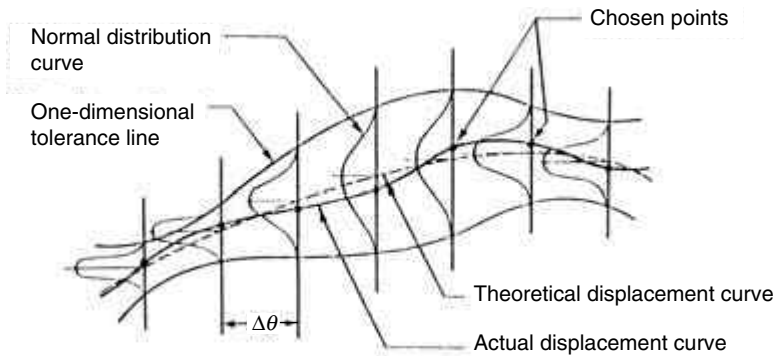


FIGURE 10.9. Combined effects of cam and follower tolerance on follower displacement curve.

#### 10.4.6 Manufacturing Discussion

Note that profile accuracy does not wholly lie in orthodoxy to or deviation from the theoretical profile. Also important are the increment deviation and its proportion to the theoretical change in increment displacement. For example, an error of 0.001 in at the beginning of a stroke, where the increment change in displacement is small, is of more concern than the same error at the middle of the stroke where the increment change is much larger. Also, the effect of a gradual error occurring over a long period is less important than the same total error in a much shorter period. Furthermore, the location of error deviation is a critical factor only if it affects the performance of the final machine. The error in dwell period may be more important than any other part of the cam action.

*Roughness* is the lack of surface smoothness. Smoothness can be increased (roughness decreased) by pressure grinding of the cam surface. Roughness in the cam profile always produces high-frequency and low-amplitude vibrations. The only practical way to improve this outcome requires the expense of more accurate fabrication and checking (preferably dynamic characteristics) of surface smoothness. Reduced roughness on surface-ground

cams has in some instances reduced wear. However, it has been observed that cam surface finishes better than  $15\mu\text{inrms}$  can induce errors in the cam profile that will affect cam dynamic loading (acceleration curve shape) and as a result nullify the result of the improved surface finish. The limit on finishing can be determined by experience and by cost.

*Finishing* of cams is the most critical of the fabrication operations. The basic point for consideration is how smooth the surface must be for the ultimate fatigue life and follower performance. This subject was discussed in Chap. 9.

A milled cam surface finish can be held to  $125\mu\text{inrms}$ . Grinding is the most accurate cam-finishing operation and surface finishes as fine as  $15\mu\text{inrms}$  can be obtained. Figure 10.5 shows a DRD ground cam acceleration curve with high-frequency oscillations at points of maximum acceleration. Barkan (1953) showed that analog ground cams tend to have high-frequency inaccuracies. However, these high-frequency inaccuracies have very little effect on the dynamic action of the cam-follower system at moderate speeds.

Roller followers have been finished as smooth as  $4\mu\text{inrms}$ . Polishing of automotive sliding followers as high as  $50\mu\text{inrms}$  is acceptable. *Lapping* is sometimes utilized to correct minute heat treatment distortion errors in multiple hardened cams. An abrasive lapping compound is used to fit mating cams and followers. Sometimes if a surface needs improvement a shear polish, lapping operation, or controlled run-in period is employed, all limited by cost.

*Machine frames* should be chosen to be as rigid as possible so as not to detract in any way from the proper, accurate function of the cam-follower mechanism. If the frame is "soft," it may store and release energy in every cycle of operation.

Next, let us discuss the cam curve mathematical analysis as it relates to the accuracy of manufacturing the actual cam. It should be noted that there is a limit in design to control the higher order derivatives of the cam curve. In cam analysis, it is conventional to use the smooth acceleration curve  $\ddot{y}$  as a basis for analysis. The curve choice is selected accordingly. This is compatible with the usual manufacturing tolerance of  $\pm 0.001$  in. It has been shown by Kim and Newcombe (1983), Barkan (1953), and Weiderrich (1973) that extreme manufacturing limits of  $\pm 0.0001$  in tolerances cannot control the jerk. In general, for industrial production machinery the jerk curve is used basically as a guide and not as a design tool. Hence, given normal manufacturer tolerance, it is not possible to control higher order deviation. Thus, it is not significant to elaborate on the jerk curve since it cannot be controlled in manufacturing easily.

Last, let us discuss the total machine tolerance analysis to reduce the accumulated error in the system. This method consists of a *weighting* factor for each of the connected parts of the machine. In this manner the engineer can determine and control the tolerance of each member that contributes most to the error. The manufacturing tolerances can then be modified to improve the machine performance. Sometimes a change in manufacturing methods is helpful.

## 10.5 CAM SHAPES VERSUS ACCELERATION CURVE

---

A cam may appear smooth to the touch or sight and yet be composed of vibratory imperfections. It may be dimensionally acceptable yet dynamically poor. In this section, the blending of the cam profile shapes will be observed to establish their effect on the cam velocity  $\dot{y}$  and acceleration  $\ddot{y}$  curves.

In Fig. 10.10a, a cam is cut from a circle that has a  $0.0001$  in flat sliced from its surface. As the cam rotates on the circular portion, the velocity  $\dot{y} = 0$  and acceleration  $\ddot{y} = 0$ . When the follower reaches point *a* it receives a velocity shock since the velocity instantaneously

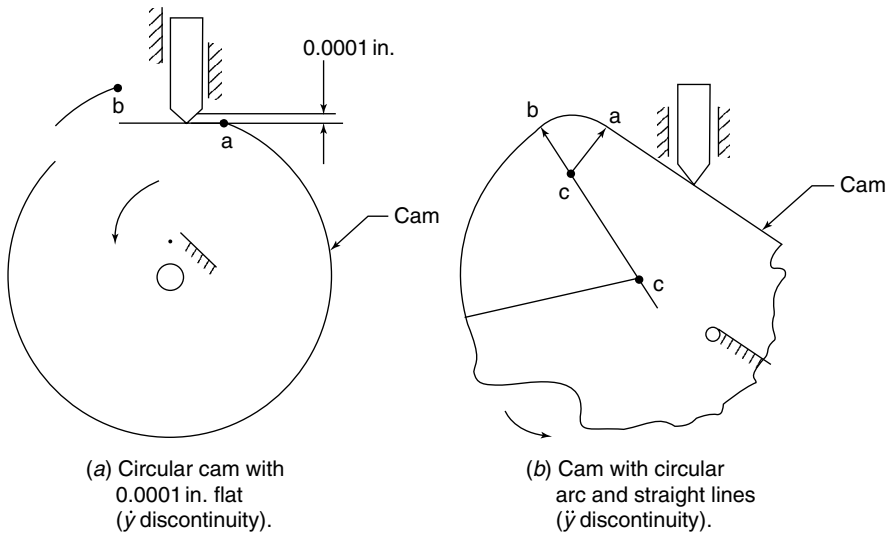


FIGURE 10.10. Cam shape dynamic discontinuities.

changes its value. The acceleration at point  $a$  accordingly is  $\ddot{y} = \infty$ . This velocity shock is not acceptable in any design. At point  $b$ , the same situation exists as at point  $a$ . It is to be observed that the depth of the slice has no effect on the phenomenon.

In Fig. 10.10*b*, a cam is formed by blending circular arcs and a flat side. Points  $c$  are the centers of curvature of the circular arcs. At point  $a$ , the radius of curvature instantaneously goes from infinity (flat) to a finite value. This yields a discontinuity in the acceleration since the acceleration is related to the radius of curvature at any point. Similarly, at point  $b$ , there are two instantaneous radii of curvature, which also yield a discontinuity in the follower acceleration.

Thus, circular arcs and straight lines for cams have poor dynamic properties because of their acceleration curve discontinuities. Such cams are not acceptable for moderate to high-speed dynamic performances. However, this acceleration curve discontinuity cannot be seen on the cam.

## 10.6 DYNAMIC ERRORS BY FINITE DIFFERENCES

Inspecting the accuracy of a cam contour can be accomplished in many ways. A few of the methods of inspection are:

- laser beam electronic equipment
- Windows-based process control for milling and grinding operations
- attaching an accelerometer to the functioning cam-follower mechanism
- measuring the cam profile displacements in small increments and converting this data by finite difference techniques

The last two procedures of inspecting the cam contour obtain the cam-follower acceleration curve and both can be compared with each other as a check. It should be acknowledged that measuring the cam profile and applying finite differences, Johnson (1995), is somewhat costly and time-consuming. Applying the method of finite differences, we can establish the acceleration effect of simple profile inaccuracies. The acceleration of any point  $b$  midway between two other points  $a$  and  $c$  as a small angle interval  $\Delta\theta$  is

$$\ddot{y}_b \cong \left(\frac{\omega}{\Delta\theta}\right)^2 (y_a + y_c - 2y_b) \quad \text{in/sec}^2 \tag{10.2}$$

where  $y$  = follower displacement, in  
 $\sigma$  = error or deviation from the theoretical cam profile, in  
 $\omega$  = cam speed rad/sec

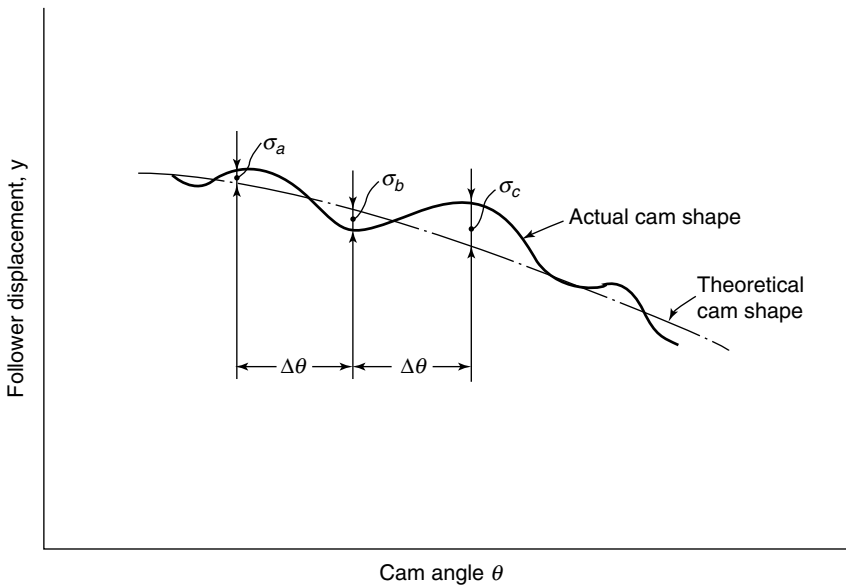
Equation (10.2) may be rewritten for the three points (Fig. 10.11) that have deviations from the theoretical cam curve. The deviation of the follower acceleration from the theoretical or primary value

$$\ddot{y}_\sigma \cong \pm \left(\frac{\omega}{\Delta\theta}\right)^2 (\sigma_a + \sigma_c - 2\sigma_b). \tag{10.3}$$

Two general error cases may be approximated. The first is with the errors at each point the same value ( $\sigma_a = \sigma_b = \sigma_c$ ) and gives the acceleration, substituting in Eq. (10.3)

$$\ddot{y}_\sigma \cong \pm 4\sigma \left(\frac{\omega}{\Delta\theta}\right)^2. \tag{10.4}$$

The second error type is a single “dip” at point  $b$  with  $\sigma_a = \sigma_c = 0$  and yields acceleration



**FIGURE 10.11.** Displacement diagram showing cam profile deviation.

$$\ddot{y}_\sigma \cong \pm 2\sigma \left( \frac{\omega}{\Delta\theta} \right)^2 \quad (10.5)$$

Equations (10.3) through (10.5) provide the actual cam profile deviation from the theoretical cam shape. A smoother acceleration curve can be found by utilizing *average weighted values* (Olderfield, 1958).

In Fig. 10.12 the cam acceleration curves of a high-speed aircraft engine valve gear linkage are shown. Superimposed on this curve—Fig. 10.12a—is the acceleration trace of a cam profile with a single smooth nonperiodic error of 0.0005 in in 0.020 in length of cam profile. Furthermore, the error was introduced at the top of the cam rise and the acceleration profile trace shows that this error is only slightly larger than other profile imperfections.

In Fig. 10.12b we see the acceleration trace of a cam having a more abrupt 0.002 in error in the same profile length of 0.020 in. This magnitude of error causes a more appreciable disturbance in the acceleration curve.

It is suggested for satisfactory performance at high speeds that the allowable acceleration error be

$$\ddot{y}_\sigma \leq (10 \text{ to } 20\%) \ddot{y}_m \quad (10.6)$$

where  $\ddot{y}_m$  = maximum follower acceleration, in/sec<sup>2</sup>

Obviously, the error location with respect to the theoretical cam acceleration curve may affect the performance and life of a cam-follower surface. In a cycloidal cam as an example, an error of a few thousandths of an inch in initial and final stages of the rise will definitely affect the follower performance.

Many types and sizes of errors were investigated to determine the correlation of the two techniques of obtaining cam-follower acceleration curves. The test cams employed the cycloidal curve as a theoretical shape. The example in Fig. 10.13 shows a cam that rotates at 300 rpm in 45° of cam falling action from the dwell position. The greatest error exists at about the 40° cam angle. Correlation is observed between the finite difference and experimental results. The theoretical maximum acceleration was calculated from the cycloidal formula to be 19.5 g and the maximum acceleration of the cam with errors is about 34 g. On a broad average the maximum acceleration difference for the error is 12 g per 0.001 in error at a speed of 300 rpm.

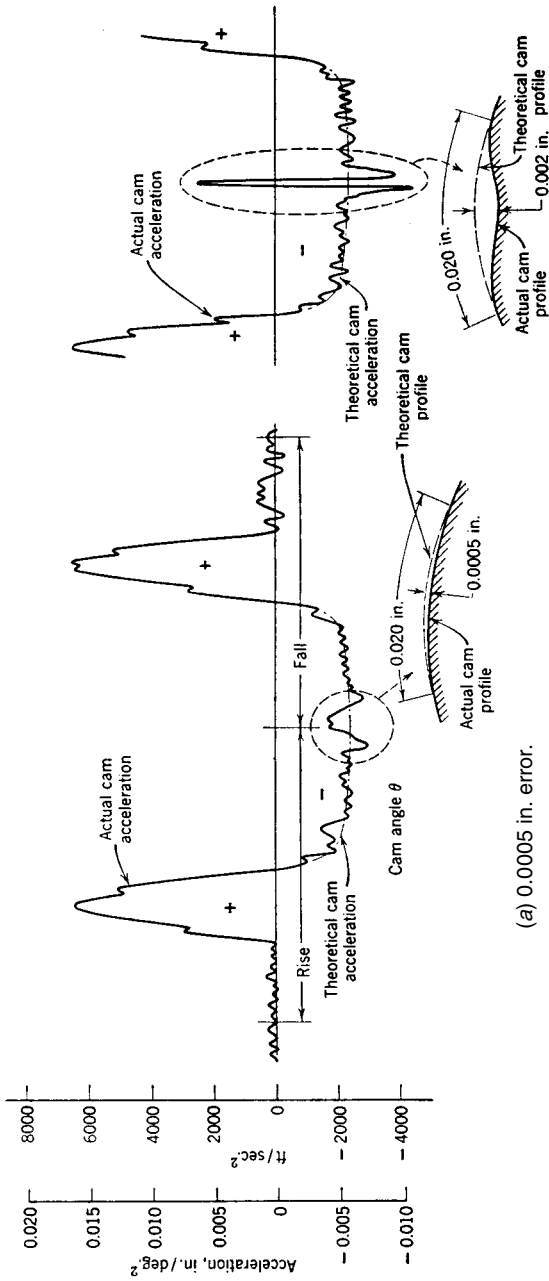
**EXAMPLE** By finite differences, verify the test results of Fig. 10.13.

**Solution** In Fig. 10.12a, the 0.0005 in error has a measured acceleration  $\ddot{y}_\sigma = 8400 \text{ in/sec}^2$ . By Eq. (10.5)

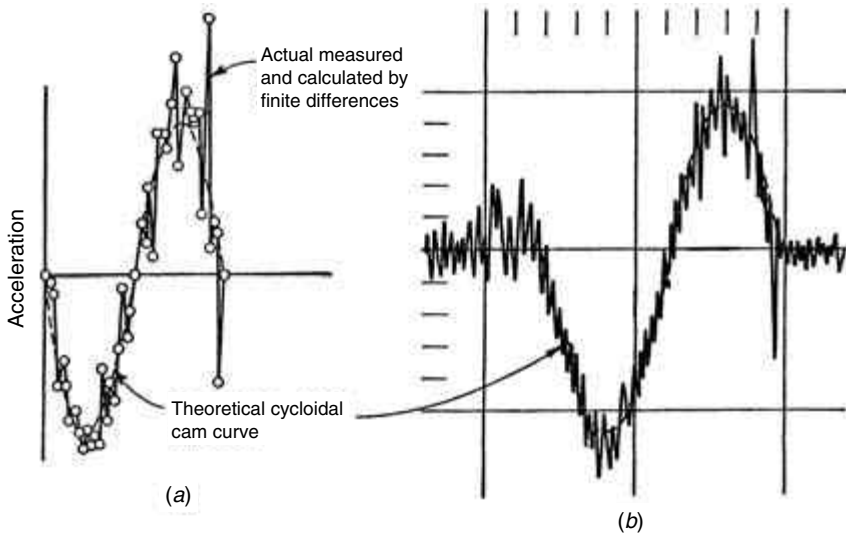
$$\begin{aligned} \ddot{y}_\sigma &\cong \pm 2\sigma \left( \frac{\omega}{\Delta\theta} \right)^2 \\ &\cong \pm 2(0.0005) \left( \frac{340 \times 2\pi}{60 \times \frac{3}{4} \times \pi/180} \right)^2 = 7400 \text{ in/sec}^2 \end{aligned}$$

This shows good correlation between test and calculated values. In Fig. 10.13b, the 0.002 in error has a measured acceleration  $\ddot{y}_\sigma = 45,000 \text{ in/sec}^2$ . Again substituting in Eq. (10.5)

$$\ddot{y}_\sigma \cong \pm 2(0.002) \left( \frac{540 \times 2\pi}{60 \times \frac{3}{4} \times \pi/180} \right)^2 = 29,600 \text{ in/sec}^2$$



**FIGURE 10.12.** Dynamic effect of single errors arbitrarily located on a 14-in-diameter four-lobe high-speed aircraft valve gear cam. Linkage weighs 4.25 lb. Maximum lift = 0.600 in; maximum follower velocity = 11.9 ft/sec. Designed cam speed = 340 rpm. (Note 0.020-in arc is 75°.)



**FIGURE 10.13.** Accuracy investigation of cam turning 300 rpm;  $45^\circ$ , rise =  $\frac{3}{4}$  in. (a) Finite-difference calculation. (b) Experimental with accelerometer and oscilloscope.

which shows an acceptable discrepancy between the test and calculated values.

We see that the 0.002-in error gives a dynamically excessive effect, whereas the 0.0005-in error provides reasonable acceleration values.

## 10.7 MATERIAL PROCESSES

Research literature has reported on the metallurgical variables for rolling-element bearings and gears. As mentioned previously, cams are similar to bearings and gearing as loaded contacting surface materials in the hertzian stress field. All three have similar resultant shearing stresses and their surface fatigue behavior will be similar. Since no official information is recorded for cams, the following is presented as applicable to cams. It has been found that rolling-element bearings and gearing have shown increased wear life of up to 60 times with the use of proper material process controls and improvements. The metallurgical processing variables to be considered are:

- Melting practice, such as air, vacuum induction, consumable electrode vacuum melt (CVM), vacuum degassing, electroslag (electroflux) remelt, and vacuum induction-melting vacuum arc remelting (VIM-VAR)
- Heat treatment which gives hardness and residual stress
- Metalworking to increase wear life

These factors significantly affect cam life. Other factors affecting cam fatigue life not included are: trace elements, retained austenite, gas content, inclusion type, and content. However, these factors are not controllable by normal quality control procedures. One mode of rolling-element fatigue is due to nonmetallic inclusions. These inclusions act as

stress raisers. Incipient cracks emanate from these inclusions and enlarge and propagate under repeated stresses, forming a network of cracks that develops into a fatigue spall or pit. Inclusion location with respect to the maximum shear stress is of primary importance, as are size and orientation.

### 10.7.1 Melting Practice

Both sufficient data and practical experience exist which indicate that the use of vacuum-melted materials, and, specifically, CVM, can increase cam surface-pitting fatigue life beyond that obtainable by air-melted materials. However, it is recommended that conservative estimates for life improvements be considered, such as a factor of 3 for CVM processing and a factor of 10 for VIM-VAR processing.

Data available on other melting techniques such as a vacuum induction, vacuum degassing, and electroslag remelting indicate that the life improvement approaches or equals that of the CVM process. However, it is also important to differentiate between CVM and CVD (carbon vacuum degassing). The CVM process yields cleaner and more homogenous steels than CVD does.

### 10.7.2 Heat Treatment

Heat treatment of cams is employed to improve cam surface-fatigue life. At present, no controls exist over heat treatment to produce a consistent, finished product. The thermal cycle is left to the individual producer for grain size and hardness ranges. Hardness is discussed, but in the case of grain size, lack of definitive data precludes discussing here.

Heat treatment is accomplished by furnace hardening, carburizing, induction hardening, or flame hardening. Cams are either case-hardened, through-hardened, nitrided, or precipitation-hardened for the proper combination of roughness and hardness.

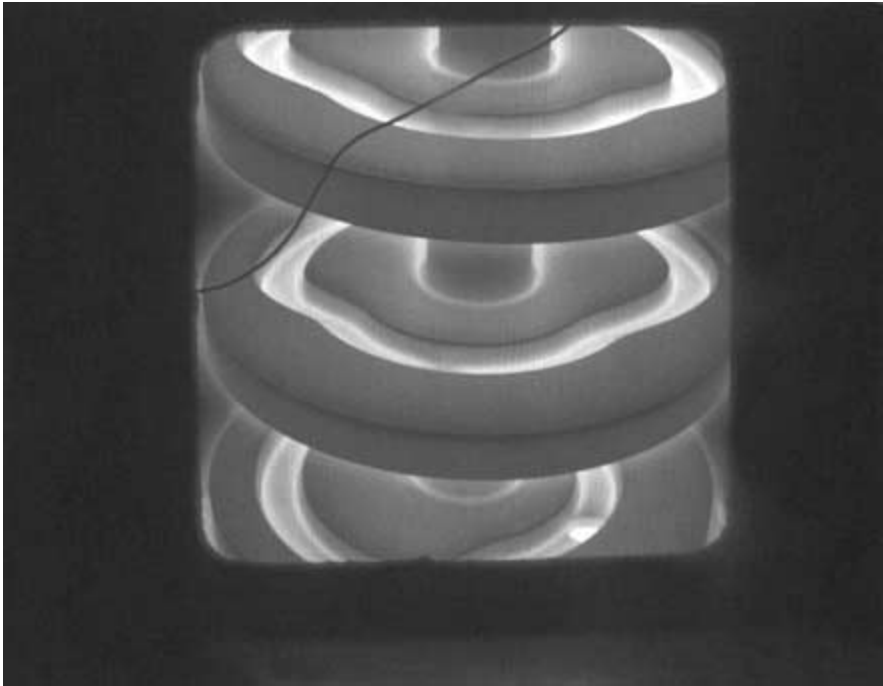
Heat-treatment distortion must be minimized if the cam is to have increased service life. Several hardening techniques have proved useful. For moderate service life increases, the cams are hardened but kept within the range of machinability so that distortion produced by heat treatment can be machined away.

Where maximum durability is required, surface hardening is necessary. Carburizing, nitriding, and induction hardening are generally used. However, precision cams can be ensured only by finishing after hardening. Full-contour induction hardening is an economical and effective method for surface-hardening cams. The extremely high but localized heat allows small sections to come to hardening temperatures while the balance of the gear dissipates heat. Thus, major distortions are eliminated. Conventional methods such as flame hardening can be employed.

Nitriding is a satisfactory method of hardening small-and medium-size cams. Distortion is minimal because furnace temperatures are comparatively low. The hardening pattern is uniform but depth of hardness is limited. Best results are achieved when special materials, suited to nitriding, are specified. Also, cam contour cross-sections should be thick enough to withstand distortion from heat treatment. Figure 10.14 shows the plasma/ion nitriding of a cast iron cam drive for the graphic arts industry. The glow is a result of the iron nitriding process. The thin dark line is a thermocouple wire utilized in the process.

### 10.7.3 Metalworking

Proper grain flow or fiber orientation can significantly affect pitting-fatigue life. Proper fiber orientation can be defined as grain flow parallel to the cam shape. Standard forging of cams as opposed to machining a forged disk is one way of obtaining proper fiber



**FIGURE 10.14.** Nitriding cast iron drive cams for the graphic arts industry. (Courtesy Advanced Heat Treat Corporation, Waterloo, Ia.)

orientation. A controlled-energy-flow forming (CEFF) technique can be used for this purpose. This technique is a high-velocity metalworking procedure that has been a production process for several years.

*Ausforging*, a thermomechanical fabrication method, has potential for improving the strength and life of cams. The suitability of candidate steels to the ausforging process must be individually evaluated.

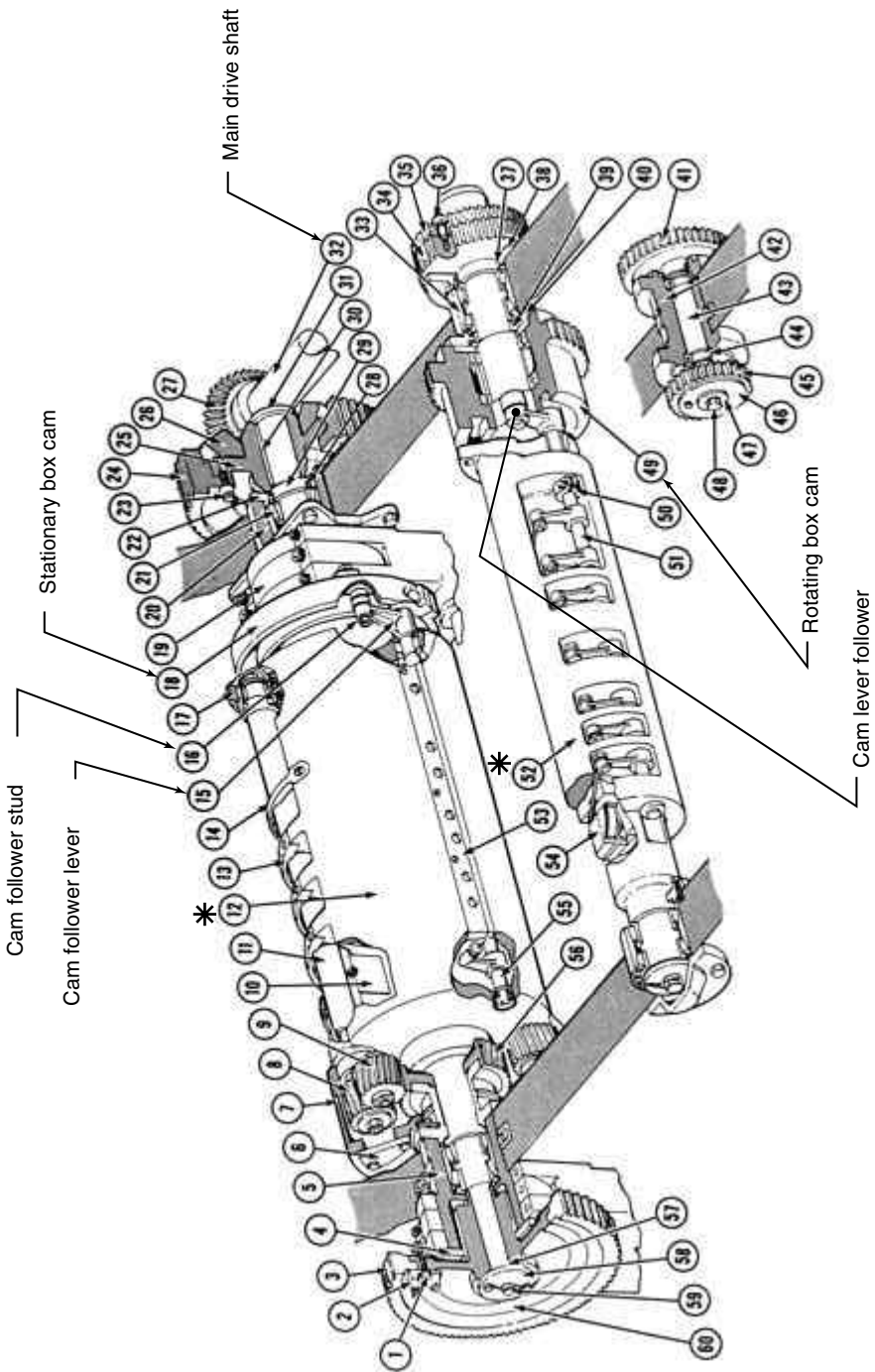
Most cam manufacturing specifications do not designate heat treatment, but rather call for material characteristics, i.e., hardness and grain size, that are controlled by the heat-treatment cycle. Hardness is the most influential heat-treatment-induced variable. It is recommended that RC 55-58 be considered the minimum hardness required for critical cam applications.

Residual stresses can be reduced by the heat-treatment process or shot peening. No analytical method can predict the amount of residual stress in the subsurface region, although  $\pm 50,000$  psi alternating shear stress has been accepted in the industry for indefinite cam life.

## **10.8 SPARE PARTS LISTING**

---

In machinery production, a listing of spare parts is a necessary requirement to replace the worn or broken members of a machine. In this section we will show an example that illustrates the recording of this information. Figure 10.15 shows the subassembly mechanism



**FIGURE 10.15.** Newspaper press subassembly (folding couple), 70,000 per hour. (Courtesy Doss Printing Press Co., Chicago, Ill.)

**TABLE 10.1** Spare Parts List, Newspaper Press Subassembly Folding Couple

Key	Name	Key	Name	Key	Name
FC-1.	Stud	FC-21.	Roller Bearing	FC-41.	Gear for Pin Cam
FC-2.	Adjusting Lug	FC-22.	Bearing Plate	FC-42.	Eccentric Bushing
FC-3.	2nd Fold Roller Gear	FC-23.	Adjusting Lug	FC-43.	Shaft
FC-4.	End Plate	FC-24.	Folding Cylinder Gear Rim	FC-44.	Bearing
FC-5.	Sleeve	FC-25.	Gear Rim Hub	FC-45.	Gear for Pin Cam
FC-6.	Plate On Gear Housing	FC-26.	Bevel Drive Gear	FC-46.	Gear Hub
FC-7.	Gear Housing	FC-27.	Bevel Gear On Shaft	FC-47.	Washer
FC-8.	Folding Blade Shaft Gear	FC-28.	Oil Seal	FC-48.	Stud
FC-9.	Intermediate Gear	FC-29.	Spacer	FC-49.	Rotating Pin Cam
FC-10.	Folding Blade	FC-30.	Key	FC-50.	Collar
FC-11.	Folding Blade Shaft	FC-31.	Washer	FC-51.	Pin Lever Shaft
FC-12.	Folding Cylinder	FC-32.	Horizontal Drive Shaft	FC-52.	Cutting Cylinder
FC-13.	Bridge	FC-33.	Roller Bearing	FC-53.	Cutting Rubber
FC-14.	Bridge	FC-34.	Cutting Cylinder Drive Gear	FC-54.	Knife Bar Assembly
FC-15.	Pin Cam Lever	FC-35.	Backlash Gear	FC-55.	Pin Lever Shaft
FC-16.	Stud and Roller	FC-36.	Adjusting Stud	FC-56.	Gear Rim
FC-17.	Folding Cylinder Yoke	FC-37.	Oil Seal	FC-57.	Shim
FC-18.	Folding Pin Cam	FC-38.	Plate for Cutting Cylinder	FC-58.	End Plate
FC-19.	Second Fold Roller Levers	FC-39.	Spacer	FC-59.	Capscrew
FC-20.	Folding Cylinder Sleeve	FC-40.	Plate for Cutting Cylinder	FC-60.	Gear Hub

Courtesy Goss Printing Press Co. Chicago, Ill.

of a 3-story high, 90-foot-long newspaper printing press that runs at a production rate of 70,000 completely folded newspapers per hour. This subassembly consists of the paper-folding cylinder (part 12) and the paper-cutting cylinder (part 52). These cylinders run at about 500rpm. Table 10.1 lists the number parts. Incidentally, part 32 is the main drive shaft for the subassembly shown. It connects to the various other series of drives in the press, making a complex system. Note that in this mechanism a flywheel is not necessary since the two heavy cylinders act as their own flywheels.

## 10.9 CAM FOLLOWERS

### 10.9.1 Roller Followers

There are two kinds of cam followers: roller and sliding followers. The roller follower is commonly used because of its low friction, low wear, low cost, easy replacement, and small size. The sliding follower may have a flat or spherical-shaped surface in contact with the cam profile.

As stated in the Chap. 9, the primary basis of design is that the roller may wear relatively quickly and need to be replaced often, while wear on the cam is minimized. In this

manner, machine life cycle cost is controlled since a cam is much more complicated and expensive than a roller-follower assembly. The roller is measured and replaced when a reduction in diameter is observed. This approach to cam-follower life has yielded permanently installed high-speed and high-load cams that last over 40 years.

Roller followers are commercially obtainable and comprise an assembly of separate parts—a drilled stud (for bearing lubrication), an outer race, and a set of rollers. The outer race is hardened to Rockwell C 60-62, having a highly polished hardened steel surface for good wear life and a tough case for absorption of dynamic and shock loads. The rollers are usually *needle* bearings. Sometimes *cylindrical* rollers are employed. Both kinds supply purely radial loads.

Needle bearings have an advantage over cylindrical bearings when they are used alone as cam followers; the large number of small-diameter, closely spaced rollers appreciably reduces the bending stress in the outer bearing race. Needle bearings have a low misalignment tolerance and moderate speed limits but use a smaller low-mass, low-inertia roller assembly which is excellent in cam followers. Reduced slipping of the roller on the cam surface is effected. Needle bearings are speed limited because the rollers skew at high speeds. The bearings are made of AJSI 52100.

The cam roll mountings available are the *stud* type, which is cantilever supported, and the *yoke* or *straddle* type. Figure 10.16*a* shows the stud type supported on a steel stem carrying needle bearings. Seals are included to return the grease which is inserted through a grease nipple. Heavy stud types are commercially available (not shown) for heavy load, shock loading, or applications requiring minimum deflection. Figure 10.16*b* shows a yoke-supported type using needle bearings and used in the automobile industry as valve tappet and fuel injection rollers. The yoke mounting is a better support and has reduced deflection and misalignment of the roller on the cam. The seals are excluded when external oil lubrication is available. This is desirable also to reduce seal friction in bearings. Because a yoke mounting distributes load uniformly over the bearing, the load limit of a yoke is about equal to that of a heavy stud follower. Cylindrical roller cam followers are employed for heavy loaded systems. They are also available in double-roller assemblies for extra-heavy installations.

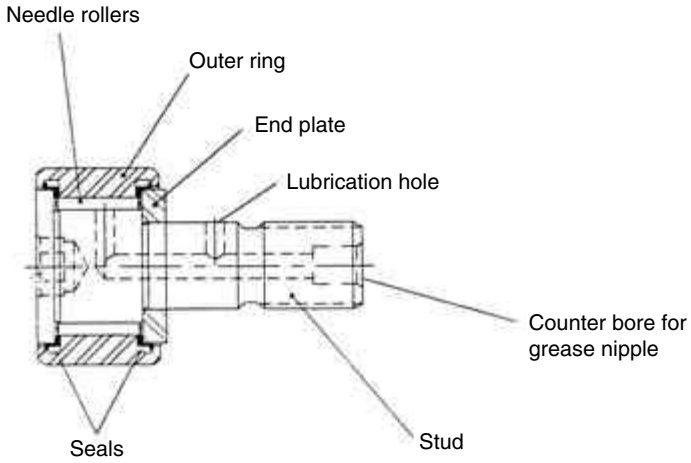
Sometimes standard ball, cylindrical roller, or needle bearings are utilized with the outer race specially built. Figure 10.17 shows a needle roller follower with a laminated thermoset resin outer roller used on a textile machine to reduce shock.

The cam-follower roller in contact with the cam will produce geometric stress concentrations that are dependent on the length of the contact. Figure 10.18*a* shows a straight roller resting on a cam. The roller will deflect slightly into the cam surface, producing the stress curve shown. Higher stresses will be induced at the ends and thus stress concentrations occur. Fatigue pitting or spalling will initiate at the ends. Crowned rollers, having a large radius of curvature, are used to distribute the stress more evenly. In Fig. 10.18*b*, partial crown rollers and logarithmic rollers have been employed with impunity. Also, a proper lubricated cam surface is required to minimize follower wear. If grease is used, it must be “tacky” enough to cause the follower to roll instead of slide.

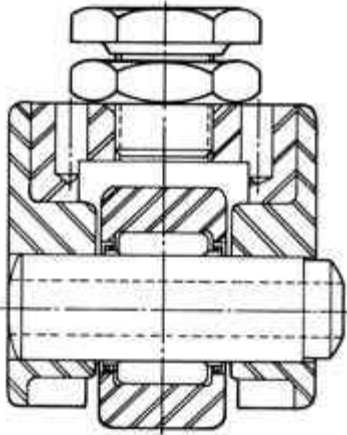
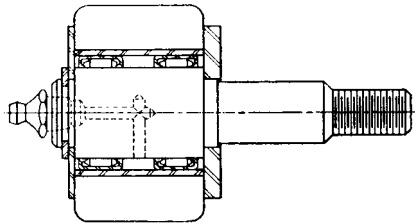
### 10.9.2 Roller-Follower Installations

Rolling function is explained in terms of the energy required to overcome the interfacial slip that occurs due to the curved shape of the contacting area between the roller and the cam surface. A portion of the elastic energy in rolling is lost because of hysteresis.

As stated, a roller is used because of its low friction and low rolling wear. Pure rolling action is desired, although a tolerable amount of sliding is always evident. However, certain difficulties may arise in which the roller, when running on a cam, may have a



(a) Cantilever stud bearing.

(b) Yoke support pin mounted bearing.  
(Courtesy RBC Bearings  
Trenton, N.J.).**FIGURE 10.16.** Commercial roller followers (needle bearings).**FIGURE 10.17.** Roller follower constructed of standard needle bearings with laminated thermoset resin outer race.

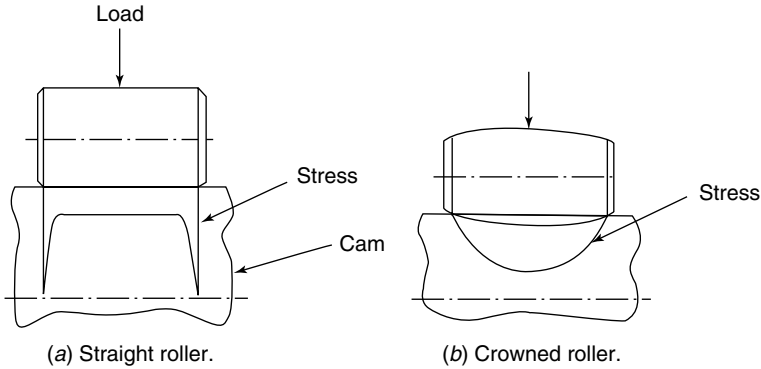


FIGURE 10.18. Roller stress concentrations.

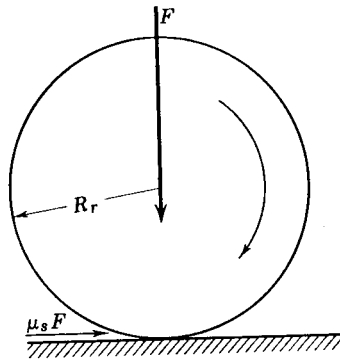


FIGURE 10.19. Rolling action.

considerable amount of detrimental sliding. Some of the factors are a jammed or dirty bearing race, fluctuations in the cam peripheral speed (especially in starting and stopping), backlash, misalignment, and the proportions of the positive-drive grooved roller follower, if used. Let us discuss these conditions, assuming that the roller is running properly on the cam surface, i.e., with its bearing lubricated and free of contaminants.

The peripheral speed of a cam rotating at a constant speed, or starting and stopping, is continuously changing. This alternately accelerates and decelerates the cam roller, inducing a torque reaction that for pure rolling (Fig. 10.19) must be less than the moment of the static frictional force. Thus

$$I\alpha < \mu_s FR_r \tag{10.7}$$

where  $I$  = moment of inertia of roller assembly, including needle or cylindrical roller bearing elements, lb-in-sec<sup>2</sup>

$\alpha$  = angular acceleration of roller, rad/sec<sup>2</sup>

$\mu_s$  = static coefficient of friction between cam and roller

$F$  = normal force, lb

$R_r$  = roller radius, in

Therefore to maintain rolling and reduce sliding at high speeds, a small lightweight roller is required to minimize inertia. The angular acceleration cannot be changed easily because it is inherent in the design. Also, the smallest cam gives the largest roller acceleration, since the ratio of roller speeds (roller acceleration) is increased for the same rise and same cam angle of rotation. Reducing sliding by increasing the coefficient of static friction or the normal force  $F$  is limited, since wear and stress will be further increased.

Followers are held in contact with the cam in four ways:

1. preloaded compression spring
2. single roller in cam groove
3. double rollers in cam groove
4. external double rollers on cam

In commercial machinery, the preloaded compression spring is rarely used, primarily because the spring adds an additional load to the system throughout its cycle, see Sec. 9.

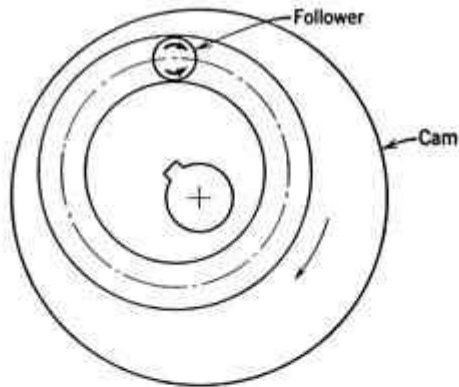
**SINGLE ROLLER IN CAM GROOVE:** Figure 10.20 shows a single roller follower in an internal groove in a radial cam (Fig. 10.20*a*) and a cylindrical cam (Fig. 10.20*b*). The roller has necessary backlash for free movement in the cam groove. Sliding occurs at the crossover point when the roller suddenly changes its contact cam, picking up the backlash. Wear and shock occur also. A kind of flutter movement sometimes exists with both rolling and sliding for all single-roller positive drive cams.

For the cylindrical groove cam, another type of sliding may exist, depending on the kind of follower. As mentioned previously, the cylindrical cam has either a cylindrical or a conical follower. A cylindrical roller is preferred primarily because of the ease of cutting the groove. In the end view of Fig. 10.20*b*, we see a cylindrical roller in contact with surfaces between radii  $r_1$  and  $r_2$ . This means that the velocity of the path of travel in contact with the surface at  $r_2$  is more than the velocity of the path in contact at  $r_1$ . Sliding must occur to compensate for the velocity difference, which depends on the roller length. Obviously, this length should be kept as small as possible. In general, this kind of sliding is not a seriously detrimental factor in the problem of surface life as compared to the action at the radial cams or cylindrical crossover point.

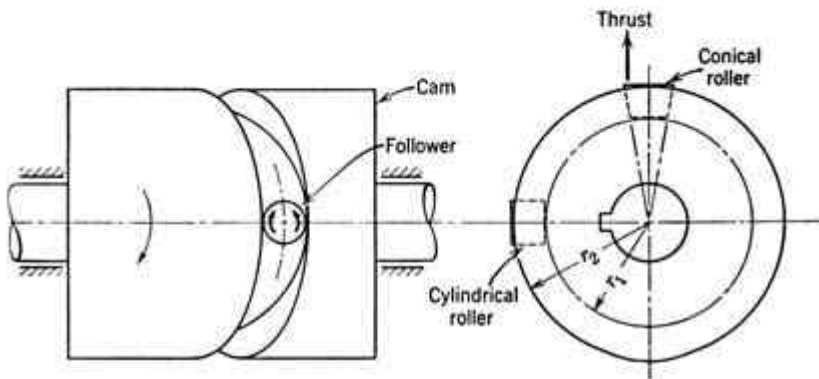
To improve this sliding action in the cylindrical cam, a conical roller (frustum) may be utilized. The vertex of this roller should be located at the center of the cam for best action (Fig. 10.20*b*). Thus, all points on the roller follower will be theoretically driven at their proper linear velocities. The conical roller has been applied largely for small cams in lieu of the simpler plain cylindrical type, because of the large ratio of radius  $r_1$  to radius  $r_2$  for the same groove depth. A special cutter must be employed to obtain the groove for the conical roller follower. Also, the conical roller in contact with a cam has a separating force component that must be overcome to keep the roller in place. However, the conical roller has the natural advantage that it can be moved radially inward to adjust for wear in the roller and groove.

**DOUBLE ROLLER IN CAM GROOVE:** Double roller or dual rollers in opposition with positive-drive grooved cams have been employed. While this option has an advantage of reduced rolling slipping compared to single roller, it also has limitations. The predominant shortcoming is the cantilever follower which deflects under load. This increases the possibility of misalignment of the loaded roller on the cam surface and thus excessive wear and reduced life. Figure 10.21 shows three different groove designs.

Figure 10.21*a* shows two eccentric rollers in a single groove. These rollers are of equal diameter; they are free to rotate and ride on opposite groove surfaces. An eccentric

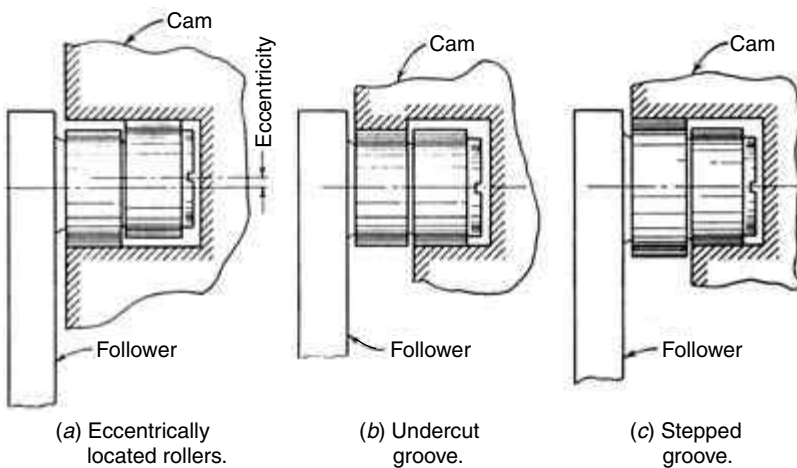


(a) Radial cam.



(b) Cylindrical cam.

**FIGURE 10.20.** Groove cams with single roller followers.

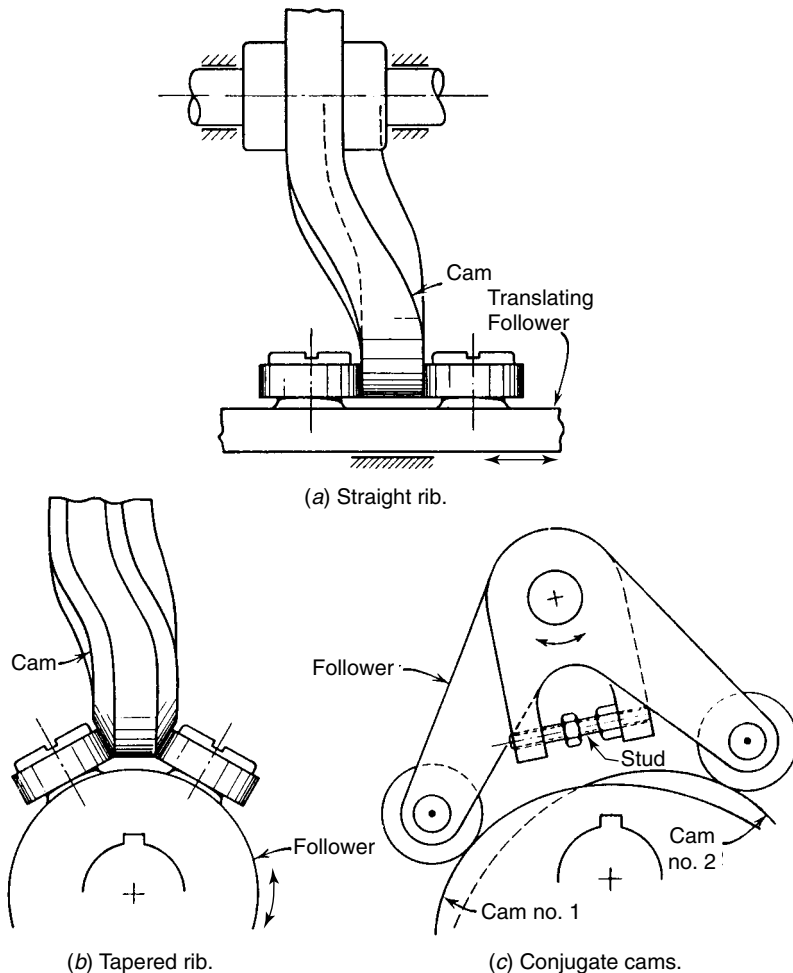


(a) Eccentrically located rollers.

(b) Undercut groove.

(c) Stepped groove.

**FIGURE 10.21.** Roller and groove designs.



**FIGURE 10.22.** External double roller on cam.

adjustment is sometimes provided for reducing backlash and preloading the roller. In Fig. 10.21*b* we see concentric rollers of the same diameter but in a relieved groove. The undercut is difficult to produce accurately. The last type, and the most acceptable, is shown in Fig. 10.21*c*, where we see two concentric rollers of different diameters in a stepped groove.

**EXTERNAL DOUBLE ROLLER ON CAM:** In Fig. 10.22 are shown positive-drive double rollers on double surfaces. Figure 10.22*a* indicates a globoidal cam having a straight rib and a translating follower. Figure 10.22*b* has a tapered rib with a globoidal cam and an oscillating follower. An excellent choice for radial cams is realized by the application of conjugate or complementary cams, Fig. 10.22*c*. This arrangement is flexible and accurate and minimizes misalignment of contacting parts. It is also reliable for high-speed, high-mass systems giving low noise and low vibration. In all three cam followers shown, pre-

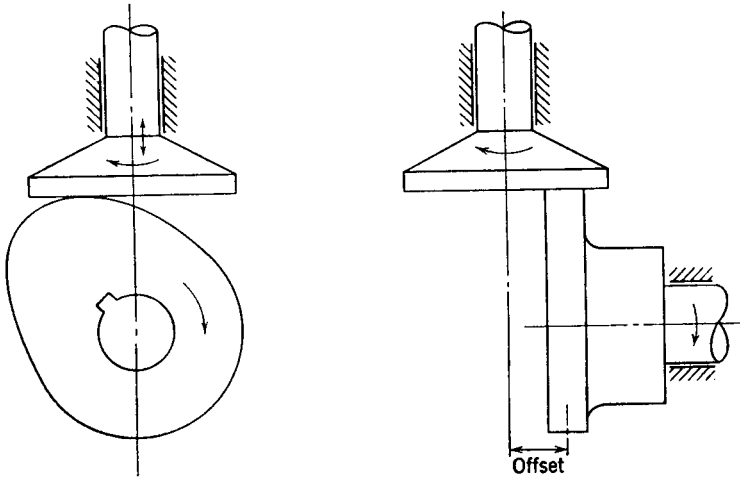


FIGURE 10.23. Flat-faced follower (may be offset to distribute wear).

loading or reducing the clearances and tolerances may be accomplished by use of the adjustable stud shown or by an eccentric roller stud, or by (in rare cases) a compression spring. The preload of the rollers depends on the cam size, with  $-0.001$  in interference fit, a usually acceptable amount.

### 10.9.3 Sliding Followers

Sliding followers may be either *flat-faced* or *spherical faced* and are sometimes called mushroom followers. These followers in general weigh less than roller followers for the same application and have the additional advantages of simplicity of maintenance and ease of lubrication. Lubrication is with high-viscosity oil or with EP lubrication. Automobile makers are the largest users of flat-faced followers, although some manufacturers are switching to roller followers. The spherical follower face has a large radius of curvature, 30 to 300 in, which corrects for wearing and misalignment and provides longer fatigue wear. Obviously this sliding follower cannot be used with concave cam surfaces. These sliding followers also are employed with small cams only, because of the prohibitive high sliding with large cams. With small cams the fluctuating cam-follower contacting surface speed maintains an oil film largely in the hydrodynamic regime discussed in Chap. 8.

Sometimes the mushroom follower is offset to reduce the sliding action (Fig. 10.23). The rise or fall of the follower is unaffected by the offset. However, the follower is now rotating and translating (corkscrew action), giving sliding and rolling of the cam. The area of contact and wear life is thus increased. The magnitude of the unbalanced forces on the follower stem, tending to deflect and jam it in its guide, limits the amount of offset. The practical net improvement of offsetting in this manner is subject to controversy.

## 10.10 CONCLUSION

All machined surfaces (with the exception of MEMS, Chap. 15) are generated and functionally operated under the influence of impact and impulsive forces of variable

intensities and frequencies. These dynamic forces, which are of indeterminable magnitude, affect the cam profile, accuracy, surface quality, and life. Moreover, the magnitude of these factors and the performance of the cam-follower systems are greatly influenced by the fabrication of the cam profile. The interrelated factors of accuracy, cost, and time are pertinent to the study. Poor manufacturing techniques can seriously impede the functional ability of the mechanism. Under most methods of fabrication, the actual and the theoretical cams rarely agree. Accuracies as close as  $\pm 0.0001$  in may be necessary in high-speed machinery. The following are some brief thoughts:

- Make parts as rigid as possible to keep flexibility to a minimum. Use laminated thermoset resins, carbides, and new materials if possible and practicable.
- Make the component moving parts of the machine as light as possible. Use new materials such as titanium, magnesium, and aluminum, if feasible. We should aspire for a high natural frequency of the follower linkage. If resonance occurs in a given speed range, it will be with a higher harmonic number and consequently smaller amplitude harmonics.
- Surface finish and accuracy of fabrication are of prime importance. Be sure that cams are cut accurately in accordance with the theoretical contours so that benefit from the mathematics is not lost. Keep surface errors to a minimum.
- Backlash in parts should be held to a minimum. Preloaded bearings and followers are a possible solution.
- Use low-friction bearings, and lubricate all mating surfaces.
- Balance the cams with intelligent proportioning of the mass.
- For high-speed production machinery DRD cam curve choices are the modified sine and the modified trapezoid. These yield low accelerations and no discontinuities. Both have excellent follower vibration performance.

## REFERENCES

---

- Barkan, P., *The Calculation of High-Speed Motion of a Flexible Cam Actuated System*, Ph.D. disse., Pennsylvania State University, 1953.
- Grewal, P.S., and Newcombe, W.R., "Dynamic Performance of High-Speed Semi-Rigid Follower Cam Systems—Effects of Cam Profile Errors," *Mech. Mach. Theory*, 23 (2): 121, 1988.
- Harris, T.A., "Rolling Bearing Analysis," John Wiley and Sons, New York, 1991.
- Johnson, R.C., "Method of Finite Differences in Cam Design," *Machine Design*, 27: 195, 1955.
- Kim, H.E., and Newcombe, W.R., "Stochastic Error Analysis in Cam Mechanisms," *Mech. Mach. Theory*, 13, 1978.
- Kim, H.E., and Newcombe, W.R., "The Effect of Cam Profile Errors and System Flexibility on Cam Mechanism Output," *Trans. ASME, Mechanism and Machine Theory*, 17 (1): 57, 1982.
- Newcombe, H.R., and Kim, H.E., "Some Results of the Effect of Waviness in Cam Profiles on the Output Motion," *Trans. 8<sup>th</sup> OSU Applied Mechanisms Conference*. St. Louis, Mo., 1983.
- Norton, R.L., "Effect of Manufacturing Method on Dynamic Performance of Cams," *Mechanism and Machine Theory, Parts 1 and 2*, 23 (3): 291–208, 1988.
- Olderfield, J., "On Application of Finite-Difference Method for Kinematics of Mechanisms," *Zastosowania Matematyki IV* (in Polish.), p. 176, 1958.
- Wiederrich, J.L., *Design of Cam Profiles for Systems with High Inertial Loadings*, Ph.D. thesis, Stanford University, Palo Alto, Calif. 1973.

*This page intentionally left blank.*

---

# CHAPTER 11

---

# CAM SYSTEM MODELING

---

**J. Christian Gerdes, Ph.D.**

*Assistant Professor of Mechanical Engineering, Design Division  
Stanford University  
Palo Alto, California*

<p>11.1 INTRODUCTION 316</p> <p>11.2 DYNAMIC SYSTEM MODELING AND REDUCTION 317</p> <p style="padding-left: 20px;">11.2.1 Natural Frequencies and Modes of Vibration 317</p> <p style="padding-left: 20px;">11.2.2 Model Sufficiency and Model Reduction 321</p> <p>11.3 MASS, INERTIA, AND KINETIC ENERGY 324</p> <p style="padding-left: 20px;">11.3.1 Finding Mass and Moment of Inertia 327</p> <p style="padding-left: 20px;">11.3.2 Moving Moments of Inertia to Other Points 329</p> <p style="padding-left: 20px;">11.3.3 Equivalent Mass or Inertia 329</p> <p>11.4 SPRINGS AND POTENTIAL ENERGY 332</p>	<p>11.4.1 Coil Springs 334</p> <p>11.4.2 Compliance of Other Mechanical Elements 335</p> <p>11.4.3 Combinations of Springs 338</p> <p>11.4.4 Equivalent Springs and Mechanical Advantage 340</p> <p>11.4.5 Massive Springs 341</p> <p>11.5 DAMPERS AND DISSIPATION 342</p> <p style="padding-left: 20px;">11.5.1 Viscous or Speed-Dependent Damping 343</p> <p style="padding-left: 20px;">11.5.2 Coulomb or Dry Friction 344</p> <p style="padding-left: 20px;">11.5.3 Mechanical Efficiency 345</p> <p style="padding-left: 20px;">11.5.4 Combinations and Equivalent Dampers 346</p> <p>11.6 EXAMPLE: MODELING AN AUTOMOTIVE VALVE-GEAR SYSTEM 348</p>
--	---

---

## **SYMBOLS**

---

$b$	Damping coefficient	lbf/(in/s)	(N/(m/s))
$b_r$	Rotary damping coefficient	ft-lbf/(rad/s)	(Nm/(rad/s))
$J_o$	Mass moment of inertia about O (or moment of inertia of body O)	lbm-in <sup>2</sup>	(kgm <sup>2</sup> )
K or k	Stiffness or spring rate	lbf/in	(N/m)
$K_r$	Rotary stiffness or spring rate	ft-lbf/rad	(Nm/rad)
$L_f$	Free length of spring	in	(m)
M or m	Mass	lbm	(kg)
N	Number active coils		
$\mathbf{v}_p$	Velocity vector at point P	in/s	(m/s)
$v_p$	Magnitude of velocity at point P	in/s	(m/s)
$\mathbf{r}_o$	Vector from O to given point	in	(m)
$\delta$	Deflection or relative displacement	in	(m)
$\dot{\delta}$	Relative velocity	in/s	(m/s)
$\Delta\theta$	Angular deflection or displacement	rad	(rad)
$\eta$	Mechanical efficiency	%	—
$\omega$	Angular velocity vector	rad/s	(rad/s)
$\omega_n$	Natural frequency	rad/s or Hz	(rad/s or Hz)

## 11.1 INTRODUCTION

---

*“All models are wrong. Some models are useful.”—George Box*  
*“Everything should be made as simple as possible, but not simpler.”—Albert Einstein*

Engineering modeling is the art of reducing a physical system to a mathematical description in order to analyze system performance. Unlike many familiar problems in mathematics and engineering, the problem of producing a mathematical model for a given system does not possess a unique solution. Many models of various degrees of complexity and detail can be derived for any physical system, and the selection of the *right* model for a given purpose can at times seem a bit overwhelming. The concepts of usefulness and simplicity outlined in the quotes above prove to be helpful guides when faced with such a challenge. As the quotes above suggest, the goal is rarely to create the most detailed or realistic model conceivable, but instead to produce a representation that captures the details of interest in a simple, concise manner. Transforming a system from physical reality to a set of equations invariably involves some simplification in the description and some uncertainty in the measurement or calculation of model parameters. Since it is therefore impossible to reproduce the physical system perfectly in the mathematical world, the proper evaluation of a model's quality is really an evaluation of its usefulness and not its detail. The operative question thus becomes: can the model explain the behavior it was developed to explain to the degree of accuracy desired?

Given a choice among models that pass this test of usefulness, there are often advantages to using the simplest possible representation. These advantages stem not from computational efficiency (after all, many commercially available computer codes allow the engineer to build multibody dynamic models of cam-follower systems that are more complex than those discussed here), but rather from the engineering insight provided by simple models. Often, simple models enable the engineer to develop analytical results that save time in the design process. Instead of running a battery of simulations on a complex model to see how the frequency of an oscillation in the system varies with the length of one element, a simple model could provide an algebraic relationship indicating that the frequency changes with the square root of the length. Simple models also enable the engineer to apply intuition from very simple systems (for instance, the idealized mass-spring-damper) to more complex systems (such as an automotive valve train). The danger is that the model will be too simple and some relevant behavior will be ignored. In the design of engineering systems, therefore, different models with varying complexity each have a role to play. Complex models offer the comfort of additional completeness and a closer match to experiment while simple models provide intuition and a means of separating primary and secondary effects. Knowing which model to use when is indeed a challenge, but one that can be greatly reduced with the help of a few concepts discussed in later sections.

This chapter provides the basic tools necessary to produce dynamic models of cam-follower systems (and many other mechanical systems), simplify the models through some physical arguments, and roughly assess whether or not such models are useful or too simple. The models developed may be used to analyze dynamic phenomena (Rothbart, 1956) such as cam hop (where the cam and follower actually separate), the dynamic forces that occur in each component, and the noise generated by the system while in operation. The particular modeling approach taken is known as “lumped parameter” modeling since the physical characteristics of components are combined, or lumped, to produce simpler representations. All components of the cam-follower system possess some mass or inertia, exhibit some compliance or spring-like behavior, and dissipate some energy from the system. For modeling purposes, it is convenient to separate these effects into a series of

idealized elements: point masses or lumped inertias, massless springs that provide force as some function of displacement, and massless dampers that produce force as a function of some velocity in the system. Once the properties of the individual components have been identified, the individual masses, springs, and dampers can be lumped together to produce simple models of the complete system. This process of lumping in many cases requires making judgments about which elements of the system are dominant and which can be ignored. For instance, elements with very little compliance can often be assumed rigid and elements with very small mass can often be assumed massless in order to simplify the modeling process.

The chapter begins by presenting some fundamental concepts from vibrations and system dynamics that prove useful in model reduction and assessment. The next three sections treat each of the basic modeling elements—mass or inertia elements, spring elements, and dampers—individually and discuss the rules for obtaining equivalent elements when multiple elements are lumped or combined. The final section of the chapter applies all of the concepts of modeling, simplification, and evaluation to produce a simple model of an automotive valve-gear system.

## **11.2 DYNAMIC SYSTEM MODELING AND REDUCTION**

---

This section introduces a few concepts from the fields of vibrations and system dynamics that provide useful vocabulary and intuition for developing and reducing models of dynamic systems. Obviously, it is impossible to cover the entire field of vibrations in a few pages, so only the aspects most relevant to later discussions in this chapter are included. For a more complete treatment of these concepts and the field of vibrations in general, useful resources are Ungar (1985) and the texts by De Silva (2000) and Meirovich (2001). Although not discussed in this chapter, the concepts of lumped parameter modeling and model reduction applied here to mechanical systems can also be applied to systems that include electrical, thermal, and fluidic elements. More general treatments of this material that include all of these energy domains can be found in Cannon (1967), Layton (1998), and Karnopp et al. (2000).

### **11.2.1 Natural Frequencies and Modes of Vibration**

One concept that proves useful in discussing any system modeled as a combination of masses, springs, and dampers is the natural frequency associated with a given mode of vibration. Figure 11.1 illustrates the simplest such system, consisting of a single mass and a single spring with the displacement  $x$  measured from the equilibrium position of the spring. Invoking Newton's second law

$$F = m\ddot{x} \quad (11.1)$$

and assuming that the spring provides a force proportional to its displacement from equilibrium,

$$F = -kx \quad (11.2)$$

a force balance of this system gives

$$m\ddot{x} = -kx \quad (11.3)$$

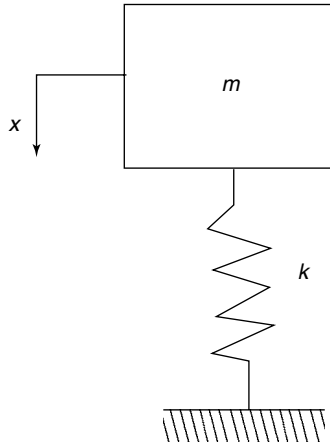


FIGURE 11.1. A simple mass-spring system.

as the equation of motion. If moved from its equilibrium position by a distance  $x_0$  and released from rest, the system illustrated in Fig. 11.1 will execute simple harmonic motion and move in a sinusoidal trajectory given by

$$x = A \cos(\omega_n t + \phi) \quad (11.4)$$

for some amplitude  $A$ , frequency  $\omega_n$ , and phase shift  $\phi$ . Using this expression in the equation of motion gives

$$m\ddot{x} = -mA\omega_n^2 \cos(\omega_n t + \phi) = -kA \cos(\omega_n t + \phi). \quad (11.5)$$

The frequency of oscillation, or natural frequency, is thus given by

$$\omega_n = \sqrt{\frac{k}{m}} \quad (11.6)$$

in units of radians/second. Note that this formula works directly when the stiffness and mass are in SI units ( $\text{N} \cdot \text{m}$  and  $\text{kg}$ , respectively), but when English units of  $\text{lb}/\text{in}$  and  $\text{lbm}$  are used a conversion is necessary

$$\omega_n = \sqrt{32.2 \times 12 \times \frac{k}{m}}. \quad (11.7)$$

The amplitude and phase can be determined from the initial conditions. Since the initial conditions assumed here are

$$x(0) = A \cos(0 + \phi) = x_0 \quad \dot{x}(0) = -A \sin(0 + \phi) = 0$$

the amplitude and phase are given by

$$A = x_0 \quad \phi = 0.$$

Unlike the amplitude and phase, the frequency of vibration is a property of the system and depends only upon the mass and stiffness, not the initial conditions. For this reason, it is called

the “natural frequency” of the system. A stiffer spring (higher spring constant  $k$ ) results in a higher natural frequency while a larger mass produces a lower natural frequency.

More complex systems consisting of multiple masses will possess several frequencies at which components will vibrate. This basic idea of simple harmonic motion and natural frequencies can be adapted to more complex systems by considering individual modes of vibration. Figure 11.2 provides an example of a two-mass system commonly used to represent the suspension at one corner of an automobile for ride quality analysis (Gillespie, 1992). Mass  $M$  represents the vehicle body (the “sprung mass”) while mass  $m$  represents the tire and wheel assembly (the “unsprung mass”). These masses are both clearly lumped parameters that combine masses of a number of individual components on the car. Associated with these two masses are two position coordinates (or degrees of freedom) and two second-order differential equations describing the motion. These equations of motion can be put into the form

$$\mathbf{M}\ddot{\mathbf{x}}(t) + \mathbf{K}\mathbf{x}(t) = 0 \quad (11.8)$$

where

$$\mathbf{M} = \begin{bmatrix} M & 0 \\ 0 & m \end{bmatrix} \quad \mathbf{K} = \begin{bmatrix} K_s & -K_s \\ -K_s & K_s + K_t \end{bmatrix} \quad (11.9)$$

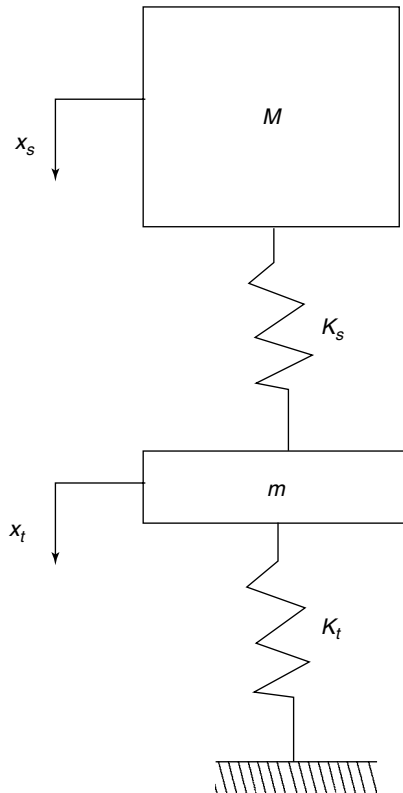


FIGURE 11.2. Quarter car suspension model.

and the vector  $\mathbf{x} = [x_s \ x_t]^T$ . As with the single degree of freedom system, solutions of the form

$$\mathbf{x}(t) = A \cos(\omega_n t + \phi) \mathbf{u} \quad (11.10)$$

exist to these equations for some constant modal vector  $\mathbf{u}$  which represents the shape of the system motion. Solving this equation of motion for the exact natural frequencies of this system gives:

$$\omega_n^2 = \frac{K_s m + (K_s + K_t) M}{2Mm} \pm \frac{\sqrt{[K_s m + (K_s + K_t) M]^2 - 4K_s K_t M m}}{2Mm}. \quad (11.11)$$

There are thus two natural frequencies for the two degrees of freedom system, each associated with its own modal vector  $\mathbf{u}$ . The exact shape of the system's motion at a particular natural frequency (known as a mode shape) can be determined analytically by solving for the vector  $\mathbf{u}$ . In this case, solving the equation above for  $\mathbf{u} = [u_s \ u_t]^T$  gives:

$$\frac{u_t}{u_s} = \frac{K_s - \omega_n^2 M}{K_t}. \quad (11.12)$$

Like the natural frequencies, the mode shapes are properties of the system. The exact amplitude of the motion requires knowledge of the initial conditions, but the *ratio* of the motions associated with each mass remains fixed.

To put some physical intuition behind this example, consider specific parameter values of  $M = 890$  lbm,  $m = 100$  lbm,  $K_s = 97$  lbf/in, and  $K_t = 1140$  lbf/in which are reasonable numbers for passenger car suspensions. Equation (11.11) indicates that for this choice of parameters, free vibrations will occur at frequencies of about 1 Hz and 11 Hz. The mode shape corresponding to the low frequency mode is given by  $u_t/u_s = 0.079$  and the mode shape corresponding to the high frequency mode is  $u_t/u_s = -110$ . This indicates that the low frequency mode consists mainly of motion of the larger mass while the high frequency mode consists mainly of motion of the smaller mass. The negative sign indicates that the two motions are  $180^\circ$  out of phase with each other. Physically, these mathematical results describe two modes of vibration: the sprung mass bouncing on the suspension spring with the tire remaining relatively rigid (the body mode), and the tire bouncing between the road and the vehicle body while the body remains approximately stationary (the tire hop mode). The effects of vibrations at these modes are familiar to most drivers or passengers. The 1 Hz mode represents the slow body bounce that can occur with particular spacings of pavement joints while the body mode produces the "slapping" sound as the tire bounces on a rough stretch of pavement.

Unlike the single mass-spring-damper system, the two-mass system possesses two degrees of freedom and two natural frequencies. Loosely speaking, whenever a system consists of lumped masses and springs, each mass that is connected to other masses or the environment through a spring generates one degree of freedom and one natural frequency (for a more formal treatment of the number of variables needed to characterize a general dynamic system see Layton, 1998 or Karnopp, 2000). While the presence of damping alters the system somewhat in that oscillations die out instead of continuing indefinitely, it does not change the basic number of degrees of freedom or natural frequencies. Damping will slightly change the exact numerical value of the natural frequencies relative to calculations made in the undamped case, but not the underlying intuition.

As demonstrated above, natural frequencies and mode shapes are concepts that can be formulated in a rigorous mathematical framework. From the standpoint of modeling, however, the qualitative use of these concepts in judging the complexity and sufficiency of a given model is often as important (or more important) than exact quantitative calculations.

For simple systems like this suspension model and many cam-follower systems, the vibrational modes can often be analyzed intuitively and this information used to simplify models.

### 11.2.2 Model Sufficiency and Model Reduction

Natural frequencies provide some insight into the applicability or sufficiency of the model. For mechanical systems, if the system is forced at the natural frequency, resonance (the maximum amplification of the forcing input) will occur. Intuitively, since the system naturally tends to vibrate at certain frequencies and in certain modes, motion at these frequencies is, in a sense, easier to initiate and maintain. Resonance is an important feature to capture in a mathematical model since it is not uncommon for the ratio of system motion to input magnitude to increase by an order of magnitude or more at resonance if the system is lightly damped. In a cam follower system, therefore, if the cam rotates at speeds up to 3000 rpm (or 50 Hz), the dynamic model of the follower system must, as a bare minimum, include all natural frequencies up to 50 Hz to capture the basic motion of the follower with reasonable fidelity. Similarly, if experiments show a resonance at 1000 Hz but the highest natural frequency predicted by the model is 100 Hz, the model requires additional refinement. It is “too simple” to predict the observed behavior.

Continuing with the example of the suspension in Fig. 11.2, this two-mass model is sufficient for simulating the vehicle response to road excitations in the range of around 0 to 15 Hz. If a test driver complains about road vibrations being amplified around 50 or 60 Hz, the model is too simple, since the mass responsible for this vibration has been lumped into either the body or the tire in the two-mass model. Conversely, if the goal of the modeling process is to capture the fundamental response of the vehicle to vibrations in the range of 1 Hz, information about the resonance at 11 Hz is extraneous and the model is more complex than needed. Of course the more complex model could still be used. Instead of retaining the additional complexity in the model, however, it is often beneficial to look for a simpler model that retains the important characteristics of the original model. This process is known as model reduction. In this case, the objective of the reduction is to create a model with a single natural frequency that predicts the resonance associated with the low-frequency mode (the sprung mass bouncing on the tire). The task then is to choose an equivalent mass and stiffness for a simplified model with a single natural frequency that resembles Fig. 11.3a. It cannot be emphasized enough that since any model will be an approximation of the real system, there is no unique or correct way to simplify. Simplification is again part of the art of engineering modeling.

The idea of natural frequencies can provide some guidance, however. Since natural frequencies are associated with masses and stiffnesses (more formally, with mass and stiffness matrices) and the goal is to remove the higher natural frequencies, the model can be simplified by ignoring masses or replacing certain spring elements with rigid links (thus assuming infinite stiffness). These assumptions remove degrees of freedom from the system and reduce the number of natural frequencies and the complexity of the resulting equations of motion. It is also possible, in the manner suggested by Chen (1982), to lump masses and stiffnesses together without explicitly assuming any of these to be zero or infinite. Three possible ways to apply these concepts to the suspension system are:

**Approach 1: Assume Infinite Tire Stiffness.** Assume that the stiffer spring (the tire) is rigid and use the mass of the car and the stiffness of the suspension spring to determine natural frequency. In this model, the mass of the tire and the degree of freedom associated with the tire are neglected since the rigid spring prevents the tire from moving relative to the road. This simplification is illustrated in Fig. 11.3b. The natural frequency in this case is given by

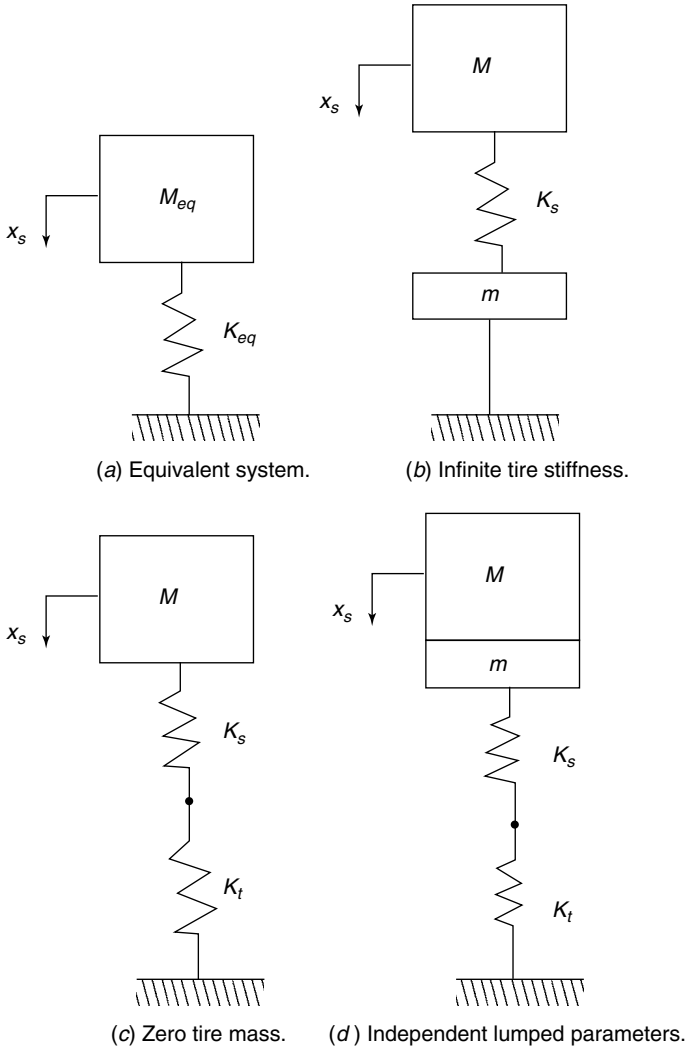


FIGURE 11.3. Reductions of the suspension model.

$$\omega_n = \sqrt{\frac{K_s}{M}} = 6.49 \text{ rad/s} = 1.03 \text{ Hz.}$$

**Approach 2: Assume Zero Tire Mass.** Assume that the tire has no mass so that the system takes the form of Fig. 11.3c. Neither the tire mass nor its degree of freedom are necessary for modeling, but the tire stiffness does influence the system through an equivalent stiffness of the springs in series (discussed in Section 11.4.3.2) defined by

$$K_{eq} = \frac{K_s K_t}{K_s + K_t}. \quad (11.13)$$

The resulting natural frequency is

$$\omega_n = \sqrt{\frac{K_{eq}}{M}} = 6.22 \text{ rad/s} = 0.990 \text{ Hz}.$$

**Approach 3: Lump Mass and Stiffness Independently.** Assume that a single mass and spring are required and independently combine masses and springs into a single equivalent mass and a single equivalent spring using techniques discussed in later sections. This is the approach suggested by Chen (1982) for reducing models of cam-follower systems and is illustrated schematically in Fig. 11.3*d*. The equivalent stiffness is again given by Eq. (11.13) while the equivalent mass is simply the sum of the masses

$$M_{eq} = M + m. \quad (11.14)$$

The natural frequency of the simplified system is

$$\omega_n = \sqrt{\frac{K_{eq}}{M_{eq}}} = 5.09 \text{ rad/s} = 0.940 \text{ Hz}.$$

Relative to the exact model, the error in natural frequency prediction for the three approaches is about 4.2 percent, 0.03 percent, and 5.1 percent, respectively. While none of these simplifications give exactly the same result as the exact model, all are close and the error involved in approach 2 is below the error introduced by any reasonable measurement system. Strictly speaking, all of these simplifications are wrong in that they do not precisely predict the natural frequency. Nevertheless, they are useful since they reduce complexity, produce reasonable approximations, and demonstrate which physical parameters are significant in determining the natural frequency of the body mode. For instance, it is much clearer from these simple models that the sprung mass and the suspension spring stiffness are the major determinants of the body mode natural frequency. While it would be possible to choose the equivalent mass above and then choose an equivalent stiffness that produced a value numerically equal to the exact natural frequency of the body mode, this stiffness would lose its connection to physical parameters. Hence its usefulness as a design tool would be reduced and the model would be valid only for the one specific system for which it was developed.

The fact that the three approaches above all produce similar results provides some measure of confidence in removing the tire degree of freedom. In this case, it follows from the fact that the tire mass is an order of magnitude smaller than that of the body, while the tire stiffness is about an order of magnitude larger. Hence, assuming that the mass is zero or the stiffness is infinite are both reasonable assumptions to make. In other systems, only one of these assumptions may be appropriate, based upon the physical parameters.

A reasonable approach to producing dynamic models of cam-driven systems, therefore, is to start with some understanding of the mass and stiffness of each component in the system. With this information, the model can be reduced such that the most compliant (least stiff) or most massive components are retained and the models ignore natural frequencies above the frequency range of interest. This ensures that the model remains as simple as possible. Of course, it is then necessary to verify (by verifying that the natural frequencies associated with the components assumed to be rigid are outside the region of interest or, preferably, through experimental validation) that the model is not too simple. Models can be scaled up in complexity by replacing some of the stiffnesses or masses

removed by model reduction, thus generating additional degrees of freedom and additional natural frequencies at successively higher frequencies.

### 11.3 MASS, INERTIA, AND KINETIC ENERGY

The ultimate goal of modeling a dynamic system is to produce equations of motion that may be used for simulation and analysis. These equations can be produced by relying on either Newtonian dynamics or analytical dynamics such as Lagrange's equations of motion Layton (1998). In the case of the former, the basic approach is to use Newton's second law to relate force and acceleration; in the latter, the basic equations of motion are derived from expressions of the kinetic and potential energy of the system. In either case, the concepts of mass and inertia are fundamental to the derivation of equations of motion and, therefore, to dynamic systems modeling. From the Newtonian perspective, mass and inertia provide the link between the forces acting on the system (kinetics) and the acceleration (kinematics) experienced by the system (or more rigorously, between the forces and the change of momentum). From the perspective of analytical dynamics, mass and inertia are essential in forming the kinetic energy of the system. The following section develops relationships among mass, inertia, and kinetic energy for a variety of cases involving rigid body motion.

The kinetic energy of a single particle of mass  $m$  (with units of lbm or kg) is given by

$$KE = \frac{1}{2} m \mathbf{v} \cdot \mathbf{v} = \frac{1}{2} m v^2 \quad (11.15)$$

where  $\mathbf{v}$  is the velocity vector of the particle in a three-dimensional space and  $v$  is the magnitude of the velocity (a scalar). Clearly, the kinetic energy depends only upon the magnitude of velocity and not on the direction. The kinetic energy of a system of particles or a rigid body can be derived by integrating over all of the particles that comprise the body, giving

$$KE = \frac{1}{2} \int_{\text{rigid body}} \mathbf{v} \cdot \mathbf{v} dm. \quad (11.16)$$

This equation is rather cumbersome, but a number of simplified forms exist for the common cases of motion needed in modeling cam systems. For a rigid body that translates without rotating, the angular velocity is zero and the linear velocity at every point on the body is the same since the distance between points on a rigid body cannot change. In this case, if  $\mathbf{v}$  represents the velocity vector at any point on the body,  $v$  is its magnitude and  $m$  is the total mass of the body, the kinetic energy takes the familiar form

$$KE = \frac{1}{2} \int_{\text{rigid body}} \mathbf{v} \cdot \mathbf{v} dm = \frac{1}{2} \mathbf{v} \cdot \mathbf{v} \int_{\text{rigid body}} dm = \frac{1}{2} m v^2. \quad (11.17)$$

Analysis of the kinetic energy is simplified greatly if the rigid body is restricted to move in a single plane of motion. Under this assumption, the motion can be generally described by the linear velocity at one point and the angular or rotational velocity of the body. While the linear velocity can, in general, vary from point to point in the body, the angular velocity is the same anywhere on the body and should always be described in units of radians/s in both SI and English systems of units. A further simplification may be made if the body rotates in the plane about some point on the body. A body rotates about a point if that point on the body remains stationary with respect to an iner-

tial frame while the body moves. In this case, the velocity at any point  $p$  on the body can be given by

$$\mathbf{v}_p = \boldsymbol{\omega} \times \mathbf{r}_o \quad (11.18)$$

where  $\boldsymbol{\omega}$  is the angular velocity vector and  $\mathbf{r}_o$  is the position vector from the point around which the body is rotating to the point where the velocity is being calculated (Fig. 11.4). Since for planar motion the angular velocity vector is at right angles to the position vector  $\mathbf{r}_o$ , the magnitude of the vector  $\mathbf{v}_p$  is simply the scalar product of the magnitude  $\omega$  of  $\boldsymbol{\omega}$  and the length  $r_o$  of vector  $\mathbf{r}_o$ .

$$v_p = \omega r_o \quad (11.19)$$

so the kinetic energy expression is

$$KE = \frac{1}{2} \int_{\text{rigid body}} \omega^2 r_o^2 dm = \frac{1}{2} \omega^2 \int_{\text{rigid body}} r_o^2 dm. \quad (11.20)$$

Defining the integral term as the moment of inertia about the fixed point,

$$J_o = \int_{\text{rigid body}} r_o^2 dm \quad (11.21)$$

this can be rewritten as:

$$KE = \frac{1}{2} J_o \omega^2. \quad (11.22)$$

So in this case, the kinetic energy can be described solely in terms of the moment of inertia of the body about the fixed point  $O$  (often called the polar moment of inertia about the point  $O$ ). The moment of inertia has units of mass  $\times$  length<sup>2</sup> such as lbm-in<sup>2</sup> or kg<sup>2</sup>.

Planar motion is typically described by a combination of the velocity at the body's center of mass (or center of gravity) and the angular velocity of the body. There is an

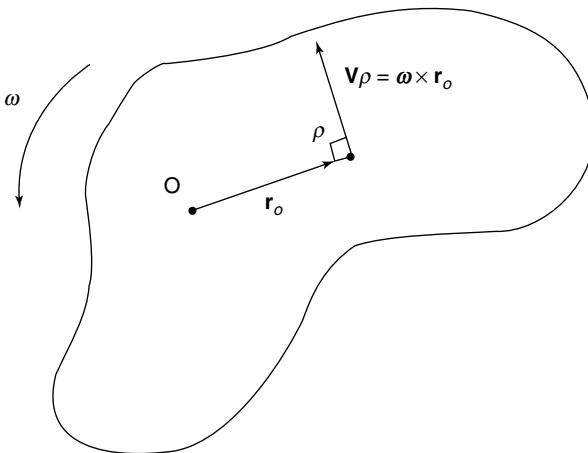


FIGURE 11.4. Rigid body planar motion: rotation about point  $O$ .

extremely good reason to do this in terms of the kinetic energy. The coordinates of the mass center are described by

$$x_{CR} = \frac{1}{m} \int_{\text{rigid body}} x dm = \frac{1}{m} \int_{\text{rigid body}} x \rho dV \quad y_{cg} = \frac{1}{m} \int_{\text{rigid body}} y dm = \frac{1}{m} \int_{\text{rigid body}} y \rho dV \quad (11.23)$$

for any coordinate system  $(x,y)$  in the plane of motion. If the object has constant density, this can be expressed solely in terms of the volume  $V$

$$x_{cg} = \frac{1}{V} \int_{\text{rigid body}} x dV \quad y_{cg} = \frac{1}{V} \int_{\text{rigid body}} y dV \quad (11.24)$$

in which case the mass center is said to coincide with the volume centroid of the body. Rearranging Eq. 11.23,

$$\int_{\text{rigid body}} (x - x_{cg}) dm = \int_{\text{rigid body}} (y - y_{cg}) dm = 0 \quad (11.25)$$

from which it follows that

$$\int_{\text{rigid body}} \mathbf{r}_{cg} dm = \int_{\text{rigid body}} \begin{bmatrix} (x - x_{cg}) \\ (y - y_{cg}) \end{bmatrix} dm = 0 \quad (11.26)$$

where the vector  $\mathbf{r}_{cg}$  represents the vector from the center of mass to an arbitrary point on the body. This relationship, in turn, enables the kinetic energy for the general case of translation and rotation in a plane (Fig. 11.5) to be simplified by splitting it into three terms:

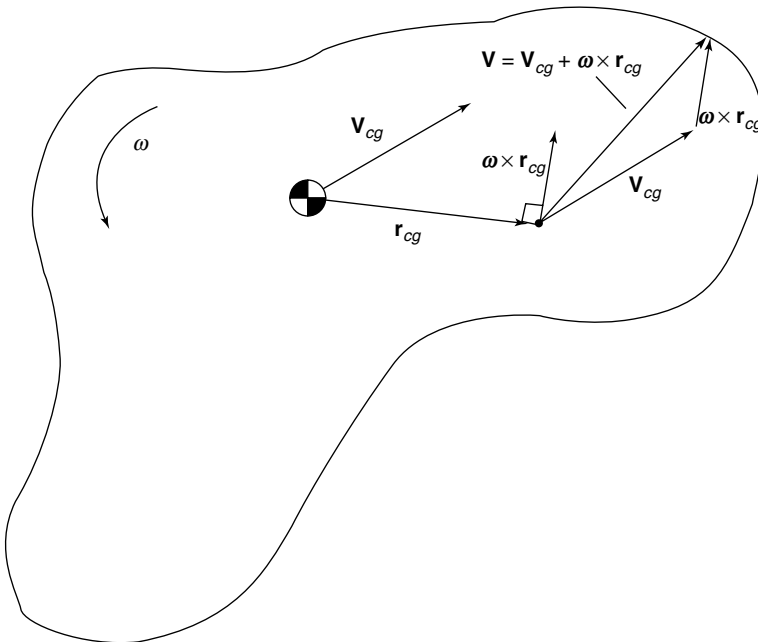


FIGURE 11.5. Rigid body planar motion: translation with rotation.

$$\begin{aligned}
 KE &= \frac{1}{2} \int_{\text{rigid body}} (\mathbf{v}_{cg} + \boldsymbol{\omega} \times \mathbf{r}_{cg}) \cdot (\mathbf{v}_{cg} + \boldsymbol{\omega} \times \mathbf{r}_{cg}) dm \\
 &= \frac{1}{2} \int_{\text{rigid body}} [(\mathbf{v}_{cg} \cdot \mathbf{v}_{cg}) + (\boldsymbol{\omega} \times \mathbf{r}_{cg}) \cdot (\boldsymbol{\omega} \times \mathbf{r}_{cg}) + 2(\mathbf{v}_{cg} \cdot (\boldsymbol{\omega} \times \mathbf{r}_{cg}))] dm \\
 &= \frac{1}{2} m v_{cg}^2 + \frac{1}{2} J_{cg} \omega^2 + \int_{\text{rigid body}} \mathbf{v}_{cg} \cdot (\boldsymbol{\omega} \times \mathbf{r}_{cg}) dm \\
 &= \frac{1}{2} m v_{cg}^2 + \frac{1}{2} J_{cg} \omega^2 + 0.
 \end{aligned} \tag{11.27}$$

The first term is simply the translational kinetic energy of the body, the second term is the rotational kinetic energy of the body and the third term goes to zero because of the property of the center of mass given in Eq. 11.26. As a result, the kinetic energy of a body can be described in terms of the mass of the body, the velocity at the center of mass, the moment of inertia about the center of mass and the angular velocity. In modeling, this result provides justification for describing a rigid body or a collection of rigidly connected rigid bodies by a single point mass at the center of mass and a moment of inertia about the center of mass.

In terms of Newtonian mechanics, mass and inertia play integral roles in the formation of equations of motion. For translation, mass gives the relationship

$$\mathbf{F} = m\mathbf{a} = m\ddot{\mathbf{r}} \tag{11.28}$$

between the force vector  $\mathbf{F}$  applied to the rigid body and the acceleration vector  $\mathbf{a}$  located at the body's center of gravity. The acceleration can also be expressed in terms of the second derivative of the vector  $\mathbf{r}$ , which represents the vector from any fixed inertial frame of reference to the center of mass of the body. For rotation in the plane, the equivalent expression is derived from the rate of change of angular momentum, giving

$$T_{cg} = J_{cg} \dot{\omega} \tag{11.29}$$

where  $T_{cg}$  is the net torque about the center of mass and  $\omega$  is the angular velocity. Since motion is restricted to the plane, rotation can occur only about one axis, so this is a scalar equation in contrast to Eq. 11.28. When motion of the body does not lie in a single plane, the situation becomes a bit more complicated, since the proper representation of inertia is then a tensor, not a scalar.

### 11.3.1 Finding Mass and Moment of Inertia

Finding the mass of a component is straightforward. The element may either be weighed directly on a scale or the mass can be determined from knowledge of the element's density and geometry. In this latter case, the mass is given simply by integrating the density over the volume of the body:

$$m = \int_{\text{rigid body}} \rho dV. \tag{11.30}$$

Similarly, Eq. 11.21 can be directly used to obtain the moment of inertia of a body about a given point. Moments of inertia of simple geometries can often be found in tables, Popov (1976), Fenster and Gould (1985). As a first approximation, complex objects can often be broken into one or more simple shapes and the moments of inertia (about the center of mass of the combination of shapes) summed. Moments of inertia can also be obtained experi-

mentally. While there are several ways to accomplish this, one of the more common methods is to calculate the natural frequency of a pendulum made from the object (an interesting application of this to moment of inertia calculation for passenger cars is described by Garrott and Monk (1988)). The following simple example describes the direct use of the formulas for determining the mass, center of mass, and moment of inertia of a flat plate.

**EXAMPLE** Consider the square plate with sides of length  $s$ , a thickness  $t$ , and a density  $\rho$  shown in Fig. 11.6. The mass of the plate is given by

$$m = \int_{\text{rigid body}} \rho dV = \rho t \int_{x=0}^s \int_{y=0}^s dx dy = \rho t xy \Big|_{\substack{x=s \\ y=s}} = \rho s^2 t.$$

The coordinates of the center of gravity of the plate are given by

$$y_{cg} = x_{cg} = \frac{1}{m} \int_{x=0}^s x \rho(st) dx = \frac{\rho st}{m} \frac{x^2}{2} \Big|_{x=0}^s = \frac{\rho s^3 t}{2m} = \frac{\rho s^3 t}{2\rho s^2 t} = \frac{s}{2}$$

which, of course, describe the center of the plate. The moment of inertia about the center of the plate is

$$\begin{aligned} J_{cg} &= \int_{\text{plate}} r_{cg}^2 dm = \int_{x=-s/2}^{s/2} \int_{y=-s/2}^{s/2} (x^2 + y^2) \rho t dx dy \\ &= \rho t \int_{x=-s/2}^{s/2} \int_{y=-s/2}^{s/2} x^2 dx dy + \rho t \int_{x=-s/2}^{s/2} \int_{y=-s/2}^{s/2} y^2 dx dy \\ &= \rho t s \int_{x=-s/2}^{s/2} x^2 dx + \rho t s \int_{y=-s/2}^{s/2} y^2 dy = 2\rho t s \frac{x^3}{3} \Big|_{x=-s/2}^{s/2} = \frac{\rho t s^4}{6} = \frac{1}{6} m s^2. \end{aligned}$$

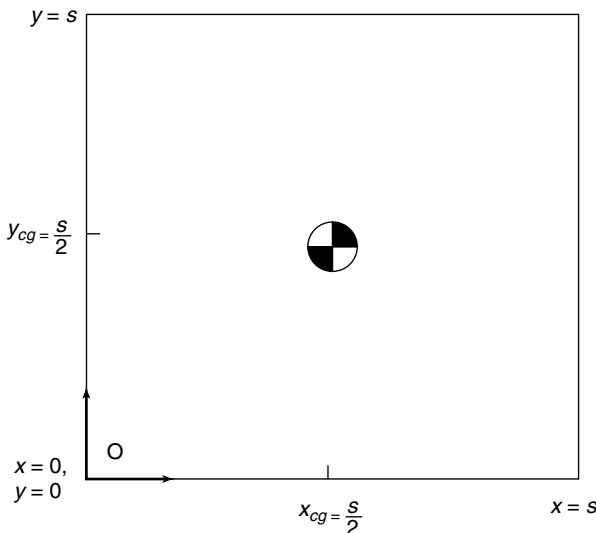


FIGURE 11.6. Square plate of uniform density.

### 11.3.2 Moving Moments of Inertia to Other Points

Sometimes the moment of inertia about the center of mass is known, but the moment of inertia about another point on the body is required. While the moment of inertia about the desired point could be calculated directly, it is often easier to simply move the moment of inertia. If the distance between the center of mass and the point  $O$  where the moment of inertia is desired is given by  $d$ , the two moments of inertia are related by the parallel-axis theorem

$$J_o = J_{cg} + md^2. \quad (11.31)$$

As with the previous results, planar motion is assumed (though an analogous result holds for spatial motion with proper definition of the distance  $d$  and the axes of rotation). This relationship can be proven easily by substituting the expression

$$x_o = x_{cg} + \bar{x} \quad y_o = y_{cg} + \bar{y} \quad (11.32)$$

into Eq. 11.21 and realizing that

$$d^2 = \bar{x}^2 + \bar{y}^2. \quad (11.33)$$

**EXAMPLE** Continuing with the example of the flat plate in Fig. 11.6, suppose that the plate is pinned to rotate around point  $O$ . From the discussion above, the kinetic energy can be described in terms of the angular velocity and the moment of inertia about point  $O$ . To derive the moment of inertia about point  $O$  from the moment of inertia about the center of mass, the parallel axis theorem can be used

$$J_o = J_{cg} + m\left(\frac{s}{\sqrt{2}}\right)^2 = J_{cg} + \frac{1}{2}ms^2.$$

As a check, the moment of inertia about  $O$  can be derived using the basic formula:

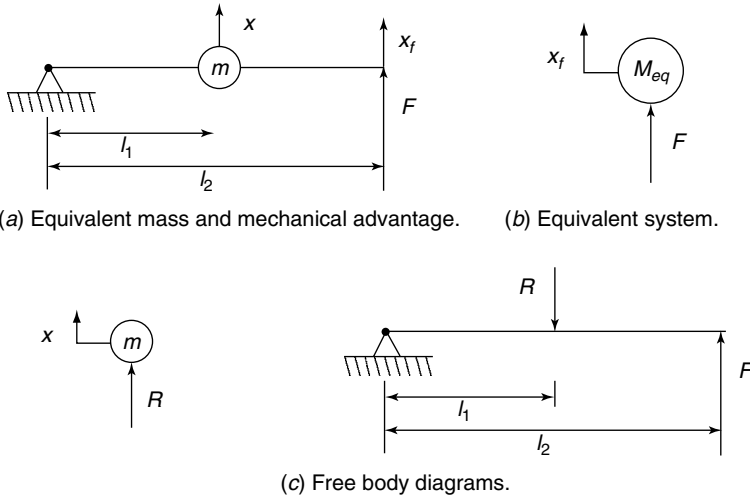
$$\begin{aligned} J_o &= \int_{\text{plate}} r_o^2 dm = \int_{y=0}^s \int_{x=0}^s (x^2 + y^2) \rho t dx dy \\ &= 2\rho t s \frac{x^3}{3} \Big|_{x=0}^s = \frac{2\rho t s^4}{3} = \frac{2}{3}ms^2 = J_{cg} + \frac{1}{2}ms^2 \end{aligned}$$

which gives the same result, albeit with a fair amount more work.

### 11.3.3 Equivalent Mass or Inertia

While the mass and inertia of each component in the system can be determined, the mass of interest in dynamic modeling is generally not the mass of each individual component, but rather the “equivalent mass” of the components connected as they are in the system. This is particularly true when model reduction is used to reduce the number of degrees of freedom and lump multiple masses and inertias together. The equivalent mass is, loosely speaking, the mass “felt” by an observer at a particular reference point in the system. While this may seem to be a somewhat abstract concept, it is nothing more than a consequence of the familiar concept of mechanical advantage.

Figure 11.7 demonstrates this. Suppose that the mass  $m$  is rigidly attached to a massless rod a distance  $l_1$  from the pivot and a force  $F$  is applied to the rod a distance  $l_2$  from



(a) Equivalent mass and mechanical advantage. (b) Equivalent system.

(c) Free body diagrams.

**FIGURE 11.7.** Equivalent mass and mechanical advantage.

the pivot as in Fig. 11.7a. For simplicity, assume that the rod swings in a horizontal plane (so that gravity acts normal to the page and does not enter this analysis) and that only small motions occur (so that the motion may be treated as linear and small angle approximations used). Since there is only one degree of freedom in this case, the system can be replaced by the equivalent system in Fig. 11.7b and the equation of motion given by

$$F = M_{eq} \ddot{x}_f. \tag{11.34}$$

Because of the mechanical advantage provided by the rod and pivot, the equivalent mass is not simply the mass  $m$ . One way to derive the equivalent mass is to separate the mass and rod by a reaction force  $R$  as shown in Fig. 11.7c. The equation of motion of the mass can then be given by

$$R = m\ddot{x}. \tag{11.35}$$

Similarly, a moment balance on the massless rod gives

$$F = R \frac{l_1}{l_2} \tag{11.36}$$

and the kinematics of the rod and pivot determine the relationship between  $x$  and  $x_f$

$$\frac{x}{l_1} = \frac{x_f}{l_2}. \tag{11.37}$$

Combining these expressions gives:

$$F = m\ddot{x} \left( \frac{l_1}{l_2} \right) = m \left( \frac{l_1}{l_2} \right) \ddot{x}_f \left( \frac{l_1}{l_2} \right) = m \left( \frac{l_1}{l_2} \right)^2 \ddot{x}_f. \tag{11.38}$$

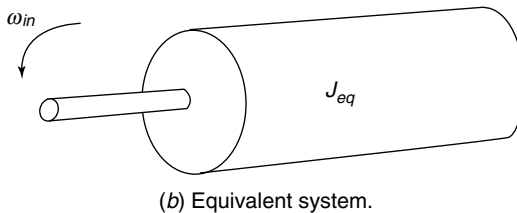
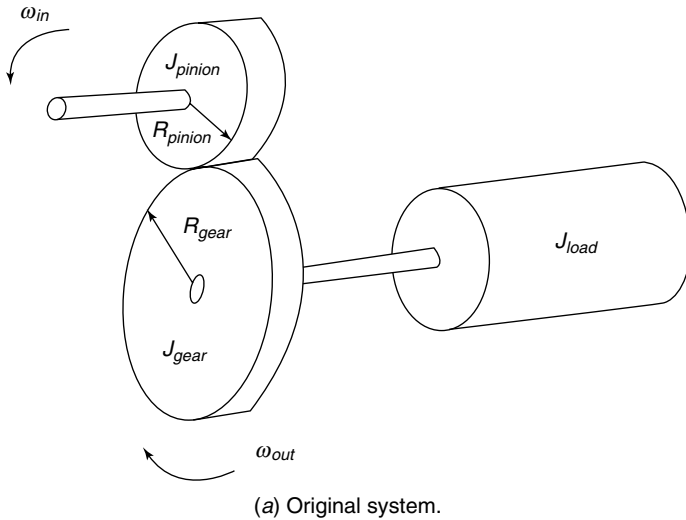
So the equivalent mass is

$$M_{eq} = m \left( \frac{l_1}{l_2} \right)^2. \quad (11.39)$$

The mass associated with the equivalent model therefore depends upon the amount of mechanical advantage provided by the lever formed by the rod and the pivot.

There are two ways to calculate the equivalent mass of a system. The first is to balance reaction forces as in the example above. This method has an advantage in that the equations of motion are developed concurrently, though it is the more tedious of the two approaches. The other method is to consider the kinetic energy of the original model and the lumped model. Masses and inertias store energy in the form of kinetic energy, so for the lumped model to represent the original, the kinetic energy of the two systems must be the same. This works not only for masses but also for inertias, as demonstrated in the following example.

**EXAMPLE** Figure 11.8a illustrates a simple model of a geared system with an inertial load. Each gear and the load are assumed to have inertia and the desired model is an equivalent inertia reflected to the input shaft (Fig. 11.8b). The kinetic energy of the original system is



**FIGURE 11.8.** Geared system.

$$KE = \frac{1}{2} J_{pinion} \omega_{in}^2 + \frac{1}{2} (J_{gear} + J_{load}) \omega_{out}^2$$

and the kinetic energy of the lumped parameter system is

$$KE = \frac{1}{2} J_{eq} \omega_{in}^2.$$

The equivalent inertia can be obtained by equating the two expressions for the kinetic energy and incorporating the kinematics of the system. In this case, the kinematic relationship is simply the gear ratio or

$$\omega_{out} = \left( \frac{R_{pinion}}{R_{gear}} \right) \omega_{in}.$$

This gives

$$\frac{1}{2} J_{eq} \omega_{in}^2 = \frac{1}{2} J_{pinion} \omega_{in}^2 + \frac{1}{2} (J_{gear} + J_{load}) \left( \frac{R_{pinion}}{R_{gear}} \right)^2 \omega_{in}^2$$

so

$$J_{eq} = J_{pinion} + (J_{gear} + J_{load}) \left( \frac{R_{pinion}}{R_{gear}} \right)^2.$$

This would be the inertia felt by a motor or person turning the input shaft. Conversely, if the motor were attached to the output shaft, the elements in Fig. 11.8 would have an equivalent inertia of

$$J_{eq} = J_{gear} + J_{load} + \left( \frac{R_{gear}}{R_{pinion}} \right)^2 J_{pinion}.$$

Because of the analogy to mechanical advantage, it is not surprising that the equivalent inertia of a system depends upon the reference point chosen.

## 11.4 SPRINGS AND POTENTIAL ENERGY

In system modeling, the term “spring” refers not only to machine elements such as coil, torsional, or leaf springs, but to any component of the system that deflects in response to load. In other words, every part of the system that is not assumed to be perfectly rigid acts as a spring for the purposes of modeling. Springs selected from a catalog and compliant elements share several properties. Most fundamentally, they are described by some relationship between deflection and the force applied at either end of the spring. This is most commonly modeled as a linear relationship

$$F = K\delta \tag{11.40}$$

keeping in mind that the force exerted by the spring always acts to oppose the compression or extension. The value  $K$  is known as the spring stiffness or spring rate and has units of force/distance with lbf/in and N-m being common. In Eq. 11.40, the deflection  $\delta$  is measured from the free or unstretched length,  $L_f$ , of the spring and  $F$  is the force exerted on the spring (Fig. 11.9).

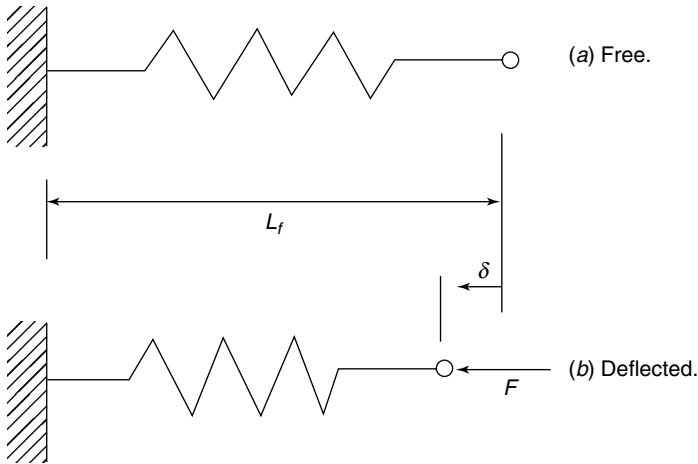


FIGURE 11.9. Spring deflection.

There are several reasons why a linear spring model is a useful approximation. First, systems described by combinations of masses, linear springs, and linear dampers possess linear equations of motion. These are more readily analyzed than general nonlinear forms. The linear description is also compact, requiring only a single parameter (the rate of stiffness) to describe the spring. From a practical standpoint, linearity proves to be a reasonable assumption for most physical springs, at least within a small range of deflection. If more accuracy is desired, however, springs can instead be represented as a general nonlinear function such as:

$$F = f_s(\delta). \quad (11.41)$$

Such expressions can be useful in describing the bottoming out behavior of coil springs, for instance. The only constraint is that the function must be a nondecreasing function of displacement in order to capture the desired physical characteristics of a spring.

A second property that mechanical springs and compliant elements share is the storage of energy. It requires work to displace a spring from its free length and, if the spring is assumed ideal, all of that work is stored in the spring. As a result, the amount stored (the spring's potential energy) can be found by integrating the work done on the spring. For the general nonlinear spring form given above,

$$PE(\delta) = \int_0^{\delta} f_s(\eta) d\eta. \quad (11.42)$$

For the linear spring in Eq. 11.41, displaced a distance  $x$  from its unstretched length, this translates to the familiar expression

$$PE = \int_0^{\delta} K\eta d\eta = \frac{1}{2}K\delta^2. \quad (11.43)$$

As with the force, the only spring properties needed to determine the amount of energy stored are the spring rate and the unstretched length. Spring rates can be determined experimentally by applying a known force and measuring deflection (or deflecting a

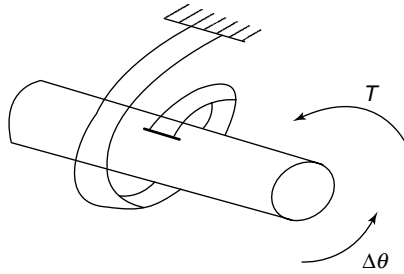


FIGURE 11.10. A Torsional Spring.

known amount and measuring force) but can also be determined analytically for a number of simple geometries.

Torsional springs (Fig. 11.10) are completely analogous to the linear springs described above but relate torque and angular deflection instead of torque and linear deflection. The corresponding expressions for torsional springs are:

$$T = K_r \Delta\theta \quad (11.44)$$

where  $K_r$  is the torsional spring rate (in units of torque/angle such as in-lbf/rad or Nm/rad)  $T$  is the torque exerted by the spring and  $\Delta\theta$  is angle through which the spring is turned, relative to its equilibrium position. The potential energy in the spring is given by:

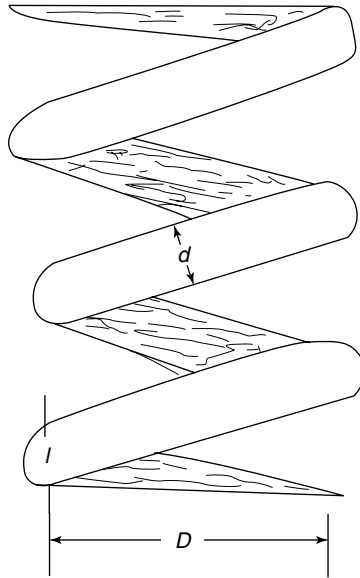
$$PE = \int_0^{\Delta\theta} K_r \eta d\eta = \frac{1}{2} K_r \Delta\theta^2. \quad (11.45)$$

### 11.4.1 Coil Springs

While many types of manufactured springs exist, coil springs are one of the most commonly used springs in cam systems. Coil springs may be used in either extension or compression, depending upon the design of their ends. Figure 11.11 illustrates a typical compression coil spring such as the type used in automotive suspensions. The spring rate for a coil spring in axial tension or compression is given by

$$K = \frac{Gd^4}{8D^3N} \quad (11.46)$$

where  $d$  is the diameter of the spring wire,  $D$  is the diameter of the spring coil (measured from the center of the spring wire),  $G$  is the shear modulus of the material, and  $N$  is the number of active coils.  $N$  does not need to be an integer and does not include ground ends that are pressed against the mating surface at either end of the spring since these do not participate in the compression or extension of the spring. Values of  $G$  for various spring materials may be found in engineering handbooks: a typical value used for steel springs when no additional information is available is  $11.0 \times 10^6$  psi. Coil springs may be designed in such a way that the diameters  $d$  and  $D$  change over the length of the spring. As a first order approximation, spring rates in such cases can be estimated by using the average values of these parameters.



**FIGURE 11.11.** Coil spring (2.5 active coils illustrated).

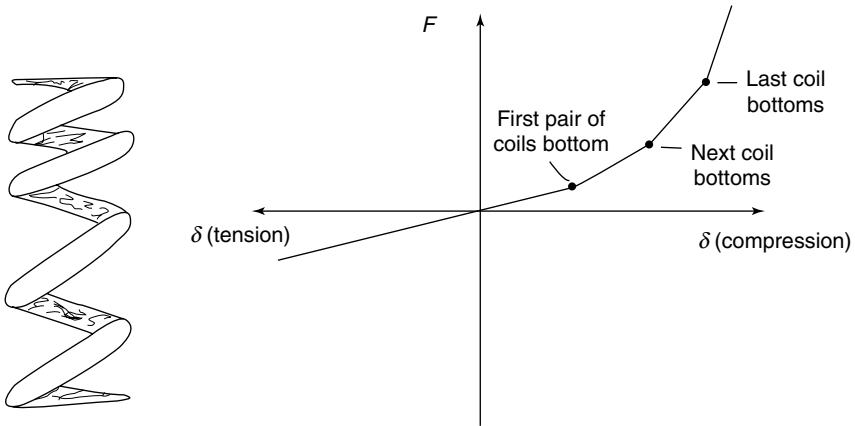
A coil spring reaches its maximum compression when all coils have been pushed tightly together. For a compression spring with ground (flat) ends, this happens at a length of

$$L = N_s d \quad (11.47)$$

where  $N_s$  is the total number of coils in the spring. When a spring is compressed to its minimum length, it is said to have *bottomed out*. At the point where a spring bottoms out, the spring rate increases greatly, since further compression requires deformation in the packed spring wires. This characteristic is sometimes exploited to create progressive springs in which the spring rate increases as the spring is compressed. Figure 11.12a illustrates a compression spring with varying pitch. Unlike the constant pitch spring, where all coils bottom out at once, the more closely spaced coils on a variable pitch spring bottom out at a lower spring deflection than the more widely spaced coils. When a coil bottoms out, the effective number of coils is reduced, so the spring displays a stiffening characteristic in compression, as illustrated in Fig. 11.12b. Note that the bottoming out effect only occurs in compression, since the coils continually move further apart when a coil spring is placed in tension.

#### 11.4.2 Compliance of Other Mechanical Elements

Spring rates for any element in the system can be obtained through experimental testing of the force-displacement relationship or, for simple geometries, from basic results from mechanics of materials. A few common force-deflection relationships for simple geometries and their corresponding spring rates are listed in Table 11.1; many more can be found in engineering handbooks or textbooks on the mechanics of materials (Popov, 1976, Chen, 1982, Relvas, 1985, Ungar, 1985). If the desired relationship is not readily available, spring



(a) Shape of spring.

(b) Force-deflection curve.

**FIGURE 11.12.** Variable-pitch coil spring.

rates can be easily derived from a basic stress analysis. First, choose a simplified geometry that approximates the shape of the element in question. Next, calculate the stress arising in the element as a result of the applied load. If it is assumed that the element is acting in the region of elastic deformation (a reasonable assumption for the systems in question here since they must be designed to survive cyclic motion and loading), the stress can then easily be related to strain. Finally, the deflection can be calculated from the strain and the spring rate determined from this relationship between force and deflection. This procedure is illustrated by a simple example.

**EXAMPLE** Suppose a system uses a long rod (Fig. 11.13) loaded axially to transmit force between members (this is in fact the case in pushrod engines). The rod does not in fact remain perfectly rigid, but deflects as a result of the applied load. The axial stress that arises in the rod is given by

$$\sigma = \frac{F}{A}$$

where  $A$  is the cross-sectional area of the rod. In the linear region, the strain is proportional to the stress through Young's modulus, so

$$\varepsilon = \frac{\sigma}{E} = \frac{F}{EA}$$


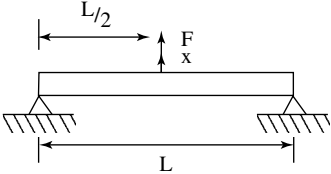
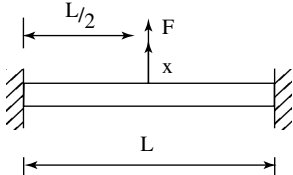
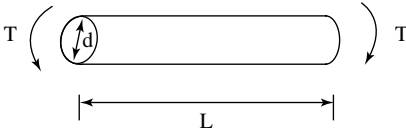
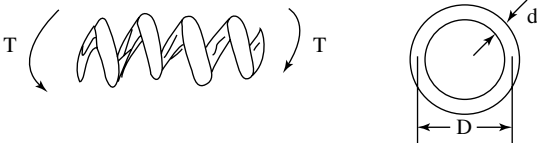
Finally, the strain is simply deflection per unit length, so the deflection of the rod is

$$\delta = L\varepsilon = \frac{FL}{EA}$$

The spring rate follows directly from this expression, so for the axially loaded rod

$$K = \frac{F}{\delta} = \frac{EA}{L}$$

**TABLE 11.1** Equivalent Linear and Rotary Spring Constants

Linear system	Spring constant ( $K = F/x$ )
Cantilever Beam	
	$\frac{1}{4}Eb \left(\frac{h}{L}\right)^3$
Simply Supported Beam	
	$4Eb \left(\frac{h}{L}\right)^3$
Beam Clamped at Both Ends	
	$16Eb \left(\frac{h}{L}\right)^3$
Rotary system	Spring constant ( $K_1 = T/\Delta\theta$ )
Circular Bar in Torsion	
	$\frac{\pi Gd^4}{32L}$
Coil Spring in Torsion	
	$\frac{Ed^4}{64ND}$

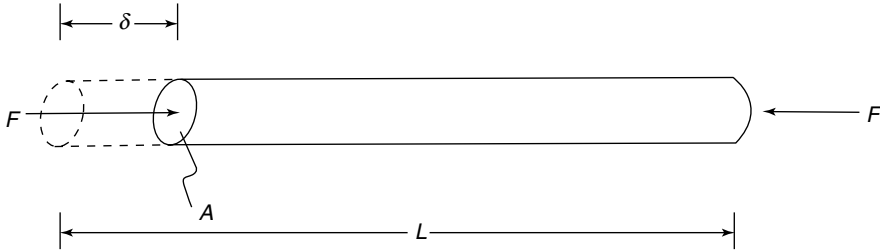
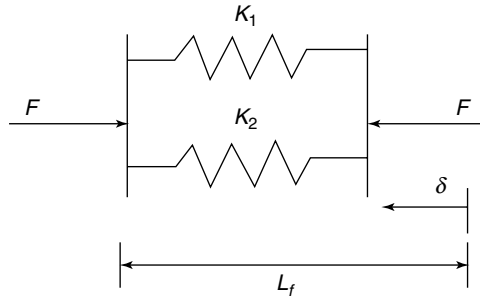
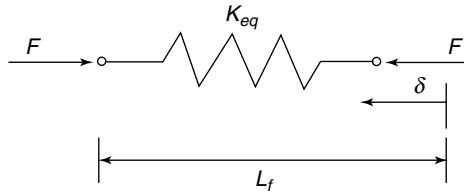


FIGURE 11.13. Rod in axial compression.



(a) Springs in parallel.



(b) Equivalent single spring.

FIGURE 11.14. Parallel spring equivalence.

### 11.4.3 Combinations of Springs

If combinations of springs are connected by elements that are assumed to be massless, the combination can be replaced with a single spring of equivalent stiffness and free length. The need for this often arises as a result of model reduction where a mass has been assumed to be zero (as with the suspension in Fig. 11.3c). There are two possible ways to connect springs, known as parallel and series connections.

**11.4.3.1 Springs in Parallel.** Two springs connected in parallel, as shown in Fig. 11.14a, can be replaced by the single spring in Fig. 11.14b to simplify modeling. The spring constant for the equivalent spring can be found by realizing that two springs in parallel are constrained to have the same deflection. Thus, if the two springs deflect by a distance  $\delta$  in response to an applied force  $F$ , the first spring will produce a force

$$F_1 = K_1 \delta \quad (11.48)$$

while the second spring produces a force

$$F_2 = K_2 \delta. \quad (11.49)$$

The sum of these forces must equal the applied force  $F$  so

$$F = F_1 + F_2 = (K_1 + K_2) \delta = K_{eq} \delta. \quad (11.50)$$

Clearly, the equivalent spring stiffness is therefore

$$K_{eq} = K_1 + K_2. \quad (11.51)$$

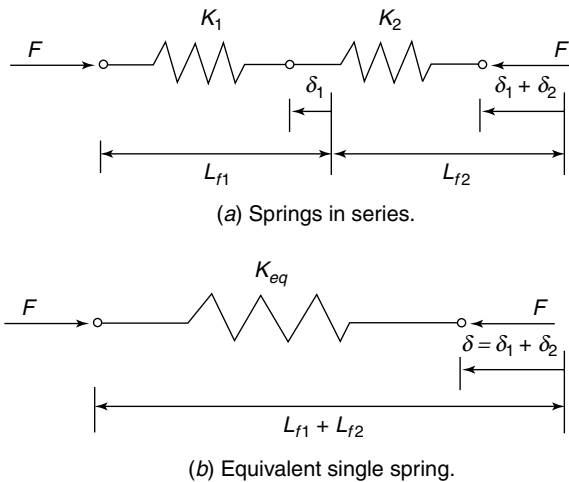
Since the equivalent stiffness is simply the sum of the two individual spring stiffnesses, if the two springs have very different stiffnesses, the equivalent stiffness will be dominated by the spring with higher stiffness.

**11.4.3.2 Springs in Series.** Two springs connected end-to-end, as shown in Fig. 11.15a, are defined to be connected in series. These springs can also be replaced by a single equivalent spring in Fig. 11.15b. The stiffness of the equivalent spring can be derived by realizing that the forces must sum to zero at the point where the springs connect for the spring to be in equilibrium. As a result, the force exerted on each spring is the same

$$F_1 = F_2 = F. \quad (11.52)$$

The deflection in each spring is different with the total deflection of the system equal to the sum of the two spring deflections. Taking this information together with the spring stiffnesses,

$$\delta = \delta_1 + \delta_2 = \frac{F_1}{K_1} + \frac{F_2}{K_2} = F \left( \frac{1}{K_1} + \frac{1}{K_2} \right) = \frac{F}{K_{eq}}. \quad (11.53)$$



**FIGURE 11.15.** Series spring equivalence.

So

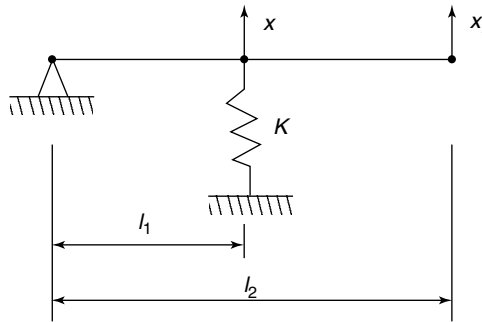
$$\frac{1}{K_{eq}} = \left( \frac{1}{K_1} + \frac{1}{K_2} \right). \tag{11.54}$$

In contrast to springs in parallel, if two springs connected in series have very dissimilar stiffnesses, the equivalent stiffness will be dominated by (yet even lower than) the spring with the lower stiffness. The same rules for series and parallel connections hold for torsional springs.

**11.4.4 Equivalent Springs and Mechanical Advantage**

A spring combined with some mechanical advantage has an equivalent spring constant that is directly analogous to the equivalent mass or inertia discussed previously. Instead of equating the kinetic energy to determine the equivalent mass, however, the potential energies of the two systems are equated to give an equivalent stiffness or spring rate.

**EXAMPLE** Figure 11.16a shows a lever arm with a spring attached. To get the equivalent system of Fig. 11.16b, which is referred to the displacement  $x_f$ , it is necessary to equate the potential energies of the two systems. Assuming small displacements, the potential energy of the original system is



(a) Original system.



(b) Equivalent system.

**FIGURE 11.16.** Equivalent spring stiffness and mechanical advantage.

$$PE = \frac{1}{2} Kx^2$$

while the potential energy of the equivalent system is

$$PE = \frac{1}{2} K_{eq} x_f^2.$$

Since for small angles, the relationship between  $x$  and  $x_f$  is

$$\frac{x}{l_1} = \frac{x_f}{l_2}.$$

Using this expression for  $x$  above gives

$$K_{eq} = K \left( \frac{l_1}{l_2} \right)^2.$$

When  $l_1 > l_2$ , the spring appears stiffer than its physical stiffness, while for  $l_1 < l_2$ , the equivalent stiffness is less than the physical stiffness of the spring because of the mechanical advantage.

### 11.4.5 Massive Springs

Up to this point, the springs considered have been ideal springs and have had no mass associated with them. In practice, it is often acceptable to model real springs as ideal springs if the mass of other elements in the system dominates the mass of the springs. This is not always the case, however, and real springs may need to be modeled as a combination of an ideal spring and a lumped mass. The equivalent mass of a massive spring (Fig. 11.17) can be derived by applying the concepts used in the previous section.

Since the spring is a continuum, the kinetic energy is given by

$$KE = \frac{1}{2} \int_{spring} v^2(x) dm. \quad (11.55)$$

If the mass is evenly distributed along the length of the spring,

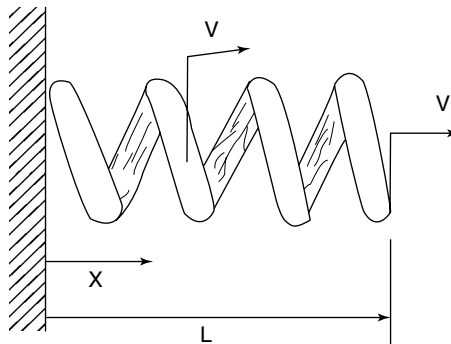


FIGURE 11.17. Spring with mass.

$$dm = \frac{m_s}{L} dx. \quad (11.56)$$

Assuming that the spring compresses uniformly, the velocity profile along the spring can be interpolated between the end points. At  $x = 0$ , the spring is fixed, so the velocity is zero; at  $x = L$ , define the velocity as  $v_L$ . The velocity at any point  $x$  between 0 and  $L$  is therefore

$$v = \frac{x}{L} v_L. \quad (11.57)$$

Putting these together, the expression for kinetic energy gives

$$KE = \frac{1}{2} \int_0^L \frac{x^2}{L^2} v_L^2 \frac{m_s}{L} dx = \frac{1}{2} \frac{m_s v_L^2}{L^3} \int_0^L x^2 dx = \frac{1}{2} \frac{m_s v_L^2}{L^3} \frac{L^3}{3} = \frac{1}{2} \frac{m_s}{3} v_L^2. \quad (11.58)$$

Equating this expression with the kinetic energy of a single equivalent mass attached at the end of the spring ( $x = L$ ), the equivalent mass is simply

$$m_{eq} = \frac{m_s}{3}. \quad (11.59)$$

So a spring with mass can be represented by a combination of an ideal spring with the same spring constant and an equivalent mass of one-third of the spring mass attached to the moving end of the spring. Similar techniques can be used to obtain equivalent masses for other distributed masses for which the rigid body assumption is not a good approximation. Such systems are better analyzed using other techniques, however (Ungar, 1985), so this is not detailed here.

## 11.5 DAMPERS AND DISSIPATION

---

Unlike mass or inertia elements, which store kinetic energy, and springs, which store potential energy, damping elements cannot store energy at all. Instead, they remove energy from the system. Without dampers, systems modeled as combinations of masses and dampers would always conserve energy. Since real systems can, at best, only approximate conservative systems, models without dampers tend to underestimate the force or energy needed to produce a certain system motion. The main reason for including dampers in a system model is to capture this energy dissipation effect and more accurately describe the magnitude of input necessary to produce a given output or the amplification at resonance. As noted before, the addition of damping does not reduce the number of natural frequencies or degrees of freedom of a system.

As with springs, damping elements describe both components intentionally designed to remove energy from the system (such as dashpots and automotive shock absorbers) and the inherent energy dissipation of other system elements. All elements contribute in some way to energy dissipation, either through material damping in springs and structural members or, more importantly, through friction in bearings and other surface contacts. In contrast to mass and compliance (or spring) properties, it is generally extremely difficult to obtain simple analytical expressions for the amount of damping in a system. Damping in a gearbox, for instance, will depend upon a number of factors including the type and condition of lubricant, the alignment of the shafts, and the condition and quality of the gears. Unless data is available for the element from the manufacturer (as is the case with

shock absorbers) or the system fits a form easily modeled as with the examples in Chen (1982), damping results are usually obtained experimentally.

Damping results from motion, and as such, experimental determination of damping is complicated by the fact that the system must be maintained in motion in order to generate damping forces. As a result, it is rarely worth the effort to fixture each component separately to estimate its damping. Furthermore, since frictional effects occur at the interface between components, it may even be impossible to determine the amount of damping by looking at components individually. Because of these issues, damping is usually determined experimentally by choosing a form or forms of damping and using experimental data from the overall system to fit the parameters in those forms. Thus damping is often added to a system model after masses and stiffnesses have been determined and the appropriate reductions made. Accordingly, the approach of this section is somewhat different than the previous sections. Instead of the main focus being on the combination of individual damping elements, this section focuses on describing the broad classes of damping models commonly encountered and appropriate conditions for the use of each.

### 11.5.1 Viscous or Speed-Dependent Damping

The most common form of damper applied in linear systems modeling is a damping force that is proportional to the relative velocity of two coordinates in the system. A typical schematic for such a damper is illustrated in Fig. 11.18. The damping force thus takes the form

$$F = b\dot{\delta} \quad (11.60)$$

where  $b$  is known as the damping coefficient, which has units of force/velocity such as lbf/(in/s) or N/(m/s). As with spring forces, the force exerted by a damper always acts to oppose the relative motion. This form of damping is often called viscous friction since it captures the effects of damping due to viscosity effects in fluids quite well. For instance, given a moving plate sliding over a fixed plate as in Fig. 11.19, the force exerted by the fluid on the plate is

$$F = \frac{\mu A}{h} \dot{\delta} \quad (11.61)$$

where  $\mu$  is the coefficient of absolute viscosity and  $A$  is the surface area (Chen, 1982). This clearly fits the form of Eq. 11.60. Viscous friction is a good model for damping in bearings and other lubricated parts of the cam-follower system. Rotary versions of the damper in Fig. 11.18 can be defined analogously by

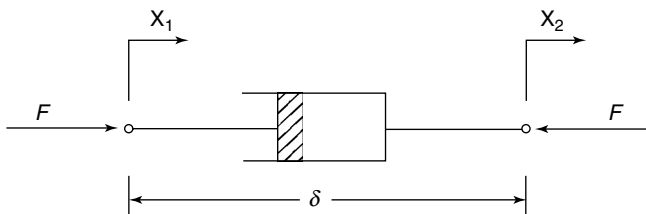


FIGURE 11.18. Schematic illustration of a damper.

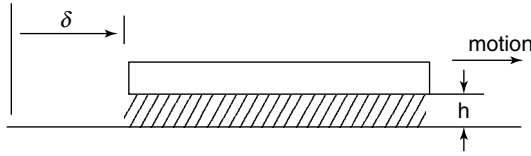


FIGURE 11.19. Sliding plate with viscous friction.

$$T = b_r \omega \quad (11.62)$$

as illustrated in the example later in this section. In this case, the units of the damping coefficient,  $b_r$ , take the form of torque/angular velocity, such as ft-lbf/(rad/s) or Nm/(rad/s). More general damping laws can also be used. For instance, a power-law dependence upon position may be added, giving a damping force of

$$F = b \delta^n \dot{\delta} \quad (11.63)$$

as is commonly done for simulating damping due to impact (Hunt and Crossley, 1975; Herbert and McWhannell, 1977).

The dissipated power, or the rate at which a linear viscous damper of the form in Eq. 11.60 dissipates energy, is

$$P_{\text{viscous}} = F \dot{\delta} = b \dot{\delta}^2. \quad (11.64)$$

From this expression, it is clear that power is dissipated regardless of the direction of motion since the damping force always acts to oppose the relative motion of the two moving parts in the damper. No power is dissipated when the system is at rest. Furthermore, the power dissipated depends only upon the velocity of the system and grows as the square of the velocity. Damping factors are the most difficult to pin down in analysis. The choice of the value of a damping factor of 0.03 for structural damping and 0.04 to 0.08 for well-lubricated machine (closed lubrication) components is considered reasonable. For open lubrication systems the damping factors are higher depending on the contaminants.

### 11.5.2 Coulomb or Dry Friction

In contrast to viscous friction, where the damping force depends upon the relative velocity between the two elements, friction between dry surfaces depends only upon the direction of the velocity and not its magnitude. The amplitude of the damping force is determined by the normal force at the interface and the coefficient of friction between the surfaces. For the system in Fig. 11.20, therefore, the damping force can be represented by

$$F = \mu F_n \text{sgn}(\dot{\delta}) \quad (11.65)$$

where  $\text{sgn}(x)$  denotes the sign of  $x$  (positive or negative) since the force always acts to oppose motion. The power dissipated by this model is

$$P_{\text{coulomb}} = F \dot{\delta} = \mu F_n \text{sgn}(\dot{\delta}) \dot{\delta}. \quad (11.66)$$

As with the viscous friction model, the power dissipated depends upon the velocity. Unlike the viscous friction model, this dependence is linear, not quadratic. The power also scales

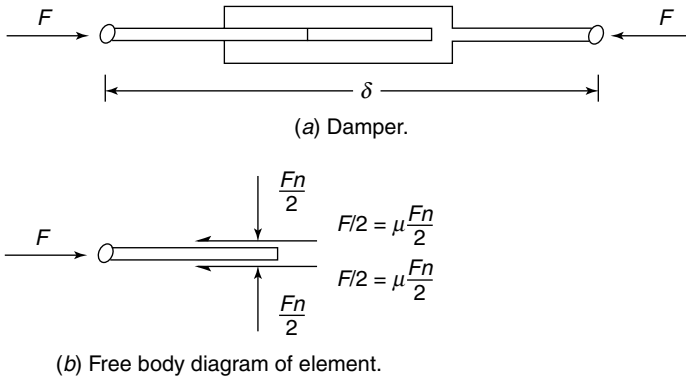


FIGURE 11.20. Dry friction damper.

with the normal force, meaning that more power will be dissipated if a heavier load is moved. From the standpoint of choosing an appropriate friction model, these characteristics can be used to determine whether a viscous friction or Coulomb friction model is a closer representation. As the term “dry friction” implies, Coulomb friction models are often useful when dry lubricants are used between moving surfaces. The usefulness of the model is not limited to such cases, however, since transmissions with grease or oil lubricants also exhibit Coulomb friction. Consequently, a combination of models is often used to capture the behavior of real systems. For example, Pisano (1984) and Hanachi and Freudenstein (1986) demonstrated the need for Coulomb friction models in high-speed cam modeling despite the presence of lubricating oil.

It is commonly known that the friction coefficient in Eq. 11.65 is higher when the system is at rest (static friction) than when the system is moving (dynamic friction). This relationship can be captured in a smooth manner by a slightly more complicated version of the friction force (Friedland, 1996).

$$F = (\mu_k + (\mu_s - \mu_k)e^{-c|\dot{\delta}|})F_n \operatorname{sgn}(\dot{\delta}) \quad (11.67)$$

where  $\mu_k$  is the kinetic coefficient of friction,  $\mu_s$  is the static coefficient of friction and  $c$  is a positive number used to produce a smooth transition between the two coefficients (the larger the value of  $c$ , the more abrupt the change between static and dynamic friction). This model is still not sufficient to capture “sticktion” or “stick-slip” friction where the difference between static and dynamic friction values causes a system to move intermittently. Capturing such effects is challenging because of the discontinuity involved as the system transitions between stasis and motion. Models for stick-slip friction are available, Karnopp (1985), Haessig and Friedland (1991) but can be numerically difficult to implement.

### 11.5.3 Mechanical Efficiency

Although mechanical efficiency does not take the form of the damping element illustrated in Fig. 11.18, it does represent a form of system damping and can often be an effective way to model dissipation in the system. Mechanical efficiency,  $\eta$ , is defined in terms of the ratio of input power to output power for a certain subsystem such as a gear train

$$\eta = \frac{P_{out}}{P_{in}}. \quad (11.68)$$

To make physical sense, the value of  $\eta$  must lie between zero (completely inefficient) and one (perfectly efficient). The power lost due to dissipation is simply the difference between the input and output power or

$$P_{eff} = P_{in} - P_{out} = (1 - \eta)P_{in}. \quad (11.69)$$

The power dissipated depends upon the amount of power being transmitted through the subsystem and so, like Coulomb friction, depends upon both the applied load and the speed of the system. Gearboxes, lead screws, and other transmission devices are often successfully modeled using an overall efficiency to account for system damping. Mechanical efficiency is somewhat different than the viscous or dry friction models presented above since its inclusion alters the effective mass, stiffness, and damping of the system. Qualitatively, the loss of efficiency associated with an inefficient transmission makes everything downstream of the transmission “feel” heavier, stiffer, and more damped. This effect is illustrated in the example in the following section.

### 11.5.4 Combinations and Equivalent Dampers

As mentioned before, one of the most common ways of adding damping to a system is to choose an appropriate form for the damping and determine the parameters experimentally. If, however, damping values are known for individual dampers in the system, these elements may be combined according to the same rules as springs. If two dampers have damping coefficients of  $b_1$  and  $b_2$ , a single equivalent damper has a damping coefficient of

$$b_{eq} = b_1 + b_2 \quad (11.70)$$

if the dampers are combined in parallel and

$$\frac{1}{b_{eq}} = \frac{1}{b_1} + \frac{1}{b_2} \quad (11.71)$$

if the dampers are combined in series. The same relations hold for rotary dampers combined in series or parallel. Furthermore, if dampers are integrated into a system in a way that incorporates mechanical advantage, this must also be taken into account to determine an equivalent damping coefficient.

**EXAMPLE** Consider a modification to the gear example in Sec. 11.3 with viscous damping added to both the input and output shafts and an overall mechanical efficiency assigned to the gear pair (Fig. 11.21a). Assume for simplicity that the inertia of the gears are small enough relative to the inertia of the load that they may be ignored and the goal is to reduce this system to the equivalent system in Fig. 11.21b. The power into the gearbox is

$$P_{in} = (T_{in} - b_{rin}\omega_{in})\omega_{in}$$

while the power out of the gearbox is

$$P_{out} = (b_{rou}\omega_{out} + J_{load}\dot{\omega}_{out})\omega_{out}.$$

Using the definition of efficiency from Eq. (11.67), the input and output power expressions give

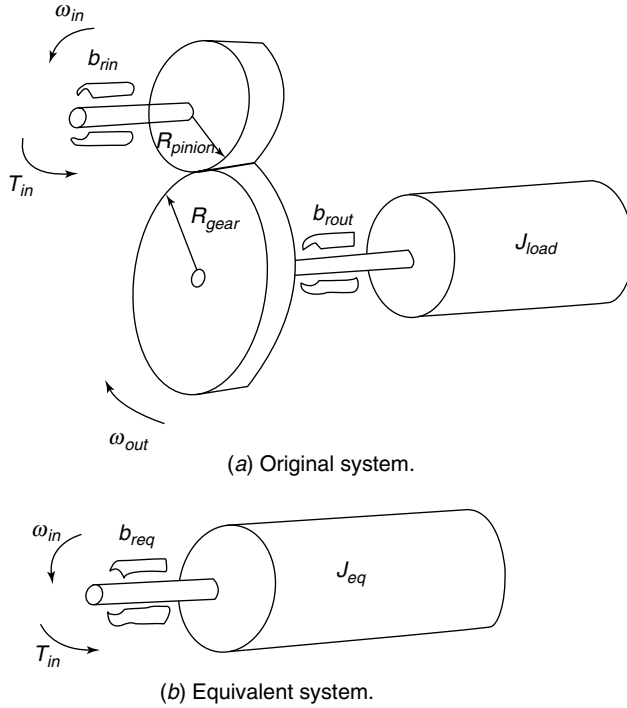


FIGURE 11.21. Geared system with damping.

$$(b_{rout}\omega_{out} + J_{load}\dot{\omega}_{out})\omega_{out} = \eta(T_{in} - b_{rin}\omega_{in})\omega_{in}$$

so

$$T_{in} = \frac{1}{\eta} \left[ \left( \frac{\omega_{out}}{\omega_{in}} \right) (b_{rout}\omega_{out} + J_{load}\dot{\omega}_{out}) + b_{rin}\omega_{in} \right].$$

Since the angular velocities are related by

$$\omega_{out} = \left( \frac{R_{pinion}}{R_{gear}} \right) \omega_{in}$$

this can be rewritten as

$$T_{in} = \frac{J_{load}}{\eta} \left( \frac{R_{pinion}}{R_{gear}} \right)^2 \dot{\omega}_{in} + \left( b_{rin} + \frac{b_{rout}}{\eta} \left( \frac{R_{pinion}}{R_{gear}} \right)^2 \right) \omega_{in}.$$

Equating this expression with the equation of motion for the equivalent system in Fig. 11.21b

$$T_{in} = J_{eq}\dot{\omega}_{in} + b_{req}\omega_{in}$$

it is clear that the equivalent inertia and damping terms are

$$J_{eq} = \frac{J_{load}}{\eta} \left( \frac{R_{pinion}}{R_{gear}} \right)^2$$

$$b_{req} = b_{rin} + \frac{b_{rout}}{\eta} \left( \frac{R_{pinion}}{R_{gear}} \right)^2.$$

The equivalent damping and inertia both involve the mechanical advantage provided by the gear ratio as before. The mechanical efficiency, however, alters not only the equivalent damping of the system, but also its inertia.

## 11.6 EXAMPLE: MODELING AN AUTOMOTIVE VALVE-GEAR SYSTEM

As an example application of the ideas presented in this chapter, consider the process of producing a simple model of an automotive valve-gear system, the mechanism that connects the engine valves to the camshaft. This system not only illustrates a large number of the concepts discussed in this chapter, but has also been the focus of a number of previous modeling efforts (Barkan 1953, Rothbart 1956, Chen 1982, Pisano and Freudenstein 1983; Pisano, 1984; Hanachi and Freudenstein, 1986). The variety of approaches and levels of detail involved in these models provide a valuable reminder that engineering models are not unique descriptions of the system and that no single model can satisfy all needs. The models by Barkan (1953) and Chen (1982), in particular, include many more degrees of freedom than the one presented here, though they can ultimately be reduced. Hanachi and Freudenstein (1986) produce some interesting analytical models for specific types of damping in this system so the model can be used as a design tool without the need for experimental determination of damping. They also explicitly consider the operation of the hydraulic valve lifter, assumed here to be a solid mass.

Figure 11.22 illustrates the physical components of the valve-gear system used in the LS-1 engine on a Chevrolet Corvette and Fig. 11.23 shows a schematic of the assembly. Beginning the model after the cam, five moving masses can be identified: the lifter, the pushrod, the rocker arm, the valve and the spring. The mass of each component can be obtained by weighing each element separately and the moment of inertia of the rocker arm about its axis (a fixed point of rotation) can be obtained from experiment or analysis of a solid model. Values for each of these are listed in Table 11.2 and represent roughly the values for the real system. To shorten the modeling process a bit, the rocker arm and lifter are assumed to be rigid (Pisano and Freudenstein, 1983). Given the complex geometry of these shapes, it should of course be verified from finite element models or from experiment that these components do have the highest stiffness. For the remaining elements, some estimates of the stiffness can be obtained from basic mechanics of materials. The coil spring has 5.5 active coils, a wire diameter of 0.175 in, a spring diameter of 1.0 in and an assumed shear modulus of  $11 \times 10^6$  psi for a steel spring. The stiffness is therefore

$$K_{cs} = \frac{Gd^4}{8D^3N} = \frac{(11 \times 10^6 \text{ psi})(0.175 \text{ in})^4}{8(1 \text{ in})^3(5.5)} = 230 \text{ lb/in}$$

The valve stem and the pushrod resemble long, slender rods of circular cross-section. Both are made of steel with a cross-sectional area of  $0.075 \text{ in}^2$ . The valve stem has a length of 4.75 in while the pushrod has a length of 7.4 in. The stiffnesses of these components are

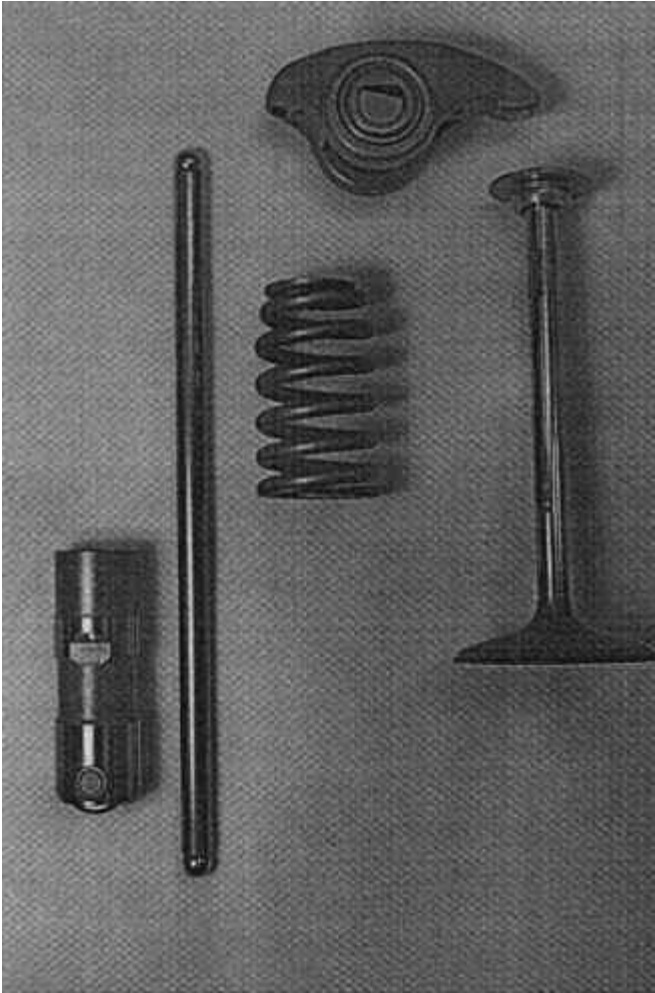


FIGURE 11.22. Valve-gear components.

$$K_{vs} = \frac{EA}{L} = \frac{(30 \times 10^6 \text{ psi})(0.075 \text{ in}^2)}{4.75 \text{ in}} = 4.7 \times 10^5 \text{ lb/in}$$

$$K_{pr} = \frac{EA}{L} = \frac{(30 \times 10^6 \text{ psi})(0.075 \text{ in}^2)}{7.4 \text{ in}} = 3.0 \times 10^5 \text{ lb/in}$$

All of the compliances act like springs in series, and hence are dominated by the spring with the smallest spring rate. Since the lowest rate belongs to the coil spring, this spring becomes the most important spring element to retain in any single degree of freedom model. The other two stiffnesses are so large relative to the coil spring that the pushrod and valve stem may be reasonably modeled as rigid bodies. With the valve stem, the rocker

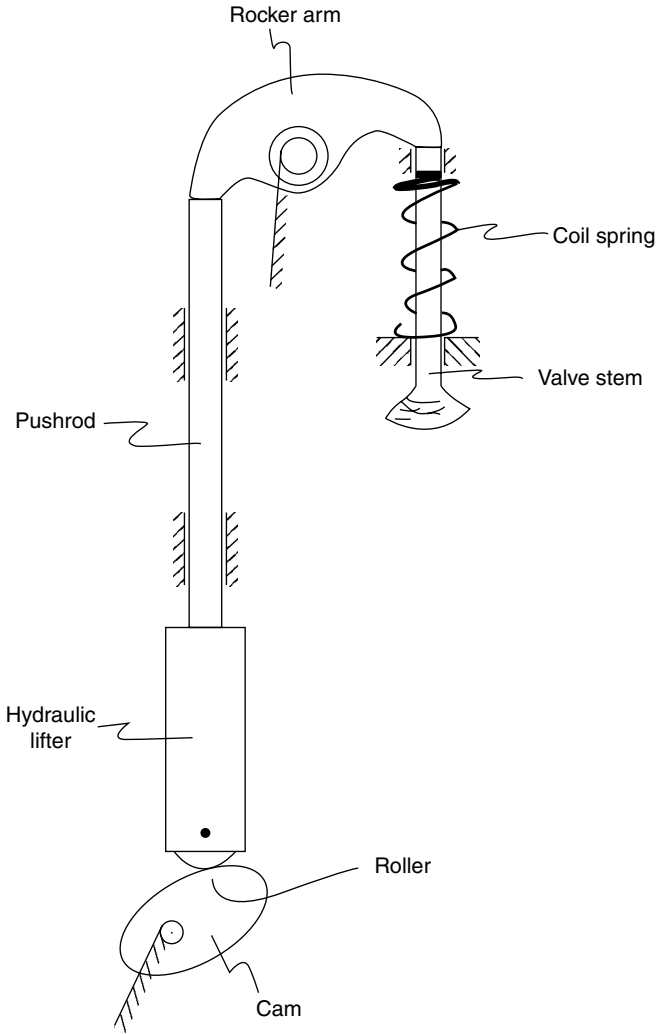


FIGURE 11.23. Valve-gear component assembly.

TABLE 11.2 Inertial Parameters of Valve-gear System

Component	Mass or Inertia
Hydraulic Lifter	$m_l = 0.270 \text{ lbm}$
Pushrod	$m_{pr} = 0.114 \text{ lbm}$
Rocker Arm	$J_{ra} = 0.132 \text{ lbm-in}^2$
Valve Stem	$m_{vs} = 0.251 \text{ lbm}$
Coil Spring	$m_{cs} = 0.153 \text{ lbm}$

arm, the pushrod and the lifter now assumed rigid, the system takes on the schematic form of Fig. 11.24a. To obtain the equivalent system of Fig. 11.24b reflected to the lifter, it is necessary to equate the kinetic energy of the original system to that of the equivalent system to account for the mechanical advantage of the rocker arm. Recalling that the mass contribution of a spring fixed at one end is a third of its mass at the free end, equating the kinetic energy of the equivalent system and the original system gives

$$\frac{1}{2} m_{eq} v_l^2 = \frac{1}{2} m_f v_l^2 + \frac{1}{2} m_{pr} v_{pr}^2 + \frac{1}{2} J_{ra} \omega_{ra}^2 + \frac{1}{2} m_{vs} v_{vs}^2 + \frac{1}{2} \frac{1}{3} m_{cs} v_{vs}^2.$$

Kinematically, there are several relationships between velocities that follow from the modeling assumptions made earlier. Since the lifter and pushrod are assumed to be rigid, their velocities are the same, so

$$v_{pr} = v_l.$$

Assuming small angles of rotation on the rocker arm, the rocker arm rotational velocity can be obtained from

$$\omega_{ra} = \frac{v_l}{l_{ra,pr}} = \frac{v_{vs}}{l_{ra,vs}}.$$

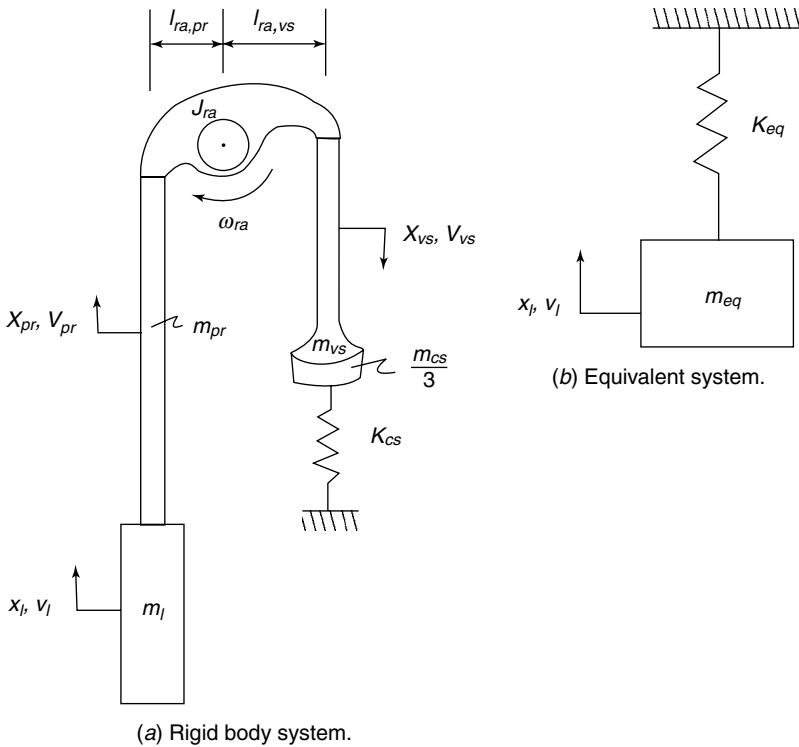


FIGURE 11.24. Valve-gear system after rigid body assumptions.

this also gives the relationship between the linear velocities of the pushrod and valve as

$$\frac{v_l}{v_{vs}} = \frac{l_{ra,pr}}{l_{ra,vs}} = \frac{1}{r_{ra}}$$

where  $r_{ra}$  is the rocker arm ratio. For this rocker arm,  $l_{ra,pr} = 0.875$  in.,  $l_{ra,vs} = 1.4875$  in and  $r_{ra} = 1.7$ . Putting this all together gives:

$$\begin{aligned} m_{eq} &= m_l + m_{pr} + \frac{J_{ra}}{l_{ra,pr}^2} + m_{vs} r_{ra}^2 + \frac{m_{cs}}{3} r_{ra}^2 \\ &= 0.270 \text{ lbm} + 0.114 \text{ lbm} + \frac{0.132 \text{ lbm} \cdot \text{in}^2}{(0.875 \text{ in})^2} + 0.251 \text{ lbm}(1.7)^2 + \frac{0.153 \text{ lbm}}{3}(1.7)^2 \\ &= 1.43 \text{ lbm} \end{aligned}$$

Since the system is referred to the lifter, the spring rate of the coil spring must be modified to account for the pushrod ratio. Equating the potential energy of the equivalent model and the original model

$$\frac{1}{2} k_{eq} x_l^2 = \frac{1}{2} k_{cs} x_{vs}^2 = \frac{1}{2} k_{cs} r_{ra}^2 x_l^2$$

so the equivalent stiffness is

$$K_{eq} = K_{cs} r_{ra}^2 = (230 \text{ lb/in})(1.7)^2 = 660 \text{ lb/in.}$$

Although the pushrod and valve stem were considered rigid, it is reasonable to consider adding their stiffnesses in series to that of the coil spring as Chen (1982) suggests in reducing a similar model. In this case, it makes very little difference since there is such a vast discrepancy in the stiffnesses of the pushrod and valve stem and that of the coil spring. If these springs are added in series with proper accounting for the rocker arm ratio,

$$\begin{aligned} \frac{1}{K_{eq}} &= \left( \frac{1}{r_{ra}^2 K_{cs}} + \frac{1}{r_{ra}^2 K_{vs}} + \frac{1}{K_{pr}} \right) \\ &= \left( \frac{1}{(1.7)^2 (230 \text{ lb/in})} + \frac{1}{(1.7)^2 (4.7 \times 10^5 \text{ lb/in})} + \frac{1}{3.0 \times 10^5 \text{ lb/in}} \right) \end{aligned}$$

so  $K_{eq} = 660$  lb/in, which is exactly the same as  $K_{vs}$  to two significant figures (the values differ by about 0.3 percent). The fact that the equivalent stiffness resembles that of the coil spring provides additional justification for assuming these elements to be rigid.

Thus a simplified model of this system can be obtained by using these equivalent mass and stiffness values. Over what frequency range is this model likely to be valid? To get a rough idea, consider that the natural frequency of the system with this mass and stiffness is

$$\omega_n = \sqrt{32.2 \times 12 \times \frac{K_{eq}}{M_{eq}}} = 420 \text{ rad/s} = 67 \text{ Hz}$$

This makes sense since redline for the engine corresponds to a camshaft rotational speed on the order of 3000rpm (or 50Hz) and resonance in this basic operating region should be avoided. To get a rough idea of the next resonance in the system, consider treating the

pushrod (the next lowest spring rate) as a flexible element. The model then takes the shape of Fig. 11.25a, where the mass of the pushrod has been divided equally between the elements on either side of it, the lifter and the rocker arm (Chen, 1982; Hanachi and Freudenstein, 1986). The parameter values then become

$$m_1 = m_l + \frac{1}{2} m_{pr}$$

$$= 0.270 \text{ lbm} + (0.5)0.114 \text{ lbm} = 0.327 \text{ lbm}$$

$$m_2 = \frac{1}{2} m_{pr} + \frac{J_{ra}}{l_{ra,pr}^2} + m_{vs} r_{ra}^2 + \frac{m_{cs}}{3} r_{ra}^2$$

$$= (0.5)0.114 \text{ lbm} + \frac{0.132 \text{ lbm} \cdot \text{in}^2}{(0.875 \text{ in})^2} + 0.251 \text{ lbm}(1.7)^2 + \frac{0.153 \text{ lbm}}{3}(1.7)^2 = 1.10 \text{ lbm}$$

$$K_1 = K_{pr} = 3.0 \times 10^5 \text{ lb/in}$$

$$K_2 = K_{eq} = 660 \text{ lb/in}$$

Since this is exactly the same form as the suspension model discussed earlier, the natural frequencies of this two-mass system can be calculated and occur at 67 Hz (as predicted by the one degree of freedom model) and 3400 Hz. This suggests two things. First, the next natural frequency is significantly higher than the first so there is ample justification for using a single-mass model for basic analysis. Secondly, while the single mass

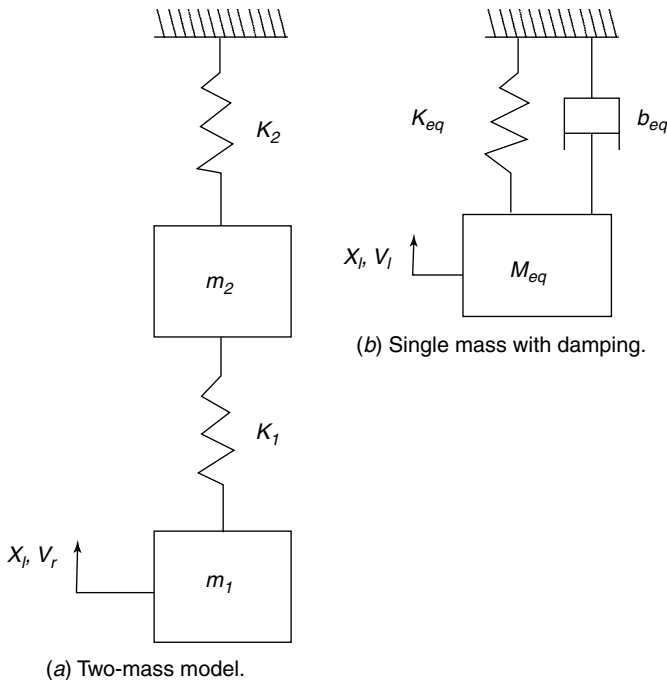


FIGURE 11.25. Other simple models of the valve-gear system.

model is likely a reasonable model for frequency ranges around 0–200 Hz, it would not be appropriate to use at high frequencies near the resonance at 3400 Hz. While the additional complexity of the two-mass system is not required to reproduce the low frequency behavior of the valve-gear system, damping should be added to the model if accurate reproduction of the resonance around 67 Hz is desired. This could take the form of an analytical prediction of friction (Pisano, 1984; Hanachi and Freudenstein, 1986) or a simple equivalent damper added in parallel to the equivalent spring (Fig. 11.25*b*) and identified through experiment, Chen (1982).

## REFERENCES

- Barkan, P., "Calculation of High-Speed Valve Motion with a Flexible Overhead Linkage," *Society of Automotive Engineers Transactions*, (61): 687–700, 1953.
- Cannon, R.H., *Dynamics of Physical Systems*, McGraw-Hill, New York, 1967.
- Chen, F.Y., *Mechanics and Design of Cam Mechanisms*, Pergamon Press, New York, 1982.
- De Silva, C.W., *Vibration: Fundamentals and Practice*, CRC Press, London, 2000.
- Fenster, S.K., and Gould, H.H., "Mathematics," in Rothbart, H.A. (ed) *Mechanical Design and Systems Handbook*, second edition, McGraw-Hill, New York, 1985.
- Friedland, B., *Advanced Control System Design*, Prentice-Hall, Englewood Cliffs, N.J., 1996.
- Garrott, W.R., and Monk, M.W., Vehicle Inertial Parameters—Measured Values and Approximations, *Society of Automotive Engineers Paper 881767*, 1988.
- Gillespie, T.D., *Fundamentals of Vehicle Dynamics*, Society of Automotive Engineers, Warrendale, Pa., 1992.
- Haessig, D.A., and B. Friedland, "On the Modelling and Simulation of Friction," *American Society of Mechanical Engineers Journal of Dynamic Systems, Measurement and Control*, (113): 354–362, 1991.
- Hanachi, S., and Freudenstein, F., "The Development of a Predictive Model for the Optimization of High-Speed Cam-Follower Systems with Coulomb Damping, Internal Friction and Elastic and Fluidic Elements," *American Society of Mechanical Engineers Journal of Mechanisms, Transmissions and Automation in Design*, (108): 506–515, 1986.
- Herbert, R.G., and McWhannell, D.C., "Shape and Frequency Composition of Impulses from an Impact Pair," *American Society of Mechanical Engineers Journal of Engineering for Industry*, (99): 513–518, 1977.
- Hunt, K.H., and Crossley, F.R.E., "Coefficient of Restitution Interpreted as Damping in Vibroimpact," *American Society of Mechanical Engineers Journal of Applied Mechanics*, (97): 440–445, 1975.
- Karnopp, D., Margolis, D.L., and Rosenberg, R.C., *System Dynamics: Modeling and Simulation of Mechatronic Systems*, John Wiley & Sons, New York, 2000.
- Karnopp, D., "Computer Simulation of Stick-Slip Friction in Mechanical Dynamic Systems," *American Society of Mechanical Engineers Journal of Dynamic Systems, Measurement and Control*, (107): 100–103, 1985.
- Layton, R.A., *Principles of Analytical System Dynamics*, Springer-Verlag, New York, 1998.
- Meirovich, L., *Fundamentals of Vibrations*, McGraw-Hill, New York, 2001.
- Pisano, A.P., and Freudenstein, F., "An Experimental and Analytical Verification of a High-Speed Cam-Follower System," *American Society of Mechanical Engineers Journal of Mechanisms, Transmissions and Automation in Design*, (105): 692–704, 1983.
- Pisano, A.P., "Coulomb Friction in High-Speed Cam-Follower Systems," *American Society of Mechanical Engineers Journal of Mechanisms, Transmissions and Automation in Design*, (106): 470–474, 1984.

Popov, E.P., *Mechanics of Materials*, Prentice-Hall, Englewood Cliffs, N.J., 1976.

Relvas, A.A., Springs, in Rothbart, H.A., (ed) *Mechanical Design and Systems Handbook*, second edition, McGraw-Hill, New York, 1985.

Ungar, E.E., Mechanical Vibrations, in Rothbart, H.A., (ed.) *Mechanical Design and Systems Handbook*, second edition, McGraw-Hill, New York, 1985.

*This page intentionally left blank.*

---

# CHAPTER 12

---

## CAM SYSTEM DYNAMICS—ANALYSIS

---

Harold A. Rothbart, D. Eng.

12.1 INTRODUCTION	357	12.4 CAM DRIVE DYNAMICS—ELASTIC CAMSHAFT	374
12.2 SYSTEM VIBRATIONS	358	12.4.1 Introduction to Elastic Camshaft	374
12.3 CAM-FOLLOWER DYNAMICS—RIGID CAMSHAFT	360	12.4.2 Single-Degree-of-Freedom Torsional System	374
12.3.1 Single-Degree-of-Freedom System	360	12.4.2.1 <i>Open-Track Cam System</i>	375
12.3.2 Single-Degree-of-Freedom System Compliance	363	12.4.2.2 <i>Closed-Track Cam System</i>	378
12.3.3 Harmonic/Fourier Analysis	367	12.4.3 Two-Degree-of-Freedom System	384
12.3.4 Two-Degree-of-Freedom System	370	12.4.4 Four-Degree-of-Freedom System	386
12.3.5 Some Cam-System Dynamic Phenomena	372	12.4.5 Multi-Degree-of-Freedom System	389
12.3.5.1 <i>Balancing</i>	372	12.5 SUMMARY	396
12.3.5.2 <i>Crossover Shock (Backlash)</i>	373		
12.3.5.3 <i>Spring Surge</i>	374		

---

### 12.1 INTRODUCTION

---

In this chapter we submit the dynamic analysis of cam-follower systems that are inherently *compliant*. A measure of system compliance is the extent of the deviation between the dynamic response and the intended kinematic response, which is the vibration level. This deviation tends to increase (1) as any of the input harmonics of cam motion approaches the fundamental frequency of the mechanism and (2) with the increase of the maximum value of the cam function third-time derivative (jerk). Also, the deleterious effects of vibration are well known. Vibration causes motion perturbations, excessive component stresses, noise, chatter, wear, and cam surface fatigue. This wear and cam surface erosion feeds back to further exacerbate the problem. For more on the subject of cam system dynamics, the reader is referred to Freudenstein (1960), Chen (1982), Erdman (1993), and Koster (1970).

In designing cam-follower systems, the compliancy of the system can be obtained by (1) the application of mathematical theoretical formulas, (2) testing prototypes, or (3) constructing detailed models. It has been found that the stiffnesses obtained by simple models is more than double the actual stiffness. The analytical inaccuracies are due to differences between assumed and actual stress distributions (largely near the applied loads) and deflection modes that were ignored in the analysis.

This chapter presents the analysis of two kinds of systems: (1) high-speed systems and (2) highly compliant systems. The models are:

- models with a rigid camshaft
- models with an elastic camshaft
- coupled combinations of elastic camshaft and follower

Models with a relatively rigid camshaft are the most general. Models with an elastic camshaft are an occasional requirement. Models with an elastic camshaft are coupled to the follower resulting in nonlinear second-order differential equations, since the cam movement on the shaft is not a direct function of time.

Multi-degree-of-freedom systems are shown, but note that they are shown to be complicated and difficult to apply, time-consuming, and thus costly. It has been found that the one-degree-of-freedom model is satisfactory as long as the excitations of the second and higher modes are much less than those near the first mode, which is usually true. The representation of a cam-follower mechanism by means of a single-degree-of-freedom model having a natural frequency equal to the fundamental natural frequency of the actual system is satisfactory. The fundamental natural frequency dominates the transient follower responses, which are treated in Chap. 13. Most researchers involved with the dynamics of cam-follower systems use linear one-degree-of-freedom spring-mass models with either open or closed-track cams for constraint of the follower. The closed-track cam is predominantly utilized for production machinery, and the open-track cam (spring force loaded) is specifically used for automotive valve gear systems. Nonlinear stiffness models have rarely been used, since the nonlinear component of the stiffness is usually relatively small. In addition, nonlinearities caused by passive parameters are not addressed in this book. These nonlinearities are damping of various kinds (e.g., Coulomb friction, quadratic damping, stiction, and combinations), backlash, and tolerances in mechanical components. The nonlinear models must be solved numerically with Runge-Kutta and Adams Bulirsch-Stoer algorithms. The Runge-Kutta Methods are the most popular; for other choices, Chen (1982), Chen and Polvanich (1975a,b), and Koster (1970) have employed computer simulations using models of complex cam systems including multiple nonlinear component effects.

The following are the commercially available computer programs:

TK Solver, Universal Technical Services  
1220 Rock Street  
Rockford, Ill. 61101  
[www.uts.com](http://www.uts.com)

Mathcad, Mathsoft, Inc.  
101 Main Street  
Cambridge, Mass. 02142  
[www.mathsoft.com](http://www.mathsoft.com)

MATLAB/SIMULINK, The Mathworks, Inc.  
2W Prime Parkway  
Natick, Mass. 01760  
[www.mathworks.com](http://www.mathworks.com)

## **12.2 SYSTEM VIBRATIONS**

---

This section looks at the practical and theoretical sources of vibration that may occur in the design and study of high-speed cam-follower mechanisms. This information is itemized to enhance the knowledge of the theoretical simplified modeling that is used. Although simplified models are invaluable, the designer should not be “trapped” totally by conclusions that models reveal. One should always maintain freedom of thought in the process of designing high-speed machinery. All vibrations are not always what the model reveals

since a model is not a *real* representation of the performing machine. There is no real model, only approximate representations of values. Since vibration is generally an undesirable side effect, it seldom controls the primary design of the cam-follower machine system. Such systems are designed first to fulfill their main function and are then analyzed from a vibration viewpoint possibly for equipment damage or malfunction, noise, or human discomfort or annoyance.

The most severe effects of vibration generally occur at resonance; therefore, one usually is concerned first with determination of the resonance frequencies of the preliminary design. Damping is usually neglected in the pertinent calculations for all but the simplest systems. If resonance frequencies are found to lie within the intended range of driving frequencies, one should attempt a redesign of the cam and follower system to shift the resonances out of the driving frequency range. Added stiffness with little addition of mass results in shifting of the resonances to higher frequencies. Added mass with little addition of stiffness results in lowering of the resonance frequencies. Damping generally has little effect on the resonance frequencies.

Excitation reduction of vibration may take the form of running a machine at reduced power, isolating the resonating system from the source of excitation, or shielding the system from exciting inputs. Also, increased damping may be obtained by addition of energy-dissipating devices or structures. For example, one might use metals with high internal damping for the primary structure or attach coatings or sandwich media with large energy-dissipation capacities to a primary structure of common materials.

In addition to the basic vibrations that result from compliant systems as discussed in this chapter, vibrations may occur in the cam follower for the following reasons:

- *As a result of separation of the cam and follower with backlash.* With closed-track cams impact of the roller on the cam is produced and is called crossover shock. With open-track cams vibrations are due to the “jump” condition of the follower leaving the cam surface.
- *Because of surface imperfections or irregularities.* These can affect the performance of the machine depending on the loads or speeds.
- *Due to the rate and phase of application of the external load.* For example, a cam-driven punch-indexing mechanism has its load applied suddenly as the punch starts into the workpiece. This quick-load application cannot be eliminated, and therefore the design by necessity must include it. Note that sometimes the application of load during the minus acceleration period tends to reduce or even eliminate the reversal of forces acting on the cam surface.
- *Due to cam or linkage unbalance.* These may be fabricated with blowholes or nonhomogenous contaminants.
- *Due to installation of improper and worn parts and misalignment.*
- *Due to support structures (frame) being either too light in weight or elastic.* These vibrations may occur at high speed and may be of significant magnitude to affect the design action. Incidentally, the author has observed a textile machine that performed properly and used an elastic frame to its advantage. In other words, the machine only worked utilizing the compliancy of the frame.
- *Vibrations transmitted to the cam from a relatively external power source.* These may arise from electrical motor, gearing, or other machinery action as part of the whole system.
- *Due to moving parts of complex linkages affecting the vibration mounts and substructures of the machine.*

- *As a result of the machine systems being old.* Generally the older the machine is, the more vibrations, noise, and lack of smoothness of operation occur.
- *As result of periodic change in power input voltage of the electrical motor or prime mover.* This has occurred in the performance of a high-speed textile machine in which the function had transient energy malfunction.
- *Due to the inclusion of belts and chains in the torsional drive.* This may produce large backlash and high compliancy in the system, seriously reducing the effective performance.

Note that in cases where the vibrating system cannot be modified satisfactorily, one may avoid resonance effects by not operating the machine at excitation frequencies at which resonances are excited. This may be accomplished by speed controls on a machine or by prescribing limitations on use of the system, e.g., “red lines” on engine tachometers to show operating speeds to be avoided.

## 12.3 CAM-FOLLOWER DYNAMICS—RIGID CAMSHAFT

---

### 12.3.1 Single-Degree-of-Freedom System

Modeling, as discussed in Chap. 11, transforms the system into a set of tenable mathematical equations that describe the system in sufficient detail for the accuracy required. Various tools of analysis are at the disposal of the designer-analyst and range in complexity from classical linear analysis for single-degree-of-freedom systems to complex multiple-degree-of-freedom nonlinear computer programs.

In this section we present a single-degree-of-freedom system (DOF) with a rigid camshaft. The cam mechanism consists of a camshaft, cam, follower train including one or more connecting links, and springs terminating in a load mass or force. For lumped systems, linkages and springs are divided into two or more ideal mass points interconnected with weightless springs and dampers.

*Springs.* The spring force generally follows the law

$$F = kx \pm \sum_{n=1}^4 a_n x^{2n+1}$$

where terms under the  $\Sigma$  sign are nonlinear.

*Dampers.* Damping takes the general form

$$C(\dot{x}) = C\dot{x}|\dot{x}|^{r-1}$$

$$\text{For } r = \begin{cases} 0 & C(\ddot{x}) \text{ is Coulomb damping} \\ 1 & C(\dot{x}) \text{ is viscous damping} \\ 2 & C(\dot{x}) \text{ is quadratic damping} \end{cases}$$

“Stiction” is accounted for as the breakaway force,  $\mathfrak{S}$ , in one element  $i$  sliding along another element  $j$ .

$$\begin{aligned} F_{st} &= 0 && \text{for } \dot{x}_i \neq \dot{x}_j \\ &\leq \mathfrak{S} && \text{for } \dot{x}_i = \dot{x}_j \\ &= \mathfrak{S} && \text{at breakaway} \end{aligned}$$

Damping value ranges from 4 to 8 percent in most cam-and-follower systems; it is the *transient response* of the follower that is of basic concern. Steady-state vibration in most systems rarely occurs, because in practice the angular velocity of the camshaft is low in comparison with the natural frequency of the follower system. We assume that the vibration damps out during the dwell period and does not carry over to the next motion cycle.

The model is the one-degree-of-freedom system, which lumps the follower train and mass load into a single equivalent mass with equivalent springs and dampers connected to the closed-track cam, as shown in Fig. 12.1.

Let

$m$  = mass, lb

$b$  = damping coefficient, lb/in/sec

$k$  = spring rate, lb/in

$x$  = follower displacement, in

$\dot{x}$  = follower velocity, in/sec

$\ddot{x}$  = follower acceleration, in/sec<sup>2</sup>

$y$  = cam displacement, in

$\dot{y}$  = cam velocity, in/sec

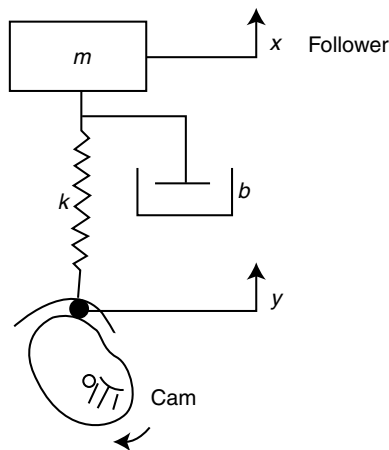
$\ddot{y}$  = cam acceleration, in/sec<sup>2</sup>

Utilizing Newton's second law, we see that

$$m\ddot{x} + b(\dot{x} - \dot{y}) + k(x - y) = 0. \quad (12.1)$$

The vibration form of Eq. (12.1) is

$$m(\ddot{x} - \ddot{y}) + b(\dot{x} - \dot{y}) + k(x - y) = -m\ddot{y}. \quad (12.2)$$



**FIGURE 12.1.** Single-degree-of-freedom system (closed-track cam).

Substituting  $z = x - y$  yields

$$m\ddot{z} + b\dot{z} + kz = -m\ddot{y} \quad (12.3)$$

which places in evidence the prominent role of cam function acceleration  $y$  on the vibrating system, similar to a system response to a shock input at its foundation.

The general solution to Eq. (12.3) consists of the complementary or transient solution plus the particular solution. The complementary solution is the solution to the homogeneous equation

$$\begin{aligned} m\ddot{z} + b\dot{z} + kz &= 0 \\ \ddot{z} + 2\zeta\omega_n\dot{z} + \omega_n^2 z &= 0 \\ \text{where } \omega_n &= (k/m)^{1/2} \\ \zeta &= \frac{1}{2}b(1/km)^{1/2} \end{aligned}$$

and is

$$z_c = Ae^{-\zeta\omega_n t} \sin[(1-\zeta^2)^{1/2}\omega_n t] + Be^{-\zeta\omega_n t} \cos[(1-\zeta^2)^{1/2}\omega_n t] \quad (12.4)$$

where  $A$  and  $B$  are determined in conjunction with the particular solution and the initial conditions. One form of the particular solution is derivable from the impulse response

$$z_p = \frac{1}{(1-\zeta^2)^{1/2}\omega_n} \int_0^t \ddot{y} e^{-\zeta\omega_n(t-\tau)} \sin[(1-\zeta^2)^{1/2}\omega_n(t-\tau)] d\tau. \quad (12.5)$$

For finite  $\ddot{y}$ , the case here,  $z_p(0) = \dot{z}_p(0) = 0$ , so that the general solution to Eq. (12.3) is

$$z = z_p + \left\{ \frac{\dot{z}(0) + z(0)\zeta\omega_n}{(1-\zeta^2)^{1/2}\omega_n} \sin[(1-\zeta^2)^{1/2}\omega_n t] + z(0) \cos[(1-\zeta^2)^{1/2}\omega_n t] \right\} e^{-\zeta\omega_n t} \quad (12.6)$$

where the initial conditions  $z(0)$  and  $\dot{z}(0)$  are subsumed in  $z_c$ . Accordingly, for a system initially at rest, the  $z_p$  solution becomes the complete solution. However, the difficulty with this solution is that  $\ddot{y}$  is periodic and integration would have to be performed over many cycles depending on the amount of damping present. Solutions would be analyzed first to determine the input “transient” peak response, which is important in cam-follower system performance. Incidentally, the “steady-state” response would be reached when

$$z(nt) = (n+1)T \quad \text{and} \quad \dot{z}(nt) = \dot{z}(n+1)T.$$

Typical transient-response curves for one-degree-of-freedom systems are shown in Fig. 12.2, where  $\beta$  is the cam angle for maximum displacement, radians. Hrones (1948) mathematically analyzed and Mitchell (1940) tested the vibrations resulting from three basic dwell-rise-dwell curves with a high-rigidity system (follower). They investigated the transient dynamic magnification, providing the measure of the spring-dashpot coupling effect on the follower. In Fig. 12.2, the dynamic magnification is equal to 2 at any discontinuity of the two curves, parabolic and simple harmonic. However, the cycloidal curve has a smaller magnification, about 1.06 to 1. Thus a discontinuity means a sudden or transient application of the inertia load that produces a shock (twice the value of the inertia load) in the cam-follower system. In design, this phenomenon is often called a “suddenly applied load.”

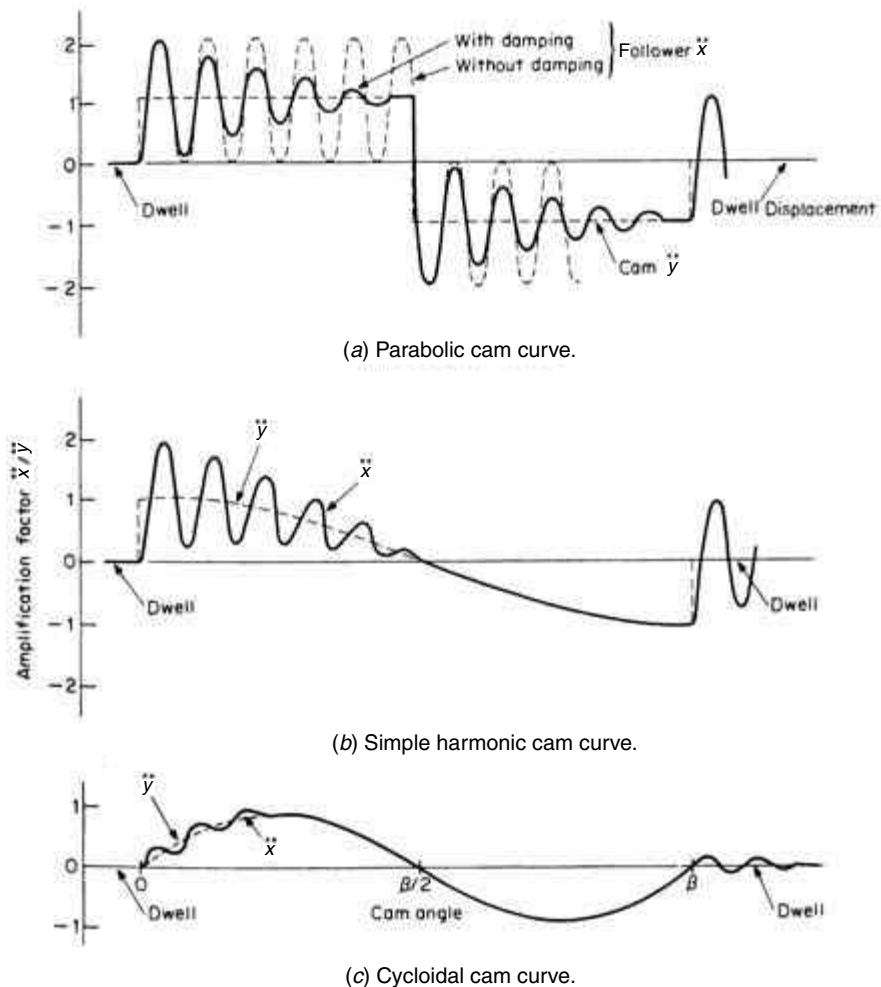
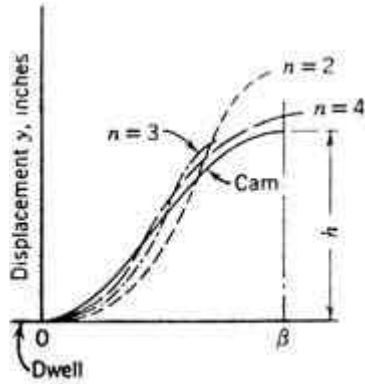


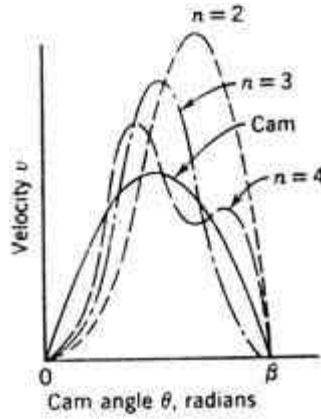
FIGURE 12.2. Single-degree-of-freedom response of basic dwell-rise-dwell cam acceleration curves.

### 12.3.2 Single Degree-of-Freedom System Compliance

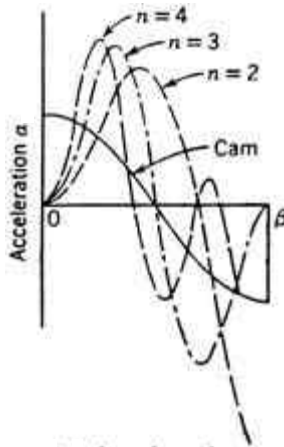
The solution of the single-degree-of-freedom cam-follower system is shown in the previous section. In this section we investigate the analysis and response of highly elastic systems such as the high-speed automotive valve-gear system and some special textile machines. Figures 12.3 and 12.4 show the displacement, velocity, and acceleration follower response curves of the simple harmonic and cycloidal basic cam curves. The curves show the response for small values of  $n$ , where  $n = \frac{\omega_n}{\omega}$ , the ratio of the natural frequency to the excitational frequency. For more rigid systems ( $n > 4$ ) the analysis and the curves will be similar, having higher frequencies and smaller amplitudes. In both figures we see that the follower mass catches up with and overshoots the forcing cam dis-



(a) Displacement.



(b) Velocity.



(c) Acceleration.

FIGURE 12.3. Transient time response for simple harmonic motion  $n = \frac{\omega}{\omega_n}$  and no damping.

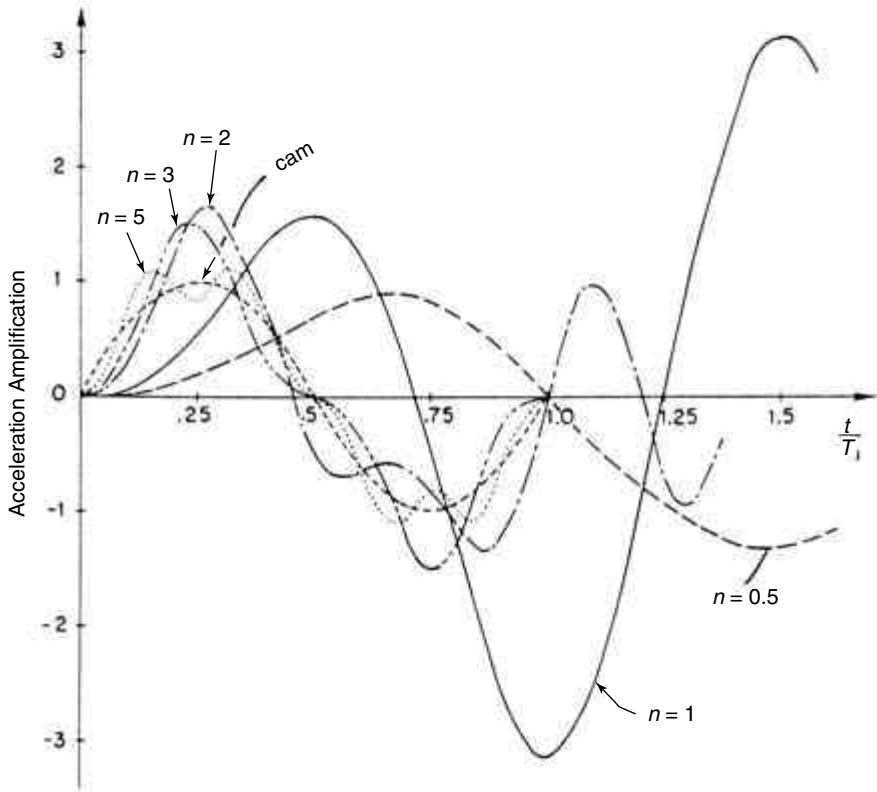


FIGURE 12.4. Time response of excitation period (cycloidal motion),  $n = \frac{\omega_n}{\omega}$ .

placement. Here, the dynamic compression of the highly flexible follower linkage results in a subsequent release of energy that causes the end of the follower to surge ahead of or fall behind the cam lift. When damping is present, the amplitudes produced by this action will be somewhat reduced.

Dresner et al. in Erdman (1993) discussed some rules of thumb to be applied to systems with significant compliance. They establish the critical speed as the operating speed for which the time duration of the positive acceleration interval of the lift event equals the fundamental period of vibration. The points suggested are:

- Maximize the fundamental natural frequency of system vibration. The amplitude of vibration is minimized when the fundamental period of vibration is as short as possible. Some researchers simply state that vibrations become excessive at just above critical speed.
- When acceleration varies smoothly over the positive acceleration interval, vibrations will be tolerable as long as the operating speed is below 50 percent of the critical speed.

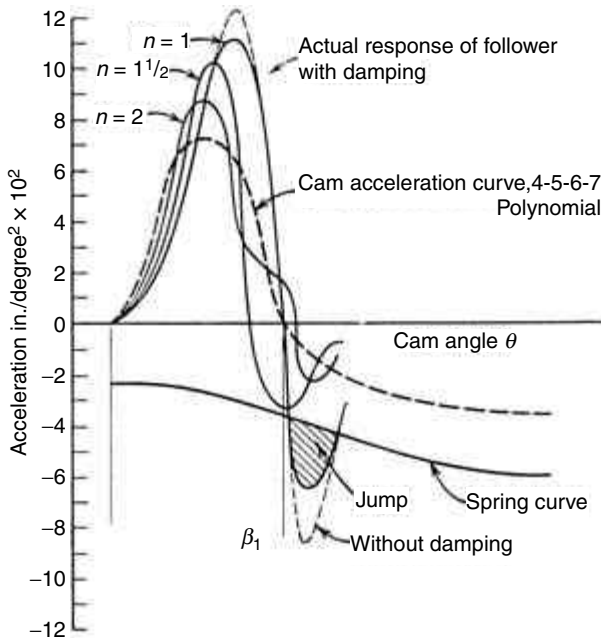
Although manufacturing tolerances do not allow the high-order derivatives of the lift curves to be controlled, these tolerances are usually only about one-thousandth of the total cam lift. Thus, the amplitudes of any harmonics caused by these tolerances are likely to

be less than one-thousandth of the amplitude of the first harmonic and thus are unlikely to cause major problems. These observations also imply that accurate control of the high-order derivatives is not critical in controlling system vibration.

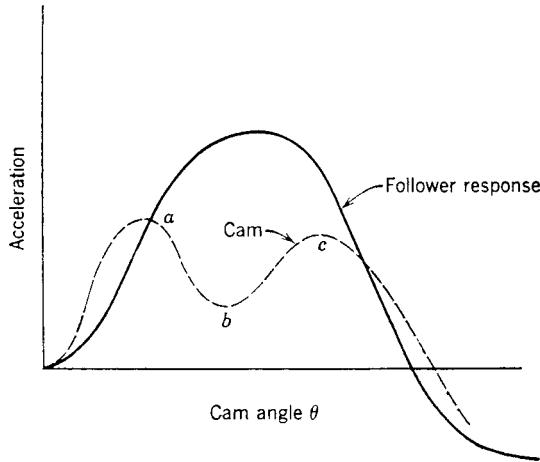
With the open-track cam-follower system we may have a condition called jump or bounce. It is a transient condition that occurs with high-speed and highly flexible systems. With jump, the cam and the follower separate owing to excessively unbalanced forces exceeding the spring force during the period of negative acceleration. This is undesirable since the fundamental function of the cam-follower system, the constraint and control of follower motion, is not maintained. Also related are short life of the cam flank surface, high noise, vibrations, and poor action.

Figure 12.5 depicts high-speed, highly flexible cam mechanism running at 2100rpm with  $\beta_1 = 27$  degrees and a follower natural frequency of 42,000 cycles per minute. Figure 12.5 shows the asymmetrical cam acceleration curve with the positive acceleration period of the 4-5-6-7 polynomial. Superimposed is the natural follower acceleration for various values of the frequency ratio. Also shown is the compression spring curve below the negative acceleration values to maintain constraint of the follower on the cam. Jump occurs when the response curve falls below the spring curve. Turkish (1953) in his excellent article verifies this by tests. We see that jump becomes more predominant with smaller values of  $n$  (Baratta and Bluhm, 1954).

A direct approach for establishing the minimum allowable value of  $n$  to prevent jump is shown by Karman and Biot (1940). Increasing the spring load is a poor way to eliminate jump, since greater surface stresses and shorter life result. A design method



**FIGURE 12.5.** Jump phenomenon—transient response of follower (cam rotates 2100rpm,  $\beta_1 = 27$  degrees, follower natural frequency = 42,000 cycles/min).



**FIGURE 12.6.** Polydyne cam design (note dip *a-b-c* to oppose “jump”).

for eliminating this detrimental condition with highly flexible systems is to use the polydyne procedure of Chap. 11. In Fig. 12.6, we see the highly flexible follower acceleration curve and the cam acceleration curve necessary to fulfill the polydyne requirement of Chap. 11. Note the negative acceleration dip *a-b-c* that opposes the jump condition. It may be mentioned, however, that this phenomenon may be difficult to fabricate.

### 12.3.3 Harmonic/Fourier Analysis

In Sec. 12.3, we showed the general expression for a cam-follower system to be, Eq. (12.3),

$$m\ddot{z} + b\dot{z} + kz = -m\ddot{y}$$

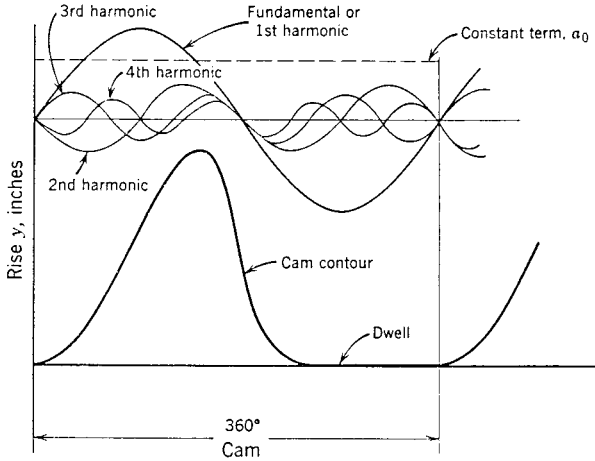
or

$$m\ddot{z} + b\dot{z} + kz = F(t)$$

showing a periodical disturbing force as a function of time,  $F(t)$ . This force can be represented in the form of a trigonometric series of sinusoidal functions (Timoshenko, 1955; Kármán and Biot, 1940) such as

$$\begin{aligned} m\ddot{z} + b\dot{z} + kz \\ = a_0 + a_1 \cos \omega t + b_1 \sin \omega t + a_2 \cos 2\omega t + b_2 \sin 2\omega t + \dots \end{aligned} \quad (12.7)$$

In Fig. 12.7, we see the harmonic analysis of the first four components of a cam contour where the harmonic numbers are 1, 2, 3, and 4. The coefficients  $a$  and  $b$  can be calculated if  $F(t)$  is known analytically. As before, the general solution of this equation will consist of two parts, free vibration and forced vibration. Steady-state solution may be found by ignoring the free vibrations and solving for the follower response by superimposing the



**FIGURE 12.7.** Harmonic analysis (resolving into sinusoidal components).

effects of the magnitudes of components  $a_1, b_1, a_2, b_2, a_3, b_3, \dots$  at each point. Also, large forced vibrations may occur when the period (sec) of one of the terms of the series coincides with (or is a multiple of) the period (sec) of the natural frequency of the system. This is called resonance, which occurs at the critical speed of the respective harmonic number, i.e., when  $n$  equals an integer.

Furthermore, the magnitude of the response at resonance depends primarily on the magnitude of the components  $a_1, b_1, a_2, b_2, a_3, b_3, \dots$  for that harmonic. Vibration is caused by a force, and thus the harmonics of the acceleration curve rather than the displacement curve are responsible for it. For any contour the acceleration and displacement harmonics are proportional.

Harmonic analysis of the acceleration forces produced by a given cam design will give an indication of the performance to be expected. As before, the natural frequency  $\omega_n$  should be as high as possible so that resonance at a given speed range will occur with a higher harmonic number of consequently smaller amplitude harmonics. Fortunately only a few of the low numbers cause excessive vibratory amplitudes. Some of the higher numbers appear as noise and may be objectionable. Last, the amplitude of the forced oscillation is small if the frequency of the external force is different from the natural frequency and, of course, depends on the proximity to the natural frequency of the system.

Also, it should be remembered that a smooth, "bumpless" acceleration curve generally gives weaker harmonics and thus a smaller response. By *smooth* is meant few points of inflection, i.e., the DRD acceleration curve has one point of inflection. A refinement would be to have all derivatives of the acceleration curve  $\ddot{y}, \dot{y}, \dots$  continuous functions. However, in practice it is impossible to fabricate the cam to the accuracy demands of these higher derivatives and their practical value has never been verified.

If  $F(t)$  (cam curve) is given numerically or graphically because no analytical expression is available, some approximate numerical method for calculating harmonics can be employed to analyze trigonometric series curves.

Let us elaborate on the Fourier analysis of cam-follower systems. The solution for Eq. (12.7) may be put into the form:

$$R = kz = k \sum_{n=0}^{\infty} \frac{F_n}{m} \frac{\cos(w_n t - \alpha)}{\left[ (w_o^2 - w_n^2) + \frac{b}{m^2} w_n^2 \right]^{1/2}} \quad (12.8)$$

where

- $\alpha$  = phase angle
- $b$  = clamping factor
- $R$  = resultant dynamic force
- $F(t)$  = external driving force
- $F_n$  = amplitude of nth harmonic of harmonic analysis of  $F(t)$
- $k$  = system elasticity
- $m$  = effective mass of cam-follower system from equilibrium position
- $z$  = deflection of cam-follower system
- $w_o = (\mathbf{k})^{1/2}$  = natural frequency of system, rad/sec
- $w_n$  = frequency of nth harmonic, rad/sec

Examination of the equation shows that resonance occurs at speeds that are multiples of the natural frequency of the system. With small  $b$ , the value under the square-root sign becomes very small when  $w_o = w_n$ ; consequently, the contribution of that member which is in resonance to the complete solution is by far the largest. With a given cam-follower system, the magnitude of the response at resonance will depend primarily on the magnitude of the component  $F_n$ . By performing a harmonic analysis of the forces acting on the system, it is possible to predict the response with a given cam operating at a given speed. The principal force acting on the system is the acceleration force. Therefore, a harmonic analysis of the acceleration forces produced by a given cam design will give an indication of the performance to be expected.

In general, any periodic function, provided that it contains no more than a finite number of discontinuities, has a convergent Fourier series that represents it. However, the number and extent of the discontinuities have an important bearing on the rapidity of the convergence, i.e., the rate at which the harmonics approach zero as  $n$  becomes large. If a function itself has discontinuities, the coefficients will decrease in general as  $1/n$ , whereas if discontinuities do not exist in the function itself but only in its first derivative, the coefficients will fall off approximately as  $1/n^2$ .

Examination of the three acceleration forms considered, namely constant acceleration, simple harmonic, and cycloidal, shows that only the cycloidal is completely continuous. It was stated in Mitchell (1950) that the cycloidal curve cam-follower system used has a natural frequency of 162.5 cycles per sec. At a cam speed of 140 rpm, resonance occurs with the harmonic  $9750/140 = 70$ th harmonic. Therefore, we would anticipate that the resonant response of the system to the cycloidal cam profile would be on the order of 1/70 of the response to the other two profiles at this speed.

**EXAMPLE** A closed-track radial cam turning once every 4 sec operates a roller follower on a push rod. This rod moves a rocking lever and, by means of a connecting link, a sliding table weighing 185 lb. Some basic dimensions of the roller follower displacement from dwell to dwell are shown in Table 12.1. The strength of the connecting members are: under 100 lb of compressive load, the push rod deflects 0.0012 in, the connecting link 0.0165 in, and the rocking lever bends 0.237 in. The masses of these members are small in comparison with the table. While the cam is operating, a troublesome chatter develops in the table. Find the cause. Note: it is recognized that the machine is very old and the cam surface is worn and has serious surface imperfections.

**TABLE 12.1** Example of Harmonic Analysis

Cam angle, deg	10	20	30	40	50	60	70	80	90
Displacement, in	0.080	0.215	0.439	0.730	1.112	1.500	1.898	2.250	2.561
Cam angle, deg	100	110	120	130	140	150	160	170	180
Displacement, in	2.789	2.949	3.049	3.155	3.410	3.781	4.132	4.422	4.500

Note: The return action is symmetrical.

**Solution** *The overall (equivalent) spring constant for a system in series is*

$$\begin{aligned}\frac{1}{k} &= \frac{1}{k_1} + \frac{1}{k_2} + \frac{1}{k_3} + \dots \\ &= \frac{1}{100/0.0012} + \frac{1}{100/0.0165} + \frac{1}{100/0.237} \\ k &= 392 \text{ lb/in.}\end{aligned}$$

*The natural frequency of the follower*

$$= \frac{1}{2\pi} \left( \frac{k}{m} \right)^{1/2} = \frac{1}{2\pi} \left( \frac{392}{185/386} \right)^{1/2} = 4.55 \text{ cycles/sec}$$

*Plotting the displacement of the follower in Fig. 12.8, we can find the velocity and acceleration curves by employing the method of finite differences.*

*We find a strong imposed frequency of acceleration of 4½ cycles/sec.*

*It may be seen that the frequency ratio*

$$= \frac{4.50 \text{ cycles/sec}}{\frac{1}{4} \text{ rev/sec}} = 18$$

*Thus, by observation of Fig. 12.8, we see that the chatter is caused by (a) resonance between natural frequency and the strong eighteenth harmonic number and (b) excessive jerk values, especially at the dwell ends of the cam curve. A new cam designed with a smoother acceleration curve with smaller maximum jerk values solved the problem by yielding weaker higher harmonics.*

### 12.3.4 Two-Degree-of-Freedom System

Let us consider a two-degree-of-freedom linear, closed-track cam-follower system as shown in Fig. 12.9. For other applications of two DOF systems, see Hanachi and Freudenstein (1986) and Eliss (1964).

Let

$m_1, m_2$  = respective mass: 1, 2, lb

$k_1, k_2$  = respective spring, 1, 2, lb/in

$b_1, b_2$  = respective damping coefficient, 1, 2, lb/(in/sec)

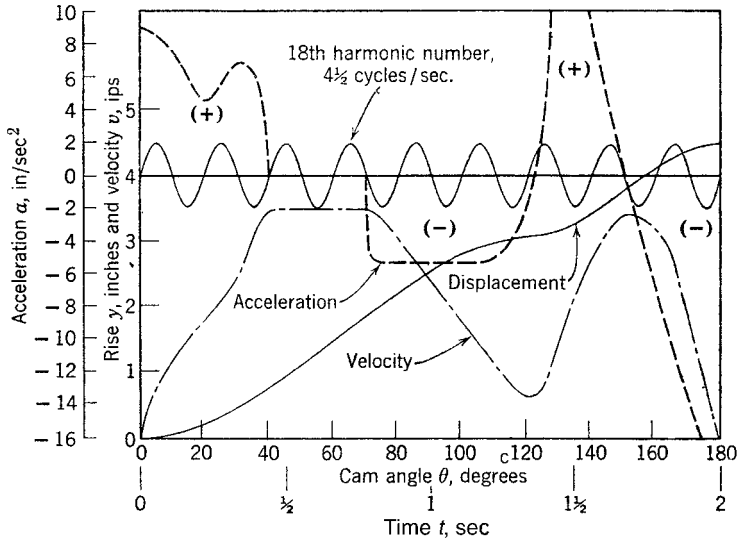


FIGURE 12.8. Cam example (chatter resulted from resonance with strong 18th harmonic number).

Based on the free-body diagrams, applying Newton’s second law, we obtain

$$\begin{aligned} m_1 \ddot{x}_1 &= b_2 \dot{z}_2 + k_2 z_2 - b_1 \dot{z}_1 - k_1 z_1 \\ m_2 \ddot{x}_2 &= -b_2 \dot{z}_2 - k_2 z_2 \end{aligned} \tag{12.9}$$

where  $z_1 = x_1 - y$  and  $z_2 = x_2 - x_1$  are the relative coordinates.

Eq. (12.9) can be rearranged as

$$\begin{aligned} m_1 \ddot{z}_1 + b_1 \dot{z}_1 + k_1 z_1 &= b_2 \dot{z}_2 + k_2 z_2 - m_1 \ddot{y} \\ m_2 \ddot{z}_2 + b_2 \dot{z}_2 + k_2 z_2 &= -m_2 (\ddot{z}_1 + \ddot{y}). \end{aligned} \tag{12.10}$$

Substituting the first expression for  $\ddot{z}_1$  into the second Eq. (12.10) leads to the following

$$\begin{aligned} \ddot{z}_1 + 2\zeta_1 \omega_1 \dot{z}_1 + \omega_1^2 z_1 &= -\omega_1^2 \delta_1 \\ \ddot{z}_2 + 2\zeta_2 \omega_2 \dot{z}_2 + \omega_2^2 z_2 &= -\omega_2^2 \delta_2, \end{aligned} \tag{12.11}$$

where

$$\begin{aligned} \delta_1 &= \frac{\ddot{y}}{\omega_1^2} - \frac{b_2}{k_1} \dot{z}_2 - \frac{k_2}{k_1} z_2 \\ \delta_2 &= -\frac{b_1}{m_1 \omega_2^2} \dot{z}_1 + \frac{b_2}{m_1 \omega_2^2} \dot{z}_2 - \frac{\omega_1^2}{\omega_2^2} z_1 + \frac{m_2}{m_1} z_2 \\ \omega_1^2 &= \frac{k_1}{m_1}, \quad \omega_2^2 = \frac{k_2}{m_2} \end{aligned}$$

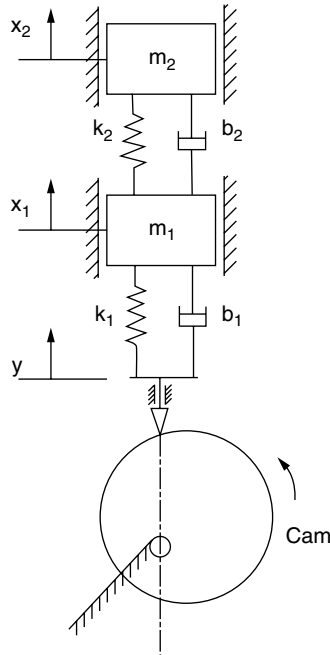


FIGURE 12.9. Model of two DOF elastic follower, closed-track cam-follower system.

$$\zeta_1 = \frac{b_1}{2\sqrt{k_1 m_1}}, \quad \zeta_2 = \frac{b_2}{2\sqrt{k_2 m_2}}.$$

### 12.3.5 Some Cam-System Dynamic Phenomena

**12.3.5.1 Balancing.** In this section miscellaneous subjects of interest in the dynamics of cam-follower systems are covered, such as the balancing of rotating elements of the cam body, the crossover shock that occurs in closed-track cam-follower systems, the spring surge (resonance) that occurs with open-track cams, and harmonic analysis of cams.

The balance of the dynamic members of all complex machinery is a critical factor in the performance. Thus it is with high-speed cam-follower systems. The imbalance of the asymmetrical cam mass itself with respect to the center of rotation is the first issue of concern. Obviously, strong vibrations are induced in the system at the cam speed fundamental harmonic. This vibration can be kept to a minimum, although not completely eliminated, by intelligent practical cam proportions, using a well-ribbed, low-mass structure with designed counterweights as part of the cam body.

Some of the other sources of vibration due to imbalance that may be investigated for cam-follower systems are:

- dissymmetry such as core shifts in castings and rough surfaces on forgings
- nonhomogeneous material; blowholes in castings, slag inclusions or variations in crystalline structure
- distortions at design speed in buildup design
- eccentricity in which the journals are not concentric or matching holes are not circular
- misalignment of bearings
- improperly installed parts or misalignment

Balancing problems can be minimized by careful design in which imbalance is controlled. Large amounts of imbalance require large corrections. If such corrections are made by removal of material, additional cost is involved and part strength may be affected. If corrections are made by addition of material, cost is again a factor and space requirements for the added material may be a problem.

Manufacturing processes are a major source of conditions that create imbalance. Unmachined portions of castings or forgings that cannot be made concentric and symmetrical with respect to the shaft axis introduce substantial imbalance. Manufacturing tolerances and processes that permit any eccentricity or lack of squareness with respect to the shaft axis are sources of imbalance.

Almost all machinery contains a flywheel as an energy reservoir. The flywheel is generally installed on the camshaft close to the cam body. The balance of the flywheel is also a factor to be considered. Flywheels are composed of steel, cast iron, aluminum graphite, and other materials, depending on the application; see Shigley and Mischke (1996).

**12.3.5.2 Crossover Shock (Backlash).** Let us now consider a phenomenon called crossover shock. Crossover shock exists with roller-follower closed-track cams when the contact of the follower shifts from one side to the other. Thus, the clearance or backlash between the follower and the cam are taken up with resulting impact. We know that crossover shock exists in all roller cam followers. The greater the clearance, the greater is the shock. The cumulative backlash is the sum of all the clearance, play, or slack in both the input and output transmissions, adjusted if necessary by gearing ratios, and in the cam track and cam follower. Typical examples are slack chain drives, gear tooth clearances, oversized enclosed cam tracks, and worn follower roller bearings; there are many others. Backlash occurs at a point where the acceleration of the follower changes from positive to negative or vice versa. This is also the point of maximum follower velocity. The crossover shock and the maximum velocity of the mechanism become less as the follower is made stiffer. Crossover shock can be kept to a minimum by using a rigid follower system with a high natural frequency or by maintaining high manufacturing clearance tolerances, which is expensive. Preloading of the follower by utilizing dual rollers, Chap. 10, is a practical means of alleviating this detrimental condition in which backlash is removed from the system. Preloading is a design possibility only for lightly loaded mechanisms. In heavily loaded machines, however, it is usually not practical for preloading to avoid crossover shock. Van der Hoek (1966) and Koster (1970) have considered the problem of backlash traversal based on the model of nonlinear film squeeze effect, a damping phenomenon. The reduction of backlash is essential to decrease undesirable roller sliding and skidding action, vibrations, wear, and noise. It cannot be totally eliminated, however. Proper choice of lubricant and reduction of clearance between the roller and its groove will aid considerably in this problem.

Backlash with open-track systems can often be eliminated by applying sufficient external force with a spring or the payload weight, or even a friction force, to ensure that there

is no force reversal at the operating speed. For spring-loaded open-track cam systems to be fully effective in eliminating backlash the spring must be applied not just to the follower but also at a point in the output transmission that affects all significant clearances. In summation, the complete action of the roller follower as it rides on the cam is unknown as it rolls, slides, and impacts the cam surface during its cycle of operation.

**12.3.5.3 Spring Surge.** For open-track cam-follower systems, the force loading compression spring has the basic function of keeping the cam and follower in contact. At high speeds, a phenomenon occurs that may seriously reduce the effective force of the spring, allowing the follower to leave the cam, even though considerable surplus spring force was provided. This is called spring surge. It is a torsional wave transmitted through the wire up and down the spring at the natural frequency of the spring. It has been found to be a state of resonance at the natural frequency of the spring with the cam high-amplitude harmonics. Preventing spring surge is simple. In general, the lower the harmonic number, the higher are the vibratory amplitudes. Therefore, the natural frequency of the spring should be high enough so that if resonance occurs it will be with higher harmonic numbers and vibratory amplitudes will be kept to a minimum. The harmonic number should be 11 or higher. However, a ratio as low as 9 may be used with good follower dynamics and a smooth acceleration curve. In modeling the system, it is common practice to consider that the weight of the spring substituted should be one-third the total spring weight. The phenomenon of “jump” exists for high-speed springs as well as the linkages. For further discussion of the subject of spring surge, see Jehle and Spiller (1929).

## **12.4 CAM DRIVE DYNAMICS— ELASTIC CAMSHAFT**

---

### **12.4.1 Introduction to Elastic Camshaft**

The power input of almost all mechanisms and machinery is transmitted *torsionally* from an electric motor to the output where it performs its function. In this book, the output is a cam-follower system. Also, every torsional motion has a rotating mass or flywheel that is generally located near the cam and support bearing. The flywheel provides stability to the system and, depending on its size, aims to control fluctuations in speed as energy surges through the system.

In this section, torsionally elastic camshafts are discussed with a selection of diverse kinds of compliant shafts and followers. We will explore the dynamic phenomena of the total machine performance. The model system takes into account cam shaft compliance and leads to a set of nonlinear equations owing to the fact that the driving cam function is no longer a known function. For more on torsionally compliant cam-follower systems, see Koster (1975*a* and *b*).

### **12.4.2 Single-Degree-of-Freedom Torsional System**

In high-speed camera studies of cam-driven systems, Rothbart (1961) observed a phenomenon that was termed “shaft windup.” This phenomenon arose under the conditions of a high inertia load, a large pressure angle, and a flexible drive shaft. Although the power input end of the shaft rotates at a constant speed, the speed of the cam itself fluctuates as it twists due to the time-varying torque. During this period, the follower is at first reluctant to move and later moves slower than intended. Beyond the instant of maximum torque,

the energy stored in the shaft is released and drives the cam at an increasing speed, thus causing the follower mass to catch up with the forcing cam action and then to overshoot it. In this section (Szakallas and Savage, 1980), we will present the dynamic investigation of two basic types of models:

- The “open-track” cam-follower system uses a spring-loaded follower to constrain the follower to the cam. The spring force is transmitted to the cam at all times in which the torque on the cam drive has the same frequency as the rotation of the cam.
- The “closed-track” cam-follower system uses rollers constrained in cam grooves or, as in the conjugate design, dual rollers on two cams. It is seen that the closed-track system subjected to an inertia load will have significant compliances to yield twice the frequency of the cam speed. This phenomenon affects both the torsion and flexure in the shaft.

**12.4.2.1 Open-Track Cam System.** Figure 12.10 depicts the schematic open-track cam-follower system in which the cam rotation  $\theta_c$  differs from the camshaft input rotation  $\theta_i$  because of shaft elasticity.

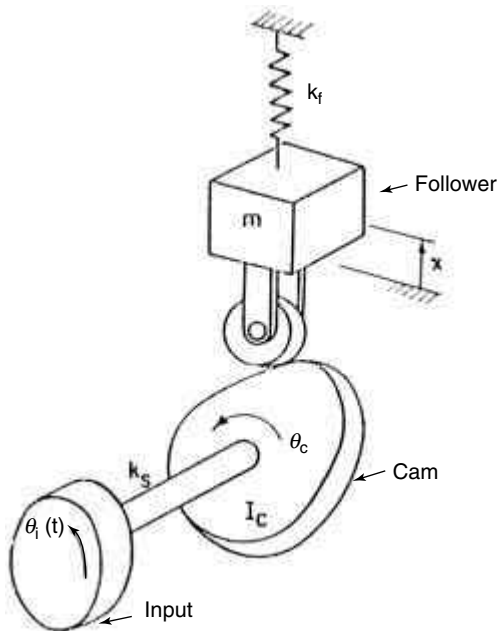
Where

$a$  = ratio of maximum return spring force to the maximum nominal follower inertia force

$F_h$  = contact force in the circumferential direction between the cam surface and the follower, lb (N)

$F_n$  = nominal cam force, lb (N)

$F_s$  = follower return spring force, lb (N)



**FIGURE 12.10.** Schematic of elastic drive, open-track cam-follower system.

$F_{sh}$  = torque on shaft, lb/in (Nm)

$F_y$  = compressive contact force in the radial direction between the cam surface and the follower, lb (N)

$I_c$  = mass moment of inertia of the cam, lb/in<sup>2</sup>/RAD (N/m/RAD)

$k_r$  = follower return spring rate, lb/in/RAD (N/m)

$k_s$  = drive system flexibility lb/in/RAD (N/m/RAD)

$m$  = follower mass, lb (kg)

$Q$  = variable reflected follower inertia ratio

$Q_m$  = maximum reflected inertia ratio

$R$  = radius from cam center to follower roller center, in (m)

$T$  = drive system torque at cam speed, lb/in (N-m)

$t$  = time, sec

$x$  = follower displacement, in (m)

$\dot{x}$  = follower velocity ( $dx/dt$ ) in/sec (m/s)

$\ddot{x}$  = follower acceleration ( $d^2x/dt^2$ ) in/sec<sup>2</sup> (m/s<sup>2</sup>)

$x'$  = cam slope ( $dx/d\theta_c$ ), in (m)

$x''$  = rate of change of cam slope ( $d^2x/d\theta_c^2$ ), in (m)

$x_f$  = final or total displacement of rise, in (m)

$y$  = normalized cam position, in (m)

$\beta$  = variable cam drive system windup ratio

$\beta_m$  = maximum cam drive system windup ratio

$\gamma$  = variable follower radial force ratio

$\gamma_m$  = maximum follower radial force ratio

$\eta$  = limiting linear frequency ratio

$\theta_c$  = cam angular position, rad

$\dot{\theta}_c$  = cam angular velocity, rad/sec

$\ddot{\theta}_c$  = cam angular acceleration, rad/sec<sup>2</sup>

$\theta_f$  = final or total duration of rise, rad

$\theta_i$  = input power source position, rad

$\dot{\theta}_i$  = input power source speed, rad/sec

$\phi$  = cam surface pressure angle, rad

$\omega_b$  = base natural frequency rad/sec

$\omega_l$  = limiting linear natural frequency, rad/sec

$\omega_n$  = variable natural frequency, rad/sec

The system takes account of camshaft flexibility and leads to a set of nonlinear equations owing to the fact that the driving-cam function is no longer a known function of time.

In Fig. 12.10, where  $\theta_i(t)$ , the input shaft rotating at a known angular rate, is not equal to the cam angle,  $\theta_c$ , or  $\theta_i \neq \theta_c$ . This is due to camshaft flexibility;  $k_s$  is the camshaft spring rate and the cam-follower rise is  $x$ . A convenient method of formulation is derivable from Lagrange's equations as follows:

$$T = \frac{1}{2} M \dot{x}^2 + \frac{1}{2} I \dot{\theta}_c^2$$

$$V = \frac{1}{2} k_s (\theta_c - \theta_i)^2 + \frac{1}{2} k_r x^2$$

$$L = T - V.$$

The follower is constrained by the cam function

$$x = x(\theta_c)$$

where  $\theta_i = \theta_i(t)$ , by the Lagrange multiplier method

$$\begin{aligned} F_n dx - F_n x' d\theta_c &= 0 & x' &= dx(\theta_c)/d\theta_c \\ F_{sh} d\theta_1 - F_{sh} \theta_1' dt &= 0 & \theta' &= d\theta_i/dt \end{aligned}$$

$$\left( \frac{d}{dt} \frac{\delta L}{\delta \dot{x}} - \frac{\delta L}{\delta x} \right) dx + F_n dx = 0 \rightarrow m\ddot{x} + kx + F_n = 0 \quad (12.12)$$

$$\left( \frac{d}{dt} \frac{\delta L}{\delta \dot{\theta}_c} - \frac{\delta L}{\delta \theta_c} \right) d\theta_c - F_n x' d\theta_c = 0 \rightarrow I_c \ddot{\theta}_c + k_s(\theta_c - \theta_i) - F_n x' = 0 \quad (12.13)$$

$$\left( \frac{d}{dt} \frac{\delta L}{\delta \dot{\theta}_i} - \frac{\delta L}{\delta \theta_i} \right) d\theta_i + F_{sh} = 0 \rightarrow k_s(\theta_i - \theta_c) + F_{sh} = 0.$$

where  $F_n$  = contact force on cam  
 $F_n x'$  = torque on cam due to contact force  
 $F_{sh}$  = torque on shaft

Eliminating  $F_n$  between Eqs. (12.12) and (12.13) and taking two time derivatives of  $x(\theta_c)$  yields

$$\begin{aligned} m\ddot{x}x' + k_f xx' + I_c \ddot{\theta}_c + k_s(\theta_c - \theta_i) &= 0 \\ \ddot{x} &= x''\dot{\theta}_c^2 + \ddot{\theta}_c x' \end{aligned}$$

whence

$$(I_c + mx'^2)\ddot{\theta}_c + mx'x''\dot{\theta}_c + k_f xx' + k_s\theta_c = k_s\theta_i(t) \quad (12.14)$$

yields the basic second degree vibration equation characterized as the spring-windup equation.

The equation is consistent with those reported in cam windup studies by Bloom and Radcliffe (1964) and Koster (1975a and b).

The problem being studied is one of self-induced torsional vibration in the cam system. The transient response is of interest with the angular velocity of the power source being a constant. Also the torque response for the open-track system fluctuates about the same rotational speed as the input system.

Four dimensionless parameters are used to characterize the dynamic response of the system. These parameters, according to Szakallas and Savage (1980), are the frequency ratio  $\eta$ , the reflected inertia ratio  $Q_m$  (measure of nonlinearity of the system), the maximum drive windup ratio  $\beta_m$ , and the maximum radial force ratio  $\gamma_m$ .

$$\begin{aligned} \eta &= \frac{\omega_i}{\omega_f} \frac{\theta_f}{2\pi\theta_i} \sqrt{\frac{k_s}{I_c}} \quad \text{where} \quad \omega_b = \frac{2\pi}{\theta_f} \dot{\theta}_i \\ Q_m &= \frac{m(x'_{\max})^2}{I_c} \\ \beta_m &= \left( \frac{\theta_i - \theta_f}{\theta_f} \right)_r \\ \gamma_m &= \frac{F_y}{F_n} = \frac{k_f x + m\ddot{x}}{mx_f \left( \frac{\dot{\theta}_i}{\theta_f} \right)^2} \end{aligned} \quad (12.15)$$

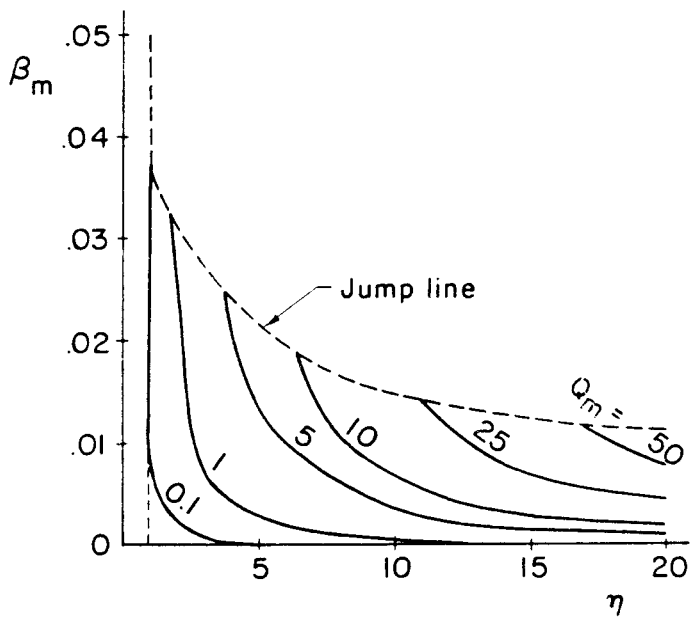
Figures 12.11 and 12.12 show for an open-track spring-loaded system a plot of the maximum windup ratio  $\beta_m$  versus  $\eta$ , with  $Q_m$  as a varying parameter for the harmonic cam curve and for the cycloidal cam curve, respectively.  $Q_m$  is a measure of the degree of severity of the drive shaft windup. For  $Q_m = 0$ , there is no windup in the drive train since the drive train vibration is caused by the accelerating and decelerating torques required to move the follower mass through its rise. Thus, the greater  $Q_m$ , the greater is this forcing function. The jump line indicates the limiting condition in which the vibration model is invalid.

From these figures, one can see that increasing the value of the frequency ratio  $\eta$  and decreasing the value of the reflected inertia ratio  $Q_m$  imply stiffer systems, thus reducing the drive system windup effect. Furthermore, the harmonic rise produces lower drive shaft windup than the cycloidal curve cam.

**12.4.2.2 Closed-Track Cam System.** Next let us consider the closed-track cam follower system, Fig. 12.13. This system has special physical phenomena when compared to the open-track system presented earlier. In the closed-track system we see

- The torsional vibration and the response frequency are two times the basic speed of the input. The follower and cam are constrained together and reflect and exchange their rotation energy throughout the whole cycle.
- Equation (12.14) is modified by the elimination of the term,  $k_r x \dot{x}' = 0$ , since there is no return spring that gives the second-degree vibration equation for the closed-track cam-follower system

$$(I_c + mx'^2)\ddot{\theta}_c + mx'x''\dot{\theta}_c^2 + k_s \theta_c = k_s \theta_i(t). \tag{12.16}$$



**FIGURE 12.11.** Maximum windup ratio  $\beta_m$  versus  $\eta$  with  $Q_m$  as varying parameter open-track (harmonic cam).

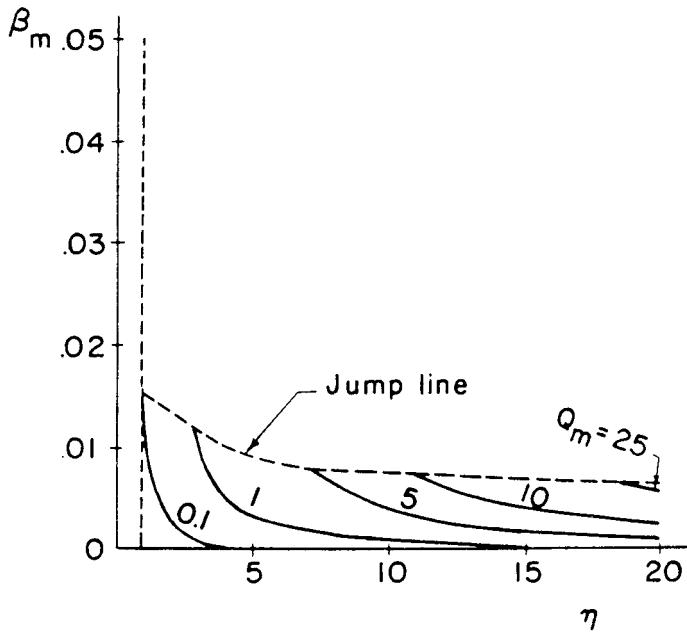


FIGURE 12.12. Maximum windup ratio  $\beta_m$  versus  $\eta$  with  $Q_m$  as varying parameter open-track (cycloidal cam).

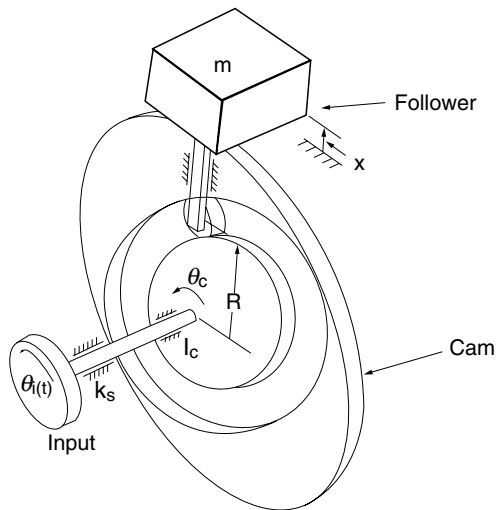
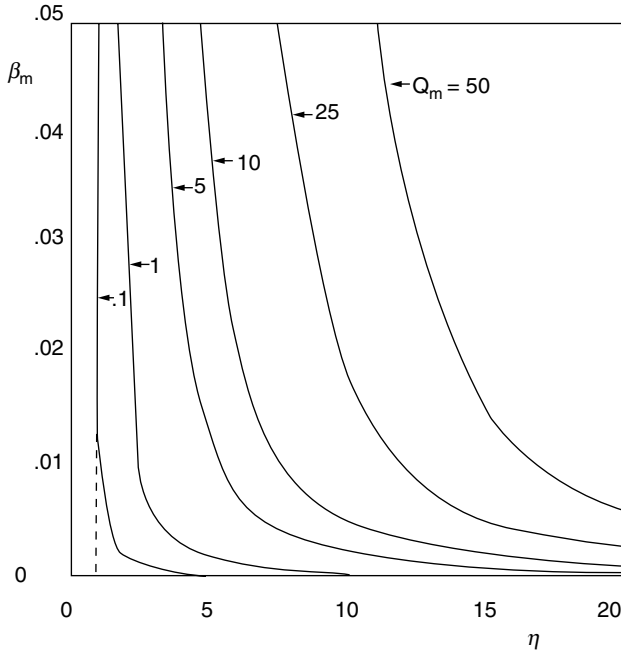


FIGURE 12.13. Schematic of elastic drive, closed-track cam-follower system.

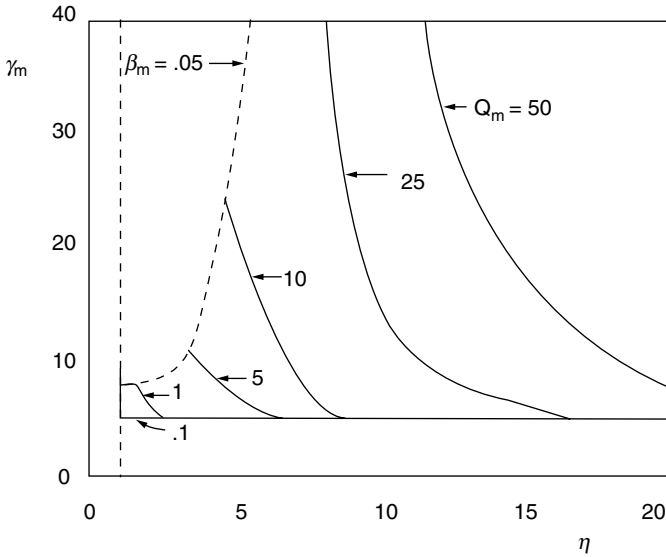


**FIGURE 12.14.** Dimensionless windup chart for closed-track cam with a harmonic rise.

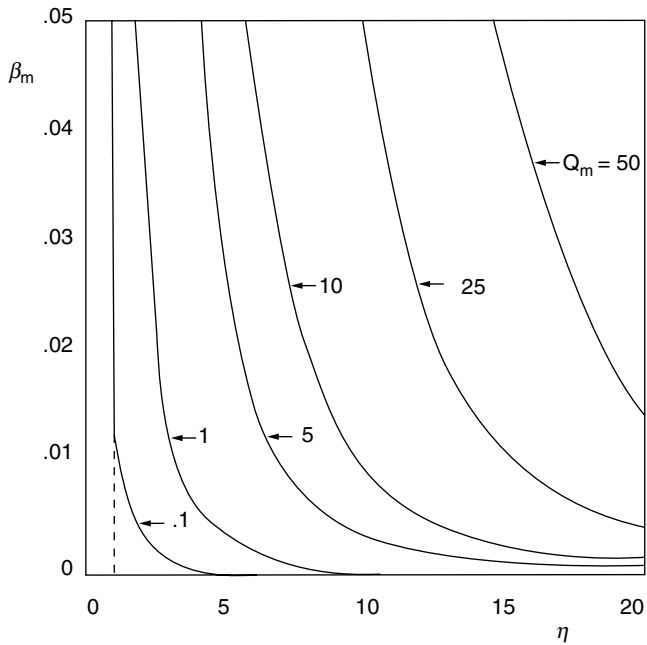
Figures 12.14 through 12.17 are the contour plots of  $\beta_m$  and  $\gamma_n$  for the harmonic and cycloidal curve investigation of this system. These charts also allow one to compare the performance of the harmonic and cycloidal cam rises. When looking at the follower system for a constant cam speed, cycloidal motion has definitely better dynamic characteristics. However, for this drive system vibration problem, the harmonic rise has lower drive system windups and lower radial follower forces than the cycloidal rise. This is true for both the closed-track cam system and the open-track cam system with a return spring. The difference is even greater than appears in a direct chart comparison because the harmonic rise has a lower maximum slope than the cycloidal rise for the same endpoints.

These charts may be used by a designer to determine at an early point in the design whether drive system windup will be a problem. Given design estimates for  $\theta_f$ ,  $x_f$ ,  $\theta_s$ ,  $I_c$ ,  $M$ , and  $k_s$  one can quickly estimate the maximum windup, dynamic drive system torque, and radial follower force for a harmonic or cycloidal cam. Also, other high-speed curves such as modified sine and modified trapezoidal offer better performance characteristics than the two basic curves studied in this section. Thus for well-designed, stiff systems, a moderate spring size will keep the follower in contact. However, for a more flexible system (low  $\eta$ ) with a degree of nonlinearity (nonzero  $Q_m$ ), follower separation is to be expected along with the other ills of vibration.

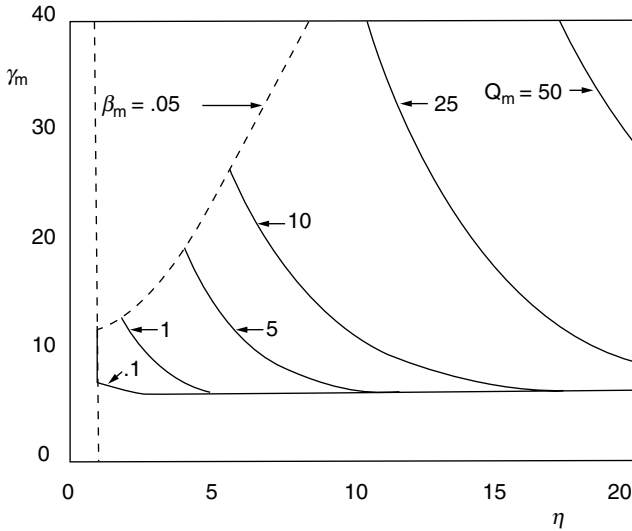
Comparing the performance of the open-track cams below the point of follower separation to the closed-track cams, the addition of the return spring affects the vibration. It increases the minimum radial force ratio but removes the effects of the reflected inertia ratio on the radial force if separation does not occur. It also increases the drive system windup at higher frequency ratios ( $\eta$ ) while decreasing the drive system windup at lower



**FIGURE 12.15.** Radial force ratio chart for closed-track cam with a harmonic rise.



**FIGURE 12.16.** Dimensionless windup chart for closed-track cam with a cycloidal rise.



**FIGURE 12.17.** Radial force ratio chart for closed-track cam with a cycloidal rise.

frequency ratios. Thus for a well-designed cam system that operates at high frequency ratios, the closed-track cam system without a return spring has better performance characteristics. Comparisons are academic because closed-track systems are utilized only in commercial production machinery, and open-track systems are best for only the automotive field.

**EXAMPLE** Consider an open-track dwell-rise-dwell cam-follower-driveshaft system having a cycloidal cam curve with the following data:

Cam speed, 350 rpm (36.65 rad/sec)

Stroke,  $h = 0.02$  m

Total cam angle,  $\beta = 90^\circ$

Follower mass,  $m = 50$  kg

Drive train spring stiffness,  $k_s = 10,000$  N-m/rad

Cam moment of inertia,  $I = 0.005$  kg-m<sup>2</sup>

Return spring coefficient (the ratio between the maximum spring force and maximum nominal follower inertia force),  $a = 1.5$

**Solution** The cycloidal cam study of the torsional windup of the system gives

$$x'_{\max} = \frac{2h}{\beta} = \frac{2(0.02)}{\frac{\pi}{2}} = 0.0255$$

$$x''_{\max} = \frac{2\pi h}{\beta^2} = \frac{2\pi(0.02)}{\left(\frac{\pi}{2}\right)^2} = 0.051.$$

Thus the return spring rate, the linear frequency ratio, and the maximum reflected inertia ratio are

$$k_r = \frac{am}{h} x''_{\max} \dot{\theta}_i^2 = \frac{1.5(50)}{0.02} (0.051)(36.65)^2 = 0.257 \times 10^6 \text{ N/m}$$

$$\eta = \frac{\omega_i}{\omega_b} \frac{\beta}{2\pi\theta_i} \sqrt{\frac{k_i}{I}} = \frac{\beta^2}{(2\pi\dot{\theta}_i)^2} \frac{k_i}{I} = \frac{\left(\frac{\pi}{2}\right)^2}{(2\pi \times 36.65)^2} \frac{10,000}{0.005} = 9.31$$

$$Q_m = \frac{m}{I} (x'_{\max})^2 = \frac{50}{0.005} (0.0255)^2 = 6.50.$$

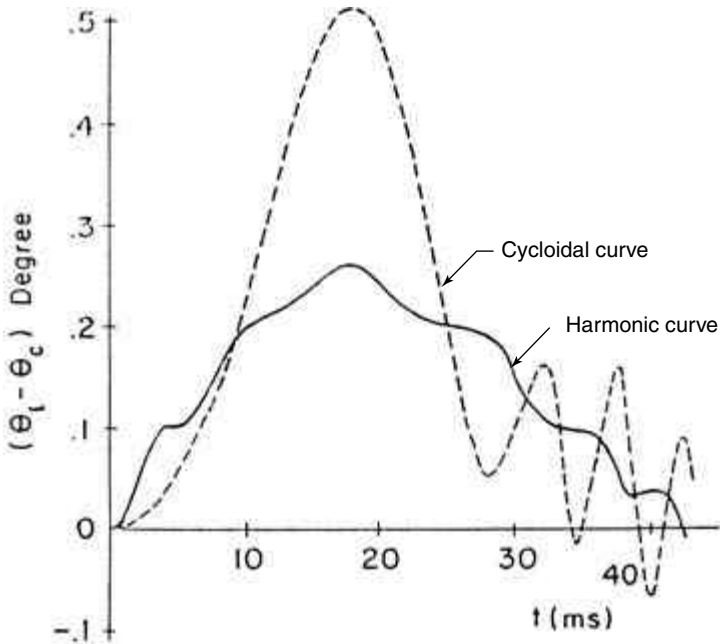
From Fig. 12.11 we obtain  $\beta_m = 0.006$ . The corresponding maximum driveshaft windup is

$$\theta_i - \theta_c = 0.006 \left(\frac{\pi}{2}\right) = 0.0094 \text{ rad } (0.54^\circ)$$

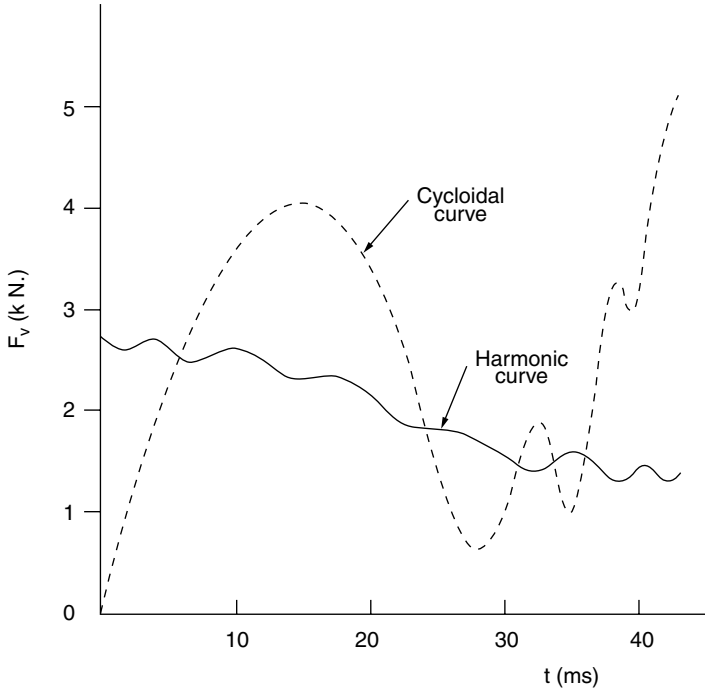
and the associated dynamic windup torque is

$$T_m = k_i \beta_m \beta = 10,000 \times 0.006 \frac{\pi}{2} = 94.2 \text{ N-m.}$$

Graphical plots of windup versus time and of radial contact force versus time are given as the dashed curves in Figs. 12.18 and 12.19.



**FIGURE 12.18.** Example comparison of shaft windup between harmonic cam and cycloidal cam.



**FIGURE 12.19.** Example comparison of contact force between harmonic cam and cycloidal cam.

If this design is unacceptable, we may replace the cycloidal cam curve with a simple harmonic curve, other modified harmonic, or modified trapezoidal curve, keeping the other condition intact. By so doing we can calculate

$$x'_{\max} = \frac{h\pi}{2\beta} = 0.02$$

$$x''_{\max} = \frac{h\pi^2}{2\beta^2} = 0.04.$$

$\eta$  will remain unchanged, but  $k_r$  becomes equal to  $0.2 \times 10^6 \text{ N/m}$ , and  $Q_m$  becomes equal to approximately 4.0.

From Fig. 12.11 we obtain  $\beta_m = 0.0025$ . Thus  $\theta_i - \theta_c = 0.25^\circ$  and its corresponding peak windup torque is  $T_m = 45 \text{ N}\cdot\text{m}$ . Therefore, a change from a cycloidal rise to a harmonic rise reduces the forcing function by about 50 percent. Charts of windup versus time and of radial contact force versus time for this harmonic cam system are given as the solid curves in Figs. 12.18 and 12.19.

### 12.4.3 Two-Degree-of-Freedom System

Let us consider a two-degree-of-freedom closed-track cam follower system with an elastic camshaft and an elastic follower. In Fig. 12.20a we see a schematic of the mechanism. In Fig. 12.20b it is observed that torque

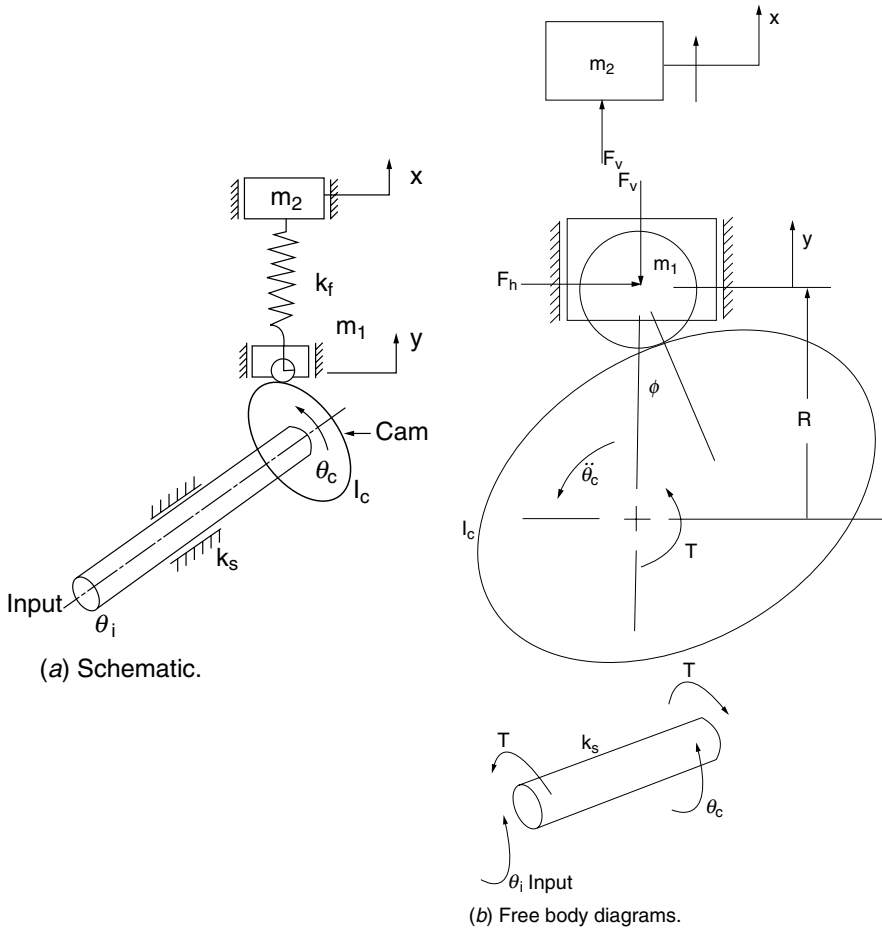


FIGURE 12.20. Two-degree-of-freedom, closed-track cam system, coupled elastic follower.

$$T = (\theta_i - \theta_c)k_s - k_f(y - x) R \tan \phi \tag{12.17}$$

where  $T$  is the net torque accelerating the cam and the bottom of the follower. Therefore, the torque

$$T = I_c \ddot{\theta}_c + m_1 \ddot{y} R \tan \phi$$

where  $m_1$  is the mass of the follower base, and rotational acceleration of the roller has been neglected. Also the follower  $m_1$  has the following characteristics of displacement, velocity, and acceleration (see Chap. 2 for symbols).

$$\begin{aligned} y &= y(\theta_c) \\ \dot{y} &= y' \dot{\theta}_c \\ \ddot{y} &= y'' \dot{\theta}_c^2 + y' \ddot{\theta}_c \end{aligned}$$

which yields

$$T = I_c \ddot{\theta}_c + m_1 R \tan \phi (y'' \dot{\theta}_c^2 + y' \ddot{\theta}_c) \tag{12.18}$$

$$\begin{aligned} y &= R \tan \phi \dot{\theta}_c = y' \dot{\theta}_c \\ y' &= R \tan \phi. \end{aligned} \tag{12.19}$$

Therefore, from Eqs. (12.17), (12.18), and (12.19)

$$(\theta_i - \theta_c) k_s + k_f (x - y) y' - m_1 y'' y' \dot{\theta}_c^2 = (I_c + m_1 y'^2) \ddot{\theta}_c.$$

Summing forces on mass  $m_2$  at the follower top

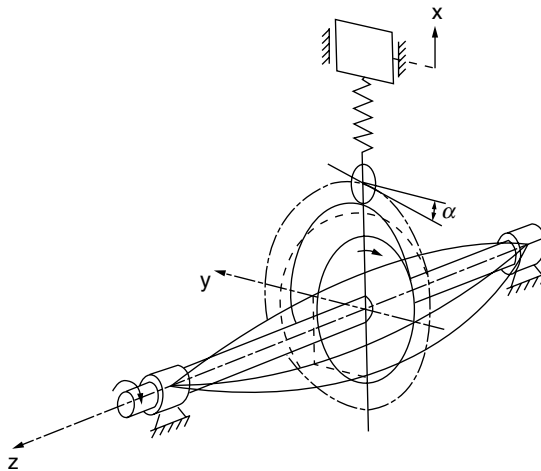
$$m_2 \ddot{x} = k_f (y - x). \tag{12.20}$$

If there is no model mass  $m_1$  those terms in the equation will be eliminated.

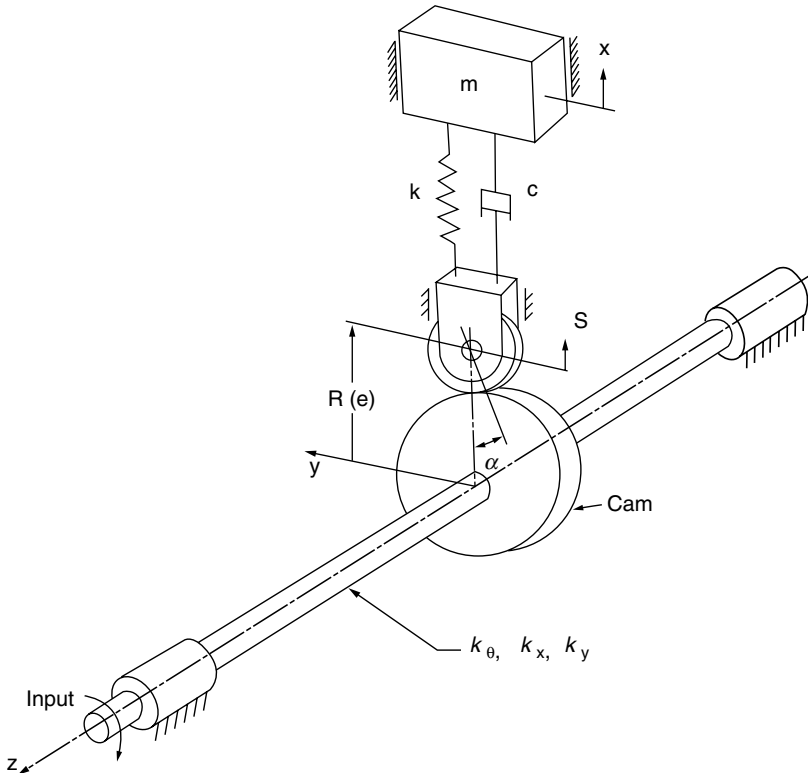
### 12.4.4 Four-Degree-of-Freedom System

Next, let us analyze a four-degree-of-freedom model with coupled elastic follower and elastic torsional and flexural camshaft (Fig. 12.21) to further study the effects of flexibility in the driveshaft on the vibratory response of the cam follower.

Figure 12.22 shows the sketch of the system which has a closed-track cam-follower system. Note in Figs. 12.21 and 12.22 that the cam is located at the middle of the elastic shaft for convenient analysis. However, it is an essence of good design not to locate the cam in the center of the shaft, permitting deflections in three directions. The cam is usually located as close to a rigid bearing as possible, largely to eliminate the flexural vibrational factors. Also, a phenomenon exists in the closed-track system, see Wiederrich



**FIGURE 12.21.** Diagram of the four-degree-of-freedom cam-follower mechanism.



**FIGURE 12.22.** Coupled system of a four DOF closed-track cam-follower and flexible driveshaft.

(1973), in which the initial effects of the follower are reflected in the elastic camshaft and thus the torsion and two-dimensional bending modes are excited at twice the frequency of other modes. Note, this phenomenon does not effect the open-track cam-follower with its constraining external spring force on the follower for the complete cycle of operation.

This model, shown in Fig. 12.22, is obtained by assuming that the equivalent mass  $m$  of the follower is lumped in one point and constrained to move in the vertical direction only. The elasticity of the follower corresponds to a linear spring, with stiffness  $k$  supporting the mass. Damping in the follower is represented by the viscous damping coefficient  $c$ . The flexible camshaft is represented by the torsional stiffness  $k_\theta$  and the transverse (bending) stiffnesses  $k_x$  and  $k_y$  in the  $x$  and  $y$  directions, respectively. Also,  $x$ ,  $\dot{x}$ , and  $\ddot{x}$  are the follower displacement, velocity and acceleration, and  $s$ ,  $\dot{s}$ , and  $\ddot{s}$  are the cam displacement, velocity, and acceleration, respectively. The input angular velocity is considered to be constant. Backlash is neglected. This model has been developed by Koster (1975) and Ardayfio (1976).

The motion of the bending of the follower roller is a function of the cam rotation  $\theta$  and the elastic deflections of the camshaft in the  $y$  and  $x$  directions. The slope of the cam can be approximated

$$\tan \alpha = \frac{1}{R(\theta)} \frac{ds}{d\theta}.$$

Thus the nominal follower velocity is

$$\dot{s} = \omega R(\tan) \alpha \quad (12.21)$$

where  $\omega$  is the constant input angular velocity of the shaft. Integrating Eq. (12.21) gives the nominal displacement at the roller

$$s = \omega \int_0^t R(\theta) \tan \alpha dt. \quad (12.22)$$

The equivalent stiffness  $k_{eq}$  of the system is derived in Koster (1975).

$$\frac{1}{k_{eq}} = \frac{1}{k_c} + \frac{1}{k_t} \tan^2 \alpha \quad (12.23)$$

where  $k_{eq}$ , the equivalent vertical spring stiffness, is

$$k_c = \frac{kk_x}{k + k_x}$$

and  $k_c$ , the equivalent tangential spring stiffness, is

$$k_c = \frac{k_y k_\theta}{k_y + k_\theta}.$$

$k_{eq}$  thus obtained is time-dependent.

The original model with four degrees of freedom may be approximated by a model with a single degree of freedom with variable stiffness, using the general application for the rule of transformation. The equation of motion of the system

$$m\ddot{x} + c(\dot{s} - \dot{x}) + k_{eq}(s - x) = 0$$

where the dots represent differentiation with respect to time.

Using Eq. (12.23) gives

$$m\ddot{x} + c(\dot{s} - \dot{x}) + \frac{k_c}{1 + \frac{k_c}{k_t} \left( \frac{1}{\omega R} \dot{s} \right)^2} (s - x) = 0. \quad (12.24)$$

The effect of the flexibility of the shaft is greatest for the position of the cam corresponding to  $\alpha = \alpha_{\max}$ . For many cam profiles this occurs at the midpoint of the cam. As a first approximation,  $R(\theta)$  can be replaced by the mean pitch radius of the cam

$$R(\theta) = R_m. \quad (12.25)$$

Eq. (12.24) can now be rewritten as

$$m\ddot{x} + c(\dot{s} - \dot{x}) + \frac{k_c}{1 + \frac{k_c}{k_t} \left( \frac{1}{\omega R_m} \dot{s} \right)^2} (s - x) = 0. \quad (12.26)$$

Next, the following nondimensional parameters are introduced:

$$\begin{aligned} \tau &= \frac{tX}{T_1} \\ \Gamma &= \frac{s}{h} \quad \dot{\Gamma} = \frac{\dot{s}T_1}{h} \\ X &= \frac{x}{h} \quad \dot{X} = \frac{\dot{x}T_1}{h} \quad \ddot{X} = \frac{\ddot{x}T_1^2}{h}, \\ T &= \frac{2\pi}{T_1} \sqrt{\frac{m}{k_c}} \\ \xi &= \frac{cT}{4\pi} \\ F &= \frac{k_c}{k_f} \left( \frac{h}{R_m \beta} \right)^2 \quad \beta = \omega T_1, \end{aligned}$$

where  $h$  is the cam lift in a dwell-rise-dwell motion input and  $T_1$  is the period of such input. Substituting these into Eq. (12.26) yields

$$(1 + \dot{\Gamma}^2 F) \ddot{X} + 2\xi(1 + \dot{\Gamma}^2 F) \left( \frac{2\pi}{T} \right) \dot{X} + \left( \frac{2\pi}{T} \right)^2 X = 2\xi(1 + \dot{\Gamma}^2 F) \left( \frac{2\pi}{T} \right) \dot{\Gamma} + \left( \frac{2\pi}{T} \right)^2 \Gamma. \quad (12.27)$$

This is a second-order linear differential equation with variable coefficients.

Figure 12.23 shows the acceleration response of a cycloidal cam with  $T = 0.15$  when damping is not taken into account. Note that when  $F = 0$  (corresponding to an infinitely rigid shaft), the curve resembles that of nominal acceleration. With  $F$  increasing, the amplitudes of the residual vibration increase markedly. The reason for this phenomenon is that at big values of  $F$ , i.e., with a relatively flexible shaft, a large amount of energy is stored in windup and bending during the first half of the cam lift. During the second half, with the decreasing slope of the cam, the shaft relaxes and acts as a catapult. At the increased angular velocity of the cam, the deceleration of the follower may appreciably exceed the nominal value, so that heavy vibrations will persist after the end of the cam rise. Figure 12.24 shows a plot of the residual amplitude of acceleration versus  $T$ , with  $F$  as a varying parameter for an undamped cycloidal cam. Damping would change the effect very little.

### 12.4.5 Multi-Degree-of-Freedom System

A complex dynamic model with eleven degrees of freedom was studied by Kim and Newcombe (1981). For more on multi-degree-of-freedom systems, see Pisano and Freudenstein (1983). Kim and Newcombe (1981) also presented a study to take into account the random nature of flexibility and fabrication errors. Figure 12.25 shows the schematic model consisting of driving torsional and driven translational subsystems. Figure 12.26 shows the three-degree-of-freedom torsional subsystem model. Figure 12.27 displays the eight-degree-of-freedom translational subsystem model. The latter is divided into two subsystems according to the vertical motion ( $y$  axis) and the horizontal motion ( $x$  axis) of the parts.

Using Newton's second law, we can write the following sets of equations of motion.

For translational movement of the follower (see Fig. 12.27) along the  $y$  axis direction

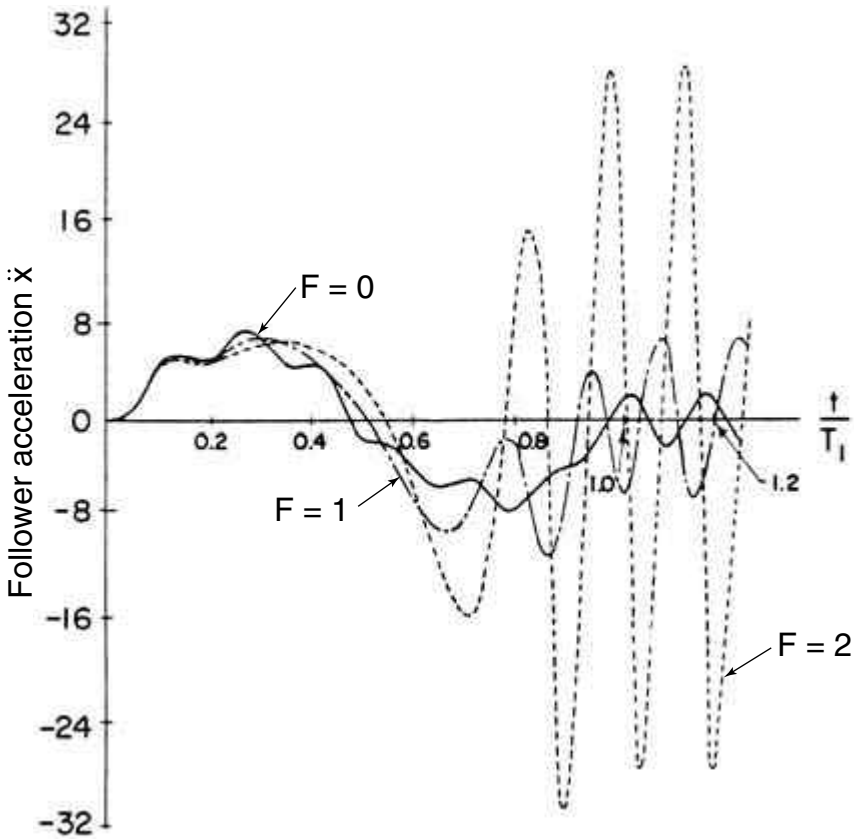


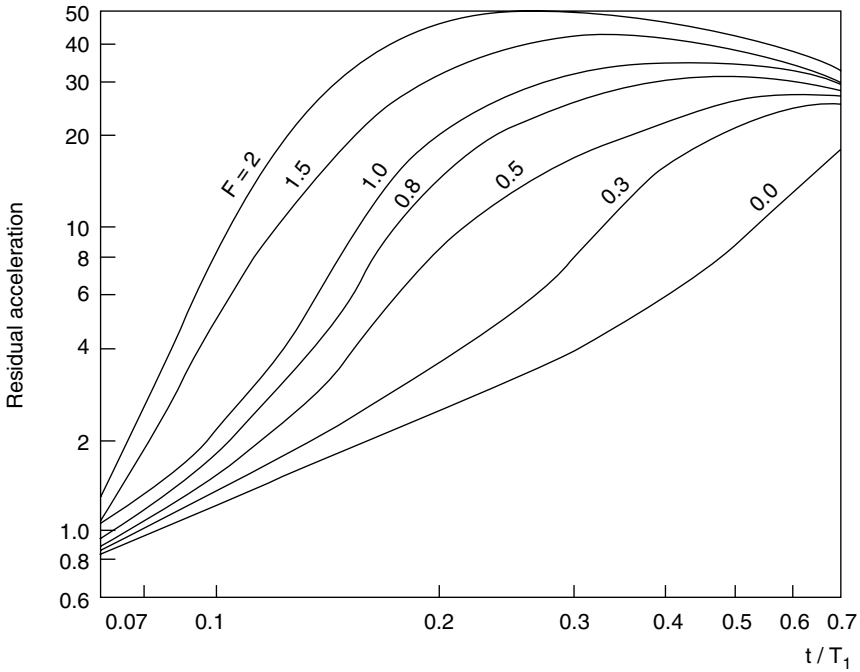
FIGURE 12.23. Acceleration response for cycloidal cam with  $T = 0.15$ , undamped, and different degrees of driveshaft flexibility.

$$\begin{aligned}
 M_l \dot{y}_5' + c_{f1}(\dot{y}_5' - \dot{y}_4') + k_f(y_5 - y_4) &= 0 \\
 M_f \dot{y}_4' - c_{f1}(\dot{y}_5' - \dot{y}_4') + \frac{1}{2}c_f \dot{y}_4' + k_{vc}(y_4 - y_3) - k_f(y_5 - y_4) &= 0 \\
 M_{fc} \dot{y}_3' + \frac{1}{2}c_f \dot{y}_3' + k_{rb}(y_3 - y_2) - k_{vc}(y_4 - y_3) + F_p + k_{rs}y_3 &= 0 \\
 M_r \dot{y}_2' - k_{rb}(y_3 - y_2) - F_n \cos \alpha &= 0 \\
 M_c \dot{y}_1' + c_{vs} \dot{y}_1' + k_{vs}y_1 + F_n \cos \alpha &= 0
 \end{aligned} \tag{12.28}$$

along the x-axis

$$\begin{aligned}
 M_{fc} \ddot{x}_3 - k_{rb}(x_2 - x_3) + k_{hc}x_3 &= 0 \\
 M_r \ddot{x}_2 + k_{rb}(x_2 - x_3) + F_n \sin \alpha &= 0 \\
 M_c \ddot{x}_1 + c_{hs} \ddot{x}_1 + k_{hs}x_1 - F_n \sin \alpha &= 0.
 \end{aligned} \tag{12.29}$$

For torsional movement of the drive shaft (see Fig. 12.26)



**FIGURE 12.24.** Residual amplitude of acceleration versus  $T$  with  $F$  as varying parameter undamped (cycloidal cam).

$$\begin{aligned}
 I_m \ddot{\theta}_m + c_{sl}(\dot{\theta}_m - \dot{\theta}_{cp}) + c_{mb} \dot{\theta}_m + k_{s1}(\theta_m - \theta_{cp}) - T_i &= 0 \\
 I_{cp} \ddot{\theta}_{cp} - c_{sl}(\dot{\theta}_m - \dot{\theta}_{cp}) + c_{s2}(\dot{\theta}_{cp} - \dot{\theta}_c) - k_{sl}(\theta_m - \theta_{cp}) + k_{s2}(\theta_{cp} - \theta_c) &= 0 \\
 I_c \ddot{\theta}_c - c_{s2}(\dot{\theta}_{cp} - \dot{\theta}_c) + c_{cc} \dot{\theta}_c - k_{s2}(\theta_{cp} - \theta_c) + T_0 &= 0.
 \end{aligned} \quad (12.30)$$

In the expressions above

$$T_o = \frac{\ddot{\theta}}{\theta} F_c \cos \alpha$$

where

$F_n$  = the contact force between the cam and follower roller  
 $\alpha$  = the pressure angle

The damping forces  $\frac{1}{2} c_f \dot{y}_4$  and  $\frac{1}{2} c_f \dot{y}_3$  are to be replaced by the friction forces  $F_1$  and  $F_2$  caused by the contact force  $F_n$ , which will be found later. To be able to simulate the simultaneous differential Eqs. (12.28) and (12.29), the parameters such as the mass, the spring stiffness, and the damping coefficient first must be determined.

If we denote  $\delta_{rs}$  as the length of the spring subjected to compression,  $F_p$  as the spring preload, and  $k_s$  as the total equivalent spring constant, then

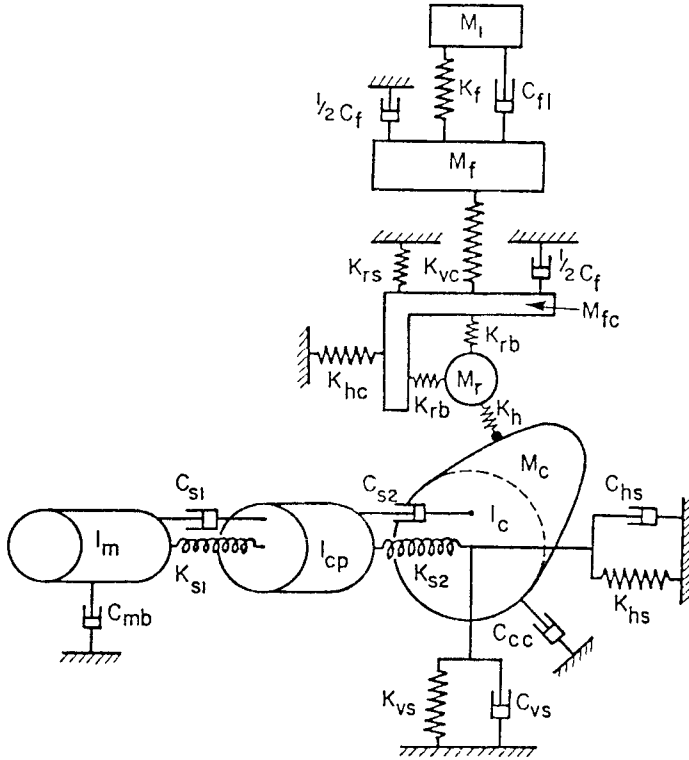


FIGURE 12.25. 11-degree-of-freedom cam-follower system model.

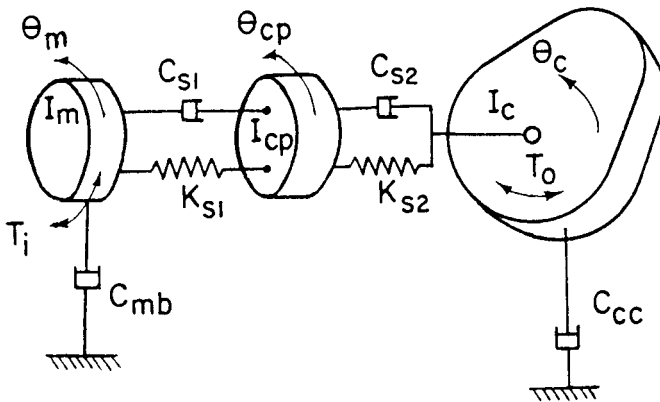


FIGURE 12.26. Three-degree-of-freedom torsional subsystem model.

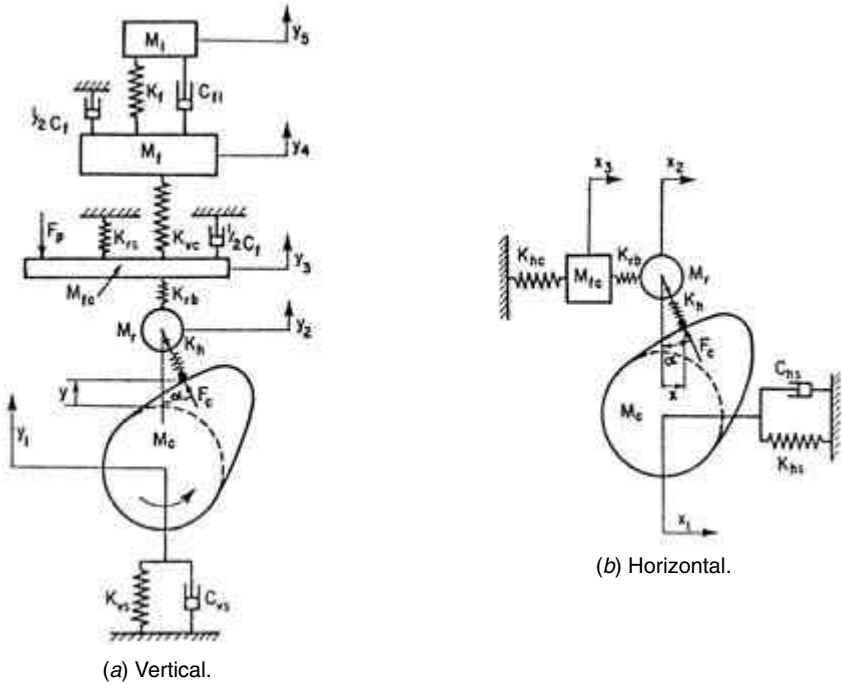


FIGURE 12.27. 8-degree-of-freedom translational subsystem models.

$$\delta_{rs} = \frac{F_p}{k_t} = \frac{F_p}{k_{rs}} + \frac{F_p}{k_{rb}} + \frac{F_p \cos^2 \alpha}{k_h} + \frac{F_p}{k_{vs}}$$

and

$$\frac{1}{k_t} = \frac{k_{rb}k_hk_{vs} + k_{rs}k_hk_{vs} + k_{rs}k_{rb}k_{vs} \cos^2 \alpha + k_{rs}k_{rb}k_h}{k_{rs}k_{rb}k_hk_{vs}}$$

Then

$$F_p = \delta_{rs} k_t = \frac{k_{rs}k_{rb}k_hk_{vs} \delta_{rs}}{k_{rb}k_hk_{vs} + k_{rs}k_hk_{vs} + k_{rs}k_{rb}k_{vs} \cos^2 \alpha + k_{rs}k_{rb}k_h}$$

The normal contact force  $F_n$  is obtained according to the criterion of separation of contact between the cam and roller,

$$y_2 \leq y + y_1 + \frac{F_p}{k_h}$$

For  $y_2 < y + y_1 + \frac{F_p}{k_h}$ , contact is maintained, thus

$$F_n = k_h(y + y_1 - y_2)\cos\alpha + F_p\cos\alpha$$

and for  $y_2 \geq y + y_1 + \frac{F_p}{k_h}$ , separation occurs, thus

$$F_n = 0.$$

Therefore, we may regard  $y_2 = y + y_1 + \frac{F_p}{k_h}$  as providing the least contact separation.

To calculate the contact force, the spring stiffness  $k_h$  for contact between the cam and the roller should be defined. We recall that for two cylinders having thickness  $w$ , the width of the rectangular contact area,  $2b$ , can be obtained from Chap. 9, the hertzian stress formula. Thus,

$$b = \left[ \frac{2P}{\pi w} \frac{\frac{1-\mu_1^2}{E_1} + \frac{1-\mu_2^2}{E_2}}{\left(\frac{1}{\rho_1} + \frac{1}{\rho_2}\right)} \right]$$

where

$\mu_1, \mu_2$  = Poisson's ratio of materials for the roller and the cam, respectively

$E_1, E_2$  = the modulus of elasticity of materials for the roller and the cam, respectively

$\rho_1, \rho_2$  = the radius of the roller and the cam, respectively

Note that  $\rho_2$  varies according to the contact position and is given

$$\rho_2 = \frac{\left[ (r_o + s)^2 + \left( \frac{ds}{d\theta} \right)^2 \right]^{3/2}}{(r_o + s)^2 + 2 \left( \frac{ds}{d\theta} \right)^2 - (r_o + s) \frac{d^2s}{d\theta^2}}$$

where  $r_o = r_b + r_1$ ,  $R_b$  is the base circle radius. Also, with reference to the geometry of Chap. 9, the depth of deformations

$$h_1 = \rho_1 - \sqrt{\rho_1^2 - b^2}$$

$$h_2 = \rho_2 - \sqrt{\rho_2^2 - b^2}.$$

Since  $k_h = \frac{P}{H}$ , and by assuming unity  $P$ , we finally get

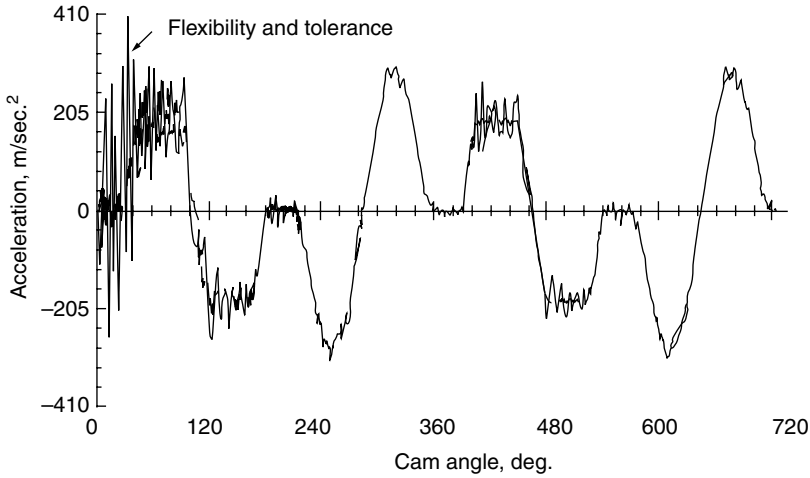
$$k_h = \frac{1}{h_1 + h_2}.$$

The frictional forces between the follower stem and the follower guide can be calculated at

$$F_1 = \mu N_1$$

$$F_2 = \mu N_2$$

where  $\mu$  is the coefficient of friction between the follower and its guide. From static force equilibrium,



**FIGURE 12.28.** Example showing the first two whole revolutions of the cam and transient accelerations over the cam.

$$N_1 = \xi F_n \sin \alpha$$

$$N_2 = (1 + \xi) F_n \sin \alpha$$

in which  $F_n$  is the normal contact force,  $\alpha$  is the pressure angle, and  $\xi$  is a dimension ratio.

The modeling of passive system parameters such as masses, moments of inertia, and spring stiffnesses is carried out in a standard way. The choice for the value of the damping factor of 0.03 for structural damping and of 0.05 to 0.07 for well-lubricated machine components is considered reasonable.

Let us analyze the dynamic response of the complex eleven-degree-of-freedom model to include some major sources of *manufacturing errors*. This was accomplished by Kim and Newcomb (1981) to include *system flexibility* with cam profile variations due to errors or tolerances. A computer simulation technique was applied for this analysis which indicated the stochastic nature of manufacturing as discussed in Chap. 10.

The cam-follower drive system was simulated to include elasticity and manufacturing with the following data: A cam rotates at 800rpm with a dwell-rise-return dwell action. The displacement is  $0^\circ$  to  $30^\circ$ , dwell;  $30^\circ$  to  $180^\circ$ , rise 0.381 m with modified trapezoidal motion;  $180^\circ$  to  $210^\circ$ , dwell; and  $210^\circ$  to  $360^\circ$ , return with 4-5-6-7 polynomial motion. The base circle radius of the cam is 0.381 m. and the follower roller radius is 0.09525 m. The tolerance of the cam profile equals  $\pm 0.27 \times 10^{-5}$  m and the tolerance of the roller follower equals  $\pm 0.254 \times 10^{-5}$  m. The v-result of the eyes figation revealed that the assumed tolerances had very little influence on the vibration of the cam-follower system. Figure 12.28 shows two whole revolutions of the cam and the transient behavior of follower acceleration. It includes the combined effects of flexibility in the system and the tolerances of the cam and follower. For more on this subject see the original reference.

## 12.5 SUMMARY

---

We conclude the chapter with a summary of both theoretical and practical design considerations for high-speed cam-follower performance.

- Vibrations in dynamic cam-follower systems are primarily due to the compliance in the system.
- Vibration may also be the result of other practical factors, i.e., errors in fabrication, worn-out (old) machine parts, misalignment in assembled parts, and imbalance of parts. Backlash should be minimized. Preloaded bearings may sometimes be applied and lubrication systems should be selected carefully for optimum performance.
- An elastic follower with a rigid camshaft in general can employ a single-degree-of-freedom model with impunity.
- The elastic follower with a rigid camshaft model presents the transient vibratory state for important primary and residual vibrations to be studied; see Chap. 13.
- The elastic camshaft presents a more complicated mathematical nonlinear relationship. The models of this cam-follower include the closed-track and open-track systems.
- Choose the lubricant properly for compatibility in the system.
- Proper choice of cam curves (acceleration curve continuity) are the modified sine, modified trapezoidal, and polynomial curves. These will minimize the effect of follower output, linear system, and cam drive nonlinear vibrations. The inertia load of the closed-track model produces vibrations that are twice the frequency of the modes of the open-track. Also, the elastic camshaft may produce vibratory resonant couple of the cam input and the follower system to produce difficulties.
- Excessive noise may accompany vibrations in cam-follower systems. This may be the result of a waviness error in the cam profile fabrication.
- For automotive camshaft (valve gear) optimization, performance proprietary software exists in all manufacturers. In App. D the designer will find a comprehensive listing of available software for design, manufacturing, and engine performance. Some of the camshaft studies are: cam profile determination, cam surface hertzian stresses, and harmonic analysis for spring surge and valve bounce.

## REFERENCES

---

- Ardayfio, D., "Dynamics of High-Speed Cam Mechanisms with Damped Flexible Followers Driven by Flexible Camshafts," ASME paper 76-DET-69, 1976.
- Baratta, F.I., and Bluhm, J.I., "When Will a Cam Follower Jump?" *Product Engineering*, 25: 156–159, July 1954.
- Barkan, P., and McGarrity, R.V., "A Spring-Actuated, Cam-Follower System: Design Theory and Experimental Results," *Transactions of the ASME, Journal of Engineering for Industry*, Paper No. 64-Mech-12, 1964.
- Bloom, D., and Radcliffe, C.W., "The Effect of Camshaft Elasticity on the Response of Cam Driven Systems," ASME paper 64-Mech-41, 1964.
- Chen, F.Y., "Analysis and Design of Cam-Driven Mechanisms with Nonlinearities," *Journal of Engineering for Industry*, pp. 685–694, 1973.
- Chen, F.Y., *Mechanics and Design of Cam Mechanisms*, Pergamon Press, N.Y. 1982.

- Chen, F.Y., and Polvanich, N., "Dynamics of High Speed Cam-Driven Mechanisms, Part I: Linear System Models," *Transactions of the ASME, Journal of Engineering for Industry*, 97E (3): 769–776, 1975a.
- Chen, F.Y., and Polvanich, N., "Dynamics of High Speed Cam-Driven Mechanisms: Part II Nonlinear System Models" *Transactions of the ASME, Journal of Engineering for Industry*, 97B: 777–784, 1975b.
- Curtis, D.F., "Flywheels," *Standard Handbook of Machine Design*, ed. by T.E. Shigley and C.R. Miske, McGraw-Hill, New York, 1996.
- Eliss, N.S., Jr., "Vibration of Cams Having Two Degrees of Freedom," *Journal of Engineering for Industry*, 86: 343–350, November 1964.
- Erdman, A.G., *Modern Kinematics—Developments in the Past Forty Years*, John Wiley, New York, 1993.
- Freudenstein, F., "On the Dynamics of High-Speed Cam Profiles," *International Journal of Mechanical Science*, I: 342–249, 1960.
- Hanachi, S., and Freudenstein, F., "The Development of a Predictive Model for the Optimization of High-Speed Cam-Follower Systems with Coulomb Damping, Internal Friction, and Elastic and Fluidic Elements," *Transactions of the ASME, Journal of Mechanisms, Transmissions, and Automation in Design*, 108: 506–515, 1986.
- Hrones, J.A., "Analysis of Dynamic Forces in a Cam-Driven System," *Transactions of the ASME*, 70: 473–482, 1948.
- Jehle, F., and Spiller, W.R., "Idiosyncrasies of Valve Mechanisms and Their Causes," *SAEJ*, 24: 133–143, 1929.
- Kim, H.R., and Newcombe, W.R., "The Effect of Cam Profile Errors and System Flexibility on Cam Mechanism Output," *Mech. Mach. Theory*, 16: 4, 1981.
- Koster, M.P., "Effect of Flexibility of Driving Shaft on the Dynamic Behavior of a Cam Mechanism," *ASME Journal of Engineering for Ind.*, 97B (2): 595–602, 1975.
- Koster, M.P., *Vibration of Cam Mechanisms*, Macmillan, London, 1970.
- Koster, M.P., "Digital Simulation of the Dynamics of Cam Follower and Camshafts," Fourth World Congress of the Theory of Machine and Mechanisms, pp. 969–974. Mechanical Engineering Publ., London, 1975a.
- Koster, M.P., "Effect of Flexibility of Driving Shaft on the Dynamic Behavior of a Cam Mechanism," *Transactions of the ASME*, 97 (2): 595–602, 1975b.
- Mitchell, D.B., "Tests on Dynamic Response of Cam-Follower-Systems," *Mechanical Engineering*, 72: 467–471, June 1950.
- Pisano, A.P., and Freudenstein, F., "An Experimental and Analytical Investigation of the Dynamic Response of a High-Speed Cam Follower System: Parts 1 & 2," *Transactions of the ASME, Journal of Mechanisms, Transmissions, and Automation in Design*, 105 (4): 692–704, 1983.
- Rothbart, H., "Cam Dynamics," Proc. Int. Conference on Mechanisms, pp. 141–155, Shoe String Press, New Haven, Conn, 1961.
- Shigley, J., and Mischke, C., *Standard Handbook of Machine Design*, Chap. 18, D. Curtis, McGraw-Hill, New York, 1996.
- Szakallas, L.E., and Savage, M., "The Characterization of Cam Drive System Windup," *Trans. ASME, J. Mech. Des.*, 102 (2): 278–285, 1980.
- Talbroudet, G.J., *The Dynamic Synthesis, Analysis, and Design of Modeled Cam Systems*, Lexington Books, Lexington, Mass., 1976.
- Timoshenko, S., *Vibration Problems in Engineering*, Third Edition, D. Van Nostrand Co., New York, 1955.
- Turkish, M.C., "The Relationship of Valve Spring Design to Valve Gear Dynamics and Hydraulic Lifter Pump-up," *Trans. SAE* 61: 707, 1953.

- Van Der Hoek, W., "Das Voraussagfu des Dynamischen Verhaltens bei Kurvenge Trieben," Vdi Ausschub Getriebetchnik, Goslar, February 1966.
- von Karman, T., and Biot, M.A., *Mathematical Methods in Engineering*, first edition, McGraw-Hill, New York, 1940.
- Wiederrich, J.L., "Design of Cam Profiles for Systems with High Inertial Loadings," Ph.D. thesis, Stanford University, 1973.

---

# CHAPTER 13

---

## CAM SYSTEM DYNAMICS— RESPONSE

---

**Thomas L. Dresner, Ph.D.**

*Consulting Engineer  
Mountain View, California*

- 13.1 INTRODUCTION TO RESPONSE 400
- 13.2 RESPONSE IN FREQUENCY DOMAIN 401
- 13.3 VIBRATION MINIMIZATION 406
  - 13.3.1 Introduction to Vibration Minimization 406
- 13.4 DYNAMIC SYNTHESIS OF CAMS USING FINITE TRIGONOMETRIC SERIES 407
  - 13.4.1 Introduction 407
  - 13.4.2 Symbols 408
  - 13.4.3 Tuned Cam Design 408
  - 13.4.4 Cam Design Based on Mean Squared Error Minimization 413
  - 13.4.5 Conclusions 416
- 13.5 APPLICATION OF OPTIMAL CONTROL THEORY TO THE SYNTHESIS OF CAM-FOLLOWER SYSTEMS 416
  - 13.5.1 Introduction 416
  - 13.5.2 Symbols 416
  - 13.5.3 Description of Dynamic Model 417
  - 13.5.4 Development of an Optimality Criterion-1: Output Criterion 418
    - 13.5.4.1 *Minimization of Rate of Change of Effective Follower-Spring Force* 418
    - 13.5.4.2 *Relative Vibration and Relative Vibrational Energy* 419
    - 13.5.4.3 *Problem Formulation Based on the Output Criterion* 419
  - 13.5.5 Development of an Optimality Criterion-2: Cam Criterion 419
    - 13.5.5.1 *General* 419
    - 13.5.5.2 *Contact Stress at Cam-Follower Interface* 419
  - 13.5.6 Formulation of Optimization Problem 420
  - 13.5.7 Introduction to System Optimization 421
  - 13.5.8 Optimization of Tuned Dwell-Rise-Dwell Cams 421
    - 13.5.8.1 *Formulation of Two-Point Boundary-Value Problems* 421
    - 13.5.8.2 *Solution of the Two-Point Boundary-Value Problem* 422
    - 13.5.8.3 *Minimization of Output Vibrations* 423
    - 13.5.8.4 *Minimization of Hertzian Cam Contact Stress* 424
  - 13.5.9 Optimization of Tuned Dwell-Rise-Return-Dwell Cams 425
    - 13.5.9.1 *General* 425
    - 13.5.9.2 *Formulation of Two-Point Boundary-Value Problem* 425
  - 13.5.10 Conclusions 427
- 13.6 USE OF THE CONVOLUTION OPERATOR TO REDUCE RESIDUAL VIBRATIONS 427
  - 13.6.1 Introduction 427
  - 13.6.2 Symbols 427
  - 13.6.3 Basic Theory 428
  - 13.6.4 Fixed Convolution 430
  - 13.6.5 Constant Velocity Convolution 431
  - 13.6.6 Conclusion 434
- 13.7 POLYDYNE CAMS 434
  - 13.7.1 Introduction 434
  - 13.7.2 Fundamental Relationships 435
  - 13.7.3 Ramp Height,  $r_a$  437
  - 13.7.4 Spring Ratio Constant,  $k_r$  437
  - 13.7.5 Dynamic Constant,  $c$  438
  - 13.7.6 Equivalent Weight,  $w$  438
  - 13.7.7 Application of Polynomials for Cam Curves 439
  - 13.7.8 Example Using the 3-4-5 Polynomial End Mass Movement 440
  - 13.7.9 4-5-6-7 and 5-6-7-8-9 Polynomials 443
  - 13.7.10 Ramps or Subcams 444
  - 13.7.11 D-R-R-D Cams 444
  - 13.7.12 Practical Vibration Discussion 446
  - 13.7.13 Summary 447
- 13.8 DISCUSSION 447
  - 13.8.1 Design Guidelines and Rules of Thumb 448
  - 13.8.2 Conclusions and Recommendations on the Use of the Methods Given in this Chapter 449
    - 13.8.2.1 *Cam Synthesis Using Trigonometric Series (Sec. 13.4)* 449
    - 13.8.2.2 *Cam Synthesis Using Optimal Control Theory (Sec. 13.5)* 449
    - 13.8.2.3 *Cam Synthesis Using the Convolution Operator (Sec. 13.6)* 450
    - 13.8.2.4 *Polydyne Cams* 450
    - 13.8.2.5 *Summary of Conclusions* 450

### 13.1 INTRODUCTION TO RESPONSE

---

In Chap. 12 mathematical models of the differential equations were employed to establish the performance of cam-follower systems. Modeling techniques were utilized to investigate the vibratory response of the follower in the time domain. In this chapter much of the dynamic study is done as an input of time transients to the cam-follower system. Also, Wiederrich (2001) has contributed in the development of this chapter. In the beginning, we will be operating in the frequency domain. The dynamic response of a cam-follower system has the following three considerations:

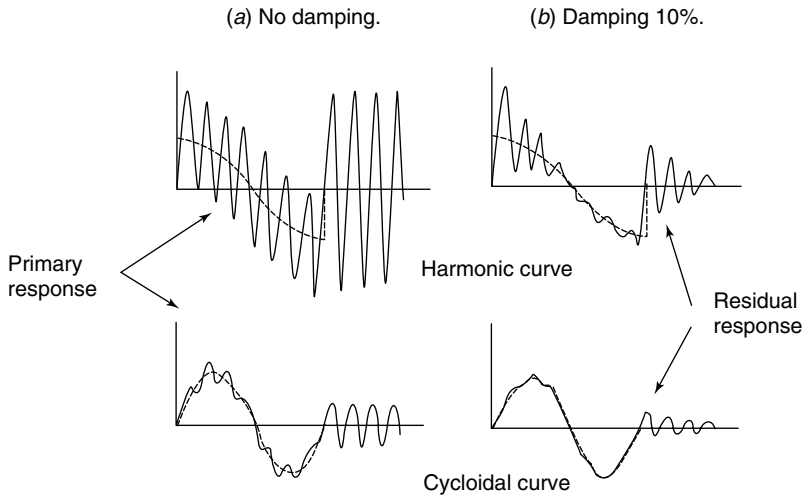
- The driving motion produced by the cam, called the base excitation. Note that other external disturbing forces may also act on the follower at the same time.
- The mass, elasticity, and damping of the system between the base excitation and the follower end point.
- The behavior of the follower caused by the excitation, which is called the response.

The studies presented in this chapter all use the single degree-of-freedom (DOF) model. As stated in Chap. 12, one DOF is sufficiently accurate to model most cam-follower systems. This DOF, the fundamental mode of the system, usually represents the great majority of the dynamic deformation of the system. In systems in which one DOF is not clearly dominant, the error in a one-DOF model may be too great. When this occurs, either a multi-DOF system must be used or the system structurally redesigned to mitigate the adverse effect of the other significant modes. Otherwise, the improvement by use of multi-DOF does not justify the additional analytical and modeling complexity or the additional data required. Multi-DOF system responses are occasionally referred to but will not be treated in this chapter.

The response of a typical dynamic system consists of both *steady state and transient* responses. For cam-follower systems it is the transient response that is pertinent. Steady state vibration is usually not a concern since the cam angular velocity is low in comparison to the natural frequency of the system. Therefore, vibrations excited by the acceleration periods are not significantly reduced or reinforced by succeeding cam cycles. For ease of analysis and simplicity to compare the different cam curve responses we usually assume that vibration damps out during the dwell period and does not carry over to the next cycle. The designer will consider

- The *primary response* produced during the application of the base excitation or stroke
- The *residual response* that remains at the start of the dwell after the removal of the excitation.

Figure 13.1 (Hrones, 1948 and Mitchell, 1950) shows the primary and residual responses of a relatively low speed cam-follower system. Note that the vibrations occur at the natural frequency of the system. Vibrations take place during the stroke and the dwell periods, with their peak magnitudes influenced by the sudden application, reversal, or removal of the excitation. The acceleration discontinuity in the harmonic cam profiles leads to the high vibrations shown. As speed is increased, the cycloidal cam vibrations will increase rapidly as the significant excitational frequencies approach the natural frequency of the system. At sufficiently high speeds the cycloidal system vibrations will approach those of harmonic profiles. As Sec. 13.4 will illustrate, we cannot generally assume that profiles with acceleration discontinuities will always perform less well than those without such discontinuities in high-speed systems. Sometimes the optimal solution will have significant discontinuities in acceleration.



**FIGURE 13.1.** Vibratory response characteristics of cam-follower for simple harmonic and cycloidal input, Hrones (1948) Mitchell (1950).

## 13.2 RESPONSE IN FREQUENCY DOMAIN

As speed increases in a cam-follower system, a rapid exchange of energy occurs within the system and the noise of operation also increases. This sudden energy shift takes place between the elastic members and the masses during operation. The energy shift is also visible as high follower vibration. This action is termed mechanical shock and its related system response a shock response.

A shock is defined as the physical manifestation of the transfer of mechanical energy from one body to another during an extremely short interval of time (see Chapter 9).

The shock response spectrum or the *response spectrum* is one of the two most commonly used methods of analyzing mechanical shock. The other method is the Fourier spectrum analysis. In both cases, the time history of the transient is converted into an amplitude versus frequency picture, or spectrum. Neklutin (1954) was the first to employ this technique in the study of cam-driven systems.

Thus, a valuable method of expressing the dynamic response of a cam-follower system is to obtain the *dynamic response spectra* (DRS) of the cam's excitations. A DRS is defined as a plot of individual peak-acceleration responses of a multitude of single-degree-of-freedom, mass-spring systems subject to a particular input transient. The ordinate is usually acceleration, or some normalized expression relating to acceleration, while the abscissa is in terms of the system natural frequency, or the ratio of pulse duration to the system natural period. Damping is a parameter, and if possible, its values should be stated; otherwise, it is usually assumed to be zero.

To illustrate the DRS, we start with a given input pulse and carry out a mathematical computation to obtain the response of a single-degree-of-freedom linear system subject to that input. It is best to first compute the follower acceleration as a function of time. Then find the maximum follower acceleration and plot it on a graph versus the fundamental period of the one DOF system. This provides one point on the diagram. By holding the damping of the system constant and varying the system's natural frequency by changing

the stiffness of the spring, the calculations are repeated to define a curve called a response spectrum. We can calculate these curves over a range of damping ratios to obtain a set of curves, each applicable for a different damping ratio. The normalized displacement, velocity, and acceleration DRSs are defined, respectively, as

$$\begin{aligned} S_{ND} &= \frac{x_m}{y_m} \\ S_{NV} &= \frac{\omega_n x_m}{\dot{y}_m} \\ S_{NA} &= \frac{\omega_n^2 x_m}{\ddot{y}_m}. \end{aligned} \quad (13.1)$$

Nomenclature for these equations and the figures:

$\omega_n$  = cam-follower system natural frequency

$x_m$  = maximum displacement of output

$y_m$  = cam maximum displacement

$\dot{y}_m$  = cam maximum velocity

$\ddot{y}_m$  = cam maximum acceleration

$T_r/T_N$  = ratio of pulse width to system natural period

Figure 13.2 shows the acceleration DRS of a modified trapezoidal cam with 5 percent critical damping. Curves with other damping values can be added if so desired. The curves peak at several values of  $\omega_n$ . From the spectra a designer can ascertain how systems of different periods relate to specific inputs. Also, it is found that damping has a greater effect on the residual vibration than on the primary response. In establishing the acceptable damping factor it is usually conservative to use a value near the low end of the choices.

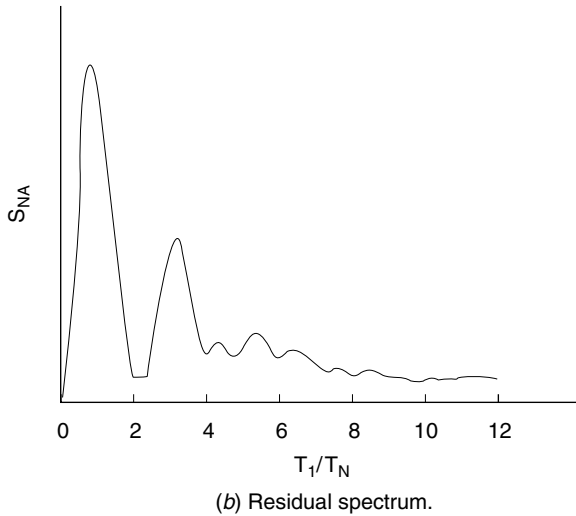
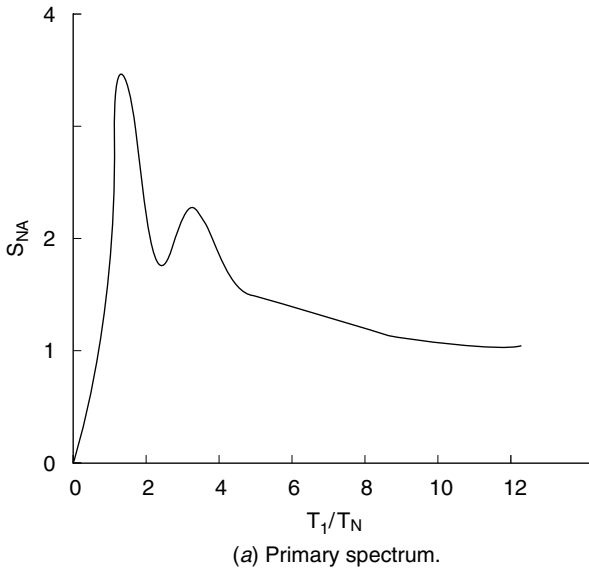
### 13.2.1 Example

*For illustration, consider a cam-follower system used in a high-speed automatic machine modeled with a single DOF, Chen (1982). The follower is actuated by a dwell-rise-dwell cam with a modified trapezoidal profile. The peak input acceleration is  $500 \text{ m/sec}^2$ , and the duration of the excitation is  $0.015 \text{ sec}$ . If the follower linkage of the system is such that it has a natural frequency of  $100 \text{ Hz}$ , what will be the peak acceleration response of the follower during the lift stroke and during the dwell period? Let us assume the damping factor is  $0.05$ .*

### 13.2.2 Solution

*With reference to Fig. 13.2 with 5 percent damping and at time ratio  $T_r/T_N = 0.015 \times 100 = 1.5$ , the primary acceleration amplification is  $2.98$ , and the residual acceleration amplification is  $1.88$ . Therefore, the primary acceleration response will be  $2.98$  times the input or  $1490 \text{ m/sec}^2$ , and the residual acceleration response will be  $1.88$  times the input or  $940 \text{ m/sec}^2$ . If the effective mass of the follower is  $40 \text{ N}$ , the corresponding inertial load of the follower is  $6075 \text{ N}$  due to primary vibration and  $3833 \text{ N}$  due to residual vibration.*

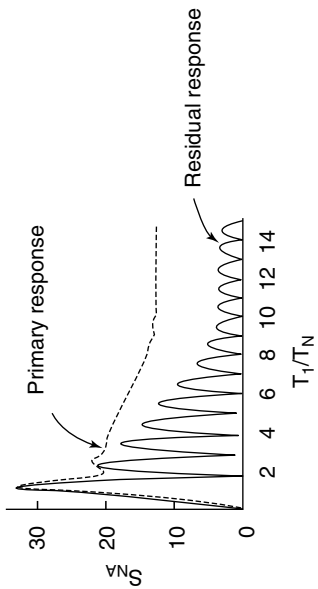
Next, a quantitative comparison (Chen, 1981) of the dynamic characteristics of various types of dwell-rise-dwell cam profiles will be shown. Based on a single-DOF model, a



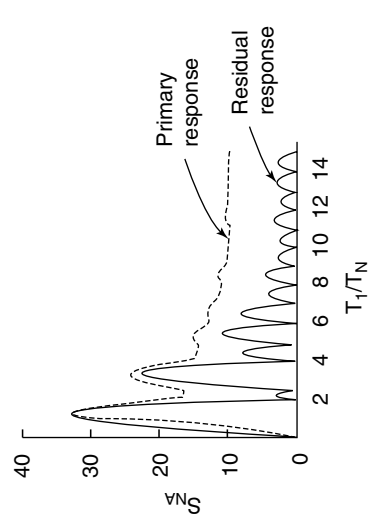
**FIGURE 13.2.** Acceleration spectrum of modified trapezoidal cam (DRS) with 5% damping.

display of the dynamic characteristics of a number of cam profiles is presented. It should be noted that damping has a significant effect on both the primary and the residual responses. The more significant effect is on the residual response. The magnitude of damping is very difficult to firmly establish. The effect of damping is to smooth out the curves and reduce the sharpness of the peaks in the residual responses.

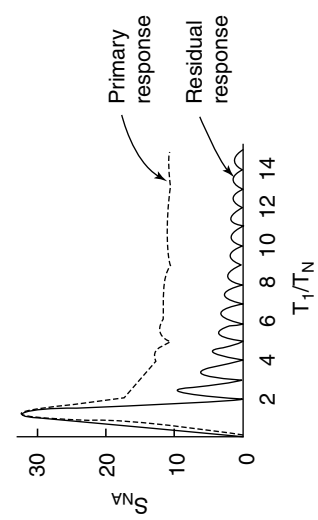
Figure 13.3 presents the  $S_{NA}$  of selected cams all having zero damping. Figure 13.4 illustrates a comparison of the maximum primary vibrations of many important cam pro-



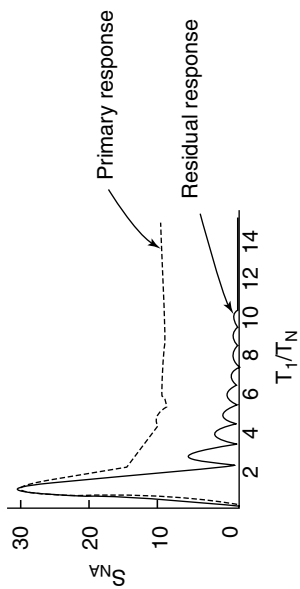
(a) Cycloidal.



(b) Modified sine.

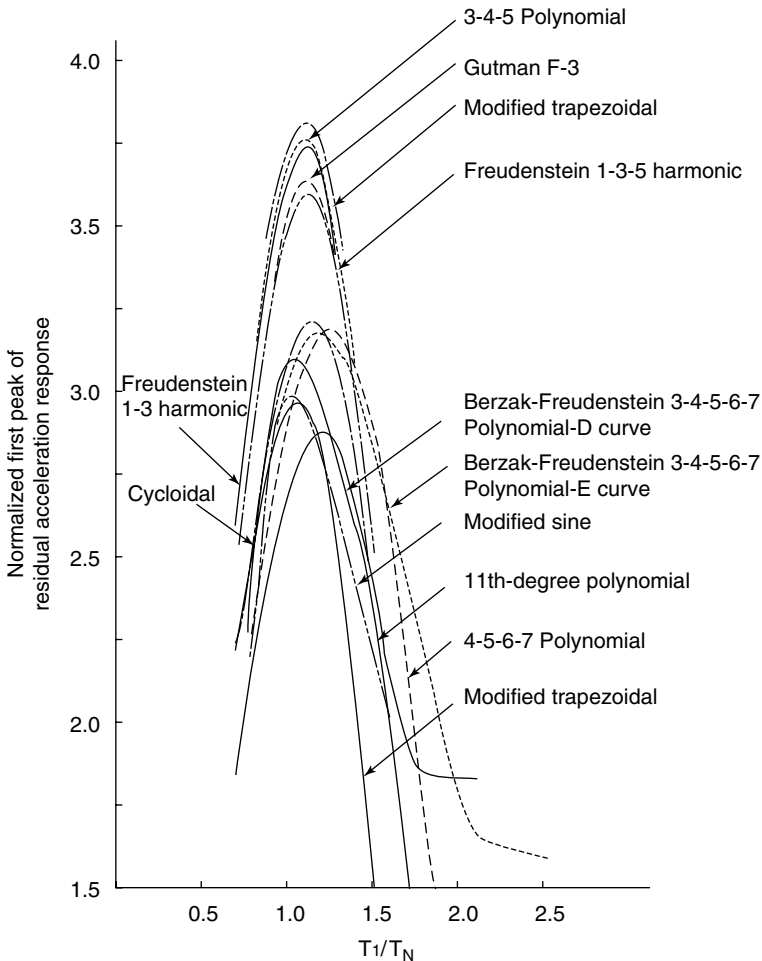


(c) Modified trapezoidal.



(d) 4-5-6-7 polynomial.

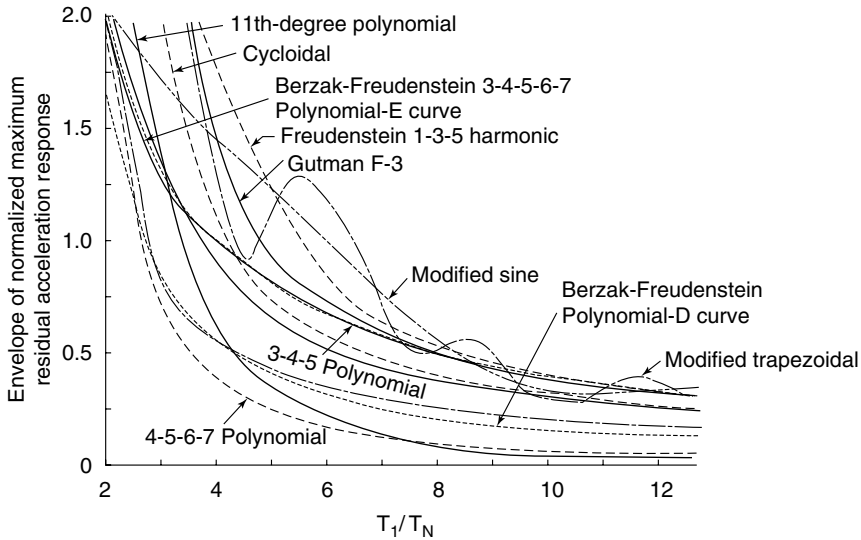
**FIGURE 13.3.** Plot of  $S_{NA}$  versus  $T_1/T_N$  for cam curves (zero damping).



**FIGURE 13.4.** Comparison of normalized first-peak acceleration magnitudes for primary vibrations.

files and Fig. 13.5 shows a comparison of the residual vibration envelopes (constructed by connecting the peaks of the residual vibrations). A study of the figures yields that some cam curves have a lower level of residual vibrations than others depending on the range of  $T_1/T_N$ .

In summation, the speeds of all cam-driven mechanisms vary. Even constant speed systems must vary in speed from zero to design speed during start-up and shutdown. Thus, resonances with one or more of the excitational frequencies will occur. The amplitude of response is proportional to the amplitude of the input harmonic. A cam acceleration curve with a limited number of harmonics avoids this coincidence if the frequency of the highest harmonic is well below the first natural frequency of the system. For example, the Gutman F-3, Freudenstein 1-3 harmonic, and cycloidal curves each have few harmonics and thus produce generally sound dynamic responses except at very high speeds.



**FIGURE 13.5.** Comparison of normalized peak acceleration magnitude envelopes for residual vibration.

No single cam form is best for all applications. A form that is optimized for its response spectrum in certain frequency regions will not be optimized for response in others. Other complicating factors that are difficult to account for are variations in external loads, torque fluctuations, fabrication errors, and alignment and other inherent factors. Good performance in the field is the final test that the system design is a good one.

### 13.3 VIBRATION MINIMIZATION

#### 13.3.1 Introduction to Vibration Minimization

Many investigators have studied optimization criteria for cam profile design. Their methods minimized many important response parameters, particularly vibration of the cam follower. One of the first presentations of a form of vibration optimization was by Hussmann (1938). He established specific harmonics near the follower natural frequency equal to zero to minimize vibrations. Chew and Chuang (1990) applied Lagrange multipliers and polynomial lift curves to minimize the integral of the end of the rise residual vibrations over the desired speed range. They developed a direct procedure for minimizing residual vibrations when designing cam motions. They concluded (as did Wiederrich and Roth, 1978) that for high-speed applications, specification of vanishing cam boundary conditions for derivatives higher than the velocity is inappropriate when using an optimization procedure that accounts for the dynamic response. Perhaps the most important feature of these optimization methods in cam design is that they can readily be applied to design the entire cam motion rather than just a segment of the motion. Cams designed in this way have been found to work well in practice. Optimization methods can also be applied to optimize the geometry of the cam and follower mechanism.

For many years much research has been directed toward identifying and tabulating suitable functions to define cam motion segments which produce good dynamic response. Neklutin (1952) contributed much in this area.

Freudenstein (1960) observed that cam dynamics could be improved by minimizing the harmonic content of the motion and developed a family of low harmonic curves that minimized the peak acceleration.

The next four sections of this chapter each explore a method for determining optimal or at least near-optimal cam curves for any particular set of requirements (mainly lift, operating speed, system natural frequency, and duration). These methods allow a designer to systematically obtain a near-optimal cam curve directly for whatever system is being developed. The designer does not have to choose a curve which is known to have good vibration characteristics and hope for the best nor must a variety of curves be selected to find the best one through analysis.

Wiederrich (1981) showed, by applying modal analysis methods, that once the cam curve has been designed using a single-DOF model to minimize vibration over the entire speed range, from zero to maximum, then the actual system, with its many degrees of freedom, has also been so optimized (i.e., the vibration of each of the modes has been minimized). However, if the one-DOF model is used to optimize only at a single speed or over a limited range of speeds, the vibration from the higher modes cannot be assumed to be optimized and their combined vibration response could be significant compared to that predicted by the single DOF analyzed. Therefore, it is generally recommended that optimization using a single-DOF model be applied over the entire speed range. Of course, the single-DOF model must also satisfy the conditions stated in Sec. 13.1 before any conclusions can be made as to the adequacy of the design.

The methods presented are all relatively complex mathematically and thus require solution by computer using a program written for that purpose. Once the computer program is available, application is relatively easy.

## **13.4 DYNAMIC SYNTHESIS OF CAMS USING FINITE TRIGONOMETRIC SERIES**

---

### **13.4.1 Introduction**

In this section, we present cam design methods originated by Wiederrich and Roth (1978). In these methods, follower or cam displacement is defined as a finite trigonometric series. One method generates a “tuned” cam design, in which the cam profile is designed to provide exactly the follower lift as a given finite trigonometric series function at one particular cam speed. With this method, the performance at other speeds can be very poor. Another method uses a finite trigonometric series function for cam lift and a mean square error minimization technique to optimize the cam performance over a range of cam speeds.

The methods employ the usual linear single degree-of-freedom mathematical system model. The original 1975 paper provides a mathematical method to estimate the limitations of such a model for any particular case. Basically, the method shows the single degree-of-freedom model to be valid when the highest significant frequency of a Fourier representation of the lift event is much lower than the second mode natural frequency of the system. This is almost always true of a good design, where the highest significant frequencies are significantly below the first mode natural frequency and therefore far below that of the second mode.

The methods presented do not rely on rules of thumb. In fact, some solutions provide motions with low vibration levels even though they violate the commonly accepted design criterion that jerk must be minimized.

### 13.4.2 Symbols

$a_i, b_i$  = Cosine and sine term coefficients, respectively, to be determined in the cam profile function  $\bar{y}$ , Eq. (13.26)

$A_1, A_2, A_3$  = User-defined coefficients in Eq. (13.22) for performance index  $\bar{P}$

$B_i$  = Coefficients of the sine series terms in the desired follower lift function  $X$ , Eq. (13.11)

$C_i, D_i$  = Cosine and sine term coefficients, respectively, to be determined in the cam profile function  $\bar{y}$ , Eq. (13.16)

$F_2 = \omega_2 \theta_0 / (\pi \omega)$  normalized inverse operating speed

$F_{2h}, F_{2l}$  = The high and low speed operating limits, respectively, of  $F_2$  for the system being analyzed

$H$  = Required follower lift at the end of the cam segment

$P$  = Performance index to be minimized to find the optimum cam lift function  $\bar{y}$  over a range of frequencies, Eq. (13.25)

$\bar{P}$  = Performance index which when minimized indicates an optimum cam lift function  $\bar{y}$  at one frequency, Eq. (13.22)

$r$  = The follower displacement relative to its static equilibrium position

$R$  = The residual vibration—the magnitude of  $r$  induced by one cycle of the cam profile as defined by Eq. (13.5)

$R_s$  = The steady state follower vibration induced by the cam profile

$t$  = Time

$T = \pi \omega t / \theta_0$ , normalized time

$T_i$  = Normalized time corresponding to  $X(T_i)$  and  $X_i$

$V_1$  = Required follower velocity at start of cam segment

$V_2$  = Required follower velocity at end of cam segment

$X(T_i)$  = Follower displacement at time  $T_i$

$X_i$  = Desired follower displacement  $X$  at time  $T_i$

$\bar{y} = (\omega_1^2 / \omega_2^2) y$ , normalized cam displacement

$\bar{y}_k$  = Desired normalized cam displacement  $\bar{y}$  at time  $T_k$ , Eq. (13.23)

$(\dot{y}) = d(\bar{y})/dT$

$\xi_1$  = Damping ratio for the cam input

$\xi_2$  = Damping ratio for the follower motion

$\theta_0$  = Angle of cam rotation over which the cam profile segment being analyzed occurs

$\omega$  = Angular rate of cam rotation

$\omega_1$  = Square root of the coefficient of  $\bar{y}$  determining the follower input, Eq. (13.2)

$\omega_2$  = No-damping follower natural frequency

### 13.4.3 Tuned Cam Design

In many applications a cam operates at a constant or nearly constant speed. It is then theoretically possible to completely control the follower motion by using dynamically compensated (i.e., tuned) cam designs. To do this, the desired motion is specified and the required cam profile determined through the equations of motion.

We here consider the problem of designing a cam profile segment to move the follower exactly from one state of position and velocity to another. To begin, we start with the usual single-degree-of-freedom linear system of the form

$$\ddot{X} + 2\xi_2\omega_2\dot{X} + \omega_2^2X = \omega_1^2y + 2\xi_1\omega_1\dot{y}. \quad (13.2)$$

Before we can proceed further, we need to mathematically define a vibration criterion. The quality of the dynamic behavior of any system is reflected by its displacement relative to its static equilibrium position. We define the relative vibration as

$$r = \frac{\omega_1^2}{\omega_2^2}y - x. \quad (13.3)$$

In terms of  $r$ , Eq. (13.2) becomes

$$\ddot{r} + 2\xi_2\omega_2\dot{r} + \omega_2^2r = \frac{\omega_1^2}{\omega_2^2}\ddot{y} + 2(\omega_1\xi_2 - \xi_1\omega_2)\frac{\omega_1}{\omega_2}\dot{y}. \quad (13.4)$$

Our primary goal is to minimize the vibration levels in the steady state operation of the cam-follower system. This level,  $R_s$ , is dependent on the magnitude  $R$  of  $r$  induced by one cycle of  $y$  and the amount of damping present. The residual vibration ( $R$ ) is defined as

$$R = \left\{ r^2(t) + \frac{r'^2(t)}{F_2^2} \right\}^{1/2} \quad (13.5)$$

where  $t$  would normally be the time at the end of the cam lift event (at the start of the dwell period that continues until the next lift event). Alternatively,  $t$  could be the time at some other critical part of the cam rotation. Then,  $R_s$  can be expressed as

$$R_s \leq R / \left\{ 1 - \exp\left[ \frac{-2\pi\xi_2\omega_2}{\omega} \right] \right\}. \quad (13.6)$$

Eq. (13.2) can be written in normalized form as

$$X'' + 2\xi_2F_2X' + F_2^2X = F_2^2\bar{y} + 2\xi_2F_2\bar{y}' \quad (13.7)$$

where we have used the definitions of  $F_2$ ,  $\bar{y}$ , and  $(\bar{\cdot})'$  given in the nomenclature and assumed that  $\xi_1\omega_2 = \xi_2\omega_1$ .

The required motion is to occur over an angle of cam rotation  $\theta_0$ , and the motion should begin and end with  $R$  identically zero so that it does not contribute to  $R_s$ . In addition we require that the motion begin and end with  $\ddot{y}$  equal to zero. Substituting these conditions into Eq. (13.7) it follows that the required motion is subject to the constraints

$$\begin{aligned} X(0) = X''(0) = X'''(0) = X''(\pi) = X'''(\pi) = 0 \\ X(\pi) = H, \quad X'(0) = V_1, \quad X'(\pi) = V_2. \end{aligned} \quad (13.8)$$

In addition, if  $\xi_1 = \xi_2 = 0$  then

$$X^{iv}(0) = X^{iv}(\pi) = 0 \quad (13.9)$$

and if  $\xi_1$  and  $\xi_2$  are not zero we must specify that

$$\bar{y}(0) = 0, \bar{y}(\pi) = H. \quad (13.10)$$

These conditions are satisfied by a motion of the form

$$X = \frac{H}{\pi}T - \sum_n \frac{B_n}{n^2} \sin(nT) \quad (13.11)$$

where the  $\beta_n$  are subject to the constraints

$$\sum_{n\text{-even}} \frac{B_n}{n} = \frac{H}{\pi} - \frac{(V_1 + V_2)}{2} \quad (13.12)$$

$$\sum_{n\text{-odd}} \frac{B_n}{n} = \frac{(V_2 + V_1)}{2} \quad (13.13)$$

$$\sum_{n\text{-even}} nB_n = 0 \quad (13.14)$$

$$\sum_{n\text{-odd}} nB_n = 0. \quad (13.15)$$

The associated cam profile tuned to operate at  $F_2 = F_{2d}$  is

$$\bar{y} = \frac{H}{\pi}T + \sum_n (C_n \cos(nT) + D_n \sin(nT)) \quad (13.16)$$

where

$$C_n = \frac{-2n\xi_2 B_n}{[F_{2d}(F_{2d}^2 + 4n^2\xi_2^2)]} \quad (13.17)$$

$$D_n = \frac{[n^2 - (F_{2d}^2 + 4n^2\xi_2^2)]B_n}{[n^2(F_{2d}^2 + 4n^2\xi_2^2)]} \quad (13.18)$$

and for a damped system Eq. (13.10) requires that

$$\sum_{n\text{-even}} C_n = 0 \quad (13.19)$$

$$\sum_{n\text{-odd}} C_n = 0. \quad (13.20)$$

As an example we consider the design of a unit rise dwell-rise-dwell motion subject to the additional constraint that maximum value of  $X''$  be minimized. Three solutions to this problem are tabulated in Table 13.1 and their acceleration profiles are shown in Fig. 13.6. Solution number 3 is the preferred one since it provides the lowest maximum value of  $X''$ .

Since we have assumed no damping in the development above, Eq. (13.4) reduces to

$$r'' + F_2^2 r = \bar{y}'', \quad r(0) = r'(0) = 0. \quad (13.21)$$

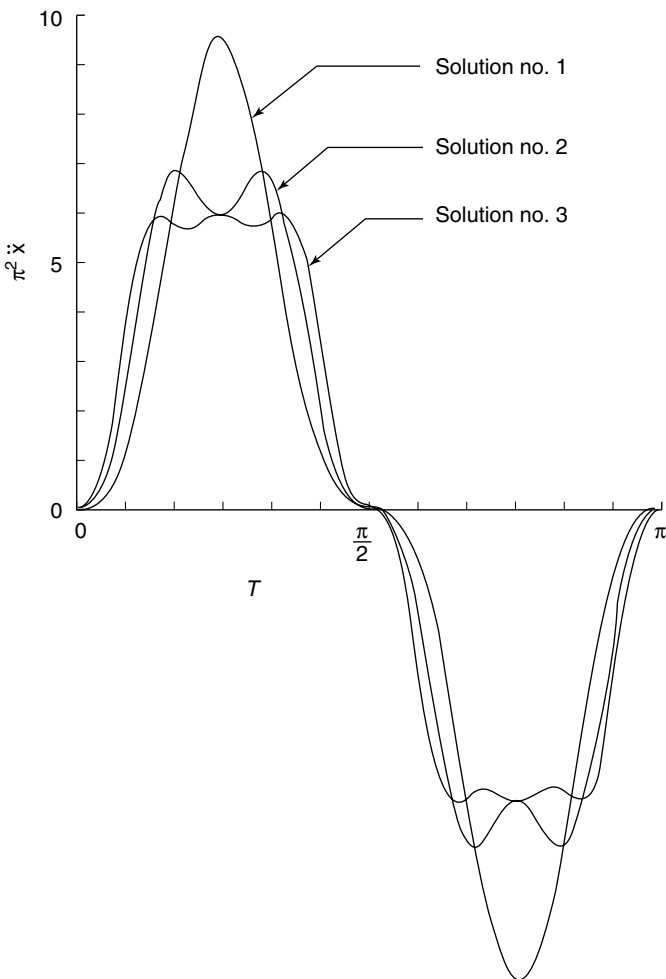
As shown by Eq. (13.6),  $R_s$  is indicative of the tendency for a motion to excite large steady-state vibrations.

Figures 13.7 and 13.8 illustrate typical residual vibration characteristics obtained using solution numbers 1 to 3 tuned for  $F_{2d} = \infty$  and 10, respectively. For comparison we have also shown the characteristics of parabolic and cycloidal motions. In plotting these curves we have only indicated the peak values of  $R$  joined by dotted lines, except in the immediate region of the designed operating point where we have plotted  $R$  exactly in order to show the sensitivity of the performance to changes in the operating conditions.

From these figures the reader may verify several general observations. First, for large values of  $F_2$  (i.e., low speeds) the residual vibration of a family of cam profiles increases

**TABLE 13.1** Problem Solutions (Fig. 13.6)

No.	Solution			
	$\pi^2 B_2$	$\pi^2 B_6$	$\pi^2 B_{10}$	$\pi^2 B_{11}$
1	7.0686	-2.3562	0	0
2	6.6260	-0.3645	-1.1065	0
3	6.4075	0.2935	-0.7490	-0.5062

**FIGURE 13.6.** Acceleration of tuned DRD cam profiles, see Table 13.1.

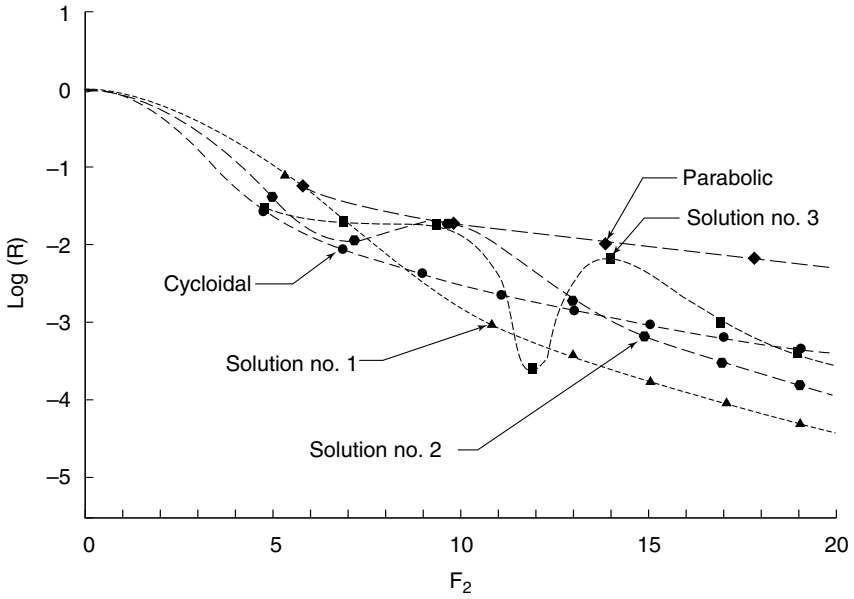


FIGURE 13.7. Vibration characteristics of cams tuned for  $F_{2d} \rightarrow \infty$ .

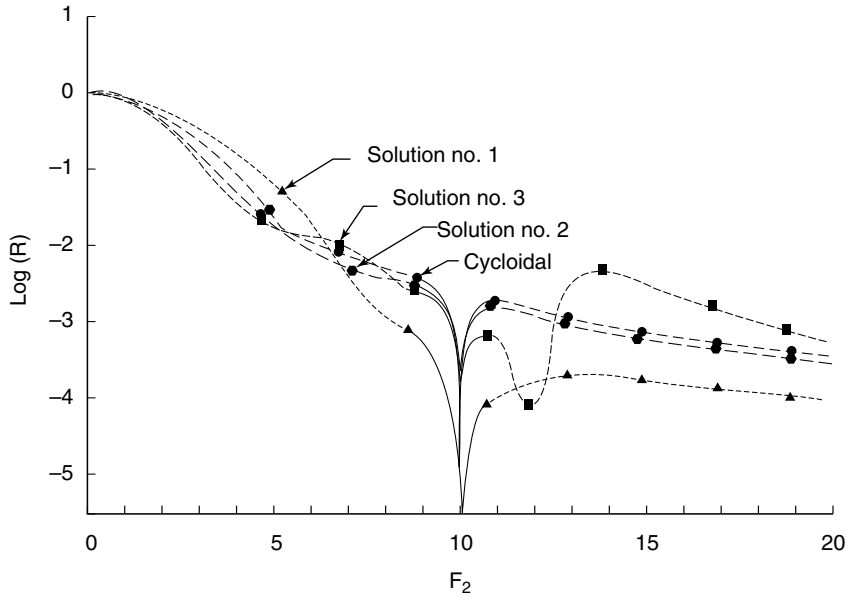


FIGURE 13.8. Vibration characteristics of cams tuned for  $F_{2d} = 10$ .

as the peak acceleration is decreased. Second, tuning a cam for higher speeds increases the tendency for the cam to excite vibrations at lower speeds. Finally, we can verify that the vibration behavior of these tuned cams is better than that of a comparable cycloidal cam for speeds below and slightly above the designed speed if the designed operating point,  $F_{2d}$ , is greater than the harmonic content of the tuned cam.

Tuned cams are appropriate for use in those systems that are intended to operate at a constant or nearly constant speed. Where applicable, the method of tuned cam design may be the most powerful method available in that it allows the designer to specify entirely the output motion at the design speed. However, the performance of the system away from the design speed may deteriorate depending on the designer's choice of optimization criteria and constraints.

In many applications, cam systems are required to operate over a wide range of operating speeds. In the next section we develop methods for designing cams to have low vibration characteristics over a range of operating speeds. A primary objective of these methods is the elimination of all unnecessary constraints to obtain the largest possible family of solutions.

### 13.4.4 Cam Design Based on Mean Squared Error Minimization

Cams are often designed to operate over a wide range of speeds. Since it is not possible to design a cam to be optimal at more than one speed at a time, the question becomes how best to design the cam for the best overall performance. This section presents a method of designing cams for optimized performance over a range of operating speeds.

The cam performance index, which reflects the deviation of the system from its desired operating conditions at any one speed, is defined as

$$\bar{P} = A_1 \sum_i (X(T_i) - X_i)^2 + A_2 \sum_j \frac{(X'(T_j) - X_j')^2}{F_2^2} + A_3 \int_0^\pi X''^2 dT. \quad (13.22)$$

Minimizing  $P$  is an indication of optimal cam design, since this is a measure of the deviation in follower position, velocity, and acceleration.

In addition, it may also be desired to impose constraints on the cam profile of the form

$$\bar{y}(T_k) = \bar{y}_k, \quad \bar{y}'(T_k) = \bar{y}'_k, \quad k = 1, \dots, l. \quad (13.23)$$

We want to optimize the performance over the operating range of speeds

$$\frac{1}{F_{21}} \leq \frac{1}{F_2} \leq \frac{1}{F_{2h}}. \quad (13.24)$$

To optimize the performance, we want to minimize the average value of the mean squared error  $\bar{P}$  over this speed range. Thus, we want to minimize

$$P = \int_{1/F_{21}}^{1/F_{2h}} \bar{P} d\left(\frac{1}{F_2}\right). \quad (13.25)$$

Assuming that

$$\bar{y} = \sum_{n=0}^{\infty} (a_n \cos(nT) + b_n \sin(nT)) \quad (13.26)$$

then the forced response of the follower for the worst case of an undamped system ( $\xi_1 = \xi_2 = 0$ ) is, from Eq. (13.7),

$$X = F_2^2 \sum_{n=0}^m \left( \frac{a_n \cos(nT) + b_n \sin(nT)}{F_2^2 - n^2} \right). \tag{13.27}$$

The required integration of Eq. (13.22) and Eq. (13.25) can now be performed exactly. The  $2m + 1$  coefficients can then be determined from the two equations, Eq. (13.23), and the  $2m + 1 - 2l$  extremum conditions

$$\frac{\delta P}{\delta a_0} = \frac{\delta P}{\delta a_i} = \frac{\delta P}{\delta b_i} = 0, \quad i = 1, \dots, m - 1. \tag{13.28}$$

Using this approach, one can design an entire cam profile at once, thereby obtaining maximum control of the motion and its harmonic content. Alternatively, for greater generality, one can design segments of low vibration motion by requiring that

$$\bar{y}(T_k) = X_k, \quad \bar{y}'(T_k) = X'_k, \quad \text{for } 0 \leq T_k \leq \pi, \tag{13.29}$$

in order to minimize  $R$ , see Eq. (13.5). These segments can then be pieced together to give a desired motion.

To obtain an optimum cam profile design to satisfy any particular case requires performing several designs using different values of  $A_2/A_1$  and  $A_3/A_1$  to find the design that appears to give the best compromise between optimizing response for accuracy of displacement and velocity responses and minimized acceleration.

As an example we consider the design of a unit rise dwell-rise-dwell motion designed to operate over the range  $F_2 \geq 9$ . Three motions designed in this way are tabulated in Table 13.2 and their associated acceleration and residual vibration characteristics are shown in Figs. 13.9 and 13.10, respectively. These motions were obtained using values of  $A_1 = A_2 = 1$  and  $A_3 = 0.0, 5 \times 10^{-8}$ , and  $7 \times 10^{-7}$  in Eq. (13.22) for examples 4, 5, and 6, respectively.

We again observe that for large values of  $F_2$ , the residual vibration of a family of cam profiles increases as the peak acceleration is decreased. In this section we have not imposed the constraints on the magnitude of jerk (i.e.,  $\bar{y}'''$ ) or continuity of  $\bar{y}''$  which are generally suggested by rules of thumb. In the absence of these constraints we observe that the peak value of jerk is relatively high and that the acceleration begins and ends with definite discontinuities that are small but increasing as  $A_3$  increases. Nonetheless the high-speed vibration characteristics of these motions represent a significant improvement over those of the cycloidal motion, and the accuracy of this predicted performance has been assured by controlling the harmonic content of the motion. The existence of such motions is contrary to

**TABLE 13.2** Problem Solutions (Figs. 13.9 and 13.10)

	No. 4	No. 5	No. 6
$a_0$	0.500000	0.500000	0.500000
$a_1$	-0.583802	-0.543883	-0.466909
$a_3$	0.095326	0.034106	-0.082227
$a_5$	-0.012015	0.011519	0.054570
$a_7$	0.000491	-0.001741	-0.005434
$b_2$	0.000000	-0.002399	-0.098142
$b_4$	0.000000	0.002835	0.078912
$b_6$	0.000000	-0.001293	-0.021730
$b_8$	0.000000	0.000152	0.001378

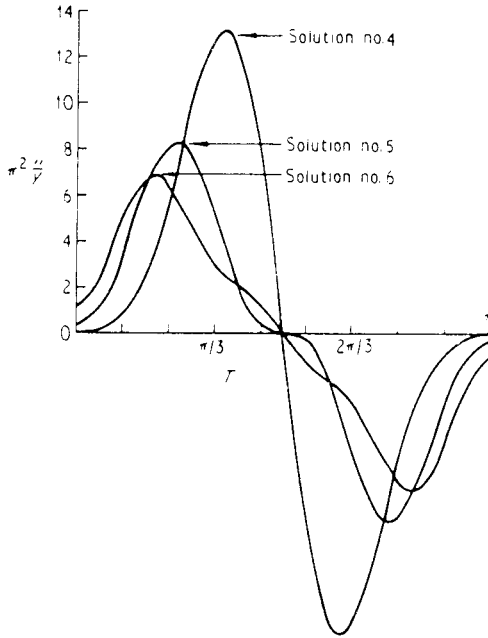


FIGURE 13.9. Acceleration of DRD cams designed for  $F_2 \geq 9$ .

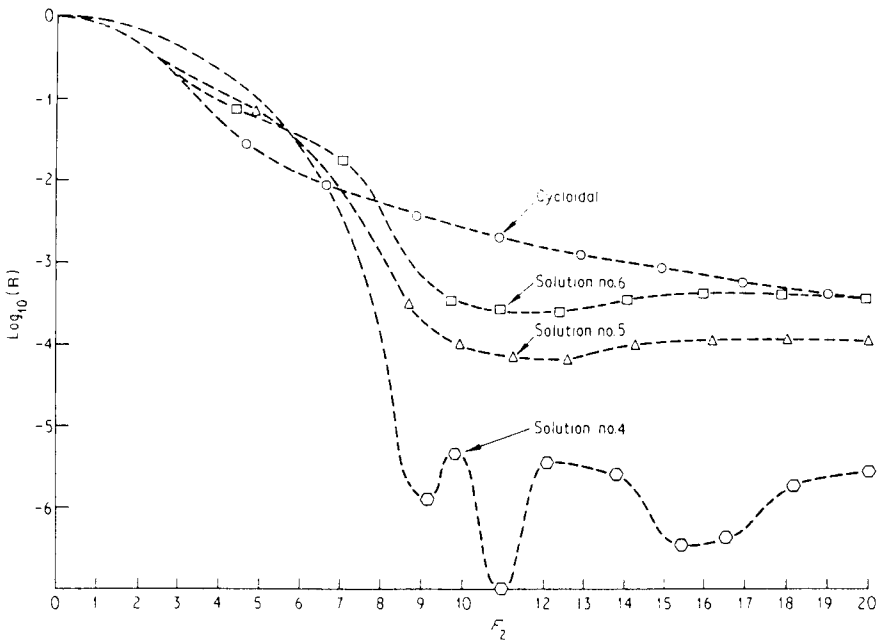


FIGURE 13.10. Vibration characteristics of DRD cams designed for  $F_2 \geq 9$ .

the usual rule of thumb that motions with discontinuous accelerations or high values of jerk always have bad vibration characteristics.

From Fig. 13.10, we see that  $\pi^2 X''_{\max} \geq 6$ , but if desired, further reduction is possible by increasing the ratios of  $A_3/A_1$  and/or  $A_3/A_2$  in Eq. (13.22).

### 13.4.5 Conclusion

The design of high-speed motions has been posed as an extremum problem. The solutions thus obtained show that a trade-off exists between minimizing the imposed inertial force and reducing the additional force and loss of control associated with large vibrations. In addition, examples were shown in which motions with discontinuous acceleration were found which have low vibration characteristics over a wide range of operating speeds, a significant contradiction to the generalized statements concerning the bad vibration characteristics of motions with high values of jerk. In view of this, it is recommended that high-speed cam designs not be based upon rules of thumb, which rather arbitrarily specify peak values of acceleration and jerk. Instead, at high speeds, each design should be evaluated separately based upon its particular requirements. The methods presented here are well-suited for high-speed cam design.

All the important system parameters needed for these analyses are rarely known in advance with extreme accuracy. In addition, damping will never be zero, as assumed in the calculations for the response to one cycle. Therefore, the tuned cam design method of Sec. 13.4.3 could well result in poor vibration characteristics at the design speed. Thus, this method should rarely be used in practice; rather, the mean squared error minimization method of Sec. 13.4.4 should be used. For a constant speed system this method should be applied over a range of speeds bracketing the design speed and large enough to accommodate possible errors in the assumed parameters. Similarly, in a variable speed system the desired speed range should be increased in the design process to account for errors.

Wiederrich (1981) showed that optimizing a design to minimize the residual vibrations over the range of speeds from zero to design speed, using the single degree of freedom model, also minimizes the response for the higher modes. This procedure minimizes the deficiencies caused by the absence of higher modes in the one-degree-of-freedom model to obtain a near-optimal solution.

## 13.5 APPLICATION OF OPTIMAL CONTROL THEORY TO THE SYNTHESIS OF CAM-FOLLOWER SYSTEMS

---

### 13.5.1 Introduction

Any cam design requires trade-offs between characteristics at the cam (such as contact stresses, lateral forces, etc.) and at the output (such as vibrations, forces, etc.). Any procedure that optimizes only one of these characteristics penalizes the others. One method that provides an approach to optimizing several of these characteristics simultaneously is based on optimal control theory (Chew et al., Parts 1 and 2, 1983). Here, we define suitable optimality criteria and show how to use them to design systems to optimize several parameters simultaneously.

### 13.5.2 Symbols

#### Dimensional parameters

$f_c$  = contact force between cam and follower

$f_{ce}$  = effective contact force between cam and follower

$f_f$  = compressive force exerted by follower spring on output mass

$f_{fe}$  = effective follower spring force =  $f_f - s_p$

$h_c, h$  = cam rise and corresponding (total) output rise

$k_s, k_f$  = stiffness of return and follower spring

$m_0, m_f$  = mass of output and of follower

$\mathbf{p}(\tau)$  = costate vector

$s_p$  = preload force of closing spring

$t_0$  = natural period of vibration of system

$t_1, t_2$  = rise, return time

$t$  = time

$\mathbf{x}(\tau)$  = state variable vector

$y, y_c$  = displacement of follower output and cam, respectively

$\eta$  = distance between axis of rotation of cam and center of roller, measured in direction of follower motion

$\sigma_c$  = Hertzian contact stress at cam-follower interface

$\sigma_{ce}$  = effective cam contact stress

$\theta_1, \theta_2$  = cam rotation during rise, return

$\omega$  = angular frequency of cam rotation

$\omega_0$  = angular frequency of vibration =  $2\pi/t_0$

$(\ )'$  = derivative with respect to time,  $t$

#### Normalized parameters

$C_F$  = nonlinear factor relating cam contact stress  $\sigma_c$  to cam contact force  $F_c$

$F_c = f_c/(k_f h)$

$F_{ce} = f_{ce}/(k_f h)$

$F_f = f_f/(k_f h)$

$F_{fe} = f_{fe}/(k_f h)$

$J$  = optimality criterion

$K_k = (k_s + k_f) / k_f$

$N_F$  = nonlinear factor relating cam contact stress  $\sigma_c$  to Follower force  $F_f$

$r_0 = (2\pi\lambda)^2$

$r_1 = 2\zeta (2\pi\lambda)$

$R_p = r_p/h_c$

$R_v = Y_c - Y$  = relative vibration

$S_F$  = factor allowing for follower guide friction, follower pressure angle, and follower mass acceleration to relate roller contact force  $F_c$  to follower force  $F_f$

$S_p = s_p/(k_f h)$

$T = (t_1 + t_2) / t_1$

$V_i$  = weight functions for  $i = 1, 2$

$W_i$  = weight factors for  $i = 1, 2, 3$

$Y = y/h$

$Y_c = y_c/h_c$

$\bar{\eta} = \eta/h_c = \sqrt{R_p^2 - \bar{\epsilon}^2}$

$\tau = t/t_1$

$\lambda = t_1/t_0$

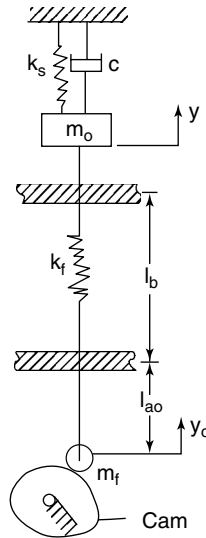
$\zeta = c/(2m_0\omega_0)$  damping ratio

$(\ )'$  = first derivative with respect to  $\tau$

$(\ )^{(n)}$  =  $n$  - th derivative with respect to  $\tau$

### 13.5.3 Description of Dynamic Model

Figure 13.11 shows a lumped-parameter model of a cam-follower system. This is a single degree-of-freedom model with two masses, two springs, and a dashpot. The model



**FIGURE 13.11.** Lumped-parameter model of a high-speed cam-follower system.

includes a roller-follower with mass to provide a realistic description of contact force and stress at the cam-follower interface. This part of the model is two-dimensional and non-linear. The equation of motion is:

$$\ddot{Y} + 2\zeta(2\pi\lambda)\dot{Y} + (2\pi\lambda)^2 Y = (2\pi\lambda)^2 Y_c. \tag{13.30}$$

### 13.5.4 Development of an Optimality Criterion-1: Output Criterion

**13.5.4.1 Minimization of Rate of Change of Effective Follower-Spring Force.** Consider now the minimization of:

$$J = \int_0^1 \ddot{F}_{fe}^2 d\tau \tag{13.31}$$

such that Eq. (13.30) as well as the following boundary conditions are satisfied:

$$Y(0) = 0, \quad Y(1) = 1, \quad Y^{(1)} = Y^{(2)} = Y^{(3)} = Y^{(4)} = 0 \quad \text{for } \tau = 0, 1. \tag{13.32}$$

The boundary conditions  $Y^{(3)}(\tau)$  for  $\tau = 0$  and  $1$  ensure that the cam velocities  $\dot{Y}_c(\tau)$  at  $\tau = 0$  and  $1$  are continuous. Otherwise, an impact exists at the cam. The boundary conditions  $Y^{(4)}(\tau)$  at  $\tau = 0$  and  $1$  ensure continuity of the cam acceleration at time  $\tau = 0$  and  $1$ .

In Part 1 of the reference papers, Chew et al. (1983), the authors also considered four alternate forms of Eq. (13.31).  $\ddot{F}_{fe}$  was replaced with  $\dot{F}_{fe}$ ,  $\dot{F}_{fc}$ ,  $F_{fe}$  and  $F_f$ . Equation (13.31) was shown to be the best option. Use of  $F_f$  gave an unacceptable reversal in the follower motion at the start of the rise. Use of  $F_{fe}$  gave a higher value of  $\dot{F}_{fe}$  at the end of the rise, meaning increased sensitivity to running speed. Use of  $\dot{F}_{fe}$  did allow continuity of the acceleration at  $t = 0$  and  $1$ . Additionally,  $\dot{F}_{fe}$  was shown to be nearly as good as  $\ddot{F}_{fe}$ .

Applying the optimality criterion discussed above requires reconciling the number of desired boundary conditions with the number specifiable by the use of optimal-control theory. To minimize the output residual vibrations, the ten boundary conditions given by Eq. (13.32) are sufficient. These ensure zero initial and end cam velocities and accelerations, thus maintaining continuity at the terminals.

**13.5.4.2 Relative Vibration and Relative Vibrational Energy.** With damping neglected and using the definition of  $R_v$ , Eq. (13.30) can be rewritten as

$$\ddot{R}_v + \frac{(K_k - 1)}{K_k} (2\pi\lambda)^2 R_v = \frac{\ddot{F}_{fe}}{K_k} \quad (13.33)$$

where

$$F_{fe} = K_k Y_c - Y. \quad (13.34)$$

After integrating Eq. (13.33) with respect to  $R_v$ , the left-hand side becomes the relative vibrational energy of the output. It follows that this vibrational energy is controllable by the parameter,  $\ddot{F}_{fe}$ . In the same way, control of the third derivative of the effective follower-spring force,  $\ddot{\ddot{F}}_{fe}$ , controls the time rate-of-change of relative vibrational energy. Hence, the continuity of this time rate-of-change of the relative vibrational energy is directly related to the continuity of the cam acceleration. The latter is specifiable through the boundary conditions given by Eq. (13.32).

**13.5.4.3 Problem Formulation Based on the Output Criterion.** From the discussion above, the problem formulation based on the output optimality criterion may be written as follows:

Minimize

$$J = \int_0^1 (W_1 \ddot{F}_{fe}^2 + W_2 \ddot{\ddot{F}}_{fe}^2) d\tau \quad (13.35)$$

such that system Eq. (13.30) and boundary conditions Eq. (13.32) are satisfied.

## 13.5.5 Development of an Optimality Criterion-2: Cam Criterion

**13.5.5.1 General.** The optimality criteria derived up to this point are for output characteristics. It is also desirable to introduce criteria for cam contact stress to allow a compromise between output performance and cam contact stress.

**13.5.5.2 Contact Stress at Cam-Follower Interface.** The Hertzian contact stress at the cam-follower interface is a nonlinear function of parameters such as pressure angles, cam offset, roller-follower mass, preload, follower-guide dimensions, follower-guide friction, and cam curvature. These parameters can be grouped into three nonlinear factors, each highlighting certain aspects of the cam contact stress.

Factor  $S_f$  allows for follower guide friction and follower pressure angle. It relates the follower-spring force  $f_f$  on the output mass to the cam contact force  $f_c$  and is given in normalized form as:

$$F_c = F_f S_f. \quad (13.36)$$

A second factor,  $C_F$ , allows for cam and roller radii and width to relate the cam contact force  $f_c$  to the cam contact stress. This factor is obtained by a Hertzian stress formula and is defined by

$$\sigma_c^2 = F_c C_F. \quad (13.37)$$

To minimize the Hertzian contact stress at the cam, the quadratic formulation is used. From Eqs. (13.36) and (13.37), the cost functional then becomes:

$$\bar{J}_c = \int_0^1 F_f N_F d\tau \quad (13.38)$$

where

$$N_F = S_F C_F. \quad (13.39)$$

The discussion after Eq. (13.31) explained that use of  $F_f$  in the minimization criterion caused reversal at the start of the motion. Similarly, the use of  $F_f$  here has been shown to do the same. Hence, the following formulation for minimizing the Hertzian cam contact stress may be used without causing reversal:

$$J_c = \int_0^1 F_{fe}^2 N_F^2 d\tau \quad (13.40)$$

where

$$\sigma_{ce}^2 = F_{fe} N_F. \quad (13.41)$$

The stress parameter,  $\sigma_{ce}$ , is that fraction of the Hertzian cam contact stress resulting from the effective follower-spring force  $F_{fe}$ , i.e., the preload effect has been eliminated as was the case in the minimization of the follower-spring force. The quadratic formulation in  $F_{fe}$  is used to ensure that a negative value for force  $F_{fe}$  is undesirable.

### 13.5.6 Formulation of Optimization Problem

At this stage it is possible to define the problem of the optimization of a high-speed cam-follower system using Eqs. (13.35) and (13.40), with weight factors  $W_i$  ( $i = 1, 2, 3$ ) as follows:

Minimize

$$J = \int_0^1 (W_1 \ddot{F}_{fe}^2 + W_2 \ddot{\ddot{F}}_{fe}^2 + W_3 F_{fe}^2 N_F^2) d\tau \quad (13.42)$$

subject to the system Eq. (13.30) and boundary conditions Eq. (13.32).

To design for desirable output characteristics, weight factor  $W_3$  may be set to zero. To design for favorable cam characteristics, weight factor  $W_3$  is chosen as large as necessary relative to weight factors  $W_1$  and  $W_2$ , with  $W_2$  nonzero. Weight factor  $W_2$  must be nonzero to provide sufficient boundary conditions to ensure continuity of the cam acceleration function.

When weight factor  $W_3$  does not vanish, the problem cannot be solved by linear methods due to the nonlinearity of parameter  $N_F$ . It can, however, be solved using optimal control theory.

### 13.5.7 Introduction to System Optimization

Having formulated an optimization criterion, we are now faced with its evaluation. Various linear techniques have been used in the design optimization of high-speed cam-follower systems.

Linear methods are certainly preferable when applicable. However, for the synthesis of cam-follower systems with nonlinearities such as contact stresses, pressure angles, cam curvature, and follower guide friction, more general methods are needed. In this section the nonlinearities are handled by means of optimal-control theory. Although this method is powerful, it requires a well-defined problem. In certain instances an optimal solution does not exist. The solution of an optimization problem using optimal control theory always results in a two-point boundary-value problem. Such problems can be tedious and time consuming. Except for simple linear problems, the vast majority require a numerical solution. Such a procedure will be described.

### 13.5.8 Optimization of Tuned Dwell-Rise-Dwell Cams

**13.5.8.1 Formulation of Two-Point Boundary-Value Problems.** The optimality criteria for high-speed cam-follower systems derived previously will now be used for the synthesis of a tuned DRD cam. The optimization problem can be stated as the optimality criterion (Eq. [13.42]) subject to the system equation (Eq. [13.30]) and boundary conditions (Eq. [13.32]).

By defining new state variables:

$$\mathbf{x}(\tau) = \begin{bmatrix} x_1 \\ x_2 \\ x_3 \\ x_4 \\ x_5 \end{bmatrix} = \begin{bmatrix} Y \\ \dot{Y} \\ Y_c \\ \dot{Y}_c \\ \ddot{Y}_c \end{bmatrix} \quad (13.43)$$

and the control variable,  $\mathbf{u} = \dot{x}_5$ , the parameters in Eq. (13.42) can be expressed as follows.

$$\left. \begin{aligned} F_{fe} &= -x_1 + K_k x_3 \\ \ddot{F}_{fe} &= r_0 x_1 + r_1 x_2 - r_0 x_3 + K_k x_5 \\ \ddot{\ddot{F}}_{fe} &= K_k u - r_0 r_1 x_1 - (r_1^2 - r_0) x_2 + r_0 r_1 x_3 - r_0 x_4 \end{aligned} \right\} \quad (13.44)$$

where

$$\begin{aligned} r_0 &= (2\pi\lambda)^2 \\ r_1 &= 2\zeta(2\pi\lambda)^2 \end{aligned}$$

and

$$N_F = S_F(x_1, x_3, x_4, x_5) C_F(x_3, x_4, x_5). \quad (13.45)$$

The system equation and boundary conditions can also be written as

$$\dot{\mathbf{x}} = \begin{pmatrix} 0 & 1 & 0 & 0 & 0 \\ -r_0 & -r_1 & r_0 & 0 & 0 \\ 0 & 0 & 0 & 1 & 0 \\ 0 & 0 & 0 & 0 & 1 \\ 0 & 0 & 0 & 0 & 0 \end{pmatrix} \mathbf{x} + \begin{pmatrix} 0 \\ 0 \\ 0 \\ 0 \\ 1 \end{pmatrix} u \quad (13.46)$$

and

$$\mathbf{x}(0) = \begin{pmatrix} 0 \\ 0 \\ 0 \\ 0 \\ 0 \end{pmatrix}, \quad \mathbf{x}(1) = \begin{pmatrix} 1 \\ 0 \\ 1 \\ 0 \\ 0 \end{pmatrix}. \quad (13.47)$$

By defining the Hamiltonian,  $H$ , of Eq. (13.42) and using the state Eq. (13.46), a two-point boundary-value problem can be obtained as follows:

State equation:

$$\dot{\mathbf{x}} = \frac{\partial H}{\partial \mathbf{p}}(\mathbf{x}, \mathbf{p}, \tau) = \begin{pmatrix} x_2 \\ -r_0 x_1 - r_1 x_2 + r_0 x_3 \\ x_4 \\ x_5 \\ \frac{r_0 r_1}{K_k} x_1 + \frac{(r_1^2 - r_0)}{K_k} x_2 - \frac{r_0 r_1}{K_k} x_3 + \frac{r_0}{K_k} x_4 - \frac{p_5}{2W_2 K_k^2} \end{pmatrix} \quad (13.48)$$

Costate equation:

$$\dot{\mathbf{p}} = \frac{\partial H}{\partial \mathbf{x}}(\mathbf{x}, \mathbf{p}, \tau) = \begin{pmatrix} -2W_1 \ddot{F}_{je} r_0 + 2W_3 F_{je} N_F^2 - 2W_3 F_{je}^2 N_F \frac{\partial N_F}{\partial x_1} + p_2 r_0 - p_5 \frac{r_0 r_1}{K_k} \\ -2W_1 r_1 \ddot{F}_{je} - p_1 + p_2 r_1 - p_5 \frac{r_1^2 - r_0}{K_k} \\ 2W_1 r_0 \ddot{F}_{je} - 2W_3 K_k F_{je} N_F^2 - 2W_3 F_{je}^2 N_F \frac{\partial N_F}{\partial x_3} - p_3 r_0 + p_5 \frac{r_0 r_1}{K_k} \\ -2W_3 F_{je}^2 N_F \frac{\partial N_F}{\partial x_4} - p_3 - p_5 \frac{r_0}{K_k} \\ -2W_1 K_k \ddot{F}_{je} - 2W_3 F_{je}^2 N_F \frac{\partial N_F}{\partial x_5} - p_4 \end{pmatrix} \quad (13.49)$$

Boundary Conditions: use Eq. (13.47).

**13.5.8.2 Solution of the Two-Point Boundary-Value Problem.** The two-point boundary-value problem given by Eqs. (13.48) and (13.49) cannot be integrated directly. A trial initial value for the costate vector,  $\mathbf{p}^{(0)}(0)$ , is chosen and the system of Eq. (13.48) and (13.49) are integrated forward in time. In general, however, the final state,  $\mathbf{x}^{(0)}(1)$  will not coincide with the boundary condition  $\mathbf{x}(1)$  specified by Eq. (13.47). It is necessary, therefore, to develop a new and hopefully improved estimate of  $\mathbf{p}^{(0)}(0)$  based on the

difference between  $\mathbf{x}^{(0)}(1)$  and  $\mathbf{x}(1)$ . The iteration formula relating the correction term for the previous initial costate to the new costate is:

$$\mathbf{p}^{(j+1)}(0) = \mathbf{p}^{(j)}(0) - \{P_x(\mathbf{p}^{(j)}(0), 1)\}^{-1} (\mathbf{x}^{(j)}(1) - \mathbf{x}(1)) \quad (13.50)$$

where  $P_x(\mathbf{p}^{(j)}(0), 1)$  is the influence function matrix and is given by

$$P_x(\mathbf{p}^{(j)}(0), 1) = \begin{pmatrix} \frac{\partial x_1(1)}{\partial p_1(0)} & \cdots & \frac{\partial x_1(1)}{\partial p_5(0)} \\ \cdot & & \cdot \\ \cdot & & \cdot \\ \cdot & & \cdot \\ \frac{\partial x_5(1)}{\partial p_1(0)} & \cdots & \frac{\partial x_5(1)}{\partial p_5(0)} \end{pmatrix} = \frac{\partial \mathbf{x}(1)}{\partial \mathbf{p}(0)}. \quad (13.51)$$

Since the explicit relationship between the vectors  $\mathbf{p}(0)$  and  $\mathbf{x}(1)$  is not known, the influence function matrix,  $P_x$ , cannot be easily calculated. One approach involves the perturbations of each of the components  $p_k(0)$ ,  $k = 1, \dots, 5$  of the costate vector  $\mathbf{p}(0)$  and the approximation

$$\frac{\partial \mathbf{x}(1)}{\partial p_k(0)} \approx \frac{\Delta \mathbf{x}(1)}{\Delta p_k(0)} \quad k = 1, \dots, 5. \quad (13.52)$$

Such a differencing procedure faces the problem of choosing the magnitude of the perturbations. Large perturbations may cause the difference approximation to be inaccurate, while small perturbations introduce numerical inaccuracies associated with integration, roundoff, and truncation errors.

Another approach is to take partial derivatives of Eqs. (13.48) and (13.49) with respect to the initial value of the costate vector,  $\mathbf{p}(0)$ , and interchange the order of differentiation (since continuity with respect to  $\mathbf{p}(0)$  and  $\tau$  is assumed). The resulting two-point boundary-value problem is derived in App. F, with each subsequent new approximation for the vector,  $\mathbf{p}^{(j+1)}(0)$  given by the iteration formula of Eq. (13.50). This approach to the solution of the two-point boundary-value problem is called the Variation of Extremals, also known as the Generalized Newton-Raphson algorithm. It is a second-order gradient technique and hence, a good initial approximation for the costate vector,  $\mathbf{p}^{(0)}(0)$ , is usually needed for convergence.

**13.5.8.3 Minimization of Output Vibrations.** To minimize output vibrations, weight factor  $W_3$  of equation (13.42) is set to zero. The other weight factors chosen are  $W_1 = 0$

**TABLE 13.3** Values of Cam-Follower System Design Parameters Used in Numerical Examples

---

$m_o = 0.75$ lb
$m_f = 0.25$ lb
$k_s = 200.0$ lb/in
$k_f = 10,000.0$ lb/in
$s_p = 75.0$ lb
$h = 0.50$ in
$\theta_1 = \pi/3$ rad
$\theta_2 = \pi/3$ rad
$\Omega = 1000$ rpm (cam speed)

---

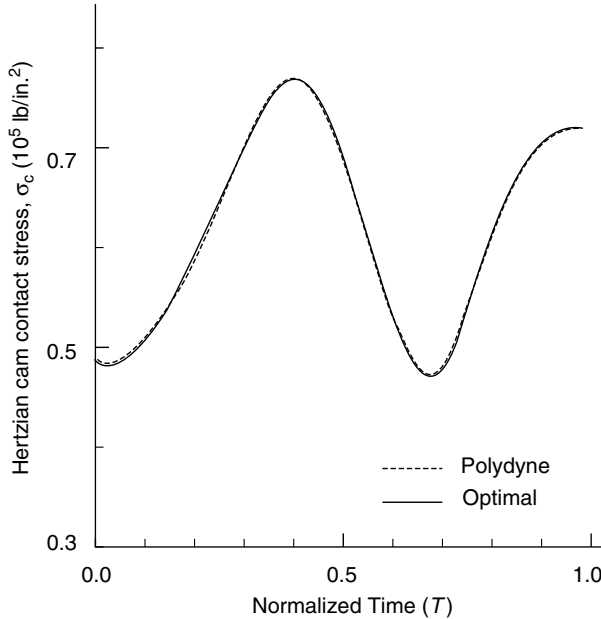


FIGURE 13.12. Hertzian cam contact stresses.

and  $W_2 = 1$ . Numerical values of the design parameters are given in Table 13.3. For simplicity, the parameters required for stress calculations only are not given in the table, and the details of the stress calculations are also not shown. With weight factor  $W_3$  set to zero, the optimization problem is linear and can be solved by linear procedures.

For linear problems, such as this, the algorithm is guaranteed to converge. Figure 13.12 shows the Hertzian cam contact stress and compares the result of using the polydyne approach. The polydyne approach used the boundary conditions given by Eq. (13.32). As can be seen, the contact stresses for the two approaches are nearly identical. Figure 13.13 shows the residual output vibrations for the optimal cam compared with the polydyne cam. The amplitude,  $S_v$ , of the residual vibrations is defined by the relationship

$$S_v = \left\{ [Y(1) - 1]^2 + [\dot{Y}(1)/(2\pi\lambda)]^2 \right\}^{1/2}. \quad (13.53)$$

For this design the cam was tuned for a speed ratio of  $\lambda = 6.6$ . The residual vibrations of the optimal cam here are lower than those of the polydyne cam. Thus, the output optimality criterion developed in Sec. 13.5.4 has been successful in minimizing the residual output vibrations at off-design speeds.

**13.5.8.4 Minimization of Hertzian Cam Contact Stress.** To design for minimum contact stresses, weight factor  $W_3$  in Eq. (13.39) is chosen as large as possible. Weight factor  $W_2$  should be small but not vanishing. For example, the following weight factors have been used:  $W_1 = 0.99$ ,  $W_2 = 0.01$ ,  $W_3 = 800$ . The required relative values of the weight factors may vary by many orders of magnitude from case to case due to variations in the design parameters, especially since the units of each term are different.

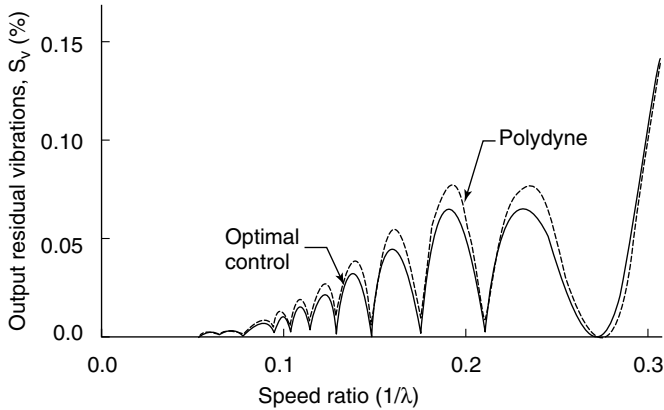


FIGURE 13.13. Output residual vibrations.

The system of Eqs. (13.48) and (13.49) is solved with the variation-of-extremals algorithm. When weight factor  $W_3$  is nonzero, the problem is nonlinear. Accurate estimates of the initial costates are then needed for convergence. For the first estimate, weight factor  $W_3$  is set to zero and the algorithm converges in one iteration. Factor  $W_3$  is then progressively increased in steps small enough to ensure the convergence of the algorithm until the desired value is achieved.

Using the same data as Sec. 13.5.8.3 above, results are obtained as shown in Fig. 13.12. The reduction in contact stress relative to the polydyne approach is seen to be relatively small. This is due to three reasons. The first is the rather high value of  $\lambda$ . To observe larger differences, a value of half the value used or less would be needed. The second reason is that the cam optimality criterion does not include (as required as described previously to obtain an acceptable solution) the effect of preload on contact stress. Therefore, only the portion of the contact stress due to system dynamics and return spring compression during the rise is minimized. Hence, contact stress is reduced less than one percent in this example. The third reason is that the ten specified boundary conditions restrict the freedom to adjust for contact stress.

The residual output vibration for the polydyne cam is somewhat lower than that for the stress-optimal cam, as depicted in Fig. 13.13. The two residual-vibration curves are similar, implying similar cam displacement curves and supporting the conclusion that the boundary conditions are at least partially responsible.

### 13.5.9 Optimization of Tuned Dwell-Rise-Return-Dwell Cams

**13.5.9.1 General.** In applying optimal control theory to the design of tuned DRRD cams, we restrict the optimization to the output criterion. The formulation of the previous sections for tuned DRD cams is modified slightly to accommodate this new class.

The return segment immediately following the rise renders the optimization procedure more difficult. It is not feasible to divide the optimization into separate dwell-rise and return-dwell portions. Doing the optimization in such a piecewise manner leads to unacceptable distortions in the cam displacement curve.

**13.5.9.2 Formulation of Two-Point Boundary-Value Problem.** Consider a modification for the cost given by Eq. (13.42) with the weight factor  $W_3$  set to zero.

$$J = \int_0^T W_1 \ddot{F}_{fe}^2 + W_2 \ddot{F}_{fc}^2 + Y_i(\tau)[Y(\tau) - Y_d(\tau)]^2 + V_2(\tau)Y^2(\tau)d\tau \quad (13.54)$$

where weight functions  $V_1(\tau)$  and  $V_2(\tau)$  are normal distributions given by

$$v_i(\tau) = \frac{k}{S_d} e^{-\frac{n}{2}} \quad i = 1, 2 \quad (13.55)$$

with

$$n = \left( \frac{\tau - 1}{S_d} \right)^2$$

$$k \approx 10^4$$

$$S_d \approx 10^{-5}$$

and the function  $Y_d(\tau)$  is a polynomial given by

$$\left. \begin{aligned} Y_d(\tau) &= 6\tau^5 - 5\tau^6 & 0 \leq \tau \leq 1 \\ Y_d(\tau) &= 6S^5 - 5S^6 & 1 < \tau \leq T \end{aligned} \right\} \quad (13.56)$$

where  $T > 1$

$$S = \frac{T - \tau}{T - 1}$$

The boundary conditions of the “interior point” at time  $\tau = 1.0$  are now indirectly specified through the introduction of weight functions  $V_1(\tau)$  and  $V_2(\tau)$  in the cost functional. To ensure convergence of the variation-of-extremals algorithm as well as reducing numerical errors in the integration, it is necessary to start the optimization with a relatively large standard deviation of about  $10^{-2}$ . With succeeding iteration, constant  $S_d$  is gradually reduced to a point at which the weighting functions  $V_i(\tau)$ ,  $i = 1, 2$  approximate a delta function. These weighting functions force the boundary conditions at this interior point to be:

$$Y(1) = 1.0$$

$$\text{and } \dot{Y}(1) = 0.0. \quad (13.57)$$

These boundary conditions are not expected to give a cam displacement,  $Y_c(1)$ , of unity at time  $\tau = 1$  since the system equation (Eq. [13.30]) is of second order. If this is a concern, an additional term  $V_3(\tau)\dot{Y}^2(\tau)$  may be introduced in the cost functional to specify the interior boundary condition  $\dot{Y}(1) = 0.0$  indirectly. Weight function  $V_3(\tau)$  is defined identically to  $V_1(\tau)$  and  $V_2(\tau)$ .

With the definition of  $T$  (see symbols), the previously used normalizations remain unchanged. This minimizes the amount of modification needed in problem formulation and computation.

The formulation of the optimization problem for a tuned D-R-R-D cam can now be given as follows.

Minimize

$$J = \int_0^T W_1 \ddot{F}_{fe}^2 + W_2 \ddot{F}_{fc}^2 + V_1(\tau)[Y(\tau) - Y_d(\tau)]^2 + V_2(\tau)Y^2(\tau) + V_3(\tau)\dot{Y}^2(\tau)d\tau \quad (13.58)$$

subject to system equation (13.30) and boundary conditions Eq. (13.32).

The derivation of the resulting two-point boundary-value problem is carried out in the same way as for the tuned D-R-D cam design. The problem is then solved using the variation-of-extremals algorithm developed previously. In this way the difficulties posed by the three-point boundary value problem have been circumvented with only slight modifications in the procedure used for tuned D-R-D cams.

### 13.5.10 Conclusions

An optimization procedure has been developed for the synthesis of high-speed cam-follower system lift curves. Trade-offs between criteria at the cam-follower interface and at the output are included. Optimal-control theory has been shown to optimize not only for traditional linear relationships, but also for nonlinear relationships, such as those needed for contact-stress minimization. However, large-scale numerical integrations are required.

The accuracy of the method for contact stress minimization is limited by the exclusion of closing-spring preload from the analysis. If the closing-spring preload is generally a small portion of the net cam load, however, the accuracy should be good. Another limitation of the contact stress minimization method is that it limits stress over the entire motion, not the maximum stress, which is usually of chief concern.

## 13.6 USE OF THE CONVOLUTION OPERATOR TO REDUCE RESIDUAL VIBRATIONS

---

### 13.6.1 Introduction

This section presents a systematic method of using the convolution operator to generate cam lift curves that minimize the residual vibration after a lift event of given displacement and duration. The method is a mathematical transformation that can be applied to any suitable motion to produce families of cam profiles of increasing continuity. For example, starting with a uniform rise curve, one sequence of modifications leads to a family of curves whose members include parabolic and various nonelementary rise curves. Another sequence starting with a simple harmonic rise curve leads to a family whose members include cycloidal and various nonelementary rise curves. An alternate application of this approach enables us to design cam curves that produce extremely low residual vibration over a range of operating speeds. This method was originated by Gupta and Wiederrich (1983).

### 13.6.2 Symbols

$a$  = cam curve acceleration

$a^*(\eta)$  = acceleration curve for any lift curve with unit rise and unit rise angle

$A$  = Fourier transform of  $a$

$A^*(\lambda)$  = Fourier transform of  $a^*(\eta)$

$d$  = cam rise

$k = \omega_r/\omega$

$R$  = amplitude of the residual vibrations induced by the rise curve

$v$  = cam curve velocity

$v^*(\eta)$  = velocity curve for any lift curve with unit rise and unit rise angle

$V$  = Fourier transform of  $v$

$V^*(\lambda)$  = Fourier transform of  $v^*(\eta)$

$w$  = an admissible cam velocity curve

$W$  = Fourier transform of admissible cam velocity curve  $w$

$y$  = cam curve displacement

$y^*(\eta)$  = displacement curve for any cam lift curve with unit rise and unit rise angle

$Y$  = Fourier transform of  $y$

$Y^*(\lambda)$  = Fourier transform of  $y^*(\eta)$

$Z$  = dynamic error of the follower response

$\beta$  = cam rise angle

$\lambda$  = parameter for Fourier transforms of functions

$\theta$  = cam angle of rotation

$\omega$  = cam rotational speed

$\omega_n$  = natural frequency of the one degree-of-freedom elastic follower model

### 13.6.3 Basic Theory

Convolution is a basic operation performed on two functions. A convolution operation in the function plane corresponds to a simple multiplication of the two functions in the transform plane (Laplace, Fourier, etc.). Gupta and Wiederrich (1983) showed that convolution can be useful in the design of cam motions for linear, moderately damped cam-follower systems. Any rise or return cam lift curve can be modified to give a new lift curve of the required rise and duration with significantly reduced residual follower vibration. Minimizing the residual vibration is of primary importance in many applications, particularly those with long periods of dwell. Knowing the residual response of the motion, one can use the principle of superposition to predict the contribution of that motion on the steady state vibration response of the system, or at least establish an upper bound on that contribution. The residual response is thus a valuable indicator of the overall dynamic quality of a motion.

Let  $y^*(\eta)$ ,  $v^*(\eta)$ , and  $a^*(\eta)$  represent displacement, velocity, and acceleration for any cam lift curve with unit rise and unit rise angle. It may be noted that

$$v^* = \frac{dv^*}{d\eta} \quad \text{and} \quad a^* = \frac{dv^*}{d\eta}.$$

When the rise is  $d$  and the rise angle is  $\beta$ , we can obtain displacement, velocity, and acceleration curves as follows:

$$\begin{aligned} y(d, \beta, \theta) &= d \cdot y^*(\theta/\beta) \\ v(d, \beta, \theta) &= \left(\frac{d}{\beta}\right) \cdot v^*(\theta/\beta) \\ a(d, \beta, \theta) &= \left(\frac{d}{\beta^2}\right) \cdot a^*(\theta/\beta) \end{aligned} \quad (13.59)$$

where  $v = dy/d\theta$  and  $a = dv/d\theta$ . Note that  $y^*(\eta) = y(1, 1, \eta)$ .

To use the Fourier transform, we define  $v^*(\eta) = 0$  for  $\eta < 0$  and  $\eta > 1$ . Likewise,  $v(d, \beta, \theta) = 0$  for  $\theta < 0$  and  $\theta > \beta$ . The Fourier transforms of  $v^*(\eta)$  and  $v(d, \beta, \theta)$  are defined as

$$\begin{aligned}
 V^*(\lambda) &= \int_{0-}^{1+} v^*(\eta) \cdot e^{-i\lambda\eta} d\eta \\
 V(d, \beta, \lambda) &= \int_{0-}^{\beta+} v(d, \beta, \theta) \cdot e^{-i\lambda\theta} d\theta.
 \end{aligned} \tag{13.60}$$

In a similar manner,  $Y^*(\lambda)$ ,  $A^*(\lambda)$ ,  $Y(d, \beta, \lambda)$ , and  $A(d, \beta, \lambda)$  are defined as the Fourier transforms of  $y^*(\eta)$ ,  $a^*(\eta)$ ,  $y(d, \beta, \theta)$ , and  $a(d, \beta, \theta)$  respectively, although for  $Y^*(\lambda)$  and  $Y(d, \beta, \lambda)$ , the upper limit of the transform integral must extend to  $+\infty$ . The analog of Eq. (13.59) in the transform plane is as follows:

$$\begin{aligned}
 Y(d, \beta, \lambda) &= d\beta Y^*(\beta\lambda) \\
 V(d, \beta, \lambda) &= dV^*(\beta\lambda) \\
 A(d, \beta, \lambda) &= \left(\frac{d}{\beta}\right) A^*(\beta\lambda).
 \end{aligned} \tag{13.61}$$

Note that  $Y^*(\lambda) = Y(1, 1, \lambda)$ .

The dynamic error  $Z$  is defined as the difference between the actual and the static follower responses. Let  $k = \omega_n/\omega$ , where  $\omega_n$  is the natural frequency of a one degree-of-freedom elastic model of the cam-follower system and  $\omega$  is the rotational speed of the cam. Neglecting damping, the governing equation of  $Z$  is assumed to be

$$Z'' + k^2 Z = a(d, \beta, \theta). \tag{13.62}$$

The absence of a damping term in Eq. 13.62, required for the method developed here, is usually conservative. The amplitude of the residual vibration induced by the rise curve is then

$$R(k) = \left| \frac{1}{k} A(d, \beta, k) \right|. \tag{13.63a}$$

Because  $v$  is defined to be zero for  $\theta < 0$  and  $\theta > \beta$ , Eq. (13.63a) becomes

$$R(k) = |V(d, \beta, k)|. \tag{13.63b}$$

The residual response spectrum is thus the Fourier spectrum of the velocity curve  $v(d, \beta, \theta)$ . The area of an admissible velocity curve between  $\theta = 0$  and  $\beta$  is equal to the follower rise  $d$ .

Convolution,  $h(\theta)$ , of two functions  $f(\theta)$  and  $g(\theta)$  is defined as

$$h(\theta) = f * g = \int_{-\infty}^{+\infty} f(\tau) \cdot g(\theta - \tau) d\tau. \tag{13.64a}$$

In the transform plane,

$$H(\lambda) = F(\lambda) \cdot G(\lambda). \tag{13.64b}$$

It can be easily verified that the area under the curve  $h$  is equal to the product of the areas under the curves  $f$  and  $g$ , i.e.,

$$(\text{area})_h = (\text{area})_f \cdot (\text{area})_g. \tag{13.65}$$

Also if  $f = 0$  when  $\theta < 0$  and  $\theta > \theta_f$ , and  $g = 0$  when  $\theta < 0$  and  $\theta > \theta_g$ , then  $h = 0$  when  $\theta < 0$  and  $\theta > \theta_n$ , where

$$\theta_n = \theta_f + \theta_g. \tag{13.66}$$

These properties of the convolution operator can be applied to cam curves as follows: let  $v_i(d, \beta, \theta)$  be an admissible velocity curve of area  $d$  corresponding to a follower motion of rise  $d$  in cam rotation  $\beta$ . Let  $w(d, \beta, \theta)$  be another admissible velocity curve. Then a new admissible velocity curve  $v_{i+1}(d, \beta, \theta)$  is constructed as

$$v_{i+1}(d, \beta, \theta) = v_i(d', \beta', \theta) * w(d'', \beta'', \theta) \quad (13.67a)$$

where the symbol  $*$  represents convolution (see Eq. [13.64a])  $d = d' d''$  (see Eq. [13.65]) and  $\beta = \beta' + \beta''$  (see Eq. [13.66]). Like ordinary integration, convolution is a smoothing operation. As a result, with each convolution additional derivatives of  $v$  vanish at the start and end of the rise.

Fourier transform of Eq. (13.67a) leads to equation (13.67b)

$$V_{i+1}(d, \beta, k) = V_i(d', \beta', k) \cdot W(d'', \beta'', k). \quad (13.67b)$$

Equation (13.67a) then gives the post convolution cam curve and Eq. (13.67b), in conjunction with Eq. (13.63b), gives the postconvolution residual response. Some specific applications of convolution to the development of cam motions are discussed in the following sections.

### 13.6.4 Fixed Convolution

Convolution can be applied in several ways to improve cam profiles. The most effective way that Gupta and Wiederrich (1983) identified they called fixed convolution. In this method we set  $d' = d$ ,  $d'' = 1$ ,  $\beta' = \beta'' = \beta/2$  in Eqs. (13.67a and b). In this case, the nature of  $w$  is not changed during the convolutions. The velocity curve is obtained from Eq. (13.67a) as

$$v_{i+1}(d, \beta, \theta) = v_i(d, \beta/2, \theta) * w(1, \beta/2, \theta) \quad (13.68)$$

and the Fourier transform from Eq. (13.67b) as

$$V_{i+1}(d, \beta, k) = V_i(d, \beta/2, k) \cdot W(1, \beta/2, k). \quad (13.69)$$

The cumulative effect of  $m$  convolutions is obtained as follows:

$$V_m(d, \beta, k) = W(1, \beta/2, k) \cdot W(1, \beta/4, k) \cdots W(1, \beta/2^m, k) \cdot V_0(d, \beta/2^m, k). \quad (13.70)$$

It is seen from Eq. (13.63b) and (13.70) that the residual response,  $R_m(d, \beta, k) = |V_m(d, \beta, k)|$ , after  $m$  convolutions is dominated by the modifier function  $w(d, \beta, \theta)$ , and the starting function  $v_0(d, \beta, \theta)$  has only a small influence.

From the definition of  $v(1, \beta, \theta)$ , it follows that  $v(1, 0, \theta)$  is a delta function (area = 1, function vanishes for  $\theta < 0-$  and  $\theta > 0+$ ). Its transform  $|V(1, 0, k)| = 1$ . As  $m \rightarrow \infty$ , a limiting residual response is thus obtained from Eq. (13.70).

$$\lim_{m \rightarrow \infty} R_m(d, \beta, k) = \left| d \cdot \prod_{r=1}^{\infty} W(1, \beta/2^r, k) \right| \quad (13.71)$$

As will be seen in the example below, the envelope of  $R_{i+1}$  always lies above that of  $R_i$  until the value of  $k$  exceeds some crossover value. Above this value of  $k$ , the envelope of  $R_{i+1}$  lies below that of  $R_i$ . In this case, a limit  $R_\infty$  is reached which provides the lowest envelope available by this method, although it is possible that other basic curves may provide a lower envelope. For the high-speed systems in which vibration is typically a major concern, however,  $k$  will be sufficiently low enough so that the lowest

envelope will be found at some limiting value of  $m$ . In this case the resulting design should be nearly optimal.

### 13.6.5 Constant Velocity Convolution

As an illustration of fixed-convolution let us consider  $w(1, \beta, \theta)$  to be the velocity curve for constant velocity. Then

$$\begin{aligned} v_{i+1}(d, \beta, \theta) &= (2/\beta) \int_0^\theta v_i(d, \beta/2, \tau) \cdot d\tau, 0 \leq \theta \leq \beta/2 \\ &= (2/\beta) \int_{\theta-\beta/2}^{\beta/2} v_i(d, \beta/2, \tau) \cdot d\tau, \beta/2 \leq \theta \leq \beta. \end{aligned} \quad (13.72)$$

The postconvolution acceleration curve is obtained by differentiation of Eq. (13.72)

$$\begin{aligned} a_{i+1}(d, \beta, \theta) &= (2/\beta) v_i(d, \beta/2, \theta), 0 \leq \theta \leq \beta/2 \\ &= (2/\beta) v_i(d, \beta/2, \theta - \beta/2), \beta/2 \leq \theta \leq \beta. \end{aligned} \quad (13.73)$$

In dimensionless form

$$\begin{aligned} v_{i+1}^*(\eta) &= 2 \int_0^{2\eta} v_i^*(\tau) d\tau, 0 \leq \eta \leq 1/2 \\ &= 2 \int_{2\eta-1}^1 v_i^*(\tau) d\tau, 1/2 \leq \eta \leq 1 \end{aligned} \quad (13.74)$$

$$\begin{aligned} a_{i+1}^*(\eta) &= 4v_i^*(2\eta), 0 \leq \eta \leq 1/2 \\ &= -4v_i^*(2\eta-1), 0 \leq \eta \leq 1. \end{aligned} \quad (13.75)$$

Let us start with a uniform rise curve as the function  $V_0^*(\eta)$ . After the first convolution, we obtain  $V_1^*(\eta)$  which corresponds to the well-known parabolic motion. Additional convolutions lead to nonelementary curves. Successive numerical integrations based upon Eq. (13.74) indicated convergence after eight convolutions. The nature of  $V_i^*(\eta)$  is shown in Fig. 13.14. For  $i \neq 0$ ,  $V_i^*(0.5) = 2$ ,  $V_i^*(0.25) = V_i^*(0.75) = 1$ . The envelopes of the residual vibration spectra,  $R_i^*(k)$  versus  $k$ , are shown in Fig. 13.15 for large  $k$ . These were obtained from an FFT analysis of  $V_i^*(\eta)$  which gave  $V_i^*(2\pi k)$  for  $k = 0, 1/2, 1, 3/2, \dots$  (Alternatively, one could have obtained these results for  $V_i^*$  from Eq. (13.70) after setting  $d = \beta = 1$  and then determined  $V_i^*$  as in Eq. (13.69). Figure 13.15 shows the crossover values of  $k$ . Although the eighth convolution appears to give the least residual vibration for  $k$  greater than  $20\pi$ , this value of  $k$  is above those which occur in medium to high-speed cam systems. In fact, the third convolution appears to be better in this range of

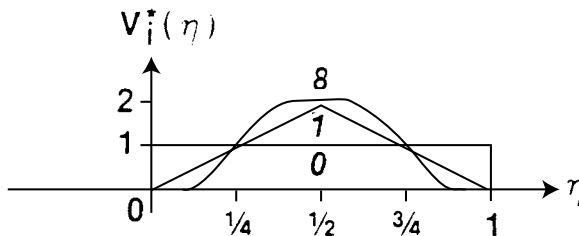


FIGURE 13.14. Uniform convolution velocities,  $v_i^*(\eta)$  for  $i = 0, 1, 8$ .

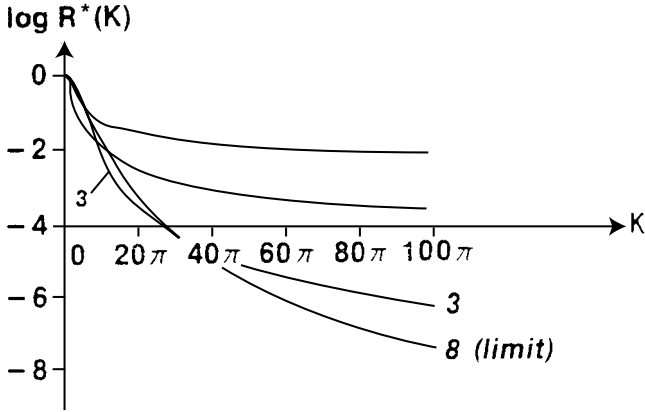


FIGURE 13.15. Uniform convolution residual vibration spectrum envelopes.

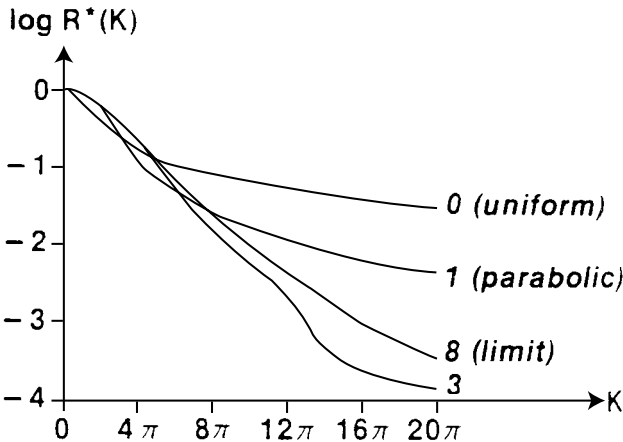


FIGURE 13.16. Uniform convolution residual vibration spectrum envelopes.

$k(1 \ll k < 20\pi)$ . This portion of  $R^*$  is shown in more detail in Fig. 13.16. It was obtained from an FFT analysis of  $V_i^*(\eta)$  which gave  $V_i^*(2\pi k)$ ,  $k = 0, 1/8, 1/4, 3/8, \dots$ . The complete residual vibration spectrum for the limiting profile (i.e.,  $v_8^*$ ) is shown in Fig. 13.17.

A convenient way to express  $V_1^*(\eta)$  is in terms of its Fourier series which is as follows

$$v_i^*(\eta) = V_i^*(0) + 2 \sum_{m=1}^M [\text{Re}(V_i^*(2\pi m)) \cdot \cos(2\pi m\eta) - \text{Im}(V_i^*(2\pi m)) \cdot \sin(2\pi m\eta)]. \quad (13.76)$$

The Fourier series coefficients for several of the  $V_i^*(\eta)$  are given in Table 13.4.

When  $V_0^*(\eta)$  is chosen as the velocity curve for simple harmonic motion, then the envelopes of the residual vibration spectra are as shown in Fig. 13.18. The Fourier series for  $V_2^*(\eta)$  is given as

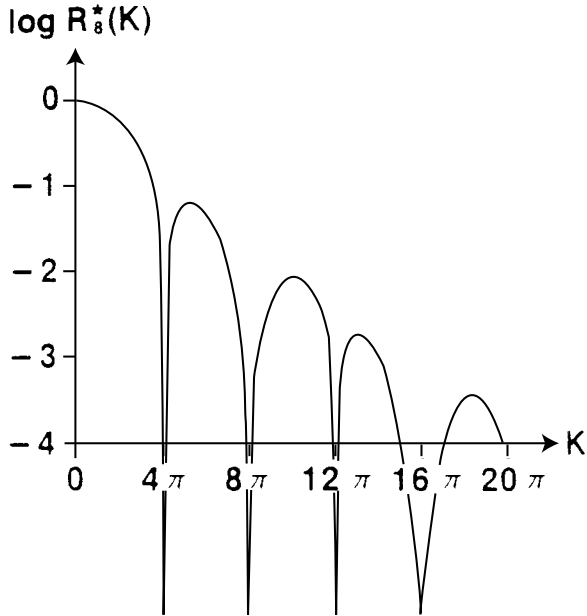


FIGURE 13.17. Uniform convolution residual vibration spectrum.

TABLE 13.4 Fourier Analysis when  $V_0^*$  is for Uniform Rise  $V_0^*(0) = 1$ .  $ImV_i^*(2\pi m) = 0$ .

$m$	$2ReV_0^*(2\pi m)$	$2ReV_1^*(2\pi m)$	$2ReV_2^*(2\pi m)$	$2ReV_3^*(2\pi m)$	$2ReV_4^*(2\pi m)$
1	0	-0.810732	-1.032049	-1.088591	-1.107524
2	0	0	0	0	0
3	0	-0.090226	0.038224	0.078330	0.092391
4	0	0	0	0	0
5	0	-0.032586	-0.008256	0.010152	0.017306
6	0	0	0	0	0
7	0	-0.016706	0.003009	-0.000453	-0.002088
8	0	0	0	0	0
9	0	-0.010171	-0.001416	-0.000166	0.000711
10	0	0	0	0	0
11	0	-0.006864	0.001550	0.000434	-0.000596
12	0	0	0	0	0
13	0	-0.004962	-0.000469	0.000222	-0.000182
14	0	0	0	0	0
15	0	-0.003770	0.000306	-0.000022	0.000013

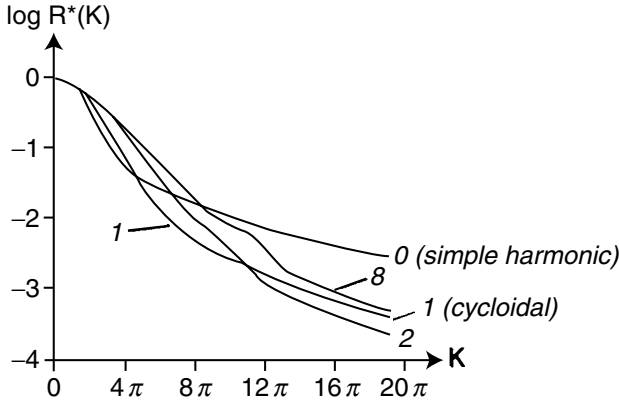


FIGURE 13.18. Uniform convolution residual vibration spectrum envelopes.

$$\begin{aligned}
 V_2^*(\eta) = & 1 - 1.080760 \cos(2\pi\eta) + 0.72051 \cos(6\pi\eta) \\
 & + 0.006176 \cos(10\pi\eta) + 0.001470 \cos(14\pi\eta) \\
 & + 0.000520 \cos(18\pi\eta) + 0.000229 \cos(22\pi\eta) \\
 & + 0.000116 \cos(26\pi\eta) + 0.000065 \cos(30\pi\eta). \quad (13.77)
 \end{aligned}$$

### 13.6.6 Conclusion

A method to mathematically manipulate cam motions with the objective of improving their residual vibration response has been presented and illustrated with examples. The families of curves thus generated are of theoretical interest, particularly since the families are seen to approach limits that are independent of the starting motion. This ability to transform motions in specified ways can also be useful in the practical design and selection of cam motions. The method presented is well suited to numerical calculation.

## 13.7 POLYDYNE CAMS

### 13.7.1 Introduction

In polydyne cams the cam profile is designed such that the follower lift curve matches a desired polynomial equation at the desired design speed given the cam-follower system dynamic characteristics. Automobile valve-gear linkages and textile machine members are prime examples of good polydyne applications. The polydyne method was originally presented by Dudley (1948) and elaborated by Stoddart (1953). This is the first method ever proposed that designs the cam shape to give the desired follower action. Polydyne's basic advantages are:

1. By direct means it can eliminate "jump" of the follower off the cam.
2. By direct calculation it provides control of the exact position of the follower end.
3. It limits vibrations to minimum amplitudes at the design speed.

Its primary shortcomings are:

1. High accuracy is needed to realize the advantage of the mathematically computed curve. Sometimes the cam calculated is impossible to cut; i.e. a “dip” in the cam is required.
2. The mathematical work is laborious and time-consuming.
3. The cam-follower system is valid at only one speed.

### 13.7.2 Fundamental Relationships

In the following sections a typical example indicating the method of attack establishes the basic equations for a high-speed cam-follower system.

First, the flexibility relationship of the linkage must be determined. Any cam-driven mechanism (assuming a single degree of freedom) may be divided into the usual dynamic equivalent system of four parts.

1. Compression spring—to hold the follower on the cam. In positive-drive cams, this spring obviously does not exist.
2. An equivalent mass at the end of the follower.
3. A spring representing the combined elasticity of the linkage.
4. A cam—The cam and follower motions may be considered the same at speeds low enough that the highest frequency of significant cam input is low compared to the system’s natural frequency.

Since damping and friction are small, they will be neglected. This will greatly simplify the mathematical relations. Let

$k_s$  = spring rate of compression spring, lb/in

$k_f$  = spring rate of follower linkage, lb/in

$m = \frac{w}{g}$  = equivalent mass at the follower end, lb-sec<sup>2</sup>/in

$w$  = equivalent weight at follower end, lb

$L$  = external load acting on follower, lb

$S_1$  = initial compression spring force with mass  $m$  at zero position, lb

$N$  = cam speed, rpm

$y$  = actual lift at follower end, in

$y_c$  = rise of cam, in. (This is not the same as  $y$  because of the linkage deflection.)

$\theta$  = cam angle of rotation at cam lift  $y_c$  and follower lift,  $y$ , deg

Mass  $m$  (Fig. 13.19) is subjected to an acceleration such that at any instant

$$\sum \text{Forces} = m \frac{d^2 y}{dt^2}. \quad (13.78)$$

The forces are

Main spring force =  $-k_s y$

Linkage force =  $-k_f (y - y_c)$

External load =  $-L$

Initial spring force =  $-S_1$

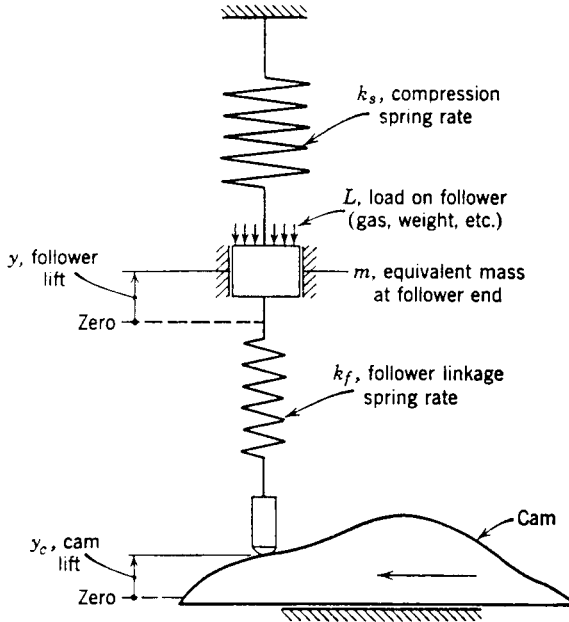


FIGURE 13.19. Dynamic model for high-speed cam-follower system.

Substituting in Eq. (13.78) gives

$$-k_s y - L - S_1 - k_f (y - y_c) = m \frac{d^2 y}{dt^2}.$$

Solving for cam displacement,

$$y_c = \frac{L + S_1}{k_f} + \frac{k_f + k_s}{k_f} y + \frac{m}{k_f} \frac{d^2 y}{dt^2}. \tag{13.79}$$

In Eq. (13.79), it is convenient to change the independent variable from time  $t$  to the cam angle  $\theta$ , degrees. We know that

$$\frac{d^2 y}{dt^2} = \omega^2 \frac{d^2 y}{d\theta^2}. \tag{13.80}$$

Substituting gives

$$\frac{d^2 y}{dt^2} = 360^2 \left( \frac{\text{deg}}{\text{rev}} \right)^2 \times \left( \frac{N}{60} \right)^2 \left( \frac{\text{rev}}{\text{sec}} \right)^2 \times \frac{d^2 y}{d\theta^2} = 36N^2 y''. \tag{13.81}$$

Substituting in Eq. (13.79) yields the cam displacement

$$y_c = \frac{L + S_1}{k_f} + \frac{k_f + k_s}{k_f} y + \frac{m}{k_f} 36N^2 y''. \tag{13.82}$$

Rewriting,

$$y_c = r_a + k_r y + c y'' \quad (13.83)$$

where  $r_a = r_s + r_k$  = the ramp height, in. (This is the initial deflection of the follower linkage to eliminate [1] preload, and [2] clearance, so that motion of the follower end is impending.)

$$r_s = \frac{L + S_1}{k_f} = \text{initial static deflection of linkage, in.}$$

$$r_k = \text{clearance or backlash in linkage, in.}$$

$$k_r = \frac{k_f + k_s}{k_f} = \text{equivalent spring rate ratio of the follower linkage.}$$

$$c = \frac{m \times 36 N^2}{k_f} = \text{dynamic constant, degrees.}$$

Equation (13.83) may be applied in either of two ways:

1. Having an arbitrary cam profile  $y_c$ , the actual motion of the follower end  $y$  may be found. This method may be used to investigate existing cam mechanisms.
2. A suitable follower motion  $y$  versus cam angle  $\theta$  may be assumed, and the cam profile  $y_c$  may be developed to fulfill that motion at the desired speed. This is the direct approach used in this chapter.

### 13.7.3 Ramp Height, $r_a$

The ramp is a small pre-cam and is of critical importance. Its function is to compensate for the clearance  $r_k$  and the static follower deflection  $r_s$ .  $r_a$  is the amount of cam lift required before the follower end moves against the preload of the compression spring holding the follower on the cam. In the high-speed, highly flexible systems of this chapter, the clearance  $r_k$  is small (held to a minimum) as compared with the static deflection  $r_s$ . The needed ramp height may be found by measurement of the actual linkage or by calculation in which deflection formulae and clearances are applied.

The required ramp height is dependent upon the clearance  $r_k$  and three other factors: the external load  $L$ , the initial spring force  $S_1$ , and the linkage rigidity  $k_f$ . The initial spring load  $S_1$  is in turn dependent on the inertia forces as well as other factors.

### 13.7.4 Spring Ratio Constant, $k_r$

The second term of Eq. (13.83) is the constant  $k_r$ , called the equivalent spring rate ratio, which is related to the stiffnesses of the follower linkage  $k_f$ , and the loading spring  $k_s$ .

Every part in the linkage acts as a spring. Therefore the follower linkage spring rate  $k_f$  in a machine may consist of the sum of many individual springs such as: (a) the bending and twisting of shafts; (b) the deflection and bowing of rods and arms; (c) the deflection of gears; (d) the deflection of bearings; and (e) the deflection of cam and follower surfaces.

The most convenient and accurate method for determining the overall value of  $k_f$  is by measurement on the actual machine or model. This is done by loading the system and accurately observing the deflection with a micrometer indicator. These values when plotted approximate a straight line. The spring rate  $k_f$  equals the slope of the plotted line. Another

approach for determining  $k_f$  is by calculation of above items (a) through (e). This method is subject to error since broad assumptions must be made in the deflection formulae.

The compression spring rigidity  $k_s$  may easily be found by the design calculations if fabrication accuracy is maintained. In the automotive and aircraft fields, typical values are

$$k_f = \text{between } 20,000 \text{ and } 60,000 \text{ lb/in}$$

$$k_s = \text{between } 100 \text{ and } 600 \text{ lb/in}$$

These values depend on engine size and speed.

### 13.7.5 Dynamic Constant, $c$

The dynamic constant

$$c = 36 \frac{m}{k_f} N^2$$

which can be rewritten as

$$c = 0.093 \frac{w}{k_f} N^2. \quad (13.84)$$

### 13.7.6 Equivalent Weight, $w$

This weight  $w$  may or may not be the total weight of the members, depending upon (1) the effect of the flexible members, (2) levers, and (3) gears. The following are suggestions for finding the equivalent weight  $w$ .

**13.7.6.1 Springs.** For both long thin rods that act as springs and actual compression springs, we do not use their weights directly. Theory and experience have shown that about one-third of their actual weight is effective. This is because flexibility prevents all the mass from being accelerated at the same rate. Thus, the acceleration above does not affect the other two-thirds of the weight.

**13.7.6.2 Levers and Gears.** A lever (Fig. 13.20) with unequal arms has its effective weight  $w$  inversely related to the square of its lever arm ratio. In this figure, we have a lever with arms  $d_1$  and  $d_2$ , follower velocities  $v_1$  and  $v_2$ , and a weight  $w_1$  to be referred to the follower end.

The kinetic energy of weight  $w_1$

$$\text{K.E.} = \frac{w_1}{2g} v_1^2.$$

This must equal the kinetic energy of the equivalent weight on the follower end

$$\text{K.E.} = \frac{w}{2g} v_2^2$$

equating gives

$$w = w_1 \left( \frac{v_1}{v_2} \right)^2 = w_1 U^2 \quad (13.85)$$

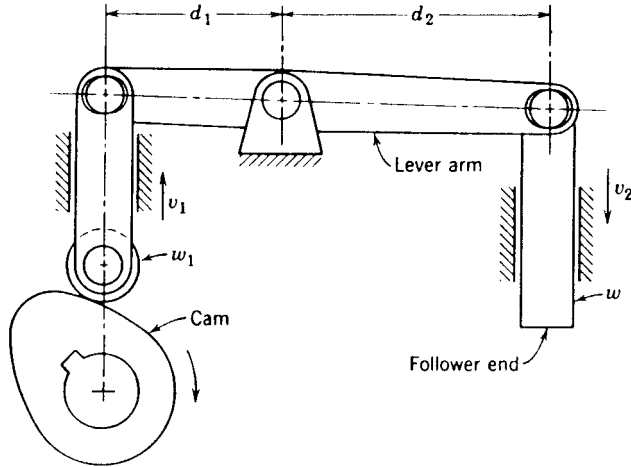


FIGURE 13.20. Lever ratio.

where  $U = d_1/d_2 =$  lever arm ratio. Similarly, it can be shown that the equivalent weight or equivalent moment of inertia for rotating gears have the same relationship in which  $U$  equals the gear ratio. Therefore, any weight or moment of inertia may be referred to the follower end by the square of the lever arm or gear ratio. It may be noted that the inertia of the oscillating arm, being special, may be found by reference to any book on mechanics.

### 13.7.7 Application of Polynomials for Cam Curves

We recall from Eq. (13.83) that the cam profile displacement is

$$y_c = r_a + k_r y + c y''.$$

Differentiating with respect to  $\theta$ , yields for the cam,

$$\text{Velocity} = y_c' + k_r y' + c y''' \quad (13.86a)$$

$$\text{Acceleration} = y_c'' + k_r y'' + c y^{IV}. \quad (13.86b)$$

The first four derivatives of the follower motion equation,  $Y = f(\theta)$ , must be continuous functions. This is required, since we want to maintain continuity of the cam profile  $y_c$ , velocity  $y_c'$ , and acceleration  $y_c''$ . Equation (13.87) shows that the cam acceleration  $y_c''$ , is a function of the fourth derivative of the follower motion,  $y^{IV}$ . Thus, combinations of basic curves cannot be used, since they are discontinuous in these higher derivatives. However, polynomial equations are feasible. These equations may be utilized to fulfill any boundary condition required simply by adding power parts to the fundamental equation.

$$y = C_0 + C_1\theta + C_2\theta^2 + C_3\theta^3 + \cdots + C_n\theta^n. \quad (13.87)$$

The number of terms is dependent on the number of boundary conditions at the end points.

With dwell-rise-dwell action, it can be shown that the 3-4-5 polynomial family for the follower end motion,  $y$ , will give finite values of velocity  $y_c'$  at the ends. The 4-5-6-7 poly-

nominal indicates finite acceleration values  $y_c''$  at the ends (infinite jerk); vibrations result. This condition can be alleviated by the use of special ramps. However, if we desire that the cam acceleration curve have finite values of jerk, a fourth-order boundary condition [for follower  $y = f(\theta)$ ] equal to zero at the ends is required. The 5-6-7-8-9 polynomial family having the following basic equation fulfills this condition:

$$y = 1 - 126\theta^5 + 420\theta^6 - 540\theta^7 + 315\theta^8 - 70\theta^9. \quad (13.88)$$

This curve gives a lift of 1.0 at the start ( $\theta = 0$ ) and a lift and first four derivatives of 0.0 at the end ( $\theta = 1$ ). This family is suggested for most high-speed, high-flexibility machinery.

The best approach is to establish basic equations with certain simplifying approximations. The significance of the approximations must be compared with the accuracy of the given data and the cutting of the cam. The procedure for design is as follows:

1. Choose a polynomial equation,  $y = f(\theta)$ , with proper control at the end points. The 5-6-7-8-9 family is often suggested.
2. Establish the follower system flexibility relationship, using equations similar to Eq. (13.83).
3. Combine steps 1 and 2, plot displacement, velocity, and acceleration curves of both the cam and the follower end to check the reasonableness of assumptions. This will give the cam shape to be cut. The reader should remember that a comparison between  $y$  and  $y_c$  must be made after the lever ratio and gear ratio are considered, if they are part of the follower linkage system.

### 13.7.8 Example Using the 3-4-5 Polynomial End Mass Movement

For simplicity we shall solve a polydyne example, using the impractical 3-4-5 polynomial (for the end mass movement) to indicate the method. We know that the cam will have finite values at the end points, requiring a special ramp to meet these values smoothly. Note that for reasonable accuracy, a larger number of significant figures is generally necessary than that shown in the calculations of this problem.

**EXAMPLE** A cam for a high-speed textile machine rotates at 1000 rpm with the follower rising 3/4 in in 60° of cam rotation. The follower linkage spring rate is 25,000 lb/in, and the helical compression spring rate is 400 lb/in. The effective weight of the follower (including the lever) is 5 1/2 lb on the cam and 3 1/2 lb on the follower end. The lever arms are 4 in and 6 in long (Fig. 13.21).

The clearance or backlash in the linkage is negligible. The external load is 100 lb, and the initial spring load is 150 lb. Plot curves of the cam and follower displacement and acceleration. Describe the ramp necessary.

**Solution** The equation for a 3-4-5 polynomial meeting the boundary conditions for this problem is

$$y = .75 - 7.5\left(\frac{\theta}{60}\right)^3 + 11.25\left(\frac{\theta}{60}\right)^4 - 4.5\left(\frac{\theta}{60}\right)^5. \quad (13.89)$$

Differentiating

$$y' = -.375\left(\frac{\theta}{60}\right)^2 + .75\left(\frac{\theta}{60}\right)^3 - .375\left(\frac{\theta}{60}\right)^4 \quad (13.90)$$

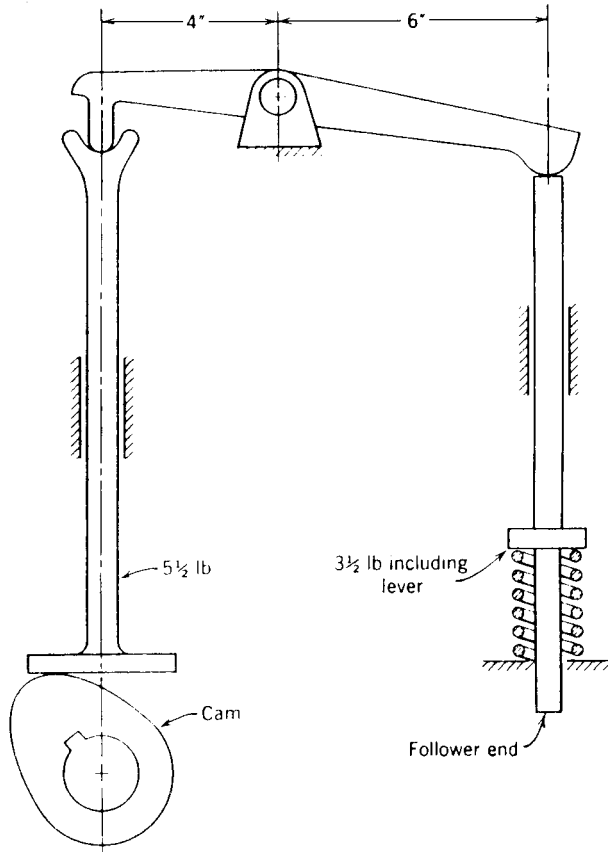


FIGURE 13.21. Textile machine example.

$$y'' = -0.0125\left(\frac{\theta}{60}\right) + .75\left(\frac{\theta}{60}\right)^2 - .025\left(\frac{\theta}{60}\right)^3. \quad (13.91)$$

Now let us find the system characteristics for the cam displacement from Eq. (13.83):

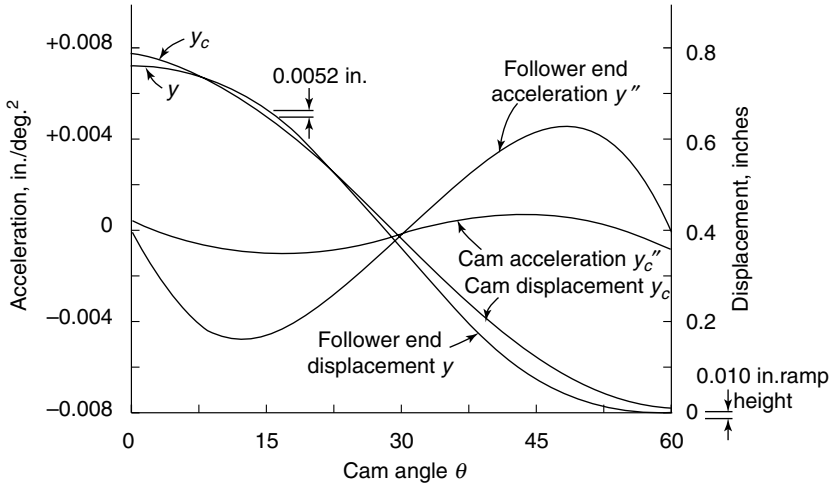
$$y_c = r_a + k_r y + cy''$$

The ramp height

$$r_a = r_k + \frac{S_1 + L}{k_f} = 0.01 \text{ in.}$$

The spring ratio

$$k_r = \frac{k_s + k_f}{k_f} = 1.016.$$



**FIGURE 13.22.** Textile machine polydyne cam example. Follower end displacement of 3-4-5 polynomial.

Assume that the helical spring weighs 0.3 lb. The effective weight

$$w = 5.5 \left( \frac{4}{6} \right)^2 + \frac{0.3}{3} + 3.5 = 6.00 \text{ lb.}$$

Therefore the dynamic constant from Eq. (13.84) is

$$C = 0.093 \frac{w}{k_f} N^2 = 22.2.$$

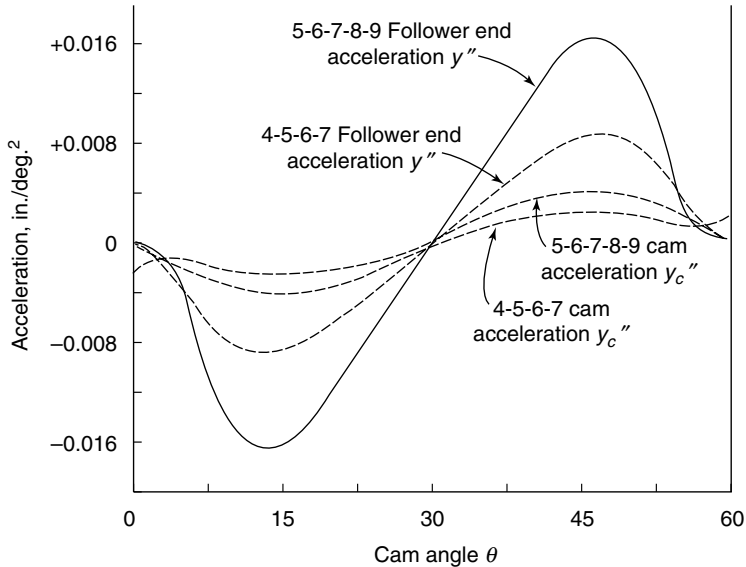
Substituting in Eq. (13.83) gives the cam profile

$$y_c = 0.010 + 1.016y + 22.2y'' \tag{13.92}$$

In Fig. 13.22, we plot the resulting displacement and acceleration curves of both the cam,  $y_c$  and  $y_c''$ , and the follower end,  $y$  and  $y''$ , respectively. The velocity curves are not shown since they are of lesser importance. It should be remembered that all these curves are compared on the same basis; i.e., the actual cam would be reduced by the lever arm ratio of 4 in/6 in or 2/3 scale.

We see that the acceleration curve of the cam  $y_c''$  has smaller values than the acceleration curve of the follower end  $y''$ . This difference is increased as the speed increases. In other words, at a low speed the two curves are practically identical. In addition, we see an infinite jerk at the ends of the cam acceleration curve  $y_c''$ . This suggests another required function of the ramp for this 3-4-5 curve, i.e., to provide velocity and acceleration values dictated by the cam, in addition to taking up the preload (initial displacement) in the system.

In the displacement curve of the follower, we see the desired 3-4-5 curve shape. The displacement of the cam indicates a ramp of 0.010 in at the beginning of the curve. However, a serious shortcoming of this design may be observed. At the 15° point, we find that the cam displacement,  $y_c$  curve, falls below the follower displacement,  $y$  curve, about 0.0052 in. If it were possible, the linkage at this point would be in tension. In other words, the cam would leave the follower. This is alleviated by subjecting the linkage to com-



**FIGURE 13.23.** Comparisons of cam and follower accelerations of the 4-5-6-7 and 5-6-7-8-9 polynomials (textile machine example).

pression at all times. In that event the valve spring force must be increased, a lower speed accepted, or other suitable means utilized. In this problem, we shall use a larger initial spring load  $S_1$  and thus a larger ramp. To recalculate, we have the relationship

$$\frac{S_1 + L}{k_f} = r_s = r_a, \quad \text{since } r_k = 0.$$

Here  $r_a$  will be increased by 0.006 in instead of 0.0052 in for a small margin of safety. Therefore

$$\frac{S_1 + 100}{25000} = 0.010 + 0.006$$

where  $S_1 = 300$  lb, the initial spring load with an initial ramp height of 0.016 in. necessary instead of the ramp height 0.010 in shown in Fig. 13.22.

If we replot this value in Fig. 13.22, the cam curve  $y_c$  will properly be above the follower curve  $y$  at all points and the linkage will always be in contact with the cam.

### 13.79 4-5-6-7 and 5-6-7-8-9 Polynomials

Taking the data of the previous example and using the 4-5-6-7 and 5-6-7-8-9 polynomials, we have the acceleration curves  $y''$  and  $y_c''$  plotted in Fig. 13.23. With the 4-5-6-7 polynomial, we see that any ramp must meet the cam with an acceleration to prevent an infinite pulse at the beginning and end of the action. The 5-6-7-8-9 family shows the best condition, having both cam acceleration and follower end acceleration equal to zero at both ends. In contrast, the ramp for this curve must provide only a rise but no initial velocity or acceleration to the follower. This 5-6-7-8-9 family is thus suggested for most designs.

It may be mentioned that higher orders are possible than 5-6-7-8-9 to control the jerk of the follower motion, but they are not justified in view of the additional effort necessary and fabrication inaccuracies that will exist. Furthermore, the changes in contour are negligible, being in the tens of thousandths of an inch.

### 13.7.10 Ramps or Subcams

In all polydyne cam designs, it is necessary to bring the linkage to its starting point with a smooth curve. This curve, as previously explained, is needed in many high-speed designs to compensate for the change in length due to temperature, wear, and flexibility of the parts. It is also sometimes needed to start the follower motion, to prevent the follower from leaving the cam, and to provide values of velocity and acceleration to the follower. We saw that the 3-4-5 polynomial required a ramp which gave the follower an initial displacement, velocity, and acceleration. We also found that the 4-5-6-7 polynomial needed a ramp for initial displacement and acceleration; the 5-6-7-8-9 polynomial requires only a displacement value from the ramp.

The design of the ramp for polydyne cams is very important. The combination dwell-rise-dwell curves are good choices to fulfill the 3-4-5 and 4-5-6-7 polynomial ramp requirements. The 5-6-7-8-9 polynomial could be provided with a ramp of the dwell-rise-dwell type, i.e., cycloidal or 3-4-5 type. Some of the ramps employed (Chap. 2) are: (1) cycloidal; (2) cubic no. 1; (3) combination curves of parabolic motion followed by constant velocity; (4) combination curves of parabolic motion followed by constant velocity and finished with cubic no. 1.

It may be mentioned that in all examples the end points had zero boundary conditions. If finite end point values are needed to suit the ramp or for another reason, it may be fulfilled by further application of the polynomial equations.

### 13.7.11 DRRD Cams

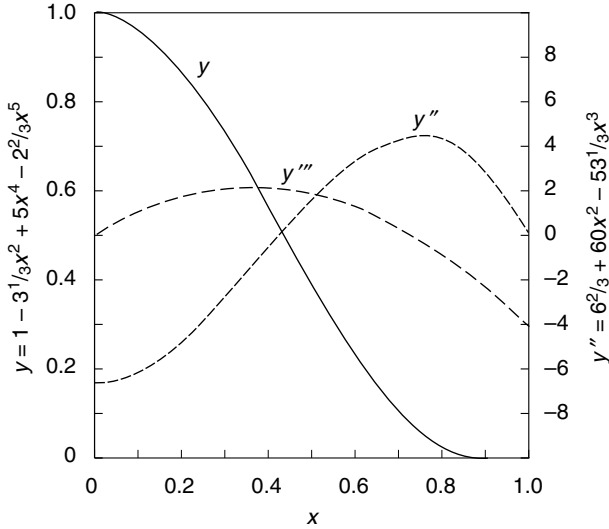
The polydyne method can also be used to design dwell-rise-return-dwell (D-R-R-D) cams. Again, displacement, velocity, and acceleration must be zero at the event terminals, but at the midevent point, velocity should be zero, displacement is 1, and acceleration is unspecified. Or, when  $x = 1$ :  $y = 0$ ,  $y' = 0$ ,  $y'' = 0$ ; when  $x = 0$ :  $y = 1$ ,  $y' = 0$ . Assuming the cam is symmetric the first half-event characteristic will be  $y(-x)$  for the function above. Additionally, if acceleration is to be smoothly continuous across the axis dividing the first and second quadrants, its rate of change must be zero. Therefore, another condition is that when  $x = 0$ ,  $y''' = 0$ . The simplest polynomial satisfying these conditions is

$$y = 1 + C_2x^2 + C_4x^4 + C_5x^5.$$

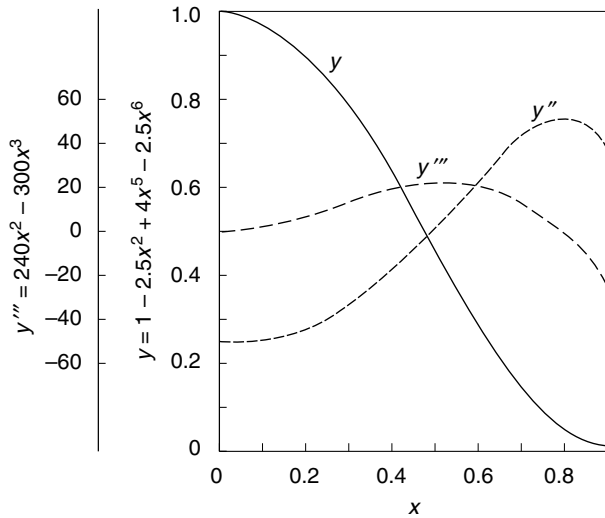
When the coefficients are evaluated, the results are the equations and characteristics of Fig. 13.24. Many alternative equations could also be used. However, the equation must always have an  $x^2$  term but no  $x^3$  term, to preserve the acceleration peak at  $x = 0$ . Another acceptable trial equation is

$$y = 1 + C_2x^2 + C_3x^5 + C_6x^6.$$

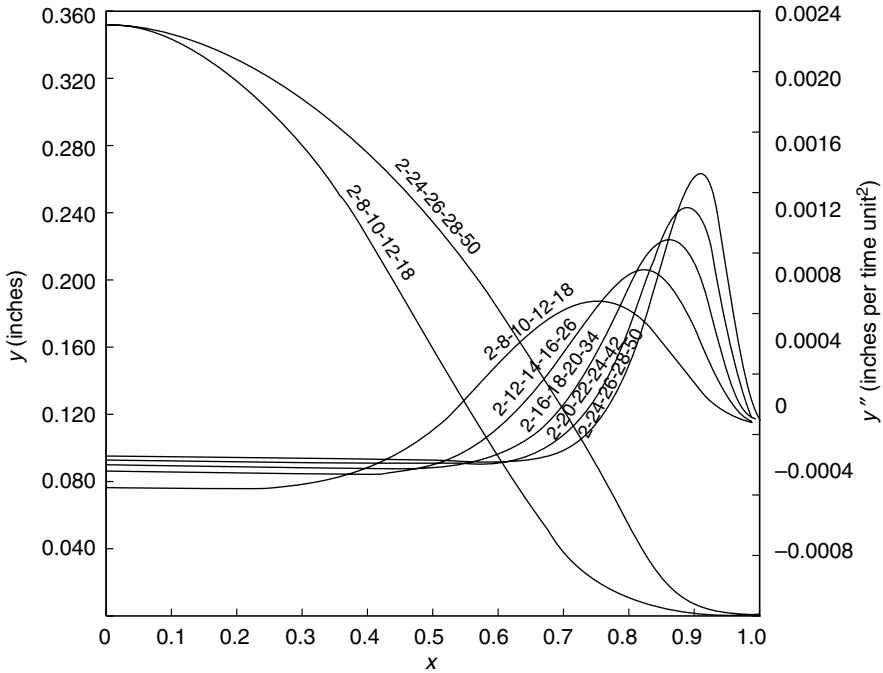
The results are shown in Fig. 13.25. Here, the maximum positive and negative accelerations are about the same, whereas in Fig. 13.24 the negative acceleration peak was significantly larger.



**FIGURE 13.24.** Simplest polynomial for DRRD profiles combining zero acceleration at the start and zero velocity with finite acceleration at juncture of rise and return phases.



**FIGURE 13.25.** Effect of changing 2-4-5 polynomial of Fig. 13.24 to 2-5-6 to obtain near equivalence of maximum positive and negative accelerations.



**FIGURE 13.26.** Effect of progressive power changes upon high-order polynomials of the DRRD type profile.

Figure 13.26 shows several higher-order polynomials applied to D-R-R-D cams. The conditions used here are: when  $x = 0$ ;  $y = 0.35$ ,  $y' = 0$ , and  $y''' = 0$ ; when  $x = 1$ ;  $y = 0$ ,  $y' = 0$ ,  $y'' = 0$ ,  $y''' = 0$ , and  $y^{iv} = 0$ . These curves characterize the type successfully adapted to automotive cams, wherein the positive accelerations are high to maximize the average valve lift and the negative accelerations are low to minimize the required closing spring preload.

### 13.7.12 Practical Vibration Discussion

Theoretically, if we run the polydyne cam-follower system at the designed speed, the action will have no vibrations. Actually, small amplitude vibrations (at the natural frequency of the system) are evident in operation. These may be due to the ramp design, the simplified assumptions, the surface inaccuracies, and the application of the external load. The ramp design may not adequately compensate for vibrations. The assumption was made with the equations that damping should be ignored for easier calculations. In actual practice, damping may go as high as 25 percent of critical damping. The surface of the cam profile may have errors in cutting or from wear. Also, the external load may be applied suddenly in machinery such as dial-feed mechanisms. All these factors affect the follower vibratory amplitudes. If a cam is to run at speeds other than the rated speed, the best approach is to employ one of the analysis methods of Chap. 12. A machine designed by the polydyne method should not be overspeeded since high vibratory amplitudes may be induced for only 10 percent excess of the designed speed.

### 13.7.13 Summary

In this section, we used an automobile and textile cam-follower system as examples. Other machines could be calculated in the same manner. The methods of this chapter represent a dynamic analysis of a high-speed, high-flexibility cam design. Vibrations at the design speed thus approach zero. We also see that any polynomial may be used, but the 5-6-7-8-9 is suggested with a 3-4-5 polynomial or cycloidal ramp. Note that proper ramp design is probably the most critical aspect of the investigation.

Although time-consuming, the justification of this method has been proved in the field. To repeat the design procedure:

1. Select a polynomial

$$y = C_0 + C_1\theta + C_2\theta^2 + C_3\theta^3 + \dots + C_n\theta^n. \quad (13.87)$$

2. Set up a cam-follower system whose characteristic is similar to

$$y_c = r_a + k_r y + c y''. \quad (13.83)$$

3. Substitute values, and plot displacement curves and their derivatives.

Be sure that the compression spring is strong enough and the ramp high enough so that cam-follower constraint is maintained. Also, the maximum cam acceleration should always exceed the maximum follower acceleration; otherwise the system may go out of control because it is too flexible.

Finally, a system with a rigid camshaft and a flexible follower was employed. Sometimes, in cam-driven mechanisms such as turret or dial cams, the camshaft is light in weight having a small inertia or flywheel effect. In addition, the follower linkage stiffness is high compared with that of the drive and support frame. Accordingly it is reasonable to consider the camshaft and frame in the same manner as that shown in deriving the characteristic equations of Eq. (13.83). A flexible torsional system will exist. Tests in the field under actual operating conditions to measure deflection and vibration (under high speeds) will verify the design.

## 13.8 DISCUSSION

---

In cam-follower systems, follower vibrations are always induced. At low speeds, they are rarely a factor for concern, but at high speeds, they can become great enough to significantly degrade system performance. At very high speeds the vibration may be sufficient to destroy the system or at least stop it from functioning.

Vibrations arise from many sources:

1. Vibrations due to the shape of the follower acceleration curve (the main source addressed in this chapter).
2. Vibrations resulting from separation of the cam and the follower. With positive-drive cams with backlash, impact of the roller on the cam is produced as the contact force changes direction. This is called cross-over shock. With spring-loaded followers separation is due to the "jump" condition that occurs when the preload force is insufficient to maintain a positive contact force.
3. Vibrations due to surface irregularities caused by deficiencies in cam and/or follower manufacturing.

4. Vibrations due to variations in the external load. For example, a cam-driven punch indexing mechanism has its load applied suddenly as the punch starts into the work-piece. This quick-load application cannot be eliminated, and, therefore, the ultimate design must account for it.
5. Miscellaneous sources. One of these sources is camshaft unbalance. In this case, intelligent practical design of the cam structure and the body to reduce the offset mass and maximize camshaft stiffness and support will keep this vibration to a minimum. Vibration may be transmitted to the cam surface from the driving mechanism through the frame from such sources as electrical motors, gears, and chains.

Vibrations may be transmitted from an external source through the foundation of a machine base or the body structure of a vehicle to the cam-follower system. For example, the vibration source could be terrain interaction on a ground vehicle or aerodynamic loads on an airplane.

To reduce vibrations in a cam-follower system, all members from the driver to the follower end should be as rigid as possible. The follower should also be as light as possible. Damping devices are rarely practical as a means of reducing vibrations in cam mechanisms.

### 13.8.1 Design Guidelines and Rules of Thumb

Some generally accepted guidelines in designing cam curves for moderate to high-speed operation are:

1. The maximum acceleration values should be kept as low as possible.
2. A continuous jerk function should be maintained, with the peak value preferably not exceeding the maximum for an equivalent cycloidal curve.
3. Modified sine, modified trapezoidal, and cycloidal cam curves are reasonable choices in most cases, usually giving lower peak forces, vibratory amplitudes, noise, stresses, and, in general, smoother performance than other basic curves.

Other cam curves have the same characteristics that make cycloidal curves good. Like cycloidal curves, they provide continuity of all derivatives throughout the lift and their lowest order of discontinuity at each end of the lift curve is at the jerk level or higher. Their peak acceleration is comparable to a cycloidal's and they do not possess unnecessary relative maxima or minima in the jerk characteristic. Other curves such as polynomials, for example, are also good choices.

Most methods for the design of high-speed cam profiles that do not involve a formal optimization procedure rely strongly on rules of thumb such as those above. When a formal design optimization procedure, such as one of those discussed in this chapter, will not be performed, these guidelines are generally good ones to use. The resulting design is likely to be much better than a design obtained without use of any guidelines or formal design procedure, and will be obtained with minimal effort.

However, if an optimization procedure is employed, such as one of those given in this chapter, it will provide a better design than use of these guidelines will. The optimal solution for a high-speed system will often violate guideline 2 to a significant degree; there is a high likelihood of discontinuities in the acceleration, equivalent to infinite jerk, at the ends of the cam curve. This is particularly true when the objective of the optimization is to reduce the dynamic forces on the cam and follower while still maintaining low vibration characteristics over a wide range of operating speeds. Guideline 2 applies most accurately to low-speed systems (where the cam lift duration is very long relative to the system

period of vibration). At the highest speeds where vibration is most critical and where many systems are designed to run, its use will still lead to a reasonably good design, but not an optimal design.

### **13.8.2 Conclusions and Recommendations on the Use of the Methods Given in this Chapter**

All of the methods presented in this chapter use a single degree-of-freedom dynamic model. Such a model is adequate for almost all well-designed systems because their highest significant frequency of excitation at maximum operating speed is usually well below the natural frequency of the model. This is, in turn, well below the second and higher natural frequencies of the real system. Therefore, the dynamic amplification by the upper modes is minimal. The models are also all linear, which is accurate for almost all real systems, although the method of Sec. 13.5 does allow optimization using some nonlinear criteria.

The sections below present a review of the features of each of the methods discussed in Secs. 13.4 through 13.7 and give recommendations on how best to use them. Guidelines for choosing the best method are given and their limitations are detailed.

**13.8.2.1 Cam Synthesis Using Trigonometric Series (Sec. 13.4).** This section presents a good general procedure for designing cam profiles to minimize residual vibration. A major advantage of this method is that the optimization can be done over any contiguous range of operating speeds the user desires. This feature is important because many real systems operate over a range of speeds. Even constant speed systems still must vary in speed for startup and shutdown. Also, there is always uncertainty in the design parameters, particularly stiffness and mass. This uncertainty is equivalent to an uncertainty in speed.

This section also presents a method to optimize a design for one speed (tuned cam). This is never recommended, however, even for constant-speed systems, because of all the factors noted above. For some cams designed for just one speed, even small variations in speed or parameters can cause large variations in vibration. Therefore, optimization should always be done over a wide enough range of speeds to allow for both the operating speed range and parameter uncertainties. It is not necessary to optimize over the range of speeds well below the maximum speed, since the energy input and primary excitation frequencies will be much lower there. However, including this low-end speed range in the optimization will have little effect on the optimal solution anyway, precisely because of its low effect on vibration.

**13.8.2.2 Cam Synthesis Using Optimal Control Theory (Sec. 13.5).** There are two significant features of this procedure for optimizing cam design. The first is that a theoretically exact optimal solution is obtained, subject to only a few constraints; it is not restricted to a user-defined set of basic functions, such as the trigonometric series used in Sec. 13.4. The method constrains the solution by requiring the first four derivatives of the follower lift to be zero at each end of the lift event and does not allow discontinuities in the acceleration at the follower or the cam. These restrictions unnecessarily constrain the solution, not allowing the acceleration discontinuities at the ends of the lift event that were found to be optimal in Sec. 13.4.

The second feature of this procedure is the ability to perform this optimization for nonlinear optimization criteria. This second feature is greatly limited in its usefulness, however, because the nonlinear optimization cannot include cam preload. Preload is important in optimization for stress, for example, due to the highly nonlinear relationship between stress and load.

Another major limitation of this method is that it cannot optimize a design over a range of operating speeds. As stated in Sec. 13.8.2.1, this also limits the usefulness of this method for constant speed systems. Applying the method at the maximum cam speed is likely to provide a good design throughout the speed range. But this should be verified by analyzing the vibration over the operating speed range (or at least over a good portion of the high-speed end of the range).

**13.8.2.3 Cam Synthesis Using the Convolution Operator (Sec. 13.6).** This procedure can be used to find a good cam profile, but it is not a true optimization like that of Secs. 13.4 and 13.5. Those methods are guaranteed to optimize the design (although limited by the choice of trigonometric series in Sec. 13.4). Convolution, on the other hand, only generates a family of curves, one member of which provides the lowest vibration response for any given cam speed. The convolution solution will usually be a good one, but will seldom be the optimal one.

To apply convolution for a system that operates over a range of speeds, determine the optimum curve to use at the maximum speed. The design thus obtained will provide a good response over the entire speed range.

**13.8.2.4 Polydyne Cams (Sec. 13.7).** This technique is limited in that it only optimizes for operation at a single speed. As stated in Sec. 13.8.2.1, this also limits the quality of the optimization even for systems that operate at only a single speed. The chosen polynomial series for the follower lift curve further limits the ability to find an optimal solution.

Techniques have been developed that use polydyne methods to optimize a cam design over a range of speeds, equivalent to the method presented in Sec. 13.4.4, but using polynomials in place of the trigonometric series used there. However, a good design can be obtained in most cases by designing for the maximum system speed and then analyzing at enough other speeds to verify the reasonableness of the result.

One feature of this method is that it makes available a variety of dwell-rise-return-dwell follower lift profiles that provide a wide range of the ratio of positive to negative acceleration. For example, for an engine valve opening profile, the area under the opening curve should be maximized, meaning a high ratio of positive to negative acceleration, within the limitations of vibration and contact stress.

**13.8.2.5 Summary of Conclusions.** Any of the methods above can be used to provide a good to optimal solution to most cam design problems. Each method has its advantages and disadvantages. The method in Sec. 13.4 can provide a near-optimal design over any given range of operating speeds. The method described in Sec. 13.5 only optimizes at one speed at a time and is the most complex to use, but it provides a true optimum, not limited to a linear combination of given trigonometric terms, as in Sec. 13.4. The method in Sec. 13.5 is also the only one that can optimize for nonlinear effects, although the accuracy of nonlinear design is greatly limited by the inability to include preload. The method in Sec. 13.6 does not provide a true optimum, but can usually find a good solution. The method in Sec. 13.7 can provide a good, but not really optimal solution for any case, and it has the advantage over the other methods of providing good control over the shape of the follower lift curve.

From the preceding paragraph and the more detailed information presented previously, the designer should be able to find the best of these methods to use for any particular design problem.

## REFERENCES

- Chen, F.Y., "Assessment of the Dynamic Quality of a Class of Dwell-Rise-Dwell Cams," *Transactions of the ASME, Journal of Mechanical Design*, 103: 793–802, October 1981.
- Chen, F.Y., *Mechanics and Design of Cam Mechanisms*, Pergamon Press, New York, 1982.
- Chew, M., and Chuang C.H., "Designing for Lower Residual Vibrations in High-Speed Cam-Follower Systems Over a Range of Speeds," *Proceedings of the 1990 ASME Design Technical Conferences-21st Biennial Mechanisms Conference, Session M4: CAMS-I*, Chicago, Ill., September 16–19, 1990. DE-Vol. 26: 23–31, 1990.
- Chew, M., Freudenstein, F., and Longman, R.W., "Application of Optimal Control Theory to the Synthesis of High-Speed Cam-Follower Systems. Part 1: Optimality Criterion and Part 2: System Optimization," *Transactions of the ASME, Journal of Mechanisms, Transmissions, and Automation in Design*, Vol. (105): 576–591, September 1983.
- Dudley, W.M., "New Methods in Valve Cam Design," *Transactions of the Society of Automotive Engineers*, 2: 19, January 1948.
- Freudenstein, F., "On the Dynamics of High-Speed Cam Profiles," *International Journal of Mechanical Science*, 1: 342–349, 1960.
- Gupta, K.C., and Wiederrich, J.L., "Development of Cam Profiles Using the Convolution Operator," *Transactions of the ASME, Journal of Mechanisms, Transmissions, and Automation in Design*, 105: 654–657, 1983.
- Hrones, J.A., "Analysis of Dynamic Forces in a Cam-Driven System," *Transactions of the American Society of Mechanical Engineers* (70): 473–482, 1948.
- Hussman, A.W., *Rechnerische Verfahren Zur Harmonischen Analyse und Synthese*, Julius Springer Verlag, Berlin 1938.
- Hussmann, A.W., "Schwingungen in Schraubenförmigen Ventililfedern," *Jahrbuch der Deutschen Luftfahrtschung*, Part 2, pp. 119–133, 1938(b).
- Mitchell, D.B., "Tests on Dynamic Response of Cam-Follower Systems," *Mechanical Engineering*, (72): 467–74, 1950.
- Neklutin, E.N., "Designing Cams for Controlled Inertia and Vibration," *Machine Design*, pp. 154–160, June 1952.
- Neklutin, C.N., "Vibration Analysis of Cams," *Transactions of the Second Conference on Mechanisms*, Penton Publishing Co., Cleveland, 1954.
- Stoddart, D.A., "Polydyne Cam Design," *Machine Design* 25: 121, January 1953; 146, February 1953; 149, March, 1953.
- Wiederrich, J.L., "Residual Vibration Criteria Applied to Multiple Degree of Freedom Cam Followers," *Transactions of the ASME, Journal of Mechanical Design*, October: 702–705, 1981.
- Wiederrich, J.L., Personal Communication, 2001.
- Wiederrich, J.L., and Roth, B., *Dynamic Synthesis of Cams Using Finite Trigonometric Series*, *Transactions of the ASME, Journal of Engineering for Industry*, pp. 287–293, February 1975.
- Wiederrich, J.L., and Roth, B., "Design of Low Vibration Cam Profiles," in Jones, J.R. (ed.) *Cams and Cam Mechanisms*, Mechanical Engineering Publications Ltd. for the Institution of Mechanical Engineers, Suffolk 1978.

*This page intentionally left blank.*

---

# CHAPTER 14

---

## SPECIAL CAM MECHANISMS

---

Harold A. Rothbart, D. Eng.

- 14.1 SLIDING BODIES 454
- 14.2 ROLLING BODIES 456
- 14.3 ROLLING BODIES OF BASIC CONTOURS 457
- 14.4 INVOLUTE CAM 459
- 14.5 ECCENTRIC CIRCLE CAM—TRANSLATING ROLLER FOLLOWER 460
- 14.6 ECCENTRIC CIRCLE CAM—TRANSLATING FLAT-FACED FOLLOWER 463
- 14.7 CONTOUR-SHAPED RADIAL CAMS 464
  - 14.7.1 Special Contour 464
  - 14.7.2 Circular Arc Cams 465
- 14.8 CIRCULAR ARC CAM—TRANSLATING ROLLER FOLLOWER 465
- 14.9 TANGENT CAM—TRANSLATING ROLLER FOLLOWER 466
- 14.10 CIRCULAR ARC CAM—TRANSLATING FLAT-FACED FOLLOWER 467
- 14.11 BALL AND GROOVE CAM 468
- 14.12 SPIRAL CAM CUTTING MECHANISM 468
- 14.13 UNIDIRECTIONAL CAM CLUTCHES 470
- 14.14 TWO INDEPENDENT CAMS IN SERIES (AUTOMOTIVE) 471
- 14.15 QUICK ACTION CAMS 471
- 14.16 VARIABLE-DWELL CAM 472
- 14.17 CAM TO CONVERT LINEAR TO ROTARY MOTION 473
- 14.18 CAM TO CONVERT ROTARY TO LINEAR MOTION 474
- 14.19 TWO-REVOLUTIONS-PER-CYCLE CAMS 474
- 14.20 INCREASED STROKE CAMS 475
- 14.21 ADJUSTABLE STROKE CAMS 475
- 14.22 CONTROLLED TRANSLATING CYCLE CAMS 477
- 14.23 CIRCULAR ARC CAMS—CONSTANT BREADTH FOLLOWER 477
- 14.24 SWASH PLATE CAM 479
- 14.25 VARIABLE-ANGULAR-VELOCITY CAM 480
- 14.26 CAM INTERMITTENT-MOTION MECHANISMS 481
  - 14.26.1 Comparison of Intermittent-Motion Mechanisms 481
  - 14.26.2 Cylindrical Cam for Intermittent Motion 484
  - 14.26.3 Grooved Concave Globoidal Cam for Intermittent Motion 486
  - 14.26.4 Spider Cam for Intermittent Motion 487
  - 14.26.5 Multiple Double-End Cam for Intermittent Motion 488
  - 14.26.6 Star-Wheel Cam for Intermittent Motion 489
- 14.27 CAM-MODULATED MECHANISMS 489
  - 14.27.1 Cam-Modulated Stamping Mechanism 489
  - 14.27.2 Cam-Modulated Worm and Worm Gear 490
  - 14.27.3 Cam-Modulated Epicyclic Gears and Moving Cam (Type 1) 492
  - 14.27.4 Cam-Modulated Epicyclic Gearing and Moving Cam (Type 2) 492
  - 14.27.5 Cam-Modulated Epicyclic Gearing and Fixed Cam 492
  - 14.27.6 Cam-Modulated Noncircular Gears 493
- 14.28 CAM COMPUTING MECHANISMS 494
  - 14.28.1 Cam Types 495
  - 14.28.2 Archimedes Spiral Gear Cam 497
  - 14.28.3 Basic Spiral Cam (Nonlinear) 498
  - 14.28.4 Basic Spiral Cam Constants 501

---

### SYMBOLS

---

- $c_e = p_o + p_i$  = distance between centers of rotation, in
- $C$  = a constant
- $D$  = effective diameter of rollers, in
- $E$  = distance from cam center to circular arc center of curvature, in
- $h = 2E$  = maximum displacement of follower, in
- $K_i, K_0$  = constants
- $M$  = equivalent mechanism connecting rod length, in
- $r$  = instantaneous radial distance from center of cam, in

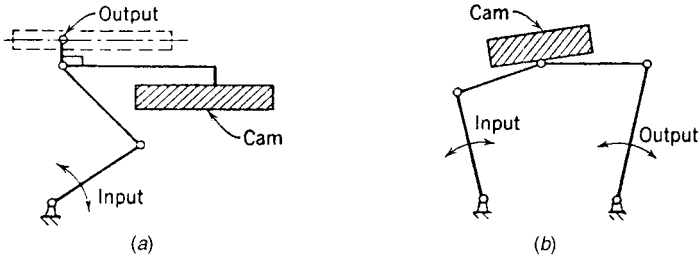


FIGURE 14.1. Cam-modulated linkages.

$R_f$  = roller-follower radius, in

$R_w$  = mean radius of pin wheel, in

$T$  = torque transmitted, tangent to the bodies, 16/in<sup>2</sup>

$V_{P/Q}$  = velocity of contact point  $P$  on body  $B$  with respect to the ground  $A$  in the tangent direction, in/sec

$V_{P/A}$  = velocity of contact point  $P$  on body  $C$  with respect to the ground  $A$ , in/sec

$x, x_1, x_2$  = input cam angular rotation, rad

$y$  = follower displacement, in

$y_\varepsilon$  = equivalent mechanism follower displacement measured from crank-end dead center, in

$Y$  = output follower angular rotation, rad

$\alpha$  = angle between tangents to cam contour

$\varepsilon$  = crank angle rotation (equivalent mechanism) for displacement  $y_\varepsilon$ , rad

$\phi$  = angle  $\tan^{-1} \mu$

$\mu$  = coefficient of friction, in

$\theta_0$  = angle rotated by the output driven member, deg

$\theta$  = cam angle rotation for displacement  $y$ , rad

$\theta_i$  = cam angle to a point on straight-side flank, deg

$\theta_i$  = the angle rotated by input driver, deg

$\rho_i$  = radius to point of contact at angle  $\theta$ , in

$\rho_0$  = radius to point of contact at angle  $\theta_0$ , in

$\tau$  = angle between connecting rod and follower motion, deg

$\omega$  = cam and equivalent mechanism angular velocity, rad/sec

In this chapter we discuss some selected special cams and their applications to various kinds of mechanisms and machinery. Mathematical theories are minimized to emphasize the practical and inventive aspect of cams as versatile design components.

The cams shown are from the simplest mechanism, the wedge, to elaborate cam-modulated systems where the follower is located remotely from the basic cam system. (Figure 14.1 is a schematic drawing of a cam-modulated linkage mechanism used in the chemical field for measurement.) Summaries of practical cam mechanisms are given by Freudenstein and Sandor (1996), Grodzinski (1947), and Jones (1967).

## 14.1 SLIDING BODIES

The action between two contacting bodies may be pure rolling, sliding, or a combination of both rolling and sliding. Rolling surfaces are a special case of cam and follower action.

The relative tangential velocity between two bodies with  $P$  and  $Q$ , the points in contact, is

$$V_{P/Q} = V_{P/A} - V_{Q/A} \tag{14.1}$$

where  $V_{P/A}$  = velocity of contact point  $P$  on body  $B$  with respect to the ground  $A$   
 $V_{Q/A}$  = velocity of contact point  $Q$  on body  $C$  with respect to the ground  $A$

Thus, given the velocity of one body at any instant, we can find the velocity of the contacting body and the relative sliding velocity given the cam-follower characteristics.

**EXAMPLE** We are given the cam and follower of Fig. 14.2 to scale. At the position shown, find the instantaneous angular velocity of the follower if the cam rotates at 500 rpm.

**Solution** In Fig. 14.2, draw the normal and tangent lines at the point of contact. The absolute velocity of point  $P$  on cam  $B$ ,

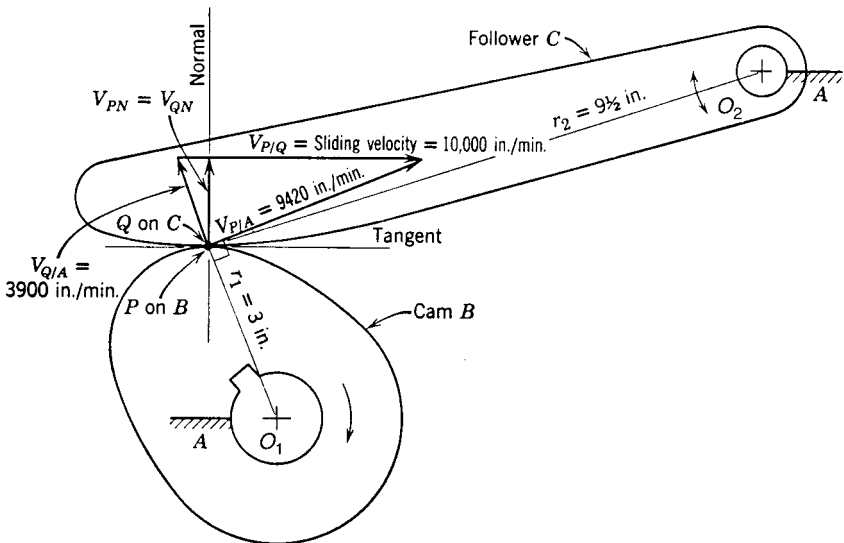
$$V_{P/A} = r_1 \omega_B = 3 \times 500 \times 2\pi = 9420 \text{ in./min}$$

Vectorially this gives the absolute velocity of point  $Q$  on follower  $C$  equal to 3900 in./min. Note that the instantaneous sliding velocity of the contacting bodies

$$V_{P/Q} = 10,000 \text{ in./min}$$

Last, we can find the instantaneous angular velocity of follower  $C$

$$\omega_c = \frac{V_{Q/A}}{r_2} = \frac{3900}{9\frac{1}{2} \times 2\pi} = 65.3 \text{ rpm.}$$



**FIGURE 14.2.** Example of sliding bodies: space scale  $\frac{5}{16}$  in = 1 in; velocity scale, 1 in = 8000 in./min.

## 14.2 ROLLING BODIES

Let us now define the term *pure rolling* as the action on a surface in which the points on the first body consecutively contact only one corresponding point on the second body; see Fig 14.3. If every point on the first body comes in contact with the same point on the second body, we have pure sliding. In Fig. 14.3, for pure rolling to occur between contacting bodies  $B$  and  $C$ , the arc  $QW$  must equal the arc  $PX$  if  $W$  meets  $X$  during the action. Also from Eq. (14.1) and Fig. 14.2 for pure rolling  $V_{P/Q} = 0$ ,  $V_{P/A}$  and  $V_{P/Q}$  are colinear and the point of contact  $PQ$  is on the line of centers  $O_1O_2$  at times.

By constructing an approximation, let us find the contour of the body  $B$  having pure rolling action with given body  $C$ . Body  $C$  drives clockwise with the initial contact  $Q$  on the line of centers. Both bodies turn through a small angle. The steps for construction are as follows:

1. To find point  $a'$  on body  $B$  corresponding to point  $a$  on body  $C$ , swing arc  $0_1a$  to line of centers, giving point  $R$ .
2. With radius  $0_2R$ , draw arc  $RS$ .
3. Since arc length  $Pa'$  is equal to arc length  $Qa$ , use chord  $Qa$  as a compass distance and draw an arc from  $P$  intersecting arc  $RS$ , giving point  $a'$ .
4. Find  $b'$  on  $C$  which contacts  $b$  on  $B$  as in steps (a) and (b). Obtain  $U$  on the line of centers by swinging arc  $0_1b$  and draw arc  $UV$  of radius  $0_2U$ .
5. Arc  $ab$  equals arc  $a'b'$ . Use chord  $ab$  as a compass distance to draw arc  $a'b'$  from  $a'$ , intersecting arc  $UV$  and giving point  $b'$ .
6. Repeat to find other points.

Note that, if body  $B$  were driven in translation, we would have  $RS$  and  $UV$  as lines perpendicular to  $0_10_2$  since arcs  $RS$  and  $UV$  would have infinite radii.

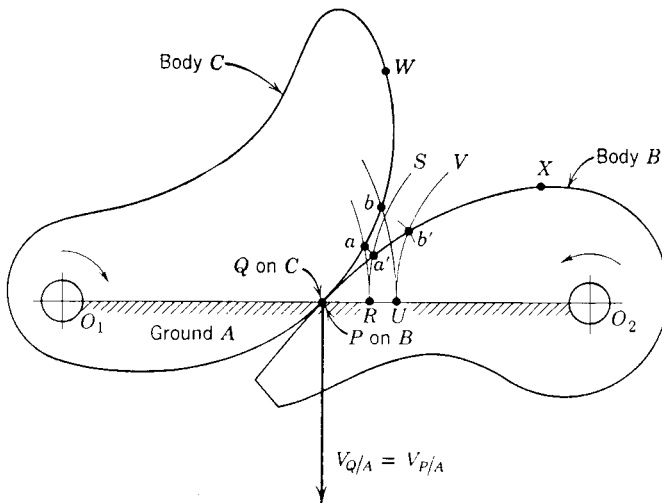


FIGURE 14.3. Pure rolling between bodies in contact.

It may be observed that engaging gear teeth do not have rolling action except where the point of contact is on the line of centers.

### 14.3 ROLLING BODIES OF BASIC CONTOURS

Pure rolling action between bodies occurs with basic contours (special cams) such as logarithmic spirals, ellipses, parabolas, and hyperbolas (see App. A). Appendix A also includes the involute and Archimedes spiral curves. Note the Archimedes spiral curve is the straight line curve in Chap. 2. The proposition for pure rolling action of curves is

- Centers of oscillation should be located at the foci of the curves.
- Lengths of the arc of action of the contacting bodies must be equal.
- Point of contact must be on the line of centers.

Figure 14.4 shows these rolling bodies in contact at point  $Q$ , and having foci  $F_1$  and  $F_2$ . The center oscillation may be at either of the foci, if two are available for each curve. We see that the ellipse is the only curve that is closed and therefore the only one that will give continuous action. All other curves in contact will have limited action, i.e., oscillation. However, sectors of logarithmic spirals may be combined to give continuous rolling action. These bodies are called lobe wheels.

*Logarithmic spirals* of equal obliquity, Figs. 14.4a and 14.4b, are shown in contact at point  $Q$ , pivoting around their foci. In Fig. 14.4a we see the bodies rotating in opposite directions, whereas in Fig. 14.4b rotation is in the same direction. The latter is obviously a more compact mechanism.

A *logarithmic spiral and translating straight-sided follower* is shown in Fig. 14.4c. It can be shown that with pure rolling the contacting curve of the straight-sided follower is a logarithmic spiral oscillating about its focus. This is so because of the inherent quality of the logarithmic spiral, i.e., a tangent at all points makes a constant pressure angle with a radial line.

A *pair of equal ellipses*, Fig. 14.4d, has pure rolling action which may occur for complete rotation of both bodies. For oscillation, sectors of ellipses are feasible.

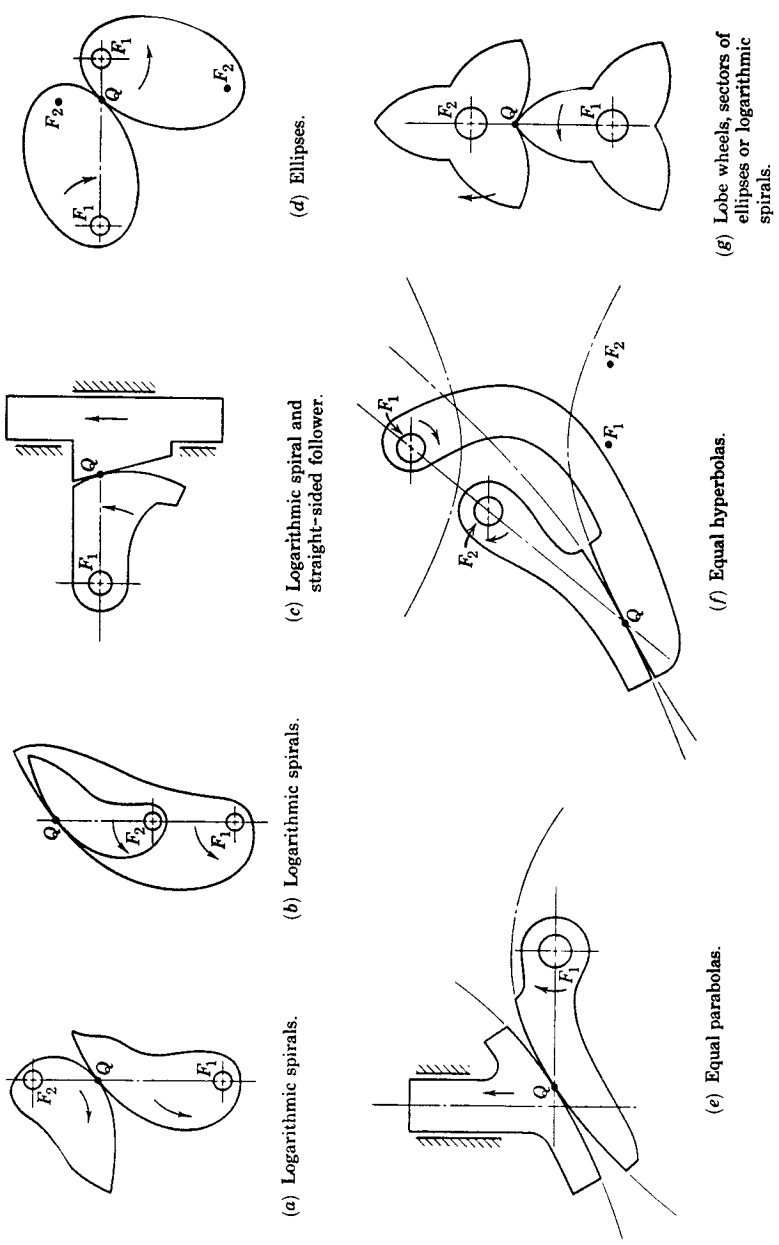
A *pair of equal parabolas* is shown in Fig. 14.4e. One parabola is oscillating about its axis. The other parabolic body is translating, having the same shape as the first. The point of contact  $Q$  is on a line through the center of oscillation perpendicular to the axis of the translating body.

A *pair of equal hyperbolas*, Fig. 14.4f, may be utilized for pure rolling action if they are properly located relative to each other. Note the location of the foci with respect to the hyperbolas' curves. Hyperbolas are an excellent choice where space is at a premium.

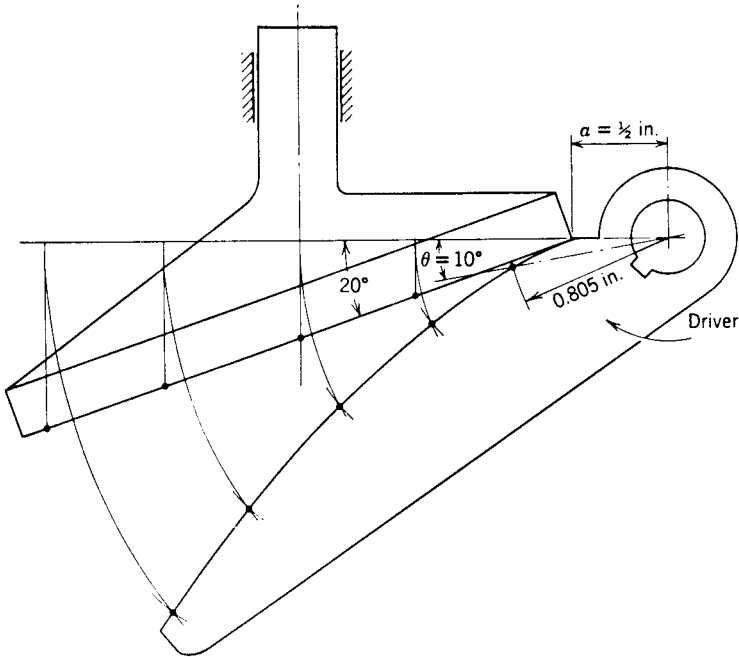
One of the shortcomings of logarithmic spirals is that complete rotation is not possible. Figure 14.4g shows a lobe wheel made up of sectors of logarithmic spirals or ellipses which will roll with continuous action. Although a trilobes area is shown, any number of lobes may be employed.

**EXAMPLE** We are given a toe-and-wiper cam mechanism having a straight-sided translating follower at an acute angle of  $20^\circ$  (Fig. 15.5). By mathematical and graphical means, plot the contour of the driver having pure rolling action. Note: the contour is a logarithmic spiral, since the tangent to the curve is at a constant angle.

**Solution** In App. A, we have the equation for the logarithmic contour



**FIGURE 14.4.** Pure rolling action of basic curves.



**FIGURE 14.5.** Example of logarithmic spiral with pure rolling action, full scale.

$$r = ae^{b\theta}.$$

Let us find a point on the contour where  $\theta = 10$  degrees. Substituting in the above

$$\begin{aligned} r &= \frac{1}{2} e^{\left(\frac{1}{\tan 20}\right) \left(\frac{10\pi}{180}\right)} \\ &= 0.805 \text{ in shown.} \end{aligned}$$

The construction method is shown for the other points on the contour; it is self-explanatory. We see that the smaller the follower face angle, the larger is the size of the logarithmic cam toe necessary for the same follower displacement.

#### 14.4 INVOLUTE CAM

The involute curve (Shaw, 1933) is generated by a string end unwinding from a fixed circle called the involute base circle. This is not the same as the cam base circle previously defined. The involute curve when chosen for a cam has certain interesting characteristics. It can be shown that the involute curve is almost identical to the straight-line (Archimedes spiral) curve. Therefore, for a close approximation, the reader is referred to Chap. 2 which discusses the straight-line displacement curve.

A frequent application of the wiper cam uses an involute curve giving intermittent action to a flat-faced follower (Fig. 14.6). A cam having two or more involute lobes, called

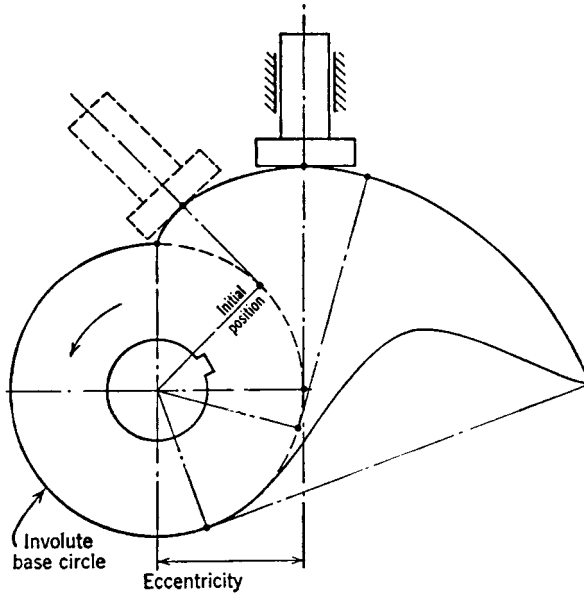


FIGURE 14.6. Involute cam (single lobe for stamp mill).

a stamp mill cam, has been employed for pulverizing crushed ore. The inherent action is that the point of contact always occurs at the same place on the follower face. Thus, this face may be made as small as possible within practical limits. Also, if we locate the point of contact on the line of follower motion, the force components are ideal because the moments tending to bend the follower stem are minimum. Other curves require large overhangs or moments that continuously change with cam rotation.

### 14.5 ECCENTRIC CIRCLE CAM—TRANSLATING ROLLER FOLLOWER

Now let us use the eccentric circle cam with a translating roller follower. In Fig. 14.7a we see an eccentric rotating about its center  $A$ , offset by a distance  $E$ . Figure 14.7b shows the equivalent mechanism, the slider crank chain. The crank radius  $E$  is distance  $AB$ , and the connecting rod length  $M$  is distance  $BC$ . Since these distances are constant, the equivalent mechanism has constant proportions for the complete action of the eccentric circle cam. Let us now derive the characteristics of this cam action. Let

- $y_\epsilon$  = equivalent mechanism follower displacement measured from crank-end dead center position, in
- $M$  = equivalent mechanism connecting rod length, in
- $R_f$  = roller follower radius, in
- $\tau$  = angle between connecting rod and follower motion, deg

In this example,  $y = y_\epsilon$  and  $\theta = \epsilon$ .

From Fig 14.7b we see the displacement of slider  $C$

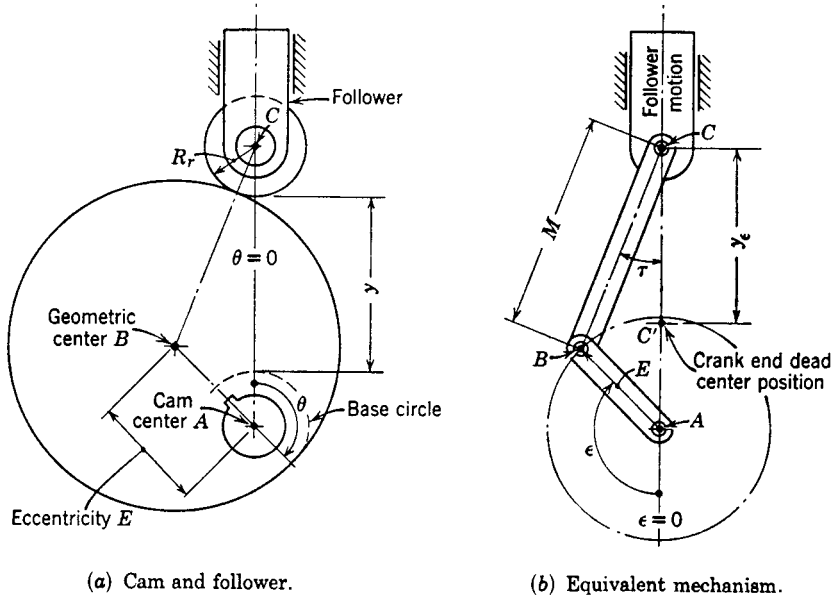


FIGURE 14.7. Eccentric circle cam—translating roller follower.

$$y_e = E - E \cos \epsilon + M \cos \tau \cos \tau - M. \tag{14.2}$$

Differentiating gives velocity

$$v = E\omega \sin \epsilon - M \sin \tau \frac{d\tau}{dt}. \tag{14.3}$$

Inspection of the figure shows the angular relationship

$$\sin \tau = \frac{E}{M} = \sin \epsilon. \tag{14.4}$$

Differentiating and solving yield

$$\frac{d\tau}{dt} = \frac{E\omega \cos \epsilon}{M \cos \tau}. \tag{14.5}$$

Substituting Eq. 14.5 in Eq. (14.3) gives the follower velocity, and differentiating to find the acceleration we have,

$$r = E\omega(\sin \epsilon - \cos \epsilon \tan \tau) \tag{14.6}$$

$$\ddot{y} = E\omega^2 \left( \cos \epsilon - \frac{E \cos^2 \epsilon}{M \cos^3 \tau} + \sin \epsilon \tan \tau \right). \tag{14.7}$$

Equations (14.2), (14.6), and (14.7) provide the characteristics of the complete follower motion. In addition, we observe that angle  $\tau$  always equals the pressure angle

of the cam-follower mechanism. Since we are concerned with the maximum pressure angle

$$\tan \alpha_m = \tan \tau_m = \frac{E}{M}. \quad (14.8)$$

**EXAMPLE** An eccentric circle cam drives a translating roller follower. This circle has an eccentricity of 0.500 in. and a diameter of 2.500 in. and rotates at 180 rpm. The roller follower has a diameter of 0.750 in. Find (1) the characteristics of the follower motion after the cam has rotated  $30^\circ$  from its lowest position and (2) the maximum pressure angle.

**Solution** The equivalent mechanism has a crank length  $E$  equal to 0.500 in. The connecting rod length equals the eccentric circle radius plus the roller radius, giving

$$M = 1.250 + 0.375 = 1.625 \text{ in.}$$

The cam angular velocity

$$\omega = 180 \times \frac{2\pi}{60} = 18.85 \text{ rad/sec.}$$

From Eq. (14.4)

$$\begin{aligned} \sin \tau &= \frac{E}{M} \sin \varepsilon \\ \tau &= \sin^{-1} \left( \frac{0.500}{1.625} \sin 30 \right) = 8.85^\circ. \end{aligned}$$

The displacement from Eq. (14.2)

$$\begin{aligned} y &= E - E \cos \varepsilon + M \cos \tau - M \\ &= 0.500 - 1.625 - 0.500 \cos 30 + 1.625 \cos 8.85 \\ &= 0.0475 \text{ in.} \end{aligned}$$

The velocity from Eq. (14.6)

$$\begin{aligned} \dot{y} &= E\omega(\sin \varepsilon - \cos \varepsilon \tan \tau) \\ &= (0.500)(18.85)(\sin 30 - \cos 30 \tan 8.85) \\ &= 3.44 \text{ lb/in}^2. \end{aligned}$$

The acceleration, Eq. (14.7)

$$\begin{aligned} \ddot{y} &= E\omega^2 \left( \cos \varepsilon - \frac{E \cos^2 \varepsilon}{M \cos^3 \tau} + \sin \varepsilon \tan \tau \right) \\ &= (0.500)(18.85)^2 \left( \cos 30 - \frac{0.500 \cos^2 30}{1.625 \cos^3 8.85} + \sin 30 \tan 8.85 \right) \\ &= 125.2 \text{ in/sec}^2. \end{aligned}$$

The maximum pressure angle from Eq. (14.8)

$$\tau_m = \tan^{-1} \frac{E}{M} = \tan^{-1} \frac{0.500}{1.625} = 17.1 \text{ deg.}$$

### 14.6 ECCENTRIC CIRCLE CAM—TRANSLATING FLAT-FACED FOLLOWER

The eccentric is a type of cam. It is a circular member having its center of rotation offset from its geometric center. The follower may be flat-faced or roller type. A translating flat-faced follower will be discussed. The eccentric represents the simplest cam mechanism possible. Its zero pressure angle eliminates the problem of the follower jamming.

In Fig. 14.8*a* we see an eccentric rotating about point *A* with its geometric center at a distance *E*. In Fig. 14.8*b* we see the equivalent mechanism which is the Scotch yoke mechanism in which the follower movement is a simple harmonic function. Let

$y$  = follower displacement, in

$y_e$  = equivalent mechanism follower displacement, in

$\theta$  = cam angle of rotation for displacement  $y$ , rad

$\epsilon$  = crank angle of rotation (equivalent mechanism) for displacement  $y_e = \text{rad}$

$E$  = distance from cam center to circular-arc center of curvature, in

$h = 2E$  = maximum displacement of follower, in

$\omega$  = cam and equivalent mechanism angular velocity, rad/sec

In this example,  $y = y_e$  and  $\theta = \epsilon$ . From Fig. 14.8*b* we see that the follower displacement

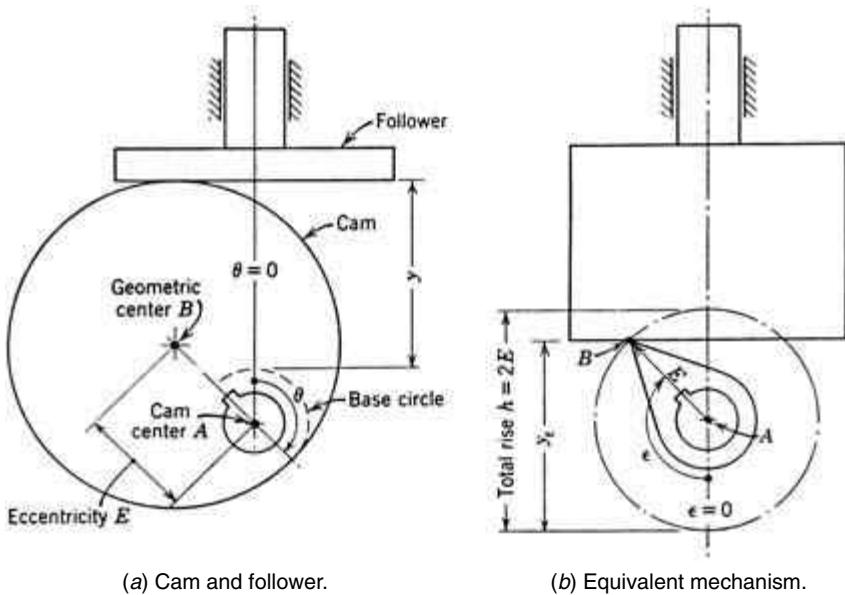


FIGURE 14.8. Eccentric circle cam—translating flat-faced follower.

$$y_e = E(1 - \cos \epsilon) \text{ in.} \quad (14.9)$$

Differentiating, we find the velocity and acceleration

$$\dot{y} = E\omega \sin \epsilon \text{ ips} \quad (14.10)$$

$$\ddot{y} = E\omega^2 \cos \epsilon \text{ in/sec}^2. \quad (14.11)$$

We see that the eccentric circle size has no effect on the follower action; only the eccentricity,  $E$  does. Furthermore, offsetting the line of follower motion from the cam center of rotation does not change the follower movement.

## 14.7 CONTOUR-SHAPED RADIAL CAMS

For the radial cams developed elsewhere in this book the desired displacement characteristics are initially established and then the shape of the cam is mathematically determined. The analysis of the shape also includes the study of the geometric pressure angle and curvature of the cam. Then the cam-follower dynamics are investigated if necessary.

In this section, we will establish the cam contours from known geometric shapes (sometimes blended with other shapes) with limited control of the cam-follower system dynamics. These shapes are rarely utilized in design. In producing a radial cam we can apply any curve or combination of curves such as straight lines, circular arcs, Archimedes spirals, involute, logarithmic spirals, ellipses, parabolas, and hyperbolas. As cam-follower mechanisms the curves can be utilized as partial or complete rotating bodies in contact with the follower.

### 14.7.1 Special Contour

In Fig. 14.9 we see some combinations of curves that have been used in cam mechanisms. A circular arc (dwell) and a circular arc nose have sometimes been combined with the

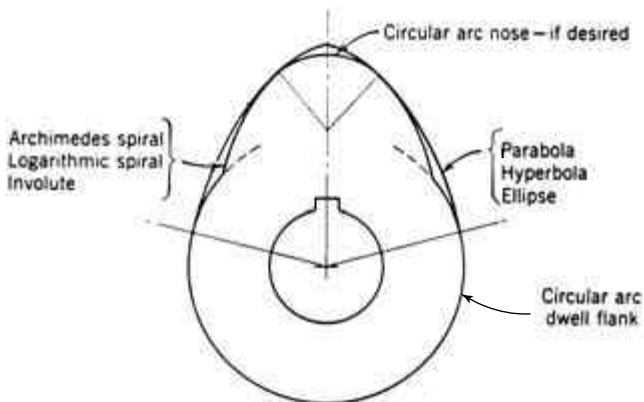
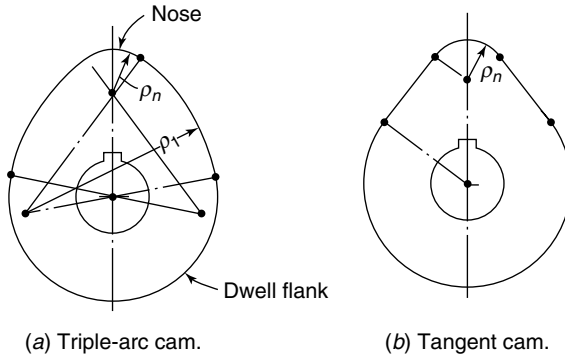


FIGURE 14.9. Radial cam composed of contour combinations.



(a) Triple-arc cam. (b) Tangent cam.

FIGURE 14.10. Circular arc cams.

other aforementioned curves. This blending of curves is not acceptable for high-speed action, since the dynamic characteristics are poor due to the discontinuities in either the velocity or the acceleration of the follower. Note that the least complex conics applied to cams such as ellipses, parabolas, and hyperbolas have a continuous evolute, i.e., continuous locus of the center of curvature, to give the acceleration curve continuity. This ensures more acceptable high-speed characteristics.

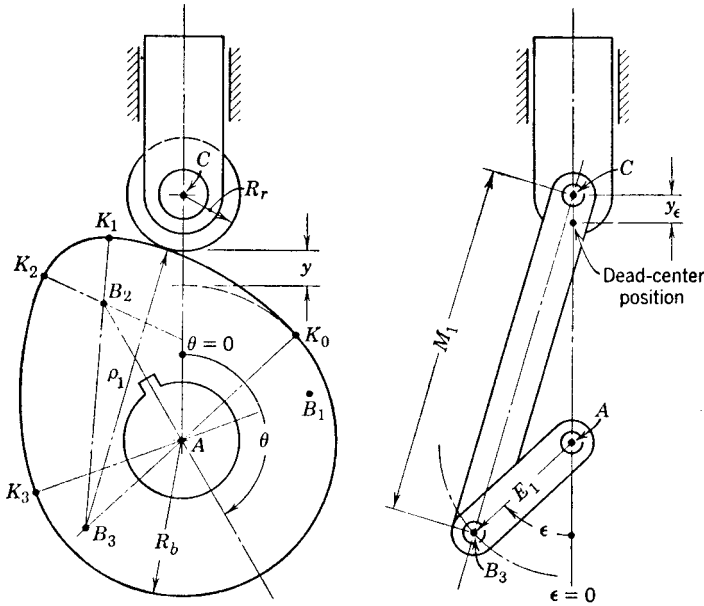
However, discontinuities in evolute and acceleration curves exist when blended with circular noses and flanks. In addition, the Archimedes spiral, logarithmic spiral, and involute start with an impractical, abrupt slope in which a “bump” occurs with a discontinuity in the velocity of the follower. Blending curves have been employed to correct this theoretical infinite acceleration. In the past, “triple curve cams” having a circular arc nose, involute flanks, and a harmonic or parabolic blend into the base circle were popular in the automotive field. Note that the logarithmic spiral has inherent qualities that make it desirable for all sorts of bodies in contact. Applied to the cam form of Fig. 14.9 it provides the smallest radial cam for a given pressure angle. Moreover, the maximum pressure angle is constant during the action.

### 14.7.2 Circular Arc Cams

In the past, the cams were of a combination of circular arcs with or without tangent straight lines. Even now, some designers utilize these cams regardless of their poor dynamic properties. In Fig. 14.10a, we see the blending of a circular arc cam having three different sized circles with  $\rho$  the radius of curvature for the circles. In Fig. 14.10b the circles are blended with straight lines (tangent cam). All cams may provide motion to roller followers or convex curved-faced followers.

## 14.8 CIRCULAR ARC CAM—TRANSLATING ROLLER FOLLOWER

In Fig. 14.11, we see a typical circular cam composed of arcs having centers at  $A$ ,  $B_1$ ,  $B_2$  and  $B_3$ . Figures 14.11a and 14.11b show the cam follower in contact over the flank arc and its equivalent slider crank mechanism. This equivalent mechanism has a crank, radius



(a) Flank action.  
 Note:  $\theta \neq \epsilon$   
 and  $y = y_\epsilon$ .

FIGURE 14.11. Circular arc cam—translating roller follower.

$E_1$  equal to distance  $AB_3$  and a connecting rod length  $M_1$  equal to  $B_3C$ . Equations (14.2), (14.6), and (14.7) can be used to give the follower action.

### 14.9 TANGENT CAM—TRANSLATING ROLLER FOLLOWER

This cam is often called a tangent cam because it consists of straight lines drawn tangent to circular arcs. On the cam in Fig. 14.12, we see straight sides for portions  $K_0K_1$  and  $K_2K_3$ . Nose arc  $K_1K_2$  is a circle with center at  $B_2$  and arc  $K_0K_3$  is the dwell base circle radius  $R_b$ . The previous results of Sec. 14.7 apply for the circular arc portions of the cam. However, additional equations are needed for the straight-side portions  $K_0K_1$  and  $K_2K_3$ . Let

$$\theta = \text{cam angle to a point on straight-side flank, deg.}$$

It can be shown that the follower displacement on straight sided range  $K_0K_1$  and  $K_2K_3$

$$y = (R_b + R_r)(\sec \theta - 1) \text{ in.} \tag{14.12}$$

Differentiating gives velocity and acceleration

$$v = (R_b + R_r)\omega \sec \theta \tan \theta \text{ ips} \tag{14.13}$$



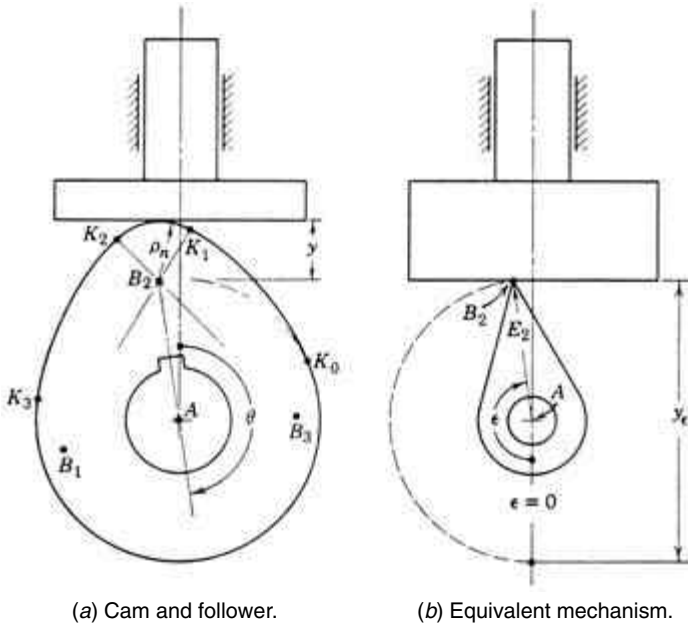


FIGURE 14.13. Circular arc cam—translating flat-faced follower (nose action).

mechanisms for each arc of contact  $K_0K_1$  and  $K_1K_2$ . For example, in contact on nose arc  $K_1K_2$  Fig. 14.13a, the center of curvature  $B_2$  gives an equivalent mechanism having a crank length  $E_2$ . Section 14.7 indicates the method for finding the cam proportions, and Eqs. (14.9), (14.10), and (14.11) should be employed to determine the follower characteristics.

### 14.11 BALL AND GROOVE CAM

Figure 14.14 shows a ball and groove follower cam mechanism that is used in a lightly loaded mechanism such as a sewing machine at speeds from 2000 to 3000 rpm. The cam groove  $C$  is a closed track cam utilizing a ball follower. A round arm  $A$  has a sliding fit in the hole of the ball and is fastened to shaft  $D$ , which is the output shaft. The ball follower runs in the groove of the closed track follower, imparting oscillating motion to output member  $A$  and shaft  $D$ . This cam follower mechanism is easy to fabricate.

### 14.12 SPIRAL CAM CUTTING MECHANISM

Many hand tools provide mechanical advantage. Examples are pliers, scissors, car jacks, and bolt cutters. They all have a design restriction in that the amount of leverage is dependent on the length of the handles. A spiral cam can be a proper choice to provide the nec-

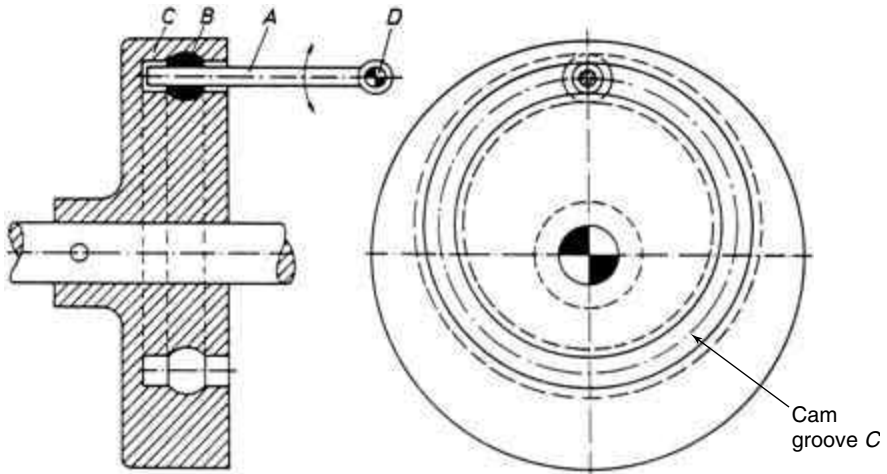


FIGURE 14.14. Ball and groove cam.

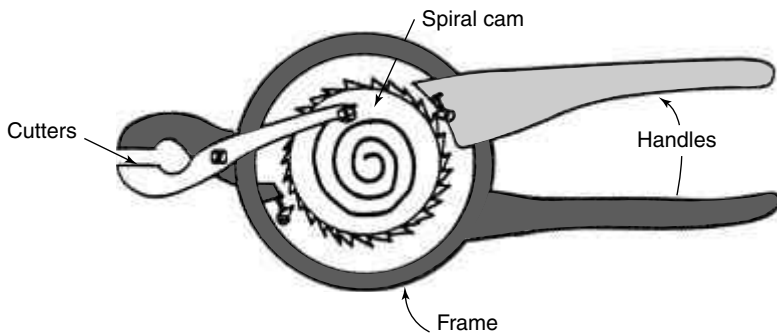


FIGURE 14.15. Spiral-cam cutting mechanism (ratchet driven).

essary mechanical advantage in which a small force rotates the cam a large distance to provide a much larger force. Figure 14.15 shows a schematic of a spiral-cam cutting mechanism doubled with a ratchet system, which is designed for three revolutions of the spiral. The frame of the tool consists of one edge of the cutting tool and one handle. Near the center of the tool, the spiral cam is ratcheted to the frame. The second handle is in turn ratcheted to this. Above the spiral cam is a pin joint to which the other cutting edge is fastened. This cutting tool is guided by a follower in the cam track.

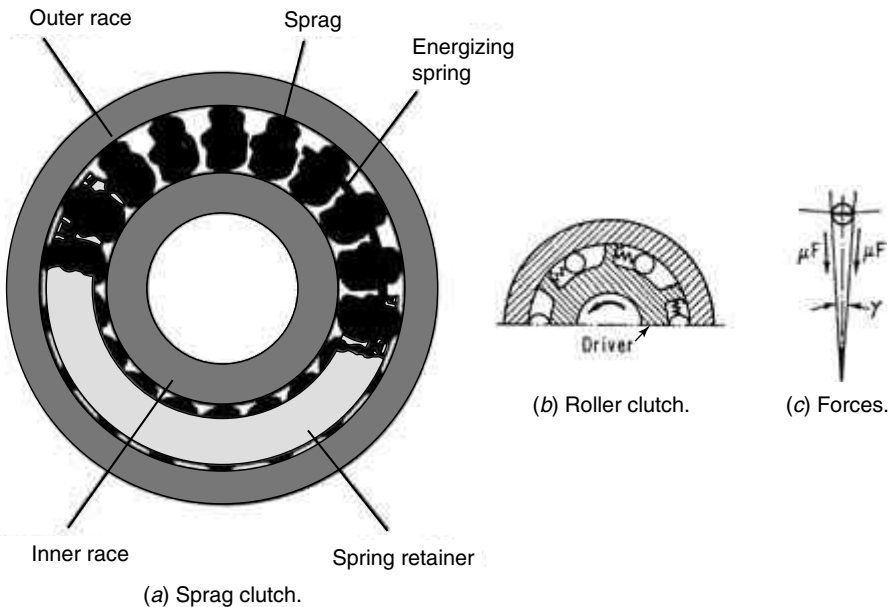
A force analysis of the cam provides interesting mechanical advantage characteristics. Simple lever devices can be modified with spiral cams of various shapes to enhance the operating characteristics of the tool. It can be shown that for a simple wire cutting device, mechanical advantage values of 300 for small hand tools can be produced. In addition to hand tools a spiral cam can lend itself to more elaborate devices such as jacks, positioners, and crimpers.

**14.13 UNIDIRECTIONAL CAM CLUTCHES**

Freewheeling or overrunning clutches are employed when torque must be transmitted in one direction only or where the driven member is to be permitted to “overrun” the driver. They can be considered simple and inexpensive substitutes for a differential drive and also be used in multiple-speed drives where they automatically disengage the lower-speed unit when the higher-speed unit is engaged. When one of the members of the overrunning clutch is fixed, the other member can rotate in only one direction and the clutch becomes “backstopping.”

The most common designs utilize the cam wedging principle. Figure 14.16a shows a commercially available “sprag” clutch, which has an inner and outer race like a ball bearing. It utilizes hardened, specially shaped wedge cam bodies called sprags to lock or free the movement. A similar result is obtained with balls or rollers in wedge-shaped chambers (having designed wedge angles of inclination) in one of the races called a roller clutch. Figure 14.16b is an application of the clutch principle in the rear wheel of a bicycle when the wheel speed exceeds that of the drive. The construction consists of a shell-shaped outer member and an inner member with wedge-shaped pockets, or flat cam profiles, around its periphery; the coupling between the two members is provided by the locking action of the rollers. Generally, instantaneous wedging action at any position without backlash or slip is required. The wedge-shaped pocket may have the disadvantage of high manufacturing costs.

For proper locking action, the condition for self-locking,  $\alpha \leq 2\phi$ , must be satisfied; see Fig. 14.16c. Here  $\alpha$  = the angle between tangents to the cam contour and to the roller surface at the point of contact. And  $\phi = \tan^{-1}\mu$  ( $\mu$  = coefficient of friction). To check the strength of the roller the crushing for



**FIGURE 14.16.** Unidirectional cam clutches.

$$F_c = F_f / \tan \alpha = 2T / D \tan \alpha \quad (14.17)$$

where  $T$  = the torque transmitted in-lb and  $D$  = the effective diameter of the rollers, inches.

#### 14.14 TWO INDEPENDENT CAMS IN SERIES (AUTOMOTIVE)

Valve cams for four-stroke-cycle internal combustion engines present special design problems. They run at speeds of up to 6000rpm with very lightweight flexible follower trains. These systems have a rise-fall-dwell program with the dwell used to keep the valve sealed during the cycle. Performance difficulties exist and the demands for high engine performance and good fuel economy have stimulated an interest in variable valve timing (VVT) for these engines. Variable valve timing is a design system that dynamically changes the valve timing to be optimized more nearly under all operating conditions. Dresner and Barkan (1989) have presented a variety of new mechanisms utilizing cams, eccentrics, and lever systems for this problem. Figure 14.17 shows one of the unique designs using two independent cams in series. The output is the sum of the two cams. Timing stages are established by varying the phase angles of the two cams relative to the crankshaft.

#### 14.15 QUICK ACTION CAMS

Sometimes machines require cam actions to provide a quick follower movement. Previously, we have indicated that a roller follower on a conventional radial cam cannot have an instantaneous return event if the cam has a sharp corner. In the earlier example the path of the roller follower was an arc of a circle of radius equal to the roller radius. Now, we shall show two practical cams that do not have this shortcoming. In Fig. 14.18a we have lugs  $C$  and  $C'$ , which are fixed to the cam shaft. The cam is free to turn (float) on the cam shaft, limited by lug  $C$  and the adjusting screw. With the cam rotating clockwise, lug  $C$

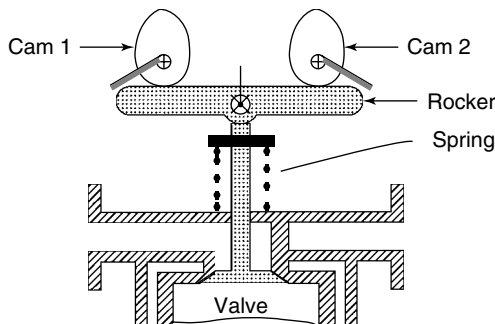
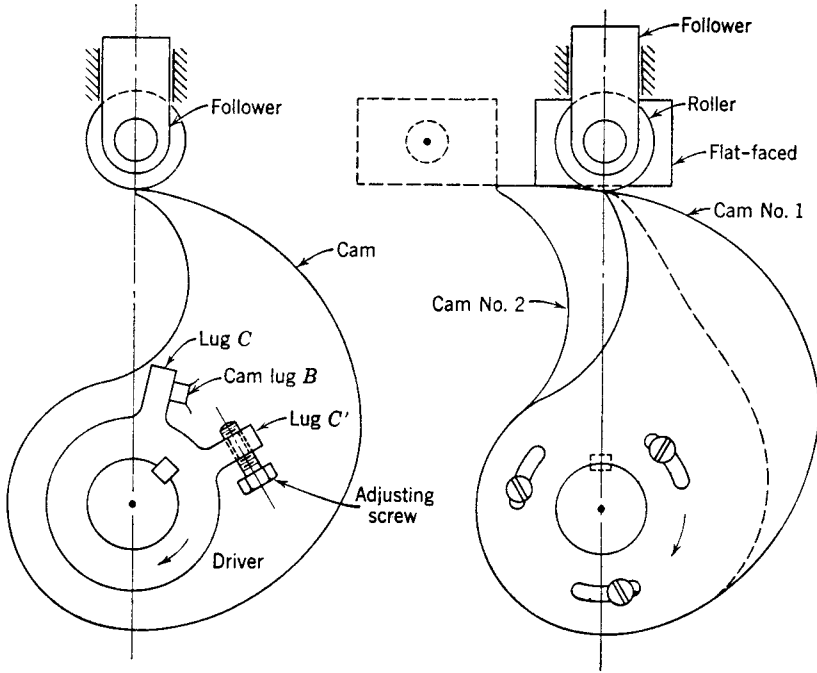


FIGURE 14.17. Two independent cams in series—automotive valve timing.



(a) Floating cam (between lugs  $C$  and  $C'$ ).

(b) Dual cams and followers.

FIGURE 14.18. Quick-acting cams.

drives the cam through the cam lug  $B$ . At the position shown the rollers will drop off the edge of the cam, which is accelerated clockwise until its cam lug  $B$  hits the adjusting screw of lug  $C'$ . The action is quick but obviously is limited by the inertia of the cam mass itself and by the amount of noise that one is willing to tolerate when the follower falls. Figure 14.18*b* shows the application of two integral cams and two followers, providing much faster action. The roller follower rides on cam 1. At the position shown, the flat-faced follower starts on cam 2. Continued clockwise rotation of the cam will move the flat-faced follower to the edge of the cam (dotted position), where it drops off the edge. Slots shown may be employed for timing adjustment.

### 14.16 VARIABLE-DWELL CAM

In some special machinery, it is necessary to vary the dwell period of the cam. This may be accomplished by adjusting and fixing the distance between two rollers in the slot, Fig. 14.19. Note that changing one dwell period (rise) effects a change in the total action in which two radial cams would provide greater control.

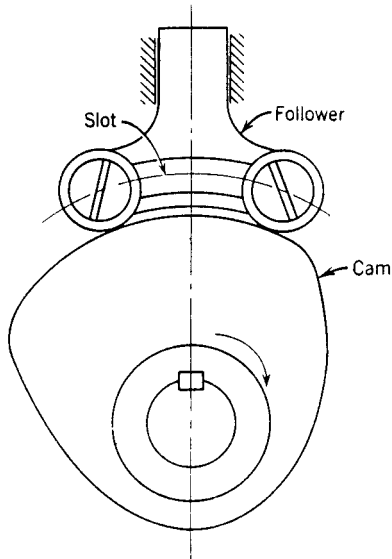


FIGURE 14.19. Variable-dwell cam.

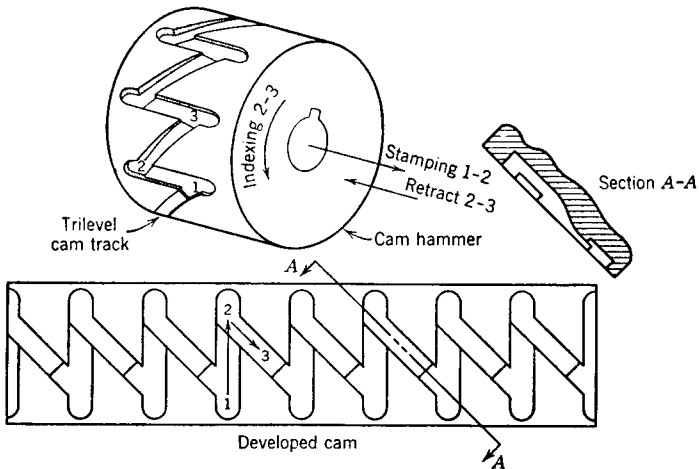


FIGURE 14.20. Cam to convert linear to rotary motion.

### 14.17 CAM TO CONVERT LINEAR TO ROTARY MOTION

Let us now analyze a novel inverse indexing cam design utilizing a continuous trilevel cam track. In this design (Fig. 14.20) a stationary cam pin rides in the cam track to convert horizontal linear motion into rotary motion. The trilevel track guarantees the proper

indexing directions without backtracking. This mechanism has been applied to index the stays on a stamping machine. A stationary pin (not shown) is in position 1 with the cam hammer assembly fully retracted. At position 2, the hammer has completed its stamping blow. As the hammer assembly retracts, the cam track follows the stationary pin to position 3 to impart rotary motion to the inverse cam.

### 14.18 CAM TO CONVERT ROTARY TO LINEAR MOTION

Six steel balls that cause an inverse-faced cam to assume an up-and-down motion result in a vibratory motion of a shaft attached to the cam (Fig. 14.21). This reciprocating movement of the shaft has been applied in the form of a high-frequency shock to the drill core of the rotary hammer. The total shaft output was 6000 blows per minute at 1000 rpm. Contoured and convex shaped, the grooved face of the cam contacts the exposed portion of the balls; the rest of the balls are housed in recesses of the ball seat, which at the same time acts as a spacer for the balls. Heat-treated Nitralloy is utilized to give required hardness and to minimize wear.

### 14.19 TWO-REVOLUTIONS-PER-CYCLE CAMS

There are two designs that can fulfill the requirements of two revolutions of the cam for one complete movement of the follower. These cams provide full lift of the follower with a cam rotation of more than 360 degrees. The mechanism shown in Fig. 14.22a utilizes a double-groove cam with an oscillating roller follower. A translating follower may also be used. This cam has movable doors or switches *A* and *B* directing the follower alternately in each groove. The grooves may be designed so that we may have follower movement or dwell as required. At the instant shown, door *B* is ready to guide the roller follower from slot 1 to slot 2. The other door positions are shown dotted.

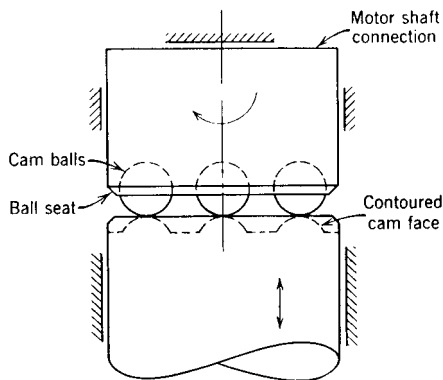
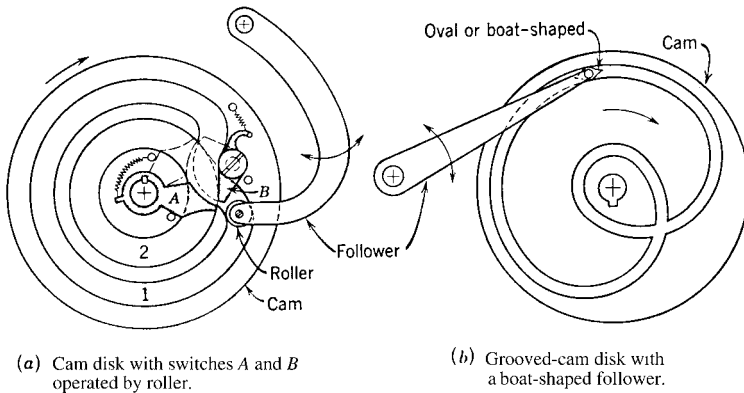


FIGURE 14.21. Cam to convert rotary to linear motion.



**FIGURE 14.22.** Two-revolutions-per-cycle cams.

In Fig. 14.22*b* we see a cam mechanism that fulfills the same requirements without the use of movable doors. As before, a groove cam is employed. However, the follower is made oval or boat-shaped to traverse the small radii of curvature and high-pressure angles that exist in this type of cam while also being able to maintain direction when traversing the crossovers in the cam groove. Although a radial cam and an oscillating follower are shown, cylindrical cams or translating followers may also be utilized.

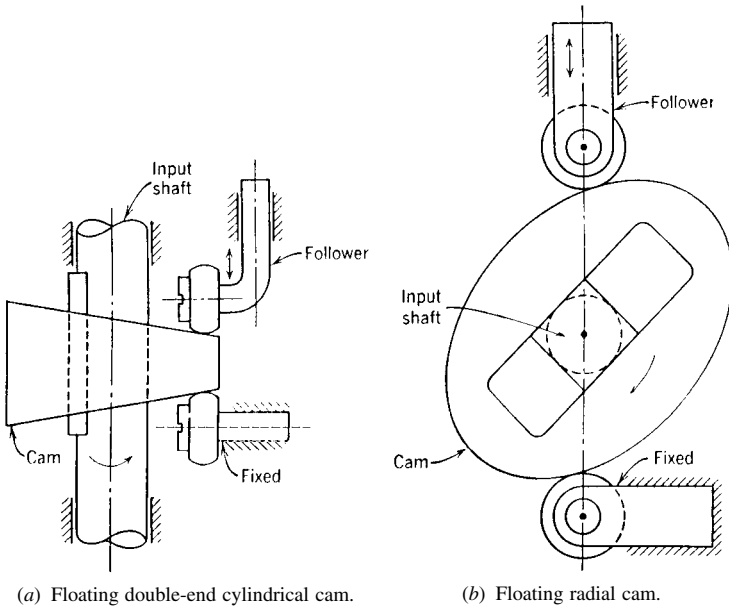
## 14.20 INCREASED STROKE CAMS

In Fig. 14.23 we see two examples of cams giving an increased stroke without increasing the pressure angle. Both examples, one a radial cam and the other a cylindrical cam, are kinematically the same design. The mechanism shown in Fig. 14.23*a* has the input shaft parallel to the follower movement, whereas in Fig. 14.23*b* the input shaft is perpendicular to the follower movement. In both examples, the cam slides on the input shaft and is in contact with a fixed roller on which the complete mechanism rides. Thus the total movement of the follower is the sum of the cam displacement on the fixed roller plus the follower displacement relative to the cam. In simplicity one may consider the cam as a “double” wedge acting on the follower.

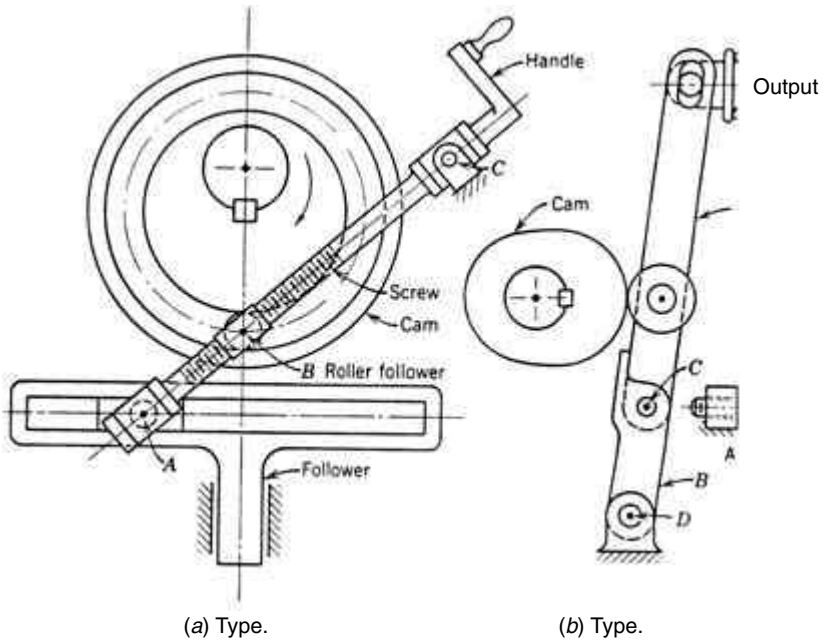
## 14.21 ADJUSTABLE STROKE CAMS

In Fig. 14.24 we see two possibilities of adjustable stroke cams (screw type) in which the total follower movement can be changed while the machine is running. In Fig. 14.24*a* we have a screw moving on its pivot at *C* and the roller follower *B* driving the follower through point *A*. The stroke adjustment is made by turning the screw handle, which changes the critical distance *AB*.

Figure 14.24*b* shows two links, *A* and *B*, that are connected at point *C*. These links either are in line pivoting about point *D* or are pivoting about *C* contacting the fixed adjustable screw. The follower stroke variation is made with the adjustable screw. The stroke depends on the relative amounts that lever *A* pivots about either points *C* or *D*.



(a) Floating double-end cylindrical cam.  
**FIGURE 14.23.** Increased stroke cams.



(a) Type.  
**FIGURE 14.24.** Adjustable stroke cams—screw type.

Therefore, minimum stroke will occur with the adjustable screw to the right. In this instance the arms, *A* and *B*, if never in contact with the screw and the lever, will always pivot about *D*. Similarly, the maximum stroke will occur when the adjustable screw is at the left so that the arms will pivot about points *C* and *D*. Thus infinite stroke adjustment is possible within these two ranges.

### 14.22 CONTROLLED TRANSLATING CYCLE CAMS

In Fig. 14.25*a* we have a special mechanism superimposing the motion of two cams, *A* and *B*. As an example, cam *A* is the main drive cam locating the follower position in steps, and cam *B* is the higher speed cam giving the follower its back-and-forth cycle for each position. In Fig. 14.25*b* we see the motion in which cam *B* turns at least 8 times faster than cam *A*. We can control the translating motion cycle by varying the relative speed ratio of cams *A* and *B*. Any combinations of motion are possible.

### 14.23 CIRCULAR ARC CAMS—CONSTANT BREADTH FOLLOWER

Let us now consider a positive-drive cam composed of circular arcs bearing against the sides of a follower track. For shapes other than a circle, the reader is referred to Shaw (1935). If the follower is stationary and completely encloses the cam, the motion of each corner of the cam will be a polygon in the shape of the follower, Figs. 14.26*a* and *b*. Usually the follower has more sides than the cam. In Fig. 14.26 we see all the cams

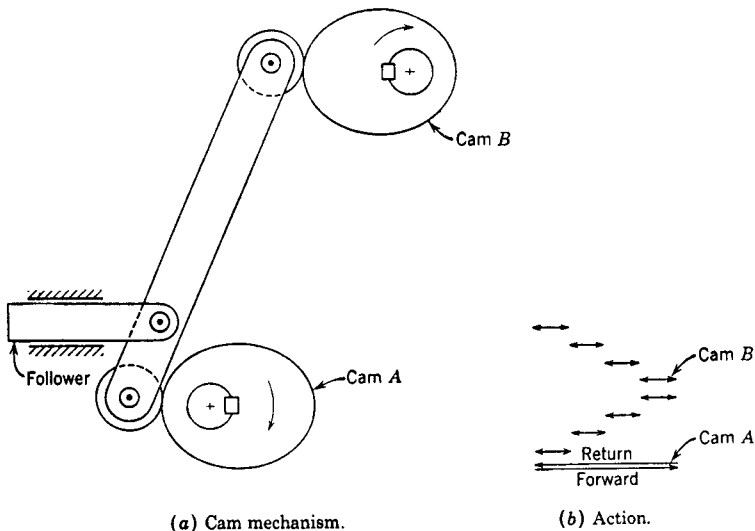


FIGURE 14.25. Cam with controlled translating cycle.

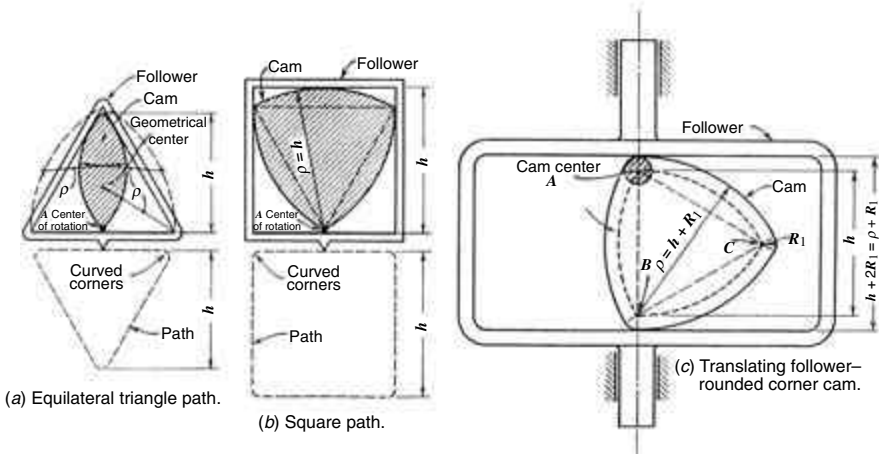


FIGURE 14.26. Circular arc cams—constant-breadth follower.

rotating about their centers,  $A$ , with the follower constrained to give a total rise,  $h$ . In Fig. 14.26a we have a two-sided cam and an equilateral triangle follower. The radius of cam curvature  $\rho$  equals the distance from the center to the corner of the triangle. The path of point  $A$  is approximately an equilateral triangle (Not exactly triangular due to the small rounded corners). In Fig. 14.26b the cam is constructed on an equilateral triangle having a circular arc radius equal to the width of the square follower,  $h$ . This follower takes a square path, again with small-radius corners. Note that the radius  $h$  is equal to the total displacement of the follower. Obviously, in a similar manner any number of sides may be used. It should be observed that a practical difficulty exists in that the center line of the shaft  $A$  is on the cam edge, which does not always provide enough space for the shaft. This shortcoming may be alleviated by the design shown in Fig. 14.26c or by employing an asymmetrical cam having a small radius at the cam center.

On the other hand, if the outer frame is fixed, the cam would be free to travel constrained by the frame track. Thus, any point on the cam would describe a similar geometric path, as shown in Figs. 14.26a and b. The size of the path depends on the distance from the cam center of rotation to the point on the cam under consideration. This principle has been applied in the drilling of holes of a polygon of any shape.

Let us analyze a triangular circular arc cam enclosed by a translating follower on two sides only, Fig. 14.26c. The design discussed here has been successfully used for sewing machines, film movement, fuel pumps, and other mechanisms. Its application is used in silent, high speed, lightly loaded, small power mechanisms. Some of these have been in excellent condition after over 20 years of operation. For further information, see Richards. (1940, 1941).

The design shown in Fig. 14.26c is more practical than the previous kinds because space has been provided for the shaft. Furthermore the cam has a radius  $R_1$  in each corner. This radius has the additional advantage of increasing the wear life over the previous cams having sharp corners. Note that the actual displacement  $h$  is unaffected by the size of this radius since the basic cam is contour  $ABC$ . The sides of the cam are shown at a radius  $\rho = h + R_1$ , and the breadth of the follower is  $h + 2R_1$ .

Using this triangular circular arc cam, we shall show that the displacement is made up of parts of the simple harmonic motion curve, Fig. 14.27. All action with circular arcs is similar. In Fig. 14.27a let  $\theta$  equal the angle of cam rotation from some original position.

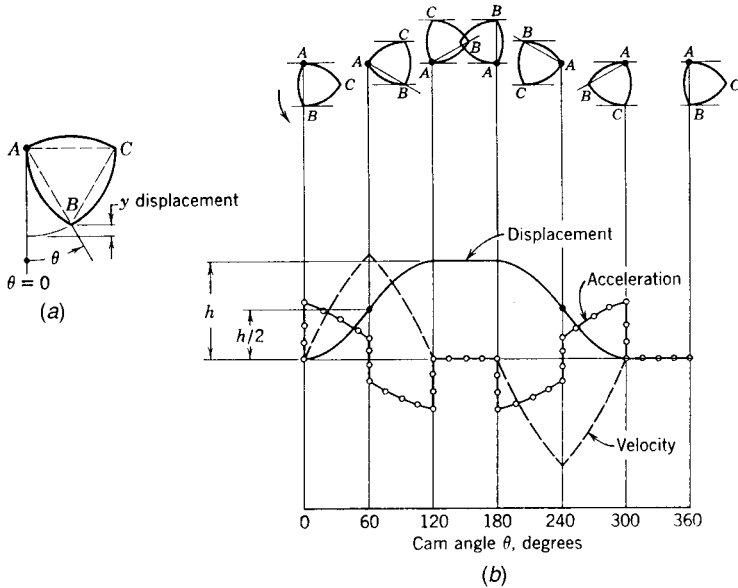


FIGURE 14.27. Triangular circular arc cam characteristics (translating follower).

If we consider the cycle in which  $\theta$  varies from  $0^\circ$  to  $60^\circ$  (the positive acceleration period of the motion), the displacement

$$y = h(1 - \cos\theta) \text{ in.} \quad (14.18)$$

This is simple harmonic motion for these  $60^\circ$  to a total lift equal to  $h/2$ .

The velocity and acceleration by differentiation

$$\dot{y} = \omega h \sin\theta \text{ ips} \quad (14.19)$$

$$\ddot{y} = \omega^2 h \cos\theta \text{ in/sec}^2. \quad (14.20)$$

The minus acceleration period is similar for the next rise portion  $h/2$ , the total lift occurring in  $120^\circ$  of cam rotation. A dwell of  $60^\circ$  of cam rotation then follows. In Fig. 14.27b we plot the curves of the complete action in which it is seen that the acceleration curve is discontinuous.

## 14.24 SWASH PLATE CAM

The swash plate cam (Fig. 14.28) is an end cam having a flat-plane disk fixed at an acute angle to a rotating shaft. This cam has been used for a multipiston pump whose piston rods ride on the swash surface. If a knife edge or point contact were employed, the follower would move with simple harmonic motion. However, with a more practical crowned roller follower, the follower has approximate simple harmonic motion, if the roller diameter is kept small. Swash-plate cams are feasible only under light loads, since the eccentricity shown causes poor bearing operation due to excessive deflections of the cam and its shaft.

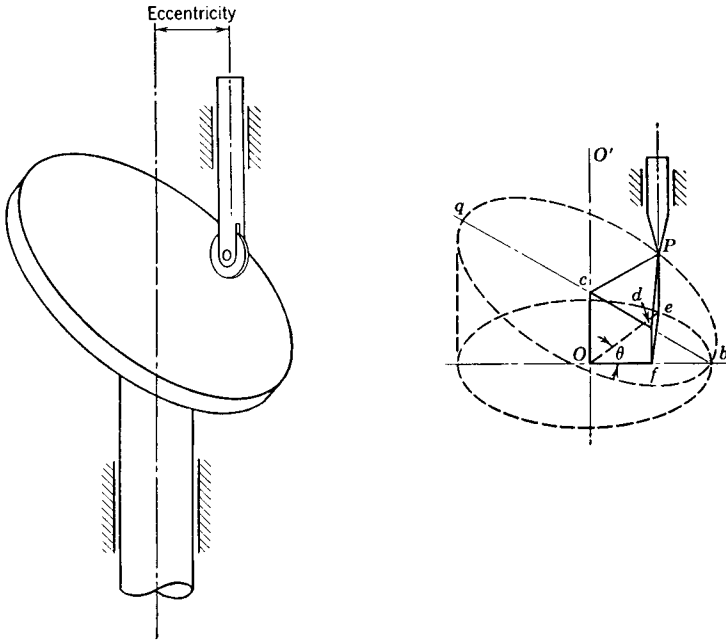


FIGURE 14.28. Swash plate cam.

Let us now verify the stated follower motion. If the axis of the shaft is  $O-O'$  with the point  $P$  of the follower in contact with the cam, we see that, as the cam rotates an angle  $\theta$  from  $Ob$  to  $Oe$ , the follower point rises a distance  $eP$ . The swash plate traces an elliptical path  $bPq$ . The rise by proportion and similar triangles is

$$eP = df = Oc \frac{bf}{bO} = Oc \left( \frac{bO - Of}{bO} \right)$$

which solves to harmonic motion

$$eP = Oc(1 - \cos\theta). \tag{14.21}$$

### 14.25 VARIABLE-ANGULAR-VELOCITY CAM

In all other cam mechanisms previously discussed in this book, we have had the cam rotating at a constant speed, since in practice, the cam is generally driven by a constant-speed prime mover, such as an engine or an electrical motor. However, particular design requirements may necessitate a variable-speed cam to drive the follower (see Fig. 14.29 and Fig. 14.30). In both cases the cam is attached to a constant speed crank. Fig. 14.30 is known as the Whitworth mechanism. The development of the cam shape provides a smaller cam, a constant pressure angle, and a compact overall mechanism.

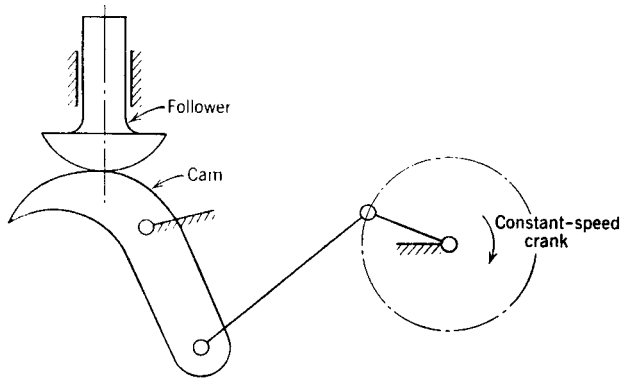


FIGURE 14.29. Variable-angular-velocity cam (schematic).

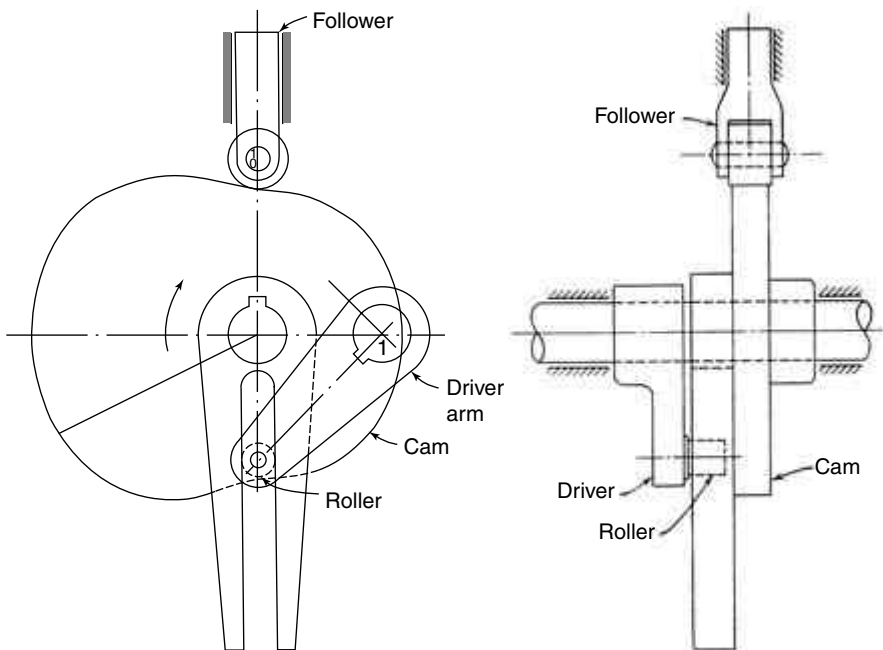


FIGURE 14.30. Variable-angular-velocity cam (Whitworth drive mechanism).

## 14.26 CAM INTERMITTENT-MOTION MECHANISMS

### 14.26.1 Comparison of Intermittent-Motion Mechanisms

Intermittent-motion mechanisms, sometimes called indexing mechanisms, are among the most useful devices available to machine engineers. These mechanisms have been applied

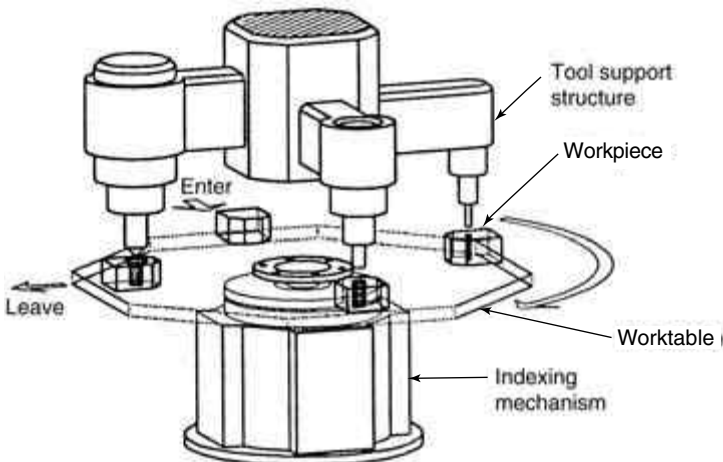
to indexing dials, carriers, conveyors, feeding mechanisms, and others. The function of these devices is to convert a continuous motion to an intermittent motion.

In Fig. 14.31 we see an indexing machine that converts the constant motion speed (not shown) to intermittent motion of the work table, allowing the process to be automated in 90° sequences. This dwell action permits various operations to take place simultaneously. Sometimes robots are employed to work on the workplace simultaneously.

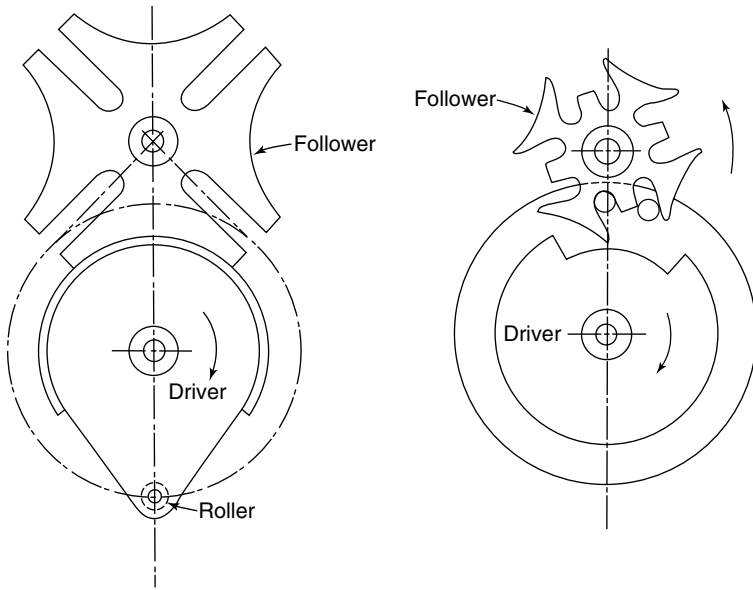
The types of intermittent-motion mechanisms available are the ratchet gear, intermittent-gear, Geneva mechanism, star-wheel mechanism, and cam-driven mechanisms. The cam mechanisms are generally the best choice at high speeds and high dynamic loads. In Fig. 14.32 we see the Geneva and the star-wheel mechanisms: Both of these mechanisms index when the driver roller enters the follower slot and are held in the dwell position by the concave portion of the follower wheel. The ratchet and intermittent gear mechanisms are not shown because they are quite common. Other mechanisms for indexing have been employed that, although ingenious, are not practical because of high fabrication cost and part complexity. A critical survey of intermittent mechanisms is presented by Lichtwitz (1951, 1952), Cheng and Lin (1995), and Fenton et al. (1994).

Now, let us analyze the characteristics of the foregoing mechanisms with special concern for the acceleration curve shape. These acceleration curves have basic shapes that are specifically inherent to each mechanism. They have high peak accelerations with either a discontinuity in acceleration or infinite acceleration values, Fig. 14.33. With the motion of the ratchet gear, usually derived from a crank since pawl and wheel are not connected directly, the pawl hits the teeth of the wheel abruptly. This gives theoretically infinite acceleration followed by a modified harmonic acceleration. Ratchet gears are used in low-speed applications where noise and accuracy of movement are not important. The intermittent gear mechanism has a similar acceleration curve and thus the same speed limitation.

Again referring to Fig. 14.33 we see that the Geneva and star-wheel mechanisms are alike in that infinite jerk exists at the beginning of the action. This, as noted in previous chapters, produces vibration, noise, and wear, which limits the speed and mass of the follower. Also, with the Geneva mechanism, the driven index wheel is given high acceleration during the middle part of the movement, as the driver acts on a very small lever arm.



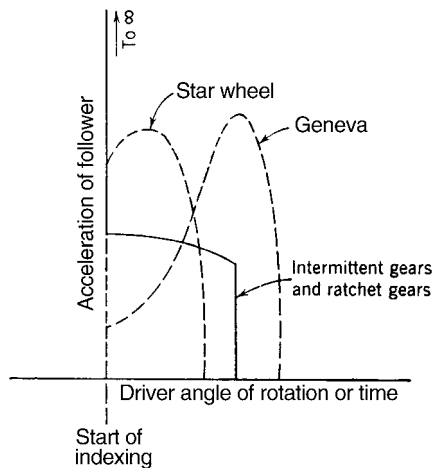
**FIGURE 14.31.** Indexing machinery for intermittent action.



(a) Four-station Geneva mechanism (locked position).

(b) Star wheel mechanism (indexing position).

**FIGURE 14.32.** Some intermittent-motion mechanisms.



**FIGURE 14.33.** Acceleration curves of intermittent mechanisms.

Therefore, driving conditions are unfavorable, particularly with large sizes and speeds. Special mechanisms have been combined with the Geneva to improve the acceleration curve. These are complicated and expensive and thus are not feasible. The star wheel is a kindred mechanism to the Geneva, having a greater range for the rotation and dwell periods.

We shall see in the following sections that cam-driven mechanisms are best. The basic advantage is that the cam can be designed for any curve (simple harmonic, parabolic, cycloidal, or trapezoidal, etc., motions) and thus the action may be selected with complete control. By choosing the proper acceleration curve with a finite jerk at all times, we can control the inertia forces and limit the vibration, noise, and wear under high-speed operation.

The indexing period for these cam mechanisms may be chosen to suit, ranging from less than 90 degrees up to 360 degrees. Shorter indexing periods require larger cams: they can be used when there are no limitations in space and when the speed is not so high as to produce prohibitively large inertia forces. A dwell period of about 180 degrees generally gives reasonable action and proportions.

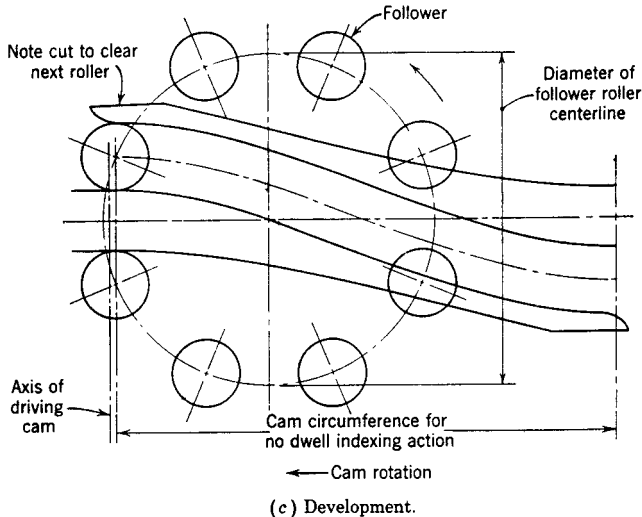
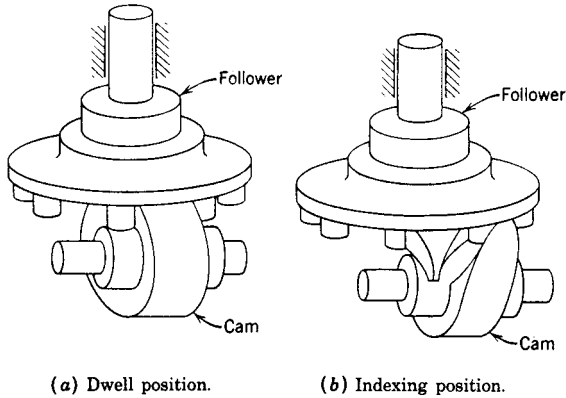
Let us discuss the following cams and cam applications: cylindrical, grooved concave globoidal, spider, multiple double-end, and the modified star wheel. All of these are positive-drive mechanisms; the multiple double-end cam and the star-wheel cam are the best for high-speed action. These latter types fulfill the requirements of minimum backlash and low follower vibration.

#### 14.26.2 Cylindrical Cam for Intermittent Motion

The first of the cam-driven indexing mechanisms to be discussed employs a cylindrical cam. This mechanism, which generally has eight or more stations, is applied to crossed or skewed shafts. Two of the many installations were with zipper-making equipment which had light loads at 3000 indexes per minute and with cigarette-packaging machinery allowing hopper-fed cigarettes to be inserted forty at a time, 300 times per minute into pockets of a 12-station turret cam, SAE 8617 carburized Rock C-56 to 60.

The driving member is a cylindrical drum having a ridge that engages the follower rollers mounted on a disk (Fig. 14.34). A part of the ridge is in a plane perpendicular to the axis of the drum. Its width is equal to the distance between the rollers, which serves to lock the driven disks. The two ends of the ridge are curved outward. The driven member is rotated by the interaction of the curved portion of the ridge with the rollers. The ridge as shown provides a positive-drive action of the driven member. However, this locking arrangement may be reversed and the basic kinematic function retained by having the two rollers guided by the curved ridge; the two straight branches of the ridge serve for locking. There is a cut in the ridge to clear the next roller as the follower is indexed.

As we have previously indicated, the kinematic properties are independent of the diameter of the roller driving cam and driven disk. These dimensions may be chosen arbitrarily. However, a large cam diameter reduces the pressure angle or inclination of the ridge in the same manner as a helix angle of a screw thread. The pressure between the cam and the follower is thus lessened. In addition, the cam size is limited by the fact that as the rollers move along an arc their axes cannot point (in every position) toward the axis of the driving cam. Cutting of the grooves becomes difficult when the attempt is made to compensate for the roller position during action. This can be decreased by having the axis of the driving shaft midway between the extreme roller positions.



**FIGURE 14.34.** Cylindrical cam for intermittent motion (eight-station indexing).

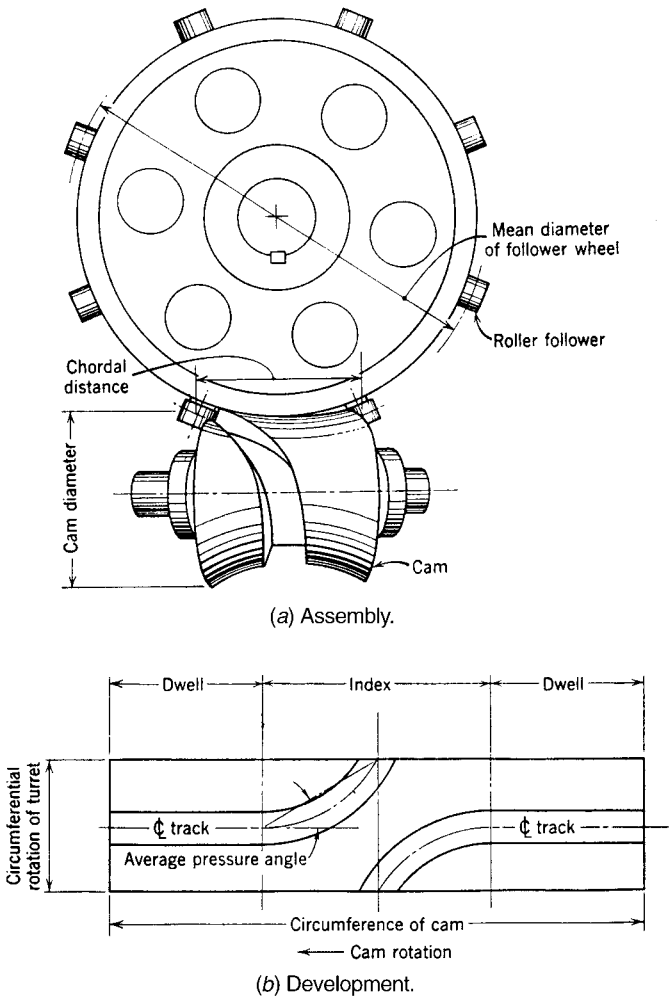
Returning to the cam-follower action, experience has shown that rapid wear due to a large amount of sliding (spalling) is evident as the rollers withdraw from large cams. Furthermore, the rollers tend to skew, owing to the end thrust. Short rollers are suggested to minimize this detrimental action. Some improvement may be made by employing conical rollers with the apex at the axis of the drum, but they are often troublesome to install.

Another hindrance of this cam mechanism is that it is often difficult to maintain locking under dwell conditions. A positive lock such as a wedge-shaped block that engages a pair of rollers during the idle period, relieving the shock load from the cam, is sometimes employed. Shock and vibration may be caused by the backlash or clearance between the rollers and their groove.

**14.26.3 Grooved Concave Globoidal Cam for Intermittent Motion**

The concave globoidal cam is often referred to as the concave barrel cam. When used for indexing, it is an improvement over the barrel cam or the cylindrical cam, Fig. 14.35*a*. The concave globoidal cam has been successfully used in the paper industry where a 1000-lb wheel, 50 inches in diameter, operates 16 hours per day, 100 indexes per minute, for two years without noticeable wear.

The follower has rollers that ride in grooves of the cam, giving positive-drive action during both indexing and dwell periods. There rollers remain at a constant depth as com-



**FIGURE 14.35.** Grooved concave globoidal cam for intermittent motion (8-station).

pared to the previous cylindrical cam, allowing a smaller follower wheel and thus reduced inertia. The only shortcoming of this type of groove cam follower is that the backlash between the roller and groove sides may produce noise, wear, and vibration.

Generally, no auxiliary members, such as locating pins or wedge locks, are necessary during the dwell periods. The number of index stations on the cam-follower turret should be eight or more, to give reasonable cam and follower wheel proportions.

Experience has shown that a dwell into the index period is desirable, the chordal distance being about 0.8 of the cam diameter and the follower diameter about twice the cam diameter. An average pressure angle of about  $30^\circ$  and a maximum pressure angle as high as  $50^\circ$  have been successful. In Fig. 14.35*b* we see a development of this cam track. For more information refer to Jacobs (1953), who utilized turrets from 24 to 60 inches in diameter weighing 200 to 2000 pounds. For small quantities, SAE 4140 forged steel billets with a cam track flame-hardened to Rock. C50-60 were chosen.

#### 14.26.4 Spider Cam for Intermittent Motion

The spider cam (Richards, 1940, 1941) derives its name from the appearance of the follower. This mechanism requires a follower having four or more indexing rollers. One of its former applications was the feeding of the film in motion-picture projectors. In Fig. 14.36 we see the drive cam rotating clockwise at a constant speed driving a four-roller follower also clockwise. In Fig. 14.36*a* the roller *a* is being moved in its slot, indexing the follower a quarter revolution with positive-drive action. In Fig. 14.36*b*, we see the dwell cycle in which the rollers are positively fixed between two contours.

The spider cam mechanism offers more accurate control of the dwell action than do the other indexing mechanisms shown. However, the limitations of backlash in the roller groove described may offer difficulty at high speeds, giving wear, noise, and vibration in the same manner as intermittent-motion cams. The design of this mechanism may vary somewhat in that the follower pivot *B* may be located outside the cam ring farther from the cam center *A*. With this construction, the follower will rotate in a direction opposite that of the cam.

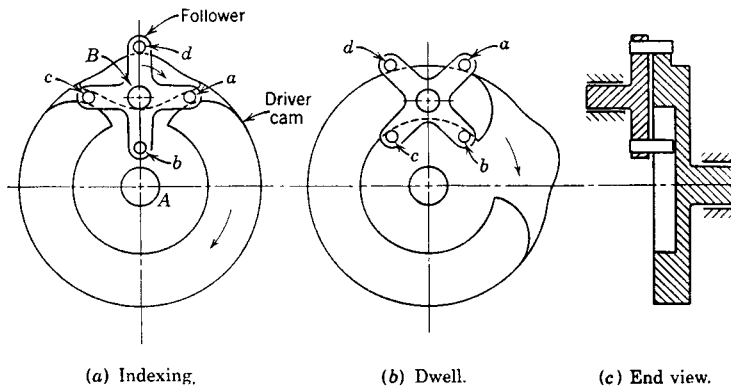


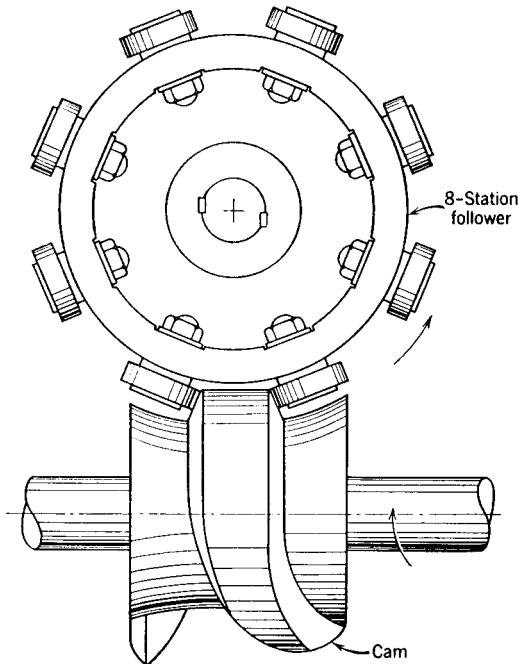
FIGURE 14.36. Spider cam for intermittent motion.

### 14.26.5 Multiple Double-End Cam for Intermittent Motion

This cam with a concave globoidal shape is often referred to as the roller gear drive (Neklutin, 1953). It is available commercially. The roller gear drive (Fig. 14.37) is similar to a worn gear driven by a worn with a varying helix angle. We see that the follower has cylindrical rollers located radially. As with other cam mechanisms, the shape of the cam rib may be made to produce any follower action with any desired acceleration curve characteristics.

A slight change of the radial position of the rollers does not affect the performance, because the rollers are moved along the axis parallel to the side of the tapered rib. The presence of the tapered rib permits proper roller loading, which is accomplished by shifting the driving and driven shafts closer. The use of the ball bearing as rollers is advantageous, because they permit preloading against each other. They also allow building the drive with minimum backlash and with a precision of about  $\pm 0.001$  inch. The roller gear is locked at the instant at which it stops moving, so that no time is lost for the locking operation. Thus, this cam mechanism having conjugate dual-opposed roller followers is excellent for high-speed drives, giving smooth, low-vibratory performance and requiring little maintenance. It is generally expensive but the cost is often justified.

Two or more stops per cam revolution are permitted. Mechanisms that make six or more stops per revolution have a number of rollers equal to the number of stops—only one roller is passed during one revolution of the cam. If the number of stops is between two and five then the followers should have more rollers than the number of stops. The necessity of passing more than one roller per stroke increases the size of the cam; there-



**FIGURE 14.37.** Multiple double-end cam for intermittent motion.

fore, the designer should by all means consider changing the design of the machine to permit the use of six or more stops per revolution of the gear.

This drive has been used on dial and roll feed at speeds up to 800 per minute. It has been applied to multicolor printing presses to feed paper webs intermittently at 10,000 impressions or more per hour, envelope folding machines, cap assembly machines, punch presses, and many others.

### 14.26.6 Star-Wheel Cam for Intermittent Motion

The conventional star-wheel mechanism is the most versatile of the intermittent mechanisms. However, it can be shown that the follower slot takes the path of an epicycloid, which gives inherently unfavorable dynamic properties. The poor acceleration curve limits high-speed application to machinery. In the conventional star-wheel mechanism, Fig. 14.38*b*, the drive roller is enclosed on both sides of the star-wheel follower slot during indexing operation. However, a physical change in the arrangement of parts may be made to permit the use of camlike surfaces. In this design, two rollers and two cam surfaces are employed.

In Fig. 14.38*a*, we see the counterclockwise-rotating driver indexing (positive acceleration) the clockwise-rotating star-wheel follower. The drive roller and the control cam are on the driving member, with the control roller and the drive cam on the driven star-wheel follower. The drive roller is in contact with the drive cam with the control roller in contact with the control cam. Note that the drive roller contacts one side of the slot only, with clearance on the other side of its slot. Positive engagement, therefore, is the only function of the control roller and its contacting control cam. Figure 14.38*b* shows an installation having the rollers on the driver and the cams on the driven member.

As with all other cam mechanisms, the cam surfaces may have any form. It has been found that proper choice of acceleration curve (trapezoidal or cycloidal) will reduce the maximum acceleration value to one-half that with the basic star-wheel mechanism. A finite jerk exists at all times. This mechanism has been used in various lithographic offset and typographic presses. In one installation, a 12-inch cylinder weighing about 1000 pounds was driven with a maximum velocity of 250rpm with one standstill period per revolution.

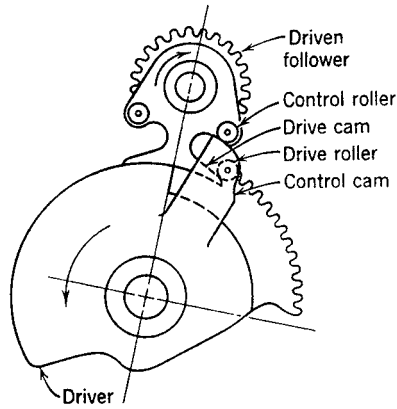
## 14.27 CAM-MODULATED MECHANISMS

---

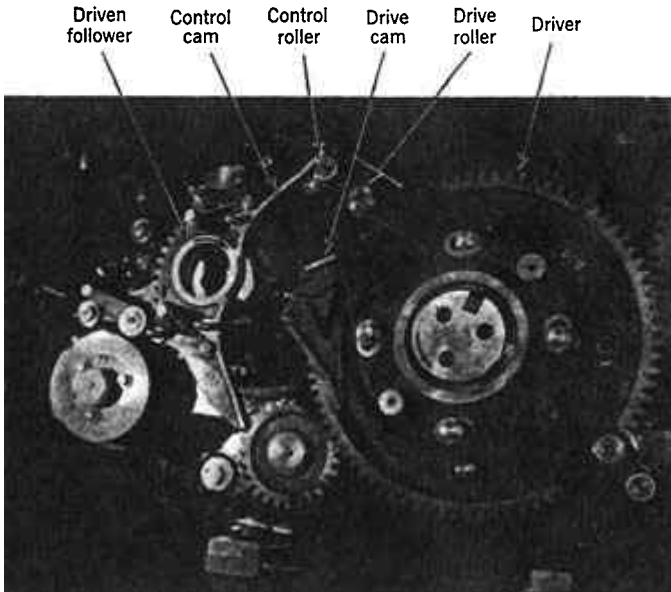
Many cam-follower systems in machinery have the follower remotely located from the cam drive. An example is the four-bar mechanism used as the input device in the electric typewriter, see Fig. 1.2. Another example is the automobile cam-driven valve operating system discussed throughout the book. Cams may be attached to linkages, gears, belts, chains, etc., to fulfill the design requirements. Combinations of linkage analysis and cam systems are necessary to establish the mechanism and action.

### 14.27.1 Cam-Modulated Stamping Mechanism

In Fig. 14.39 we see a cam-modulated stamping mechanism (Erdman and Sandor, 1984) in which stamp 1 is pressed on fixed body 2. The stamp is supported by flexure springs 3. Springs 4 and 5 maintain the roller contact on cam 6. This is one of the many possible designs depending on the design requirements of the stamping action such as speed, pressure, lift, and noise.



(a) Schematic (note cams on both)



(b) Installation

**FIGURE 14.38.** Star wheel cams for intermittent motion. Drive of a printing press (note cams on driver). Courtesy Harris-Seybold Co., Chicago, Ill.

**14.27.2 Cam-Modulated Worm and Worm Gear**

Many fields including those using cloth, wire, and paper machinery need to have the machine's speed controlled over a cycle of operation. This requirement has high power and high load, often best satisfied by combining cams with gears and all driven by a constant-speed motor or engine. Accuracy, reliability, low vibration, and low noise may be achieved even when large masses are moved at high speeds. Cams offer all the advan-

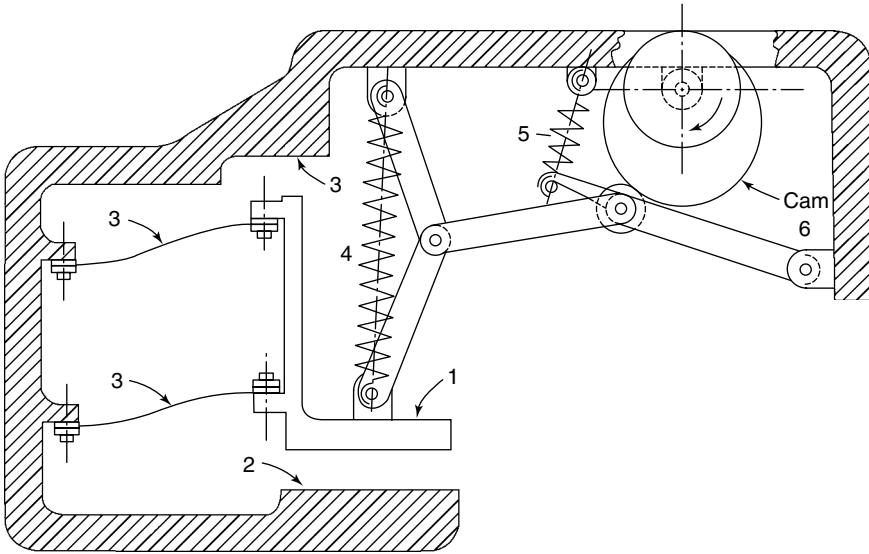


FIGURE 14.39. Cam-modulated stamping machine (Erdman and Sandor, 1984).

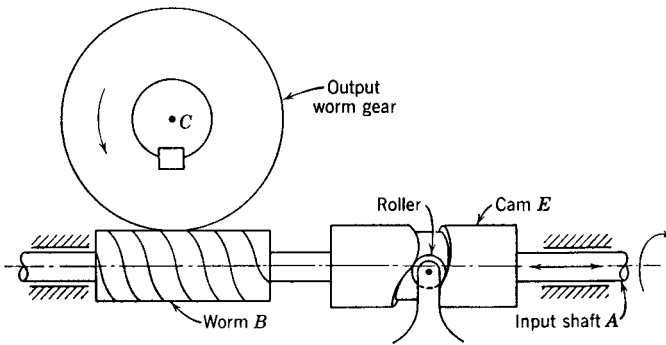


FIGURE 14.40. Cam-modulated mechanism—worm and worm gear drive.

tages of controlled design to give the best dynamic properties of the mechanism, since they allow flexibility in choice of follower action.

This section and the following four present examples of mechanisms utilizing cam-modulated systems. In the worm and worm gear design, Fig. 14.40, the input shaft *A* drives the output worm gear *C* through its meshing worm *B*. Shaft *A* rotates and is also made to reciprocate by a fixed roller in the positive-drive cam *E*. Thus the output of *C* is made up of the rotation of shaft *A* plus or minus its axial movement. Any movement of output shaft *C* may be obtained, depending on the design of the cam, *E*. Thus a zero velocity of the output gear can be the net result of the input shaft driving in the direction opposite that of the cam.

### 14.273 Cam-Modulated Epicyclic Gears and Moving Cam (Type 1)

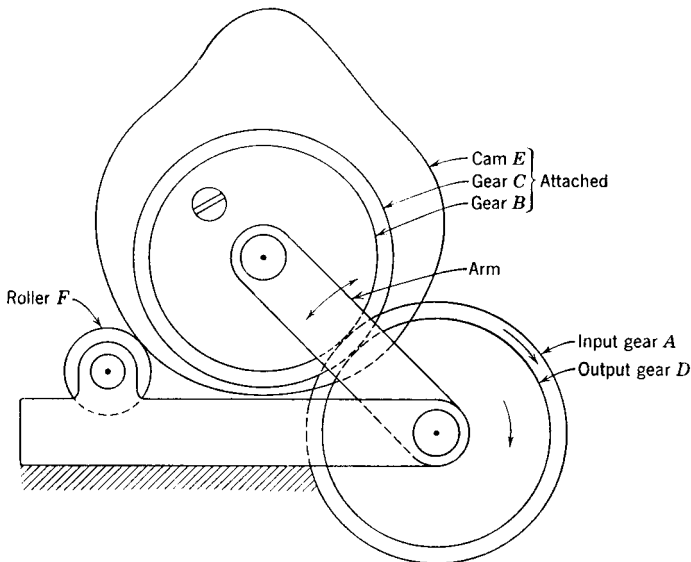
Again, the output speed is the sum of the input gear movement plus or minus the cam movement. In Fig. 14.41 we see a compound train with *A* the input gear and *D* the output gear. Gear *D* is floating or, in other words, not attached to gear *A*. Gears *B* and *C* and cam *E* are fixed to each other. Cam *E* is riding over roller *F*. When the unit rotates, gear *D* is driven by the output of gears plus or minus the movement of the arm shown. Thus we have a cam-controlled cyclical variable-speed drive.

### 14.274 Cam-Modulated Epicyclic Gearing and Moving Cam (Type 2)

This design is kinematically the same as the previous ones. As before, the output speed is the superposition of two actions (Fig. 14.42), the input gear speed and the epicyclic arm *G*, the latter driven by the cam. The main drive occurs through gear *A* into *B*, turning the epicyclic gears, *C*, meshing with the output shaft of gear *D*. Gears *C* are free to rotate on their shafts. Rack *F* attached to the cam roller drives gear *E* which is attached to arm *F*. Thus, the output is made up of the inputs of the cam and gear *A*.

### 14.275 Cam-Modulated Epicyclic Gearing and Fixed Cam

Again, the output speed is the superposition of the input gear motion plus or minus the cam-driven action. Fig. 14.43 shows the operation. The input *A* drives the arm *C* through pivot *B*. The movement of the pivot plus the movement of roller *E* in its fixed-cam track drives output gear *D*. Epicyclic action occurs in which the output gear rotation is the sum of both the rotation of input *A* and the position of roller *E* in the fixed cam track.



**FIGURE 14.41.** Cam-modulated mechanism—epicyclic gears and moving cams, type 1.

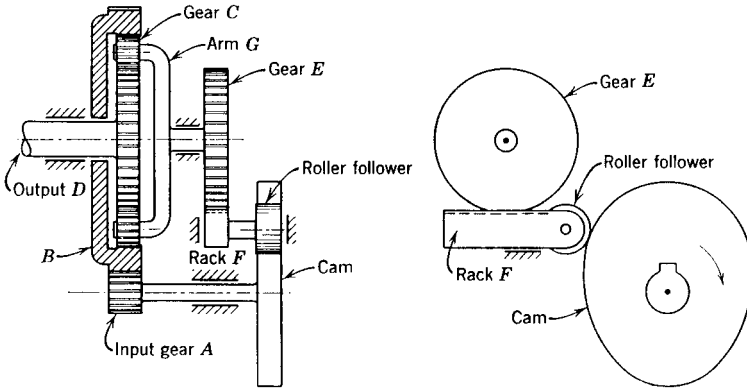


FIGURE 14.42. Cam-modulated mechanism—epicyclic gears and moving cam, type 2.

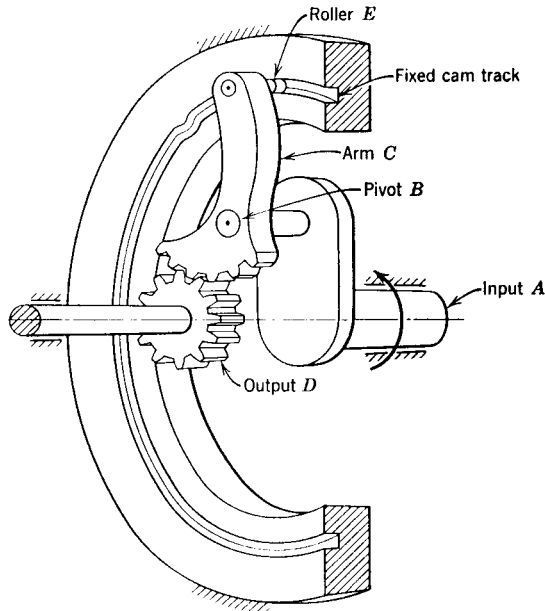
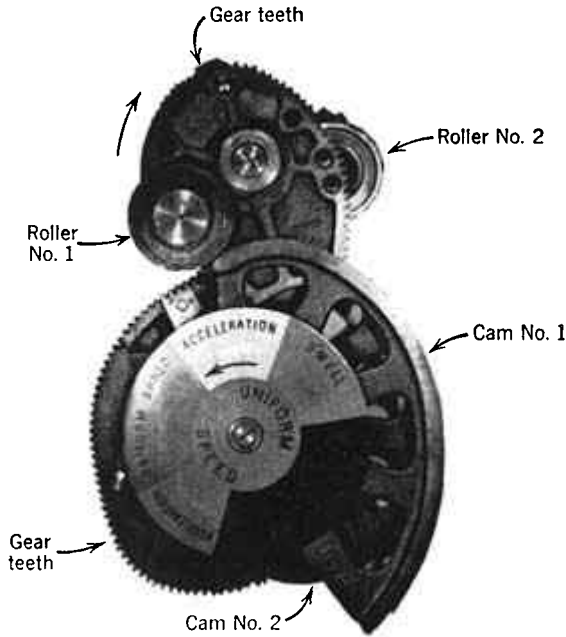


FIGURE 14.43. Cam-modulated mechanism—epicyclic gears and fixed cam.

### 14.276 Cam-Modulated Noncircular Gears

In some designs, it has been proved feasible to use noncircular gearing for a variable angular velocity ration between the driving gear and the driven gear. Generally, noncircular gears are expensive and are utilized as a last resort. However, the previous cam and link mechanisms may become too complicated and bulky. Instead, cams combined with noncircular gears are used. A dwell period exists at the beginning and at the end of the



**FIGURE 14.44.** Cam-modulated mechanism—noncircular gears (printing press transfer mechanism). (Courtesy Michle Printing Press and Manufacturing Co., Chicago, Ill.)

action in which a dwell period cannot be fulfilled by meshing gears alone, since the driver and driven gears must always move.

In Fig. 14.44, the follower is shown accelerating clockwise. Cam 1 and roller 1 are employed for the initial dwell range into the positive acceleration portion of the action, with cam 2 and roller 2 used for the negative acceleration portion of the dwell period. The gears mesh between these ranges of action. Note that conjugate cam mechanisms are utilized and backlash is kept to a minimum; see Peyrbrune (1953).

## 14.28 CAM COMPUTING MECHANISMS

Computing mechanisms are devices that solve problems automatically and quickly and are classified as either digital or analog computes. Computers today are universally of the digital type. This section is an introduction to cam analog computers, which could be of value in the recently emerging field of micromachines of (Chap. 15). The most complete survey on analog computers is by Svoboda (1948) and Fry (1945).

An analog device is one in which the numbers are changed into physical quantities (voltage, gear revolutions, etc.) that are related; they perform the mathematical operation which is translated into digital form. In the analog computer, the precision of the calculation depends on the precision with which the device is fabricated and read on calibrated scales. It is often a cam-modulated system comprising bar linkages or cams, separate or in combination, together with gears, lead screws, and other mechanical members. Applied



**FIGURE 14.45.** Computing mechanism cams. (Courtesy Ford Instrument Co., Long Island City, N.Y.).

to analog computers, cams are often used as correcting devices. In this manner, increased accuracy is obtained from the mechanisms.

The first step in the design of analog computers is the selection of the output scale, the input scale being fixed by the fact that the cam rotates usually less than  $360^\circ$  for the full range. The scale choice is an important consideration. From the standpoint of accuracy, it is desirable to have the scale as large as possible, i.e., as few units per inch per revolution as possible. In this manner, backlash and dimensional accuracy will have a lesser effect.

The second step is to establish the cam size and the sense of the follower movement, i.e., whether to move outward or inward for increasing values. This is chosen so that the steepest portion of the function curve is at the cam outer radius, permitting smaller cams for the same pressure angle limit. Generally, a maximum pressure angle of  $30^\circ$  is suggested, but angles as high as  $45^\circ$  have been successfully applied. In addition, the reader should beware of undercutting (see Chap. 6). This detrimental condition may be alleviated by increasing cam size or reducing the output scale. Figure 14.45 shows some computing mechanism cams used for precision machinery applications.

### 14.28.1 Cam Types

In computers, we denote the basic function of motion relationship between nonlinear related parameters  $X$  and  $Y$  as

$$Y = F(X). \quad (14.22)$$

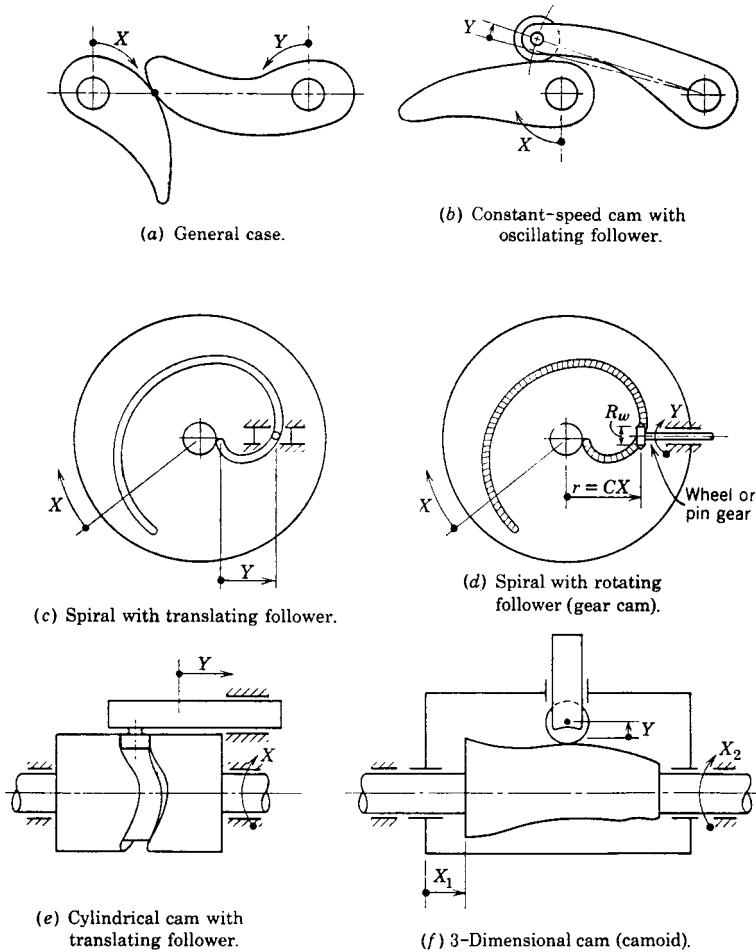


FIGURE 14.46. Cam computing mechanisms.

In this, we may call  $X$  the input parameter and  $Y$  the output parameter with the  $F(X)$  being any single-valued continuous function with a derivative held within certain limits. The latter restriction on  $F(X)$  prevents the cam from becoming too large and impractical. Among the many functions that have been cut are squares, roots, reciprocals, trigonometric functions, and empirical functions.

In Fig. 14.46 we indicate some of the possibilities of cam computer mechanisms with the nonpositive drive types held in contact by springs (not shown). Of course, any cam may be employed. In Fig. 14.46a we see the general case of two contours in contact, usually with pure rolling action. In Fig. 14.46b we see input  $X$  as a constant-speed rotating cam and output  $Y$  as an oscillating follower. In Fig. 14.46c we have a spiral rotating input  $X$  with a positive drive pin in groove output  $Y$ . Figure 14.46d, often called a gear cam, is similar to Fig. 14.46c except that the output parameter  $Y$  is a rotating pin gear meshing with grooves in the spiral input  $X$ . The primary advantage of these two spiral

cams is that more than one cam revolution is allowed, providing high accuracy. Spirals as high as eight revolutions have been used. Figure 14.46e shows a rotating cylindrical cam with input  $X$  and a translating output  $Y$ . Compared to a radial cam, cylindrical cams generally have a smaller maximum dimension for a given follower travel. Figure 14.46f differs from all the others in that it is a 3-D cam or camoid, the mechanism having two degrees of freedom. The follower is often a spherical ball in contact with the cam profile. With the camoid, we have output parameter  $Y$  a function of two parameter inputs  $X_1$  and  $X_2$

$$Y = F(X_1, X_2). \quad (14.23)$$

The input  $X_1$  and the output  $Y$  are translating with the input parameter  $X_2$  rotating. This cam is similar to a 3-D graph. In an alternative design, output  $Y$  may have oscillatory action. The 3-D cam is used in applications where the relation is so complicated that no analytical solution exists, the function being known only in the form of tabulated data or curves. An example is the computation of various exterior ballistic quantities such as the time of a projectile flight in fire control work. These 3-D cams are generally employed only as a last design possibility because of their high pressure angle, large size, high friction, and high manufacturing cost. This type cam is often cut on a profiling machine controlled by a master cutter, sometimes requiring 15,000 points with a tolerance of at least  $\pm 0.0004$  in; often higher accuracy is required. After removal from the fixture, the surface is covered with thousands of tiny protuberances between successive cuts. These projections are removed by round files properly selected to conform more or less with the cam surface at the point of filing. Last, the surface is hand-polished to 20-microns (root-mean-square) smoothness. Sometimes, to simplify fabrication, these cams have been built up of many thin disks. As with all the other computing cams of this section, the 3-D cam has been replaced by the digital computer.

### 14.28.2 Archimedes Spiral Gear Cam

Let us now take a spiral as a typical example and show how a cam similar to that in Fig. 14.46d can be established to give the square relationship between the input and the output. This mechanism is a computing tool with accuracies as high as 1 part in 30,000.

In Fig. 14.46d we have an Archimedes spiral input parameter  $X$ , rotating clockwise, driving a pin gear parameter  $Y$ . Let

- $X$  = input cam angular rotation, rad
- $Y$  = output follower angular rotations, rad
- $R_w$  = mean radius of pin wheel, in
- $r$  = instantaneous radial distance from center of cam, in
- $C$  = a constant

From the figure

$$R_w dY = r dX.$$

But we know for the Archimedes spiral

$$r = CX.$$

Therefore

$$R_w dY = CX dX$$

or

$$\begin{aligned}
 R &= \frac{C}{R_w} \int_u^{x_1} X dX \\
 &= \frac{CX^2}{2R_w}
 \end{aligned}
 \tag{14.24}$$

since  $X$  is any arbitrary endpoint. Therefore, the output is proportional to the square of the input cam rotation. It should be noted that offsetting the follower wheel from the cam axis would improve the force distribution of the mechanism. For the Archimedes spiral, it can be shown that an offset equal to the lead per radian will permit the follower wheel to be tangent to the spiral at all points. The form of this spiral is an involute.

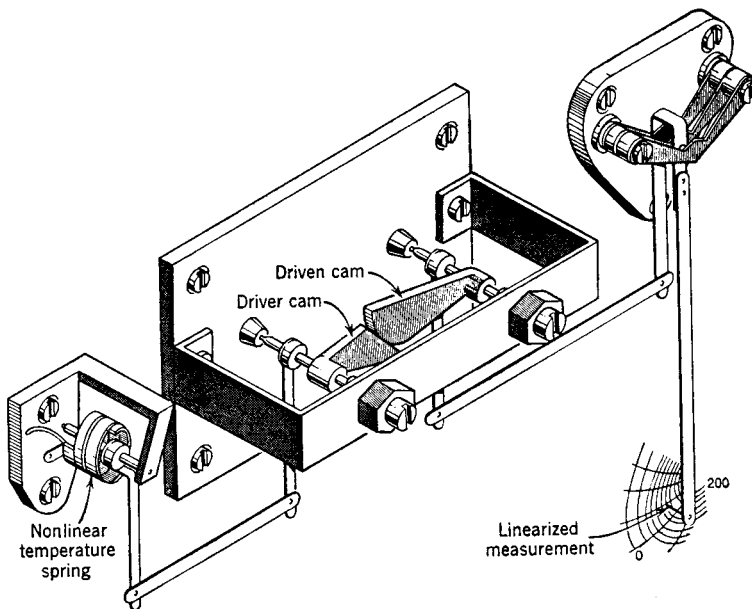
The limitation of the cam discussed occurs when successive turns allow insufficient clearance for the follower. This condition can be remedied by using several cams in series, the output of the first supplying the input to the second. For example, suppose the function to be

$$Y = X^4 = [(X^2)]^2. \tag{14.25}$$

This can be solved by compounding two squaring cams indicated in the equation.

### 14.28.3 Basic Spiral Cam (Nonlinear)

In this section, we discuss the cam and follower contour used in measuring, controlling, and computing equipment (Yavne, 1948 and Lockenvitz et al., 1935). In Fig. 14.47 we see a cam of this type applied to convert a nonlinear temperature function to a linear temper-



**FIGURE 14.47.** Basic spiral cam. (Used in measuring. Linear four-bar linkages transmit motion to and from cams. Gravity holds cams in contact.)

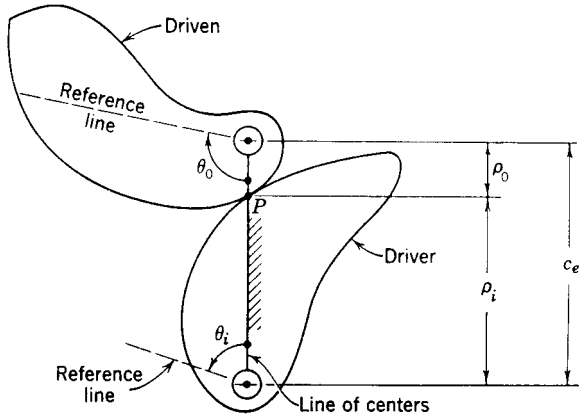


FIGURE 14.48. Basic spiral cam contour.

ature reading. Linear four-bar linkages transmit the motion to and from the cams, which are held in contact by gravity. The basic spiral contour cam mechanism has been used in instrumentation where it was necessary to generate such quantities as trigonometric functions, ballistic functions, logarithms, probability functions, etc. For example, in multiplication, the input is converted to logarithms, added, and then reconverted to a linear scale by antilogs.

This cam contour (Fig. 14.48) is the simplest, most efficient, most accurate means for linearizing input and output shafts where the motion relationship is a nonlinear function. Contacting spirals, which are generally used, have pure rolling action and are reversible. Also, for pure rolling, the contours of one curve must have an increasing radius and those of the other must be a decreasing one. In other words, the curves will not have a minimum or maximum point within the range needed. The surfaces may be plain, have cross-tapes, or have gear teeth.

As stated previously, the given related variables are nonlinear and it is necessary to make scale readings equidistant. For example, measurement of flow of a fluid may be determined by the pressure drop across an orifice. In the control field, the proportional mechanisms for control are linear, and therefore for best results we must again have equal scale measurements. Let us derive the basic relations for this contour. In Fig. 14.48 we see the two curves in contact.

Let

$\theta_0$  = angle rotated by the output driven member, deg

$\theta_i$  = the angle rotated by input driver, deg

$\rho_0$  = radius to point of contact at angle  $\theta_0$ , in

$\rho_i$  = radius to the point of contact at angle  $\theta_i$ , in

$c_e = \rho_0 + \rho_i$  = distance between centers of rotation, in.

Both the radii and the length of periphery are important. Furthermore, as shown for pure rolling action the point of contact  $P$  must lie on the line of centers. We know that the angle of the driven member

$$\theta_0 = f(\theta_i). \quad (14.26)$$

Differentiating,

$$\frac{d\theta_0}{d\theta_i} = f'(\theta_i). \quad (14.27)$$

The velocity of point  $P$  as a point on either body is equal to radius  $\rho$  multiplied by the angular velocity  $d\theta/dt$  of the respective body

$$v_p = \rho_i \frac{d\theta_i}{dt} = \rho_0 \frac{d\theta_0}{dt}.$$

Solving,

$$\frac{d\theta_0}{d\theta_i} = \frac{\rho_i}{\rho_0}. \quad (14.28)$$

Solving Eqs. (14.27) and (14.28) simultaneously and knowing that  $c_e = \rho_i + \rho_0$  gives radii

$$\rho_0 = \frac{c_e}{1 + \frac{d\theta_0}{d\theta_i}} = \frac{c_e}{1 + f'(\theta_i)} \text{ in} \quad (14.29)$$

$$\rho_i = \frac{c_e \frac{d\theta_0}{d\theta_i}}{1 + \frac{d\theta_0}{d\theta_i}} = \frac{c_e f'(\theta_i)}{1 + f'(\theta_i)} \text{ in.} \quad (14.30)$$

Equations (14.29) and (14.30) are the design equations for the contours of mating cams in terms of each radius  $\rho$  and angle  $\theta$ .

It is not necessary that the relationship be represented by any mathematical function. The calculations can be performed by approximations from a table of numerical values.

**EXAMPLE** Find the profile equations for the following exponential relationship where  $A$  and  $B$  are constants:

$$\theta_0 = A e^{\theta_i/B}.$$

**Solution** We know from Eq. 14.26

$$\theta_0 = f(\theta_i).$$

Differentiating the given expression,

$$f'(\theta_i) = \frac{A}{B} e^{\theta_i/B}.$$

Substituting in Eqs. (14.29) and (14.30) gives the radii

$$\rho_0 = \frac{c_e B}{B + \theta_0}$$

$$\rho_i = \frac{c_e \theta_0}{B + \theta_0}.$$

Thus, with the constant given, tables can be established for the cam dimensions to be cut.

### 14.28.4 Basic Spiral Cam Constants

Very often it is necessary to control the contours in which a multiple of  $\theta_0$  is a function of a multiple of  $\theta_i$ . Then it is necessary to compare scales of values. Let the functions

$$R = \frac{\theta_i}{K_i}, \quad S = \frac{\theta_0}{K_0}. \quad (14.31)$$

Differentiating

$$\frac{d\theta_i}{dR} = K_i, \quad \frac{d\theta_0}{dS} = K_0 \quad (14.32)$$

where  $K_i$  and  $K_0$  are arbitrary constants for each of the curves. Dividing

$$\frac{d\theta_0}{d\theta_i} = \frac{K_0}{K_i} \frac{dS}{dR} = \frac{K_0}{K_i} g'(R). \quad (14.33)$$

Equation (14.26) gave  $\theta_o = f(\theta_i)$ ; it is now replaced by  $S = g(R)$ . Substituting Eqs. (14.29) and (14.30) give the radii of the two contacting cams

$$\rho_0 = \frac{c_e}{1 + \frac{K_0}{K_i} g'(R)} \text{ in} \quad (14.34)$$

$$\rho_i = \frac{c_e \frac{K_0}{K_i} g'(R)}{1 + \frac{K_0}{K_i} g'(R)} \text{ in.} \quad (14.35)$$

Equations (14.31), (14.34), and (14.35) yield all the information necessary to construct any cam fulfilling the relation in which  $g'(R)$  does not equal zero. For information on fabrication and cutter location, the reader is referred to the excellent discussion by Hannula (1951).

**EXAMPLE** *It is desired to measure the temperature of a fluid A indirectly by (1) measuring the saturated vapor pressure exerted by another fluid B in a closed system subject to fluid A, and (2) then converting this pressure measurement into a linear temperature scale. The saturated vapor pressure corresponding to the temperature has been found to be of form*

$$P = 10e^{6t_m/(t_m+470)}.$$

*It is further assumed that this pressure can be converted to a uniform angular rotation of a shaft by means of a Bourdon tube or similar device. The range of pressure from 10psi to 60psi will produce a 45.5° movement of the driver cam, and the full-scale range of temperatures (0° to 200°F) will be linear over a 30° span.*

**Solution** *The center distance between the cams is chosen as 3 in, since this is the largest size that is practical within the space limitations. In the equation for the vapor pressure,*

$$P = S \text{ and } 10e^{6t_m/(t_m+470)} = g(R).$$

From Eq. (14.32)

$$K_i = \frac{45.5}{60-10} = 0.91$$

and

$$K_0 = \frac{30}{200-0} = 0.15.$$

From Eq. (14.34)

$$\rho_0 = \frac{3}{1 + \frac{0.15}{0.91} \frac{d}{dt_m} 10e^{6t_m/(t_m+470)}}.$$

Differentiating,

$$\rho_0 = \frac{3}{1 + 1.65 \left[ \frac{2820}{(t_m + 470)^2} \right] e^{6t_m/(t_m+470)}}.$$

Also we know

$$\begin{aligned} \rho_i &= c_e - \rho_0 \\ &= 3 - \rho_0 \quad \text{in.} \end{aligned}$$

From Eq. (14.31)

$$\begin{aligned} \theta_i &= K_i R = 0.91 t_m \text{ deg} \\ \theta_0 &= K_0 S = K_0 g(R) = 1.5 e^{6t_m/(t_m+470)}. \end{aligned}$$

These equations give the information necessary for the cam construction. It is necessary to substitute values of temperature  $t_m$  to determine the corresponding radii  $\rho$  and cam angles  $\theta$ . It is conventional to use a tabular notation.

## REFERENCES

- 
- Cheng, C.Y., and Lin, Y.Y., "Improving Dynamic Performance of the Geneva Mechanism Using Non-linear Spring," *Mech. Mach. Theory* 30 (1): 119–29, 1995.
- Dresner, T.L., and Barkan, P., *A Review and Classification of Variable Valve Timing Mechanisms*, SAE Paper No. 890674, *SAE Transactions*. Vol. 98, Sec. 3, *Journal of Engines*, 1278–89, 1989.
- Erdman, A.G., and Sandor, G.N., *Mechanism Design*, Vol. 1, third edition, Prentice Hall, Upper Saddle River, N.J., 1984.
- Fenton, R.G., Zang, Y., and Ku, J., "Development of a New Geneva Mechanism with Improved Kinematic Performance," *J. Mech. Design* 116 (2): 369–74, 1994.
- Freudenstein, F., and Sandor, G.N., *Kinematics of Mechanisms in Mechanical Design Handbook*, Sec. 3, H. Rothbart, Ed., McGraw-Hill Book Company, New York, 1986.

- Fry, M., "Designing Computing Mechanisms, Part III, Cam Mechanisms," *Mach. Des.* 17: 123, October 1945.
- Grodzinski, P., *A Practical Theory of Mechanisms*, Emmott & Co., Manchester, England, 1947.
- Hannula, F.W., "Designing Non-Circular Surfaces," *Mach. Des.* 23: 141, July 1951.
- Jacobs, R.J., "Indexing with Concave Barrel Cams," *Mach. Des.* 25: 197, December 1953.
- Jones, F.P., *Ingenious Mechanisms for Designers and Inventors*, Industrial Press, New York, Vol. 1, 1930; Vol. 2, 1936; Vol. 3, 1951; Vol. 4, 1967.
- Lichtwitz, O., "Mechanisms for Intermittent Motion," *Machine Design* 23: 134, December 1951; 24: 127, January 1952; 24: 146, February 1952; 24: 147, March 1952.
- Lockenvitz, E., Oliphant, J.B., Wilde, W.C., and Yong, J.M. "Geared to Compute," *Customation* 2: 37, August 1935.
- Neklutin, C.N., "Designing Cams for Controlled Inertia and Vibration," *Mach. Des.* 25: 255, April 1953.
- Peyrbrune, H.E., "Application and Design of Non-Circular Gears," *Mach. Des.* 25: 185, December 1953.
- Richards, W., "The Harmonic Motion Cam of Equilateral Triangular Form," *Mach. London* 57: 231, November 28, 1940.
- Richards, W., "The Triangular Harmonic Motion Cam with Square-Frame Follower," *Mach. London* 57: 303, January 9, 1941.
- Shaw, F.W., "Equations for the Design of Involute Cams," *Prod. Eng.* 4: 131, April 1933.
- Shaw, F.W., "Dwell Cams of Uniform Diameter," *Mech. World* 98: 329, October 4, 1935.
- Svoboda, A., *Computing Mechanisms and Linkages*, first edition, McGraw-Hill Book Company, New York, 1948.
- Yavne, R.D., "High Accuracy Contour Cams," *Prod. Eng.* 19: 134, August 1948.

*This page intentionally left blank.*

---

# CHAPTER 15

---

# CAMS IN MICROELECTROMECHANICAL SYSTEMS

---

**G. K. Ananthasuresh, Ph.D.**

*Assistant Professor of  
Mechanical Engineering and Applied Mechanics  
University of Pennsylvania, Philadelphia, Pa.*

15.1 SCOPE OF THE CHAPTER	505	15.6.3 Mechanical Lock I—Spiral Groove Cam	516
15.2 BACKGROUND ON MEMS	506	15.6.4 Micromechanical Lock II—Translating Groove Cam	518
15.3 MATERIALS FOR MEMS	507	15.6.5 Counter-meshing Gear Discriminator Device	518
15.4 MANUFACTURING OF MEMS	508	15.6.6 Microvibromotor with an Inverse Cam	520
15.5 MICROMECHANICAL TRANSMISSION	510	15.7 ACTUATORS FOR MICRO CAMS	521
15.5.1 In-Plane Revolute Joints	511	15.7.1 Electrostatic Micromotors	522
15.5.2 Out-of-Plane Revolute Joints	512	15.7.2 Electrostatic Comb Drive	523
15.5.3 Linkages	512	15.7.3 Sandia's Microengine	524
15.5.4 Gears	512	15.7.4 Other Actuators	524
15.5.5 Compliant Mechanisms	513	15.8 FRICTION AND WEAR AT THE MICROSCALE	525
15.6 CAMS IN MEMS	514	15.9 SUMMARY	527
15.6.1 Microindexing Motor with a Wedge Cam	514		
15.6.2 Torsional Ratcheting Microactuator	514		

---

## 15.1 SCOPE OF THE CHAPTER

---

Even though the word *mechanical* is prominently featured in the acronym MEMS (micro-electromechanical systems), truly mechanical applications of MEMS are still in their infancy. While it is true that moving solids and fluids, as opposed to moving electrons, distinguish MEMS from microelectronics, the research activities and applications of MEMS until now have been mostly focused on microtransducers that include microsensors and actuators. Surface contact between moving structural members is avoided or minimized in microtransducers. In this chapter, the focus is on MEMS devices with mechanical transmissions where such a contact is necessary. To make the chapter self-contained, some background on MEMS and the materials and microfabrication processes used to make them are included. A general discussion of mechanical manipulation at the micro scale is presented to describe the basic elements such as joints and also to identify the needs and challenges. There has not yet been widespread use of cams in MEMS. Since cams and gears are similar in action and to broaden the notion of cams, gear transmissions are included in this chapter in addition to devices based on the usual cam action. Micro-actuators and tribological issues, which are relevant for future application of cams in MEMS, are also discussed.

## 15.2 BACKGROUND ON MEMS

---

The field of microelectromechanical systems (MEMS), as it is called in the United States, or microsystems technology (MST), as it is called in Europe and elsewhere, deals with devices that are in the size range of micrometers. To appreciate the size of MEMS, consider the size of traditional macroscale machines, which can be seen with the naked eye and are manufactured using traditional machining methods. Some critical dimensions of the macromachinery can be very small (at the micrometer or even nanometer level), especially when they are used as precision instrumentation. Even in those cases, they are not called micromachinery or MEMS because in the micro category the general dimensions, not just the smallest and critical dimensions, are in the size range of microns. In MEMS, based on the current microfabrication technologies, the smallest dimension can be one-tenth of a micrometer and the overall size of the device can be of the order of millimeters and sometimes even a centimeter. In recent years, there has been significant interest in nanoscale systems. This third category is clearly different from MEMS just as MEMS is different from macromachinery. In nanoscale devices, the general dimensions are in the range of nanometers, and the smallest dimension can be as small as a few atoms across. Thus, this category of devices is sometimes called molecular machinery. MEMS is therefore in between macro- and nanoscale devices.

The MEMS technology is more than mere miniaturization of the macroscale devices and systems. MEMS devices are not only smaller but are also more functional, faster, and cheaper than their macro counterparts. The reasons for enhanced functionality are twofold. First, there are advantages when some physical, chemical, and biological devices are scaled down to the micro level. An example of this comes from numerous ways of modulating light using microoptomechanical devices comprising mechanical structures with feature sizes and movements in the range of wavelengths of visible light. Likewise, microchemical reactors make it easier to have an extremely well-controlled environment for the reaction to take place and also lead the way to distributed microreactor arrays. Second, complete integration of sensors, actuators, electronics, and components made of movable solids and fluids is possible to an unprecedented degree. This integration does not refer to just an assembled final product composed of a variety of subsystems but to a truly integrated product that is conceived, designed, and fabricated in a unified manner. Furthermore, MEMS devices can usually be operated at higher speeds than macrodevices because of the way in which their inertia, stiffness, and time constants of various phenomena scale when the size is decreased.

The micron-scale size of MEMS devices can be mainly attributed to the choice of material and the fabrication processes used to make them. They could be made, for example, 10 to 100 times larger while still retaining their functional advantages over macrodevices. However, the MEMS field has its origins in microelectronics, as it was natural to make micromechanical components using the same fabrication processes used to make integrated chip (IC) circuits. The economical benefits of MEMS devices are a direct consequence of batch fabrication and of the well-developed microfabrication techniques of the IC industry. As the MEMS field progressed rapidly from the late eighties, traditional microfabrication techniques for MEMS have been substantially enhanced and a number of new techniques have been developed specifically for MEMS.

The study of MEMS began with applications and is advancing rapidly with an increasing number of applications in a wide range of fields. In the mid-1960s, researchers at Westinghouse Research Laboratories developed a *resonant gate transistor* that used gold beams that are only 100 microns long. Miniaturized pressure sensors using silicon were built even before that. In the 1960s and 1970s, a number of sensors and devices that used movable micromechanical elements were developed. Tuning forks, accelerometers, projection dis-

plays, light modulators, switches, gas chromatographs, etc., are some of the many devices that appeared in that period. Some of these pioneering works are described in Trimmer (1990). An excellent review article (Petersen, 1982) also has a good description of the early applications of MEMS and the manufacturing techniques used to make them. Today, commercial applications of MEMS are in inertial measurement devices such as accelerometers and gyroscopes; microoptical devices such as displays; telecommunication devices such as mechanical filters, aligners, and switches; microfluidic devices such as valves, pumps, flowchannels for biochemical lab-on-a-chip devices, and ink-jet printer heads, to name a few. Many other applications have emerged and are likely to enter the commercial market in the near future.

From a mechanical perspective, the principle of operation of most MEMS devices is rather simple. For example, a micromechanical accelerometer consists of an inertial mass suspended with an elastic structure. It can be as simple as a cantilever with a mass attached to its free end. The movement of the mass is measured by one of a variety of means and is used to estimate the acceleration of the body on which the device is mounted. A typical MEMS pressure sensor consists of a membrane that deflects in response to increased pressure. Its deformation is measured using a transduction technique to estimate the pressure. The same membrane when actuated in a controlled manner can be used as a pump. A system of vibrating masses attached to each other with beams serves as a mechanical filter. Flat structures attached to beams that twist act as micromechanical mirrors used in projection displays. The majority of MEMS devices developed until now use very simple mechanical structures (beams, membranes, and plates) that elastically deform. Thus, the significance of such devices lies not in their mechanical structure but in the transduction scheme based on physical, chemical, and biochemical phenomena and of course micromachining. A sourcebook on micromachined transducers (Kovacs, 1998) describes them comprehensively. In contrast, the emphasis in this chapter is on those MEMS devices in which there is relative motion and motion and force transmission among rigid bodies with intermittent or sustained contact. Whether elastic deformation is used or rigid-body motion is used, materials and the processing techniques play a crucial role in the development of MEMS. These two are discussed in the following two sections.

### **15.3 MATERIALS FOR MEMS**

---

Silicon has turned out to be an excellent mechanical material, and it has played a key role in the development of MEMS technology so far. A number of other materials are also appearing in MEMS devices. The choice of a material depends largely on the fabrication technology used to make MEMS devices. In this respect, the development of MEMS materials and fabrication processes can be divided into four phases (NRC, 1997). The first phase consisted of the early years (1965 to 1985) when “old” materials and “old” processes of microelectronics were used to make MEMS devices. These materials were silicon, oxide and nitride, quartz, and some metals. The processes were deposition and photolithography-based etching of thin films. In the second phase, microelectronic processes were developed further into new micromachining processes but still used the old materials. The new processes include a sacrificial layer that enable the fabrication of releasable structures, bulk etching techniques that can also create releasable structures, some wafer-bonding techniques, and deep lithography and micromolding techniques. The third phase used “new” materials such as polymers, ceramics, metals, and some active materials but processed them with existing “old” techniques. The fourth phase will be to develop new processes for these new materials. The MEMS field is now in the third phase

and future developments constitute the fourth phase. A few commonly used MEMS materials are described next.

Single-crystal silicon is commercially available in the form of circular wafers of diameters ranging from 2 in to 12 in and thicknesses in the range of a few hundred microns. Selective chemical etching is used to carve out features in silicon wafers. The wafers are available in a number of crystallographic orientations, which are important when chemically etching patterns on them. Polycrystalline silicon, often called *polysilicon* or simply *poly* in the MEMS literature, is also used extensively as a structural material for MEMS devices. Polysilicon is deposited as a thin film on top of a substrate (e.g., the silicon wafer) using chemical vapor deposition or other techniques. In addition to being used as a structural material, polysilicon is also used to form electronic elements such as resistors, conductors, and ohmic contacts to crystalline silicon structures.

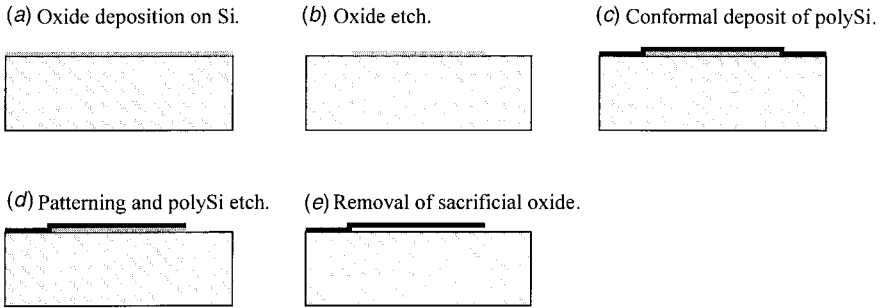
Several compounds of silicon are useful in the fabrication and operation of MEMS devices. Silicon dioxide is used as a dielectric material for electrical insulation. It is also useful in the fabrication of MEMS devices as a sacrificial layer in creating multilayered structures with movable parts. It can be either grown by thermal oxidation or deposited using a variety of methods. Silicon nitride is another useful dielectric material. It is also used as a structural material in some applications. It is usually deposited using chemical vapor deposition. Both silicon dioxide and silicon nitride are used as masks for etching silicon because many etchants are available that selectively etch only silicon but not the oxide and nitride. Silicon carbide is useful as both a dielectric material and structural material. Due to its extreme hardness, its ability to operate in high temperature, high-power, and high-radiation environments, and its resistance to chemical attack, silicon carbide, is becoming a very important material for MEMS applications in the automobile, aerospace, and power generation industries.

In addition to silicon and its compounds, metals, ceramics, and polymers are also used in MEMS. Many metals (e.g., aluminum, nickel, copper, gold) have been in use at the microscale for a long time, whereas ceramics and polymers are more recent additions to the repertoire of MEMS materials. Several active materials, such as piezoelectric, ferroelectric, conducting polymers, shape-memory alloys, etc., are also making their way into MEMS devices. These new materials call for new manufacturing techniques to make MEMS economically viable and functionally better than previous devices. Some established micromachining techniques as well as some new ones are briefly described in the next section.

## 15.4 MANUFACTURING OF MEMS

---

As in any field, it is important to know how the devices are manufactured in order to model and design them effectively or to conceive new device concepts. In a developing field like MEMS, manufacturing techniques are numerous and varied. However, they can be broadly classified into four categories: *surface micromachining*, *bulk micromachining*, *micro-molding techniques*, and *miscellaneous micromanufacturing techniques*. The first two categories are especially applicable to silicon and its compounds. Thin-film deposition, photolithography, and selective etching are the primary tools for micromachining. In photolithography, optically sensitive polymers called photoresists are exposed through a photomask consisting of transparent and opaque regions. Exposed or unexposed regions in the photoresist can be selectively washed away, leaving a photoresist mask through which a material underneath the mask can be selectively etched. Film deposition and etching by means of masks make micromachining techniques particularly suitable for batch production, as of IC chips. Many new techniques do not use photolithography and are not always amenable for batch production.



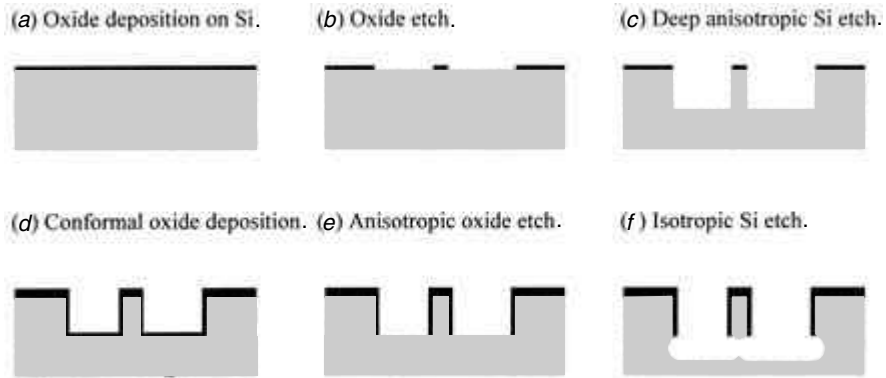
**FIGURE 15.1.** A simple cantilever example to illustrate the surface micromachining process.

In surface micromachining, thin films are deposited on a thick substrate wafer and etched using photolithographic masks to define patterns in the deposited layers. By alternating deposition and etching, several layers of different materials can be stacked to create intricate microstructures. Since lithography requires flat surfaces and the thickness of an individual layer is limited to a few microns compared to the size of the wafers (usually 2, 3, 4, 6, 8, and 12 inches in diameter), MEMS devices are generally very flat structures. In this sandwich construction, some sacrificial layers are included so that they can be dissolved at the end to create releasable (i.e., movable) mechanical structures. Figure 15.1 illustrates the surface micromachining process with a single sacrificial layer and a single movable structural layer. Multilayered structures with alternating structural and sacrificial layers can be obtained in a similar manner. MUMPs, Multi-User MEMS Processes, which were successfully made available as a foundry process for MEMS by the Microelectronic Center of North Carolina, is an example of a multilayered surface micromachining process. SUMMiT, Sandia Ultra-planar Multi-level MEMS Technology,\* process is another example. While MUMPs consisted of three structural layers, SUMMiT consists of four or five with added steps of planarization in between. Many of the devices described in Sec. 5 of this chapter are made using the SUMMiT process.

In contrast to surface micromachining, in bulk micromachining a bulk wafer whose thickness is of the order of a few hundred microns is sculpted using etching techniques to define the structures. Bulk micromachining also uses deposition and etching of thin films, but the primary feature creation is due to the substantial etching of the substrate wafer. When etched through large depths, the distinction between isotropic and anisotropic etches becomes important. Some chemicals etch certain materials equally in all directions and are called isotropic etchants for those materials, while others have different etch rates in different directions and create anisotropically etched surfaces. Both isotropic and anisotropic etches are effectively used in MEMS devices depending on the desired geometry. Since the substrate wafer is etched to a large depth, bulk micromachined MEMS devices tend to be much (about 10 times) thicker than the surface micromachined structures. A sample bulk micromachining technique is illustrated in Fig. 15.2.

One disadvantage with traditional bulk etching of silicon in building very thick microstructures (up to a few hundred microns) is the lack of vertical sidewalls of etched surfaces. While isotropic etches lead to curved sidewalls, some anisotropic etches lead to slanted surfaces, and both are undesirable in many applications. The shape of the lithographic mask and the shape of the etched pit as viewed from the top of the wafer are also

\*Sandia National Laboratory, [www.mems.sandia.gov](http://www.mems.sandia.gov)



**FIGURE 15.2.** An example of the bulk micromachining process called SCREAM (Single Crystal Reactive Ion Etching and Metallization) developed at Cornell University (metallization step is not shown here).

often very different in such cases. This is a problem when mechanical parts of complex geometry such as compound gears or compliant structures with sufficient out-of-plane stiffness are desired. To meet these and other needs, deep-vertical lithography was developed. A deep x-ray lithography-based micromolding process called LIGA (a German acronym), for example, enables microstructures as tall as 1 mm without compromising the lateral feature resolution. HEXIL is another type of molding process in which the molds are created with a photoresist material. Deep reactive ion etching (DRIE) is another widely used process to manufacture thick microstructures.

In addition to the above three categories of processes, several others span a wide variety of techniques. These include electrodischarge machining; electrochemical grinding; machining with laser, electron, and focused-ion beams; ultrasonic machining; abrasive jet machining; electro- and electroless plating, etc. A detailed description of various microfabrication techniques can be found in Madou (1998). Soft lithography, which is quite different from the traditional photolithography, is emerging as a promising technique for polymer material used in MEMS. In soft lithography, a “stamping mold” is made using a polymer material with patterned relief and is used to transfer the pattern of a coated material by stamping onto a surface. This technique is particularly useful for microfluidic and biotechnology applications.

Having described the essential features of MEMS devices, namely applications, principles of operation, materials, and manufacturing techniques, our attention now shifts to the main focus of this chapter, mechanical transmission at the microscale.

## 15.5 MICROMECHANICAL TRANSMISSION

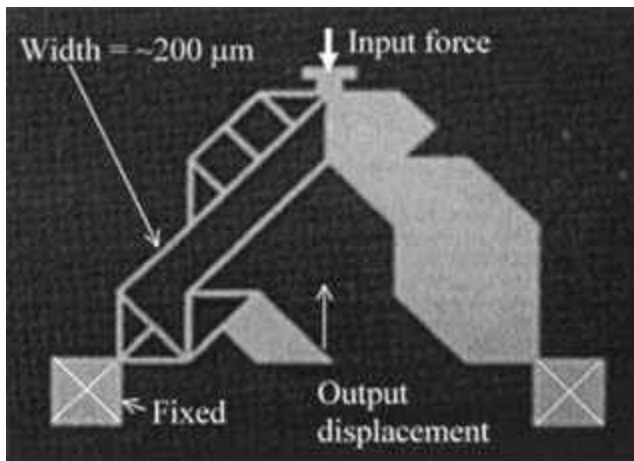
In most existing MEMS devices, mechanical elements are used for transduction. The capacitive micropressure sensor is a good example wherein mechanical pressure is converted to an electrical signal by means of a two-plate capacitor formed by a fixed electrode and deformable membrane that acts like the second electrode. In this and many other similar applications, mechanical transmission is not critical, as the mechanical elements

need to move or deform elastically in very simple ways. Thus, controlled and coordinated movement of mechanical elements is not usually required. Even when such movement is required, it is quite simple, such as holding a clamped-clamped beam in different deformed configurations. In microfluidics, fluid is moved in a controlled manner through microchannels for which valves and pumps are necessary. The mechanical structures in these are also not subject to sophisticated mechanical movement. Manipulating light beams is one application in MEMS that requires mechanical transmissions to a limited extent. A commercially available MEMS-based projection display system from Texas Instruments uses an array of micromirrors, each of which can be individually tilted between two angles about an axis. This is an example of microoptomechanical systems where mechanical movement is quite simple. There are some others, optical workbenches for example, where reasonably sophisticated mechanical movements are necessary.

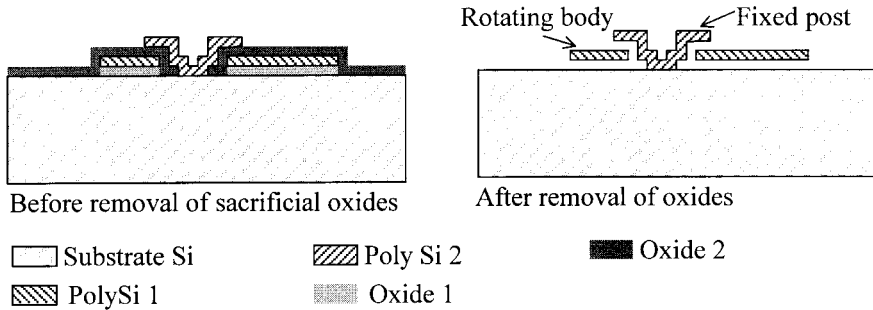
Many types of actuators use mechanical movements but those are usually quite simple, such as rotation about an axis or sliding along an axis. Compliant mechanisms (i.e., elastically flexible structures) are used widely in MEMS for achieving mechanical movements. These are referred to as rigid-link jointed mechanisms because of the ease of fabrication as a unitized structure without assembly. An example of a compliant mechanism is shown in Fig. 15.3. Several microgrippers are also demonstrated but the extent of mechanical movement in them is also quite limited. Micromechanical locks developed by Sandia National Laboratories for weapons-safety systems is a MEMS device that has substantive mechanical complexity. Some devices developed for microassembly and manipulation of micron-sized objects also exist. In the remainder of this section, generic joints, gears, and some mechanisms are described. These serve as ancillary parts to the MEMS devices built using cams. Specific applications involving cams and gears are described in detail in Sec. 15.6.

### 15.5.1 In-Plane Revolute Joints

A revolute joint whose axis is perpendicular to the wafer surface is necessary for fabricating micromechanisms with in-plane motion. Microfabricating such a joint without



**FIGURE 15.3.** A laser-micromachined displacement amplifying compliant micromechanism made using an index-card.



**FIGURE 15.4.** Formation of an in-plane revolute joint using surface micromachining.

assembly was a critical development in the MEMS field. Fan, Tai, and Muller at the University of California–Berkeley Sensor and Actuator Center first accomplished it using a sacrificial layer-based surface micromachining process in 1986 in their efforts to make a rotary electrostatic micromotor. A group at the Massachusetts Institute of Technology also accomplished this at the same time using very similar design and processing techniques. The schematic of this joint is shown in Fig. 15.4. A floating (as opposed to being fixed to the substrate) in-plane joint is also possible. The in-plane revolute joints are useful for mounting cams to the substrate or to a moving member.

### 15.5.2 Out-of-Plane Revolute Joints

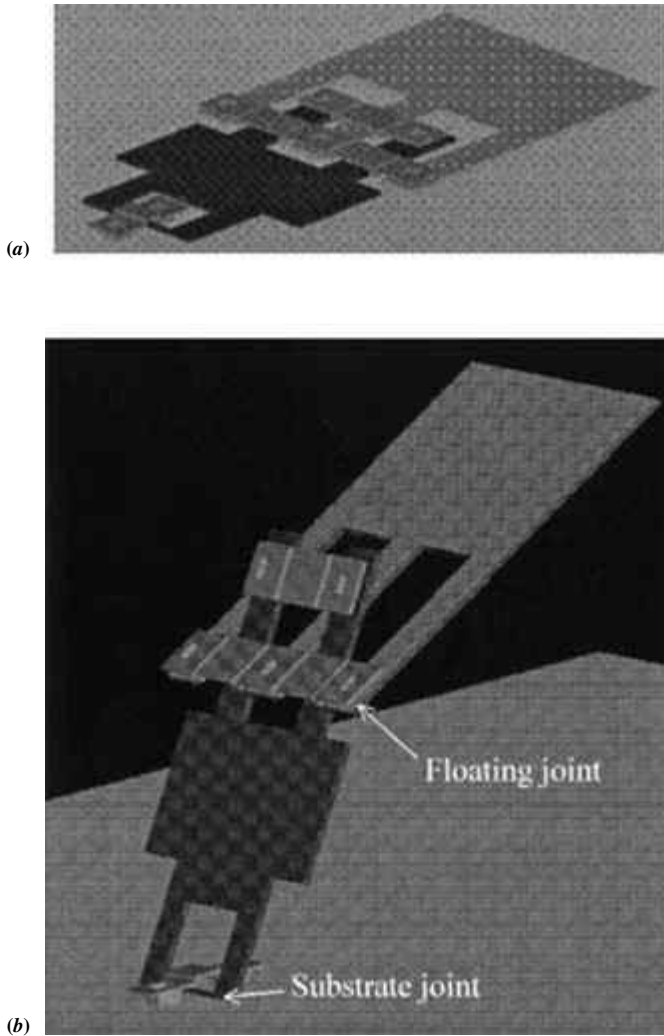
Microfabricating an out-of-plane revolute joint was another important milestone. K. Pister of Berkeley Sensor and Actuator Center accomplished this by cleverly using a sacrificial layer in the surface micromachining process. The schematics of substrate and floating joints are shown in Fig. 15.5. These joints can be used in conjunction with cams to achieve out-of-plane mechanical movement.

### 15.5.3 Linkages

A number of micromachined in-plane and out-of-plane linkages consisting of revolute joints and sliders have been demonstrated. One practical application used these in conjunction with gears and some cams to create micromechanical locks. Another application is integrated optics-on-a-chip wherein light beams can be manipulated and modulated using movable mechanical structures. A few specific linkages and mechanisms are described in Sec. 15.6.

### 15.5.4 Gears

Several micromachining processes can be used to make gears and racks in assembled or nonassembled form from the micron scale up to the millimeter scale. A proper involute profile for gear teeth is possible in photolithography masks, and deep etching techniques give reasonably smooth vertical surfaces for teeth. This means that cams also can be made easily using micromachining processes. However, cams are not yet used in MEMS in the traditional way but alternate manifestations of cams do exist. These are discussed in Sec. 15.6.



**FIGURE 15.5.** Solid models of out-of-plane surface micromachined substrate and floating revolute joints (a) as fabricated (b) after movement.

### 15.5.5 Compliant Mechanisms

At the microscale, an alternative to rigid-body jointed mechanisms is a compliant mechanism that relies on elastic deformation of a structural continuum. Figure 15.3 illustrates an example. As shown in this figure, assembly is not required to make compliant mechanisms and therefore they are well suited for MEMS applications. In fact, compliant structures such as beams and membranes are ubiquitously found in existing MEMS devices. More sophisticated mechanical motion is also possible with compliant mechanisms. Applications of this at the microscale are emerging in microoptomechanical

systems, microsurgery, microassembly, and micromanipulation of small objects such as single biological cells, to name a few.

## 15.6 CAMS IN MEMS

---

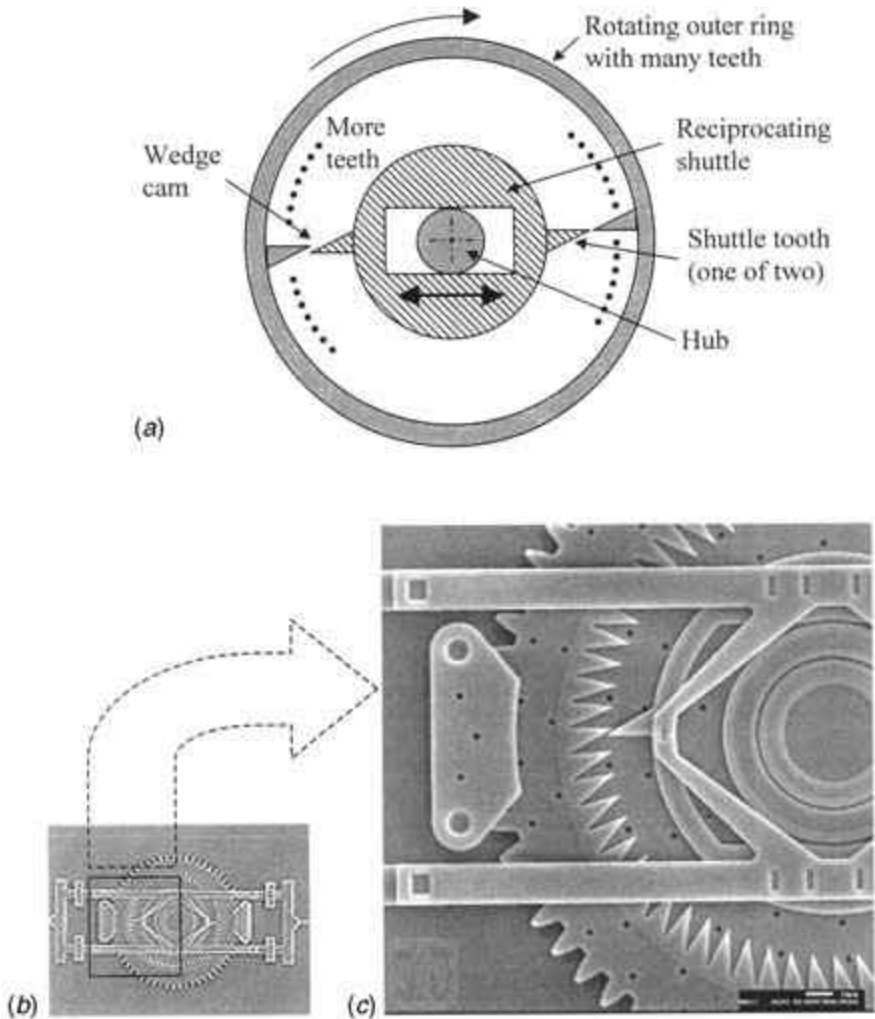
A few specific MEMS devices consisting of cams and gears will be described in this section. As stated earlier, cams used in MEMS do not belong to the same category of cams used in traditional cam-follower type mechanisms because of the entirely different objective of MEMS, which so far has been primarily transduction rather than mechanical transmission. When sophisticated, coordinated mechanical movement finds applications at the microscale level and some of the practical problems of friction and wear (discussed in Sec. 15.8) are better understood and remedied, we can expect to see more cams in MEMS. As can be seen in the examples presented later, the scope of cams is somewhat expanded in this presentation. Nevertheless, they all possess the essential features of cam-action in that the motion and force transmission take place by virtue of line or point contact between rigid bodies. In each of the devices, an association is made to a traditional cam. This may be debatable in some cases but the connection to traditional cams is necessary to promote the use of cams in MEMS.

### 15.6.1 Microindexing Motor with a Wedge Cam

The schematic in Fig. 15.6*a* shows the principle of operation of a mechanical stepper motor designed and fabricated at the Sandia National Laboratories using the SUMMiT process (Allen and Schriener, 1998). This serves as an actuator with precise indexing capability, which is useful in positioning applications in MEMS devices. It is a multilayered structure composed of an outer ring, a reciprocating shuttle, a central post, and a linear actuator for the shuttle. These components are designed in such a way that they do not interfere with each other when they move. As shown Fig. 15.6*a*, as the shuttle with two indexing teeth reciprocates from left to right, the wedge action between the two shuttle teeth and many internal teeth on the outer ring makes the outer ring rotate. Only two internal teeth on the outer gear are shown in Fig. 15.6*a* although, as indicated, many other exist. At any given time, only one shuttle tooth interacts with a single internal tooth. The shuttle is driven by a linear electrostatic comb drive, which is described in Sec. 15.7.2. A microscale prototype in which the diameter of the ring gear is about  $250\ \mu\text{m}$  with 63 internal teeth is shown in Fig. 15.6*b*. It indexes by  $2.85^\circ$  per step. An operational speed of 205 steps per second was observed. At higher speeds of operation, the indexing tooth showed a tendency to bounce over the internal teeth. It is reported that this can be overcome by adding a cover over the internal teeth, which can be easily accommodated in the SUMMiT process.

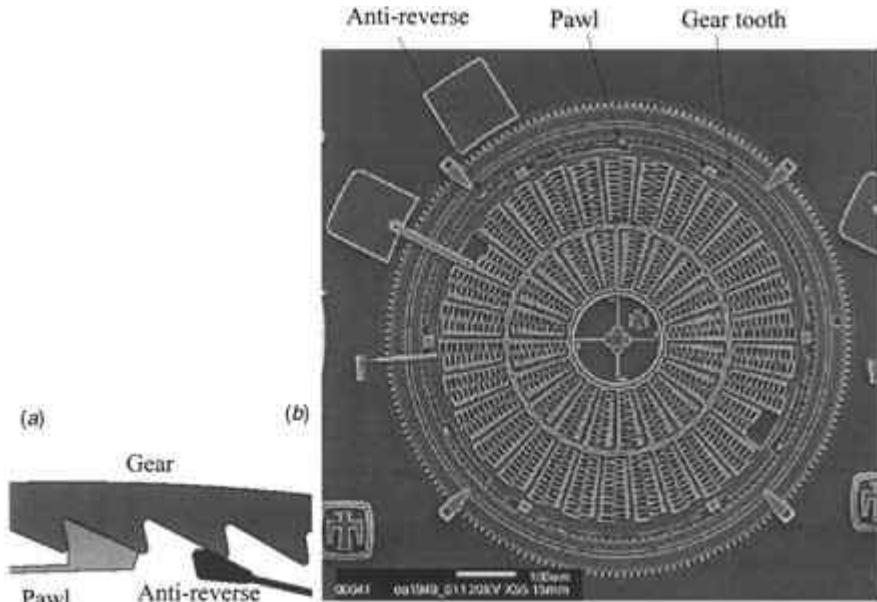
### 15.6.2 Torsional Ratcheting Microactuator

Sandia researchers have also developed a novel actuator, called an electrostatic torsional ratcheting actuator, that is compact and easy to operate and provides accurate position control without feedback. It consists of an angular comb drive with interdigitated electrostatic comb actuators, a pawl, a ring gear with ratcheting teeth, and an antireverse (see Fig. 15.7*a*). The antireverse is attached to the fixed frame by means of a flexible beam, and the pawl is attached to the angular electrostatic comb drive with a flexible beam, while the ring gear is free to rotate in the counterclockwise direction. When the angular comb



**FIGURE 15.6.** Indexing (wedge-cam) motor (a) schematic showing the principle of operation, (b) and (c) scanning electro microscope (SEM) picture of the microfabricated prototype (courtesy, Sandia National Labs—MEMS, S&T Department, [www.mems.sandia.gov](http://www.mems.sandia.gov)).

drive is rotated by  $2.5^\circ$  counterclockwise, the pawl engages the inner teeth of the ring gear and rotates it counterclockwise. When the comb drive is deactivated, its torsional spring attached to the comb drive restores it to its start orientation, which disengages the pawl. The antireverse prevents the gear from rotating clockwise. The outer involute teeth of a ring gear drive a load. A SEM image of the prototype is shown in Fig. 15.7b. Although this design intended that the gear advance by one tooth for one cycle of the oscillating angular comb drive, the fabricated microprototype exhibited some overrun caused by the impact between the pawl and the ring gear. The impact made the gear jump by two or more teeth. Therefore, an antioverrun and a riser were added in the modified design.

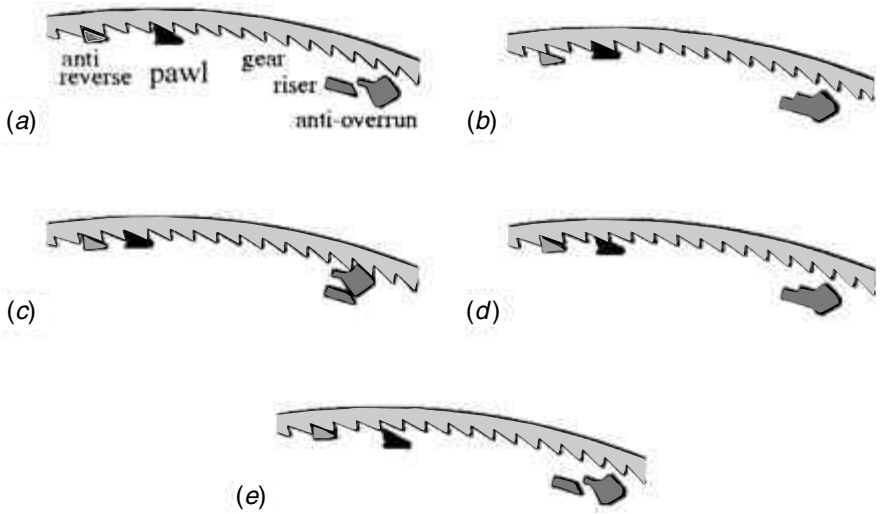


**FIGURE 15.7.** Torsional ratcheting actuator (a) schematic (courtesy, Elisha Sacks, Purdue University) (b) microfabricated prototype (courtesy, Sandia National Labs—MEMS, S&T Department, [www.mems.sandia.gov](http://www.mems.sandia.gov)).

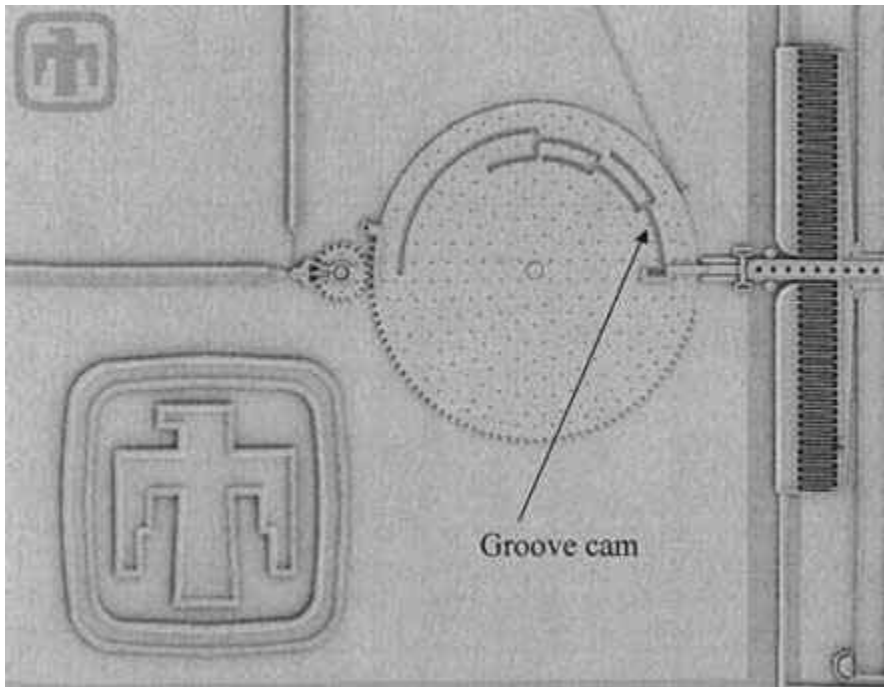
In the modified design, a riser is attached to the fixed frame and an antioverrun is attached to the comb drive with a revolute joint. A sequence of images shown in Fig. 15.8 illustrates how the modified design works. The pawl rotates with the comb drive, engages the inner teeth of the gear (Fig. 15.8*b*), and rotates it counterclockwise (Fig. 15.8*c*). The antioverrun rotates with the driver, rides over the riser (Fig. 15.8*b*), engages the gear (Fig. 15.8*c*), and prevents further gear motion. When the comb drive is deactivated, torsional springs restore it to its start position, which disengages the pawl and the antioverrun (Fig. 15.8*d* and 15.8*e*). As before, the antireverse prevents the gear from rotating clockwise. This design modification was analyzed and verified using a kinematic analysis and tolerancing software (Sacks and Barnes, 2001).

### 15.6.3 Mechanical Lock I—Spiral Groove Cam

A mechanical locking device has been developed by Sandia researchers for applications where access to or activation of some crucial components should not occur until a certain sequence of events takes place. In the device shown in Fig. 15.9, a pin runs through a maze in a specific way to unlock another component. As shown in the figure, the large gear has a spiral groove that has radial and circumferential segments. The gear is driven by Sandia's electrostatic microengine (described in Sec. 15.7.3) through a pinion that can be seen in Fig. 15.9. The pin is attached to a linear electrostatic comb drive to allow radial movements. The rotation of the large gear and the radial movement of the pin are to be coordinated in a specific manner to let the pin run through the spiral groove from the beginning to the end. Only then can the gear rotate by some angle to release a latch to activate



**FIGURE 15.8.** Schematic illustration of the modified design of Fig. 15.7a with an anti-overrun (courtesy, Elisha Sacks, Purdue University).



**FIGURE 15.9.** A micromechanical lock with a spiral groove cam (courtesy, Sandia National Labs—MEMS, S&T Department, [www.mems.sandia.gov](http://www.mems.sandia.gov)).

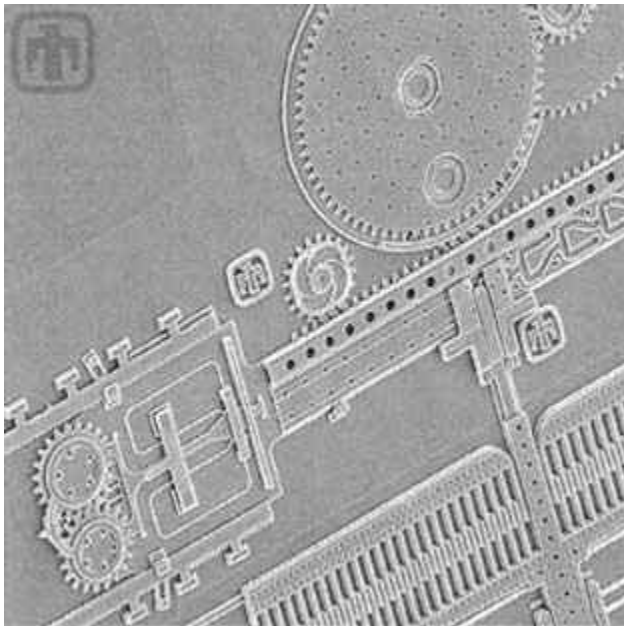
another component. If a wrong decision is made during the sequence, the pin gets stuck in the wheel. This device is equipped with an antireverse spring so that an incorrect sequence cannot be corrected by trial and error. A modified design with a translating groove cam is discussed next.

#### 15.6.4 Micromechanical Lock II—Translating Groove Cam

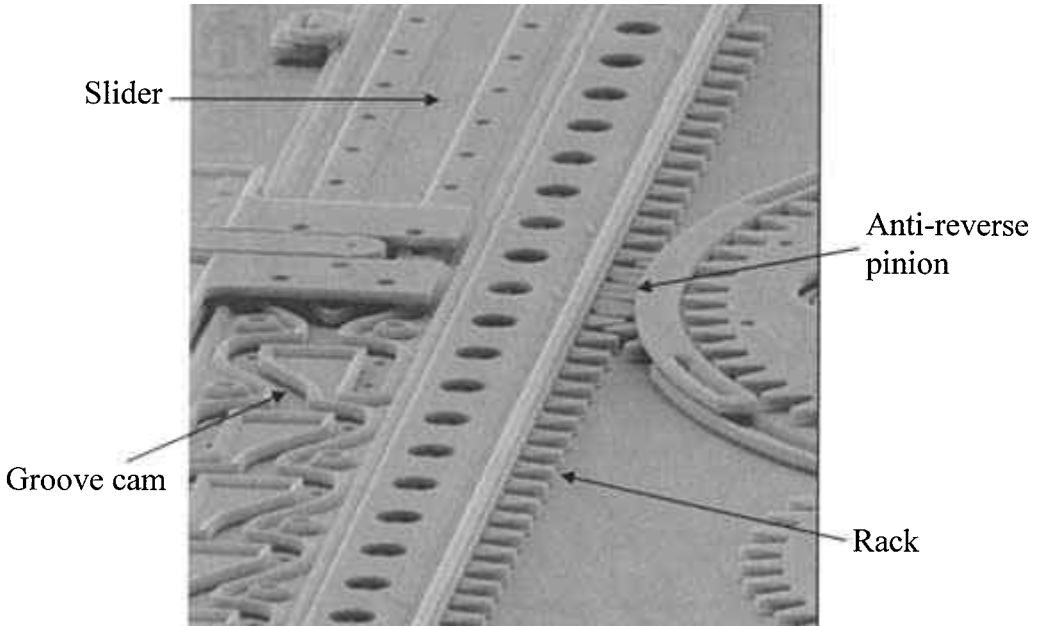
The mechanical lock shown in Fig. 15.10*a* is more sophisticated than the one just discussed. It has a slider in which there is a groove cam. The slider also has rack teeth so that it can be actuated. A pin runs in the groove and is actuated with an electrostatic comb drive. The slider is engaged with an antireverse pinion to prevent backtracking. The independent actuations of the slider and the pin are coordinated to permit the slider to move its entire course and to release another component. A detailed view of the groove cam is shown in Fig. 15.10*b*.

#### 15.6.5 Countermeshing Gear Discriminator Device

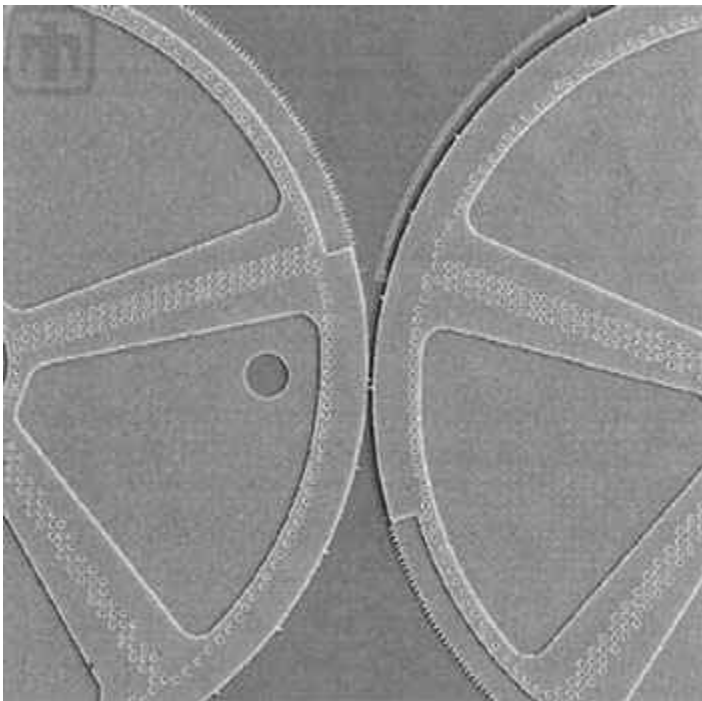
Another MEMS device that acts like a mechanical lock is the gear discriminator shown in Fig. 15.11*a*. It has three levels of gears with some teeth missing on each of them and the remaining teeth selectively placed. These gears countermesh in the sense that the meshing gear teeth approach each other from opposite directions, unlike conventional gears where the approach for both teeth is in the same direction. Consequently, they need



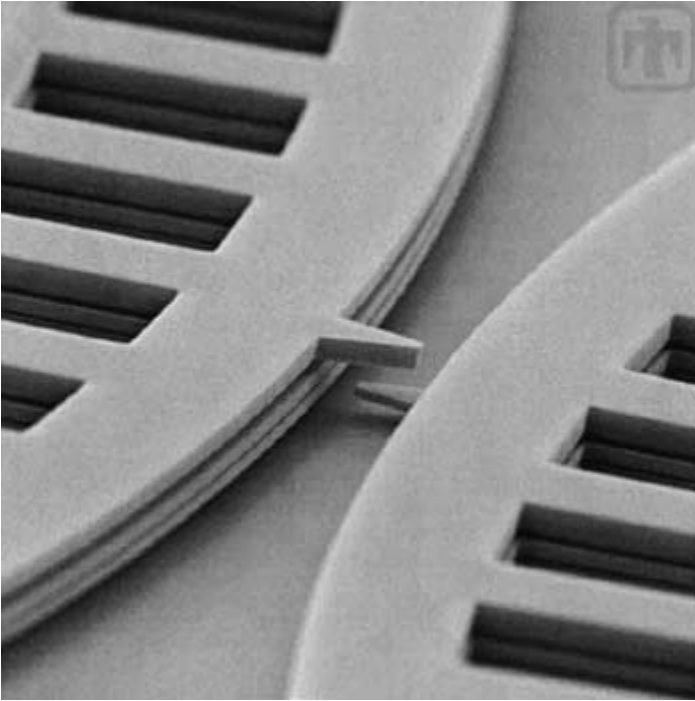
**FIGURE 15.10.** (a). A micromechanical lock with a translating groove cam.



**FIGURE 15.10.** (b). Close-up view of the translating groove cam (courtesy, Sandia National Labs—MEMS, S&T Department, [www.mems.sandia.gov](http://www.mems.sandia.gov)).



**FIGURE 15.11.** (a). Counter-meshing gear discriminator.

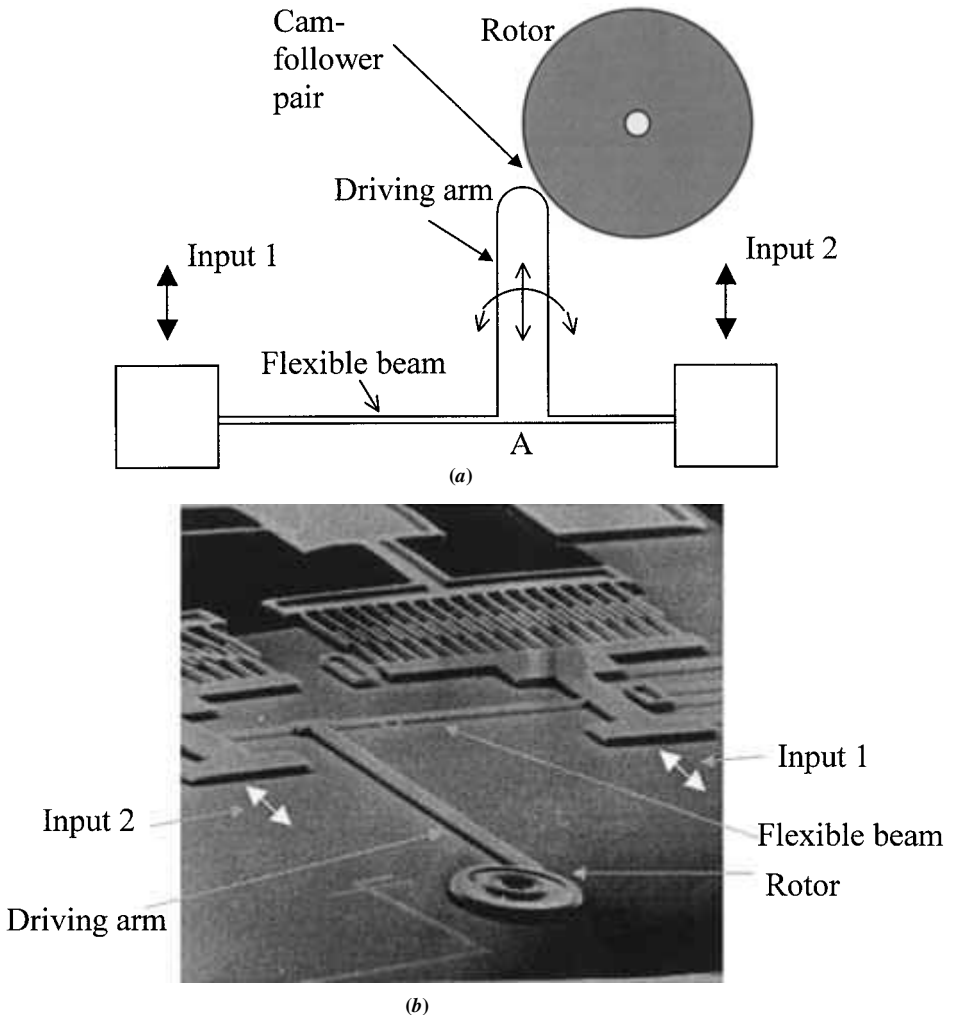


**FIGURE 15.11.** (b). Close-up view of teeth in the discriminating gears (courtesy, Sandia National Labs—MEMS, S&T Department, [www.mems.sandia.gov](http://www.mems.sandia.gov)).

to be rotated independently in a specific sequence to prevent interference between teeth located at the same level. Only when the gears are rotated according to a specific code will this device unlock and activate another component. This device also contains an anti-reverse mechanism to prevent backward rotation so that a code cannot be corrected and tried again if it is entered incorrectly. Thus, this gear discriminator device interprets a digital code as angular rotations of the countermeshing gears in a fail-safe manner.

### 15.6.6 Microvibromotor with an Inverse Cam

Researchers at the Berkeley Sensor and Actuator Center have applied the concept of a vibromotor to the microscale. One version of a microvibromotor is shown schematically in Fig. 15.12a. A scanning electron microscopic image of a fabricated prototype is shown in Fig. 15.12b. Although it resembles the traditional cam-follower arrangement, its operating principle is different. Here, the follower and the cam are not in continuous contact; the *follower* drives the cam (i.e., the rotor) by impacting it. The follower is given an upward as well as sideward motion with the help of two translating inputs at either end of a clamped-clamped beam. When the two inputs are given appropriately, point A, where the follower is attached to the beam, experiences both transverse displacement and rotation. This motor has also shown to be operational in both clockwise and counterclockwise rotations of the rotor with slight modifications and additions of more followers in other directions. The two translating inputs for this device shown in Fig. 15.12a and b come from



**FIGURE 15.12.** (a). Schematic of the angular microvibromotor. (b) Scanning electron microscope picture of a prototype (courtesy of Abraham P. Lee, National Institute of Standards and Technology).

electrostatic comb drives. This and other actuators used in MEMS are discussed in the next section.

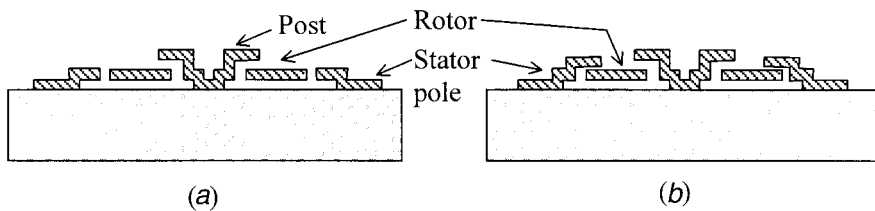
## 15.7 ACTUATORS FOR MICRO CAMS

As seen in the previous examples, both linear and rotary microactuators are available to drive microcams and other micromechanical elements. Although a very large number of actuators using a variety of transduction principles are available, only electrostatic linear

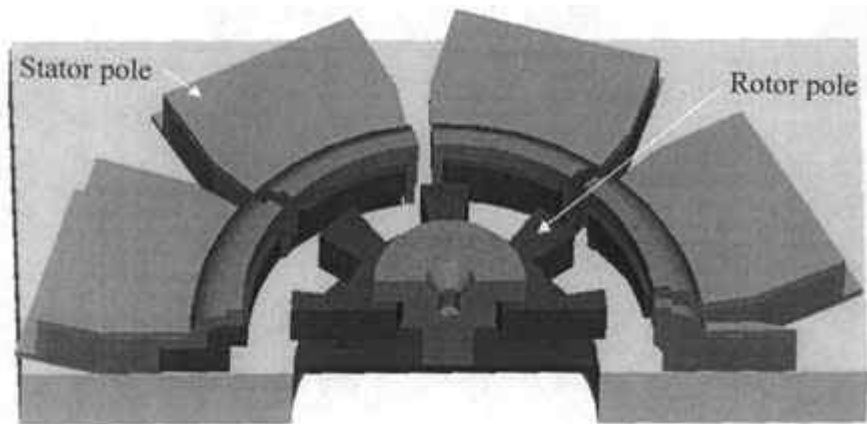
and rotary actuators are described here. It is interesting to note that it is often not practical to take power out of rotary motors to transmit to other components. The problem lies in attaching the other components. Recently this problem has been overcome by some indirect means. Such a design, called a microengine, is also described in this section.

### 15.7.1 Electrostatic Micromotors

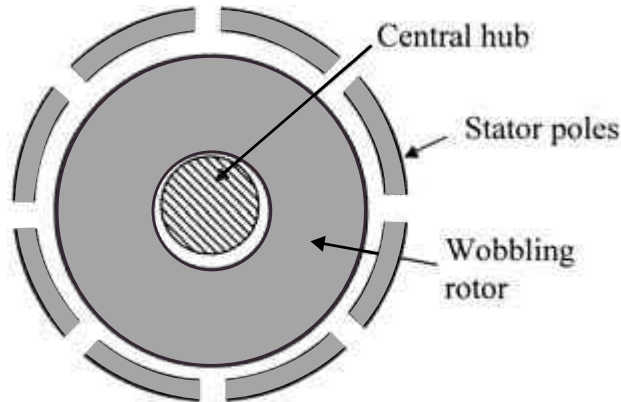
Although elastically deformable micron-scale mechanical structures existed even in the 1960s, interest in MEMS began with the development of electrostatic micromotors because they enabled rigid-body motion at the microscale. The key development was a surface micromachining batch process used to make an assembled rotor and post without explicit part-by-part assembly. This was made possible by a layered construction with structural and sacrificial materials wherein each layer was photolithographically patterned. Removal of the sacrificial layer at the end of processing creates the necessary clearance and gaps for the assembled structure. This is illustrated in Fig. 15.13*a*. Using such a freely movable rotor around a fixed post, several variations of electrostatic motors were developed. Side-



**FIGURE 15.13.** (a) Schematic of the electrostatic side-drive micromotor. (b) Schematic of the electrostatic top-drive micromotor.



**FIGURE 15.13.** (c) Cutaway view of an electrostatic side-drive micromotor.

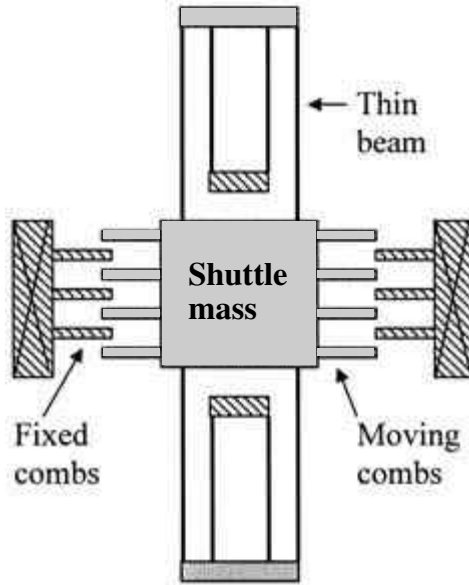


**FIGURE 15.13.** (d). Schematic of the electrostatic wobble micromotor.

drive motors, top-drive motors, and wobble motors are three such designs. In a side-drive motor, stator poles circumferentially surround the rotor. The rotor itself has its own gear-teeth-like poles. By switching the voltage on groups of alternating stator poles, the rotor is put in continuous rotation. A cutaway view of the solid model of this motor is shown in Fig. 15.13c. In a top-drive motor, the stator poles are on top of the rotor poles, which is made possible by the way polysilicon is deposited on the selectively etched sacrificial oxide layer. This is shown in Fig. 15.13b. A wobble motor, as shown in Fig. 15.13d, consists of a rotor without poles, which wobbles around the post. The wobbling distance is equal to the clearance between the rotor and the post. Its principle is similar to that of the harmonic motor in the sense that each rotation of the rotor around the post causes it to turn only by a small angle about its axis. The torque in this motor is multiplied by its inherent gear ratio, which is equal to the ratio of the bearing radius to the wobbling distance. These and other types of rotary motors have been demonstrated successfully but their significant practical applications are yet to be developed. Next, a linear microactuator that is widely used in MEMS is described.

### 15.7.2 Electrostatic Comb Drive

Figure 15.14 shows the electrostatic comb-drive-type linear microactuator. Its working principle is based on the electrostatic force generated between misaligned capacitor plates, which tends to pull them back together. In the comb-drive design several such capacitor plate pairs exist because of the interdigitated comb-finger design. This enhances the combined force generated by all of them. The combs that move relative to the fixed combs are attached to a central mass that shuttles from side to side by virtue of a symmetric design and alternating activation of the fixed combs on either side. The shuttle mass is suspended freely above the substrate by means of elastically deformable beams. The design shown in Fig. 15.14 has a folded-beam suspension, which has high flexibility in the direction of actuation and high stiffness in the perpendicular direction. This actuator is used in many MEMS devices including some commercially available products. A mechanism that converts the translational motion generated by the comb drive to rotational motion is described next.



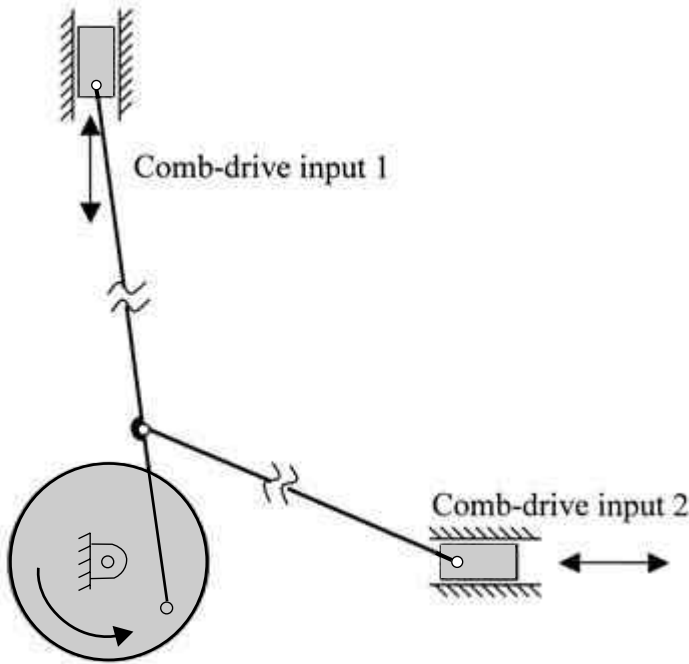
**FIGURE 15.14.** Schematic of the electrostatic comb-drive.

### 15.7.3 Sandia's Microengine

What is called a microengine by Sandia researchers is essentially an electrostatic comb drive with a linkage to convert reciprocating translational motion to continuous rotation. It is schematically shown in Fig. 15.15. Some of the revolute joints in this original design were subsequently replaced with flexible joints in later designs. The microengine is microfabricated using Sandia's SUMMiT process. It is a very successful microactuator and its use has been demonstrated in a number of applications, some of which are described in Sec. 15.6. Additionally, it has enabled Sandia researchers to conduct extensive experiments to understand failure mechanisms at the microscale.

### 15.7.4 Other Actuators

Numerous actuation techniques have been attempted at the microscale. It would not be an overstatement to say that every conceivable physical and chemical phenomenon that can be miniaturized using accessible microfabrication processes has been attempted. Kovacs (1998) contains good descriptions of most of them. The majority of the actuators developed have been demonstrated to move themselves but often do not have the force or torque to move the components connected to them. For transducer-type applications and optical applications, this is adequate. When substantive mechanical transmission becomes more prevalent, actuators will need to be greatly improved.



**FIGURE 15.15.** Kinematic sketch of the linkage in Sandia's microengine driven by two coordinated electrostatic comb-drive linear actuators.

## 15.8 FRICTION AND WEAR AT THE MICROSCALE

There is a simple, yet fundamental scaling effect to keep in mind in the design, manufacture, and operation of MEMS devices: surface area decreases as the square of the linear dimension, while volume decreases as the cube. Therefore, when the size decreases by a factor of  $10^6$  from macro- (meter) to micro- (meter) scale, the surface area decreases by a factor of  $10^{12}$  but the volume decreases by  $10^{18}$ . The implication for MEMS is that surface-dependent forces such as surface tension, friction, and viscous drag are more dominant than volume-dependent forces such as gravity and inertia. The problems associated with the detrimental surface-dependent forces were recognized at the inception of the MEMS field. When the sacrificial layer is dissolved in an etchant solution to release the movable parts of structures, the surface tension forces tend to bend the released structures down and make them stick to the newly exposed surfaces beneath. This effect, called the stiction, can be overcome using a variety of means such as adding small protrusions to the underside of the structures, supercritical drying, etc. The same stiction can also occur during the operation of the MEMS devices between surfaces that move relative to each other. Friction forces tend to be relatively larger at the microscale than they are at the macroscale because of the scaling effect described above. Wear is believed to be the dominant cause of failure of MEMS devices. It has been observed in some studies that the

major failure mechanism for microscale devices is not fatigue failure but wear between contacting surfaces. A detailed study conducted by Sandia National Laboratories on polycrystalline silicon micromechanical transmissions concluded that the major failure mechanism for operating MEMS was the wear of the rubbing surfaces.

Friction and wear can be most effectively minimized or avoided if elastically flexible structures are used. This is probably the reason for the widespread use of simple elastic structures in microtransducers. However, intermittent surface contacts are unavoidable when applications such as the ones described in the previous section involve sophisticated mechanical movement. Cams and gears suffer from the problem of friction and wear but provide the designer with numerous possibilities. As the tribological issues at the micro- and nanoscale are better understood, cams are likely to play an increasing role in MEMS devices. Some past and current studies on friction and wear pertinent to the successful operation of cams are described next.

Two early studies on in situ friction measurement on electrostatically actuated micromotors reported friction coefficients in the range of 0.21 to 0.38 for polysilicon on silicon nitride and 0.25 to 0.35 for polysilicon on silicon. In the latter study, the micromotors stopped running after 0.75 to 1 million revolutions and this was attributed to wear. Another study used a polysilicon wobble micromotor in which the wear between the rotor and the central hub changes the gear ratio of the motor. This was used to quantify wear. A very detailed three-year study (Sandia 2000) considered the effects of humidity, temperature, shock, vibration, and storage. The device on which this study focused was called a microengine, which as described earlier has many polysilicon parts that rubbed against each other. This study outlined the observed failure modes in operating and nonoperating conditions and recommended some design rules to avoid such failure. Even though the study was based entirely on a particular type of polysilicon microdevice, their findings could be generalized to any MEMS device with rubbing surfaces or surfaces in close contact. Wear was observed to be the major failure mechanism. The debris and the asperities caused by wear lead to momentary and intermittent sticking and eventually permanent adhesion and seizure. The three-body wear in which debris gets caught between the rubbing surfaces was found to be a major contributor to wear. It was also found that humidity helps to mitigate wear by acting as a lubricant. Therefore, relative humidity of 30 percent to 60 percent is recommended for operation at room temperature. Reduction of three-body wear by removing the initial debris is recommended but it may not always be practical. Minimizing rubbing surfaces by design and minimizing the impact forces at the rubbing surfaces by controlled actuation were recommended to reduce wear. All of these are relevant when cams are used in MEMS because rubbing surfaces are inevitable in cams.

Several studies have been conducted to study friction at the microscale. In one such study (Bhushan, 1999), a silicon nitride ( $\text{Si}_3\text{N}_4$ ) probe whose tip had a radius of 50 nm ( $50 \times 10^{-9}$  m) was scanned over a  $1 \times 1 \mu\text{m}$  sample area at a scanning speed of  $5 \mu\text{m/s}$  in the load range of 10 to 150 nN. Several samples of single-crystalline, polycrystalline, and oxide-coated silicon were used. It was found that the coefficient of friction was between 0.02 and 0.04 for all the samples. This is considerably smaller than the coefficient of friction at the macroscale, which was found to be about 0.18 for the same samples but using a  $\text{Si}_3\text{N}_4$  ball of radius 3 mm. Two reasons are cited for this. First, the indentation hardness and elastic modulus are higher at the microscale and this reduces wear. Second, there is a smaller apparent area of contact, which contributes less to plowing. Even though the coefficient of friction is an order of magnitude smaller than the macroscale value, it should be remembered that friction forces at the microscale are still dominant because of the scaling effect mentioned earlier.

## 15.9 SUMMARY

---

This chapter began by stating that the scope of cams has somewhat expanded to include gears and ratchets and other types of devices that involve intermittent and sustained contact between rigid bodies. The main reason for this is the limited applications where sophisticated mechanical motions are required. This has to do with the evolution of the MEMS field, where the emphasis has been on microtransducers (sensors and actuators). The slower development of MEMS applications involving mechanical transmission may also be due to the limited capabilities of micromachining techniques compared to the macroscale machining techniques. As the need for mechanical transmission at the microscale increases, linkages, gears, and cams will appear as much as beams and membranes do at present. It is also possible that future developments involving mechanical manipulation might require compliant mechanisms where there is no relative rigid-body motion but complex motions are not precluded. At this juncture, it is important to note that nature seems to avoid sliding contacts at the microscale and prefers compliant designs where there are only elastic deformations. However, engineered designs can overcome the limitations and make sliding contacts more viable even at the microscale. Whether rigid-body motions are good or elastic deformations are good definitely depends on a number of factors. These factors include materials, manufacturing processes, and an understanding of friction and wear and how to overcome them at the microscale.

## REFERENCES

---

- Allen, J.J., and Schriener, H.K., "Micromachine Wedge Stepping Motor," Micro-Electro-Mechanical Systems Symposium at the International Mechanical Engineering Congress and Exhibition, DSC-Vol. 66, ASME Press, New York, 1998.
- Bhushan, B., ed., *Handbook of Micro/Nano Tribology*, Boca Raton, Fla., CRC Press, 1999.
- Kovacs, G.T.A., *Micromachined Transducers Sourcebook*, WCB McGraw-Hill, Boston, 1998.
- Madou, M., *Fundamentals of Microfabrication*, CRC Press, Boca Raton, Fla., 1998.
- National Research Council, "Microelectromechanical Systems: Advanced Materials and Fabrication Methods," *National Research Council Report*, National Academy Press, Washington, D.C., 1997.
- Petersen, K., "Silicon as a Mechanical Material," *Proceedings of the IEEE*, 70 (2): 420–57, 1982.
- Sacks, E., and Barnes, S.M., "Computer-aided Kinematic Design of a Torsional Ratcheting Actuator," Proceedings of the Fourth International Conference on Modeling and Simulation of Microsystems, Computational Publications, Boston, 2001.
- Tanner et al., *MEMS Reliability: Infrastructure, Test, Structures, Experiments, and Failure Modes*, SAND2000-0091, Sandia National Laboratories report, Albuquerque, N.M., 2000.
- Trimmer, W.S., ed., *Micromechanics and MEMS: Classic and Seminal Papers to 1990*, IEEE Press, New York, 1990.

*This page intentionally left blank.*

---

# CHAPTER 16

---

# AUTOMOTIVE CAMSHAFT DYNAMICS

---

**Dimitri Elgin**

*D. Elgin Cams*  
*Redwood City, Calif.*  
*www.elgincams.com*

<b>16.1 BACKGROUND</b>	<b>529</b>	<b>16.3.2.2 Ductile Iron</b>	<b>535</b>
<b>16.2 INTRODUCTION</b>	<b>531</b>	<b>16.3.2.3 Miscellaneous Materials</b>	<b>535</b>
<b>16.3 CAMSHAFT MATERIALS</b>	<b>531</b>	<b>16.3.2.4 Roller Follower</b>	<b>535</b>
<b>16.3.1 Sliding Follower Camshafts</b>	<b>532</b>	<b>16.4 CAMSHAFT CURVES</b>	<b>535</b>
<b>16.3.1.1 Cast Iron</b>	<b>532</b>	<b>16.5 CAMSHAFT PROFILE GEOMETRY</b>	<b>536</b>
<b>16.3.1.2 Miscellaneous Materials</b>	<b>534</b>	<b>16.6 HARMONIC ANALYSIS</b>	<b>537</b>
<b>16.3.2 Roller-Follower Camshafts</b>	<b>534</b>	<b>16.7 ENGINE PERFORMANCE</b>	<b>541</b>
<b>16.3.2.1 Steel</b>	<b>534</b>	<b>16.8 SUMMARY</b>	<b>541</b>

---

## **16.1 BACKGROUND**

---

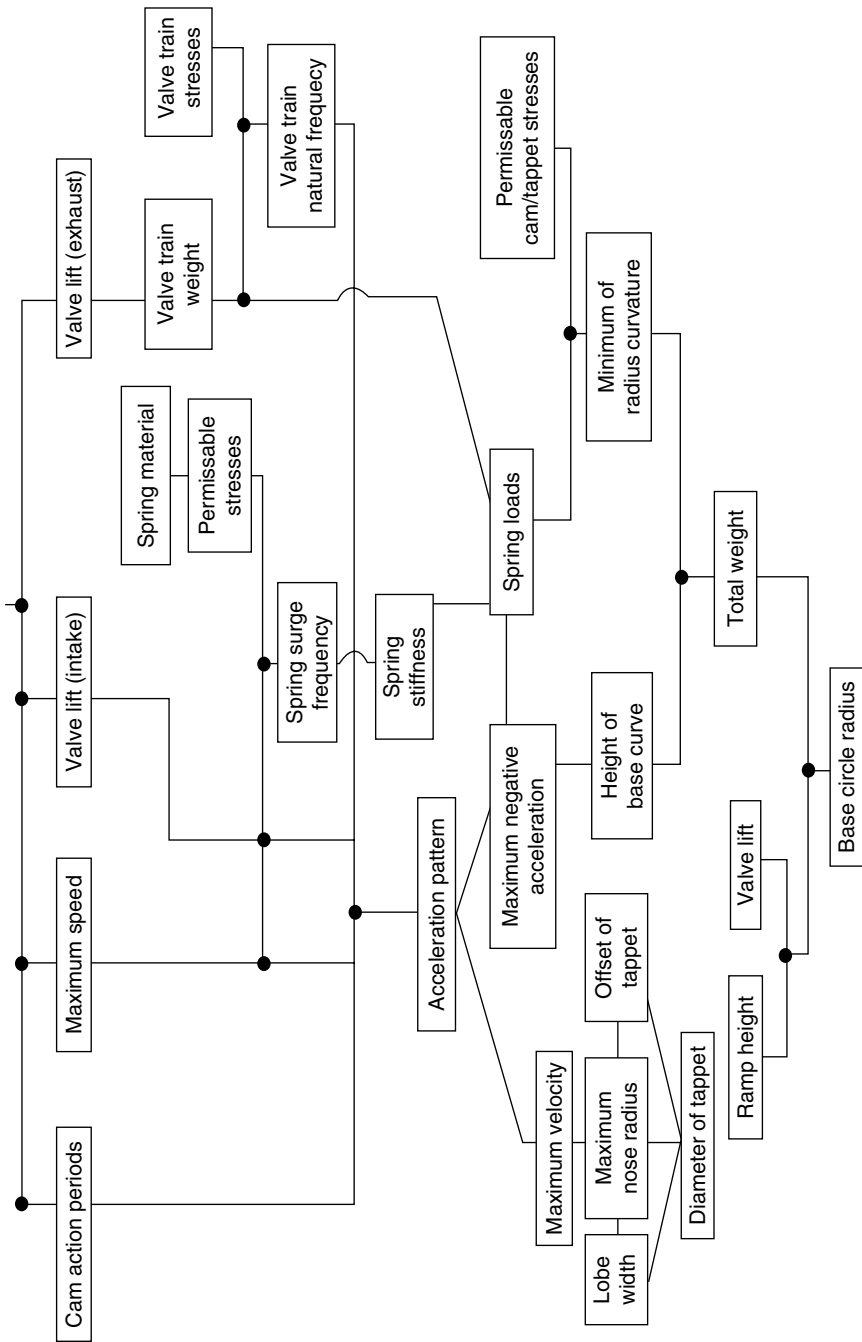
It is established that the automotive camshaft is the most influential component that governs how the engine can perform. The choice of camshaft (cam shape) has a responsibility, reliability, and durability as well as a performance impact.

Before designing the cam lobes (intake and exhaust) one must consider what the engine “wants” for a timing event diagram—seat-to-seat timing. One must address the physical limitations such as piston to valve clearance, valve-to-valve clearance, follower constraints, and spring limitations. There are at least 25 items to consider in designing the actual cam lobe (Fig. 16.1).

The writer has had the distinct advantage of having worked with two of the pioneers on the subject of automotive valve cams, Ed Winfield and Cliff Collins. These men modified the primitive circular arc and tangent cam profiles by adding ramps and reducing jerk. In addition they were aware of the demand for air and fuel in the engine and maximized the “area of the displacement the curve” *at the valve* to maximize the flow of all gases. Another development was the effective performance of the valve spring. Valve springs were always the limiting factor as to how much valve acceleration could be applied (positive and negative). Custom racing valve springs of silicon chrome wire were initiated as an improvement of the engine performance over its range of speeds.

With the advent of the computer one can simulate the engine, look at the piston and valve motion, calculate the air demand, and size the intake and exhaust systems. It has been observed that the computer modeling methods utilized in this chapter can predict the horsepower and torque values within about 2 to 5 percent of that of the actual engine.

Also, it is not the horsepower of the engine that wins races but the amount of torque and horsepower under their respective curves that accelerates the automobile and makes it a winner. Also, one might say that the automotive cam functions to make the engine “breathe.”



**FIGURE 16.1.** Factors to be considered in automotive valve-gear design.

## 16.2 INTRODUCTION

---

In this chapter we present the latest techniques necessary to design a cam-follower valve gear system for a new automobile internal combustion engine or to replace a cam in an existing engine. Included in this broad subject are automotive engines for public transportation, racing cars, motorcycles, and diesel engines. The presentation will largely utilize computer software which is listed in App. D.

Curve information in Chaps. 2, 3, and 4 and the material lubrication and manufacturing information of Chaps. 9 and 10 are particularly pertinent. Also, the reader should refer to Chapters 11, 12, and 13 which present the dynamic study of compliant high-speed cam systems applied to automotive internal-combustion valve-control systems. An excellent reference for the subject of automotive camshaft design is Hubbard (2000). Valuable information was shared with Crane (2000) and Dour (2002).

Automotive cam valve-gear systems are of two types:

- Open-track cam system
- Closed-track cam system (desmodromic)

The open-track cam follower, which is most popular, has a spring to maintain constraint of the mechanism. The closed-track follower is held on the cam by virtue of its mechanism design. This type of follower system is largely applied to motorcycles.

The following types of cam-driven automotive valve installations are shown:

- Direct acting on valve, L-head, overhead cam (OHC)
- Push-rod rocker arm overhead valve train with flat or roller contact (OHV)
- Cam-on-rocker arm (CORA) valve train with radius or roller follower (OHC)

Most automotive engines made in the United States before World War II were flat-head (L-head) designs, Fig. 16.2. The L-head design has a short stiff-valve follower train which lessened potential dynamic problems, such as follower jump. After 1950, most United States manufacturers switched to overhead valve designs (OHV) which became the United States standard.

The OHV designs, Fig. 16.3, used an underhead camshaft which drove a long, compliant pushrod to actuate the overhead valves located above the pistons. At high speeds the long, flexible follower trains of these pushrod designs caused significant dynamic problems with the valve trains.

Postwar European and Japanese engine designers adopted the overhead camshaft design, Fig. 16.4. The camshaft is located in the head above the valves. It provides a short, light, and stiff follower train similar to the old-fashioned flathead engines. This system allowed higher speeds of engine performance since the follower train had a higher natural frequency. Accordingly, United States manufacturers are currently shifting from pushrod overhead valve designs to overhead camshaft designs in the new engines.

## 16.3 CAMSHAFT MATERIALS

---

In this section we will discuss the camshaft materials that are currently used. These materials are applied in either the sliding or rolling action of the follower; see Chaps. 9 and 10. The performance and life of mating materials is dependent on the compatibility of the materials, the lubricants selected (additives), the engine speed, the newness of the cam-

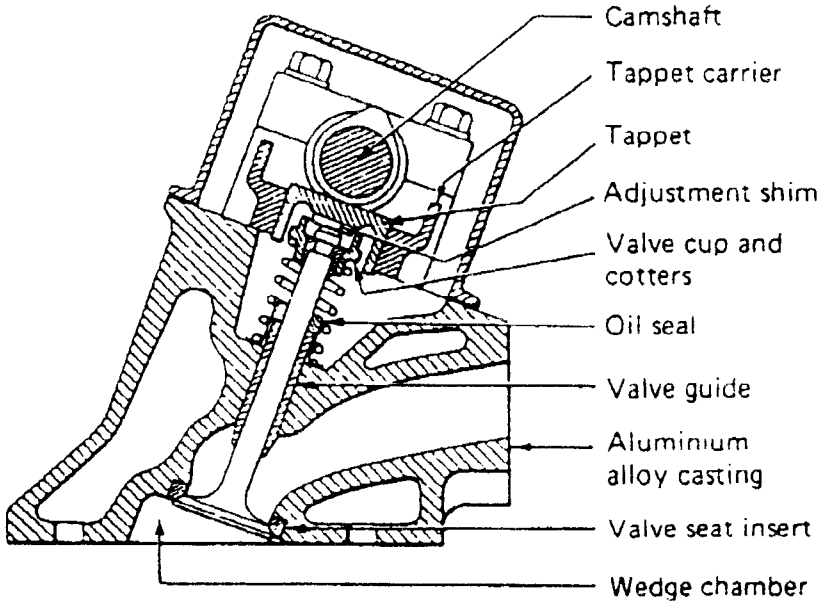


FIGURE 16.2. Direct-acting overhead cam (OHC).

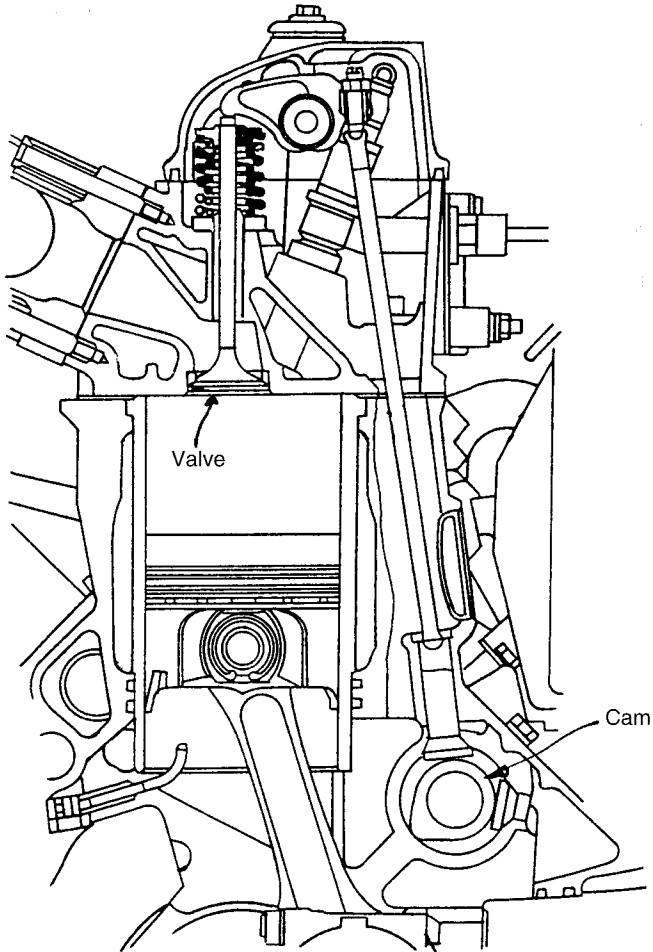
follower system, the surface smoothness and hardness, and the acceleration and jerk curves, plus other factors.

### 16.3.1 Sliding Follower Camshafts

Some engines employ a hardened steel cam lobe RC 58–61 and a hardened steel follower surface. To prevent adhesive wear or scuffing of the contacting surfaces, nitriding is required on one or more of the surfaces. A chilled iron follower is also a good material for use in contact with a hardened steel cam; the chilled iron follower is the weaker of the two surfaces and usually fails by spalling action. To resist wear, hardened steel cam lobes are sometimes used with a high chromium steel follower, and nitriding the cam lobe also provides greater durability. In special racing designs some manufacturers provide a deep-slot cam ground into the lobe face. This is filled by welding overlay high nickel material.

The material most often employed for cam lobe hard-facing is Wall Colmonoy, an alloy containing 10 percent chromium crystals RC 50–55. As mentioned in Chap. 10, cam followers that are flat and can spin about their center axis help durability because scratches and imperfections in the surfaces are worn away by this lapping action and the surface improves with use. Crowning of the follower is necessary to prevent excessive stresses that result from edge riding due to misalignment of the contacting surfaces.

**16.3.1.1 Cast Iron.** Cost is one of the main advantages of cast iron as a camshaft and follower material selection. U.S. manufacturers have used alloyed-hardened Gray Iron Grade HGI-50, having RC-50 minimum hardness on the cam lobe toe. In wear, this camshaft is compatible with chilled iron or hardened gray iron cam followers of Rock-

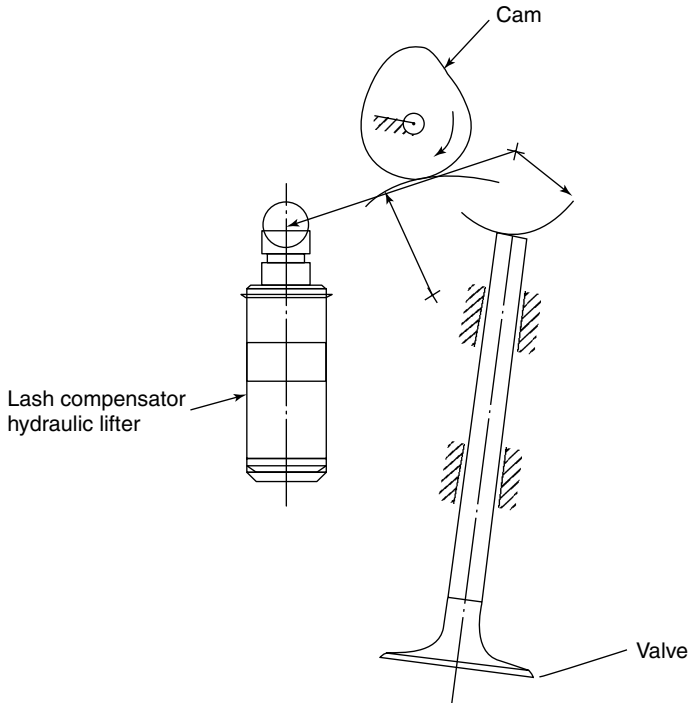


**FIGURE 16.3.** OHV push-rod rocker arm valve train with flat contact (roller similar).

well C minimum hardness. For best durability, the follower face (above 50 Rockwell C) is usually five Rockwell C numbers harder than the cam lobes.

The cast iron camshafts will normally work with chilled iron followers as long as lower stress numbers are used. Many designers want the chilled iron camshaft stress ranges to be about 20 percent lower than for comparable hardened gray iron cam lobes and hardened gray iron followers. Lobe hardening occurs as the hot metal is quickly cooled when the metal chills in the mold. This converts the iron into what is called “white iron” which is mostly iron carbides.

For example, a hardened gray iron-50 camshaft should have the hardened gray iron follower face RC-55 for the best performance. Some camshaft manufacturers have used lasers to harden cast iron cam lobes or have used TIG welding to remelt the wear surface of the cam lobes.



**FIGURE 16.4.** OHC radiused rocker arm valve train (CORA) (exhaust and intake are mirror images). (Roller follower is similar.)

**16.3.1.2 Miscellaneous Materials.** Cam lobes can be composed of a powdered metal. Some manufacturers use assembled camshafts of various powdered metal alloys and powdered metal followers that produce satisfactory sliding action. Also, powdered metal followers have been successfully used on chilled iron camshafts and hardenable camshafts.

Ductile iron and malleable iron have had some limited use in camshafts or followers. Nitrided ductile iron followers have had more success in rubbing wear with low stress replacement applications running against hardened chilled-iron camshafts. Nitrided malleable iron has been used with success on some wear camshafts and follower applications along with specially developed proprietary alloy castings. Costly laser or tungsten inert gas has been used satisfactorily to remelt and cast alloy gray iron cam lobes used in rubbing-wear applications.

Steel, chilled iron, and hardenable iron camshafts typically are cam ground after being hardened. Steel is very susceptible to surface cracking and burning when being cooled, and such imperfections make the camshaft unusable. Hardened chilled iron is almost as sensitive to the grinding operation as hardened steel.

## 16.3.2 Roller-Follower Camshafts

**16.3.2.1 Steel.** Steel is the safest and most durable material used in this type of application. There are many choices of steel alloys dependent on cost, properties required, and the methods of heat treatment employed. When roller cams fail, they do so by fatigue wear

which is a result of the tensile strength of the cam material (see Chap. 9). Steel has the highest tensile strengths (depending on the hardness) of all the alternative materials.

**16.3.2.2 Ductile Iron.** Ductile (or nodular) iron is a strong candidate for replacing steel roller cams today. Ductile iron is a form of cast iron in which the graphite (carbon) in the metal is contained in spheres (nodules) rather than the usual flakes found in normal gray iron castings.

Both austempering and postgrind induction hardening have been utilized as alternative processing methods to reduce processing costs and improve performance of ductile iron for camshafts. Austempering is a hardening and controlled quench process that makes the ductile iron stronger to absorb more stress, yet the hardness of austempered iron is less than that of iron treated with conventional heat and quench hardening. The resultant iron is not susceptible to the phenomenon of grinding-induced cracking.

Postgrind induction hardening allows the manufacturer to finish machining the camshaft completely before induction hardening the cam lobes. The unhardened casting machines and grinds rapidly without damage. Engine manufacturers using postgrind induction hardening normally allow base circle runout tolerances to increase to 0.0020 inch, and they may also allow the surface of the lobe to crown 0.0040 inch in the center of the lobe.

**16.3.2.3 Miscellaneous Materials.** The same comments are valid for sliding follower composite camshafts except that materials may be steel, powdered metal steel, powdered metal tool steel, or other powdered metal materials that show durability for roller followers. Since there are some very hard and durable powdered metal alloys, sometimes the lobe material is very difficult to grind.

**16.3.2.4 Roller Follower.** Roller followers are usually needle bearings with the roller in the follower chosen to be 52100 bearing steel on a hardened 52100 pin. Roller followers usually operate with rolling and some sliding at high speeds. The action occasionally presents a problem in that in the event of bouncing on the valve seat a flat spot may prevent the rolling action and thus significantly promote wear on the cam. This in turn affects the performance of the engine.

## 16.4 CAMSHAFT CURVES

---

Let us investigate the automobile camshaft curves applied to the system. Characteristic curves of displacement (lift), velocity, acceleration, and jerk will be studied and manipulated to yield the best performance of the follower. The total cam curve is generally composed of a ramp and the main event. The purpose of the ramp is to minimize the backlash and to control the proper valve seating velocity and seal. The ramp events that in turn are blended with sine segments (with no discontinuity) are:

- No ramp, main event only (not suggested)
- Constant velocity ramp
- Constant acceleration ramp
- Constant jerk ramp

Usually a constant-velocity ramp is chosen. The main event designs (flank of cam), which blend with a ramp, are:

- Circular-arc—see Chap. 14
- Circular-arc with straight line (tangent cam)—see Chap. 15
- High-order polynomial curve
- Composite cam designs
- Polydyne cam (rarely used)

The polynomial equation is the most popular method for blending the ramp and main event. The units of the characteristic curve equation are inches and degrees. Let us relate these units to the time base employed throughout the book. If we let

$N$  = cam speed, rpm

The follower characteristics at the cam are

*Displacement* (lift)

$$y = \text{inches}$$

*Velocity*

$$\dot{y} = \frac{1}{6N} \times \text{velocity, in/sec} = \text{in/deg}$$

*Acceleration*

$$\ddot{y} = \left(\frac{1}{6N}\right)^2 \times \text{acceleration, in/sec}^2 = \text{in/deg}^2$$

*Jerk*

$$\dddot{y} = \left(\frac{1}{6N}\right)^3 \times \text{jerk, in/sec}^3 = \text{in/deg}^3$$

In Fig. 16.5 we see the characteristic curves of an automobile camshaft (from software DESINE) with a constant velocity ramp. Figure 16.6 shows diesel intake valve curves. In these diesel curves it should be noted that the acceleration and jerk curve shape and maximum values are acceptable since diesels run at about one-half the speed of automobiles.

## 16.5 CAMSHAFT PROFILE GEOMETRY

---

In this section we investigate the camshaft geometric relationships:

- Cam profile
- Cam profile curvature
- Hertz stresses
- Follower linkage relationship

The cam profile or contour must first be established to determine the curvature of all points for an acceptable minimum radii of curvature for both fabrication and the Hertz stresses. In Chap. 9 the mathematical relationship for Hertz stresses was presented.

It is to be noted that the cam and valve have different displacement, velocity, acceleration, and jerk curves (except for direct-acting systems). This phenomenon is because of the linkage angularity and oscillations.

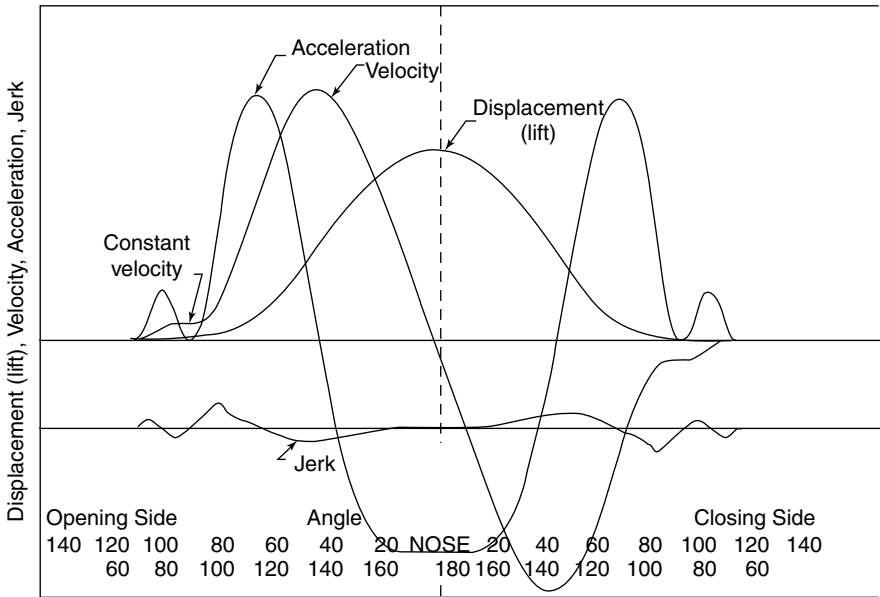


FIGURE 16.5. Automotive characteristic cam curves.

For all of the foregoing subjects the software package suggested is DESINE by Gary Matthews (see App. D). It provides excellent guidance in this profile geometry study.

### 16.6 HARMONIC ANALYSIS

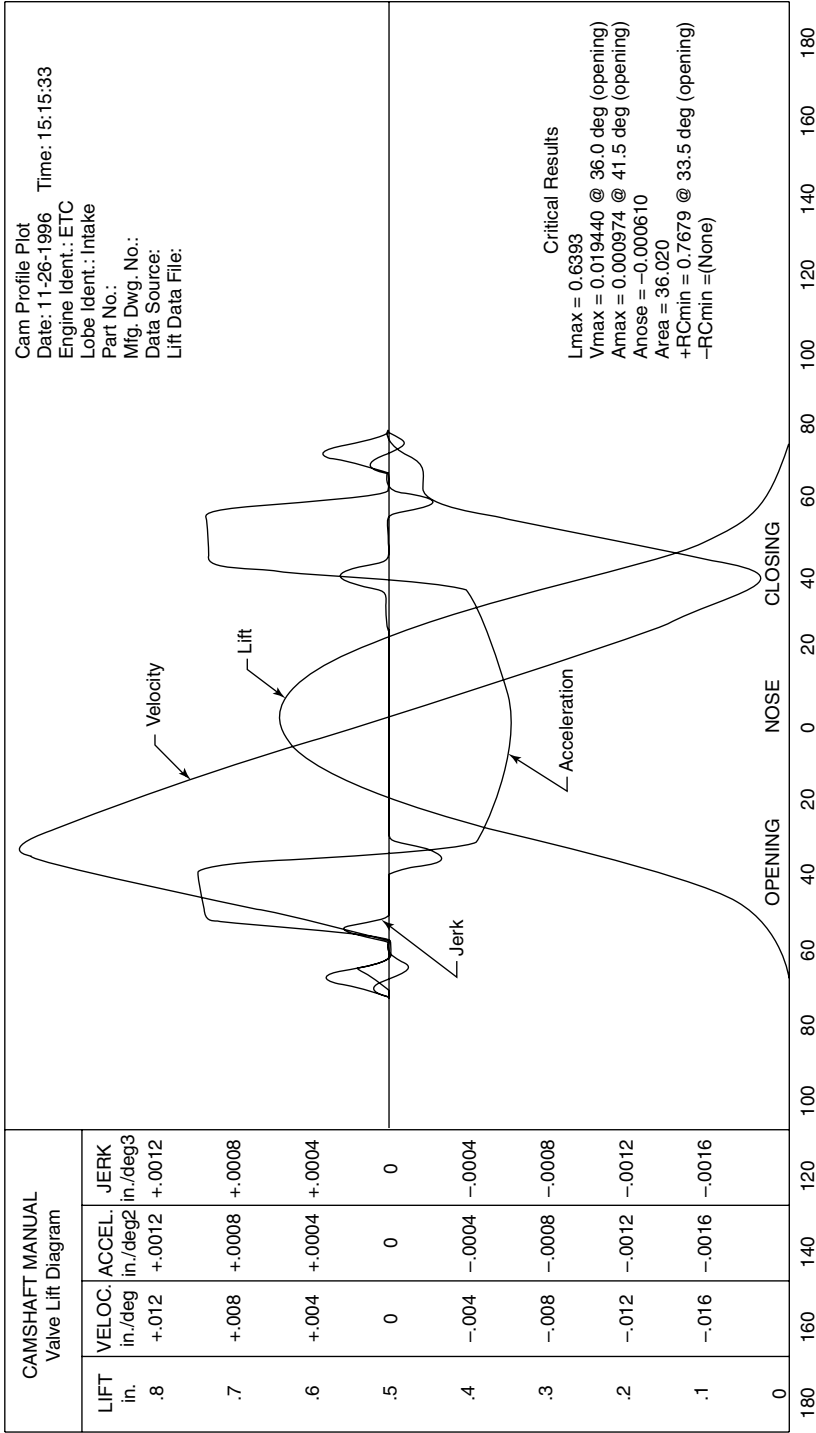
Harmonic analysis of the valve train components is pertinent to the performance of the automotive engine. Chapter 12 discusses the theoretical basis of this phenomena using Fourier analysis. The acceleration curve will be the valve acceleration curve, which is represented by a series of harmonic accelerations. Each harmonic acceleration component has an amplitude of

$$ZN^2$$

which is called the resonance factor.

There is a relationship between the valve motion, engine rpm, and the valve spring surge frequency, and it is pertinent to know how the engine valve train behaves with heat and power under actual running conditions. The limits to be applied to the harmonic analysis curves for proper engine performance with effective spring forces, controlled spring surge, reasonable spring life, and reduced noise are (Hubbard, 2000)

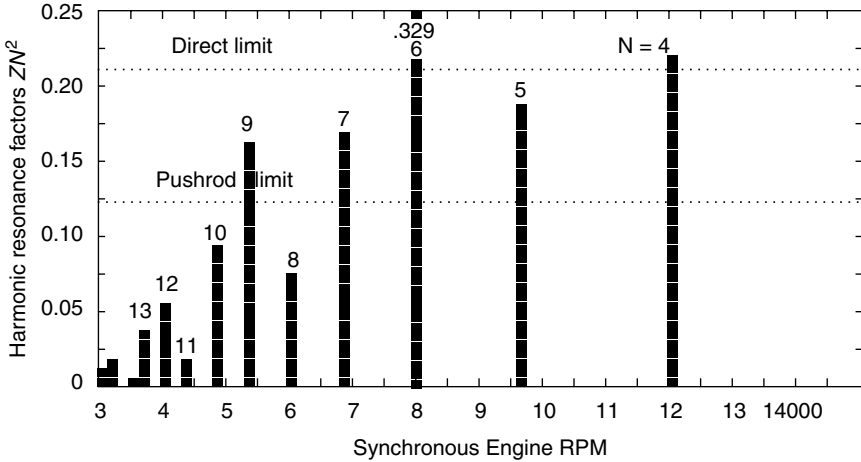
- 0.22 for direct acting (L-head) follower (OHV)
- 0.18 for cam-on-rocker arm (CORA) valve trains with radii or roller cam follower (OHC)
- 0.12 for push-rocker arm valve trains (OHV)



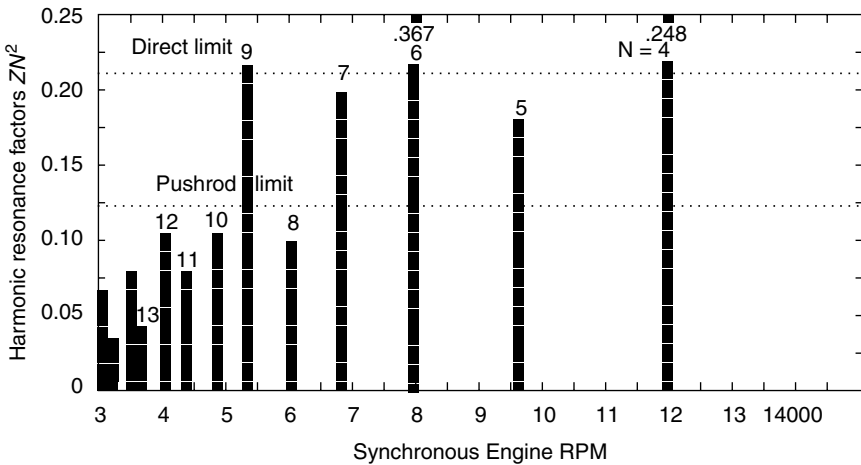
**FIGURE 16.6.** Diesel characteristic curves, (intake valve motion). Courtesy Hubbard, D., 2000.

Harmonic analysis with the lowest jerk curve values requires fine-tuning on the dynamometer to adjust the valve lash intake and exhaust system. This is to maximize the engine horsepower. To quote Crane (2000), “Do what the engine wants.”

Figure 16.7 shows the effect of increasing valve train lash on the harmonic resonance factors. Figure 16.7a shows a street rocker arm/pushrod hydraulic roller-cam profile with a valve spring having a natural frequency of 24,000cpm. It is acceptable to 5333 rpm, where it reaches 0.16, which exceeds the allowable coefficient limit of 0.12. Figure 16.7b shows the harmonic analysis of the same street rocker arm/pushrod hydraulic roller-cam profile but having lash of 0.012 inch at the follower. It looks good to 5333 rpm, where it

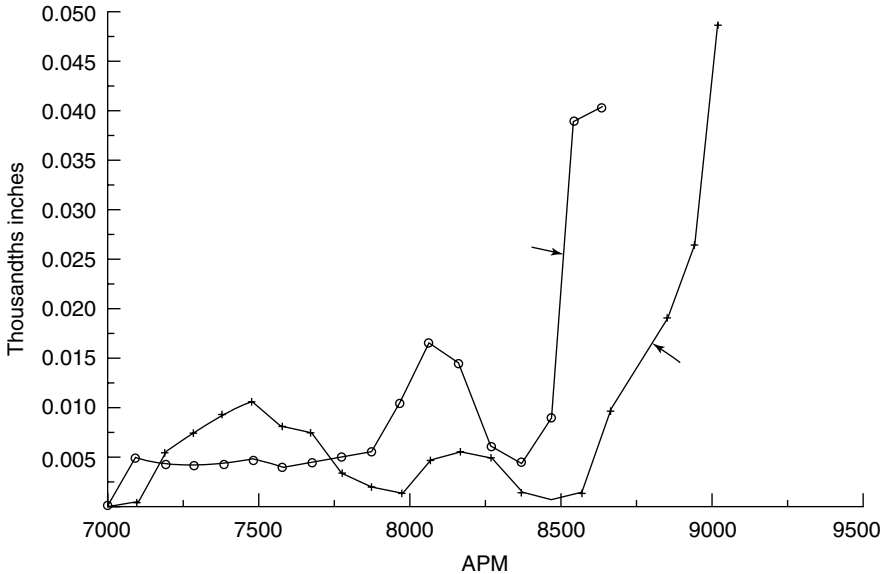


(a) Zero lash.



(b) Lash = 0.012 inches.

**FIGURE 16.7.** Harmonic resonance street performance rocker arm/pushrod hydraulic roller-cam profile (spring natural frequency of 24,000 cpm).



**FIGURE 16.8.** Valve bounce amplitude comparison.

reaches 0.217, exceeding the allowable coefficient limit of 0.12 for pushrod and 0.22 for a direct-acting valve train. This figure illustrates the effect of the added lash (less valve lift) on the harmonics of a profile design; high seating loads also result.

Figure 16.8 shows the valve bounce amplitude comparison, which was obtained by utilizing software. Also, with *SPRINGMASTER* software it is possible to select a high natural frequency spring that performs well throughout the range of speeds. Software packages *DESINE* and *DOCTOR-DOCTOR* are excellent analytical sources on this subject of harmonic analysis.

Let us elaborate on the problems involved: the procedure of selecting a good combination of spring and cam utilizing harmonic analysis of the valve-lift curve; determination of the spring frequency required to avoid resonance with bad harmonics; and selection of the spring with reference to the limitations.

The detrimental effects of valve bouncing and valve-spring surge on the power and durability of an engine and on noise are: the spring forces, as related to the speed and weight of the moving parts; the rigidity of the parts; the cam contour; and the design of the spring.

Valve bouncing affects power in several ways. It can bring about a late closure, or even a reopening, of the exhaust valve, which causes a serious overlapping with the inlet; it can bring about a late closure, or a reopening, of the inlet valve, which will result in some of the charge being backed out; or the bounce may occur while the valve is supposed to be open, in which case it increases the opening area and will not be detrimental to the power.

Spring surge is the direct result of resonance of the spring frequency with the harmonics of the valve-lift curve.

Breakage and wear of parts can be caused in two ways: by bouncing of the valve and by surging of the spring. Bouncing usually causes high valve-closing velocity and heavy impact on the seat, resulting in seat and valve wear. If the bounce occurs while the valve is open, the entire valve-operating mechanism may be overloaded. Spring surge usually

results in overstressing the spring and increasing enormously the number of stress cycles, with a consequent fatigue break of the spring, followed perhaps by breakage of other parts.

Noise, the least important result, is also caused by bouncing of the valve and surging of the spring. The former produces valve clatter, and the latter produces spring hum and coil clash.

## **16.7 ENGINE PERFORMANCE**

---

The performance of the engine is the confirmation of the camshaft valve-gear performance. Software is available to study this subject in “virtual” engines, analyzing one cylinder of the automotive engine. In the old days this requirement (see Fig 16.1) was based on experience when designing an engine. The following software packages to be utilized are listed in App. D:

AIR FLOW TESTING  
CAMPRO  
CAMPRO PLUS  
DESINE  
DOCTOR DOCTOR  
DYNOMATION  
ENGINE EXPERT  
FLOW QUIK  
SWIRL METER  
UTILITY ENGINE PROGRAMS  
SPRING MASTER  
VALVE PRO

It is to be noted that DYNOMATION and ENGINE EXPERT programs are computer simulations of dynamometer studies. Both these software programs are indeed valuable in producing a strong engine.

Last, the designer measures the air flow in the intake and exhaust systems and models the engine on the computer with empirical data based on experience. The final assembly and engine testing of the actual engine on the dynamometer will proceed quite properly.

## **16.8 SUMMARY**

---

The following are some brief thoughts on the subject of automobile camshaft dynamics:

- The subject of this chapter can be applied to any internal combustion engine with an Otto or diesel cycle, two or four stroke, such as racing cars, street cars, motorcycles, and diesel engines.
- The automotive camshaft directs the engine to “breathe.”
- Manufacturing quality is critical to the best performance. Proper alignment of the assembled parts must be achieved.
- For the ultimate manufacturing level use the newest machine tools, the highest quality materials (cost), and the most skilled and talented hands-on artisans.

- For high-level demands improved control of heat treatment and foundry production is suggested.
- Tolerances of fabrication should be  $\pm 0.0001$  to  $\pm 0.0005$  inch.
- Lubricant and additive plus the lubrication system must be chosen properly with experience.
- Frequent communication with the driver of the automobile is suggested.

## ***REFERENCES***

---

Hubbard, D., "Camshaft Reference Handbook," Don Hubbard, Publisher, Ft. Myers, Fla., 2000; dhubbard@peganet.com

Dour, J., Megacycle, San Rafael, Calif. Personal communication, 2002.

Crane, H., formerly of Crane Corporation, Daytona Beach, California. Personal communication, 2000.

---

# APPENDIXES

Harold A. Rothbart, D. Eng.

Appendix A BASIC CONTOURS 545  
Appendix B BASIC CAM CURVE FACTORS  
551  
Appendix C POLYNOMIAL COEFFICIENTS  
557  
Appendix D CAM COMPUTER SOFTWARE  
561

Appendix E CAD/CAM FOR A MEDICAL  
INSTRUMENT CAM  
MECHANISM 565  
Appendix F OPTIMAL CONTROL THEORY  
DERIVATION FOR TWO-POINT  
BOUNDARY VALUE PROBLEM  
584

*This page intentionally left blank.*

---

# APPENDIX A

---

## BASIC CONTOURS

---

A.1 ELLIPSE 545  
A.2 PARABOLA 545  
A.3 HYPERBOLA 546

A.4 LOGARITHMIC SPIRAL 548  
A.5 INVOLUTE OF A CIRCLE 549

---

### A.1 ELLIPSE

---

An ellipse is a curve generated by a point moving so that the sum of the distances from the two fixed points ( $F_1$  and  $F_2$ ) called foci is a constant. The basic equation for the ellipse is

$$\frac{X^2}{a^2} + \frac{Y^2}{b^2} = 1 \quad (\text{Eq. A.1})$$

where  $X$  = value of the curve in one direction  
 $Y$  = value of the curve in other direction  
 $a$  =  $\frac{1}{2}$  major axis  
 $b$  =  $\frac{1}{2}$  minor axis

We note that the foci of the ellipse  $F_1$  and  $F_2$  are a distance  $a$  from the ends of the minor axis. Also the major axis equals  $2a$  in length. For construction of the ellipse the reader is referred to Sec. 2.3.

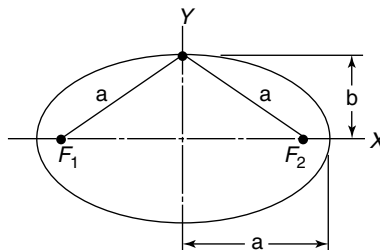


FIGURE A.1. Ellipse.

---

### A.2 PARABOLA

---

A parabola is a curve generated by a point moving so that its distance from a fixed point  $F$ , called the focus, is always equal to its distance from a fixed straight line called the directrix. In Fig. A.2, the distance  $X$ ,  $Y$ , and  $e$  are shown to any point  $P$  on the curve.  $AB$  is the directrix. Since from the definition  $X = e$ , we have the basic equation

$$Y^2 = CX$$

where  $C$  is a constant.

In addition it may be noted that with  $V$ , the vertex, the distance

$$GV = FV.$$

*Construction:*

Given, in Fig. A.3, the vertex  $V$ , the axis  $VA$ , and a point  $P$  on the curve,

- a) Enclose parabola in rectangle  $VAPB$ .
- b) Divide  $VB$  and  $BP$  into the same number of equal parts, and draw lines parallel to  $VA$ .
- c) Join division points on  $BP$  with vertex  $V$ .
- d) The intersection of these lines gives points on the parabola  $VP$ .

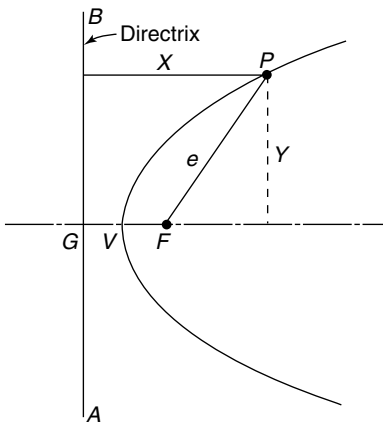


FIGURE A.2. Parabola.

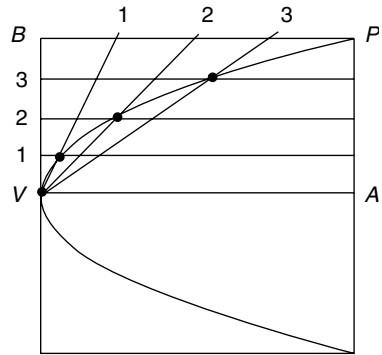


FIGURE A.3. Construction of the parabola.

### A.3 HYPERBOLA

A hyperbola is a curve generated by a point moving so that the difference of its distances from two fixed points, called the foci, is a constant.

#### 1. General Case

The equation is:

$$\frac{X^2}{a^2} - \frac{Y^2}{b^2} = 1$$

where  $a$  and  $b$  are distances shown in Fig. A.4. Also  $F_1$  and  $F_2$  are the foci. Therefore, from the definition the distance  $d - e = c$ , a constant.

*Construction:*

Given foci  $F_1$  and  $F_2$  and distance  $2a$  in Fig. A.4,

- a) With  $F_1$  and  $F_2$  as centers, draw arcs, such as  $F_1P$ .
- b) With the same centers and radius  $F_1P$  minus distance  $2a$ , strike arcs intersecting the other arcs giving points on the curve.
- c) Repeat using new radius  $F_1P$ .

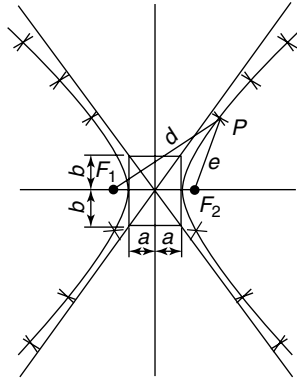


FIGURE A.4. Hyperbola.

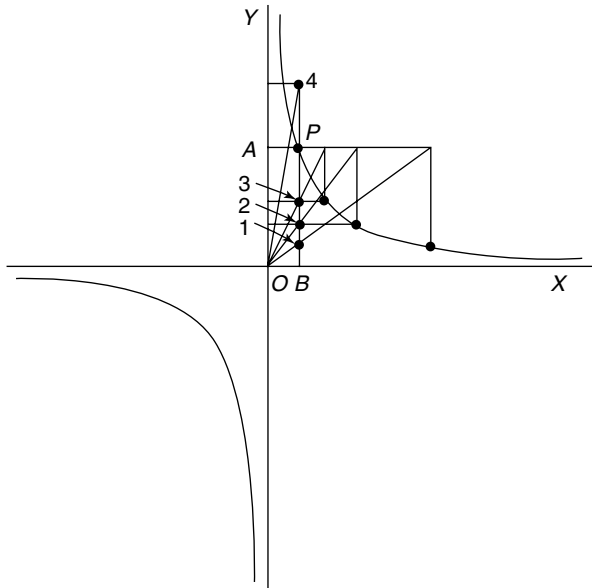


FIGURE A.5. Rectangular hyperbola.

## 2. Rectanglar

One of the most frequently employed curves in engineering is the rectangular or equilateral hyperbola (Fig. A.5).

The equation becomes

$$XY = C.$$

*Construction:*

Given  $OX$  and  $OY$  as asymptotes of the curve and any point  $P$  on the curve,

- a) Draw  $PA$  and  $PB$ .
- b) Mark any points 1, 2, and 3, etc., on  $PB$ , and through these points draw lines parallel to  $OX$ , and also lines through  $O$ .
- c) From the intersection with line  $AP$  extended draw lines parallel to  $OA$ .
- d) The intersections give the hyperbola.

### A.4 LOGARITHMIC SPIRAL

This is a radial curve having a constant pressure angle. When used on a cam, it provides the smallest radial cam for a given pressure angle limitation (Fig. A.6). The polar equation is

$$r = ae^{b\theta}$$

where  $r$  = radius to any point on curve, in  
 $a$  = spiral base-circle radius, in

$$b = \frac{1}{\tan \gamma}.$$

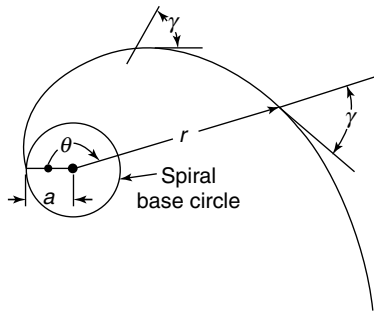


FIGURE A.6. Logarithmic spiral.

$\gamma = 90 - \alpha$  = constant angle at any point between radial line and tangent to the curve, deg.

$\alpha$  = pressure angle, deg

$\theta$  = angle between radius  $r$  and beginning point on the curve

$e = 2.718$  = base of natural logarithms

*Construction:*

Given angle  $\gamma$  and the base-circle radius in Fig. A.7,

- a) Draw lines  $MP$ ,  $PN$ , and  $OD$ .
- b) Make equal division intercepts of line  $PM$ .



- a)* Divide the circle into a convenient number of parts.
- b)* Draw tangents at these points.
- c)* Lay off on these tangents the rectified lengths of arcs from the tangency points to the starting point.
- d)* These points give the curve.

---

# APPENDIX B

---

## BASIC CAM CURVE FACTORS

---

**Table B.1 SIMPLE HARMONIC MOTION FACTORS** 552

**Table B.2 CYCLOIDAL MOTION FACTORS** 553

**Table B.3 MODIFIED TRAPEZOIDAL CURVE FACTORS** 554

**Table B.4 MODIFIED SINCE CURVE FACTORS** 555

Curve factors have been developed to establish the cam profile, the velocity, and acceleration of the follower easily. These factors are tabulated data calculated from the curve equations in Chaps. 2 and 3. In the tabulated values the cam angle factor goes from  $0^\circ$  to  $120^\circ$  and the displacement factor  $K$  goes from 0 to 1. To determine increments on a cam, the given values of  $\theta$  must be multiplied by the ratio  $\beta/120$ . For example, if  $\beta$  is  $60^\circ$ , the increment is  $60/120 = 1/2$  degree.

The following equations can be employed to establish the follower characteristics:

Displacement

$$y = Kh, \text{ in}$$

Velocity

$$y = C_v h \left( \frac{\omega}{\beta} \right), \text{ in/sec}$$

Acceleration

$$y = C_a h \left( \frac{\omega}{\beta} \right)^2, \text{ in/sec}^2$$

where  $K$ ,  $C_v$ , and  $C_a$  are the displacement factor, the velocity factor, and the acceleration factor, respectively;  $\omega$  is the camshaft speed, deg./sec.; and  $h$  is total rise in inches for cam angle  $\beta$ , degrees.

**TABLE B.1** Harmonic Factors

Pt.	K	Cv	Ca	Pt.	K	Cv	Ca	Pt.	K	Cv	Ca	Pt.	K	Cv	Ca
0	0.00000	0.0000	4.9348	30	0.14644	1.1107	3.4895	60	0.50000	1.5708	0.0000	90	0.85356	1.1107	-3.4895
1	0.00017	0.0411	4.9331	31	0.15582	1.1394	3.3969	61	0.51309	1.5703	-0.1292	91	0.86269	1.0813	-3.5796
2	0.00069	0.0822	4.9281	32	0.16543	1.1673	3.3020	62	0.52617	1.5686	-0.2582	92	0.87157	1.0511	-3.6673
3	0.00154	0.1232	4.9196	33	0.17527	1.1945	3.2049	63	0.53923	1.5660	-0.3872	93	0.88021	1.0202	-3.7525
4	0.00274	0.1642	4.9078	34	0.18543	1.2207	3.1056	64	0.55227	1.5622	-0.5158	94	0.88858	0.9885	-3.8351
5	0.00428	0.2050	4.8926	35	0.19562	1.2462	3.0041	65	0.56527	1.5574	-0.6441	95	0.89668	0.9562	-3.9150
6	0.00615	0.2457	4.8741	36	0.20611	1.2865	2.9006	66	0.57822	1.5515	-0.7719	96	0.90451	0.9233	-3.9924
7	0.00837	0.2862	4.8522	37	0.21679	1.2945	2.7951	67	0.59112	1.5469	-0.8993	97	0.91207	0.8897	-4.0669
8	0.01092	0.3266	4.8270	38	0.22768	1.3174	2.6877	68	0.60396	1.5365	-1.0260	98	0.91934	0.8555	-4.1387
9	0.01381	0.3667	4.7985	39	0.23875	1.3393	2.5784	69	0.61672	1.5274	-1.1520	99	0.92632	0.8207	-4.2076
10	0.01704	0.4066	4.7666	40	0.25000	1.3604	2.4674	70	0.62941	1.5173	-1.2772	100	0.93302	0.7854	-4.2737
11	0.02059	0.4461	4.7316	41	0.26142	1.3804	2.3547	71	0.64201	1.5061	-1.4015	101	0.93941	0.7495	-4.3368
12	0.02447	0.4854	4.6933	42	0.27300	1.3996	2.2404	72	0.65451	1.4939	-1.5250	102	0.94550	0.7131	-4.3970
13	0.02868	0.5243	4.6518	43	0.28474	1.4178	2.1245	73	0.66691	1.4807	-1.6473	103	0.95129	0.6762	-4.4541
14	0.03321	0.5629	4.6071	44	0.29663	1.4350	2.0072	74	0.67919	1.4665	-1.7685	104	0.95677	0.6389	-4.5082
15	0.03806	0.6011	4.5592	45	0.30866	1.4564	1.8884	75	0.69134	1.4564	-1.8884	105	0.96194	0.6011	-4.5592
16	0.04323	0.6389	4.5082	46	0.32081	1.4665	1.7685	76	0.70337	1.4350	-2.0072	106	0.96679	0.5629	-4.6071
17	0.04871	0.6762	4.4541	47	0.33309	1.4807	1.6473	77	0.71526	1.4178	-2.1245	107	0.97132	0.5243	-4.6518
18	0.05450	0.7131	4.3970	48	0.34549	1.4939	1.5250	78	0.72700	1.3996	-2.2404	108	0.97553	0.4854	-4.6933
19	0.06059	0.7495	4.3368	49	0.35799	1.5061	1.4015	79	0.73858	1.3804	-2.3547	109	0.97941	0.4461	-4.7316
20	0.06698	0.7854	4.2737	50	0.37059	1.5173	1.2772	80	0.75000	1.3604	-2.4674	110	0.98296	0.4066	-4.7666
21	0.07368	0.8207	4.2076	51	0.38328	1.5274	1.1520	81	0.76125	1.3393	-2.5784	111	0.98619	0.3667	-4.7985
22	0.08066	0.8555	4.1387	52	0.39604	1.5365	1.0260	82	0.77232	1.3174	-2.6877	112	0.98908	0.3266	-4.8270
23	0.08793	0.8897	4.0669	53	0.40888	1.5469	0.8993	83	0.78321	1.2945	-2.7951	113	0.99163	0.2862	-4.8522
24	0.09549	0.9233	3.9924	54	0.42178	1.5515	0.7719	84	0.79389	1.2865	-2.9006	114	0.99385	0.2457	-4.8741
25	0.10332	0.9562	3.9150	55	0.43478	1.5574	0.6441	85	0.80438	1.2462	-3.0041	115	0.99572	0.2050	-4.8926
26	0.11142	0.9885	3.8351	56	0.44773	1.5622	0.5158	86	0.81466	1.2207	-3.1056	116	0.99726	0.1642	-4.9078
27	0.11979	1.0202	3.7525	57	0.46077	1.5660	0.3872	87	0.82473	1.1945	-3.2049	117	0.99846	0.1232	-4.9196
28	0.12843	1.1511	3.6673	58	0.47383	1.5686	0.2583	88	0.83457	1.1673	-3.3020	118	0.99931	0.0822	-4.9281
29	0.13731	1.0813	3.5796	59	0.48691	1.5703	0.1292	89	0.84418	1.1394	-3.3969	119	0.99983	0.0411	-4.9331
30	0.14644	1.1107	3.4895	60	0.50000	1.5708	0.0000	90	0.85356	1.1107	-3.4895	120	1.00000	0.0000	-4.9348

**TABLE B.2** Cycloidal Factors

Pt.	K	Cv	Ca	Pt.	K	Cv	Ca	Pt.	K	Cv	Ca	Pt.	K	Cv	Ca
0	0.00000	0.0000	0.0000	30	0.09085	1.0000	6.2832	60	0.50000	2.0000	0.0000	90	0.90915	1.0000	-6.2832
1	0.00001	0.0014	0.3289	31	0.09940	1.0523	6.2746	61	0.51666	1.9886	-0.3289	91	0.91726	0.9477	-6.2746
2	0.00003	0.0055	0.6568	32	0.10839	1.1045	6.2488	62	0.53331	1.9945	-0.6568	92	0.92495	0.8955	-6.2488
3	0.00010	0.0123	0.9829	33	0.11781	1.1564	6.2059	63	0.54990	1.9877	-0.9829	93	0.93219	0.8436	-6.2059
4	0.00024	0.0218	1.3063	34	0.12766	1.2079	6.1459	64	0.56642	1.9782	-1.3063	94	0.93900	0.7921	-6.1459
5	0.00048	0.0341	1.6262	35	0.13794	1.2588	6.0691	65	0.58286	1.9659	-1.6262	95	0.94540	0.7412	-6.0691
6	0.00082	0.0489	1.9416	36	0.14864	1.3090	5.9757	66	0.59918	1.9511	-1.9416	96	0.95136	0.6910	-5.9757
7	0.00130	0.0664	2.2517	37	0.15975	1.3584	5.8659	67	0.61536	1.9336	-2.2517	97	0.95691	0.6416	-5.8659
8	0.00194	0.0865	2.5556	38	0.17128	1.4067	5.7400	68	0.63140	1.9135	-2.5556	98	0.96206	0.5933	-5.7400
9	0.00275	0.1090	2.8525	39	0.18320	1.4540	5.5984	69	0.64725	1.8910	-2.8525	99	0.96680	0.5460	-5.5984
10	0.00375	0.1340	3.1416	40	0.19550	1.5000	5.4414	70	0.66291	1.8660	-3.1416	100	0.97116	0.5000	-5.4414
11	0.00499	0.1613	3.4221	41	0.20820	1.5446	5.2695	71	0.67835	1.8387	-2.4221	101	0.97514	0.4554	-5.2695
12	0.00645	0.1910	3.6931	42	0.22124	1.5878	5.0832	72	0.69355	1.8090	-3.6931	102	0.97876	0.4122	-5.0832
13	0.00817	0.2228	3.9541	43	0.23465	1.6293	4.8830	73	0.70849	1.7772	-3.9541	103	0.98201	0.3707	-4.8830
14	0.01018	0.2569	4.2043	44	0.24840	1.6691	4.6693	74	0.72316	1.7431	-4.2043	104	0.98494	0.3309	-4.6693
15	0.01246	0.2929	4.4429	45	0.26246	1.7071	4.4429	75	0.73754	1.7071	-4.4429	105	0.98754	0.2929	-4.4429
16	0.01506	0.3309	4.6693	46	0.27684	1.7431	4.2043	76	0.75160	1.6691	-4.6693	106	0.98982	0.2569	-4.2043
17	0.01799	0.3707	4.8830	47	0.29151	1.7772	3.9541	77	0.76535	1.6293	-4.8830	107	0.99183	0.2228	-3.9541
18	0.02124	0.4122	5.0832	48	0.30645	1.8090	3.6931	78	0.77876	1.5878	-5.0832	108	0.99355	0.1910	-3.6931
19	0.02486	0.4554	5.2695	49	0.32165	1.8387	3.4221	79	0.79180	1.5446	-5.2695	109	0.99501	0.1613	-3.4221
20	0.02884	0.5000	5.4414	50	0.33709	1.8660	3.1416	80	0.80450	1.5000	-5.4414	110	0.99625	0.1340	-3.1416
21	0.03320	0.5460	5.5984	51	0.35275	1.8910	2.8525	81	0.81680	1.4540	-5.5984	111	0.99725	0.1090	-2.8525
22	0.03794	0.5933	5.7400	52	0.36860	1.9135	2.5556	82	0.82872	1.4067	-5.7400	112	0.99806	0.0865	-2.5556
23	0.04309	0.6416	5.8659	53	0.38464	1.9336	2.2517	83	0.84025	1.3584	-5.8659	113	0.99870	0.0664	-2.2517
24	0.04864	0.6910	5.9757	54	0.40082	1.9511	1.9416	84	0.85136	1.3090	-5.9757	114	0.99918	0.0489	-1.9416
25	0.05460	0.7412	6.0691	55	0.41714	1.9659	1.6262	85	0.86206	1.2588	-6.0691	115	0.99952	0.0341	-1.6262
26	0.06100	0.7921	6.1459	56	0.43358	1.9782	1.3063	86	0.87234	1.2079	-6.1459	116	0.99976	0.0218	-1.3063
27	0.06781	0.8436	6.2059	57	0.45010	1.9877	0.9829	87	0.88219	1.1564	-6.2059	117	0.99990	0.0123	-0.9829
28	0.07505	0.8955	6.2488	58	0.46669	1.9945	0.6568	88	0.89161	1.1045	-6.2488	118	0.99997	0.0055	-0.6568
29	0.08274	0.9477	6.2746	59	0.48334	1.9986	0.3289	89	0.90060	1.0523	-6.2746	119	0.99999	0.0014	-0.3289
30	0.09085	1.0000	6.2832	60	0.50000	2.0000	0.0000	90	0.90915	1.0000	-6.2832	120	1.00000	0.0000	0.0000

**TABLE B.3** Modified Trapezoidal Factors

Pt.	K	Cv	Ca	Pt.	K	Cv	Ca	Pt.	K	Cv	Ca	Pt.	K	Cv	Ca
0	0.00000	0.0000	0.0000	30	0.10451	1.0000	4.8881	60	0.50000	2.0000	0.0000	90	0.89549	1.0000	-4.8881
1	0.00001	0.0021	0.5110	31	0.11300	1.0407	4.8881	61	0.51667	1.9979	-0.5110	91	0.90370	0.9593	-4.8881
2	0.00005	0.0085	1.0163	32	0.12181	1.0815	4.8881	62	0.53328	1.9915	-1.0163	92	0.91153	0.9185	-4.8881
3	0.00016	0.0190	1.5105	33	0.13100	1.1222	4.8881	63	0.54985	1.9810	-1.5105	93	0.91900	0.8778	-4.8881
4	0.00037	0.0336	1.9882	34	0.14053	1.1629	4.8881	64	0.56623	1.9664	-1.9882	94	0.92614	0.8371	-4.8881
5	0.00073	0.0521	2.4440	35	0.15036	1.2037	4.8881	65	0.58255	1.9479	-2.4440	95	0.93294	0.7963	-4.8881
6	0.00120	0.0743	2.8731	36	0.16057	1.2444	4.8881	66	0.59873	1.9257	-2.8731	96	0.93939	0.7556	-4.8881
7	0.00198	0.0999	3.2708	37	0.17113	1.2851	4.8881	67	0.61467	1.9001	-3.2708	97	0.94555	0.7149	-4.8881
8	0.00293	0.1287	3.6326	38	0.18203	1.3259	4.8881	68	0.63036	1.8713	-3.6326	98	0.95136	0.6741	-4.8881
9	0.00413	0.1604	3.9546	39	0.19323	1.3666	4.8881	69	0.64586	1.8396	-3.9546	99	0.95679	0.6334	-4.8881
10	0.00561	0.1945	4.2333	40	0.20471	1.4073	4.8881	70	0.66101	1.8055	-4.2333	100	0.96187	0.5927	-4.8881
11	0.00738	0.2308	4.4655	41	0.21669	1.4481	4.8881	71	0.67592	1.7693	-4.4655	101	0.96666	0.5519	-4.8881
12	0.00946	0.2688	4.6489	42	0.22891	1.4888	4.8881	72	0.69053	1.7312	-4.6489	102	0.97106	0.5512	-4.8881
13	0.01186	0.3081	4.7813	43	0.24147	1.5295	4.8881	73	0.70476	1.6919	-4.7813	103	0.97517	0.4705	-4.8881
14	0.01460	0.3483	4.8613	44	0.25443	1.5703	4.8881	74	0.71873	1.6517	-4.8613	104	0.97894	0.4297	-4.8881
15	0.01767	0.3890	4.8881	45	0.26767	1.6110	4.8881	75	0.73233	1.6110	-4.8881	105	0.98233	0.3890	-4.8881
16	0.02106	0.4297	4.8881	46	0.28126	1.6517	4.8613	76	0.74557	1.5703	-4.8881	106	0.98540	0.3483	-4.8613
17	0.02483	0.4705	4.8881	47	0.29524	1.6919	4.7813	77	0.75853	1.5295	-4.8881	107	0.98814	0.3081	-4.7813
18	0.02894	0.5112	4.8881	48	0.30947	1.7312	4.6489	78	0.77109	1.4888	-4.8881	108	0.99054	0.2688	-4.6489
19	0.03334	0.5519	4.8881	49	0.32408	1.7693	4.4655	79	0.78331	1.4481	-4.8881	109	0.99262	0.2308	-4.4655
20	0.03813	0.5927	4.8881	50	0.33899	1.8055	4.2333	80	0.79529	1.4073	-4.8881	110	0.99439	0.1945	-4.2333
21	0.04321	0.6334	4.8881	51	0.35414	1.8396	3.9546	81	0.80677	1.3666	-4.8881	111	0.99587	0.1604	-3.9546
22	0.04864	0.6741	4.8881	52	0.36964	1.8713	3.6326	82	0.81797	1.3259	-4.8881	112	0.99707	0.1287	-3.6326
23	0.05445	0.7149	4.8881	53	0.38533	1.9001	3.2708	83	0.82887	1.2851	-4.8881	113	0.99802	0.0999	-3.2708
24	0.06061	0.7556	4.8881	54	0.40127	1.9257	2.8731	84	0.83943	1.2444	-4.8881	114	0.99874	0.0743	-2.8731
25	0.06706	0.7963	4.8881	55	0.41745	1.9479	2.4440	85	0.84964	1.2037	-4.8881	115	0.99927	0.0521	-2.4440
26	0.07386	0.8371	4.8881	56	0.43377	1.9664	1.9882	86	0.85947	1.1629	-4.8881	116	0.99963	0.0336	-1.9882
27	0.08100	0.8778	4.8881	57	0.45015	1.9810	1.5105	87	0.86900	1.1222	-4.8881	117	0.99984	0.0190	-1.5105
28	0.08847	0.9185	4.8881	58	0.46672	1.9915	1.0163	88	0.87819	1.0815	-4.8881	118	0.99995	0.0085	-1.0163
29	0.09630	0.9593	4.8881	59	0.48333	1.9979	0.5110	89	0.88700	1.0407	-4.8881	119	0.99999	0.0021	-0.5110
30	0.10451	1.0000	4.8881	60	0.50000	2.0000	0.0000	90	0.89549	1.0000	-4.8881	120	1.00000	0.0000	0.0000

**TABLE B.4** Modified Sine Factors

Pt.	K	Cv	Ca	Pt.	K	Cv	Ca	Pt.	K	Cv	Ca	Pt.	K	Cv	Ca
0	0.00000	0.0000	0.0000	30	0.11718	1.0997	4.7874	60	0.50000	1.7596	0.0000	90	0.88282	1.0997	-4.7874
1	0.00000	0.0024	0.5778	31	0.12650	1.1392	4.6380	61	0.51466	1.7588	-0.1929	91	0.89182	1.0594	-4.8809
2	0.00005	0.0096	1.1493	32	0.13616	1.1778	4.5829	62	0.52931	1.7564	-0.3856	92	0.90048	1.0184	-4.9685
3	0.00018	0.0215	1.7082	33	0.14613	1.2156	4.4722	63	0.54393	1.7523	-0.5778	93	0.90880	0.9767	-5.0501
4	0.00042	0.0380	2.2484	34	0.15642	1.2524	4.3561	64	0.55851	1.7467	-0.7693	94	0.91676	0.9343	-5.1255
5	0.00083	0.0589	2.7640	35	0.16701	1.2882	4.2347	65	0.57304	1.7395	-0.9599	95	0.92436	0.8912	-5.1946
6	0.00142	0.0840	3.2493	36	0.17788	1.3229	4.1081	66	0.58750	1.7307	-1.1493	96	0.93161	0.8477	-5.2574
7	0.00224	0.1130	3.6989	37	0.18905	1.3566	3.9765	67	0.60178	1.7204	-1.3373	97	0.93849	0.8036	-5.3138
8	0.00331	0.1455	4.1081	38	0.20049	1.3892	3.8401	68	0.61617	1.7084	-1.5237	98	0.94500	0.7592	-5.3638
9	0.00467	0.1813	4.4723	39	0.21220	1.4206	3.6989	69	0.63035	1.6950	-1.7082	99	0.95114	0.7143	-5.4072
10	0.00634	0.2199	4.7874	40	0.22417	1.4508	3.5553	70	0.64442	1.6800	-1.8907	100	0.95690	0.6691	-5.4440
11	0.00834	0.2610	5.0501	41	0.23638	1.4798	3.4034	71	0.65835	1.6635	-2.0708	101	0.96229	0.6236	-5.4742
12	0.01069	0.3040	5.2574	42	0.24883	1.5075	3.2493	72	0.67214	1.6455	-2.2484	102	0.96730	0.5778	-5.4977
13	0.01341	0.3484	5.4072	43	0.26150	1.5340	3.0912	73	0.68577	1.6260	-2.4233	103	0.97192	0.5320	-5.5145
14	0.01650	0.3939	5.4977	44	0.27439	1.5590	2.9294	74	0.69924	1.6051	-2.5952	104	0.97611	0.4860	-5.5246
15	0.01998	0.4399	5.5280	45	0.28748	1.5828	2.7640	75	0.71252	1.5828	-2.7640	105	0.98002	0.4399	-5.5280
16	0.02389	0.4860	5.5246	46	0.30076	1.6051	2.5952	76	0.72561	1.5590	-2.9294	106	0.98350	0.3939	-5.4977
17	0.02808	0.5320	5.5145	47	0.31423	1.6260	2.4233	77	0.73850	1.5340	-3.0912	107	0.98659	0.3484	-5.4072
18	0.03270	0.5778	5.4977	48	0.32786	1.6455	2.2484	78	0.75117	1.5075	-3.2493	108	0.98931	0.3040	-5.2574
19	0.03771	0.6236	5.4742	49	0.34165	1.6635	2.0708	79	0.76362	1.4798	-3.4034	109	0.99166	0.2610	-5.0501
20	0.04310	0.6691	5.4440	50	0.35558	1.6800	1.8907	80	0.77583	1.4508	-3.5553	110	0.99366	0.2199	-4.7874
21	0.04886	0.7143	5.4072	51	0.36965	1.6950	1.7082	81	0.78780	1.4206	-3.6989	111	0.99533	0.1813	-4.4722
22	0.05500	0.7592	5.3638	52	0.38383	1.7084	1.5237	82	0.79951	1.3892	-3.8401	112	0.99669	0.1455	-4.1081
23	0.06151	0.8036	5.3138	53	0.39812	1.7204	1.3373	83	0.81095	1.3566	-3.9765	113	0.99776	0.1130	-3.6989
24	0.06839	0.8477	5.2574	54	0.41250	1.7307	1.1493	84	0.82212	1.3229	-4.1081	114	0.99858	0.0840	-3.2493
25	0.07564	0.8912	5.1946	55	0.42696	1.7395	0.9599	85	0.83299	1.2882	-4.2347	115	0.99917	0.0589	-2.7640
26	0.08324	0.9343	5.1255	56	0.44149	1.7467	0.7693	86	0.84358	1.2524	-4.3561	116	0.99958	0.0380	-2.2484
27	0.09120	0.9767	5.0501	57	0.45607	1.7523	0.5778	87	0.85387	1.2156	-4.4722	117	0.99982	0.0215	-1.7082
28	0.09952	1.0184	4.9685	58	0.47069	1.7564	0.3856	88	0.86384	1.1778	-4.5829	118	0.99995	0.0096	-1.1493
29	0.10818	1.0594	4.8809	59	0.48534	1.7588	0.1929	89	0.87350	1.1392	-4.6880	119	1.00000	0.0024	-0.5778
30	0.11718	1.0997	4.7874	60	0.50000	1.7596	0.0000	90	0.88282	1.0997	-4.7874	120	1.00000	0.0000	0.0000

*This page intentionally left blank.*

---

# APPENDIX C

---

# POLYNOMIAL COEFFICIENTS

---

**(Chapter 7, Geometry of Planar Cam Profiles)**

This appendix contains the polynomial coefficients appearing in the formulas derived in Chap. 7, Sec. 7.4 for the computation of the geometric properties of cams. For ease of presentation, the subscript  $i$  of the spline coefficient,  $A_{xi}, \dots, D_{yi}$  is omitted throughout.

**TABLE C.1**

$a_{ij}$	Expression
$a_{i1}$	$\frac{1}{2}(C_y D_x - C_x D_y)$
$a_{i2}$	$\frac{1}{2}(B_y D_x - B_x D_y)$
$a_{i3}$	$\frac{1}{6}(3A_y D_x - 3A_x D_y + B_y C_x - B_x C_y)$
$a_{i4}$	$\frac{1}{4}(A_y C_x - A_x C_y)$
$a_{i5}$	$\frac{1}{10}(A_y B_x - A_x B_y)$

**TABLE C.2**

$q_{xij}$	Expression
$q_{xi1}$	$C_y T_7$
$q_{xi2}$	$C_y T_6 + B_y T_7$
$q_{xi3}$	$\frac{1}{2}(C_y T_4 + B_y T_5 + 3A_y T_6)$
$q_{xi4}$	$\frac{1}{3}(C_y T_5 + 4B_y T_6 + 3A_y T_7)$
$q_{xi5}$	$\frac{1}{5}(C_y T_3 + 4B_y T_4 + 3A_y T_5)$
$q_{xi6}$	$\frac{1}{3}(C_y T_2 + B_y T_3 + 3A_y T_4)$
$q_{xi7}$	$\frac{1}{7}(C_y T_1 + 4B_y T_2 + 3A_y T_3)$
$q_{xi8}$	$\frac{1}{4}(B_y T_1 + 3A_y T_2)$
$q_{xi9}$	$\frac{1}{3}A_y T_1$

TABLE C.3

$T_i$	Expression
$T_1$	$A_x^2 + A_y^2$
$T_2$	$A_x B_x + A_y B_y$
$T_3$	$B_x^2 + B_y^2 + 2(A_x C_x + A_y C_y)$
$T_4$	$A_x D_x + A_y D_y + B_x C_x + B_y C_y$
$T_5$	$C_x^2 + C_y^2 + 2(B_x D_x + B_y D_y)$
$T_6$	$C_x D_x + C_y D_y$
$T_7$	$D_x^2 + D_y^2$

TABLE C.4

$h_i^{(1)}$	Expression
$h_1^{(1)}$	$C_x D_x T_7$
$h_2^{(1)}$	$2C_x D_x T_6 + Q_x T_4$
$h_3^{(1)}$	$C_x D_x T_5 + 2Q_x T_6 + 3B_x C_x T_7$
$h_4^{(1)}$	$2C_x D_x T_4 + Q_x T_5 + 6(B_x C_x + A_x D_x) T_6 + 2P_x T_7$
$h_5^{(1)}$	$C_x D_x T_3 + 2Q_x T_4 + 3B_x C_x T_5 + 4P_x T_6 + 5A_x B_x T_7$
$h_6^{(1)}$	$2C_x D_x T_2 + Q_x T_3 + 6B_x C_x T_4 + 2P_x T_5 + 10A_x B_x T_6 + 3A_x^2 T_7$
$h_7^{(1)}$	$C_x D_x T_1 + 2Q_x T_2 + 3B_x C_x T_3 + 4P_x T_4 + 5A_x B_x T_5 + 6A_x^2 T_6$
$h_8^{(1)}$	$Q_x T_1 + 6(B_x C_x + A_x D_x) T_2 + 2P_x T_3 + 10A_x B_x T_4 + 3A_x^2 T_5$
$h_9^{(1)}$	$3B_x C_x T_1 + 4P_x T_2 + 5A_x B_x T_3 + 6A_x^2 T_4$
$h_{10}^{(1)}$	$2P_x T_1 + 10A_x B_x T_2 + 3A_x^2 T_3$
$h_{11}^{(1)}$	$5A_x B_x T_1 + 6A_x^2 T_2$
$h_{12}^{(1)}$	$A_x^2 T_1$

TABLE C.5

$h_i^{(2)}$	Expression
$h_1^{(2)}$	$C_y D_y T_7$
$h_2^{(2)}$	$2C_y D_y T_6 + Q_y T_4$
$h_3^{(2)}$	$C_y D_y T_5 + 2Q_y T_6 + 3B_y C_y T_7$
$h_4^{(2)}$	$2C_y D_y T_4 + Q_y T_5 + 6(B_y C_y + A_y D_y) T_6 + 2P_y T_7$
$h_5^{(2)}$	$C_y D_y T_3 + 2Q_y T_4 + 3B_y C_y T_5 + 4P_y T_6 + 5A_y B_y T_7$
$h_6^{(2)}$	$2C_y D_y T_2 + Q_y T_3 + 6B_y C_y T_4 + 2P_y T_5 + 10A_y B_y T_6 + 3A_y^2 T_7$
$h_7^{(2)}$	$C_y D_y T_1 + 2Q_y T_2 + 3B_y C_y T_3 + 4P_y T_4 + 5A_y B_y T_5 + 6A_y^2 T_6$
$h_8^{(2)}$	$Q_y T_1 + 6(B_y C_y + A_y D_y) T_2 + 2P_y T_3 + 10A_y B_y T_4 + 3A_y^2 T_5$
$h_9^{(2)}$	$3B_y C_y T_1 + 4P_y T_2 + 5A_y B_y T_3 + 6A_y^2 T_4$
$h_{10}^{(2)}$	$2P_y T_1 + 10A_y B_y T_2 + 3A_y^2 T_3$
$h_{11}^{(2)}$	$5A_y B_y T_1 + 6A_y^2 T_2$
$h_{12}^{(2)}$	$A_y^2 T_1$

**TABLE C.6**

$h_i^{(3)}$	Expression
$h_1^{(3)}$	$C_x D_y T_7$
$h_2^{(3)}$	$2C_x D_y T_6 + Z_x T_7$
$h_3^{(3)}$	$C_x D_y T_5 + 2Z_x T_6 + W_x T_7$
$h_4^{(3)}$	$2C_x D_y T_4 + Z_x T_5 + 2W_x T_6 + V_x T_7$
$h_5^{(3)}$	$C_x D_y T_3 + 2Z_x T_4 + W_x T_5 + 2V_x T_6 + U_x T_7$
$h_6^{(3)}$	$2C_x D_y T_2 + Z_x T_3 + 2W_x T_4 + V_x T_5 + 2U_x T_6 + 3A_x A_y T_7$
$h_7^{(3)}$	$C_x D_y T_1 + 2Z_x T_2 + W_x T_3 + 2V_x T_4 + U_x T_5 + 6A_x A_y T_6$
$h_8^{(3)}$	$Z_x T_1 + 2W_x T_2 + V_x T_3 + 2U_x T_4 + 3A_x A_y T_5$
$h_9^{(3)}$	$W_x T_1 + 2V_x T_2 + U_x T_3 + 6A_x A_y T_4$
$h_{10}^{(3)}$	$V_x T_1 + 2U_x T_2 + 3A_x A_y T_3$
$h_{11}^{(3)}$	$U_x T_1 + 6A_x A_y T_2$
$h_{12}^{(3)}$	$A_x A_y T_1$

**TABLE C.7**

$h_i^{(4)}$	Expression
$h_1^{(4)}$	$C_y D_x T_7$
$h_2^{(4)}$	$2C_y D_x T_6 + Z_y T_7$
$h_3^{(4)}$	$C_y D_x T_5 + 2Z_y T_6 + W_y T_7$
$h_4^{(4)}$	$2C_y D_x T_4 + Z_y T_5 + 2W_y T_6 + V_y T_7$
$h_5^{(4)}$	$C_y D_x T_3 + 2Z_y T_4 + W_y T_5 + 2V_y T_6 + U_y T_7$
$h_6^{(4)}$	$2C_y D_x T_2 + Z_y T_3 + 2W_y T_4 + V_y T_5 + 2U_y T_6 + 3A_y A_x T_7$
$h_7^{(4)}$	$C_y D_x T_1 + 2Z_y T_2 + W_y T_3 + 2V_y T_4 + U_y T_5 + 6A_y A_x T_6$
$h_8^{(4)}$	$Z_y T_1 + 2W_y T_2 + V_y T_3 + 2U_y T_4 + 3A_y A_x T_5$
$h_9^{(4)}$	$W_y T_1 + 2V_y T_2 + U_y T_3 + 6A_y A_x T_4$
$h_{10}^{(4)}$	$V_y T_1 + 2U_y T_2 + 3A_y A_x T_3$
$h_{11}^{(4)}$	$U_y T_1 + 6A_y A_x T_2$
$h_{12}^{(4)}$	$A_y A_x T_1$

**TABLE C.8**

Coef <sub>x</sub>	Expression
$P_x$	$B_x^2 + 2A_x C_x$
$Q_x$	$C_x^2 + 2B_x D_x$
$U_x$	$2A_y B_x + 3A_x B_y$
$V_x$	$A_y C_x + 2B_x B_y + 3A_x C_y$
$W_x$	$B_y C_x + 2B_x C_y$
$Z_x$	$C_x C_y + 2B_x D_y$

*This page intentionally left blank.*

---

# APPENDIX D

---

## CAM COMPUTER SOFTWARE

---

D.1 INTRODUCTION	561	Profiles	562
D.2 COMPUTER SOFTWARE LISTING	561	Chapter 12, Cam System Dynamics—	
Chapter 5, Cam Motion Synthesis Using		Analysis	563
Spline Functions	561	Chapter 13, Cam System Dynamics—	
Chapter 6, Elements of Cam Profile		Response	563
Geometry	561	Chapter 16, Automotive Camshaft	
Chapter 7, Geometry of Planar Cam		Dynamics	563

---

### D.1 INTRODUCTION

---

The development and application of computer resources has significantly contributed to the understanding of the cam-follower system complete design. The personal computer with its appropriate software can create in either graphical or tabular form the cam profile on the screen. With the graphics workstation the designer can study and optimize the motion and geometry of the cam mechanism over an entire range of operating speeds. Networked machine tools direct the geometric data from the CAD system to the manufacturing of the actual cam. Much of the drudgery of compilation and the possibility of errors are greatly reduced. Also, computer resources have made available more detailed modeling techniques for the dynamic analysis of cam-follower mechanisms. Cam shaft flexibility, follower friction and nonlinearities, oil-film effect, lubricant selection, effect of contaminants, and life of functions parts are a few of the many factors of the computer use for potential value.

Most manufacturers of industrial machinery have developed proprietary software packages for their specific needs. However, this section presents a short compilation of software that is available commercially. The software choices listed are the most recent and popular. It is the responsibility of the designer to investigate the application to a specific problem. This section also lists the software for both general industrial applications and automobile software packages available for automobile designers and racing car enthusiasts.

---

### D.2 COMPUTER SOFTWARE LISTING

---

#### Chapter 5, Cam Motion Synthesis Using Spline Functions

Many software packages contain procedures for evaluating B-splines (de Boor, 1977, and Foy, 1977).

de Boor, C. "Package for Calculating with B-Splines," *Siam Journal of Numerical Analysis*, 14 (3): 441–472, June 1977.

Foy, P. A., Ed., *The Port Mathematical Subroutine Library*, Bell Laboratories, Murray Hill, N.J., 1977.

#### Chapter 6, Elements of Cam Profile Geometry

*PARADE*: pressure angle and radius of curvatures

*CAMPA*: cam pressure angle

*RAD1*: radius of curvature 1

*RAD2*: radius of curvature 2

F. Y. Chen, "Mechanics and Design of Cam Mechanisms," Pergamon Press, New York 1982, appendix: Fortran listed programs of foregoing

*CAM DESIGNER SE*, Delta Engineering Corporation, [www.delta-eng.com](http://www.delta-eng.com): Design and fabricate plate and barrel cams with translating, oscillating, and indexing up to 40th order polynomial; presents geometric properties, CNC file for most machines.

## Chapter 7, Geometry of Planar Cam Profiles

The synthesis and design of cam mechanisms can be eased by using the capabilities offered by CAD packages. Extensive CAD software is commercially available, and new packages and new features appear every year. Among these features, we can mention the plotting of functions, the rotation and translation of planar rigid figures, and the determination of intersections of lines, curves, and surfaces. This is important, since to start the design process, we assume that the displacement program of the follower is given as a smooth, explicit function of the input variable so that its derivative is available.

If only a discrete set of points is specified for the functions needed in the synthesis procedures, an interpolation is needed. This can be implemented by using software packages as well.

Two representative commercial packages are:

### *AUTOCAD*

Comprehensive package for mechanical design and geometric analysis. Runs mostly on Windows. Old versions run also on Unix. Vendor: Autodesk, Inc. Web site is: <http://infoautodesk.com/>

### *VERSACAD*

Basically, this is production-level CAD software. However, the 3DJoy module is a modeler that offers high-powered spline-based modeling. Also, the Rhino module can create, edit, analyze, and translate NURBS, surfaces, and solids. Runs on Windows. Vendor: Archway Systems, Inc. Web site is: <http://www.versacad.com/>

Other pertinent CAD software packages have more advanced features in terms of solid modeling, assembly, and motion animation, e.g.:

### *PRO/ENGINEER*

Comprehensive package for mechanical design and analysis at large. Its PRO/MECHANICA module provides motion analysis, simulation, and animation of fairly complex mechanisms. Runs on Windows and Unix. Vendor: Parametric Technology, Inc. Web site is: <http://www.ptc.com/>

### *CATIA*

This software package has advanced features that can be used for creating and modifying freeform surfaces, complex solids, parametric modifications, and the use of solids in a multimodel environment. Vendor: TBM Technologies. Web site is: <http://www.catia.com/>

### *UNIGRAPHICS*

High-end, comprehensive package with modules for finite-element analysis, CAD/CAM, and so on. It features ADAMS, a general tool for mechanism and multibody-system analysis. No synthesis features are supported. Vendor: Unigraphics Solutions. Web site is: <http://www.openitx.com/>

## Chapter 12, Cam System Dynamics—Analysis

*DYNACAM*, M. P. Koster, “Vibration of Cam Mechanisms,” Macmillan Publishers, London 1970.

A program to simulate a complex multidegree of freedom model for linear and non-linear effects.

The following are the commercially available computer programs:

TK Solver, Universal Technical Services

1220 Rock Street  
Rockford, Ill. 61101  
www.uts.com

Mathcod, Mathsoft, Inc  
101 Main St.  
Cambridge, Mass. 02142  
www.mathsoft.com

MATLAB/SIMULINK, The Mathworks, Inc.  
2W Prime Parkway  
Natick, Mass. 01760  
www.mathworks.com

## Chapter 13, Cam System Dynamics—Response

*SPEC1, SPEC2, SPEC3*, F. Y. Chen, “Mechanics and Design of Cam Mechanisms” Pergamon Press, New York, 1982

Appendix: Fortran-listed programs for frequency spectra solution investigation.

## Chapter 16, Automotive Camshaft Dynamics

(For more software listings, see “Camshaft Reference Handbook” by D. Hubbard, Fort Myers, Fla., 2000 dhubbard@peganet.com)

*AIR FLOW TESTING*, Audie Technology Inc.

<http://www.audietech.com/cpinfo.htm>

Combines with Flow Quick for Air Flow Testing.

*CAMPRO* and *CAMPRO PLUS*, Audie Technology Inc.

<http://www.audietech.com/cpinfo.htm>

Shows high-resolution graphics to visualize cam lobes, valve lift, base circle runout, overlap, velocity, acceleration, and jerk.

*DESINE*, Gary Matthews, Gainesville, Fla., GKMatthew@aol.com

The main emphasis of this software is for the design of the camshaft and valve train system. The polynomial powers are not restricted to integers. It also accepts internal conditions by techniques that avoid “runoff” on flat follows.

*DOCTOR DOCTOR*, Gary Matthews, Gainesville, Fla., GKMatthew@aol.com

Accepts lift files from any source for complete analysis of lift curves (cam or valve), can be overlaid allowing for resources quality control data corrected for runout, and can be filtered to remove manufacturing noise.

*DYNOMATION*, Allan H. Lookheed, Golden, Colo.; (303) 238-2415

Computer modeling of internal combustion engine dynamics plus optional data inputs from most files.

*ENGINE EXPERT*, Allen H. Lockheed, Golden, Colo.; (303) 238-2415  
will predict air flow requirements and valve timing events.

*EZCAM*, Andrews Products, Inc., Rosemont, Ill.

<http://www.andrewsproducts.com/camshaft/ezcam/index.html>

Provides camshaft inspection for measurement and analysis. Inspect one, two lobes on entire camshaft for lift, velocity, acceleration, jerk, radius of curvature, and lobe timing.

*FLOW QUIK*, Audie Technology Inc.

<http://www.audietech.com/cpinfo.htm>

Portable air flow tester.

*FLOW PRO*, Audie Technology Inc.

<http://www.audietech.com/cpinfo.htm>

Software for processing and analysis of flow bench data.

*LOCAM, RADCAM*, James Amick, Ann Arbor, Mich., (734-663-3956)

Provides a quick method for designing a low-lift valve motion. It is able to design a low profile with a negative radius of curvature.

*MOTOR DRIVE*, Audie Technology Inc.

<http://www.audietech.com/cpinfo.htm>

Motor drive option for cam flow process.

*SPRING MASTER*, Steve Gruenwold, Dundas, Minn.

[www.integralcams.com](http://www.integralcams.com)

Compares the natural frequency of the spring to the harmonics of the cam and yields the forces on the valve.

*SWIRL METER*, Audie Technology Inc.

<http://www.audietech.com/cpinfo.htm>

Computer ready, RPM-based design to study swirl conditions.

*UTILITY ENGINE PROGRAMS*, Don Hubbard, Ft. Myers, Fla., [dhubbard@peganet.com](mailto:dhubbard@peganet.com)

Contains an assortment of engine programs that boulders may apply.

*VALVE PRO*, Audie Technology Inc.

<http://www.audietech.com/cpinfo.htm>

Kinematically models valve train to produce accurate valve motion profile from measured cam data.

---

# APPENDIX E

---

## CAD/CAM FOR A MEDICAL INSTRUMENT CAM MECHANISM

---

E.1 INTRODUCTION 565  
E.2 KINEMATIC DESIGN 565

E.3 MANUFACTURING 566  
E.4 INSPECTION 566

---

### ***E.1 INTRODUCTION***

---

In this section part-program files are presented containing the kinematic design, manufacturing data, and inspection of a cam for a medical instrument mechanism. Presented are the CAD/CAM steps taken to study the cam geometric data of pressure angle, radius of curvature, and CNC machining of the cam profile. The material was submitted by Commercial Cam Co. Inc. (CAMCO), Wheeling, Illinois, Division of Emerson Electric Corp. It includes a copy of their worksheets for their fabrication plant. The data for incremental values is for:

- pressure angle and also the maximum pressure angle
- radii of curvature and minimum radius of curvature
- milling and grinding machine tools to be stored in the machining center in preparation for the fabrication and inspection of the cam.

The information contained herein refers to Chap. 7, Geometry of Planar Cam Profiles, which contains the algorithms for developing the data to be downloaded for Chap. 10, Cam Manufacturing. A sample plate cam is shown that contains kinematic listings and contour plots necessary in analyzing and manufacturing the proper cam contour to the desired accuracy. Note that 1 deg increments (2 deg is usually acceptable) are employed for the kinematic study, while the cam profile is manufactured at  $1/4$ -degree increments for this small-size cam. The cam profile data at  $1/4$ -degree increments can easily be tabulated and is not included here. After the cam is machined, some polishing and burr removal may be necessary.

---

### ***E.2 KINEMATIC DESIGN***

---

A customer detailed print or the preliminary CAD information is used to verify the cam contour geometric parameters including pressure angle, radii of curvature, dwell, and motion time. If linkages are involved through computer software the cam contour is reproduced by placing the required motions at the endpoint and working the motions back through the linkage to the cam surface. CAMCO employs its own Fortran-based programs, digital microfax for cam, and linkage analysis which includes the cam curve choice, with the necessary computer software. In this stage of investigation the materials, tolerances, and lubrication are selected.

### E.3 MANUFACTURING

---

If no design issues such as undercutting, very small radii of curvature, or extreme pressure angles exist designers next produce a single file for use with a “universal post” which creates a part program for the requested machining center. The universal post stores the coordinate file for the cam and forwards it to whatever machine runs the part program. This “runs on the fly” in local machine memory. Depending on the need for grinding, a cam is typically milled, sent for heat treating, and then ground using various types of 3-axis linear to 5-axis linear/rotary machining center. The post processor creates the individual part program locally for transfer into the machine memory. This system basically saves computer disk space because only the file is required for manufacturing regardless of the type of machining center used. Note that the grinding operation will employ a rotary machine having a two-axis turret. The last operation consists of hand removing the “burrs” on the cam-edges.

### E.4 INSPECTION

---

After manufacturing, basic cam parameters such as (a) dwell time, (b) cam profile radii, (c) clearances and tolerances for the follower roller, and (d) the keyway location are verified. If needed a full contour analysis can be made by utilizing a “Leitz PMM” coordinate measuring machine (Brown & Sharpe Corp., North Kingston, RI). A theoretical “edge of track” coordinate file is produced and is graphically plotted and tabulated against the theoretical curve. This yields an accurate point-to-point analysis throughout the entire contour.

**EXAMPLE** *A customer in the medical instrument field indicates a need for a plate cam that is low speed at 60 rpm with a radial translating roller follower. It is a DRDRD cycle of 90°, each showing the steps necessary in the kinematic study of the pressure angle and radii of curvature plus the manufacturing data to be forwarded to the shop.*

**Solution** *The cam curve selected was the popular modified sine curve with simple harmonic curve sector at 75 percent of the cycle and the cycloidal ends of 12.5 percent each. Also, a grinding operation was chosen with a cam contour tolerance of  $\pm 0.001$  inch. Figures E.9 and E.10 summarize the coordinate information developed by CAMCO for the B-12345 sample cam.*

Figure E.1 B-12345 Sample cam, milling part-program files (shows milling operation tools to be used in machining center).

Figure E.2 B-12345 Sample cam, grinding part-program files (lists grinding operation tools).

Figure E.3 Plate cam stock (shows the selected body for the cam).

Figure E.4 Drawing with cam contour (preliminary drawing of cam shape).

Figure E.5 Drawing with cam contour and check (presents basic data picture of coordinates and visual track of locus of roller follower).

Figure E.6 Custom plate specifications (shows coordinate file for use with universal post; record check for part position).

Figure E.7 B-12345 Sample cam—plot of coordinate file (coordinate check).

Figure E.8 B-12345 Sample cam—kinematic listing (contains basic kinematic data).

```

O1
N2T20
N3M6
N4D30H20
N5M98P100
N6T21
N7M6
N8D31H21
N9M98P100
N10T22
N11M6
N12D32H22
N13M98P100
N14M30
O100
N101G20G17
N102G00G90G55X0Y0
N103X-29149Y-2559
N104G41X-24923Y-11622
N105S300M3
N106G43Z10000M8
N107G91Z-8000
N108G1Z-2000F1000
N109M98P200
N110M9
N111G40
N112G28Z0M19
N113M99
O200
N201X50Y-109Z-1
N202X52Y-108Z-7
N203X52Y-108Z-18
N204X52Y-108Z-34
N205X53Y-108Z-52
*****
N990X81Y-88Z146
N991X82Y-88Z128
N992X82Y-88Z110
N993X82Y-87Z91
N994X83Y-87Z72
N995X83Y-86Z52
N996X84Y-86Z34
N997X84Y-86Z18
N998X84Y-85Z7
N999X85Y-85Z1
N1000Z2000
N1001M99

```

**FIGURE E.1.** B-12345 Sample cam milling part-program file.

```

%MPF100
(CAMCO, B-12345)
N5M95
N10G04X.5
/N15(PROGRAM-STOP)M00
N20G60G90S2000
N25G00Z250
N30U0.0V69.8500
N35C205.0000
N40Z235.725
N45M03
N50G01G94F150
/N55M00
N60M26
N65G64G90
N70G04X15.0
N71V69.8500Z235.723C205.2500
N72V69.8500Z235.705C205.5000
N73V69.8500Z235.658C205.7500
N74V69.8500Z235.572C206.0000
N75V69.8500Z235.440C206.2500
****
N860V69.8500Z234.423C222.7500
N861V69.8500Z234.749C223.0000
N862V69.8500Z235.028C223.2500
N863V69.8500Z235.258C223.5000
N864V69.8500Z235.440C223.7500
N865V69.8500Z235.572C224.0000
N866V69.8500Z235.658C224.2500
N867V69.8500Z235.705C224.5000
N868V69.8500Z235.723C224.7500
N869V69.8500Z235.725C225.0000
N874G90G00
N879Z250
N884M05M27
N889G60
N894C360.000
N899@123R0R1K9995
N904@621R0
N909G91B=R2
N914@100K-5
N9995B0
N9999M30

```

**FIGURE E.2.** B-12345 Sample cam, grinding part-program file.

Figure E.9 B-12345 Sample cam—kinematic coordinate values (Note: radii of curvature is for the pitch contour, i.e., center of roller. The minimum radius of curvature is  $-1.4054$  at  $55^\circ$  and  $305^\circ$  and also  $+1.2913$  at  $123^\circ$  and  $237^\circ$ . Also the maximum pressure angle is  $38.2842$  at  $82^\circ$ . This pressure angle is accepted since a small cam is desired because only a small space is available. For use in the universal post the  $1/2$ -degree increments would be forwarded for the cam fabrication. Also note that the velocity and acceleration values are listed as a check on the data).



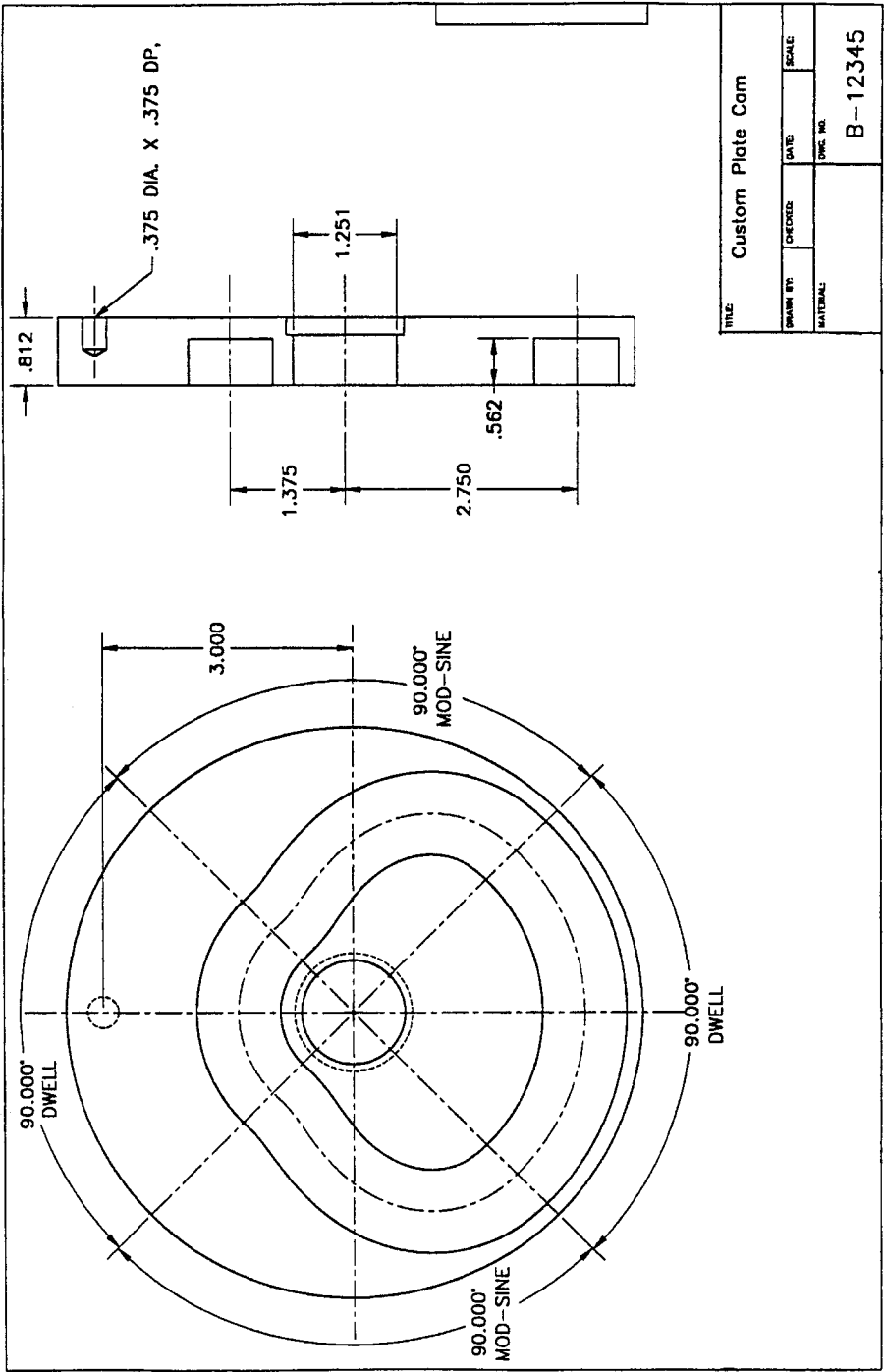


FIGURE E.4. Drawing with cam contour.

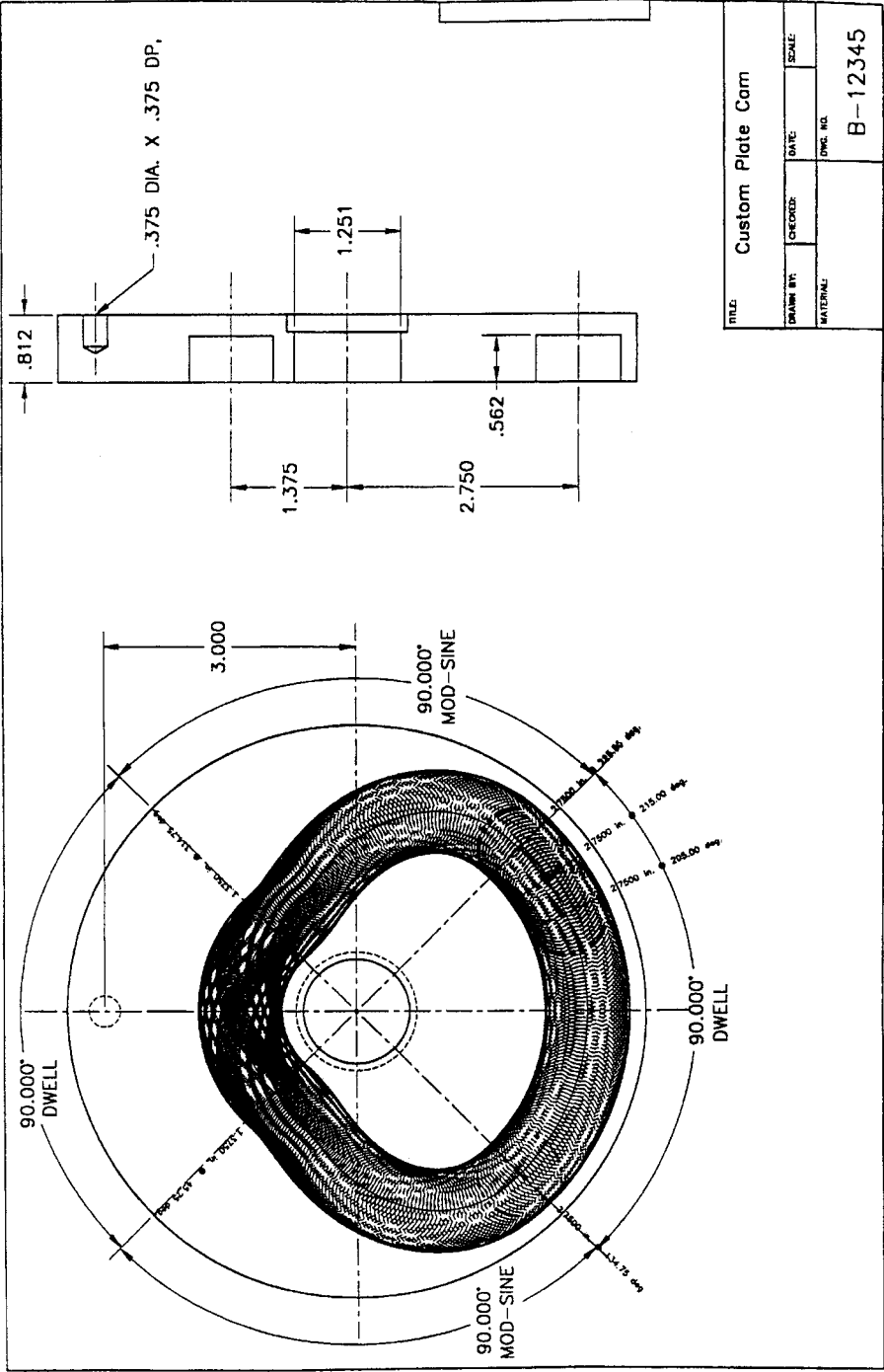


FIGURE E.5. Drawing with cam contour and check.

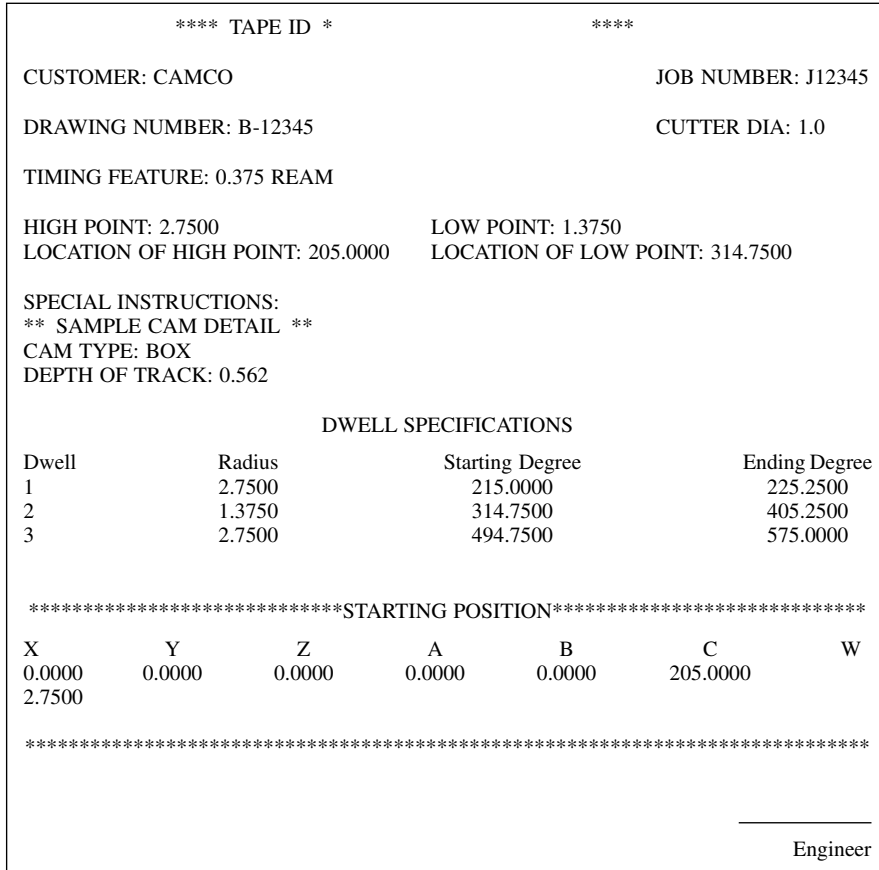


FIGURE E.6. Custom plate specifications.

Figure E.10 Loading study (summarizes the study and presents minimum radii of curvature to present small, sharp cam corners that could produce brittle heat-treatment cracks. Also the limiting speed of 10,000rpm is the recommendation by McGill Manufacturing Co., the roller manufacturer).

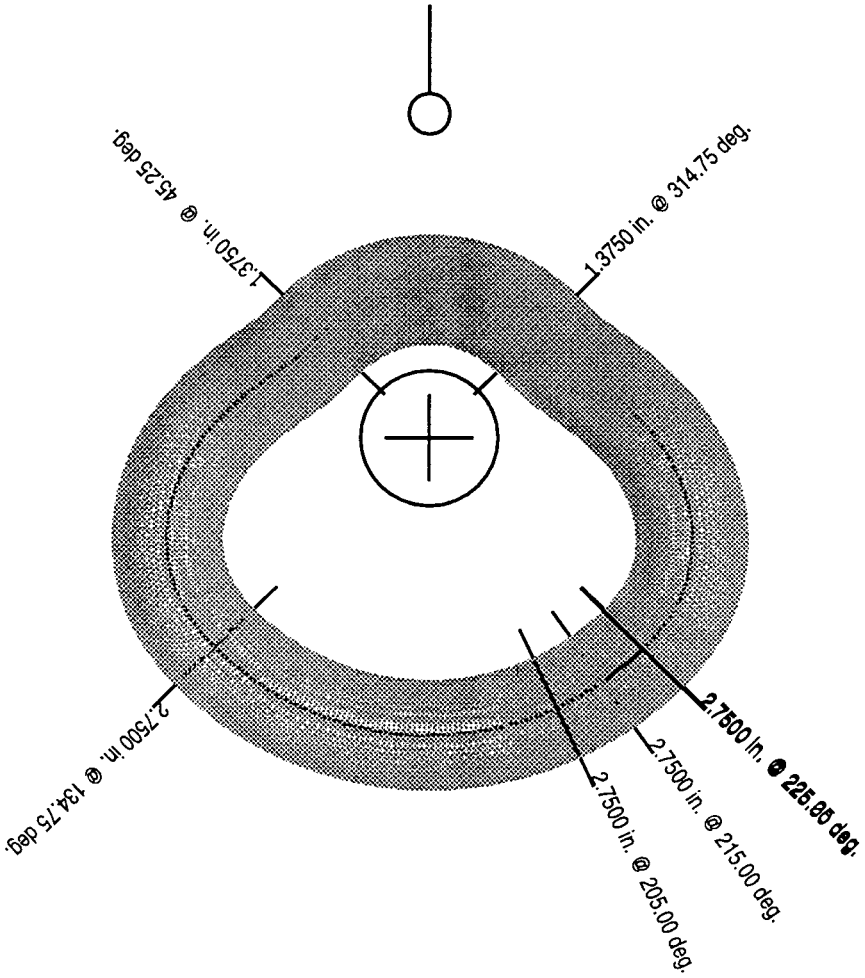


FIGURE E.7. B-12345 Sample cam plot of coordinate file.

```

*****
*
* IN-LINE PLATE CAM ANALYSIS
*
*****

-APPLICATION-

B-12345

MAXIMUM RADIUS      = 2.7500 INCHES
MINIMUM RADIUS      = 1.3750 INCHES
MOTION PERIOD       = 360.0000 DEGREES
FOLLOWER DIAMETER   = 1.0000 INCHES
CAMSHAFT SPEED      = 60.0000 RPM

```

FIGURE E.8. B-12345 Sample cam—kinematic listing.

CAMCO B-12345 (SAMPLE)						
CAMSHAFT ANGLE (DEGREES)	FOLLOWER ANGLE (DEGREES)	FOLLOWER RADIUS (INCHES)	FOLLOWER VELOC (INCHES/SEC)	FOLLOWER ACCEL (INCH/SEC/SEC)	PRESSURE ANGLE (DEGREES)	RADIUS OF CURV (INCHES)
0.0000	0.0000	1.3750	0.0000	0.0000	0.0000	1.3750
1.0000	1.0000	1.3750	0.0000	0.0000	0.0000	1.3750
2.0000	2.0000	1.3750	0.0000	0.0000	0.0000	1.3750
3.0000	3.0000	1.3750	0.0000	0.0000	0.0000	1.3750
4.0000	4.0000	1.3750	0.0000	0.0000	0.0000	1.3750
5.0000	5.0000	1.3750	0.0000	0.0000	0.0000	1.3750
6.0000	6.0000	1.3750	0.0000	0.0000	0.0000	1.3750
7.0000	7.0000	1.3750	0.0000	0.0000	0.0000	1.3750
8.0000	8.0000	1.3750	0.0000	0.0000	0.0000	1.3750
9.0000	9.0000	1.3750	0.0000	0.0000	0.0000	1.3750
10.0000	10.0000	1.3750	0.0000	0.0000	0.0000	1.3750
11.0000	11.0000	1.3750	0.0000	0.0000	0.0000	1.3750
12.0000	12.0000	1.3750	0.0000	0.0000	0.0000	1.3750
13.0000	13.0000	1.3750	0.0000	0.0000	0.0000	1.3750
14.0000	14.0000	1.3750	0.0000	0.0000	0.0000	1.3750
15.0000	15.0000	1.3750	0.0000	0.0000	0.0000	1.3750
16.0000	16.0000	1.3750	0.0000	0.0000	0.0000	1.3750
17.0000	17.0000	1.3750	0.0000	0.0000	0.0000	1.3750
18.0000	18.0000	1.3750	0.0000	0.0000	0.0000	1.3750
19.0000	19.0000	1.3750	0.0000	0.0000	0.0000	1.3750
20.0000	20.0000	1.3750	0.0000	0.0000	0.0000	1.3750
21.0000	21.0000	1.3750	0.0000	0.0000	0.0000	1.3750
22.0000	22.0000	1.3750	0.0000	0.0000	0.0000	1.3750
23.0000	23.0000	1.3750	0.0000	0.0000	0.0000	1.3750
24.0000	24.0000	1.3750	0.0000	0.0000	0.0000	1.3750
25.0000	25.0000	1.3750	0.0000	0.0000	0.0000	1.3750
26.0000	26.0000	1.3750	0.0000	0.0000	0.0000	1.3750
27.0000	27.0000	1.3750	0.0000	0.0000	0.0000	1.3750
28.0000	28.0000	1.3750	0.0000	0.0000	0.0000	1.3750
29.0000	29.0000	1.3750	0.0000	0.0000	0.0000	1.3750
30.0000	30.0000	1.3750	0.0000	0.0000	0.0000	1.3750

**FIGURE E.9.** B-12345 Sample cam kinematic coordinate values.

CAMCO B-12345 (SAMPLE)						
CAMSHAFT ANGLE (DEGREES)	FOLLOWER ANGLE (DEGREES)	FOLLOWER RADIUS (INCHES)	FOLLOWER VELOC (INCHES/SEC)	FOLLOWER ACCEL (INCH/SEC/SEC)	PRESSURE ANGLE (DEGREES)	RADIUS OF CURV (INCHES)
31.0000	31.0000	1.3750	0.0000	0.0000	0.0000	1.3750
32.0000	32.0000	1.3750	0.0000	0.0000	0.0000	1.3750
33.0000	33.0000	1.3750	0.0000	0.0000	0.0000	1.3750
34.0000	34.0000	1.3750	0.0000	0.0000	0.0000	1.3750
35.0000	35.0000	1.3750	0.0000	0.0000	0.0000	1.3750
36.0000	36.0000	1.3750	0.0000	0.0000	0.0000	1.3750
37.0000	37.0000	1.3750	0.0000	0.0000	0.0000	1.3750
38.0000	38.0000	1.3750	0.0000	0.0000	0.0000	1.3750
39.0000	39.0000	1.3750	0.0000	0.0000	0.0000	1.3750
40.0000	40.0000	1.3750	0.0000	0.0000	0.0000	1.3750
41.0000	41.0000	1.3750	0.0000	0.0000	0.0000	1.3750
42.0000	42.0000	1.3750	0.0000	0.0000	0.0000	1.3750
43.0000	43.0000	1.3750	0.0000	0.0000	0.0000	1.3750
44.0000	44.0000	1.3750	0.0000	0.0000	0.0000	1.3750
45.0000	45.0000	1.3750	0.0000	0.0000	0.0000	1.3750
46.0000	46.0000	1.3750	0.0235	16.9255	0.1562	1.9980
47.0000	47.0000	1.3752	0.0937	33.5217	0.6215	3.5933
48.0000	48.0000	1.3756	0.2092	49.4653	1.3864	15.2457
49.0000	49.0000	1.3764	0.3676	64.4462	2.4343	-7.5652
50.0000	50.0000	1.3777	0.5660	78.1727	3.7414	-3.2338
51.0000	51.0000	1.3796	0.8005	90.3776	5.2765	-2.1751
52.0000	52.0000	1.3821	1.0665	100.8235	7.0014	-1.7288
53.0000	53.0000	1.3855	1.3588	109.3069	8.8718	-1.5126
54.0000	54.0000	1.3897	1.6718	115.6628	10.8388	-1.4174
55.0000	55.0000	1.3948	1.9993	119.7674	12.8512	-1.4054
56.0000	56.0000	1.4008	2.3350	121.5410	14.8579	-1.4676
57.0000	57.0000	1.4078	2.6728	121.5410	16.8131	-1.5981
58.0000	58.0000	1.4157	3.0100	121.2119	18.6955	-1.7724
59.0000	59.0000	1.4245	3.3459	120.6203	20.4972	-2.0030
60.0000	60.0000	1.4343	3.6799	119.7674	22.2122	-2.3123
61.0000	61.0000	1.4449	4.0111	118.6552	23.8360	-2.7375

FIGURE E.9. (Continued)

CAMCO B-12345 (SAMPLE)

CAMSHAFT ANGLE (DEGREES)	FOLLOWER ANGLE (DEGREES)	FOLLOWER RADIUS (INCHES)	FOLLOWER VELOC (INCHES/SEC)	FOLLOWER ACCEL (INCH/SEC/SEC)	PRESSURE ANGLE (DEGREES)	RADIUS OF CURV (INCHES)
62.0000	62.0000	1.4565	4.3388	117.2860	25.3656	-3.3453
63.0000	63.0000	1.4690	4.6624	115.6628	26.7994	-4.2677
64.0000	64.0000	1.4824	4.9812	113.7891	28.1369	-5.8063
65.0000	65.0000	1.4967	5.2943	111.6689	29.3788	-8.8364
66.0000	66.0000	1.5118	5.6013	109.3069	30.5262	-17.3939
67.0000	67.0000	1.5278	5.9014	106.7081	31.5813	-185.7170
68.0000	68.0000	1.5446	6.1939	103.8783	32.5464	23.2065
69.0000	69.0000	1.5622	6.4783	100.8235	33.4244	11.3671
70.0000	70.0000	1.5806	6.7538	97.5503	34.2181	7.7297
71.0000	71.0000	1.5997	7.0200	94.0658	34.9308	5.9720
72.0000	72.0000	1.6196	7.2762	90.3776	35.5657	4.9406
73.0000	73.0000	1.6402	7.5219	86.4937	36.1259	4.2652
74.0000	74.0000	1.6614	7.7566	82.4224	36.6146	3.7902
75.0000	75.0000	1.6832	7.9797	78.1727	37.0347	3.4391
76.0000	76.0000	1.7057	8.1907	73.7536	37.3893	3.1696
77.0000	77.0000	1.7287	8.3893	69.1748	37.6810	2.9567
78.0000	78.0000	1.7523	8.5749	64.4462	37.9126	2.7843
79.0000	79.0000	1.7764	8.7472	59.5780	38.0864	2.6421
80.0000	80.0000	1.8009	8.9058	54.5807	38.2049	2.5227
81.0000	81.0000	1.8258	9.0503	49.4653	38.2702	2.4209
82.0000	82.0000	1.8511	9.1805	44.2427	38.2843	2.3330
83.0000	83.0000	1.8768	9.2960	38.9243	38.2491	2.2561
84.0000	84.0000	1.9028	9.3966	33.5217	38.1663	2.1882
85.0000	85.0000	1.9290	9.4822	28.0464	38.0376	2.1275
86.0000	86.0000	1.9554	9.5524	22.5103	37.8644	2.0727
87.0000	87.0000	1.9820	9.6072	16.9255	37.6480	2.0229
88.0000	88.0000	2.0088	9.6464	11.3041	37.3898	1.9772
89.0000	89.0000	2.0356	9.6700	5.6582	37.0909	1.9349
90.0000	90.0000	2.0625	9.6778	0.0000	36.7523	1.8955
91.0000	91.0000	2.0894	9.6700	-5.6582	36.3751	1.8586
92.0000	92.0000	2.1162	9.6464	-11.3041	35.9602	1.8239

FIGURE E.9. (Continued)

CAMCO B-12345 (SAMPLE)						
CAMSHAFT ANGLE (DEGREES)	FOLLOWER ANGLE (DEGREES)	FOLLOWER RADIUS (INCHES)	FOLLOWER VELOC (INCHES/SEC)	FOLLOWER ACCEL (INCH/SEC/SEC)	PRESSURE ANGLE (DEGREES)	RADIUS OF CURV (INCHES)
93.0000	93.0000	2.1430	9.6072	-16.9255	35.5085	1.7909
94.0000	94.0000	2.1696	9.5524	-22.5103	35.0206	1.7596
95.0000	95.0000	2.1960	9.4822	-28.0464	34.4975	1.7297
96.0000	96.0000	2.2222	9.3966	-33.5217	33.9399	1.7010
97.0000	97.0000	2.2482	9.2960	-38.9243	33.3483	1.6735
98.0000	98.0000	2.2739	9.1805	-44.2427	32.7236	1.6470
99.0000	99.0000	2.2992	9.0503	-49.4653	32.0664	1.6215
100.0000	100.0000	2.3241	8.9058	-54.5807	31.3774	1.5969
101.0000	101.0000	2.3486	8.7472	-59.5780	30.6573	1.5732
102.0000	102.0000	2.3727	8.5749	-64.4462	29.9067	1.5503
103.0000	103.0000	2.3963	8.3893	-69.1748	29.1264	1.5283
104.0000	104.0000	2.4193	8.1907	-73.7536	28.3171	1.5071
105.0000	105.0000	2.4418	7.9797	-78.1727	27.4797	1.4868
106.0000	106.0000	2.4636	7.7566	-82.4224	26.6150	1.4673
107.0000	107.0000	2.4848	7.5219	-86.4937	25.7239	1.4486
108.0000	108.0000	2.5054	7.2762	-90.3776	24.8074	1.4309
109.0000	109.0000	2.5253	7.0200	-94.0658	23.8664	1.4141
110.0000	110.0000	2.5444	6.7538	-97.5503	22.9022	1.3982
111.0000	111.0000	2.5628	6.4783	-100.8235	21.9158	1.3833
112.0000	112.0000	2.5804	6.1939	-103.8783	20.9086	1.3694
113.0000	113.0000	2.5972	5.9014	-106.7081	19.8818	1.3565
114.0000	114.0000	2.6132	5.6013	-109.3069	18.8370	1.3447
115.0000	115.0000	2.6283	5.2943	-111.6689	17.7757	1.3339
116.0000	116.0000	2.6426	4.9812	-113.7891	16.6994	1.3243
117.0000	117.0000	2.6560	4.6624	-115.6628	15.6098	1.3159
118.0000	118.0000	2.6685	4.3388	-117.2860	14.5087	1.3087
119.0000	119.0000	2.6801	4.0111	-118.6552	13.3980	1.3027
120.0000	120.0000	2.6907	3.6799	-119.7674	12.2795	1.2979
121.0000	121.0000	2.7005	3.3459	-120.6203	11.1552	1.2944
122.0000	122.0000	2.7093	3.0100	-121.2119	10.0272	1.2922
123.0000	123.0000	2.7172	2.6728	-121.5410	8.8975	1.2913

FIGURE E.9. (Continued)

CAMCO B-12345 (SAMPLE)

CAMSHAFT ANGLE (DEGREES)	FOLLOWER ANGLE (DEGREES)	FOLLOWER RADIUS (INCHES)	FOLLOWER VELOC (INCHES/SEC)	FOLLOWER ACCEL (INCH/SEC/SEC)	PRESSURE ANGLE (DEGREES)	RADIUS OF CURV (INCHES)
124.0000	124.0000	2.7242	2.3350	-121.5410	7.7683	1.2922
125.0000	125.0000	2.7302	1.9993	-119.7674	6.6478	1.3029
126.0000	126.0000	2.7353	1.6718	-115.6628	5.5560	1.3274
127.0000	127.0000	2.7395	1.3588	-109.3069	4.5138	1.3668
128.0000	128.0000	2.7429	1.0665	-100.8235	3.5412	1.4229
129.0000	129.0000	2.7454	0.8005	-90.3776	2.6570	1.4984
130.0000	130.0000	2.7473	0.5660	-78.1727	1.8781	1.5972
131.0000	131.0000	2.7486	0.3676	-64.4462	1.2195	1.7246
132.0000	132.0000	2.7494	0.2092	-49.4653	0.6937	1.8887
133.0000	133.0000	2.7498	0.0937	-33.5217	0.3108	2.1010
134.0000	134.0000	2.7500	0.0235	-16.9255	0.0781	2.3791
135.0000	135.0000	2.7500	0.0000	0.0000	0.0000	2.7500
225.0000	225.0000	2.7500	0.0000	0.0000	0.0000	2.7500
226.0000	226.0000	2.7500	-0.0235	-16.9255	0.0781	2.3791
227.0000	227.0000	2.7498	-0.0937	-33.5217	0.3108	2.1010
228.0000	228.0000	2.7494	-0.2092	-49.4653	0.6937	1.8887
229.0000	229.0000	2.7486	-0.3676	-64.4462	1.2195	1.7246
230.0000	230.0000	2.7473	-0.5660	-78.1727	1.8781	1.5972
231.0000	231.0000	2.7454	-0.8005	-90.3776	2.6570	1.4984
232.0000	232.0000	2.7429	-1.0665	-100.8235	3.5412	1.4229
233.0000	233.0000	2.7395	-1.3588	-109.3069	4.5138	1.3668
234.0000	234.0000	2.7353	-1.6718	-115.6628	5.5560	1.3274
235.0000	235.0000	2.7302	-1.9993	-119.7674	6.6478	1.3029
236.0000	236.0000	2.7242	-2.3350	-121.5410	7.7683	1.2922
237.0000	237.0000	2.7172	-2.6728	-121.5410	8.8975	1.2913
238.0000	238.0000	2.7093	-3.0100	-121.2119	10.0272	1.2922
239.0000	239.0000	2.7005	-3.3459	-120.6203	11.1552	1.2944
240.0000	240.0000	2.6907	-3.6799	-119.7674	12.2795	1.2979
241.0000	241.0000	2.6801	-4.0111	-118.6552	13.3980	1.3027
242.0000	242.0000	2.6685	-4.3388	-117.2860	14.5087	1.3087
243.0000	243.0000	2.6560	-4.6624	-115.6628	15.6098	1.3159

FIGURE E.9. (Continued)

CAMCO B-12345 (SAMPLE)						
CAMSHAFT ANGLE (DEGREES)	FOLLOWER ANGLE (DEGREES)	FOLLOWER RADIUS (INCHES)	FOLLOWER VELOC (INCHES/SEC)	FOLLOWER ACCEL (INCH/SEC/SEC)	PRESSURE ANGLE (DEGREES)	RADIUS OF CURV (INCHES)
244.0000	244.0000	2.6426	-4.9812	-113.7891	16.6994	1.3243
245.0000	245.0000	2.6283	-5.2943	-111.6689	17.7757	1.3339
246.0000	246.0000	2.6132	-5.6013	-109.3069	18.8370	1.3447
247.0000	247.0000	2.5972	-5.9014	-106.7081	19.8818	1.3565
248.0000	248.0000	2.5804	-6.1939	-103.8783	20.9086	1.3694
249.0000	249.0000	2.5628	-6.4783	-100.8235	21.9158	1.3833
250.0000	250.0000	2.5444	-6.7538	-97.5503	22.9022	1.3982
251.0000	251.0000	2.5253	-7.0200	-94.0658	23.8664	1.4141
252.0000	252.0000	2.5054	-7.2762	-90.3776	24.8074	1.4309
253.0000	253.0000	2.4848	-7.5219	-86.4937	25.7239	1.4486
254.0000	254.0000	2.4636	-7.7566	-82.4224	26.6150	1.4673
255.0000	255.0000	2.4418	-7.9797	-78.1727	27.4797	1.4868
256.0000	256.0000	2.4193	-8.1907	-73.7536	28.3171	1.5071
257.0000	257.0000	2.3963	-8.3893	-69.1748	29.1264	1.5283
258.0000	258.0000	2.3727	-8.5749	-64.4462	29.9067	1.5503
259.0000	259.0000	2.3486	-8.7472	-59.5780	30.6573	1.5732
260.0000	260.0000	2.3241	-8.9058	-54.5807	31.3774	1.5969
261.0000	261.0000	2.2992	-9.0503	-49.4653	32.0664	1.6215
262.0000	262.0000	2.2739	-9.1805	-44.2427	32.7236	1.6470
263.0000	263.0000	2.2482	-9.2960	-38.9243	33.3483	1.6735
264.0000	264.0000	2.2222	-9.3966	-33.5217	33.9399	1.7010
265.0000	265.0000	2.1960	-9.4822	-28.0464	34.4975	1.7297
266.0000	266.0000	2.1696	-9.5524	-22.5103	35.0206	1.7596
267.0000	267.0000	2.1430	-9.6072	-16.9255	35.5085	1.7909
268.0000	268.0000	2.1162	-9.6464	-11.3041	35.9602	1.8239
269.0000	269.0000	2.0894	-9.6700	-5.6582	36.3751	1.8586
270.0000	270.0000	2.0625	-9.6778	0.0000	36.7523	1.8955
271.0000	271.0000	2.0356	-9.6700	5.6582	37.0909	1.9349
272.0000	272.0000	2.0088	-9.6464	11.3041	37.3898	1.9772
273.0000	273.0000	1.9820	-9.6072	16.9255	37.6480	2.0229
274.0000	274.0000	1.9554	-9.5524	22.5103	37.8644	2.0727

FIGURE E.9. (Continued)

CAMCO B-12345 (SAMPLE)

CAMSHAFT ANGLE (DEGREES)	FOLLOWER ANGLE (DEGREES)	FOLLOWER RADIUS (INCHES)	FOLLOWER VELOC (INCHES/SEC)	FOLLOWER ACCEL (INCH/SEC/SEC)	PRESSURE ANGLE (DEGREES)	RADIUS OF CURV (INCHES)
275.0000	275.0000	1.9290	-9.4822	28.0464	38.0376	2.1275
276.0000	276.0000	1.9028	-9.3966	33.5217	38.1663	2.1882
277.0000	277.0000	1.8768	-9.2960	38.9243	38.2491	2.2561
278.0000	278.0000	1.8511	-9.1805	44.2427	38.2843	2.3330
279.0000	279.0000	1.8258	-9.0503	49.4653	38.2702	2.4209
280.0000	280.0000	1.8009	-8.9058	54.5807	38.2049	2.5227
281.0000	281.0000	1.7764	-8.7472	59.5780	38.0864	2.6421
282.0000	282.0000	1.7523	-8.5749	64.4462	37.9126	2.7843
283.0000	283.0000	1.7287	-8.3893	69.1748	37.6810	2.9567
284.0000	284.0000	1.7057	-8.1907	73.7536	37.3893	3.1696
285.0000	285.0000	1.6832	-7.9797	78.1727	37.0347	3.4391
286.0000	286.0000	1.6614	-7.7566	82.4224	36.6146	3.7902
287.0000	287.0000	1.6402	-7.5219	86.4937	36.1259	4.2652
288.0000	288.0000	1.6196	-7.2762	90.3776	35.5657	4.9406
289.0000	289.0000	1.5997	-7.0200	94.0658	34.9308	5.9720
290.0000	290.0000	1.5806	-6.7538	97.5503	34.2181	7.7297
291.0000	291.0000	1.5622	-6.4783	100.8235	33.4244	11.3671
292.0000	292.0000	1.5446	-6.1939	103.8783	32.5464	23.2065
293.0000	293.0000	1.5278	-5.9014	106.7081	31.5813	-185.7170
294.0000	294.0000	1.5118	-5.6013	109.3069	30.5262	-17.3939
295.0000	295.0000	1.4967	-5.2943	111.6689	29.3788	-8.8364
296.0000	296.0000	1.4824	-4.9812	113.7891	28.1369	-5.8063
297.0000	297.0000	1.4690	-4.6624	115.6628	26.7994	-4.2677
298.0000	298.0000	1.4565	-4.3388	117.2860	25.3656	-3.3453
299.0000	299.0000	1.4449	-4.0111	118.6552	23.8360	-2.7375
300.0000	300.0000	1.4343	-3.6799	119.7674	22.2122	-2.3123
301.0000	301.0000	1.4245	-3.3459	120.6203	20.4972	-2.0030
302.0000	302.0000	1.4157	-3.0100	121.2119	18.6955	-1.7724
303.0000	303.0000	1.4078	-2.6728	121.5410	16.8131	-1.5981
304.0000	304.0000	1.4008	-2.3350	121.5410	14.8579	-1.4676
305.0000	305.0000	1.3948	-1.9993	119.7674	12.8512	-1.4054

FIGURE E.9. (Continued)

CAMCO B-12345 (SAMPLE)						
CAMSHAFT ANGLE (DEGREES)	FOLLOWER ANGLE (DEGREES)	FOLLOWER RADIUS (INCHES)	FOLLOWER VELOC (INCHES/SEC)	FOLLOWER ACCEL (INCH/SEC/SEC)	PRESSURE ANGLE (DEGREES)	RADIUS OF CURV (INCHES)
306.0000	306.0000	1.3897	-1.6718	115.6628	10.8388	-1.4174
307.0000	307.0000	1.3855	-1.3588	109.3069	8.8718	-1.5126
308.0000	308.0000	1.3821	-1.0665	100.8235	7.0014	-1.7288
309.0000	309.0000	1.3796	-0.8005	90.3776	5.2765	-2.1751
310.0000	310.0000	1.3777	-0.5660	78.1727	3.7414	-3.2338
311.0000	311.0000	1.3764	-0.3676	64.4462	2.4343	-7.5652
312.0000	312.0000	1.3756	-0.2092	49.4653	1.3864	15.2457
313.0000	313.0000	1.3752	-0.0937	33.5217	0.6215	3.5933
314.0000	314.0000	1.3750	-0.0235	16.9255	0.1562	1.9980
315.0000	315.0000	1.3750	0.0000	0.0000	0.0000	1.3750
316.0000	316.0000	1.3750	0.0000	0.0000	0.0000	1.3750
317.0000	317.0000	1.3750	0.0000	0.0000	0.0000	1.3750
318.0000	318.0000	1.3750	0.0000	0.0000	0.0000	1.3750
319.0000	319.0000	1.3750	0.0000	0.0000	0.0000	1.3750
320.0000	320.0000	1.3750	0.0000	0.0000	0.0000	1.3750
321.0000	321.0000	1.3750	0.0000	0.0000	0.0000	1.3750
322.0000	322.0000	1.3750	0.0000	0.0000	0.0000	1.3750
323.0000	323.0000	1.3750	0.0000	0.0000	0.0000	1.3750
324.0000	324.0000	1.3750	0.0000	0.0000	0.0000	1.3750
325.0000	325.0000	1.3750	0.0000	0.0000	0.0000	1.3750
326.0000	326.0000	1.3750	0.0000	0.0000	0.0000	1.3750
327.0000	327.0000	1.3750	0.0000	0.0000	0.0000	1.3750
328.0000	328.0000	1.3750	0.0000	0.0000	0.0000	1.3750
329.0000	329.0000	1.3750	0.0000	0.0000	0.0000	1.3750
330.0000	330.0000	1.3750	0.0000	0.0000	0.0000	1.3750
331.0000	331.0000	1.3750	0.0000	0.0000	0.0000	1.3750
332.0000	332.0000	1.3750	0.0000	0.0000	0.0000	1.3750
333.0000	333.0000	1.3750	0.0000	0.0000	0.0000	1.3750
334.0000	334.0000	1.3750	0.0000	0.0000	0.0000	1.3750
335.0000	335.0000	1.3750	0.0000	0.0000	0.0000	1.3750
336.0000	336.0000	1.3750	0.0000	0.0000	0.0000	1.3750

FIGURE E.9. (Continued)

CAMCO B-12345 (SAMPLE)							
CAMSHAFT ANGLE (DEGREES)	FOLLOWER ANGLE (DEGREES)	FOLLOWER RADIUS (INCHES)	FOLLOWER VELOC (INCHES/SEC)	FOLLOWER ACCEL (INCH/SEC/SEC)	PRESSURE ANGLE (DEGREES)	RADIUS OF CURV (INCHES)	
337.0000	337.0000	1.3750	0.0000	0.0000	0.0000	1.3750	
338.0000	338.0000	1.3750	0.0000	0.0000	0.0000	1.3750	
339.0000	339.0000	1.3750	0.0000	0.0000	0.0000	1.3750	
340.0000	340.0000	1.3750	0.0000	0.0000	0.0000	1.3750	
341.0000	341.0000	1.3750	0.0000	0.0000	0.0000	1.3750	
342.0000	342.0000	1.3750	0.0000	0.0000	0.0000	1.3750	
343.0000	343.0000	1.3750	0.0000	0.0000	0.0000	1.3750	
344.0000	344.0000	1.3750	0.0000	0.0000	0.0000	1.3750	
345.0000	345.0000	1.3750	0.0000	0.0000	0.0000	1.3750	
346.0000	346.0000	1.3750	0.0000	0.0000	0.0000	1.3750	
347.0000	347.0000	1.3750	0.0000	0.0000	0.0000	1.3750	
348.0000	348.0000	1.3750	0.0000	0.0000	0.0000	1.3750	
349.0000	349.0000	1.3750	0.0000	0.0000	0.0000	1.3750	
350.0000	350.0000	1.3750	0.0000	0.0000	0.0000	1.3750	
351.0000	351.0000	1.3750	0.0000	0.0000	0.0000	1.3750	
352.0000	352.0000	1.3750	0.0000	0.0000	0.0000	1.3750	
353.0000	353.0000	1.3750	0.0000	0.0000	0.0000	1.3750	
354.0000	354.0000	1.3750	0.0000	0.0000	0.0000	1.3750	
355.0000	355.0000	1.3750	0.0000	0.0000	0.0000	1.3750	
356.0000	356.0000	1.3750	0.0000	0.0000	0.0000	1.3750	
357.0000	357.0000	1.3750	0.0000	0.0000	0.0000	1.3750	
358.0000	358.0000	1.3750	0.0000	0.0000	0.0000	1.3750	
359.0000	359.0000	1.3750	0.0000	0.0000	0.0000	1.3750	
360.0000	360.0000	1.3750	0.0000	0.0000	0.0000	1.3750	

FIGURE E.9. (Continued)

Maximum pressure angle	=	38.3	degrees	
Min. (+) rad. of curvature	=	1.291	inches	To avoid cam undercut, roc > 0.5600
Min. (-) rad. of curvature	=	-1.405	inches	To avoid cam undercut, roc < -0.5600
Maximum cam follower vel.	=	331.5	rpm	<10,000 recommended by McGill

**FIGURE E.10.** Loading study.

*This page intentionally left blank.*

## APPENDIX F

# OPTIMAL CONTROL THEORY DERIVATION FOR TWO-POINT BOUNDARY VALUE PROBLEM

(Chapter 13, Cam System Dynamics—Response)

Since the explicit relationship between the vectors  $\mathbf{p}(0)$  and  $\mathbf{x}(1)$  is not known, the influence function matrix,  $P_x$ , cannot easily be calculated. One approach is to take partial derivatives of Eqs. (13.48) and (13.49) with respect to the initial value of the costate vector,  $\mathbf{p}(0)$  and interchange the order of differentiation (since continuity with respect to  $\mathbf{p}(0)$  and  $\tau$  is assumed). The resulting two-point boundary-value problem is derived as follows.

$$\begin{aligned}\dot{x}(\tau) &= f(x(\tau), \mathbf{p}(\tau), \tau) \\ \dot{\mathbf{p}}(\tau) &= \mathbf{g}(x(\tau), \mathbf{p}(\tau), \tau) \\ \dot{P}_x(\mathbf{p}^1(0), \tau) &= \left[ \frac{\partial^2 H}{\partial \mathbf{p} \partial x} \right] P_x(\mathbf{p}^1(0), \tau) + \left[ \frac{\partial^2 H}{\partial \mathbf{p}^2} \right] P_p(\mathbf{p}^1(0), \tau) \\ \dot{P}_p(\mathbf{p}^1(0), \tau) &= \left[ -\frac{\partial^2 H}{\partial x^2} \right] P_x(\mathbf{p}^1(0), \tau) + \left[ -\frac{\partial^2 H}{\partial x \partial \mathbf{p}} \right] P_p(\mathbf{p}^1(0), \tau)\end{aligned}$$

with the following initial conditions

$$\begin{aligned}x(0) &= x_0 \\ \mathbf{p}(0) &= \mathbf{p}^1(0) \quad \text{jth guess} \\ P_x(\mathbf{p}^1(0), \tau) &= 0 \quad (\text{a } 5 \times 5 \text{ square matrix}) \\ P_p(\mathbf{p}^1(0), \tau) &= 1 \quad (\text{a } 5 \times 5 \text{ identity square matrix})\end{aligned}$$

where

$$\begin{aligned}P_x(\mathbf{p}^1(0), \tau) &\triangleq \begin{pmatrix} \frac{\partial x_1(\tau)}{\partial p_1(0)} & \dots & \frac{\partial x_1(\tau)}{\partial p_5(0)} \\ \vdots & & \vdots \\ \frac{\partial x_5(\tau)}{\partial p_1(0)} & \dots & \frac{\partial x_5(\tau)}{\partial p_5(0)} \end{pmatrix} \equiv \frac{\partial x(\tau)}{\partial \mathbf{p}(0)} \\ P_p(\mathbf{p}^1(0), \tau) &\equiv \frac{\partial \mathbf{p}(\tau)}{\partial \mathbf{p}(0)}\end{aligned}$$

and the (ij)th element, written as  $[\ ]_{ij}$ , is given by

$$\left[ \frac{\partial^2 H}{\partial \mathbf{p} \partial x} \right]_{ij} = \frac{\partial^2 H}{\partial p_i \partial x_j}$$

$$\left[ \frac{\partial \mathbf{p}(\tau)}{\partial \mathbf{p}(\tau)} \right]_{ij} = \frac{\partial p_i(\tau)}{\partial p_j(0)}, \text{ etc.}$$

Each subsequent new approximation for the vector,  $\mathbf{p}^{(i+1)}(0)$ , is given by the iteration formula of Eq. (13.50). This approach to the solution of the two-point boundary-value problem is called the variation of extremals, also known as the generalized Newton-Raphson algorithm. It is a second-order gradient technique and hence a good initial approximation for the costate vector,  $\mathbf{p}^{(0)}(0)$ , is usually needed for convergence.

---

# INDEX

---

Page numbers followed by *f* and *t* refer to figures and tables, respectively.

- Abrasive wear, 260, 263
- Acceleration
  - in automotive cams, 536, 537*f*, 538*f*
  - in constant acceleration curve, 35–36, 35*f*, 50*t*, 51*f*, 58*t*
    - skewed, 37*f*, 38
  - in constant velocity curve, 33, 33*f*, 50*t*
  - continuity of, B-splines and, 109, 110, 132
  - in cubic no. 1 curve, 39, 39*f*, 50*t*, 51*f*
  - in cubic no. 2 curve, 40, 41*f*, 50*t*, 51*f*
  - in curve factor calculations, 551
  - in cycloidal curve, 45, 45*f*, 50*t*, 52*f*, 58*t*, 78*f*, 83*f*
  - discontinuities in, 30, 296–297, 297*f*, 400, 448–449
  - in dwell-rise-dwell curves, 94–96
  - in dwell-rise-return-dwell curves, 78, 80*f*
  - in elliptical curves, 48, 49*f*
  - equation for, 29
  - in harmonic curves
    - double, 46, 46*f*, 50*t*, 51*f*
    - Freudenstein 1-3, 104, 405
    - Freudenstein 1-3-5, 105, 405*f*, 406*f*
    - Gutman 1-3, 103, 405, 405*f*, 406*f*
    - simple, 42–44, 42*f*, 50*t*, 52*f*, 58*t*, 82*f*
  - importance of, 30
  - minimization of, in cam profile design, 103
  - in polynomial curves, 90
    - 2-3, 91, 91*f*
    - 3-4-5, 58*t*, 91–92, 92*f*
    - 4-5-6-7, 58*t*, 93, 94*f*, 95*f*, 95*t*
    - eighth degree, 84*f*
    - fifth order, 99*f*
    - seventh order, 100*f*
    - simple, 32
  - sign of, 29
  - in sine curve, modified, 58*t*, 73, 73*f*, 76, 78*f*
  - spline weight sequence and, 123–124
  - in trapezoidal curve, 58*t*
    - modified, 58*t*, 61–67, 62*f*, 68*f*, 78*f*
    - skewed modified, 70–73, 71*f*
    - and vibration, 362, 368
- Acceleration curve
  - cam profile and, 30
  - in combining curves, 57
  - design of, 21
  - in finite difference techniques, 298–301
  - importance of, 30
  - positive and negative area of action, 31
  - slope of, 29
- Actuators
  - in microelectromechanical systems, 521–524
  - torsional ratcheting microactuator, 514–516, 516*f*, 517*f*
- ADAMS software, 562
- Adhesive bonding, 262
- Adhesive wear, 260, 261–262, 262*f*
- Adjustable mechanisms, industrial, 20
- Adjustable stroke cams, 475–477, 476*f*
- Aircraft engine, cam profile error in, 299, 300*f*
- AIR FLOW TESTING software, 541, 563
- Alignment. *See* Misalignment
- Analog computing mechanisms, 494–502
  - Archimedes spiral gear cam, 497–498
    - basic spiral cam, 296–297, 296*f*, 498–501, 498*f*, 499*f*
    - cam types in, 495–497, 495*f*, 496*f*
    - design of, 495
- Applied loads. *See* Working loads
- Archimedes spiral, 33
- Archimedes spiral gear cam, 497–498
- Area, in planar contours, 184, 194–197
- Asperities, surface, 260–261, 261*f*
- Assembly of cam mechanisms, 291
- Asymmetrical dwell-rise-return-dwell cams, 53*f*, 54, 54*f*
- Ausforging, 303
- Austempering, 535
- AUTOCAD software, 203, 562

## Automobiles

- cam-on-rocker arm design (CORA), 531, 534*f*, 537
- cams
  - design of
    - factors in, 529, 530*f*
    - polydyne, 434
    - software packages, 537, 540, 541, 563–564
    - sources on, 25
  - manufacturing of, 541–542
  - materials, 531–535
  - most-popular, 6
  - motion of, vs. valve, 536
  - open-track, 14, 531
  - profiles
    - characteristic, 54, 54*f*
    - geometry of, 536–537
    - harmonic analysis of, 537–541
    - polynomial curves for, 99
    - types used, 535–536
  - stress in, 258
  - tolerances in, 291
- cam series in, 471, 471*f*
- camshafts, 6, 7*f* (*See also* Camshaft(s))
- L-head cam design, 531, 532*f*, 537
- overhead cam design (OHC), 531, 534*f*, 537
- overhead valve design (OHV), 1, 2*f*, 489, 531, 533*f*, 537
- suspension, modeling of, 319–324, 319*f*
- tailgate cams, 234–235, 234*f*
- valve systems, 348, 349*f*, 350*f*, 350*r*
  - model of, 348–354
  - software design packages, 537, 540, 541, 563–564
  - springs for, 529
  - spring surge in, 540–541
  - types of, 531
  - valve train lash, 539–540, 539*f*

## Backlash

- in automobile valve systems, 539–540, 539*f*
- control of, 24
- vibration and, 359

## Backlash errors, in manufacturing, 293

## Balancing, 372–373

Ball and groove cams, 468, 469*f*Barrel cams, 9, 486–487, 486*f*Base circle, 18, 19*f*, 162*f*Basis splines. *See* B-splines

## Bearings

- linear ball, 222, 222*f*
- needle, 306, 307*f*

Berkeley Sensor and Actuator Center, 511–512, 512*f*, 513*f*, 520Berzak-Freudenstein 3-4-5-6-7 harmonic, 405*f*, 406*f*

## Bezier curves, vs. splines, 109

## Bonding, adhesive, 262

Bounce. *See* JumpBoundary lubrication, 273–274, 273*f*

## Boundary, piecewise-linear approximation of, 195–202

Bronze alloy, 266*f*, 270–271, 271*f*

## B-splines

## constraints, large number of, 115–116

## continuity and, 109, 110, 132

## nonrational, 109–117

## derivatives, evaluation of, 111

## evaluation of, 111

## expression for, 109–110

## in nonrigid cam-follower systems, 127–144

## rational, 117–127

## definition of, 119–120

## derivatives, evaluation of, 121–122

## evaluation of, 119–121

## expression for, 117–118

## properties of, 117–118, 120–121, 126–127

## software packages for, 561

## in 3-D cams, 144–152

## vs. Bezier curves, 109

CAD. *See* Computer-aided designCAM. *See* Computer-aided manufacturing

## Cam(s)

adjustable stroke, 475–477, 476*f*

## automotive

## design of

factors in, 529, 530*f*

## polydyne, 434

## software packages, 537, 540, 541,

## 563–564

## sources on, 25

## manufacturing of, 541–542

## materials, 531–535

## most popular, 6

## motion of, vs. valve, 536

## open-track, 14, 531

## profiles

characteristic, 54, 54*f*

## geometry of, 536–537

## harmonic analysis of, 537–541

- polynomial curves for, 99
  - types used, 535–536
- stress in, 258
- tolerances in, 291
- ball and groove, 468, 469*f*
- barrel, 9, 486–487, 486*f*
- circular arc, 9, 465, 465*f*
  - constant breadth follower, 477–479, 478*f*, 479*f*
  - tangent cams, translating roller follower, 466–467, 467*f*
  - translating flat-faced follower, 467–468, 468*f*
  - translating roller follower, 465–466, 466*f*
- classification of
  - by constraint method, 14–15
  - by follower motion, 15, 15*f*
  - by shape, 6–14
- closed-track, 14
  - automotive, 531
  - uses of, 358
  - vibration in, 378–384, 379*f*, 380*f*, 381*f*, 382*f*
- complementary, 8–9
- computer simulation, 529–542
- concave, 170, 171*f*, 172, 182, 183*f*
  - barrel, 486–487, 486*f*
  - grooved globoidal, 486–487, 486*f*
- conical, 11, 12*f*
- conjugate, 8–9, 9*f*
- controlled translating cycle, 477, 477*f*
- convex, 170, 171*f*, 172, 182, 183*f*
- cylindrical, 9–10, 10*f*
  - elastic contact theory for, 255, 256*f*
  - in intermittent motion mechanisms, 484–485, 485*f*
- cylindrical blade, 10, 11*f*
- definition of, ix, 1, 2
- disk, 7
  - contact stresses in, 258–259, 259*f*
  - double-disk, 8–9
- drum, 9
- eccentric circle
  - translating flat-faced follower, 463–464, 463*f*
  - translating roller follower, 460–463, 461*f*
- flat-plate, 6
- gear, in computing mechanisms, 296, 296*f*
- globoidal, 10, 11*f*, 12*f*
  - concave, grooved, 486–487, 486*f*
  - indexing, 10–11, 12*f*
  - groove, 4–5, 7*f*
    - in micromechanical lock, 518, 518*f*, 519*f*
  - history of, 1
  - hub design, 173–174
  - increased-stroke, 475, 476*f*
  - indexing globoidal, 10–11, 12*f*
  - industrial production, most popular, 6, 6*f*
  - intermittent motion mechanisms, 482*f*
    - concave globoidal cams, grooved, 486–487, 486*f*
    - cylindrical cams, 484–485, 485*f*
    - multiple double-end cam, 488–489, 488*f*
    - spider cams, 487, 487*f*
    - star-wheel cam, 489, 490*f*
    - types and uses of, 481–484
  - inverse, 13–14, 14*f*
    - in microvibromotor, 520–521, 521*f*
    - rotatable, 236–250
  - involute, 459–460, 460*f*
  - linear to rotary conversion, 473–474, 473*f*
  - in microelectromechanical systems, 514–521
    - actuators for, 521–524
  - multiple double-end, 488–489, 488*f*
  - open-track, 14
    - automotive, 14, 531
    - uses of, 358
    - vibration in, 375–378, 375*f*, 378*f*, 379*f*
- plate, 7
  - flat-plate, 6
  - swash plate, 479–480, 480*f*
- quick action, 471–472, 472*f*
- radial, 7, 8*f*
  - contour-shaped, 464–465, 464*f*, 465*f*
  - displacement diagrams of, 18
- rolling, 9
- rotary to linear conversion, 474, 474*f*
- in series, 471, 471*f*
- size of
  - design of, 21
  - in flat-faced followers, 173
  - minimization of, 204–208
  - pressure angle and, 162
  - and radius of curvature, 169
  - roller acceleration and, 309
- spherical, 12, 12*f*
- spider, 487, 487*f*
- spiral, 9, 10*f*
  - in analog computing mechanisms, 296–297, 296*f*, 498–501, 498*f*, 499*f*
  - in cutter mechanism, 468–469, 469*f*
  - in micromechanical lock, 516–518, 517*f*

- star-wheel, 489, 490*f*
- stationary, 14
- surface of. *See* Surface(s)
- swash plate, 479–480, 480*f*
- tangent, translating roller follower, 466–467, 467*f*
- torque-controlled, 232–235, 233*f*, 234*f*
  - wrapping, 235–236
- translating, 5*f*, 6, 7*f*
  - linear ball bearings for, 222, 222*f*
- trapezoidal, acceleration DRS of, 402, 403*f*
- two-revolution-per-cycle, 474–475, 475*f*
- variable-angular-velocity, 480, 481*f*
- variable-dwell, 472, 473*f*
- wedge
  - definition of, 6
  - in microindexing motor, 514, 515*f*
- wiper, 9
- wrapping, torque-controlled, 235–236
- yoke, 7–8, 8*f*
- Cam angle rotation, in polynomial equation, 90
- Cam clutches, unidirectional, 470–471, 470*f*
- CAMCO. *See* Commercial Cam Co., Inc.
- Cam computing mechanism, 494–502
  - Archimedes spiral gear cam, 497–498
  - basic spiral cam, 296–297, 296*f*, 498–501, 498*f*, 499*f*
  - cam types in, 495–497, 495*f*, 496*f*
  - design of, 495
- Cam contours. *See* Cam profiles
- CAM DESIGNER SE software, 562
- Cam-follower system
  - alternatives to, 20
  - applications of, 1
  - closed, 14–15
  - design of, general considerations, 21–25
  - dynamics of, rigid camshafts, 362–374
  - forces in. *See* Force(s)
  - general form of, 2–4, 3*f*
  - high speed designs, 413, 448–449 (*See also* Polydyne design)
  - as mechanical information device, 1
  - nomenclature of, 17–19, 19*f*, 162*f*
  - nonrigid
    - cam design in
      - overview of, 127–128
      - spline functions, 127–144
    - model for, 129–130, 136*f*
  - open, 14–15
  - rigidity of, 296, 359, 448
- Camiod. *See* 3-D cams
- Cam-modulated linkages, 454*f*
- Cam-modulated mechanisms, 489–494
- Cam-on-rocker arm (CORA) design, 531, 534*f*, 537
- CAMPA software, 561
- Cam performance index, 413
- Cam profiles
  - acceleration curve radius and, 30
  - accuracy of
    - cutter tolerances and, 294, 294*f*, 295*f*
    - grinding to improve, 295–296
    - importance of,  $x$ , 21, 286, 287, 287*f*, 291
    - inspection for
      - methods of, 291, 297–301
      - real-world example, 566–572, 573*f*–583*f*
    - quality control, 285–286, 287
    - tolerances, typical, 291
  - automotive
    - characteristic, 54, 54*f*
    - geometry of, 536–537
    - harmonic analysis of, 537–541
    - polynomial curves for, 99
    - types used, 535–536
  - basic curves, 27–54, 58*f*, 545–550
  - curvature. *See* curvature
  - definition of, 18
  - design of (*see also* Combination of curves)
    - constant speed cams, 413
    - dynamic objectives in, 103
    - guidelines for, 21, 448–449
    - high-speed, 413, 448–449 (*see also* Polydyne design)
    - with polydyne design. *See* Polydyne design
    - real-world example, 565
    - tuned cam design, 408–413, 416
    - using convolution operator, 427–434, 450
    - using finite trigonometric series, 407–416, 449
    - using mean squared error minimization, 413–416
    - using optimal control theory, 416–427, 449–450, 585–586
    - varying speed cams, 413
  - errors in, 293–294. *See also* Errors
  - factors for, 551, 552*t*–555*t*
  - geometric properties of. *See* Geometric properties
  - graphical layout of
    - graphical layout method, 160, 161*f*
    - manual method, 15–16, 16*f*, 17*f*, 28

- inspection of
  - methods, 291, 297–301
  - real-world example, 566–572, 573*f*–583*f*
- modeling of
  - probabilistic model, 294, 294*f*, 295*f*
  - 3-D model, 22, 24*f*
- nomenclature of, 19*f*, 162*f*
- planar contours
  - geometric properties of, 184–185, 194–198
  - piecewise-linear approximation of
    - boundary, 195–198
  - pressure angle. *See* Pressure angle
  - probabilistic model of, 294, 294*f*, 295*f*
  - sample, 22, 23*f*
  - tangent, determination of, 178–179, 178*f*
- CAMPRO PLUS software, 541, 563
- CAMPRO software, 541, 563
- Camshaft(s)
  - balancing of, 209–215
  - elastic
    - system dynamics in, 374–395
  - vibration models of
    - one-degree-of-freedom, 374–384
    - two-degrees-of-freedom, 384–386, 385*f*
    - four-degrees-of-freedom, 386–389, 386*f*, 387*f*, 390*f*, 391*f*
    - multi-degrees-of-freedom, 389–395, 392*f*, 393*f*, 395*f*
- rigid
  - dynamic phenomena in, 322–374
  - vibration models of
    - one-degree-of-freedom, 360–370, 361*f*, 363*f*, 364*f*, 365*f*
    - two-degrees-of-freedom, 370–371, 372*f*
- Carbon vacuum degassing (CVD), 302
- Cast iron, 265*f*–266*f*, 271, 532–533
- CATIA software, 203, 562
- Cavitation wear, 260
- CEFF (controlled-energy-flow forming)
  - technique, 303
- Center of mass, 326
- Centroid, 184, 185–186
- Centroid moments of inertia, 185
- Centroid position vector, 194–197, 198–202
- Chain rule, 178–179
- Circle, involute of, 549–550, 549*f*
- Circular arc cams, 9, 465, 465*f*
  - constant breadth follower, 477–479, 478*f*, 479*f*
  - tangent cams, translating roller follower, 466–467, 467*f*
  - translating flat-faced follower, 467–468, 468*f*
  - translating roller follower, 465–466, 466*f*
- Closed cam systems, 14–15
- Closed-track cams, 14
  - automotive, 531
  - uses of, 358
  - vibration in, 378–384, 379*f*, 380*f*, 381*f*, 382*f*
- Clutches, unidirectional cam, 470–471, 470*f*
- CNC. *See* Computer numerical control
- Coil flutter, 223
- Coil springs
  - progressive, 335, 336*f*
  - standard, 334–335, 335*f*
- Collings, Cliff, 529
- Combination of curves. *See also* Cam profiles, design of; *specific curves*
  - basic curves, 27–54, 58*t*, 545–550
  - fundamentals of, 57
  - modified curves, 55–87
  - overview of, 56
  - simplified method for, 81–87
  - splines in. *See* Spline(s)
- Commercial Cam Co., Inc. (CAMCO), 565
- Complementary cam, 8–9
- Compliance
  - measure of, 357
  - in one-degree-of-freedom systems, 363–367, 365*f*, 374*f*
- Compliant mechanisms, in MEMS, 511, 511*f*, 513–514
- Composite roughness, 276
- Computer-aided design (CAD)
  - advantages of, 561
  - automotive cams and, 529
  - in cam synthesis, 22
  - curve-fitting methods, 109
  - definition of, 1
  - example of, 565
  - impact of, ix
  - software packages, 203
- Computer-aided manufacturing (CAM)
  - in cam synthesis, 22
  - definition of, 1
  - example of, 565–572
  - impact of, ix
- Computer numerical control (CNC), ix, 286, 288–291, 290*f*
- Computing mechanism, analog, 494–502
  - Archimedes spiral gear cam, 497–498
  - cam types in, 495–497, 495*f*, 496*f*
  - design of, 495
  - spiral cam, 296–297, 296*f*, 498–501, 498*f*, 499*f*

- Concave cams, 170, 171*f*, 172, 182, 183*f*  
 barrel, 486–487, 486*f*  
 grooved globoidal, 486–487, 486*f*
- Conical cam, 11, 12*f*
- Conical rollers, 309, 310*f*
- Conjugate cam, 8–9, 9*f*
- Constant acceleration (parabolic) curve  
 acceleration, maximum, in, 103  
 characteristics of, 545–546, 546*f*  
 in DRD cams, 34–36, 35*f*, 50*t*, 51*f*, 58*t*  
 in DRRD cams, 53, 53*f*  
 harmonic content, 103  
 modification of  
   with constant velocity curve, 57–60, 60*f*  
   with cubic curve, 61  
   with cycloidal curve, 61–70, 62*f*, 68*f*,  
     78–81, 80*f*  
 rolling in, 457, 458*f*  
 spring forces and, 223, 224*f*  
 transient-response curves, 362, 363*f*
- Constant velocity convolution, 431–434
- Constant velocity curve  
 in dwell-rise-dwell cams, 33–34, 33*f*, 50*t*  
 modified, 57–60, 60*f*
- Constant velocity polynomial, 90
- Constraint(s), in design  
 nonrational, 110–117  
 in non-rigid systems, 131–133  
 rational, 117–127  
 in 3-D cams, 147–148, 150, 152, 153*t*–154*t*
- Constraint method, cam classification by,  
 14–15
- Consumable electrode vacuum melt (CVM),  
 302
- Contact mechanics  
 contact stresses in, 256–260, 257*f*, 258*f*  
 definition of, *x*  
 elastic contact theory, 253–255, 254*f*  
 failure mechanisms in, *x*, 252–253  
 systems studied in, 252
- Contact stresses, 256–260, 257*f*, 258*f*  
 in flat-faced followers, 258, 258*f*  
 minimization of, 419–420, 424–425  
 in nonrigid systems, 131
- Contaminants, in lubrication, 281
- Continuity  
 in acceleration curves, 30, 296–297, 297*f*,  
   400, 448–449  
 in basic curves, 29  
 B-splines and, 109, 110, 132
- Contour-shaped radial cams, 464–465, 464*f*,  
 465*f*
- Control, in polynomial curves  
 DRD cams, 94–96  
 DRRD cams, 96–98
- Controlled-energy-flow forming (CEFF)  
 technique, 303
- Controlled translating cycle cams, 477, 477*f*
- Convex cams, 170, 171*f*, 172, 182, 183*f*
- Convolution  
 constant velocity, 431–434  
 definition of, 428, 429  
 fixed, 430–431
- Convolution operator  
 cam design using, 427–434, 450  
 definition of, 428
- Corrosion fatigue, 264
- Corrosive wear, 263
- Coulomb (dry) friction, 344–345
- Crossover point. *See* Transition point
- Crossover shock, 359, 373–374, 447
- Crowned rollers, 253–255, 254*f*, 258–259,  
 259*f*, 306, 308*f*
- Cubic curves  
 blending of, with parabolic curves, 61  
 no. 1, in dwell-rise-dwell cams, 38–39, 39*f*,  
   50*t*, 51*f*  
 no. 2, in dwell-rise-dwell cams, 40, 41*f*, 50*t*,  
   51*f*
- Cubic splines, 187–189, 193–194, 197–198
- Curvature  
 calculation of, 193–194  
 definition of, 19, 180  
 design of, 21  
 determination of, 180–184  
 of flat-faced follower, 190, 190*f*, 191*f*  
 of roller followers, 191*f*, 192, 193*f*  
 of translating knife-edge follower, 191*f*,  
   192
- Curves. *See also* Cam profiles; *specific*  
*curves*  
 basic curves, 27–54, 58*t*, 545–550  
 combination of  
   fundamentals of, 57  
   modified curves, 55–87  
   overview, 56  
   simplified method for, 81–87  
   splines in, *See* Spline(s)
- Customers, communication with, 25
- Cutters, spiral-cam, 468–469, 469*f*
- Cutter tolerances, error and, 294, 294*f*, 295*f*
- CVD. *See* Carbon vacuum degassing
- CVM. *See* Consumable electrode vacuum  
 melt

- Cyclic errors, in manufacturing, 293
- Cycloidal curve  
 acceleration, maximum, in, 103  
 characteristics of, 76, 77*f*–78*f*  
 in dwell-rise-dwell cam, 44–46, 44*f*, 45*f*, 50*t*,  
 52*f*, 58*t*  
 in dwell-rise-return-dwell cams, 53, 53*f*,  
 78–81, 80*f*  
 dynamic characteristics of, 404*f*, 405  
 factors for, 553*t*  
 harmonic content, 103  
 high-speed systems and, 448  
 modified  
   with parabolic curve, 61–70, 62*f*, 68*f*,  
   78–81, 80*f*  
   Wildt curve, 76–78, 79*f*  
 segment characteristics, 83*f*  
 shaft windup in, 383, 383*f*, 384*f*  
 spring forces and, 223, 224*f*  
 torque in, 230, 231*f*  
 transient-response curves, 362, 363, 363*f*,  
 365*f*, 389, 390*f*, 391*f*  
 vibratory response in, 400
- Cylindrical blade cam, 10, 11*f*
- Cylindrical cams, 9–10, 10*f*  
 elastic contact theory for, 255, 256*f*  
 in intermittent motion mechanisms, 484–485,  
 485*f*
- D'Alembert's principle, 219
- Damping  
 dynamic response spectra and, 401–403  
 modeling of, 342–348  
   dry (Coulomb) friction, 344–345  
   equivalent dampers, 346–348  
   mechanical efficiency, 345–346  
   reasons for including, 342  
   values in, determining, 342–343  
   viscous (speed-dependent) damping,  
   343–344  
 natural frequencies and, 320
- Damping coefficient, 343
- D-Curve, 102, 405*f*, 406*f*
- Deep reactive ion etching (DRIE), 510
- Deep-vertical lithography, 510
- DESINE software, 537, 540, 541, 563
- Diesel intake valve curves, 536, 538*f*
- Discontinuities  
 in acceleration curves, 30, 296–297, 297*f*,  
 400, 448–449  
 in basic curves, 29  
 B-splines and, 109, 110, 132
- Disk cam, 7  
 contact stresses in, 258–259, 259*f*  
 double-disk, 8–9
- Displacement  
 in automotive cams, 536, 537*f*, 538*f*  
 in combining curves, 57, 63  
 in constant acceleration curve, 34–36, 35*f*,  
 50*t*, 51*f*  
   skewed, 37*f*, 38  
 in constant velocity curve, 33, 33*f*, 50*t*  
 in cubic no. 1 curve, 39, 50*t*, 51*f*  
 in cubic no. 2 curve, 40, 50*t*, 51*f*  
 in curve factor calculations, 551  
 in cycloidal curve, 45, 45*f*, 50*t*, 52*f*, 77*f*,  
 83*f*  
 definition of, 30  
 in dwell-rise-dwell curves, general  
   derivation, 94–96  
 in elliptical curve, 48, 49*f*  
 equation for, 28, 62  
 in harmonic curve  
   double, 46, 46*f*, 50*t*, 51*f*  
   simple, 42–44, 42*f*, 50*t*, 52*f*, 82*f*  
 in polynomial curves  
   eighth degree, 84*f*  
   simple, 32  
 in polynomial equation, 90  
 in sine curve, modified, 73, 73*f*, 75–76, 77*f*  
 in trapezoidal curve  
   modified, 61–70, 62*f*, 68*f*, 77*f*  
   skewed modified, 70–73, 71*f*, 72*f*
- Displacement diagrams, 17–18, 17*f*
- DOCTOR DOCTOR software, 540, 541, 563
- Double-disk cams, 8–9
- Double harmonic curves  
 in dwell-rise-dwell cam, 46, 46*f*, 50*t*, 51*f*  
 in dwell-rise-return-dwell cams, 53, 53*f*  
 spring forces and, 223, 224*f*
- DRD. *See* Dwell-rise-dwell cam
- DRDRD. *See* Dwell-rise-dwell-return-dwell  
 cam
- DRIE (deep reactive ion etching), 510
- DRRD. *See* Dwell-rise-return-dwell cam
- DRS. *See* Dynamic response spectra
- Drum cam, 9
- Dry (Coulomb) friction, 344–345
- Dwell  
 in 2-3-polynomial curve, 91*f*  
 in 3-4-5 polynomial curve, 92*f*  
 definition of, 15  
 error during, 295  
 variable, 472, 473*f*

- Dwell-rise-dwell cam (DRD), 15, 15*f*  
 dynamic response spectra of, 402–406, 404*f*, 405*f*, 406*f*  
 polydyne design of, 439–444  
 tuned, optimization of, 421–425
- Dwell-rise-dwell curves  
 comparison of, 48–49, 50*t*, 51*f*–52*f*  
 constant acceleration (parabolic) curve, 34–36, 35*f*, 50*t*, 51*f*, 58*t*  
 skewed, 37–38, 37*f*  
 constant velocity curve, 33–34, 33*f*, 50*t*  
 cubic curves  
   no. 1, 38–39, 39*f*, 50*t*, 51*f*  
   no. 2, 40, 41*f*, 50*t*, 51*f*  
 cycloidal curve, 44–46, 44*f*, 45*f*, 50*t*, 52*f*, 58*t*  
 derivative control in, 94–96  
 Fourier series, 103–105  
 harmonic curves  
   double, 46, 46*f*, 50*t*, 51*f*  
   simple, 40–44, 41*f*, 42*f*, 50*t*, 52*f*, 58*t*  
 polynomial curves  
   2-3, 90–91, 91*f*  
   3-4-5, 58*t*, 91–92, 92*f*, 93, 94*t*, 95*f*  
   4-5-6-7, 58*t*, 92–93, 94*f*, 95*f*, 95*t*  
   general derivation, 94–96  
   simple, 32–40  
 sine curve, 58*t*, 73–76, 73*f*  
 trigonometric curves, 32, 40–48
- Dwell-rise-dwell-return-dwell cam (DRDRD), 15, 15*f*  
 blending DRD curves to produce, 56, 56*f*
- Dwell-rise-return-dwell cam (DRRD), 15, 15*f*  
 polydyne design, 444–446, 445*f*, 450  
 symmetrical and asymmetrical, 53–54, 53*f*, 54*f*  
 tuned, optimization of, 425–427
- Dwell-rise-return-dwell curves, 49–54, 53*f*, 54*f*  
 constant acceleration (parabolic) curve, 53, 53*f*  
 cycloidal curve, 53, 53*f*, 78–81, 80*f*  
 derivative control in, 96–98  
 development of, 78–81, 80*f*  
 harmonic curves  
   double, 53, 53*f*  
   simple, 53, 53*f*  
 high order, 99, 100*f*
- DYNACAM software, 563
- Dynamic constant, in polydyne design, 438
- Dynamic error, 429
- Dynamic response. *See* Vibration
- Dynamic response spectra (DRS), 401–402  
 of dwell-rise-dwell cams, 402–406, 404*f*, 405*f*, 406*f*
- DYNOMATION software, 541, 563
- Eccentric circle cams  
 translating flat-faced follower, 463–464, 463*f*  
 translating roller follower, 460–463, 461*f*
- E-curve, 102, 406*f*
- EDM. *See* Electrodischarge machining
- EHD. *See* Elastohydrodynamic lubrication
- Eighth-degree polynomial curve, 84*f*, 100–101
- Elastic camshafts, vibration models of  
 one-degree-of-freedom, 374–384  
 two-degrees-of-freedom, 384–386, 385*f*  
 four-degrees-of-freedom, 386–389, 386*f*, 387*f*, 390*f*, 391*f*  
 multi-degrees-of-freedom, 389–395, 392*f*, 393*f*, 395*f*
- Elastic contact  
 stresses in, 256–260, 257*f*, 258*f*  
 theory of, 253–255, 254*f*
- Elasticity of materials, in cam system design, 24
- Elastohydrodynamic lubrication (EHD), 273–277, 273*f*, 276*t*, 280*f*
- Electrodischarge machining (EDM), 286–287
- Electroslag remelting, 302
- Electrostatic comb drive, 523, 524*f*
- Electrostatic micromotor, 522–523, 522*f*, 523*f*
- Eleventh-degree polynomial curves, 101–102, 405*f*, 406*f*
- Elliptical curve  
 characteristics of, 545, 545*f*  
 in dwell-rise-dwell cam, 47–48, 47*f*, 49*f*  
 rolling in, 457, 458*f*
- Emergency stop forces, 224
- Energy dissipation. *See* Damping; Friction
- ENGINE EXPERT software, 541, 564
- Epicyclic gears, cam-modulated, 492, 492*f*, 493*f*
- EP lubrication. *See* Extreme-pressure (EP) lubrication
- Equivalent dampers, 346–348
- Equivalent inertia, 331–332
- Equivalent mass, 329–332
- Equivalent springs, 340–341, 340*f*
- Equivalent weight, in polydyne design, 438–439
- Erosive wear, 260
- Errors  
 acceleration discontinuities, 30, 296–297, 297*f*, 400, 448–449

- accumulated, in system, 296
- cutter tolerances and, 294, 294*f*, 295*f*
- impact of, vs. cam displacement, 295
- inspection for
  - methods of, 291, 297–301
  - real-world example, 566–572, 573*f*–583*f*
- in manufacturing, 291–296
- performance and, 299–301, 300*f*, 301*f*
- Exponent manipulation, in polynomial curves, 99–102, 99*f*, 100*f*
- Extreme-pressure (EP) lubrication, 278–279, 280*f*
- EZCAM software, 564
- Fail-safe design, 267
- Fatigue
  - subsurface, 263
  - surface, 263–269, 263*f*
    - causes of, 263–264
    - prevention through design, 264–269
    - testing on, 264–269, 265*t*–266*t*
- Ferguson drive, 10
- Fiber orientation, 302–303
- Fifth-order polynomial curves, acceleration in, 99*f*
- Finishing, importance of, 296
- Finite difference techniques, 297–301
- First moment, in planar contours, 184–185, 194
- 5-6-7-8-9 polynomial curves, in polydyne design, 440, 443–444
- Fixed convolution, 430–431
- Flat-faced followers, 4*f*, 5, 213*f*, 312
  - circular arc cams, 467–468, 468*f*
  - contact stresses in, 258, 258*f*
  - curvature of, 190, 190*f*, 191*f*
  - in eccentric circle cams, 463–464, 463*f*
  - friction in, 221
  - pressure angle forces in, 168–169, 168*f*, 189–190
  - torque in, 230–232, 231*f*
  - undercutting in, 173, 173*f*
- Flat-plate cam, 6
- FLOW PRO software, 564
- FLOW QUIK software, 541, 564
- Flywheels, 24
  - balance of, 373
  - purpose of, 374
- Follower(s). *See also* Cam-follower system
  - classification of, by motion, 15, 15*f*
  - constraint methods, 14–15
  - definition of, ix, 1, 2
  - flat-faced, 4*f*, 5, 213*f*, 312
  - circular arc cams, 467–468, 468*f*
  - contact stresses in, 258, 258*f*
  - curvature of, 190, 190*f*, 191*f*
  - in eccentric circle cams, 463–464, 463*f*
  - friction in, 221
  - pressure angle forces in, 168–169, 168*f*, 189–190
  - torque in, 230–232, 231*f*
  - undercutting in, 173, 173*f*
- translating
  - curvature of, 191*f*, 192
  - pressure angle of, 191*f*, 192
  - relevance of, 190–192
- movement in, types of, 4
- mushroom, 4*f*, 5, 312
- in nonrigid systems, dynamic response of, 138–139 (*See also* Nonrigid cam-follower systems)
- offset, 5, 5*f*
- radial, 5
- roller, 4–5, 4*f*, 221*f*
  - automotive, materials for, 534–535
  - cam contact maintenance, 309–312, 310*f*, 311*f*
  - crowned, 253–255, 254*f*, 258–259, 259*f*, 306, 308*f*
  - curvature of, 191*f*, 192, 193*f*
  - double roller, 309–312, 310*f*
  - in eccentric circle cams, 460–463, 461*f*
  - friction in, 221–222
  - installations, 306–312, 310*f*, 311*f*
  - mountings, 306, 307*f*
  - oscillating
    - curvature of, 192, 193*f*
    - pressure angle forces in, 166–168, 167*f*
    - pressure angle of, 192, 193*f*
  - pressure angle of, 191*f*, 192, 193*f*
  - rollers replacement, 252, 267
  - single roller, 309, 310*f*
  - sliding in
    - causes of, 306–308
    - reduction of, 308–312
  - tangent cams, 466–467, 467*f*
  - translating
    - pressure angle forces in, 163–166, 164*f*, 166*f*
    - torque in, 228–230, 230*f*, 308–309
  - undercutting in, 170–172, 172*f*
  - wear and, 305–306
- sliding
  - automotive, materials for, 532–534

- installations, 312, 312*f*
- lubrication of, 312
- spherical, 4*f*, 5, 312
  - contact stresses in, 258–259, 259*f*
  - friction in, 221
- surface of. *See* Surface(s)
- types of, 4–5, 4*f*
- Force(s), 218–236
  - friction, 220–222 (*see also* Wear)
    - dry (Coulomb), 344–345
    - in microelectromechanical systems, 525–526
    - stick-slip, 345
    - stiction, 345, 360, 525
    - viscous, 343–344
  - impact force (mechanical shock), 219, 400–406
  - inertia, 219–220
    - equivalent, 331–332
  - operating forces, 224–225
  - of rotating body, 327
  - spring forces, 222–223, 418–419
  - surface loads, 225–228
  - vibratory forces, 220 (*see also* Vibration)
  - working loads, 218–219
- 4-5-6-7 polynomial curves
  - in dwell-rise-dwell cam, 58*t*, 92–93, 94*f*, 95*f*, 95*t*
  - dynamic characteristics of, 404*f*, 405*f*, 406*f*
  - in polydyne design, 439–440, 443–444
- Fourier analysis
  - of mechanical shock, 401
  - of vibration models, 367–370, 368*f*
- Fourier series polynomial curves, 103–105
- Fourier transforms, 428–429
- Frames, rigidity of, 296, 359, 448
- Frenet-Serret formulas, 180–181
- Frequency of oscillation. *See* Natural frequency
- Fretting corrosion wear, 260
- Freudenstein 1-3-5 harmonic curve, 104–105, 405*f*, 406*f*
- Freudenstein 1-3 harmonic curve, 104, 405
- Friction, 220–222. *See also* Wear
  - dry (Coulomb), 344–345
  - in microelectromechanical systems, 525–526
  - stick-slip, 345
  - stiction, 345, 360, 525
  - viscous, 343–344
- Function generation, as design criteria, 2–4, 3*f*
- Galling, 261
- Gauss divergence theorem (GDT), 194, 200–201
- GDT. *See* Gauss divergence theorem
- Gear(s)
  - epicyclic, cam-modulated, 492, 492*f*, 493*f*
  - equivalent weight of, 438–439
  - in MEMS, 512
  - noncircular, cam-modulated, 493–494, 494*f*
  - worm, cam-modulated, 490, 491*f*
- Gear cam, in computing mechanisms, 296, 296*f*
- Gear discriminator, in MEMS, 518–520, 519*f*
- Gear drive, roller, 10, 488–489, 488*f*
- Geneva mechanism, 482–483, 483*f*
- Geometric properties
  - case studies, 204–215
  - computational schemes, 186–202
  - global, 184–186, 194–202
  - local, 177–184, 189–194
  - overview of, 177
  - of planar contours, 184–185, 194–198
  - software packages, 203, 561–562
  - of solid regions, 198–202
- Globoidal cams, 10, 11*f*, 12*f*
  - concave grooved, 486–487, 486*f*
  - indexing, 10–11, 12*f*
- Grain flow, 302–303
- Graphical layout of cam profile
  - graphical layout method, 160, 161*f*
  - manual method, 15–16, 16*f*, 17*f*, 28
- Graphical-slope differentiating method, 29, 31
- Grease, 277–278, 278*f*
- Grinding, cam finish and, 295–296
- Groove cams
  - defined, 4–5, 7*f*
  - in micromechanical lock, 518, 518*f*, 519*f*
- Gutman 1-3 harmonic curve, 103, 405, 405*f*, 406*f*
- Hardening. *See* Heat treatment
- Hardness
  - recommended, 303
  - of roller follower, 306
  - and wear, 269–270
- Harmonic content, minimization of, 103
- Harmonic curves, 103–105. *See also* Double harmonic curves; Simple harmonic curves
  - Berzak-Freudenstein 3-4-5-6-7, 405*f*, 406*f*
  - factors for, 552*t*
  - Freudenstein 1-3, 104, 405
  - Freudenstein 1-3-5, 104–105, 405*f*, 406*f*
  - Gutman 1-3, 103, 405, 405*f*, 406*f*

- shaft windup in, 383, 383*f*, 384*f*
- vibratory response characteristics, 400
- Heat treatment
  - distortions and, 291, 302
  - methods of, 302, 303*f*
- HEXIL, 510
- High-speed cam-follower systems
  - design of, 413, 448–449 (*see also* Polydyne design)
  - vibration in, 447 (*see also* Vibration)
- Hub design, 173–174
- Hydraulic cylinders, servo valve-controlled, 20
- Hydrodynamic lubrication, 273, 273*f*
- Hyperbolic curves
  - characteristics of, 546–548, 547*f*
  - rolling in, 457, 458*f*
- Impact forces. *See* Mechanical shock
- Implicit Runge-Kutta method, 137
- IMSL software, 111
- Increased stroke cams, 475, 476*f*
- Indexing cams. *See also* Intermittent motion mechanisms
  - globoidal, 10–11, 12*f*
  - operating forces and, 225, 225*f*
- Industrial adjustable mechanisms, performance characteristics of, 20
- Industrial production cams, most-popular, 6, 6*f*
- Inertia
  - equivalent, 331–332
  - as force, 219–220
- Inertia matrix
  - in planar contours, 184–185, 194–198
  - in solid regions, 185–186, 198–202
- Inspection
  - methods of, 291, 297–301
  - real-world example, 566–572, 573*f*–583*f*
- Integrals, truncation errors and, 177, 187
- Interior control, in DRRD curves, 97–98, 98*f*
- Intermittent motion mechanisms, 482*f*
  - concave globoidal cams, grooved, 486–487, 486*f*
  - cylindrical cam, 484–485, 485*f*
  - multiple double-end cam, 488–489, 488*f*
  - spider cams, 487, 487*f*
  - star-wheel cam, 489, 490*f*
  - types and uses of, 481–484
- Interrupted drive forces, 224–225
- Inverse cam, 13–14, 14*f*
  - in microvibromotor, 520–521, 521*f*
  - rotatable, 236–250
- Involute cams, 459–460, 460*f*
- Involute, of circle, 549–550, 549*f*
- Iron
  - cast, 265*f*–266*f*, 271, 532–533
  - ductile, 535
- Jerk
  - in automotive cams, 536, 537*f*, 538*f*
  - in constant acceleration curve, 35*f*, 58*f*
  - skewed, 37*f*
  - in cubic no. 1 curve, 39, 39*f*
  - in cubic no. 2 curve, 40, 41*f*
  - in cycloidal motion curve, 45, 45*f*, 58*t*
  - equation for, 29
  - extreme tolerances and, 296
  - in harmonic curves
    - double, 46, 46*f*
    - Freudenstein 1-3, 104
    - Freudenstein 1-3-5, 105
    - Gutman 1-3, 103
    - simple, 42, 42*f*, 58*t*
  - pertinence of, 31
  - in polydyne design, 440
  - in polynomial curves
    - 2-3, 91, 91*f*
    - 3-4-5, 58*t*, 92, 92*f*
    - 4-5-6-7, 58*t*, 92–93, 93
  - in polynomial equation, 90
  - in sine curve, modified, 58*t*, 76
  - in trapezoidal motion curve, 58*t*
  - modified, 58*t*
- Jump, 366, 366*f*
  - prevention of, 366–367, 367*f*
  - vibration and, 359
- Kinetic energy
  - of particle, 324
  - in planar motion, 325–327
  - of rotating body, 324–325
  - of system of particle, 324
  - of translating body, 324
- Knife-edge follower
  - definition of, 4, 4*f*
  - translating
    - curvature of, 191*f*, 192
    - pressure angle of, 191*f*, 192
    - relevance of, 190–192
- Knot sequence, 110, 114, 125–127
- Lapping, 296
- Leonardo da Vinci, 1
- Levers, equivalent weight of, 438–439
- L-head cam design, 531, 532*f*, 537

- LIGA, 510
- Linear ball bearings, 222, 222*f*
- Linear motion
- conversion from rotary, 474, 474*f*
  - conversion to rotary, 473–474, 473*f*
- Linear spring systems, 337*t*
- Linkage mechanisms
- cam-modulated, 454*f*
  - in MEMS, 512
  - performance characteristics of, 20
- Lithography, soft, 510
- Loads
- surface, 225–228
  - working, 218–219
- Lobe wheels, 457, 458*f*
- LOCAM, RADCAM software, 564
- Locking devices, in MEMS, 516–520, 517*f*, 518*f*, 519*f*
- Logarithmic spirals
- characteristics of, 548–549, 548*f*, 549*f*
  - rolling in, 457, 458*f*, 459*f*
- Lubrication, 273–281
- abrasive wear and, 263
  - adhesive bonding and, 262
  - boundary, 273–274, 273*f*
  - contaminants in, 281
  - corrosion protection and, 264
  - corrosive wear and, 263
  - elastohydrodynamic (EHD), 273–277, 273*f*, 276*t*, 280*f*
  - extreme-pressure (EP), 278–279, 280*f*
  - film thicknesses, 280*f*
  - follower wear and, 306
  - functions of, 277
  - grease, 277–278, 278*f*
  - hydrodynamic, 273, 273*f*
  - importance of, *x*
  - liquid systems, 278
  - mineral oil, 278, 278*t*
  - mixed-regime, 273, 273*f*
  - selection of, 277–281, 279*t*, 280*f*
  - self-lubrication, 270
  - of sliding followers, 312
- Lubrication film parameter, 276–277
- Lumped parameter modeling, 316–317
- Machine frames, rigidity of, 296, 359, 448
- MACSYMA software, 203
- Manual control, 286
- Manufacturing
- accuracy in
  - cutter tolerances and, 294, 294*f*, 295*f*
  - grinding to improve, 295–296
  - importance of, *x*, 21, 286, 287, 287*f*, 291
  - inspection
    - methods, 291, 297–301
    - real-world example, 566–572, 573*f*–583*f*  - quality control in, 285–286, 287
  - tolerances, typical, 291
- balance and, 363
- computers in. *See* Computer-aided design (CAD); Computer-aided manufacturing (CAM); Computer numerical control (CNC)
- errors in, 291–296
- finishing, importance of, 296
- material processes, 301–303
- materials. *See* Materials
- methods of, 286–287
- computer numerical control (CNC), 286, 288–291, 290*f*
  - master cam analog duplication method, 287–288, 288*f*, 289*f*
- real-world example, 566–572, 567*f*–583*f*
- toolmakers, knowledge of, 25
- MAPLE, 203
- Mass
- definition of, 327
  - equivalent, 329–332
  - in spring models, 341–342, 341*f*
- Massachusetts Institute of Technology, 512
- Mass-spring system
- complex model of, 319–321
  - simple model of, 317–319, 318*f*
- Master cam analog duplication method, 287–288, 288*f*, 289*f*
- Materials
- for automotive cams, 531–535
  - bronze alloy, 266*f*, 270–271, 271*f*
  - compatibility of
    - adhesion and, 262
    - designing for, 264–272, 265*t*–266*t*
    - importance of, 24  - elasticity of, in system design, 24
  - hardness, and wear, 269–270
  - iron
    - cast, 265*f*–266*f*, 271, 532–533
    - ductile, 535  - plastics, 270, 270*f*
  - processing of, 301–303
  - steels, hardened, 265*f*, 271–272, 532, 534–535
- Materials parameter, 276, 276*t*
- Mathcod software, 563

- MATHEMATICA software, 203
- MATLAB/SIMULINK software, 563
- MATLAB software, 111, 203
- Matthews, Gary, 537
- Mean squared error minimization, 413–416
- Mechanical advantage, equivalent springs and, 340–341, 340*f*
- Mechanical efficiency, damping and, 345–346
- Mechanical locking devices, in MEMS, 516–520, 517*f*, 518*f*, 519*f*
- Mechanical shock (impact force), 219, 400–406
- Melting practices, wear and, 302
- MEMS. *See* Microelectromechanical systems
- Metalworking, 302–303
- Microelectromechanical systems (MEMS)
- analog computing devices and, 494
  - applications for, 506–507, 510–511
  - cams in, 514–521
    - actuators for, 521–524
    - compliant mechanisms, 511, 511*f*, 513–514
    - friction and wear in, 525–526
    - manufacturing processes, 508–510, 509*f*, 510*f*
    - materials for, 507–508
    - mechanical structures in, 511–514
    - size of, 506
- Microelectronic Center of North Carolina, 509
- Micromachines. *See* Microelectromechanical systems (MEMS)
- Micromachining, 508–510, 509*f*, 510*f*
- Micromotors
- electrostatic, 522–523, 522*f*, 523*f*
  - electrostatic comb drive, 523, 524*f*
  - microindexing, 514, 515*f*
  - microvibromotor, 520–521, 521*f*
  - Sandia microengine, 524, 525*f*
- Microsystems technology (MST). *See* Microelectromechanical systems (MEMS)
- Microvibromotor, 520–521, 521*f*
- Mineral oil, as lubricant, 278, 278*t*
- Misalignment
- contact stresses and, 258–259, 258*f*, 259*f*
  - sources and effects of, 24, 294
  - vibration and, 359
- Mixed-lubrication regime, 273, 273*f*
- Model(s) and modeling
- of damping, 342–348
    - dry (Coulomb) friction, 344–345
    - equivalent dampers, 346–348
    - mechanical efficiency, 345–346
    - values in, determining, 342–343
  - viscous (speed-dependent) damping, 343–344
  - limitations of, 358–359
  - lumped parameter modeling, 316–317
  - mass, equivalent, in, 329–332
  - of natural frequency
    - complex systems, 319–321
    - model reduction, 321–324
    - simple systems, 317–319, 318*f*
    - sufficiency of, 321, 323
  - one-degree-of-freedom, adequacy of, 358, 400, 407, 449
  - purpose of, 316
  - selection criteria for, 316
  - sources on, 317
  - of springs, 331–342
    - coil springs, 334–335, 335*f*
    - equivalent springs, 340–341, 340*f*
    - linear, usefulness of, 331–332
    - mass in, 341–342, 341*f*
    - nonlinear, 333
    - spring combination, 338–340, 338*f*, 339*f*
  - valve-gear system, automotive, 348–354
  - of vibration
    - in elastic camshaft
      - one-degree-of-freedom, 374–384
      - two-degrees-of-freedom, 384–386, 385*f*
      - four-degrees-of-freedom, 386–389, 386*f*, 387*f*, 390*f*, 391*f*
      - multi-degrees-of-freedom, 389–395, 392*f*, 393*f*, 395*f*
    - in rigid camshaft
      - one-degree-of-freedom, 360–370, 361*f*, 363*f*, 364*f*, 365*f*
      - two-degrees-of-freedom, 327*f*, 370–371
- Mode shapes, 320
- Modified curves. *See* Combination of curves
- Moment of inertia
- of body, 327–328
  - kinetic energy and, 325
  - moving to other points, 329
  - in planar contours, 184–185
  - in solid regions, 186
- Motion, as design criteria, 2, 3*f*
- MOTOR DRIVE software, 564
- Motor(s), micro
- electrostatic, 522–523, 522*f*, 523*f*
  - electrostatic comb drive, 523, 524*f*
  - microindexing, 514, 515*f*
  - microvibromotor, 520–521, 521*f*
  - Sandia microengine, 524, 525*f*
- Mountings, for roller followers, 306, 307*f*

- MST (microsystems technology). *See*  
 Microelectromechanical systems (MEMS)
- Multiple double-end cams, 488–489, 488*f*
- Multi-User MEMS Processes (MUMPs), 509
- MUMPs (Multi-User MEMS Processes), 509
- Mushroom followers, 4*f*, 5, 312
- Natural frequency  
 in compliance models, 358  
 equations for, 318  
 models of  
   complex, 319–321  
   model reduction, 321–324  
   simple system, 317–319, 318*f*  
   sufficiency of, 321, 323
- NC machines. *See* Numerically controlled (NC) machines
- Needle bearings, 306, 307*f*
- Newspaper folding machine, 303–305, 304*f*, 305*t*
- Nitriding, 302, 303*f*
- Nomenclature, of cam-follower system, 17–19, 19*f*, 162*f*
- Nonadhesive wear, 260
- Noncircular gears, cam-modulated, 493–494, 494*f*
- Nonmetal inclusions, wear and, 301–302
- Nonparametric splines, 187
- Nonrigid cam-follower systems  
 cam design in  
   overview of, 127–128  
   spline functions in, 127–144  
 model for, 129–130, 136*f*
- Numerically controlled (NC) machines, 1, 286.  
*See also* Computer numerical control (CNC)
- Offset followers, 5, 5*f*
- OHC. *See* Overhead cam design
- OHV. *See* Overhead valve design
- Open cam systems, 14–15
- Open-track cams, 14  
 automotive, 14, 531  
 uses of, 358  
 vibration in, 375–378, 375*f*, 378*f*, 379*f*
- Operating forces, 224–225
- Optimal control theory, cams synthesis using, 416–427, 449–450, 585–586
- Orthogonal polynomials, 187
- Oscillating roller followers  
 curvature of, 192, 193*f*  
 pressure angle forces in, 166–168, 167*f*  
 pressure angle of, 192, 193*f*
- Overhead cam design (OHC), 531, 534*f*, 537
- Overhead valve design (OHV), 1, 2*f*, 489, 531, 533*f*, 537
- Oxidation, 263
- Parabolic curve. *See* Constant acceleration (parabolic) curve
- PARADE software, 561
- Parametric splines, 187
- Parts, spare, listing of, 303–305, 304*f*, 305*t*
- Path, as design criteria, 2, 3*f*
- Photolithography, 508
- Piecewise approximation of boundaries, 195–202
- Pitch circle, 19, 19*f*, 162*f*
- Pitch curve (pitch profile), 18, 19*f*, 162*f*, 192
- Pitch point, 19, 19*f*, 162*f*
- Pitch profile. *See* Pitch curve
- Pitting, 263, 263*f*, 306
- Planar contours. *See also* Cam profiles  
 geometric properties of, 184–185, 194–198  
 piecewise-linear approximation of boundary, 195–198
- Plastics, 270, 270*f*
- Plate cam, 7  
 flat-plate cam, 6  
 swash plate cams, 479–480, 480*f*
- PMM. *See* Precision measuring machine
- Polar moment of inertia, 185
- Polydyne design, 434–447  
 dwell-rise-dwell cams, 439–444  
 dwell-rise-return-dwell cams, 444–446, 445*f*, 450  
 jump reduction and, 366–367, 367*f*  
 ramps in, 437, 444, 446, 447  
 uses of, 450  
 vibration and, 446
- Polymide, 270
- Polynomial(s), orthogonal, 187
- Polynomial curves  
 2-3, 90–91, 91*f*  
 3-4-5  
   in dwell-rise-dwell cam, 58*t*, 91–92, 92*f*, 93, 94*t*, 95*f*  
   dynamic characteristics of, 405*f*, 406*f*  
   in polydyne design, 439, 440–443  
 3-4-5-6-7, 102  
 4-5-6-7  
   in dwell-rise-dwell cam, 58*t*, 92–93, 94*f*, 95*f*, 95*t*  
   dynamic characteristics of, 404*f*, 405*f*, 406*f*  
   in polydyne design, 439–440, 443–444

- 5-6-7-8-9, in polydyne design, 440, 443–444
- control
  - DRD cams, 94–96
  - DRRD cams, 96–98
- D-Curve, 102, 405*f*, 406*f*
- E-Curve, 102, 406*f*
- eighth degree, 84*f*, 100–101
- eleventh degree, 101–102, 405*f*, 406*f*
- exponent manipulation, 99–102, 99*f*, 100*f*
- fifth order, acceleration in, 99*f*
- Fourier series, 103–105
- general derivation, DRD cam, 94–96
- high order, 99, 100*f*, 109, 446, 446*f*
- in polydyne design, 439–440
- seventh order, acceleration in, 100*f*
- simple, in dwell-rise-dwell cam, 32–40
- Polynomial equation
  - constant velocity, 90
  - in curve generation, 109
  - degree of, 109
  - general form of, 89–90
- Polysilicon, 508
- Positive drive action, in followers, 4
- Potential energy, in spring, 333–334
- Precision measuring machine (PMM), 291, 292*f*
- Press, cam-operated, 21, 22*f*
- Pressure angle
  - calculation of, 193–194
  - definition of, 18, 162
  - determination of, 179, 180*f*
  - maximum, 18–19, 20*f*
  - of roller followers, 191*f*, 192, 193*f*
  - software for, 561
  - of translating knife-edge follower, 191*f*, 192
- Pressure angle forces
  - in oscillating roller follower, 166–168, 167*f*
  - in translating flat-faced follower, 168–169, 168*f*, 189–190
  - in translating roller follower, 163–166, 164*f*, 166*f*
- Pressure-viscosity coefficient, 275, 276, 276*t*
- Prime circle, 18, 19*f*
- Prime profile, 162*f*
- PRO/ENGINEER software, 203, 562
- Progressive coil springs, 335, 336*f*
- PRO/MECHANICA software, 562
- Quick-action cams, 471–472, 472*f*
- Quintic spline functions, 187
- RAD1 software, 562
- RAD2 software, 562
- Radial cams
  - contour-shaped, 464–465, 464*f*, 465*f*
  - definition of, 7, 8*f*
  - displacement diagrams of, 18
- Radial followers, 5
- Radius of curvature
  - cam size and, 169
  - definition of, 180
  - determination of, 180–184
  - equations for, 169–170
  - of pitch curve, 19
  - software for, 561–562
  - and undercutting
    - in cam-roller follower, 170–172, 172*f*
    - in flat-faced follower, 173, 173*f*
- Ramps
  - in automotive cams, 535–536
  - in polydyne design, 437, 444, 446, 447
- Rectangular hyperbolic curves, 547, 547*f*
- Resonance, 321
  - factors affecting, 368
  - reduction of, 405
  - shifting of, 359
  - vibration effects and, 359
- Resonance factor, 537
- Response spectrum
  - definition of, 401–402
  - of dwell-rise-dwell cams, 402–406, 404*f*, 405*f*, 406*f*
- Revolute joints, in MEMS, 511–512, 512*f*, 513*f*
- Rigid camshafts
  - dynamic phenomena in, 322–374
  - vibration models of
    - one-degree-of-freedom, 360–370, 361*f*, 363*f*, 364*f*, 365*f*
    - two-degrees-of-freedom, 370–371, 372*f*
- Rise-return-rise cam (RRR), 15, 15*f*
- Roller, conical, 309, 310*f*
- Roller followers, 4–5, 4*f*, 221*f*
  - automotive, materials for, 534–535
  - cam contact maintenance, 309, 309–312, 310*f*, 311*f*
  - in circular-arc cam, 465–466, 466*f*
  - contact stresses in, 255, 256–258, 256*f*, 257*f*, 258*f*
  - crowned, 253–255, 254*f*, 258–259, 259*f*, 306, 308*f*
  - curvature of, 191*f*, 192, 193*f*
  - double roller, 309–312, 311*f*
  - in eccentric circle cams, 460–463, 461*f*

- friction in, 221–222
- installations, 306–312, 310*f*, 311*f*
- mountings, 306, 307*f*
- oscillating
  - curvature of, 192, 193*f*
  - pressure angle forces in, 166–168, 167*f*
  - pressure angle of, 192, 193*f*
  - pressure angle of, 191*f*, 192, 193*f*
- rollers replacement, 252, 267
- single roller, 309, 310*f*
- sliding in
  - causes of, 306–308
  - reduction of, 308–312
- tangent cams, 466–467, 467*f*
- translating
  - pressure angle forces in, 163–166, 164*f*, 166*f*
  - torque in, 228–230, 230*f*, 308–309
- undercutting in, 170–172, 172*f*
- wear and, 305–306
- Roller gear drive, 10, 488–489, 488*f*
- Rolling
  - in basic contours, 457–459, 458*f*
  - mechanics of, 456–457, 456*f*
  - pure, defined, 456
- Rolling cam, 9
- Rotary motion
  - conversion from linear, 473–474, 473*f*
  - conversion to linear, 474, 474*f*
- Rotary spring systems, 337*t*
- Rotatable inverse cam mechanism, 236–250
- Roughness
  - composite, 276
  - grinding to remove, 295–296
- RRR. *See* Rise-return-rise cam
  
- Sandia Laboratories, 509, 514, 516, 524, 526
- Sandia Ultra-planar, Multi-level MEMS Technology (SUMMiT), 509, 514, 524
- Scoring, 261
- Scotch yoke, 14
- Scuffing, 261
- Second moment, in planar contours, 185. *See* Variable valve timing, VVT
- Self-lubrication, 270
- Series, cams in, 471, 471*f*
- Servo valve-controlled hydraulic cylinders, 20
- Seventh-order polynomial curves, acceleration in, 100*f*
- Shaft windup, 374–375, 380
  - in closed-track systems, 378–384, 379*f*, 380*f*, 381*f*, 382*f*
  - in open-track systems, 375–378, 375*f*, 378*f*, 379*f*
- Shape, cam classification by, 6–14
- Shock, definition of, 400
- Shock response spectrum. *See* Response spectrum
- Side thrust
  - in oscillating roller follower, 167
  - in translating flat-faced follower, 168
  - in translating roller follower, 163–166, 164*f*, 166*f*
- Silicon, 507–508
- Simple harmonic curves
  - in dwell-rise-dwell cam, 40–44, 41*f*, 42*f*, 50*t*, 52*f*, 58*t*
  - for dwell-rise-return-dwell cams, 53, 53*f*
  - segment characteristics, 82*f*
  - spring forces and, 223, 224*f*
  - torque in, 230, 231*f*
  - transient-response curves, 362, 363, 363*f*, 364*f*
- Sine curve
  - in dwell-rise-dwell cam, modified, 58*t*, 73–76, 73*f*
  - modified
    - characteristics of, 76, 77*f*–78*f*, 404*f*, 405*f*, 406*f*
    - factors for, 555*t*
    - high-speed systems and, 448
    - torque in, 230, 231*f*
- Size of cam
  - design of, 21
  - in flat-faced followers, 173
  - minimization of, 204–208
  - pressure angle and, 162
  - and radius of curvature, 169
  - roller acceleration and, 309
- Skewed constant acceleration curves, 37–38, 37*f*
- Skewed modified trapezoidal curves, 70–73, 71*f*, 72*f*
- Sliding
  - causes of, 306–308
  - mechanics of, 454–455, 455*f*
  - pure, defined, 456
  - reduction of, 308–309
  - wear and, 264–267, 265*t*–266*t*, 268*f*
- Sliding followers
  - automotive, materials for, 532–534
  - installations, 312, 312*f*
  - lubrication of, 312

- Slope  
 of acceleration curve, 29  
 of velocity curve, 29
- Soft lithography, 510
- Software packages  
 automotive design, 537, 540, 541, 563–564  
 CAD, 203, 561–563  
 mathematics and geometry, 203, 561–562
- Solid regions, geometric properties of,  
 185–186, 198–202
- Spalling, 263, 263*f*, 306
- Spare parts, listing of, 303–305, 304*f*, 305*r*
- SPEC1 software, 563
- SPEC2 software, 563
- SPEC3 software, 563
- Speed-dependent (viscous) damping,  
 343–344
- Speed of cam-follower system, design of, 21
- Speed-reduction mechanism, camshaft  
 balancing in, 209–215
- Spherical cam, 12, 12*f*
- Spherical followers, 4*f*, 5, 312  
 contact stresses in, 258–259, 259*f*  
 friction in, 221
- Spider cams, intermittent motion mechanisms,  
 487, 487*f*
- Spiral(s)  
 Archimedes spiral, 33  
 logarithmic, 548–549, 548*f*, 549*f*  
 rolling in, 457, 458*f*, 459*f*
- Spiral cams, 9, 10*f*  
 in analog computing mechanisms, 296–297,  
 296*f*, 498–501, 498*f*, 499*f*  
 in cutter mechanism, 468–469, 469*f*  
 in micromechanical lock, 516–518, 517*f*
- Spline(s)  
 B-splines  
 constraints, large number of, 115–116  
 continuity and, 109, 110, 132  
 nonrational, 109–117  
 derivatives, evaluation of, 111  
 evaluation of, 111  
 expression for, 109–110  
 in nonrigid cam-follower systems,  
 127–144  
 rational, 117–127  
 definition of, 119–120  
 derivatives, evaluation of, 121–122  
 evaluation of, 119–121  
 expression for, 117–118  
 properties of, 117–118, 120–121,  
 126–127  
 software packages for, 561  
 in 3-D cams, 144–152  
 vs. Bezier curves, 109  
 cubic, 187–189, 193–194, 197–198  
 definition of, 187  
 nonparametric, 187  
 parametric, 187  
 quintic functions, 187
- Spline collocation method  
 nonrational splines, 109–117  
 in nonrigid systems, 128, 136–144  
 rational splines, 117–127
- Sprag clutch, 470, 470*f*
- Spring(s)  
 in automotive cams, 529  
 bottoming out of, 335  
 design of, 223–224  
 energy storage in, 333–334  
 equivalent weight of, 438  
 follower contact maintenance and, 309  
 force in, 222–223, 418–419  
 models of, 331–342  
 coil springs, 334–335, 335*f*  
 combinations, 338–340, 338*f*, 339*f*  
 equivalent springs, 340–341, 340*f*  
 linear, usefulness of, 331–332  
 mass in, 341–342, 341*f*  
 nonlinear, 333  
 stiffness (spring rate), 332, 337*t*  
 of coil spring, 334  
 determination of, 333–334, 335–338  
 equivalent, 340–341, 340*f*  
 of parallel springs, 339  
 of series springs, 339–340
- SPRINGMASTER software, 540, 541, 564
- Spring rate, 332, 337*t*  
 of coil spring, 334  
 determination of, 333–334, 335–338  
 equivalent, 340–341, 340*f*  
 of parallel springs, 339  
 of series springs, 339–340
- Spring ratio constant, 437–438
- Spring surge, 374, 540–541
- Stamping mechanism, 489, 491*f*
- Startup forces, 224
- Star-wheel cam, 489, 490*f*
- Star-wheel mechanism, 482–483, 483*f*
- Stationary cam, 14
- Steels, hardened, 265*f*, 271–272, 532, 534–535
- Stick-slip friction, 345
- Stiction, 345, 360, 525
- Stop forces, 224

- Straddle (yoke) mountings, 306, 307*f*
- Stress
- contact, 256–260, 257*f*, 258*f*
    - in flat-faced followers, 258, 258*f*
    - minimization of, 419–420, 424–425
    - in nonrigid systems, 131
  - subsurface, industry standard for, 303
- Stress corrosion, 264
- Stribeck-Hersey curve, 273, 273*f*
- Structural errors, in manufacturing, 293
- Stud mountings, 306, 307*f*
- Subsurface stress, industry standard for, 303
- SUMMiT (Sandia Ultra-planar, Multi-level MEMS Technology), 509, 514, 524
- Surface(s), cam and follower
- asperities on, 260–261, 261*f*
  - contact stresses. *See* Contact stresses
  - design of
    - factors in, 252
    - methodology, general, 252
    - wear and, 264–272
  - elastic contact theory, 253–255, 254*f*
  - materials for. *See* Materials
  - roughness
    - composite, 276
    - grinding to remove, 295–296
  - surface films, 260
  - surface loads, 225–228
  - waviness in, 293–294, 294*f*, 295*f*
  - wear. *See* Wear
- Surface fatigue, 263–269, 263*f*
- causes of, 263–264
  - prevention through design, 264–269
  - testing on, 264–269, 265*t*–266*t*
- Surface loads, 225–228
- Surface micromachining, 509, 509*f*
- Surging, 223
- Swash plate cams, 479–480, 480*f*
- SWIRL METER software, 541, 564
- Symmetrical dwell-rise-return-dwell cams, 53, 53*f*
- Synthesis of motion programs
- displacement programs, 193–194
  - overview of, 108–109
- Tangent cam, translating roller follower, 466–467, 467*f*
- Tangent, determination of, 178–179, 178*f*
- 3-D cams, 12–13, 13*f*, 149*f*
- applications, 144–145
  - in computing mechanisms, 496*f*, 497
  - offset surface, expression for, 146–147
  - surface, expression for, 145–146
  - synthesis of motion, B-splines in, 144–152
- Three-dimensional cams. *See* 3-D cams
- 3-4-5 polynomial curves
- in dwell-rise-dwell cam, 58*t*, 91–92, 92*f*, 93, 94*t*, 95*f*
  - dynamic characteristics of, 405*f*, 406*f*
  - in polydyne design, 439, 440–443
- 3-4-5-6-7 polynomial curves, 102
- Time charts
- in graphical layout method, 160, 161*f*
  - uses of, 18, 18*f*
- Timing diagrams. *See* Time charts
- TK Solver software, 563
- Tolerances
- accumulated error and, 296
  - extreme, jerk and, 296
  - probabilistic error and, 294, 294*f*, 295*f*
  - typical, 291
- Toolmakers, input from, 25
- Torque, 219–220, 228–236
- in cycloidal curve, 230, 231*f*
  - in flat-faced followers, 230–232, 231*f*
  - in roller followers, 228–230, 230*f*, 308–309
  - in simple harmonic curves, 230, 231*f*
  - in sine curve, modified, 230, 231*f*
- Torque-controlled cams, 232–235, 233*f*, 234*f*
- Torque-controlled wrapping cams, 235–236
- Torque curve, in cam-follower design, 21
- Torsional ratcheting microactuator, 514–516, 516*f*, 517*f*
- Torsional springs, 334, 334*f*
- Trace point, 18, 19*f*, 162*f*
- Transition point, 17*f*, 18, 19
- Translating cams
- characteristics of, 5*f*, 6, 7*f*
  - linear ball bearings for, 222, 222*f*
- Translating flat-faced followers
- curvature of, 190, 190*f*, 191*f*
  - pressure angle forces in, 168–169, 168*f*, 189–190
  - torque in, 230–232, 231*f*
- Translating knife-edge follower
- curvature of, 191*f*, 192
  - pressure angle of, 191*f*, 192
  - relevance of, 190–192
- Translating roller follower
- pressure angle forces in, 163–166, 164*f*, 166*f*
  - torque in, 228–230, 230*f*, 308–309
- Trapezoidal cam, acceleration DRS of, 402, 403*f*

- Trapezoidal curves, 58*t*, 61, 61*f*  
 building of, 61  
 factors for, 554*t*  
 modified, 58*t*, 61–70, 62*f*, 68*f*  
   characteristics of, 76, 77*f*–78*f*  
   dynamic characteristics of, 404*f*, 405*f*,  
   406*f*  
   high-speed systems and, 448  
   skewed modified, 70–73, 71*f*, 72*f*
- Trigonometric curves  
 characteristics of, 32, 40–48  
 comparison of, 48–49, 50*t*, 51*f*–52*f*
- Trigonometric series, finite, cams synthesis  
 using, 407–416, 449
- Troubleshooting, general approach to, 24
- Truncation errors, integrals and, 177, 187
- Tuned cam design, 408–413, 416
- Tuned dwell-rise-dwell cams, optimization of,  
 421–425
- Tuned dwell-rise-return-dwell cams,  
 optimization of, 425–427
- Two-revolutions-per-cycle cams, 474–475, 475*f*
- 2-3 polynomial curve, 90–91, 91*f*
- Undercutting  
 in cam-roller follower, 170–172, 172*f*  
 in flat-faced follower, 173, 173*f*
- Unidirectional cam clutches, 470–471, 470*f*
- Uniform displacement curve. *See* Constant  
 velocity curve
- UNIGRAPHICS software, 203, 562
- UTILITY ENGINE PROGRAMS software,  
 541, 564
- Vacuum degassing, 302
- Vacuum induction, 302
- Vacuum induction-melting vacuum arc  
 remelting (VIM-VAR), 302
- Valve bounce, 540–541, 540*f*
- VALVE PRO software, 541, 564
- Valve train lash, 539–540, 539*f*
- Variable-angular-velocity cams, 480, 481*f*
- Variable-dwell cam, 472, 473*f*
- Variable valve timing (VVT), 471
- Vector first moment, of solid region, 185,  
 194–197
- Velocity  
 in automotive cams, 536, 537*f*, 538*f*  
 in combining curves, 57, 63  
 in constant acceleration curve, 35–36, 35*f*,  
   50*t*, 51*f*, 58*t*  
   skewed, 37*f*, 38
- in constant velocity curve, 33, 33*f*, 50*t*  
 in cubic no. 1 curve, 39, 39*f*, 50*t*, 51*f*  
 in cubic no. 2 curve, 40, 41*f*, 50*t*, 51*f*  
 in curve factor calculations, 551  
 in cycloidal curve, 45, 45*f*, 50*t*, 52*f*, 58*t*, 77*f*,  
   83*f*  
 in dwell-rise-dwell curves, general  
   derivation, 94–96  
 in eighth-degree polynomial curves, 84*f*  
 in elliptical curve, 48, 49*f*  
 equation for, 28–29  
 factors in, 30  
 in Freudenstein 1-3-5 harmonic, 104–105  
 in Freudenstein 1-3 harmonic, 104  
 in Gutman 1-3 harmonic, 103  
 in harmonic curve  
   double, 46, 46*f*, 50*t*, 51*f*  
   simple, 42–44, 42*f*, 50*t*, 52*f*, 58*t*, 82*f*  
 in polynomial curves  
   2-3, 90–91, 91*f*  
   3-4-5, 58*t*, 91–92, 92*f*  
   4-5-6-7, 58*t*, 93, 94*f*  
   simple, 32  
 in polynomial equation, 90  
 relative tangential, 455  
 sign of, 29  
 in sine curve, modified, 58*t*, 76, 77*f*  
 spline weight sequence and, 123–124  
 in trapezoidal curve, 58*t*  
   modified, 58*t*, 61–67, 62–63, 68*f*, 77*f*  
   skewed modified, 70–73, 71*f*, 72*f*
- Velocity curve, slope of, 29
- VERSACAD software, 203, 562
- Vibration  
 in closed-track cams, 378–384, 379*f*, 380*f*,  
   381*f*, 382*f*  
 as compliance measure, 357 (*see also*  
   Compliance)  
 dynamic response spectra  
   definition of, 401–402  
   of dwell-rise-dwell cams, 402–406, 404*f*,  
   405*f*, 406*f*  
 factors affecting, 372–374, 400  
 forces in, 220  
 in high-speed systems, 447  
 minimization of  
   in cam profile design, 103  
   overview of, 406–407  
   with polydyne design, 434–447, 450  
 models of  
   in elastic camshaft  
     one-degree-of-freedom, 374–384

- two-degrees-of-freedom, 384–386, 385*f*
- four-degrees-of-freedom, 386–389, 386*f*, 387*f*, 390*f*, 391*f*
- multi-degrees-of-freedom, 389–395, 392*f*, 393*f*, 395*f*
- rigid camshaft
  - one-degree-of-freedom, 360–370, 361*f*, 363*f*, 364*f*, 365*f*
  - two-degrees-of-freedom, 370–371, 372*f*
- natural frequency
  - complex model of, 319–321
  - model reduction, 321–324
  - model sufficiency, 321, 323
  - simple model of, 317–319, 318*f*
- in nonrigid systems, 138–139
- in open-track cams, 375–378, 375*f*, 378*f*, 379*f*
- primary vs. residual, 400, 401*f*
- reduction of, 359
  - using convolution operator, 427–434, 450
  - using finite trigonometric series, 407–416, 449
  - using optimal control theory, 416–427, 449–450, 585–586
- resonance. *See* Resonance
- software for, 563
- sources of, 357–368, 447–448
- steady state vs. transient, 400
- VIM-VAR. *See* Vacuum induction-melting vacuum arc remelting (VIM-VAR)
- Viscous (speed-dependent) damping, 343–344
- Volume, calculation of, 185, 198–199
- VVT. *See* Variable valve timing
- Waviness in cam surface, 293–294, 294*f*, 295*f*
- Wear, 260–272
  - abrasive, 260, 263
  - adhesive, 260, 261–262, 262*f*
  - in automotive valve trains, 540–541
  - cavitation, 260
  - corrosive, 263
  - designing to minimize, 264–272
  - erosive, 260
  - examination for, 260
  - fretting corrosion, 260
  - material processes and, 301–303
  - in microelectromechanical systems, 525–526
  - nonadhesive, 260
  - roller-follower shape and, 306, 308*f*
  - in single roller followers, 309
  - sliding and, 264–267, 265*t*–266*t*, 268*f*
  - statistical data on, 264
  - types of, 260
- Wedge cam
  - definition of, 6
  - in microindexing motor, 514, 515*f*
- Weight, equivalent, in polydyne design, 438–439
- Weight sequence, of rational spline, 120–121, 123–127
- Westinghouse Research Laboratories, 506
- Whitworth mechanism, 480, 481*f*
- Wildt curve, 76–78, 79*f*
- Winfield, Ed, 529
- Wiper cam, 9
- Working loads, 218–219
- Worm/worm-gear, cam-modulated, 490, 491*f*
- Wrapping cams, torque-controlled, 235–236
- Yoke cam, 7–8, 8*f*
- Yoke mountings, 306, 307*f*
- Zeroth moment, in planar contours, 185

## **ABOUT THE EDITOR**

---

Harold A. Rothbart is a noted consulting engineer and lecturer, and is the author of numerous books including McGraw-Hill's *Mechanical Design Handbook*. He is the former Dean of the College of Science and Engineering at Fairleigh Dickinson University in New Jersey.